PROGRAMA DE PÓS-GRADUAÇÃO EM CIÊNCIAS BIOLÓGICAS: BIOQUÍMICA
DEPARTAMENTO DE BIOQUÍMICA
INSTITUTO DE CIÊNCIAS BÁSICAS DA SAÚDE
UNIVERSIDADE FEDERAL DO RIO GRANDE DO SUL

Tese de Doutorado

O envolvimento da proteína fosfatase 2A e do sistema glutamatérgico em processos neurodegenerativos relacionados à doença de Alzheimer: mecanismos e biomarcadores de imagem

Eduardo Rigon Zimmer

Porto Alegre

2015

PROGRAMA DE PÓS-GRADUAÇÃO EM CIÊNCIAS BIOLÓGICAS: BIOQUÍMICA
DEPARTAMENTO DE BIOQUÍMICA
INSTITUTO DE CIÊNCIAS BÁSICAS DA SAÚDE
UNIVERSIDADE FEDERAL DO RIO GRANDE DO SUL

O envolvimento da proteína fosfatase 2A e do sistema glutamatérgico em processos neurodegenerativos relacionados à doença de Alzheimer: mecanismos e biomarcadores de imagem

Tese apresentada ao Programa de Pós-Graduação em Ciências Biológicas – Bioquímica da Universidade Federal do Rio Grande do Sul, como requisito parcial à obtenção do grau de Doutor em Bioquímica.

Eduardo Rigon Zimmer

Orientador: Prof. Luis Valmor Cruz Portela

Porto Alegre

2015

“We are all agreed that your theory is crazy.

The question which divides us is whether it

is crazy enough to have a chance

of being correct.”

Niels Bohr

Aos meus pais,

pelo ombro, pelo choro,

pelo sorriso, pelo abraço e

pelo suporte incondicional.

Agradecimentos

Ao meu orientador, Professor Luis Valmor Cruz Portela, um grande pesquisador e amigo, por ter me iniciado na ciência e ser meu maior guia científico durante todos estes anos.

Ao Professor Pedro Rosa-Neto, um grande neurocientista e amigo, pela orientação, liberdade científica e as discussões intermináveis.

Ao Professor Diogo Onofre Gomes de Souza, o "Mestre", por ser um exemplo de amor a vida e a pesquisa científica, sem dúvidas um dos meus maiores incentivadores nesta caminhada.

Ao Professor Marcelo de Oliveira Dietrich, um pesquisador genial e amigo, por todos estes anos de orientação científica e de "normalidade".

Ao pessoal dos laboratórios 26 e 28 do Departamento de Bioquímica da UFRGS e do *Translational Neuroimaging Laboratory* da McGill, pela ajuda nos procedimentos científicos e por terem me ensinado muito sobre amizade.

A Fabiana de Melo, minha vida, por ter me ensinado o significado do amor verdadeiro, e por ter sido minha maior companheira durante esta caminhada. Agradeço diariamente por fazeres parte de minha vida.

Aos meus irmãos, Aline, Karine e Marcelo, grandes pesquisadores, pelo amor e apoio durante todos estes anos. Sem vocês eu nada seria.

A minha mãe, Arlete, pelo amor incondicional, apoio constante e força nas horas difíceis. Tu és meu maior pilar.

Ao meu Pai, Nelson, que teve o sonho de vida acadêmica interrompido, pelo apoio incondicional e por ter sido meu maior incentivador. Esta tese também és tua.

APRESENTAÇÃO

Esta tese está organizada em três **Partes**, cada uma sendo constituída dos seguintes itens:

Parte I: Resumo, Resumo em inglês (*abstract*), Lista de abreviações, Introdução e Objetivos;

Parte II: Resultados, que estão divididos em capítulos, sendo cada que capítulo contém um breve prefácio seguido de um artigo científico;

Parte III: Discussão, Conclusão, anexos e Referências bibliográficas citadas na Introdução da Parte I e Discussão da Parte III.

Na seção “anexos” estão os artigos científicos que foram realizados durante o período de doutoramento que tem conteúdo associado a tema da tese (Anexo I) e que não são diretamente associados com o tema da tese (Anexo II). Os trabalhos elaborados nesta tese foram desenvolvidos no laboratório de Neurotrauma, no Departamento de Bioquímica da Universidade Federal do Rio Grande do Sul (UFRGS), sob a orientação do Dr. Luis Valmor Cruz Portela, como também no Laboratório de Neuroimagem translacional da Universidade McGill (Canada), sob a orientação do Dr. Pedro Rosa-Neto.

Sumário

PARTE I

Resumo

Zimmer, Eduardo Rigon**. O envolvimento da proteína fosfatase 2A e do sistema glutamatérgico em eventos neurodegenerativos relacionados a doença de Alzheimer: mecanismos e biomarcadores de imagem.** Tese de Doutorado, Programa de Pós-graduação em Ciências Biológica: Bioquímica, Universidade Federal do Rio Grande do Sul. Porto Alegre, Brasil, 2015.

A doença de Alzheimer (DA) é uma patologia neurodegenerativa progressiva e a forma de demência mais prevalente no mundo. As alterações fisiopatológicas da DA têm sido associadas a dois marcadores neuropatológicos clássicos: a deposição de placas de β-amilóide e a formação de emaranhados neurofibrilares da proteína tau hiperfosforilada. Porém, devido a complexidade da DA, outros mecanismos têm sido propostos como coadjuvantes no processo neurodegenerativo, entre eles eventos neuroinflamatórios, a quebra da homeostasia de sistemas de neurotransmissão e disfunção sináptica. Esta pletora de eventos patológicos parece preceder a fase de demência por um longo período onde a doença age de forma silenciosa, ou seja, onde não existem evidências sintomatológicas. Na presente tese, avançamos no entendimento de vias de sinalização associadas com a hipersforforilação da proteína tau envolvendo a disfunção da proteína fosfatase 2A e neurotoxicidade do sistema glutamatérgico. Além disso, avaliamos os radiofármacos de tomografia de emissão de pósitrons (PET) disponíveis para visualização *in vivo* e não invasiva da fisiopatologia da DA. Finalmente, avaliamos um novo biomarcador de PET, o [^{11}C]ABP688, para visualizar flutuações no sistema glutamatérgico e avançamos no entendimento do impacto das células gliais no sinal do PET [^{18}F]FDG, o radiofármaco mais utilizado na clínica atualmente para visualizar metabolismo de glicose cerebral. O [^{11}C]ABP688 pode ser diretamente incluído em estudos clínicos e a reconceptualização do [^{18}F]FDG proposta nesta tese pode alterar a maneira atual como vemos o metabolismo de glicose na DA e em outras doenças neurodegenerativas. Finalmente, nesta tese, avançamos em termos de mecanismos, e no contexto da busca por um diagnóstico precoce e acurado da DA.

Palavras-chave: Doença de Alzheimer; glutamato; proteína fosfatase 2A; taupatia; tomografia por emissão de pósitrons.

Abstract

Zimmer, Eduardo Rigon. **The involvement of protein phosphatase 2A and glutamatergic system in neurodegenerative processes related to Alzheimer's disease: mechanisms and imaging biomarkers.** PhD Thesis, Post-graduation Program of Biological Sciences: Biochemistry, Universidade Federal do Rio Grande do Sul. Porto Alegre, Brazil, 2015.

Alzheimer's disease (AD) is a progressive neurodegenerative disorder and the most prevalent cause of dementia worldwide. The AD pathophysiological features have been associated to two main classic neuropathological markers: depositon of β-amyloid plaques and formation of neurofibrillary tangles of hyperphosphorylated tau. Due to AD complexity, however, additional mechanisms have been proposed as contributors to the neurodegenerative process, such as neuroinflammatory changes, altered neurotransmission, and synaptic dysfunction. These pathological events seem to precede the dementia phase by many years, resulting in a long silent period, i.e., a preclinical phase. In this thesis, we advanced in the understanding of signaling pathways associated with tau hyperphosphorylation, which includes dysfunction of protein phosphatase 2A (PP2A) and glutamatergic neurotoxicity. Furthermore, we underscored radiopharmaceuticals currently available for imaging AD pathophysiology *in vivo* and non-invasively with positron emission tomography (PET). Finally, we evaluated a new PET biomarker, [^{11}C]ABP688, for visualizing glutamatergic fluctuations and advanced in the understating of how glial cells contribute to the [^{18}F]FDG signal, the widely used radiopharmaceutical in clinical settings for visualizing cerebral glucose metabolism. Our findings have high translational value and direct impact in clinical settings, which can potentially alter the way we interpret glucose metabolism in AD and other neurodegenerative disorders. In summary, in this thesis, we have advanced in terms of molecular mechanisms, and in the use of PET biomarkers toward an early and accurate diagnosis of AD.

Keywords: Alzheimer's disease; glutamate; positron emission tomography; protein phosphatase 2A; tauopathy.

Lista de abreviaturas

[^{11}C]PIB	[^{11}C] Composto B de Pittsburgh
[^{18}F]FDG	[^{18}F] Fluoro-deoxi-glicose
AMPA	Alfa-amino-3-hidroxi-metil-5-4-isoxazolpropiónico
APP	Proteína precursora de amilóide
Aβ	β-amilóde
CAT	Catalase
CDK5	Ciclina dependente de cinase 5
CN	Cognitivamente normal
DA	Doença de Alzheimer
EPM	Labirinto em cruz elevado
FDA	Food and Drug Administration
FTDs	Demências frontotemporais
GLAST	Transportador Glutamato-aspartato
GLT-1	Transportador de Glutamato Tipo 1
GM	Substância cinzenta
GSH-Px	Glutationa peroxidase
GSK-3β	Glicogênio sintase cinase 3-beta
ICV	Intracerebroventricular
IH	Intrahipocampal
KA	Cainato
IL-1	Interleucina 1
IL-6	Interleucina 6

LCR	Líquido cefalorraquiano
LDB	Teste do claro-escuro
MAP	Proteína associada de microtúbulo
MARK	Proteína reguladora associada a microtúbulo
MCI	Declínio cognitivo leve
mGluR	Receptores metabotrópicos de glutamato
MRI	Imagem por ressonância magnética
MWM	Labirinto aquático de Morris
NFTs	Emaranhados neurofibrilares
NIH	National Institutes of Health
NMDA	N-metil D-Aspartato
OKA	Ácido ocadáico
P-tau	Tau fosforilada
PET	Tomografia por emissão de pósitrons
PKA	Proteína cinase dependente de cAMP
PP2A	Proteína fosfatase 2A
PS1	Presenilina 1
PS2	Presenilina 2
sAPPα	Fragmento solúvel da proteína precursora de amilóide
Ser	Serina
SNC	Sistema nervoso central
SOD	Superóxido Dismutase
t-tau	Tau total

TNF-alfa	Fator tumoral de necrose alfa
Tre	Treonina
TSPO	Proteína translocadora de 18 kDa
WM	Substância branca

Introdução

O envelhecimento é um fenômeno natural que pode ser definido como as alterações biológicas de um determinado organismo em função do tempo. Este processo favorece a danificação de moléculas, células e tecidos, e ultimamente leva a fragilidade e morte (Heemels, 2010). Neste sentido, o aumento da expectativa de vida da população tem sido associado aos avanços na medicina e a processos evolutivos (Vaupel, 2010). De fato, segundo o *Global AgeWatch* dados de 2012 demonstram que cerca de 11% da população mundial tem mais de 60 anos. Estima-se que em 2030 este número chegue a 16%, e a massivos 22% da população em 2050, ou seja, cerca de 2,3 bilhões de pessoas com mais de 60 anos (http://www.helpage.org/global-agewatch/). É importante ressaltar que o envelhecimento é um dos principais fator de risco para o desenvolvimento de diversas patologias, que incluem o câncer e doenças cardiovasculares.

Entretanto, os maiores mistérios do envelhecimento se concentram nas alterações produzidas no sistema nervoso central (SNC). Neste sentido, estudos clínicos de grande escala estão em andamento, entre eles o *Harvard Aging Brain Study (http://nmr.mgh.harvard.edu/lab/harvardagingbrain)* e *A4 study (http://a4study.org)*, e tem como principal objetivo entender o envelhecimento normal do cérebro e identificar pacientes em risco de desenvolver doenças neurodegenerativas, como a doença de Alzheimer (DA). Neste sentido o foco total é na DA, pois ela é responsável por mais de 50% de todos os casos de demência e caminha a passos largos para números considerados epidêmicos, assim sendo, um dos maiores desafios globais na área da saúde (Alzheimer's, 2015).

A doença de Alzheimer

A DA foi descrita a mais de um século atrás, em 1906, pelo Psiquiatra alemão Alois Alzheimer na 37ª Reunião dos Psiquiatras do Sudoeste Alemão (do inglês *37th Assembly of Southwest German Psychiatrists)* em Tubingen. A palestra do Dr. Alzheimer intitulada "Uma doença característica do Córtex Cerebral" (do inglês *A Charateristic Disease of the Cerebral Cortex)* descrevia os sintomas de Auguste Deter (**figura 1a**), uma mulher de 51 anos que exibia declínio cognitivo progressivo, alucinações e incompetência psicossocial. A autopsia do cérebro de Auguste Deter revelou a deposição evidente de "substâncias peculiares" espalhadas pelo córtex cerebral (**figura 1b**) (Jucker *et al.*, 2006).

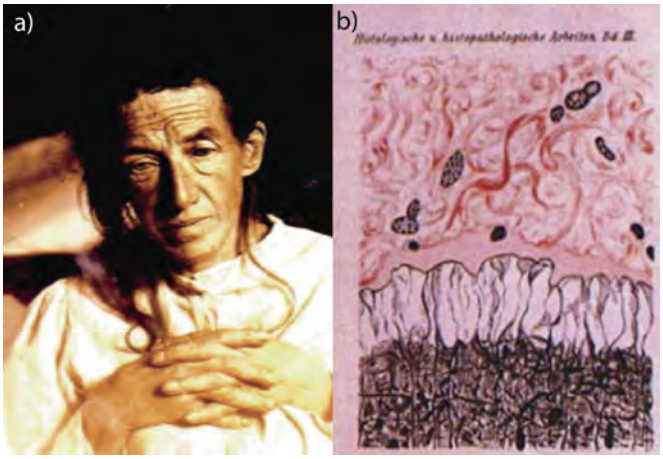

Figura 1. Auguste Deter e a "substância peculiar" no córtex. a) Retrato de Auguste Deter com 51 anos. b) Desenhos feitos com auxílio da câmera lúcida[1] da substância peculiar depositada no córtex de Auguste Deter. Figuras adaptadas de (Jucker *et al.*, 2006).

Abaixo uma tradução do caderno de anotações do Dr. Alzheimer em uma de suas consultas com a paciente Auguste Deter (trecho adaptado de (Jucker *et al.*, 2006)):

[1] Câmera lúcida: dispositivo óptico utilizado para auxiliar artistas durante o desenho, que foi descrito em 1611 por Johannes Kepler.

*"*Anotação do Dr. Alzheimer*: Ela se sentou na sua cama com uma expressão de impotência.*

Dr. Alzheimer: Qual o seu nome?

Auguste Deter: Auguste.

Dr. Alzheimer: Sobrenome?

Auguste Deter: Auguste.

Dr. Alzheimer: Qual o nome do seu marido?

Auguste Deter: Auguste, eu acho."

Atualmente as chamadas "substâncias peculiares" encontradas no cérebro de Auguste Deter são as principais características neuropatológicas da DA: a deposição de placas de beta(β)-amilóide e a formação de emaranhados neurofibrilares (NFTs, do *inglês neurofibrillary tangles*) (Nisbet *et al.*, 2015; Thal *et al.*, 2015). Segundo a hipótese da cascata de amilóide, acredita-se que a DA é um processo iniciado pela acúmulo de placas de β-amilóide que desencadeia uma cascata de processos neurodegenerativos (Hardy e Higgins, 1992; Hardy e Selkoe, 2002). Atualmente, acredita-se que estes processos fisiopatológicos estejam relacionados com a progressão dinâmica do quadro clínico da DA, onde um paciente assintomático passa por uma fase de declínio cognitivo leve (MCI, do inglês *mild cognitive impairment*) e finalmente chega a demência (Dubois *et al.*, 2010).

A forma genética da DA, que acomete menos de 5% dos pacientes antes dos 65 anos, corrobora a hipótese da cascata de amilóide, e é causada por mutações patogênicas em genes envolvidos no metabolismo da proteína precursora de amilóide (APP, do inglês do *amyloid precursor protein*). De fato, mutações nos genes APP e presenilinas 1 (PS1) e 2 (PS2) causam uma deposição agressiva de placas de β-amilóide (Wu *et al.*, 2012). O tipo mais comum da DA, chamada de esporádica, tem causa multifatorial e não apresenta

mutações nos genes citados acima. Na DA esporádica, a idade é o maior fator de risco, afetando normalmente pacientes com mais de 65 anos (Goedert e Spillantini, 2006). Os mecanismos envolvidos na DA esporádica parecem ser muito mais complexos e ainda não foram precisamente elucidados.

Mecanismos envolvidos na doença de Alzheimer

Nas seções seguintes vamos discutir brevemente os principais mecanismos moleculares já descritos e seu envolvimento na fisiopatologia da DA. Mais especificamente, discutiremos os marcadores neuropatológicos clássicos (β-amilóide e os NFTs), processos neuroinflamatórios e vias de sinalização envolvidas na disfunção sináptica na DA.

A deposição de β-amilóide

Avanços recentes mapearam mecanismos relacionados com a deposição extracelular de placas de β-amilóide. As placas de β-amilóide são a conformação final do processo amiloidogênico iniciado pela quebra da APP pela ação sequencial de duas secretases: β-secretase e γ-secretase, que levam a formação de peptídeos de β-amilóde (Aβ), sendo os mais comuns o $A\beta_{1-40}$ e o $A\beta_{1-42}$ (Nunan e Small, 2000). Estes peptídeos de Aβ sofrem processos de oligomerização e finalmente de fibrilogênese formando placas maduras e insolúveis de β-amilóide. Atualmente, acredita-se que os oligômeros de Aβ são as formas mais tóxicas de β-amilóide e parecem orquestrar a disfunção sináptica na DA (Haass e Selkoe, 2007). Baseado em estudos recentes, os oligômeros de Aβ parecem interagir com um complexo de receptores pós-sinápticos que incluem o receptor

glutamatérgico N-metil-D-Aspartato (NMDA) e o receptor metabotrópico de glutamato 5 (mGluR5), porém estes mecanismos ainda não foram precisamente elucidados (Benilova e De Strooper, 2011). Cabe salientar a existência de uma via denominada não-amiloidogênica, onde a quebra sequencial da APP é feita sequencialmente pela α-secretase e pela γ-secretase, liberando no meio extracelular um fragmento solúvel (sAPPα, do inglês *soluble amyloid precursor protein α*) que não forma placas (Suh e Checler, 2002).

Acredita-se que o processo de deposição de β-amilóide pela via amiloidogênica leve a diversos mecanismos de neurodegeneração associados a formação de emanharados neurofibrilares contendo a proteína tau hiperfosforilada, e ultimamente desencadeia disfunção sináptica associada a morte celular (**figura 2**).

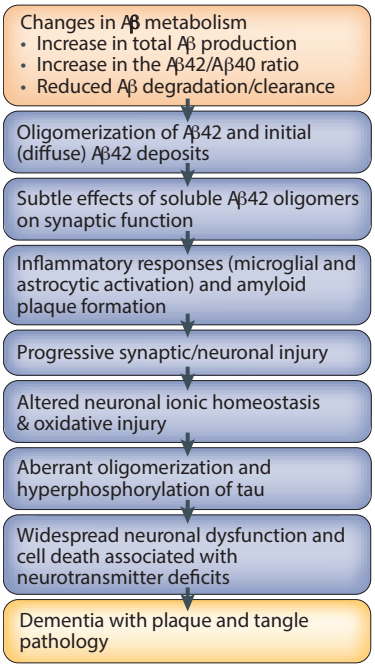

Figura 2. Atual hipótese da cascata β-amilóide. Representação atualizada dos processos neurodegenerativos iniciados pelo acúmulo de β-amilóide, que induzem processos neurodegenerativos, e ultimamente levam a demência. Figura adaptada de (Haass e Selkoe, 2007).

A proteína tau

A tau é uma proteína associada aos microtúbulos (MAPs, do inglês *microtubule associated proteins*) que fisiologicamente é uma das responsáveis pela manutenção da estabilidade do citoesqueleto (Williams, 2006). Resíduos de serina (Ser) e treonina (Tre) aceptores de fosfato, alvos de diversas proteínas cinases[2], são os principais reguladores da função da tau (Buee *et al.*, 2000). Neste sentido, quatro cinases são consideradas reguladoras chave da fosforilação de tau: glicogênio sintase cinase 3-beta (GSK-3β, do inglês *glycogen synthase kinase* 3β), ciclina dependente de cinase 5 (CDK5, do inglês *cyclin-dependent kinase 5*), proteína cinase dependente de cAMP (PKA, do inglês *cAMP-dependent protein kinase*) e proteína reguladora associada a microtúbulo (MARK, do *microtubule-affinity-regulating-kinase*). Além de mediar a estabilidade do citoesqueleto, a fosforilação da proteína tau está envolvida em diversos processos que incluem plasticidade neuronal e sinalização intraneuronal (Johnson e Stoothoff, 2004; Gendreau e Hall, 2013). O ajuste fino da fosforilação de tau também depende da atividade de proteínas fosfatases[3], em particular da proteína fosfatase 2A (PP2A, do inglês *protein phosphatase 2A*). A PP2A é a mais abundante proteína fosfatase do cérebro, e a mais envolvida na defosforilação dos sítios aceptores da proteína tau (cerca de 70%) (Gong e Iqbal, 2008).

A fosforilação exacerbada da proteína tau leva a instabilidade dos microtúbulos e neurodegeneração, e é um dos eventos neuropatológicos bem estabelecidos na DA. Mais especificamente, a hiperfosforilação dos resíduos Ser199/Ser202/Thr205 (AT8), Tre212/Ser214/Thr217 (AT100), Tre231/235 (AT180) e Ser396/Ser404 (PHF-1) é

[2] Proteína cinase: enzima que transfere grupos fosfatos de moléculas doadoras para moléculas-alvo específicas (aceptores).

[3] Proteína fosfatase: enzima que remove grupamentos fosfato de moléculas-alvo específicas.

invariavelmente um processo patológico e dá origem aos depósitos intracelulares chamados de NFTs (Augustinack *et al.*, 2002; Ballatore *et al.*, 2007; Spires-Jones *et al.*, 2009) **(figura 3)**. A agregação da proteína tau, é uma característica encontrada não só na DA mas em diversas outras doenças neurodegenerativas que incluem as demências frontotemporais (FTDs, *frontotemporal dementias*), e são denominadas taupatias.

Além do β-amilóide, diversos mecanismos parecem induzir a hiperfosforilação patológica da proteína tau (Inestrosa e Arenas, 2010; Tu *et al.*, 2014). Entre eles, está a atividade reduzida da PP2A, que é um característica fisiopatológica comumente encontrada no cérebro de pacientes na DA e em outras taupatias (Gong *et al.*, 1993; Gong *et al.*, 1995; Arif *et al.*, 2014). Neste sentido, evidências experimentais com o uso de uma neurotoxina que inibe a atividade da PP2A, chamada de ácido ocadáico (OKA, do inglês *okadaic acid*), demonstraram que a inibição da PP2A é capaz de replicar diversos processos fisiopatológicos relacionados a hiperfosforilação da proteína tau, que incluem estresse oxidativo cerebral e declínio cognitivo em modelos experimentais (Tian *et al.*, 2004; Zhang e Simpkins, 2010; Kamat *et al.*, 2011; Zimmer *et al.*, 2012).

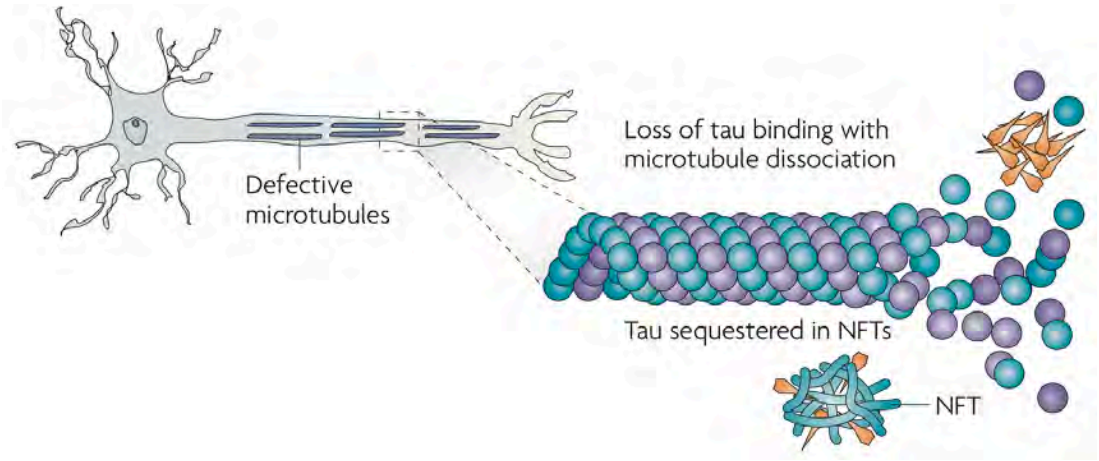

Figura 3. Hiperfosforilação da proteina tau. A hiperfosforilação da proteína tau desestabiliza os microtúbulos, liberando filamentos helicais emparelhados compostos de tau hiperfosforilada, que ultimamente formam os emaranhados neurofibrilares (NFTs). Adaptado de (Brunden *et al.*, 2009).

Na DA, a propagação cerebral dos NFTs constituídos de tau hiperfosforilada tem um padrão bem definido que foi descrito pelos anatomistas Heiko Braak e Eva Braak. O chamado estagiamento de Braak (do inglês *Braak staging*) define a deposição de NFTS em seis estágios: da camada trans-entorrinal (estágios I-II) via regiões límbicas (estágios III-IV) para áreas isocorticais (estágios V-VI) (Braak e Braak, 1991). É importante ressaltar que diversos estudos demostram uma significante correlação linear entre a propagação dos agregados de proteína tau e a severidade da DA, ou seja, com o grau de declínio cognitivo, disfunção sináptica e atrofia cerebral (Arriagada *et al.*, 1992; Guillozet *et al.*, 2003; Hampel *et al.*, 2005).

Neuroinflamação

Além das características neuropatológicas clássicas da DA, muitos estudos têm apontado para processos neuroinflamatórios como coadjuvantes importantes na progressão da DA. O envolvimento de processos inflamatórios foi primeiramente descrito pela presença de fatores de complemento, como o C1q, C4 and C3, encrustrados nas placas de β-amilóide (Eikelenboom e Stam, 1982; Eikelenboom *et al.*, 1989). Logo após, ativação microglial e elevados níveis de interleucina 1 (IL-1) foram encontrados em pacientes com DA (Griffin *et al.*, 1989; Eikelenboom e Van Gool, 2004). Atualmente, sabe-se que a ativação das células astrogliais – microglia e astrócitos – e a liberação de citocinas inflamatórias como o IL-1, interleucina 6 (IL-6) e o fator tumoral de necrose alfa (TNF-alfa, do inglês *tumor necrosis factor alpha*) são respostas inflamatórias presentes durante toda a progressão da DA (Akiyama *et al.*, 2000; Ferreira *et al.*, 2014). Além disso, diversos estudos demonstram que os depósitos de placas de β-amilóide e

NFTs estão comumente cercados de células gliais ativadas ou reativas (Serrano-Pozo *et al.*, 2011; Serrano-Pozo *et al.*, 2013).

De fato, apesar de estar bem estabelecido que estes processos inflamatórios fazem parte da fisiopatologia da DA, ainda não se sabe ao certo se são processos benéficos ou prejudiciais. Acredita-se que a inflamação no início da doença seja uma reação adaptativa com finalidade de proteger a integridade cerebral (Wyss-Coray e Mucke, 2002), enquanto a inflamação crônica parece exacerbar o processo neurodegenerativo (Mrak e Griffin, 2005; Hoozemans *et al.*, 2011). Neste sentido, estudos sugerem que a inflamação cerebral crônica pode contribuir para a quebra da homeostasia na sinapse glutamatérgica tripartite, e subsequentemente exacerbar eventos neurotóxicos (Schaeffer e Gattaz, 2008; Fuller *et al.*, 2010).

Neurotransmissão glutamatérgica

O glutamato é o principal neurotransmissor excitatório cerebral em mamíferos e está envolvido em funções cerebrais fisiológicas, como desenvolvimento, plasticidade sináptica, migração celular e diferenciação (Danbolt, 2001). Uma vez liberado pelas vesículas sinápticas, o glutamato age na fenda sináptica pela sua interação com receptores metabotrópicos e inotrópicos (Hollmann e Heinemann, 1994). Os receptores inotrópicos – alfa-amino-3-hidroxi-metil-5-4-isoxazolpropiónico (AMPA), cainato (KA) e NMDA – são canais iônicos de resposta excitatória rápida, enquanto os receptores glutamatérgicos metabotrópicos (mGluR1-8, tipo 1 ao 8) são acoplados a proteína G e exercem um importante papel modulatório (Schaeffer e Duplantier, 2010). Como o glutamato não é degradado no compartimento extracelular, dois transportadores astrocitários,

transportador de glutamato tipo 1 (GLT-1, do inglês *glutamate transporter 1*) e transportador glutamato-aspartato (GLAST, do inglês *glutamate-aspartate transporter*), são responsáveis por removerem o glutamato da fenda sináptica e cessar o estímulo excitatório (Danbolt, 2001).

A disfunção deste mecanismo de controle de transmissão sináptica causa um aumento nos níveis de glutamato na fenda sináptica e consequente hiperativação dos receptores glutamatérgicos, um processo patológico denominado excitotoxicidade. Acredita-se que a excitoxicidade tenha um papel chave em processos neurodegenerativos na DA e em outras doenças cerebrais (Mark *et al.*, 2001; Mehta *et al.*, 2013).

Neste sentido, os oligômeros de β-amilóide parecem interagir com os receptores glutamatérgicos e assim desencadear processos excitotóxicos (Paula-Lima *et al.*, 2013). Mais especificamente, estudos mostram que os oligômeros de β-amilóide induzem abertura do canal inotrópico do receptor NMDA, o que resulta em aumento do influxo de cálcio, ativação de vias de sinalização associadas com a fosforilação da proteína tau e consequente morte neuronal (Revett *et al.*, 2013). No contexto da DA o receptor ionótropico NMDA tem sido o mais explorado nos últimos anos. Este receptor é um tetrâmero formado por subunidades GluN1, GluN2 (A/B/C/D) e GluN3 (A/B) (Schoepfer *et al.*, 1994; Cull-Candy *et al.*, 2001). O receptor NMDA é o alvo molecular da memantina, uma droga aprovada pelo *Food and Drug Administration* (FDA) para o tratamento da DA. Mais especificamente, o mecanismo de ação da memantina envolve um bloqueio de baixa afinidade do canal iônico do receptor NMDA, e age somente quando o mesmo está aberto (**figura 4**). Isto leva a um bloqueio parcial do

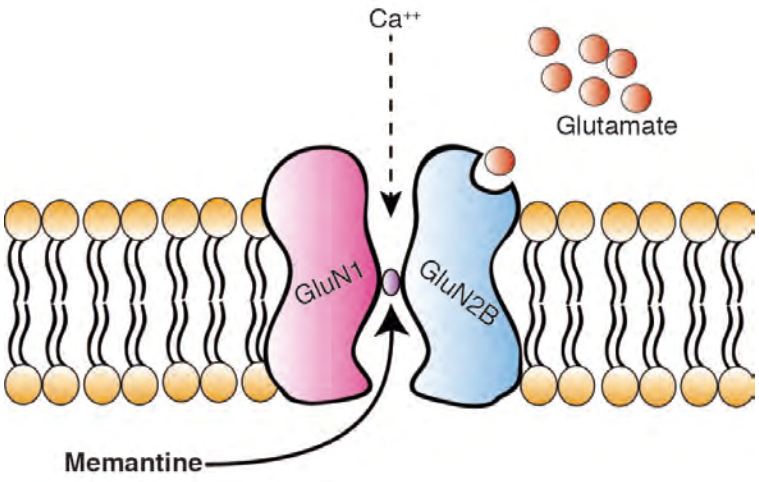

Figura 4. Mecanismo de ação da mematina. O mecanismo de ação da mematina envolve o bloqueia do canal ionico do receptor NMDA quando o receptor está ativado. Figura original baseada em (Lipton e Chen, 2004).

influxo excessivo de cálcio decorrente da abertura exacerbada do canal iônico, mas ao mesmo tempo é capaz de manter a atividade do receptor em níveis fisiológicos (Johnson e Kotermanski, 2006; Lipton, 2007). A memantina produz uma melhora global nos aspectos comportamentais e cognitivos dos pacientes com DA (Winblad e Poritis, 1999; Reisberg *et al.*, 2003; Tariot *et al.*, 2004; Peskind *et al.*, 2006; Van Marum, 2009). Porém, ela não consegue retardar ou impedir a progressão da DA. De fato, acredita-se que um dos fatores responsáveis pela falta de estratégias terapêuticas efetivas para o tratamento da DA é a ausência de uma diagnóstico acurado e precoce.

Biomarcadores

O diagnóstico definitivo da DA por muito tempo se ateve a busca dos agregados de β-amilóide e tau em tecido cerebral de pacientes *post-mortem* (Mckhann *et al.*, 1984). Cerca de uma década atrás, foi publicado o primeiro estudo demonstrando placas de β-amilóide *in vivo* com a utilização do radiofármaco denominado Composto B de Pittsburgh ([^{11}C]PIB, do inglês *Pittsburgh Compound B*) via neuroimagens com

tomografia por emissão de pósitrons (PET, do inglês *Positron emission tomography*) (Klunk *et al.*, 2004). Nos anos seguintes o uso deste biomarcador de imagem trouxe avanços sem precedentes em termos de diagnóstico da DA. Neste sentido, cabe salientar a natureza progressiva da DA e o fato de que as alterações fisiopatológicas começam muitos antes do aparecimento dos sintomas (Reiman *et al.*, 2012; Jack *et al.*, 2013b). De fato, duas meta-análises recentemente publicadas sugerem que o depósito de β-amilóde precede os primeiros sintomas clínicos na DA em cerca de 30 anos (Jansen *et al.*, 2015; Ossenkoppele *et al.*, 2015). Dado o exposto, acredita-se que o uso de biomarcadores é a melhor estratégia para um melhor entendimento da DA antes do sintomas, o que potencialmente pode levar a um diagnóstico precoce.

O uso de biomarcadores na doença de Alzheimer

De acordo com o grupo de estudos de biomarcadores do *National Institutes of Health* (NIH) nos EUA, biomarcadores são características que podem ser medidas e avaliadas objetivamente como um indicador de um processo biológico normal, processo patológico, ou resposta farmacológica a uma intervenção farmacêutica (Biomarkers Definitions Working, 2001). Na DA, os biomarcadores foram definidos como ferramentas capazes de detectar características clássicas da DA de maneira precisa e confiável (Consensus report of the Working Group on: "Molecular and Biochemical Markers of Alzheimer's Disease". The Ronald and Nancy Reagan Research Institute of the Alzheimer's Association and the National Institute on Aging Working Group, 1998). Atualmente duas modalidades de biomarcadores são as mais utilizadas: biomarcadores de fluído, que envolvem a análise bioquímica de sangue ou líquido cefalorraquiano (LCR); e

biomarcadores de imagem, que incluem o PET e a imagem por ressonância magnética (MRI, do inglês *magnetic resonance imaging*). Estes biomarcadores impulsionaram estudos clínicos de grande escala de caráter longitudinal e multimodal, como o *Dominantly Inherited Alzheimer Network* (DIAN, http://dian-info.org/) e o *Alzheimer's Disease Neuroimaging Initiave* (ADNI, http://adni.loni.usc.edu/), que visam definir a progressão da DA, avançar em um diagnóstico precoce e desvendar novos alvos terapêuticos analisando uma vasta gama de biomarcardores de imagem e fluído em associação com testes neuropsicológicos. Levando em consideração a fisiopatologia da DA, estes biomarcadores podem ser divididos em duas classes: biomarcadores de β-Amilóide e biomarcadores de neurodegeneração (Jack *et al.*, 2010). Nas próximas seções discutiremos os principais biomarcadores utilizados na DA e o advento de modelos hipotéticos que visam explicar a progressão da DA em função da análise de biomarcadores.

Biomarcadores de β-Amilóide

Existem dois tipos principais de biomarcadores de β-Amilóide: análises bioquímicas de LCR que medem os produtos da quebra do APP e a tecnologia de PET que quantifica a deposição de placas de β-Amilóide no cérebro por imagem (Blennow *et al.*, 2015).

Diversos produtos envolvidos na via amiloidogênica do APP podem ser quantificados, porém o mais estudado até o momento é o $A\beta_{1-42}$ (Blennow *et al.*, 2015). De fato, os níveis de $A\beta_{1-42}$ no LCR chegam a estar 50% reduzidos na DA (Blennow e Vanmechelen, 2003). Apesar dos níveis de $A\beta_{1-40}$ (que é quase 10 vezes mais abundante

no LCR do que $A\beta_{1-42}$) não estarem alterados na DA, razão entre os níveis de $A\beta_{1-42}/A\beta_{1-40}$ no LCR têm sido proposta como uma estratégia ainda mais sensível em termos de diagnóstico, pois ela balanceia a variabilidade interindividual na produção total de Aβ, ou seja, evita falso negativo em pacientes que naturalmente produzem pouco Aβ (Hansson *et al.*, 2007; Lewczuk *et al.*, 2015).

Entre os biomarcadores de imagem para β-amilóide, o [^{11}C]PIB é de longe o mais estudado. O [^{11}C]PIB apresenta retenção em regiões corticais relacionadas com o acúmulo de placas de β-amilóide em pacientes com DA (Klunk *et al.*, 2004; Jack *et al.*, 2013a). Além do [^{11}C]PIB, diversos radiofármacos para placas de β-amilóide foram desenvolvidos com o radioisótopo flúor 18 ([^{18}F]): [^{18}F]florbetapir (Wong *et al.*, 2010), [^{18}F]flutemetamol (Nelissen *et al.*, 2009), [^{18}F]florbetaben (Rowe *et al.*, 2008) e o [^{18}F]NAV4694 (Rowe *et al.*, 2013) (**figura 5**). É importante salientar que estes radiofármacos se correlacionam apenas modestamente com o declínio cognitivo, pois se ligam somente na estrutura folha-beta (do inglês *beta-sheet*) de placas maduras de β-amilóide (Hampel, 2013).

Esforços têm sido feitos para o desenvolvimento de metodologias não invasivas que possam identificar as formas mais tóxicas de β-amilóide, os oligômeros, que ofereceriam oportunidades sem precedentes para o monitoramento de terapias e o diagnóstico precoce na DA (Viola et al., 2015).

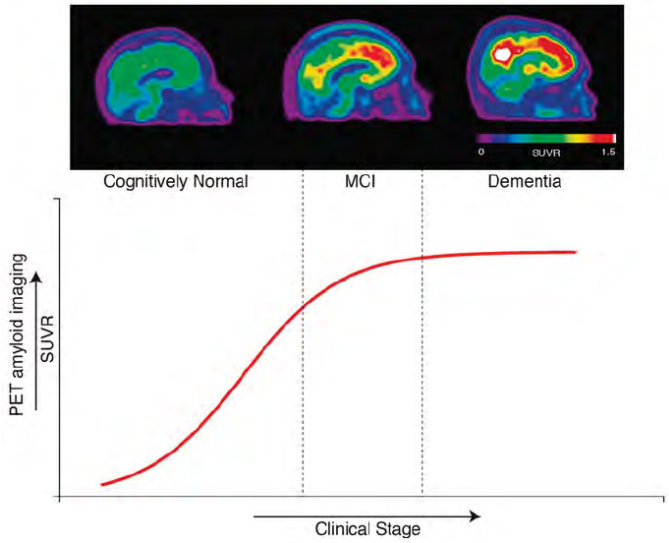

Figura 5. Visualização de placas de β-amiloides via PET: A esquerda, a imagem do cérebro de um paciente assintomático (*cognitively normal*), no centro, um paciente com declínio cognitivo leve (*MCI*) e a direita, um paciente com demência do tipo Alzheimer (*Dementia*). Adaptado de (Leuzy *et al.*, 2014c).

Biomarcadores de Neurodegeneração

Os biomarcadores clássicos de neurodegeneração incluem análises bioquímicas de LCR que medem os níveis da proteína tau total (t-tau, do inglês *total tau*) e fosforilada (p-tau, do inglês *phosphorylated tau*), e tecnologias de imagem como PET e MRI para medir o metabolismo de glicose e a atrofia cerebral, respectivamente.

Os níveis de t-tau e p-tau no LCR são marcadores dinâmicos de dano cerebral e correlacionam-se com o estagiamento clínico na DA (Buerger *et al.*, 2002; Samgard *et al.*, 2010). Cabe salientar que aumentos de até 300% na concentração de t-tau e p-tau no LCR são encontrados em pacientes com DA (Blennow, 2004). Além disso, recentemente foram desenvolvidos diversos radiofármacos direcionados para marcar os agregados de proteína tau (Zimmer *et al.*, 2014c). É esperado que estes radiofármacos sejam rapidamente integrados a estudos clínicos, e a sua utilização tem potencial de revelar informações topográficas da propagação *in vivo* dos NFTs no cérebro.

O [^{18}F]Fluoro-deoxi-glicose ([^{18}F]FDG) PET, um radiofármaco análogo da glicose, tem sido utilizado para estimar o metabolismo de glicose cerebral a mais de 30

anos, e nos dias atuais é amplamente utilizado não somente na pesquisa mas também em âmbito clínico (Mazzilotta *et al.*, 1981; Silverman, 2004; Toyama *et al.*, 2004). Acredita-se que a captação de [^{18}F]FDG PET sirva como uma espécie de index metabólico da atividade neuronal (Rocher *et al.*, 2003). Pacientes com DA apresentam uma consistente redução no consumo de glicose cerebral em regiões corticais específicas particularmente nas áreas parietal, temporal e do cingulado posterior (**figura 6**), e estas reduções correlacionam-se com a severidade do quadro clínico (Mosconi, 2005). Além disso, estudos recentes demostram que reduções no metabolismo hipocampal de glicose (captação de [^{18}F]FDG) parecem predizer a transição de um paciente normal, para MCI e demência na DA (De Leon *et al.*, 2001; Mosconi *et al.*, 2008).

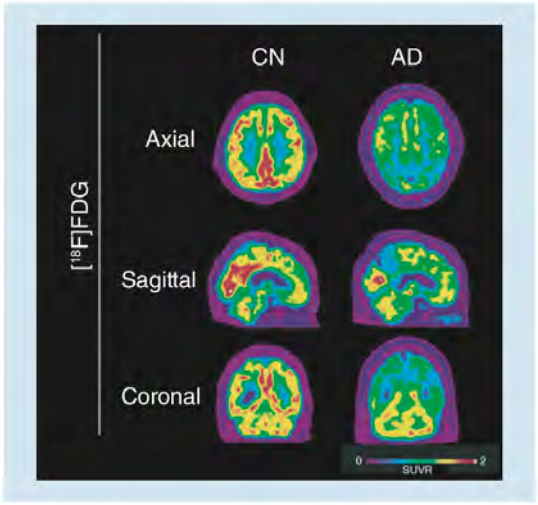

Figura 6. Assinatura metabólica via PET. Imagem representativa de [^{18}F]FDG de um paciente cognitivamente normal (CN) e um paciente com a DA (AD), mostrando uma característica redução na captação de [^{18}F]FDG nos córtices parietal, temporal e posterior cingulado. Figura adaptado de (Schilling *et al.*, 2014).

Além do PET, a aquisição de imagens por MRI estrutural tem sido utilizada para estimar taxas de atrofia cerebral (Frisoni *et al.*, 2010). Na DA, existe um padrão estereotipado de atrofia cerebral que começa no córtex entorrinal, hipocampo e córtex

posterior cingulado, e é seguido por uma atrofia tardia do neorcortex (temporal, parietal e frontal). É importante ressaltar que o grau de atrofia se correlaciona com o declínio cognitivo (Scahill *et al.*, 2002; Thompson *et al.*, 2003; Mcdonald *et al.*, 2009). Neste sentido, atrofia do hipocampo é a mais evidente, e consegue aumentar o grau de sensibilidade do diagnóstico da DA (Horn *et al.*, 1996).

Outros biomarcadores

Apesar de não específicos, uma vasta gama de biomarcadores atualmente disponíveis tem potencial de servir como coadjuvantes no diagnóstico e monitoramento da DA. Entre eles estão os radiofármacos para medir ativação microglial, que são considerados biomarcadores de neuroinflamação no contexto da DA (Zimmer *et al.*, 2014b). Além disso, existe uma vasta gama de radiofármacos capazes de identificar alterações em sistemas de neurotransmissão com potencial uso o diagnóstico e monitoramento da DA (Schilling *et al.*, 2014). É importante salientar mais uma vez que apesar de não específicos, estes radiofármacos têm potencial de identificar assinaturas topográficas da DA, como é o caso do [^{18}F]FDG, e por isso são de grande interesse.

Apesar de não fornecem informações topográficas, biomarcadores de LCR também podem ajudar na caracterização da DA. Neste sentido, uma pletora de marcadores podem ser avaliados. Entre os mais promissores estão biomarcadores neuroinflamatórios e de estresse oxidativo (Blennow *et al.*, 2012). Recentemente, dois novos biomarcadores de LCR foram propostos: I) ferritina, uma proteína que reflete a concentração de ferro no cérebro, e seus níveis parecem predizer a progressão da DA

(Ayton *et al.*, 2015); II) d-serina, um co-agonista do receptor NMDA, que parece estar até 5 vezes mais concentrado no LCR de pacientes com DA (Madeira *et al.*, 2015).

Modelos hipotéticos de biomarcadores

Estudos anteriores com a utilização destes biomarcadores impulsionaram o desenvolvimento de modelos hipotéticos da progressão da DA. Entre eles o de maior aceitação é o modelo desenvolvido pelo Dr. Clifford Jack em 2010 e atualizado em 2013 (Jack *et al.*, 2013b). O chamado modelo hipotético dinâmico de biomarcadores da cascata patológica da DA (do inglês, *hypothetical model of dynamic biomarkers of the Alzheimer's pathological cascade*) propõe a progressão clínica da DA em função da magnitude de anormalidades de biomarcadores multimodais (**figura 7**).

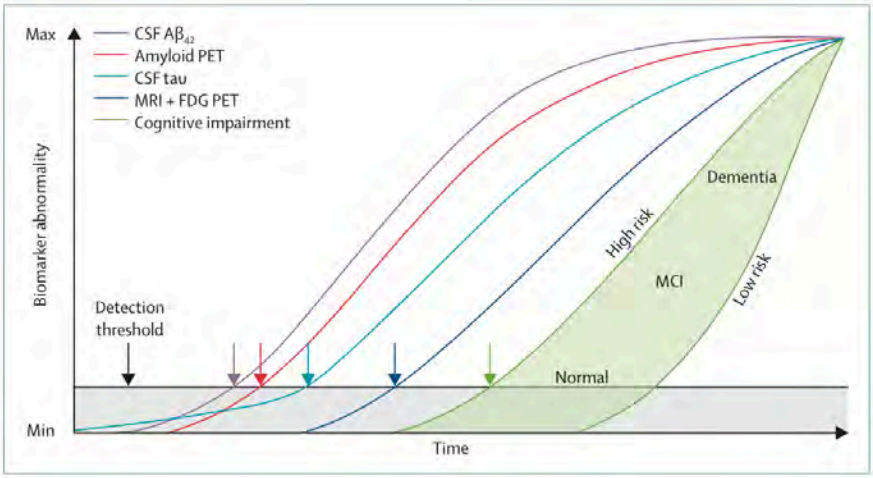

Figura 7. Atual modelo hipotético dinâmico de biomarcadores da cascata patológica da DA. Anormalidades no metabolismo de β-amiloide podem ser identificado via amilóide-PET ou LCR ($A\beta_{1-42}$). Neurodegeneração relacionada com a proteína tau pode ser analisada por LCR (t-tau e p-tau) e via [^{18}F]FDG PET. A atrofia cerebral pode ser avaliada por imagens de MRI estrutural. O declínio cognitivo é precedido por um longo e silencioso período onde os biomarcadores de β-amilóide e neurodegeneração já se encontram em níveis anormais. Figura adaptada de (Jack *et al.*, 2013b).

Apesar de todos estes avanços em mecanismos e biomarcadores na DA, nenhuma estratégia terapêutica consegue impedir a progressão da DA. Neste sentido, se faz necessário o aprofundamento do estudo dos mecanismos fisiopatológicos e a busca por novos biomarcadores que possam identificar o início da DA, e assim, possivelmente, iniciar o tratamento da DA antes do aparecimento dos sintomas.

Objetivo

Investigar mecanismos fisiopatológicos relacionados com a PP2A, a proteína tau e o sistema glutamatérgico e avaliar biomarcadores de imagem no contexto da DA.

Objetivos específicos

- Investigar os efeitos da inibição da PP2A na fosforilação da tau, sistema glutamatérgico, estresse oxidativo e função cognitiva.
- Avaliar o potencial preventivo e neuroprotetor da memantina frente a inibição da PP2A.
- Avaliar os efeitos do tratamento de longo-prazo com memantina em animais saudáveis.
- Revisar criticamente e propor direções futuras no uso dos radiofármacos atualmente disponíveis para visualização de placas de β –amilóide via PET.
- Revisar os radiofármacos recentemente desenvolvidos para visualização de NFTs via PET e seu emprego em pesquisas translacionais.
- Revisar o potencial dos biomarcadores de neuroinflamação via PET como possíveis coadjuvantes no diagnóstico e monitoramento da DA.
- Avaliar os estudos utilizando biomarcadores de PET em modelos animais transgênicos carregando mutações humanas nos genes APP, PS1 e tau.

- Investigar o possível uso do radiofármaco [^{11}C]ABP688 na identificação de anormalidades na neurotransmissão glutamatérgica.
- Investigar a contribuição dos astrócitos no sinal do PET [^{18}F]FDG.

PARTE II

Nesta seção os resultados serão apresentados em capítulos. Os capítulos são compostos por um breve prefácio seguido de um artigo científico. Os capítulos I-IV demonstram os resultados de estudos experimentais desta tese visando o entendimento de mecanismos moleculares e alvos terapêuticos na DA. Os capítulos V-IX demonstram os estudos visando um maior entendimento dos biomarcadores de imagem a nível clínico no contexto da DA. Os capítulos X-XIII demonstram os estudos experimentais com microPET com a finalidade de avançar em termos de biomarcadores de imagem.

Capítulo II. *Pretreatment with Memantine Prevents Alzheimer-Like Alterations Induced by Intrahippocampal Okadaic Acid Administration in Rats.*

No **capítulo II** apresentamos o artigo publicado no periódico *Current Alzheimer Research*.

No capítulo anterior (Capítulo I) demonstramos uma série de alterações fisiopatológicas envolvidas com a inibição da PP2A. Neste estudo, queríamos investigar o envolvimento do sistema glutamatérgico frente a inibição da PP2A. Para isto, utilizamos um protocolo de pré-tratamento com memantina seguido de uma infusão intrahipocampal de OKA em ratos. O OKA causou um aumento nos níveis de glutamato no LCR em conjunto com o aumento do imunoconteúdos de CDK5, p25 (ativador patológico de CDK5) e hiperfosforilação de tau, que se refletiram em déficit cognitivo. O pré-tratamento com memantina foi capaz de impedir a ação neurotóxica do OKA e prevenir o aumento nos níveis de glutamato no LCR, CDK5 e p25, e assim manteve integra a memória dos animais submetidos a infusão do OKA. A partir destes resultados sugerimos que o sistema glutamatérgico, em especial o receptor NMDA, pode ser um alvo para intervenções farmacológicas na DA na longa fase que precede os primeiros sintomas de déficit cognitivo.

Send Orders of Reprints at reprints@benthamscience.org

Pretreatment with Memantine Prevents Alzheimer-Like Alterations Induced by Intrahippocampal Okadaic Acid Administration in Rats

Eduardo Rigon Zimmer, Eduardo Kalinine, Clarissa Branco Haas, Vitor Rocco Torrez, Diogo Onofre Souza, Alexandre Pastoris Muller and Luis Valmor Portela*

Departamento de Bioquímica, ICBS, UFRGS. Programa de Pós Graduação em Ciências Biológicas - Bioquímica. Rua Ramiro Barcelos, 2600 anexo, CEP 90035-003, Porto Alegre, RS, Brasil

Abstract: Cerebral okadaic acid (OA) administration induces Alzheimer's disease (AD)-like phenotype in rats. Alterations in glutamate levels associated with hyperactivation of cyclin dependent kinase 5 (Cdk5) signaling pathway downstream Tau phosphorylation may participate in the genesis of this pathological phenotype. Here, we examined the efficacy of memantine (MN) pretreatment on reducing OA-induced AD-like phenotypes in rats. Wistar rats were given daily intraperitoneal injections of MN for 3 days and then given an intrahippocampal infusion of OA. Animals were divided into four groups: control (CO), MN, OA and MN/OA. Spontaneous locomotion and spatial memory performance were assessed by open field and Morris water maze respectively. Additionally, we measured glutamate levels in the cerebrospinal fluid (CSF) and the immunocontent of Cdk5, p35, p25 and phosphorylated Tau ($pTau^{Ser199/202}$) in the hippocampus. Spontaneous locomotion did not differ between groups. The OA group showed a significant decrease in spatial memory performance compared to all groups. The OA infusion also increased CSF glutamate levels and the immunocontents of Cdk5, p25 and $pTau^{Ser199/202}$ in the hippocampus. Conversely, pretreatment with MN prevented OA-induced spatial memory deficits and the increment of CSF glutamate level; which paralleled with normal immunocontents of Cdk5, p25 and $pTau^{Ser199/202}$ proteins. There were positive correlations between spatial memory performance and the neurochemical parameters. In summary, pretreatment with MN prevents spatial memory deficits induced by intrahippocampal OA administration in rats. The prevention of increase CSF glutamate levels, along with the reduced hippocampal phosphorylation of $Tau^{Ser199/202}$ by Cdk5/p25 signaling pathway, are the mechanisms proposed to participate in the prophylactic effects of MN in this AD-like model.

Keywords: Alzheimer´s disease, okadaic acid, memantine, glutamate, Cdk5, tau, learning and memory.

1. INTRODUCTION

Alzheimer's disease (AD) is an aging-associated neurodegenerative disease that causes important structural and neurochemical alterations and is associated with the progressive deterioration of cognitive function [1-3]. The neuropathological characterization of AD includes the accumulation of senile plaques (deposits of amyloid-β) and the aggregation of abnormal filaments of Tau protein into neurofibrillary tangles. These pathologies are present in brain regions involved in memory and cognition [4, 5].

For many years, acetyl cholinesterase inhibitors were the first choice in drugs for the treatment AD, but recently the glutamatergic system has also been shown to be a possible target for new drug therapies [6, 7]. Glutamate is the major excitatory neurotransmitter in the brain and plays fundamental roles in neurodevelopment, neuronal survival and in learning and memory processes through its interactions with ionotropic (AMPAr, KAr and NMDAr) and metabotropic receptors (mGluR) [8-10]. However, high amounts of glutamate in the synaptic cleft may cause receptor hyperactivation and neuronal death by excitotoxicity [11]. In this context, the N-methyl-D-aspartate receptor (NMDAr), a heterodimeric calcium ion channel, exerts a major role in a variety of neurodegenerative disorders, including AD [12, 13]. Excessive calcium influx through the ion channel activates the signaling pathways involved in neurodegeneration [10]. The cyclin dependent kinase (Cdk5) signaling pathway is physiologically regulated by p35 or p39 proteins. However, under conditions of high intracellular calcium concentrations, p35 is cleaved by calpain into p25. This cleavage allows the formation of the complex Cdk5/p25, which causes downstream aberrant phosphorylation of Tau. Indeed, several lines of evidence have associated the Cdk5 pathway with AD pathogenesis [14-16].

Memantine (MN), a non-competitive antagonist with a low affinity for the NR2B subunit of NMDAr, has been used in the treatment of AD to delay neurodegenerative processes and improve cognitive function [17-21]. The mechanism of MN action involves the blockade of an excessive influx of calcium through the NMDA receptor caused by glutamate hyper stimulation [22]. Recently, a pretreatment protocol with MN was shown to reverse neurochemical and behav-

*Address correspondence to this author at the Departamento de Bioquímica, ICBS, UFRGS, Rua Ramiro Barcelos, 2600 anexo, CEP 90035-003, Porto Alegre, RS, Brasil; Tel: 55 51 33085558; Fax: 55 51 33085544;
E-mail: roskaportela@gmail.com

1875-5828/12 $58.00+.00 © 2012 Bentham Science Publishers

ioral alterations caused by an ischemic insult in rats [23]. Furthermore, when administered post-insult, MN improved the spatial memory deficit caused by a bilateral injection of okadaic acid (OA) [24]. These data provide support to the idea that MN could be used in prophylactic protocols to diminish the harmful effects of glutamate excitotoxicity in experimental models of neurological diseases.

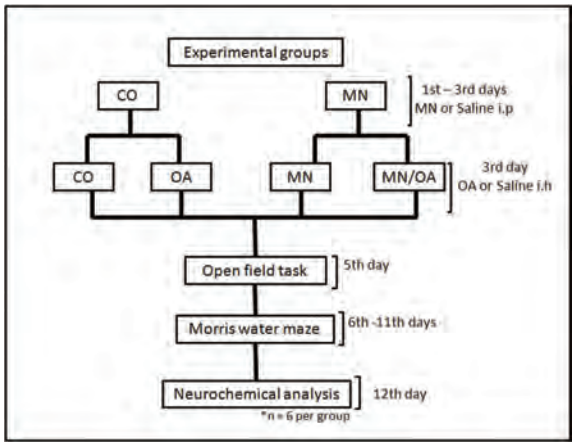

Fig. (1). Experimental Model. Animals received a daily intraperitoneal (i.p.) injection of MN (20 mg/kg) or saline (NaCl, 0.9%) over 3 consecutive days. On the third day, an intrahippocampal (i.h.) infusion of okadaic acid (100 ng) or saline (NaCl 0.9%) was made into the right hemisphere in the CA1. By the third day post-surgery, rats were considered suitable for behavioral experiments. After the *in vivo* experiments we choose randomly 6 animals per group for the neurochemical assays.

The intracerebral administration of OA causes a selective inhibition of the serine/threonine phosphatase 1(PP1) and 2A (PP2A) and exacerbates kinase activities [25]. This imbalance in phosphorylation/ dephosphorylation status induces AD-like phenotype including cognitive deficits, and hyperphosphorylation of NMDAr receptor subunits and Tau protein [16, 26-28]. Tau is a major microtubule-associated protein whose hyperphosphorylated form is considered one of the hallmark alterations reported in neurons of Alzheimer's disease patients. The increase in Tau phosphorylation is believed to cause neuronal death by destabilization of the cytoskeleton, disruption of axonal transport, microglial activation, mitochondrial dysfunction and increased generation of reactive oxygen species [24, 29-31].

This study aimed to investigate whether the prophylactic use of MN is capable of preventing AD-like phenotype induced by OA in rats. Our data demonstrate that MN prevented spatial memory deficits through the modulation of brain glutamate levels and phosphorylation of Tau by Cdk5/p25 signaling pathway.

2. MATERIAL AND METHODS

2.1. Animals

Male Wistar rats (400-500 g), 4-5 months old, were obtained from the State Foundation for Health Science Research (FEPPS, Porto Alegre/RS, Brazil). Animals were placed into a controlled temperature room (22 ºC) under a 12 h light/12 h dark cycle (lights on at 7 am) and had free access to food and water. A total of fifty-nine (n=59) rats were divided into four groups: control (CO, n=17), memantine (MN,n=14), okadaic acid (OA,n=14) and memantine/okadaic acid (MN/OA, n=14). To avoid social isolation, we kept 4 animals per cage [32]. All behavioral tests were performed in normal cycle between 9:00 a.m. and 5:00 p.m. All experiments were in agreement with the Committee on the Care and Use of Experimental Animal Resources, UFRGS, Brazil.

2.2. Drugs

Memantine (Ref. M-9292, Sigma, USA) and okadaic acid (Ref. O8010, Sigma, USA) were dissolved in saline (NaCl, 0.9%) at a concentration of 20mg/ml and 50ng/μL, respectively.

2.3. Treatment and Surgical Procedure

Animals received a daily intraperitoneal (i.p.) injection of memantine (20 mg/kg) or saline (NaCl, 0.9%) over 3 consecutive days. The dose of MN was based on work where MN was shown to prevent neural damage caused by focal ischemia in rats [23]. In addition, Abdel-Aal *et al.* 2011 reported that sixty days of daily MN (20 mg/kg) administration in rats prevented aluminum-induced cognitive deficits and did not cause alterations in motor integrity and coordination [33]. On the third day of MN injections, animals were anesthetized by an i.p. injection of ketamine (Cetamin, Schering-Plough Coopers, Brazil, 100 mg/kg body weight) and xylazine (Coopazine, Syntec, Brazil, 10 mg/kg body weight). An intrahippocampal (i.h.) infusion of 2uL okadaic acid (100 ng) or saline (NaCl 0.9%) was made into the right hemisphere in the CA1 region at the following coordinate location, with reference to bregma: A -3.6, L 2.0, and V 2.4 [34, 35]. This dose of OA was reported to cause spatial learning impairment and hippocampal neurodegeneration in rats [36]. Furthermore, the same dose also caused pyramidal cell loss in the CA1 neurons by apoptosis, similar to those observed in neurodegenerative diseases, like AD [37]. By the third day post-surgery, rats showed normal food intake, water consumption and spontaneous locomotion in the cage and were considered suitable for *in vivo* experiments.

2.4. Open Field Task

The open field test is commonly used to evaluate spontaneous locomotor activity. The apparatus for this test was a circular black box with a 60 cm diameter and a 50 cm height. The experiments were conducted in a sound-attenuated room under low-intensity light (12 lx). The rats (n=10 per group) were placed in the center of the arena and spontaneous locomotion, exploratory activity and anxiety-like behavior was recorded with a video camera for 10 min. In order to analyze anxiety-like behavior, we created a virtual central circular zone (30 cm of diameter) using the analysis software (for review, see Prut *et al.* 2003 [38]). Animals that spent less time in central zone were considered to display anxiety-like behavior. All analyses were performed using a computer-operated tracking system (Any-maze, Stoelting, Woods Dale, IL).

2.5. Morris Water Maze Task

To evaluate spatial memory, we conducted the Morris water maze task (MWM), as described by Muller *et al.* 2010 [39]. The apparatus was a black circular pool with a 190 cm diameter and 70 cm height and the water temperature was maintained at 21 ± 1 °C. Rats (CO: n= 17, MN n=14, OA: n=14 and MN/OA: n=14) were trained daily in a 4-trial water maze task up to 4 consecutive days. Each trial lasted up to 60 s, including 20 s of rest on a hidden black platform. During training, the animals learned to escape from the water by finding a hidden black platform submerged about 2 cm below the water surface in a fixed location. If an animal failed to find the platform in 60 s, it was removed from the water, gently placed on the platform and allowed to rest for 20 s. Rats were returned to their home cages immediately after each daily training session. The maze was located in a well-lit white room with several visual stimuli hanging on the walls to provide spatial cues. Escape latency was defined as the time to find the platform during each trial and was used as an indicator of learning. A probe test without the platform was performed on the fifth day, and the time spent in the target quadrant was used as an indicator of memory retention.

2.6. Cerebrospinal Fluid (CSF) Sampling

On the 11th day, after the last MWM session, rats (n=6 per group) were anesthetized with ketamine (Cetamin, Schering-Plough Coopers, Brazil, 100 mg/kg body weight) and xylazine (Coopazine, Syntec, Brazil, 10 mg/kg body weight) and placed in a stereotaxic apparatus. The CSF was collected (40 to 80 µL) by direct puncture of the cisterna magna with an insulin syringe (27 gauge × 1/2-inch length) and stored at - 80 °C. Samples with blood contamination were discarded.

2.7. High-Performance Liquid Chromatography (HPLC) Procedure

HPLC was performed to measure glutamate levels in the aliquots obtained from the CSF cell-free supernatants. The measurement was performed as previously described (Schmidt *et al.*, 2009). Analyses were performed with the Shimadzu Class-VP chromatography system, which consisted of a quaternary gradient pump with vacuum degassing and piston desalting modules, a Shimadzu SIL-10AF auto-injector valve with a 50 mL loop and a UV detector (Shimadzu, Kyoto, Japan). Separations were achieved on a Supelco 250 mm × 4.6 mm, 5 µm particle size column (Supelco, St Louis, MO, USA). The mobile phase flowed at a rate of 1.2 mL/min, and the column temperature was 24 °C. The buffer composition remained unchanged (Buffer A: 150 mmol/L phosphate buffer, pH 6.0, containing 150 mmol/L potassium chloride; Buffer B: 15% acetonitrile in Buffer A). The gradient profile was modified to the following content of Buffer B in the mobile phase: 0% at 0.00 min, 2% at 0.05 min, 7% at 2.45 min, 50% at 10.00 min, 100% at 11.00 min, and 0% at 12.40 min. Samples of 10 µl were injected into the injection valve loop. Absorbance was read at 360 and 455 nm (emission and excitation, respectively). CSF glutamate levels are expressed as the mean ± SEM in micromoles.

2.8. Western Blotting

For Western blot analysis, we used ipsilateral hippocampus (n=6 per group). Hippocampal homogenates were prepared in PIK buffer (1 % NP-40, 150 mM NaCl, 20 mM Tris, pH 7.4, 10 % glycerol, 1 mM $CaCl_2$, 1 mM $MgCl_2$, 400 µM sodium vanadate, 0.2 mM PMSF, 1 µg/ml leupeptin, 1 µg/ml aprotinin, and 0.1 % phosphatase inhibitor cocktails I and II from Sigma-Aldrich) and centrifuged. Supernatants were collected and the total protein was measured using Peterson's method [40]. Samples containing 40 µg of protein from the hippocampal homogenate were separated by electrophoresis on a polyacrylamide gel and electrotransferred to PVDF membranes. Protein bands within each sample lane were compared to standard molecular weight markers (Precision Plus Protein™ Dual Color Standards #161-0374), which were used to identify the molecular weight of protein of interest. We performed at least 3 replicate gels for each sample of the same animals. Non-specific binding sites were blocked with Tween–Tris buffered saline (TTBS, 100 mM Tris–HCl, pH 7.5) with 5% albumin for 2 h. Samples were incubated overnight at 4 ^{o}C with monoclonal and polyclonal primary antibodies against Cdk5 (Cell Signaling Technology, 1:1000), p25/35 (Cell Signaling Technology) pTau$^{ser199/202}$ (Invitrogen, 1:1000), Tau (Santa Cruz, 1:500) and actin (Sigma, 1:5000). Following primary antibody incubation, the membranes were incubated with secondary antibodies (anti-rabbit, Cell Signaling Technology, 1:3000; anti-mouse, Santa Cruz Technology, 1:5000) for 2 h at room temperature. The films were scanned and the band intensity was analyzed using ImageJ software [41].

2.9. Statistical Analysis

Results are presented as the means ± SEM. The data from the water maze task were analyzed with a repeated-measures analysis of variance (ANOVA), followed by Tukey's post-hoc test. Differences between all groups were analyzed with ANOVA with a Tukey's post-hoc test. Correlations between the measures of cognitive function and protein levels were analyzed by Pearson's correlation. Differences were considered statistically significant if $p<0.05$.

3. RESULTS

3.1. Effects of MN and OA On Locomotor and Exploratory Activity

To analyze the effects of MN and OA in locomotor and exploratory activity, we performed the open field task. The administration of MN and/or OA did not cause significant changes across time in the locomotor and exploratory activity in the open field task Fig. (**2A**), ($F_{[1,36\ ]} = 0.632$, $p = 0.432$). In addition, neither distance traveled Fig. (**2B**), ($F_{[3,36]}=1.418$, $p=0.2534$) nor mean speed Fig. (**2C**), ($F_{[3,36]}=1.491$, $p=0.2335$) was affected, suggesting that the treatment did not cause locomotor deficit. Furthermore, there were no statistical differences among groups in either the time spent ($F_{[3,36]}=1.917$, $p=0.1442$) or the total distance travelled in the central zone ($F_{[3,36]=}1.634$, $p= 0.1987$) suggesting no signs of anxiety-like behavior (data not shown).

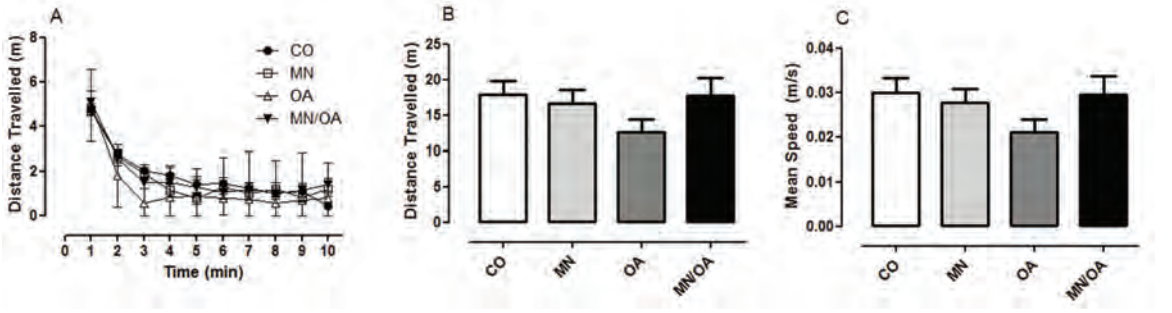

Fig. (2). Open Field Task. The spontaneous locomotor and exploratory activities were not affected by OA and MN. (**A**) Distance traveled per minute, showing exploratory and locomotor activity. (**B**) Total distance travelled. (**C**) Mean speed. Groups: control (CO), memantine (MN), okadaic acid (OA) and okadaic acid/memantine (MN/OA); n=10 per group. Data are represented as the mean ± SEM. *p<0.05 between groups.

3.2. Effects of MN and OA In Spatial Memory

To analyze the effects of MN and OA on spatial memory, we subjected the rats to the Morris water Maze Task (MWM). During the acquisition sessions (4 days), all groups showed improvements in their performances across days and took less time to find the hidden platform Fig. (**3A**), ($F_{[3,165]}$ = 47.058, p=0.0001). On the fourth day, the OA group reached a performance plateau and took more time to find the platform compared to other groups Fig. (**3A**), ($F_{[3,55]}$= 4,191, p= 0.0096). Further, MN prevented the impairment caused by OA on the fourth day Fig. (**3A**), ($F_{[1,55]}$ = 4.428, p=0.040). In the retention session (day 5), the OA group showed impaired spatial memory performance compared to the other groups Fig. (**3B**), ($F_{[3,55]}$= 5.161, p=0.0032). There were no statistical differences among groups regarding total distance traveled Fig. (**3C**), ($F_{[3,55]}$= 0.6523, p=0.5849) or mean speed Fig. (**3D**), ($F_{[3,55]}$= 0.7080, p=0.5514).

3.3. Effects of MN and OA Administration on Hippocampal Cdk5 Signaling, Tau Phosphorylation (Ser199/202) and Glutamate CSF Levels

The i.h. infusion of OA increased the hippocampal immunocontent of Cdk5 and p25/p35 ratio; however, three days of pretreatment with MN prevented these increases Fig. (**4A**) ($F_{[3,20]}$=6.061, p= 0.0042) Fig. (**4B**) and ($F_{[3,20]}$=3.764, p=0.0272). Further, OA administration significantly enhanced CSF glutamate levels, which was prevented by MN Fig. (**4C**) ($F_{[3,20]}$= 10.88, p=0.0002). Finally, intrahippocampal OA infusion caused an increase in the immunocontent of $pTau^{Ser199/202}$ but pretreatment with MN prevented this augmentation Fig. (**4D**) ($F_{[3,20]}$= 4.769 , p= 0.0115).

3.4. Correlation Between MWM and Neurochemical Assays

There were positive correlations between the latency to find the platform on day 4 of MWM and the immunocontent of Cdk5 Fig. (**5A**, R=0.6224, p=0.0012), ratio p25/p35 Fig. (**5B**, R=0.5624, p=0.0042) and $pTau^{Ser199/202}$ Fig. (**5C**, R=0.4126, p=0.0451). Moreover, CSF glutamate level was strongly correlated with increased latency on day 4 Fig. (**5**, R= 0.7302, p=0.0001).

4. DISCUSSION

Alzheimer's disease is multifactorial and heterogeneous, and thus offers multiple therapeutic opportunities [42]. The present study showed the potential of MN pretreatment as a strategy for preventing AD-like alterations induced by intrahippocampal OA infusion in rats. Indeed, MN prophylaxis prevented spatial memory impairment on Morris water maze task (MWM), which paralleled decreased expression of Cdk5, p25 and $pTau^{Ser199/202}$, and CSF glutamate levels.

Inhibition of PP2A activity by OA seems to have no effect on locomotor speed, motor coordination or sensorimotor ability [37, 43]. In fact, our results showed no significant statistical differences between groups in the spontaneous locomotion, mean speed and exploratory activities in the open field task. Although the data appear to indicate a slower speed in the open field in the OA group, the mean speed did not reach statistical significance (p=0.2335).The lack of significant locomotor deficits in the open field task permits further assessment in MWM. Zhang and Simpkins (2010) have already reported impaired performance in the Morris water maze task after an intra hippocampal OA administration. Similarly, we showed impaired spatial memory performance on MWM after intra hippocampal OA infusion. Although rats treated with MN appear to show a decreased time spent in the target quadrant, this observation is not supported by the statistical analysis. Of note, rats treated with MN after a bilateral intracerebroventricular infusion of OA showed improved performance on MWM [24].

By using a prophylactic approach we showed that MN prevented the course of molecular alterations involved in the development of memory deficits induced by OA. It has been suggested that protein phosphatase (PP1 and PP2A) activity plays an important role in normal brain physiology by controlling the neuronal dephosphorylation system, which, when dysfunctional, results in the hyperphosphorylation of Tau protein and memory deficits [44]. Although a normal PP1 activity is implicated in the improvement of learning and memory processes [45], it does not account for the majority of phosphatase activity inhibited by OA. The inhibition of PP2A by OA is achieved at concentrations up to 100 times lower than those required to inhibit PP1[46]. Considering the dose used in this work, we believe that OA is preferentially

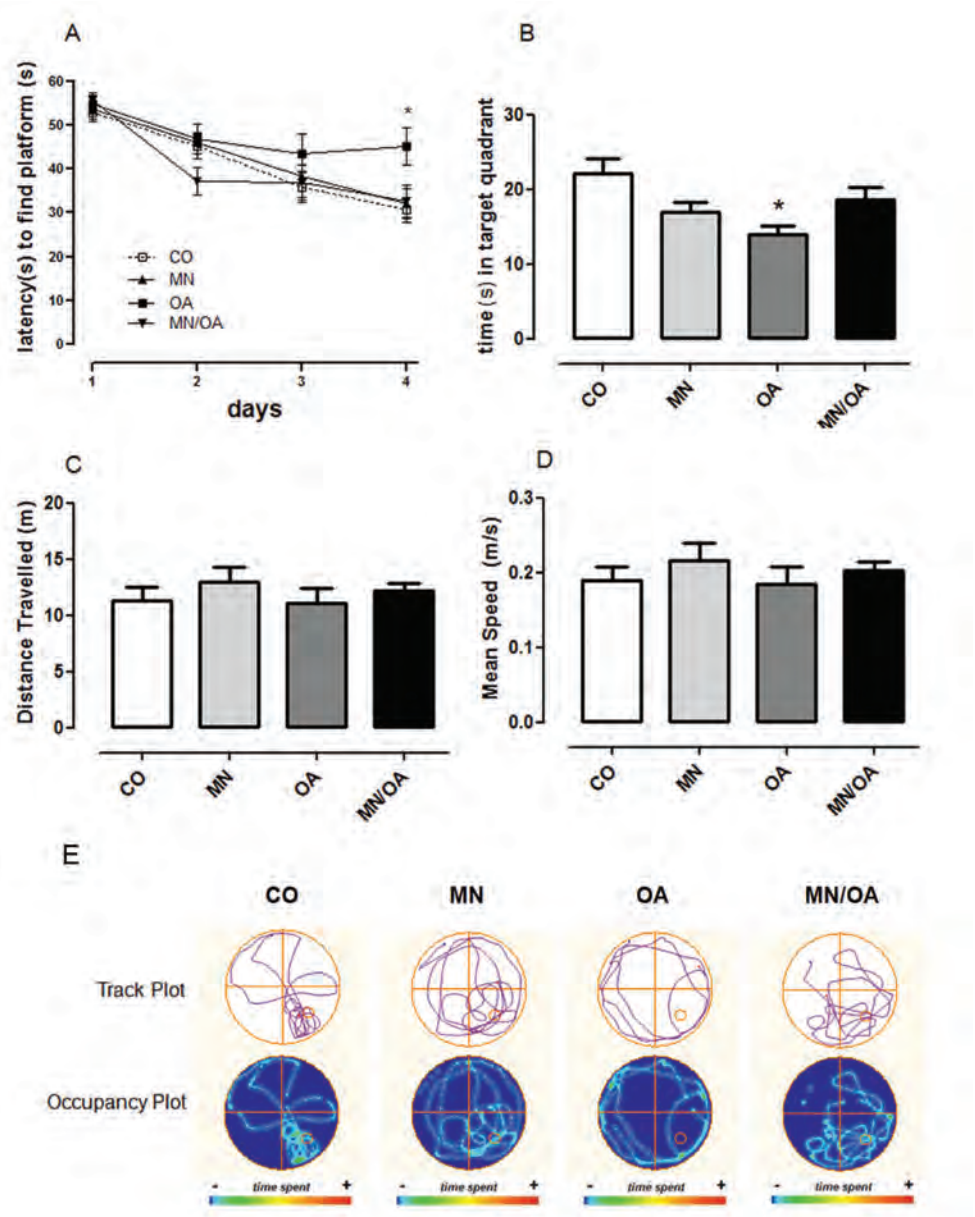

Fig. (3). Morris water maze task. OA impaired both the acquisition and retention memory performances and MN prevented these deficits. (**A**) Acquisition task: the latency to find the platform was used to assess learning ability. (**B**) Retention task: the time in the target quadrant was used to assess memory retention. (**C**) Total distance travelled. (**D**) Mean speed. (**E**) Representative track and occupancy plots obtained by video-tracking software (ANY-mazeH, Stoelting CO, USA), during the retention task. Groups: control (CO, n= 17), memantine (MN, n = 14), okadaic acid (OA, n = 14) and okadaic acid/memantine (MN/OA, n = 14). Data are represented as the mean ± SEM. *p<0.05 between groups.

inhibiting PP2A activity. Interestingly, it was demonstrated that the inhibition of PP2A by a hippocampal infusion of OA caused a transient impairment of the spatial memory performance and a persistent neurodegeneration [36, 37]. In contrast, we detected persistent spatial memory deficits that affected distinct phases of the MWM task (acquisition and retention).

One of the remarkable characteristics of AD is the progressive neurodegeneration associated with cognitive decline [1-3]. The mechanisms underlying brain degeneration and

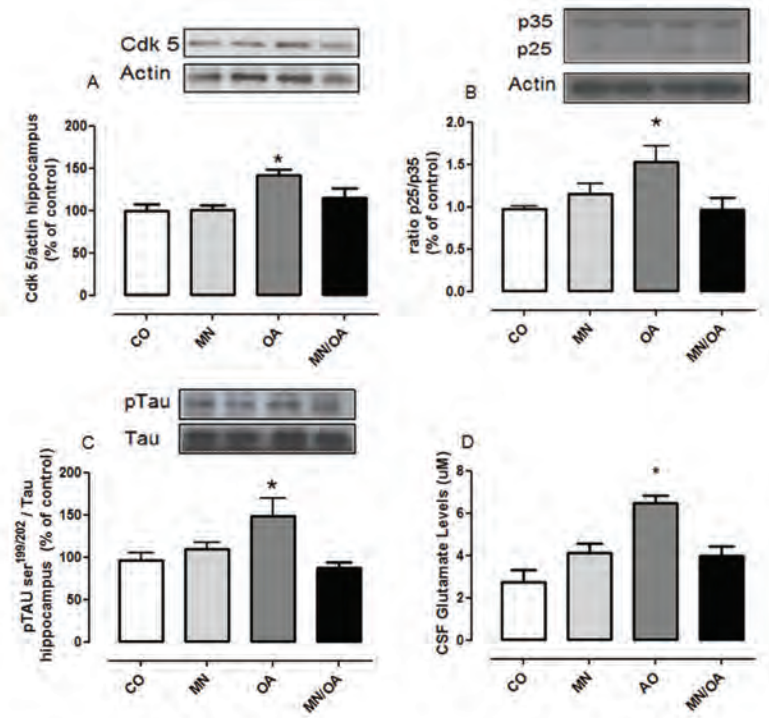

Fig. (4). MN prevent neurochemical alterations (Cdk5, p25, pTau$^{Ser199/202}$, glutamate) induced by i.h. OA administration. Western blots of proteins involved in Cdk5 signaling pathway obtained from hippocampal homogenates: (**A**) immunocontent of Cdk5, (**B**) ratio p25/p35 (**C**) Phosphorylation state of Tau$^{Ser199/202}$. (**D**) Glutamate levels in cerebrospinal fluid. Groups: control (CO), memantine (MN), okadaic acid (OA) and okadaic acid/memantine (MN/OA); n=6 per group. Data are represented as the mean ± SEM. *p<0.05 between groups.

memory deficits in AD include the hyperactivation of the glutamatergic system caused by high levels of glutamate in the synaptic cleft [47]. The infusion of OA, in turn, disrupts the balance between phosphorylation and dephosphorylation, such that there is a disproportionate level of regulatory proteins in a phosphorylated state [28, 44], which negatively affects neuronal function and activates neurodegenerative processes probably due to Tau hyperphosphorylation (Sun *et al.*, 2003). In this sense, MN therapy has been addressed to inhibit Tau hyperphosphorylation, neuronal death, and to prevent the inhibition of PP2A activity [48].

Moreover, among the putative targets of OA neurotoxicity is the persistent activation of NMDA glutamate receptor caused by increased glutamate levels. We can speculate that under these circumstances, there is an increased calcium influx through the ion channel of the NMDA receptor. Indeed, we showed that OA increases CSF glutamate levels suggesting a mechanism that mimics glutamate excitotoxicity. Similarly, glutamate levels have been found to be significantly elevated in the CSF of AD patients [49]. On the other hand, three days of MN administration prevented the increases in CSF glutamate levels caused by OA, thus suggesting that MN modulates the neuronal/glial mechanisms involved in synthesis, release and uptake of glutamate. Accordingly, it has been suggested that the neuroprotective effect of MN involves the depression of glutamate release by neurons specially when excessive glutamate release occurs [50]. We also demonstrated that MN prevented the aberrant expression of pTau$^{Ser199/202}$ induced by OA. Interestingly, these sites are downstream phosphorylated by abnormal Cdk5 activity [51, 52].

We also observed increases in hippocampal expression of Cdk5 and its pathological activator p25 after OA injection. As stated above, these increments were accompanied by an increased phosphorylation status of Tau$^{Ser199/202}$. In contrast, MN pretreatment prevented the increase expression of Cdk5, p25 and pTau$^{Ser199/202}$ in the hippocampus. Considerable evidence suggests that Cdk5 is required for the proper development of the mammalian central nervous system [14] but may also be implicated in neuronal death in neurodegenerative disorders [53, 54]. For instance, Cdk5 physiologically modulates NMDA activity by the phosphorylation of NR2A and NR2B subunits [16, 47, 55], however the pathological activation of NMDAr by Cdk5/p25 causes excessive calcium influx into neurons and functional deficits/death [56]. In support of these data, we showed that the immunocontent of Cdk5 and p25/p35 in hippocampus positively correlates with memory deficits on day 4 of the MWM. In fact, many studies demonstrate the importance of Cdk5 signaling pathway and its effectors in the learning and memory function and suggest this protein as a novel therapeutic target in neurodegenerative diseases [57]. Similarly, CSF glutamate levels and immunocontent of pTau$^{Ser199/202}$ were correlated with spatial

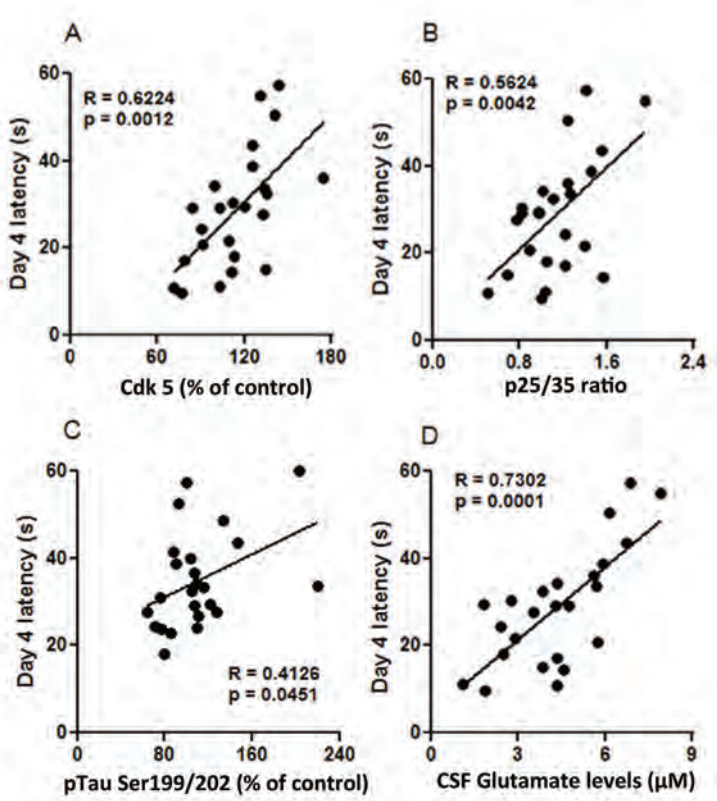

Fig. (5). Correlation analysis between memory performance on MWM task and neurochemical assays: **A**) Latency to find the platform on day 4 and Cdk5 levels in hippocampus. **B**) Latency to find the platform on day 4 and p25/p35 ratio in hippocampus. **C**) Latency to find the platform on day 4 and $pTau^{Ser199/202}$ levels in hippocampus. **D**) Latency to find the platform on day 4 glutamate levels in cerebrospinal fluid; n = 24. Data represented by one animal per point.* $p < 0.05$.

munocontent of $pTau^{Ser199/202}$ were correlated with spatial memory deficits, reinforcing the idea that these elements are active participants in the pathological processes that culminate in AD. Interestingly, some clinical studies already showed positive correlations between cognitive deficits with Tau and glutamate CSF levels [58-60].

The prophylactic use of MN is not typical in clinical practice; however, experimental evidence supports the notion that the molecular and cellular mechanisms involved in etiology of neuropathological changes and cognitive deficits can be targeted by a prophylactic regimen before the onset of dementia symptoms. In this context, there is increasing interest in the search for new tools, methods and molecular markers to enable an early diagnosis of AD or to detect, prior to symptom onset, individuals who are at risk of developing AD [61-66]. An early diagnosis coupled with a pretreatment could provide opportunities to prevent and/or delay the behavioral, neurochemical and neuroanatomical alterations associated with neurodegenerative disorders.

5. CONCLUSION

In summary, pretreatment with MN prevents spatial memory deficits induced by intrahippocampal OA administration in rats. The prevention of increase CSF glutamate levels, along with the reduced hippocampal phosphorylation of $Tau^{Ser199/202}$ by Cdk5/p25 signaling pathway, are the mechanisms proposed to participate in the prophylactic effects of MN in this AD-like model.

CONFLICT OF INTEREST

The author(s) confirm that this article content has no conflicts of interest.

ACKNOWLEDGEMENTS

This work was supported by the following Brazilian agencies and grants: CNPq, CAPES, FAPERGS, Brazilian Institute of Neuroscience - IBNnet FINEP, INCT - Excitotoxicity and Neuroprotection.

REFERENCES

[1] Ho YS, KF So, RC Chang. Anti-aging herbal medicine--how and why can they be used in aging-associated neurodegenerative diseases? Ageing Res Rev 9(3): 354-62 (2010).

[2] Katzman R. Alzheimer's disease. N Engl J Med 314(15): 964-73 (1986).

[3] Delbeuck X, M Van der Linden, F Collette. Alzheimer's disease as a disconnection syndrome? Neuropsychol Rev 13(2): 79-92 (2003).

[4] Citron, M. Alzheimer's disease: strategies for disease modification. Nat Rev Drug Discov 9(5): 387-98 (2010).
[5] McGeer PL, McGeer EG. NSAIDs and Alzheimer disease: epidemiological, animal model and clinical studies. Neurobiol Aging 28(5): 639-47 (2007).
[6] Nicolakakis NE Hamel. Neurovascular function in Alzheimer's disease patients and experimental models. J Cereb Blood Flow Metab (2011).
[7] Sonkusare SK, Kaul CL, Ramarao P. Dementia of Alzheimer's disease and other neurodegenerative disorders--memantine, a new hope. Pharmacol Res 51(1): 1-17 (2005).
[8] Hollmann M, Heinemann S. Cloned glutamate receptors. Annu Rev Neurosci 17: 31-108 (1994).
[9] Headley PM, Grillner S. Excitatory amino acids and synaptic transmission: the evidence for a physiological function. Trends Pharmacol Sci 11(5): 205-11 (1990).
[10] Danbolt NC. Glutamate uptake. Prog Neurobiol 65(1): 1-105 (2001).
[11] Maragakis NJ, Rothstein JD. Glutamate transporters: animal models to neurologic disease. Neurobiol Dis 15(3): 461-73 (2004).
[12] Dingledine R, Borges K, Bowie D, Traynelis SF. The glutamate receptor ion channels. Pharmacol Rev 51(1): 7-61 (1999).
[13] Filali M, Lalonde R, Rivest S. Subchronic memantine administration on spatial learning, exploratory activity, and nest-building in an APP/PS1 mouse model of Alzheimer's disease. Neuropharmacology 60(6): 930-6 (2011).
[14] Patrick GN, Zukerberg L, Nikolic M, de la Monte S, Dikkes P, Tsai LH, *et al.* Conversion of p35 to p25 deregulates Cdk5 activity and promotes neurodegeneration. Nature 402(6762): 615-22 (1999).
[15] Crews L, Masliah E. Molecular mechanisms of neurodegeneration in Alzheimer's disease. Hum Mol Genet 19(R1): R12-20 (2010).
[16] Zhang S, Edelmann L, Liu J, Crandall JE, Morabito MA. Cdk5 regulates the phosphorylation of tyrosine 1472 NR2B and the surface expression of NMDA receptors. J Neurosci 28(2): 415-24 (2008).
[17] Peskind ER, Potkin SG, Pomara N, Ott BR, Graham SM, Olin JT, *et al.* Memantine treatment in mild to moderate Alzheimer disease: a 24-week randomized, controlled trial. Am J Geriatr Psychiatry 14(8): 704-15 (2006).
[18] Tariot PN, Farlow MR, Grossberg GT, Graham SM, McDonald S, Gergel I, *et al.* Memantine treatment in patients with moderate to severe Alzheimer disease already receiving donepezil: a randomized controlled trial. JAMA 291(3): 317-24 (2004).
[19] Reisberg B, Doody R, Stoffler A, Schmitt F, Ferris S, Möbius HJ, *et al.* Memantine in moderate-to-severe Alzheimer's disease. N Engl J Med 348(14): 1333-41 (2003).
[20] Winblad B, Poritis N. Memantine in severe dementia: results of the 9M-Best Study (Benefit and efficacy in severely demented patients during treatment with memantine). Int J Geriatr Psychiatry 14(2): 135-46 (1999).
[21] van Marum RJ. Update on the use of memantine in Alzheimer's disease. Neuropsychiatr Dis Treat 5: 237-47 (2009).
[22] Johnson JW, Kotermanski SE. Mechanism of action of memantine. Curr Opin Pharmacol 6(1): 61-7 (2006).
[23] Babu CS, Ramanathan M. Pre-ischemic treatment with memantine reversed the neurochemical and behavioural parameters but not energy metabolites in middle cerebral artery occluded rats. Pharmacol Biochem Behav 92(3): 424-32 (2009).
[24] Kamat PK, Tota S, Saxena G, Shukla R, Nath C. Okadaic acid (ICV) induced memory impairment in rats: a suitable experimental model to test anti-dementia activity. Brain Res 1309: 66-74 (2010).
[25] Arendt T, Holzer M, Fruth R, Bruckner MK, Gartner U. Paired helical filament-like phosphorylation of tau, deposition of beta/A4-amyloid and memory impairment in rat induced by chronic inhibition of phosphatase 1 and 2A. Neuroscience 69(3): 691-8 (1995).
[26] Arendt T, Holzer M, Bruckner MK, Janke C, Gartner U. The use of okadaic acid in vivo and the induction of molecular changes typical for Alzheimer's disease. Neuroscience 85(4): 1337-40 (1998).
[27] Arias C, Montiel T, Pena F, Ferrera P, Tapia R. Okadaic acid induces epileptic seizures and hyperphosphorylation of the NR2B subunit of the NMDA receptor in rat hippocampus in vivo. Exp Neurol 177(1): 284-91 (2002).
[28] Bennecib M, Gong CX, Grundke-Iqbal I, Iqbal K. Role of protein phosphatase-2A and -1 in the regulation of GSK-3, cdk5 and cdc2 and the phosphorylation of tau in rat forebrain. FEBS Lett 485(1): 87-93 (2000).
[29] Reddy PH. Abnormal tau, mitochondrial dysfunction, impaired axonal transport of mitochondria, and synaptic deprivation in Alzheimer's disease. Brain Res 1415: 136-48 (2011).
[30] Zhang B, Carroll J, Trojanowski JQ, Yao Y, Iba M, Potuzak JS, *et al.* The microtubule-stabilizing agent, epothilone d, reduces axonal dysfunction, neurotoxicity, cognitive deficits, and Alzheimer-like pathology in an interventional study with aged tau transgenic mice. J Neurosci 32(11): 3601-11 (2012).
[31] Yoshiyama Y, Higuchi M, Zhang B, Huang SM, Iwata N, Saido TC, *et al.* Synapse loss and microglial activation precede tangles in a P301S tauopathy mouse model. Neuron 53(3): 337-51 (2007).
[32] Leasure JL, Decker L. Social isolation prevents exercise-induced proliferation of hippocampal progenitor cells in female rats. Hippocampus 19(10): 907-12 (2009).
[33] Abdel-Aal RA, Assi AA, Kostandy BB. Memantine prevents aluminum-induced cognitive deficit in rats. Behav Brain Res 225(1): 31-8 (2011).
[34] Paxinos GC Watson, *The rat brain in stereotaxic coordinates.* 2nd ed. 1986, Sydney ; Orlando: Academic Press. xxvi, 237 p. of plates.
[35] Arias C, Becerra-Garcia F, Arrieta I, Tapia R. The protein phosphatase inhibitor okadaic acid induces heat shock protein expression and neurodegeneration in rat hippocampus in vivo. Exp Neurol 153(2): 242-54 (1998).
[36] He J, Yamada K, Zou LB, Nabeshima T. Spatial memory deficit and neurodegeneration induced by the direct injection of okadaic acid into the hippocampus in rats. J Neural Transm 108(12): 1435-43 (2001).
[37] He J, Yang Y, Xu H, Zhang X, Li XM. Olanzapine attenuates the okadaic acid-induced spatial memory impairment and hippocampal cell death in rats. Neuropsychopharmacology 30(8): 1511-20 (2005).
[38] Prut L, Belzung C. The open field as a paradigm to measure the effects of drugs on anxiety-like behaviors: a review. Eur J Pharmacol 463(1-3): 3-33 (2003).
[39] Muller AP, Tort AH, Gnoatto J, Moreira JD, Vinadé ER, Perry ML, *et al.* Metabolic and behavioral effects of chronic olanzapine treatment and cafeteria diet in rats. Behav Pharmacol 21(7): 668-75 (2010).
[40] Peterson GL. A simplification of the protein assay method of Lowry et al. which is more generally applicable. Anal Biochem 83(2): 346-56 (1977).
[41] Abramoff MD, Magalhaes PJ, Ram SJ. Processing with ImageJ. Biophotonics International 11(7): 36-42 (2004).
[42] Iqbal K, Grundke-Iqbal I. Developing pharmacological therapies for Alzheimer disease. Cell Mol Life Sci 64(17): 2234-44 (2007).
[43] Zhang Z, Simpkins JW. An okadaic acid-induced model of tauopathy and cognitive deficiency. Brain Res 1359: 233-46 (2010).
[44] Sun L, Liu SY, Zhou XW, Wang XC, Liu R, Wang Q, *et al.* Inhibition of protein phosphatase 2A- and protein phosphatase 1-induced tau hyperphosphorylation and impairment of spatial memory retention in rats. Neuroscience 118(4): 1175-82 (2003).
[45] Genoux D, Haditsch U, Knobloch M, Michalon A, Storm D, Mansuy IM. Protein phosphatase 1 is a molecular constraint on learning and memory. Nature 418(6901): 970-5 (2002).
[46] Shenolikar S. Protein serine/threonine phosphatases--new avenues for cell regulation. Annu Rev Cell Biol 10: 55-86 (1994).
[47] Hu NW, Ondrejcak T, Rowan MJ. Glutamate receptors in preclinical research on Alzheimer's disease: Update on recent advances. Pharmacol Biochem Behav (2011).
[48] Chohan MO, Khatoon S, Iqbal IG, Iqbal K. Involvement of I2PP2A in the abnormal hyperphosphorylation of tau and its reversal by Memantine. FEBS Lett 580(16): 3973-9 (2006).
[49] Kaiser E, Schoenknecht P, Kassner S, Hildebrandt W, Kinscherf R, Schroeder J, *et al.* Cerebrospinal fluid concentrations of functionally important amino acids and metabolic compounds in patients with mild cognitive impairment and Alzheimer's disease. Neurodegener Dis 7(4): 251-9 (2010).
[50] Lu CW, Lin TY, Wang SJ. Memantine depresses glutamate release through inhibition of voltage-dependent Ca2+ entry and protein

kinase C in rat cerebral cortex nerve terminals: an NMDA receptor-independent mechanism. Neurochem Int 57(2): 168-76 (2010).

[51] Gong CX, Liu F, Grundke-Iqbal I, Iqbal K. Post-translational modifications of tau protein in Alzheimer's disease. J Neural Transm 112(6): 813-38 (2005).

[52] Liu F, Liang Z, Shi J, Yin D, El-Akkad E, Grundke-Iqbal I, *et al.* PKA modulates GSK-3beta- and cdk5-catalyzed phosphorylation of tau in site- and kinase-specific manners. FEBS Lett 580(26): 6269-74 (2006).

[53] Tsai LH, Delalle I, Caviness VS, Jr., Chae T, Harlow E. p35 is a neural-specific regulatory subunit of cyclin-dependent kinase 5. Nature 371(6496): 419-23 (1994).

[54] Lew J, Huang QQ, Qi Z, Winkfein RJ, Aebersold R, Hunt T, *et al.* A brain-specific activator of cyclin-dependent kinase 5. Nature 371(6496): 423-6 (1994).

[55] Wang J, Liu S, Fu Y, Wang JH, Lu Y. Cdk5 activation induces hippocampal CA1 cell death by directly phosphorylating NMDA receptors. Nat Neurosci 6(10): 1039-47 (2003).

[56] Dhavan R, Tsai LH. A decade of CDK5. Nat Rev Mol Cell Biol 2(10): 749-59 (2001).

[57] Barnett DG, Bibb JA. The role of Cdk5 in cognition and neuropsychiatric and neurological pathology. Brain Res Bull 85(1-2): 9-13 (2011).

[58] Stomrud E, Hansson O, Zetterberg H, Blennow K, Minthon L, Londos E. Correlation of longitudinal cerebrospinal fluid biomarkers with cognitive decline in healthy older adults. Arch Neurol 67(2): 217-23 (2010).

[59] Jimenez-Jimenez FJ, Molina JA, Gomez P, Vargas C, de Bustos F, Benito-León J, *et al.* Neurotransmitter amino acids in cerebrospinal fluid of patients with Alzheimer's disease. J Neural Transm 105(2-3): 269-77 (1998).

[60] Smith CC, Bowen DM, Francis PT, Snowden JS, Neary D. Putative amino acid transmitters in lumbar cerebrospinal fluid of patients with histologically verified Alzheimer's dementia. J Neurol Neurosurg Psychiatry 48(5): 469-71 (1985).

[61] Tan ZS, Beiser AS, Vasan RS, Roubenoff R, Dinarello CA, Harris TB, *et al.* Inflammatory markers and the risk of Alzheimer disease: the Framingham Study. Neurology 68(22): 1902-8 (2007).

[62] Reitz CR Mayeux. Use of genetic variation as biomarkers for Alzheimer's disease. Ann NY Acad Sci 1180: 75-96 (2009).

[63] van Exel E, P Eikelenboom, Comijs H, Frölich M, Smit JH, Stek ML, *et al.* Vascular factors and markers of inflammation in offspring with a parental history of late-onset Alzheimer disease. Arch Gen Psychiatry 66(11): 1263-70 (2009).

[64] Shoji M. Biomarkers of the dementia. Int J Alzheimers Dis 2011: 564321 (2011).

[65] van Harten AC, Kester MI, Visser PJ, Blankenstein MA, Pijnenburg YA, van der Flier WM, *et al.* Tau and p-tau as CSF biomarkers in dementia: a meta-analysis. Clin Chem Lab Med 49(3): 353-66 (2011).

[66] Vialatte FB, Dauwels J, Maurice M, Musha T, Cichocki A. Improving the specificity of EEG for diagnosing Alzheimer's disease. Int J Alzheimers Dis 2011: 259069 (2011).

Received: March 24, 2011 **Revised: April 04, 2012** **Accepted: April 17, 2012**

Capítulo III. *Inhibition of protein phosphatase 2A: focus on the glutamatergic system.*

No **capítulo III** apresentamos o artigo publicado no periódico *Molecular Neurobiology*.

No capítulo anterior (capítulo II) demonstramos o envolvimento da PP2A e do sistema glutamatérgico em processos neurodegenerativos. Neste capítulo, propusemos uma via de sinalização envolvendo excitotoxidade glutamatérgica e a atividade reduzida da PP2A na fisiopatologia de DA e de outras taupatias.

Mol Neurobiol
DOI 10.1007/s12035-015-9321-0

Inhibition of Protein Phosphatase 2A: Focus on the Glutamatergic System

Eduardo R. Zimmer[1] · **Antoine Leuzy**[2] · **Diogo O. Souza**[1] · **Luis V. Portela**[1]

Received: 26 February 2015 / Accepted: 24 June 2015
© Springer Science+Business Media New York 2015

Abstract In a recent review published in *Molecular Neurobiology*, Kamat and colleagues (Mol Neurobiol. 2014 Dec;50(3):852–65) highlighted the cellular and molecular mechanisms involved in Okadaic acid (OKA)-induced neurotoxicity. In this review, the authors underline a wide range of pathological signaling pathways involved in OKA-induced neurotoxicity; however, the role of glutamate was only briefly described. We believe that the hyperactivation of the glutamatergic system is a key pathophysiological player in OKA-induced neurotoxicity and deserves serious attention. In this commentary, we propose an integrative model linking glutamate and PP2A and put forward some unanswered questions.

Keywords Excitotoxicity · Glutamate · Okadaic acid · Protein phosphatase 2A · Tau hyperphosphorylation

Comment

Back in the 1990s, a series of seminal studies lead by Drs. Khalid Iqbal and Inge Grundke-Iqbal revealed the role of protein phosphatase (PP2A) activity in the regulation of tau phosphorylation [1, 2]. Currently, tau hyperphosphorylation is a key player in a range of neurodegenerative diseases, referred to collectively as tauopathies [3, 4]. More specifically, it is well known that reduced PP2A activity is a common feature in Alzheimer's disease (AD) and related non-AD tauopathies [5, 6]. However, the mechanisms underlying PP2A downregulation are still not fully understood.

In keeping with this, we have read with great interest the recent review published by Kamat et al. in *Molecular Neurobiology* [7]. In their article, the authors have highlighted the wide range of cellular and molecular mechanisms involved in Okadaic acid (OKA)-induced neurotoxicity; however, the role of glutamatergic excitotoxicity was only briefly described. A potent neurotoxin, OKA inhibits the major brain serine/threonine protein phosphatases 1 (PP1) and PP2A, but with greater affinity for PP2A [8, 9]. Importantly, PP2A accounts for more than 70% of tau phosphatase activity in the brain [10].

In a previous publication [11], we have demonstrated that PP2A inhibition by OKA was capable of increasing cerebrospinal fluid (CSF) concentrations of glutamate and the expression of the cyclin-dependent kinase-5 (CDK5)—as well as its activator P25—ultimately leading to tau hyperphosphorylation. Additionally, we showed that *N-methyl-D-aspartate* receptor (NMDAR) antagonism with memantine (MN) was able to prevent OKA-induced neurotoxicity, which highlights the key role of glutamate. Interestingly, in a recent article [12], Kamat and colleagues have shown that cerebral administration of OKA increased the expression of GluN1 and GluN2B (both subunits of the glutamatergic NMDAR), and also decreased synapsin-1 mRNA expression, leading to neurotoxicity. These combined events point to synaptic dysfunction guided by NMDAR hyperactivation. As proof of concept, the authors showed that MK801, also a non-competitive inhibitor of NMDAR, was capable of protecting against OKA-induced neurodegeneration [12], which is in line with our previous publication. In both

✉ Luis V. Portela
roskaportela@gmail.com

[1] Department of Biochemistry, ICBS, Federal University of Rio Grande do Sul (UFRGS), 2600 Ramiro Barcelos Street, 90035-003 Porto Alegre, RS, Brazil

[2] Centre for Alzheimer Research, Division of Translational Alzheimer Neurobiology, Karolinska Institutet, Stockholm, Sweden

Published online: 04 July 2015

publications, however, Kamat and colleagues did not mention the increased levels of glutamate in the CSF, which for us is a major finding and possibly the key trigger for all the disrupted signaling induced by PP2A inhibition.

The above described allow us to propose a pathway describing how OKA-induced neurodegeneration is orchestrated by the dysfunction of the glutamatergic system. In fact, it seems that the inhibition of PP2A by OKA increases levels of glutamate, leading to NMDAR hyperactivation. The high influx of calcium—due to NMDAR hyperactivation—leads to CDK5 dysfunction, which finally induces tau hyperphosphorylation (Fig. 1). Interestingly, a recent work [13] has shown that p35 is cleaved to p25 in an NMDAR-dependent manner, building on our previous findings. However, there are still several unanswered questions regarding the association of PP2A and glutamate, such us how do astroglial

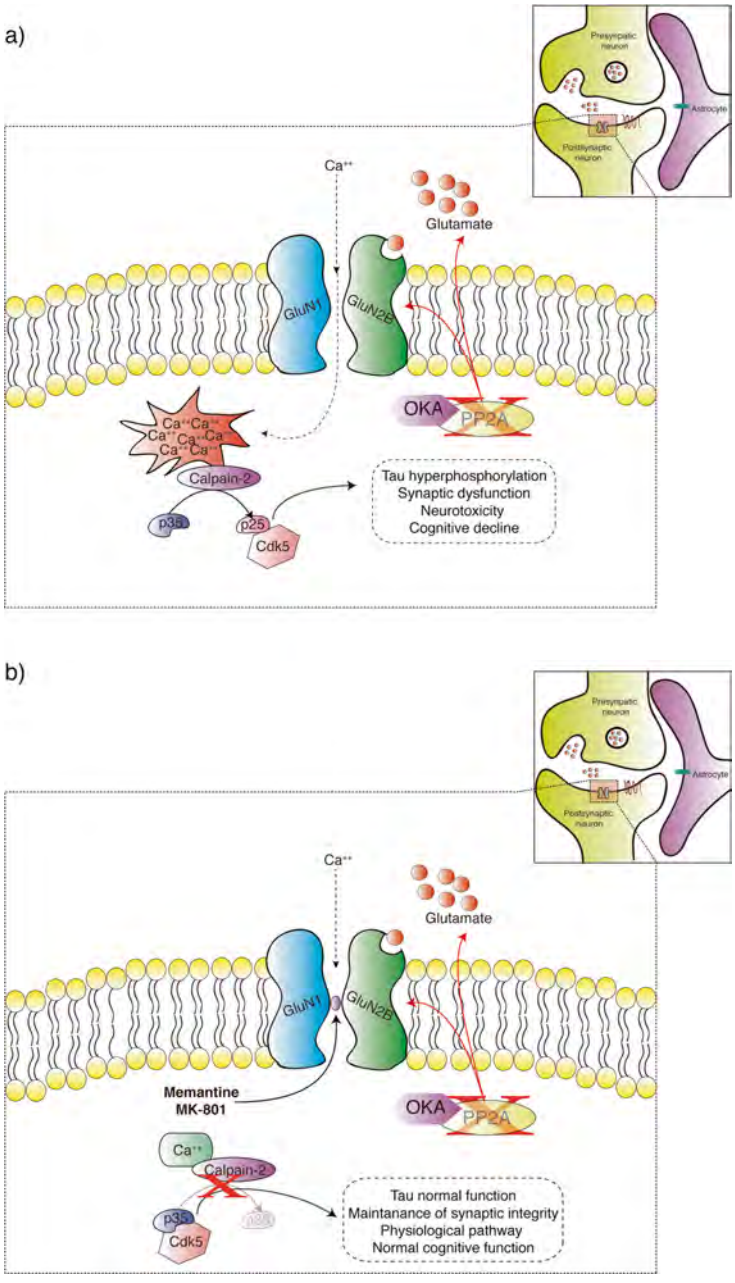

Fig. 1 Inhibition of PP2A by Okadaic acid: emphasis on the NMDAR. **a** Okadaic acid (OKA)-induced neurotoxicity via the glutamatergic NMDAR. Intracerebral administration of OKA increases extracellular levels of glutamate, leading to NMDAR hyperactivation, increased influx of calcium, and elevated rates of cleavage of p35 to p25. A potent activator of CDK5, p25, causes hyperphosphorylation of tau leading ultimately to neurotoxicity and associated synaptic dysfunction. **b** NMDAR antagonism as a protective mechanism. Administration of non-competitive NMDAR antagonists—like memantine or MK-801—regulates intracellular calcium influx, reducing calpain-2-mediated proteolytic cleavage of p35 to p25, restoring glutamate homeostasis, and protecting against OKA-induced neurotoxicity

cells react in this scenario? Or how does PP2A inhibition result in elevated levels of glutamate? The answer to this latter question, in our opinion, is the key to a better understanding of how PP2A inhibition triggers glutamatergic dysfunction.

Importantly, since MN is approved by the Food and Drug Administration (FDA) for treating AD [14] and PP2A is reduced in this condition, it seems reasonable to propose that the pathway described here can be directly translated to human neurodegenerative conditions. Though more studies are required owing to the complexity of the glutamatergic system, the body of literature presented here highlights the pivotal role of glutamatergic neurotransmission in the etiology of AD and non-AD tauopathies and suggests PP2A as a potential therapeutic target.

Conflict of Interest The authors declare that they have no competing interests.

References

1. Gong CX, Singh TJ, Grundke-Iqbal I, Iqbal K (1993) Phosphoprotein phosphatase activities in Alzheimer disease brain. J Neurochem 61(3):921–927
2. Gong CX, Grundke-Iqbal I, Damuni Z, Iqbal K (1994) Dephosphorylation of microtubule-associated protein tau by protein phosphatase-1 and -2C and its implication in Alzheimer disease. FEBS Lett 341(1):94–98
3. Iqbal K, Alonso Adel C, Chen S, Chohan MO, El-Akkad E, Gong CX, Khatoon S, Li B et al (2005) Tau pathology in Alzheimer disease and other tauopathies. Biochim Biophys Acta 1739(2–3): 198–210. doi:10.1016/j.bbadis.2004.09.008
4. Zimmer ER, Leuzy A, Bhat V, Gauthier S, Rosa-Neto P (2014) In vivo tracking of tau pathology using positron emission tomography (PET) molecular imaging in small animals. Transl Neurodegen 3(1):6. doi:10.1186/2047-9158-3-6
5. Sontag JM, Sontag E (2014) Protein phosphatase 2A dysfunction in Alzheimer's disease. Front Mol Neurosci 7:16. doi:10.3389/fnmol.2014.00016
6. Arif M, Kazim SF, Grundke-Iqbal I, Garruto RM, Iqbal K (2014) Tau pathology involves protein phosphatase 2A in parkinsonism-dementia of Guam. Proc Natl Acad Sci U S A 111(3):1144–1149. doi:10.1073/pnas.1322614111
7. Kamat PK, Rai S, Swarnkar S, Shukla R, Nath C (2014) Molecular and cellular mechanism of okadaic acid (OKA)-induced neurotoxicity: a novel tool for Alzheimer's disease therapeutic application. Mol Neurobiol 50(3):852–865. doi:10.1007/s12035-014-8699-4
8. Cohen P, Klumpp S, Schelling DL (1989) An improved procedure for identifying and quantitating protein phosphatases in mammalian tissues. FEBS Lett 250(2):596–600
9. Gong CX, Lidsky T, Wegiel J, Zuck L, Grundke-Iqbal I, Iqbal K (2000) Phosphorylation of microtubule-associated protein tau is regulated by protein phosphatase 2A in mammalian brain. Implications for neurofibrillary degeneration in Alzheimer's disease. J Biol Chem 275(8):5535–5544
10. Liu F, Grundke-Iqbal I, Iqbal K, Gong CX (2005) Contributions of protein phosphatases PP1, PP2A, PP2B and PP5 to the regulation of tau phosphorylation. Euro J Neurosci 22(8):1942–1950. doi:10.1111/j.1460-9568.2005.04391.x
11. Zimmer ER, Kalinine E, Haas CB, Torrez VR, Souza DO, Muller AP, Portela LV (2012) Pretreatment with memantine prevents Alzheimer-like alterations induced by intrahippocampal okadaic acid administration in rats. Curr Alzheimer Res 9(10):1182–1190
12. Kamat PK, Rai S, Swarnkar S, Shukla R, Nath C (2014) Mechanism of synapse redox stress in Okadaic acid (ICV) induced memory impairment: role of NMDA receptor. Neurochem Int 76: 32–41. doi:10.1016/j.neuint.2014.06.012
13. Seo J, Giusti-Rodriguez P, Zhou Y, Rudenko A, Cho S, Ota KT, Park C, Patzke H et al (2014) Activity-dependent p25 generation regulates synaptic plasticity and Abeta-induced cognitive impairment. Cell 157(2):486–498. doi:10.1016/j.cell.2014.01.065
14. Robinson DM, Keating GM (2006) Memantine: a review of its use in Alzheimer's disease. Drugs 66(11):1515–1534

Capítulo IV. *Long-term NMDAR antagonism correlates reduced astrocytic glutamate uptake with anxiety-like phenotype.*

No **capítulo IV** apresentamos o artigo publicado no periódico *Frontiers in Cellular Neuroscience*.

No capítulo II demonstramos que um pré-tratamento com memantina foi capaz de prevenir processos neurodegenerativos relacionados com a proteína tau, e sugerimos o uso de drogas glutamatérgicas na fase assintomática da DA. Cabe reenfatizar que a memantina é droga de escolha e aprovada pelo FDA para o tratamento da DA. Neste estudo queríamos investigar os efeitos de um longo tratamento com memantina. Para isso tratamos camundongos por 25 dias com memantina. A memantina causou um comportamento anxiogênico nos animais associado a uma diminuição na captação de glutamato pelos astrócitos. Estes dados apontam para um cenário de acoplamento entre neurônios e astrócitos via o antagonismo do receptor NMDA. No contexto da DA, pode-se dizer então que um diagnóstico precoce é *sine qua non* para a eficiência do tratamento com drogas glutamatérgicas.

frontiers in Cellular Neuroscience

ORIGINAL RESEARCH
published: 03 June 2015
doi: 10.3389/fncel.2015.00219

Long-term NMDAR antagonism correlates reduced astrocytic glutamate uptake with anxiety-like phenotype

*Eduardo R. Zimmer[1], Vitor R. Torrez[1], Eduardo Kalinine[1,2], Marina C. Augustin[1], Kamila C. Zenki[1], Roberto F. Almeida[1], Gisele Hansel[1], Alexandre P. Muller[1,3], Diogo O. Souza[1], Rodrigo Machado-Vieira[4,5,6] and Luis V. Portela[1]**

[1] Department of Biochemistry, Universidade Federal do Rio Grande do Sul, Porto Alegre, Brazil, [2] Department of Physiology, Universidade Federal de Sergipe, São Cristovão, Brazil, [3] Laboratory of Exercise, Biochemistry and Physiology, Universidade do Extremo Sul Catarinense, Criciúma, Brazil, [4] Laboratory of Neuroscience, LIM-27, Institute and Department of Psychiatry, Universidade de São Paulo, São Paulo, Brazil, [5] Center for Interdisciplinary Research on Applied Neurosciences (NAPNA), Universidade de São Paulo, São Paulo, Brazil, [6] Experimental Therapeutics and Pathophysiology Branch, National Institute of Mental Health, National Institutes of Health, Bethesda, MD, USA

OPEN ACCESS

Edited by:
Johann Steiner, Otto-von-Guericke University Magdeburg, Germany

Reviewed by:
Francisco Ciruela, Universitat de Barcelona, Spain
Paul Guest, University of Cambridge, UK

***Correspondence:**
Luis V. Portela, Department of Biochemistry, Universidade Federal do Rio Grande do Sul, 2600 Ramiro Barcelos Street, 90035-003, Porto Alegre, Rio Grande do Sul, Brazil
roskaportela@gmail.com

Received: *14 April 2015*
Accepted: *22 May 2015*
Published: *03 June 2015*

Citation:
Zimmer ER, Torrez VR, Kalinine E, Augustin MC, Zenki KC, Almeida RF, Hansel G, Muller AP, Souza DO, Machado-Vieira R and Portela LV (2015) Long-term NMDAR antagonism correlates reduced astrocytic glutamate uptake with anxiety-like phenotype. Front. Cell. Neurosci. 9:219. doi: 10.3389/fncel.2015.00219

The role of glutamate *N*-methyl-D-aspartate receptor (NMDAR) hypofunction has been extensively studied in schizophrenia; however, less is known about its role in anxiety disorders. Recently, it was demonstrated that astrocytic GLT-1 blockade leads to an anxiety-like phenotype. Although astrocytes are capable of modulating NMDAR activity through glutamate uptake transporters, the relationship between astrocytic glutamate uptake and the development of an anxiety phenotype remains poorly explored. Here, we aimed to investigative whether long-term antagonism of NMDAR impacts anxiety-related behaviors and astrocytic glutamate uptake. Memantine, an NMDAR antagonist, was administered daily for 24 days to healthy adult CF-1 mice by oral gavage at doses of 5, 10, or 20 mg/kg. The mice were submitted to a sequential battery of behavioral tests (open field, light–dark box and elevated plus-maze tests). We then evaluated glutamate uptake activity and the immunocontents of glutamate transporters in the frontoparietal cortex and hippocampus. Our results demonstrated that long-term administration of memantine induces anxiety-like behavior in mice in the light–dark box and elevated plus-maze paradigms. Additionally, the administration of memantine decreased glutamate uptake activity in both the frontoparietal cortex and hippocampus without altering the immunocontent of either GLT-1 or GLAST. Remarkably, the memantine-induced reduction in glutamate uptake was correlated with enhancement of an anxiety-like phenotype. In conclusion, long-term NMDAR antagonism with memantine induces anxiety-like behavior that is associated with reduced glutamate uptake activity but that is not dependent on GLT-1 or GLAST protein expression. Our study suggests that NMDAR and glutamate uptake hypofunction may contribute to the development of conditions that fall within the category of anxiety disorders.

Keywords: anxiety, astrocytes, behavior, glutamate, memantine

Introduction

Anxiety disorders are among the most prevalent psychiatric conditions worldwide. These disorders have been associated with social isolation, alcoholism, and increased suicide attempts and are also considered to be risk factors for the development of additional psychiatric disorders (Gross and Hen, 2004). Hence, it is imperative to understand the neurobiological mechanisms that are associated with anxiety disorders. It has recently been proposed that a functional imbalance of the tripartite glutamatergic synapse plays a role in anxiety disorders (Clement and Chapouthier, 1998; Nutt and Malizia, 2001; Nemeroff, 2003; Machado-Vieira et al., 2009, 2012). Indeed, glutamatergic neurotransmission offers multiple potential pharmacological targets for treating anxiety-related disorders, such as postsynaptic receptor signaling, presynaptic glutamate release, and astrocytic glutamate uptake (Szabo et al., 2009; Zarate et al., 2010; Riaza Bermudo-Soriano et al., 2012; Pilc et al., 2013).

Currently, antagonism of *N*-methyl-D-aspartate receptor (NMDAR) has been proposed as a feasible strategy for reducing the major symptoms that are linked to anxiety-like behavior (Cortese and Phan, 2005). Indeed, when memantine, an NMDAR antagonist, is administered to patients presenting with depression, anxiety or obsessive-compulsive disorder, their neuropsychiatric symptoms appear to be relieved (Tariot et al., 2004; Sani et al., 2012). By contrast, a recent work demonstrated that chronic antagonism of NMDAR induces elevated anxiety in healthy mice (Hanson et al., 2014). Overall, the current data that are available regarding the association between the use of NMDAR antagonists and the presentation of anxiety-related behaviors refute a simple model of dose-effect and instead seem to be closely related to the regimen, type of drug, or route of administration (Silvestre et al., 1997; Riaza Bermudo-Soriano et al., 2012; Schwartz et al., 2012). Additionally, it is prudent to consider that glutamatergic neurotransmission involves not only neuronal receptors (ionotropic and metabotropic) but also astroglial transporters that participate in neuron-astrocyte coupling.

Two major astroglial Na^+-dependent glutamate transporters, glutamate transporter 1 (GLT-1, also known as EAAT2) and glutamate aspartate transporter (GLAST, also known as EAAT1), take up glutamate from synapses to maintain the homeostasis that is necessary to orchestrate the physiological activity of receptors (Danbolt, 2001). Remarkably, cerebral GLT-1 and GLAST are predominately localized in astrocytes, with very low expression in other cell types (Zhou and Danbolt, 2014). Moreover, astrocytes account for 95% of the glutamate uptake activity in the brain (Danbolt et al., 1992; Lehre and Danbolt, 1998). Importantly, a recent work demonstrated that cerebral microinjection of the GLT-1 inhibitor, dihydrokainic acid (DHK), induced anhedonia and anxiety in rats (John et al., 2015). Thus, one could claim that astrocytic dysfunction may have a considerable impact on the expression of anxiety-like phenotypes (Bechtholt-Gompf et al., 2010; Schroeter et al., 2010; Lee et al., 2013). Based on the principles of neuron-astrocyte coupling, we hypothesized that long-term antagonism of NMDAR would impact astrocytic function and that this would likely affect anxiety phenotype.

In this study, we aimed to investigate the impact of long-term NMDAR antagonism by memantine on anxiety-related paradigms and their potential association with astrocytic glutamate transport.

Materials and Methods

Animals

Three-month-old CF-1 mice were housed in standard cages (48 cm × 26 cm). The animals were kept in a room with controlled temperature (22°C) under a 12 h light/12 h dark cycle (lights on at 7 am) and had free access to food and water. The mice ($n = 40$) were randomized into four groups: control (CO), memantine 5 mg (MN5), memantine 10 mg (MN10), and memantine 20 mg (MN20). To avoid social isolation, we maintained two animals per cage (Leasure and Decker, 2009). All behavioral tests were performed between 1:00 pm and 5:00 pm. All experiments were conducted in accordance with official governmental guidelines in compliance with the Federation of Brazilian Societies for Experimental Biology and were approved by the Ethical Committee of the Federal University of Rio Grande do Sul, Brazil.

Drug Administration

Memantine (Sigma, USA) was dissolved in distilled water at three different concentrations (0.5, 1.0, and 2.0 mg/mL) to standardize the volume used for oral administration and reach the desired dose. For 24 days, the animals received daily administration of either 5, 10, or 20 mg/kg of memantine, or an equivalent volume of distilled water, via oral gavage. Body weight and food intake were monitored. All groups received oral gavage at 1 h after each behavioral task.

Open Field Test

On the 22nd day, the animals were submitted to an open field task to evaluate spontaneous locomotion and exploratory activity. The apparatus was made of a black-painted box measuring 50 cm × 50 cm and was surrounded by 50 cm high walls. The experiments were conducted in a quiet room under low-intensity light (12 lx). Each mouse ($n = 10$ per group) was placed in the center of the arena, and the distance traveled (total and central zone), time spent in the central zone, and mean speed were measured over a course of 10 min (Muller et al., 2012). The experiment was recorded with a video camera that was positioned above the arena. The analysis was performed using a computer-operated tracking system (Any-maze, Stoelting, Woods Dale, IL, USA).

Light–Dark Task

On the 23rd day, the light–dark task was performed as previously described (Crawley and Goodwin, 1980) with some modifications to analyze anxiety profiles. The light–dark apparatus consisted of a wood rectangular box with two separated chambers. One chamber had black walls and floor (50 cm × 50 cm × 50 cm)

and was not illuminated. The other side had white walls and floor (50 cm × 50 cm × 50 cm) and was illuminated by a 100 W white lamp that was placed overhead. The two compartments were separated by a wall, which had a small opening at floor level. For each experiment, an animal ($n = 10$ per group) was initially placed in the white chamber and then allowed to explore the two-chamber area for a duration of 5 min. The following parameters were recorded by a trained and blinded-to-treatment observer: number of transitions between the two chambers, time spent in the light chamber, and risk assessment behavior. After each experiment, the apparatus was cleaned with 70% alcohol and dried before being used with the next animal.

Elevated Plus-Maze Task

On the 24th day, the animals were submitted to an elevated plus-maze task to evaluate further signs of anxiety-like behavior. The elevated plus-maze was performed as previously described (Pellow, 1986). The elevated plus-maze apparatus consisted of two open arms (30 cm × 5 cm) and two enclosed arms (30 cm × 5 cm × 10 cm), which were separated by a central platform (5 cm × 5 cm) with the two identical arms of each type being placed opposite to each other. The height of the maze was 70 cm, and the experiments were conducted under dim red light in a quiet room. Each mouse ($n = 10$ per group) was individually placed onto the central platform of the plus-maze, facing one of the open arms, and was observed/recorded for 5 min by a trained and blinded-to-treatment observer. The time spent in the open arms and the total distance traveled were used for further analysis. After each session, the maze was cleaned with 70% ethanol. Data analysis was performed using a computer-operated tracking system (Any-maze, Stoelting, Woods Dale, IL, USA).

Glutamate Uptake Assay

On the 25th day, the animals ($n = 6$ per group) were sacrificed/dissected and left hippocampal and left frontoparietal cortical brain slices were taken for use in a glutamate uptake assay. The glutamate uptake assay was performed according to Thomazi et al. (2004). Brain hippocampal and frontoparietal cortical slices (0.4 mm) were obtained using a McIlwain tissue chopper and were pre-incubated for 15 min at 37°C in Hank's balanced salt solution (HBSS), containing 137 mM NaCl, 0.63 mM Na_2HPO_4, 4.17 mM $NaHCO_3$, 5.36 mM KCl, 0.44 mM KH_2PO_4, 1.26 mM $CaCl_2$, 0.41 mM $MgSO_4$, 0.49 mM $MgCl_2$, and 1.11 mM glucose, at pH 7.2. Afterward, 0.66 and 0.33 Ci ml^{-1} L-[^{3}H]glutamate were added to a final 100 M concentration of glutamate for incubation with hippocampal and cortical samples, respectively. The incubations were stopped after 5 and 7 min for the hippocampal and cortical samples, respectively, with two ice-cold washes of 1 ml HBSS, which were immediately followed by the addition of 0.5 N NaOH. The samples were kept in this solution overnight. Nonspecific uptake was measured using the same protocol as described above, with differences in temperature (4°C) and medium composition (*N*-methyl-D-glucamine instead of sodium chloride). Na^+-dependent uptake was considered as the difference between the total uptake and the non-specific uptake. Note that astrocytic transport mediated by GLAST and GLT-1 is responsible for the Na^+-dependent glutamate uptake (Anderson and Swanson, 2000). Both uptakes were performed in triplicate. Any radioactivity that was incorporated into the slices was measured using a liquid scintillation counter.

Western Blotting

For western blot analysis, right hippocampal and right frontoparietal cortical homogenates ($n = 6$, per group) were prepared in PIK buffer (1% NP-40, 150 mM NaCl, 20 mM Tris, pH 7.4, 10% glycerol, 1 mM $CaCl_2$, 1 mM $MgCl_2$, 400 μM sodium vanadate, 0.2 mM PMSF, 1 μg/ml leupeptin, 1 μg/ml aprotinin, and 0.1% phosphatase inhibitor cocktails I and II from Sigma–Aldrich) and centrifuged (Zimmer et al., 2012). Supernatants were collected and total protein was measured using Peterson's method (Peterson, 1977). Samples containing 20 μg of protein from the hippocampal homogenate were separated by electrophoresis on a polyacrylamide gel and electrotransferred to PVDF membranes. Protein bands within each sample lane were compared to standard molecular weight markers (Precision Plus Protein™ Dual Color Standards, Bio-Rad), which were used to identify the molecular weights of proteins of interest. Non-specific binding sites were blocked using Tween–Tris buffered saline (TTBS, 100 mM Tris–HCl, pH 7.5) with 5% albumin for 2 h. Samples were incubated overnight at 4°C with primary antibodies against GLT-1 (Abcam, 1:1000), GLAST (Abcam, 1:1000), and β-actin (Sigma, 1:5000). Following primary antibody incubation, the membranes were incubated with secondary antibodies (anti-rabbit, GE life sciences, 1:3000; anti-mouse, GE life sciences, 1:5000) for 2 h at room temperature. Films were scanned, and band intensity was analyzed using Image J software (Abramoff et al., 2004).

Statistical Analysis

Differences between groups were analyzed with analysis of variance (ANOVA) followed by Tukey's *post hoc* test. Correlations between behavioral assessments and glutamate uptake were analyzed by Pearson's correlation coefficient. The results are presented as mean values ± SEM. Differences were considered significant at $p < 0.05$.

Results

Long-Term NMDAR Antagonism does not Alter Spontaneous Locomotion but Induces Anxiety-Like Behavior

Administration of memantine did not cause significant changes in either distance traveled [**Figure 1A**; $F_{(3,36)} = 1.642$, $p = 0.1967$] or time spent in the central zone [**Figure 1B**; $F_{(3,36)} = 0.1697$, $p = 0.9162$] in the open field. Occupancy plots are used to illustrate the similarities between groups in the open field test (**Figure 1C**).

Long-Term NMDAR Antagonism Reduced Time Spent in the Light Compartment of the Light–Dark Box

In the light–dark box (**Figure 1G**), all of the doses of memantine that were tested significantly reduced the time spent in the light

compartment by the memantine-administered mice compared to the CO group [**Figure 1D**; $F_{(3,36)} = 7.364$, MN5: $p = 0.03$, MN10: $p = 0.002$, MN20: $p = 0.01$]. However, transition numbers (light to dark) were unrelated to memantine administration [**Figure 1E**; $F_{(3,36)} = 0.8257$, $p = 0.4884$]. Additionally, there were no differences among groups in risk assessment index [**Figure 1F**; $F_{(3,36)} = 1.129$, $p = 0.3519$].

Long-Term NMDAR Antagonism Decreased Time Spent in the Open Arms of the Elevated Plus-Maze

The administration of memantine reduced the time spent by mice in the open arms of the elevated plus-maze (**Figure 1J**) when compared to the CO group [**Figure 1H**; $F_{(3,36)} = 6.974$, MN5: $p = 0.007$, MN10: $p = 0.002$, MN20: $p = 0.004$]; however, there were no changes in total distance traveled [**Figure 1I**; $F_{(3,36)} = 2.227$, $p = 0.1018$].

Long-Term NMDAR Antagonism Decreased Glutamate Uptake in the Frontoparietal Cortex and Hippocampus without Affecting the Immunocontents of GLAST and GLT-1

The administration of memantine significantly decreased glutamate uptake in slices of frontoparietal cortex [**Figure 2A**; $F_{(3,20)} = 11.458$, MN5: $p = 0.026$, MN10: $p < 0.001$, MN20: $p < 0.001$] and hippocampus [**Figure 2D**; $F_{(3,20)} = 15.008$, MN5: $p = 0.015$, MN10: $p < 0.001$, MN20: $p < 0.001$]. However, memantine did not alter the immunocontent of GLAST in either the frontoparietal cortex [**Figure 2B**; $F_{(3,20)} = 1.300$, $p = 0.3020$] or the hippocampus [**Figure 2E**; $F_{(3,20)} = 0.6174$, $p = 0.6118$]. Additionally, no alterations were found in the immunocontent of GLT-1 in either the frontoparietal cortex [**Figure 2C**; $F_{(3,20)} = 2.225$, $p = 0.1167$] or the hippocampus [**Figure 2F**; $F_{(3,20)} = 0.1520$, $p = 0.9272$].

Correlation Between Anxiety-Like Behavior and Glutamate Uptake

A positive correlation was found between time spent in the light compartment of the light dark-box and glutamate uptake in the frontoparietal cortex (**Figure 3A**; $p < 0.0001$, $R = 0.7289$) and hippocampus (**Figure 3C**; $p = 0.03$, $R = 0.4337$). Time spent in the open arms of the elevated plus-maze test was also correlated with glutamate uptake in the frontoparietal cortex (**Figure 3B**; $p = 0.03$, $R = 0.4313$) and hippocampus (**Figure 3D**; $p = 0.01$, $R = 0.4815$).

Discussion

Our results demonstrated that long-term antagonism of NMDAR by memantine induces anxiety-like behavior in healthy CF-1 mice. Additionally, memantine decreased glutamate uptake activity in the frontoparietal cortex and in the hippocampus

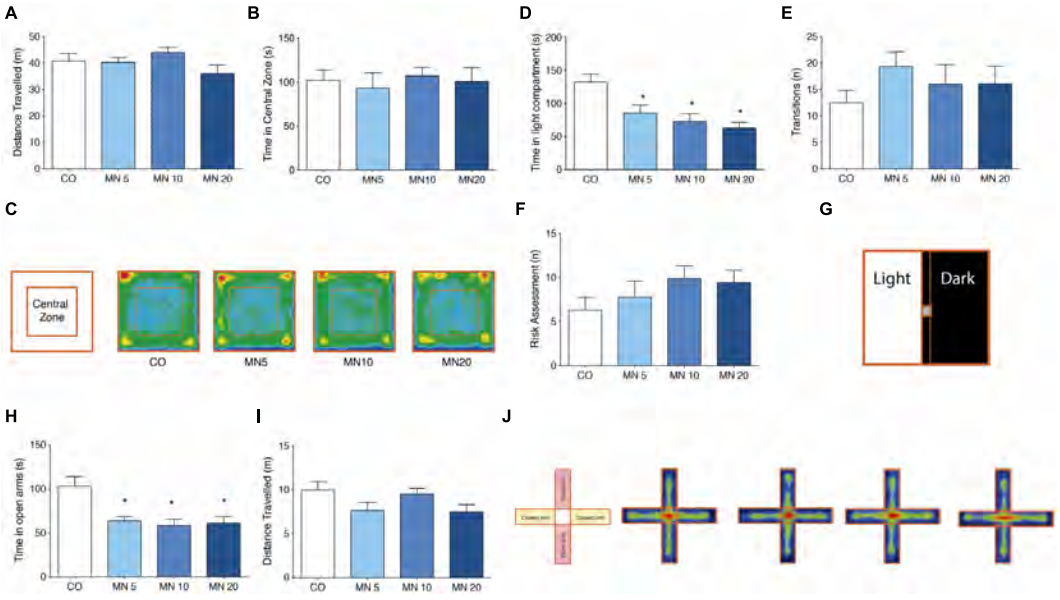

FIGURE 1 | Long-term NMDAR antagonism does not alter spontaneous locomotor and exploratory behavior, but induces anxiety-like behavior. (A) Total distance traveled in the open field. **(B)** Time in central zone in the open field. **(C)** Open field apparatus and occupancy plots. **(D)** Time in light compartment in the light–dark box. **(E)** Number of transitions in the light–dark box. **(F)** Risk assessment index in the light–dark box. **(G)** Light–dark box apparatus. **(H)** Time in open arms in the elevated plus-maze. **(I)** Distance traveled in the elevated plus-maze. **(J)** Elevated plus-maze apparatus and occupancy plots. Groups: control (CO), memantine 5 mg (MN 5), memantine 10 mg (MN 10), and memantine 20 mg (MN 20); $n = 10$ per group. Data are presented as mean values ± SEM.

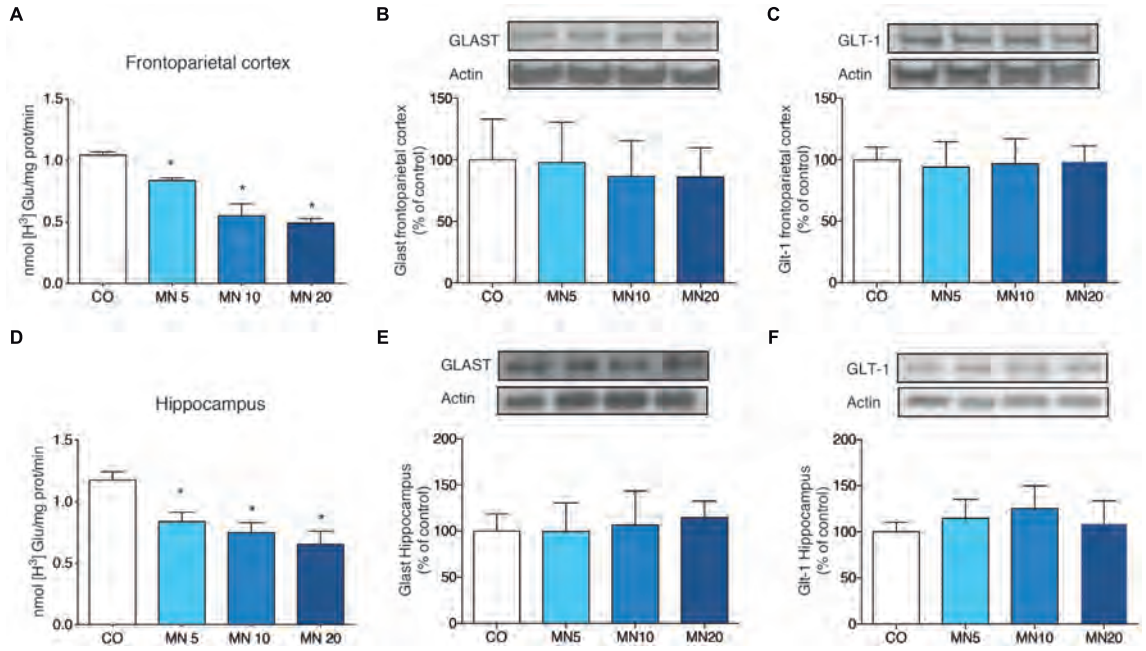

FIGURE 2 | Long-term NMDAR antagonism decreases glutamate uptake in the frontoparietal cortex and hippocampus, but does not alter astroglial transporter immunocontent. (A) Glutamate uptake in slices of frontoparietal cortex. **(B)** Immunocontent of GLAST in the frontoparietal cortex. **(C)** Immunocontent of GLT-1 in the frontoparietal cortex. **(D)** Glutamate uptake in slices of hippocampus. **(E)** Immunocontent of GLAST in the frontoparietal cortex. **(F)** Immunocontent of GLT-1T in the frontoparietal cortex. Groups: CO, memantine 5 mg (MN 5), memantine 10 mg (MN 10), and memantine 20 mg (MN 20); $n = 6$ per group. Data are presented as mean values ± SEM. $^*p < 0.05$ among groups.

with this phenomenon correlating with anxiety-like behavior. By contrast, the immunocontents of the astroglial glutamate transporters GLT-1 and GLAST were not affected.

Long-term administration of memantine did not induce significant changes in the spontaneous locomotion and exploratory activity of mice in the open field test. These findings imply that neither the dose nor the regimen of memantine that was used in our work led to non-specific effects such as sedation, which can potentially impair performance in anxiety-like tasks. This finding is in agreement with previous reports that have demonstrated that memantine administration does not alter locomotion or exploratory profiles (Reus et al., 2010). Conversely, we also showed that long-term memantine administration at doses of 5, 10, or 20 mg/kg leads to an anxiogenic phenotype that is manifested by decreased time spent in the light compartment (light–dark box) and reduced time spent in open arms (elevated plus-maze). Interestingly, a previous work showed that the administration of MK801, another non-competitive NMDAR antagonist, to rats induced an anxiety-like phenotype in the elevated plus-maze (Solati, 2011). In contrast to MK801, high doses of memantine (100 mg/kg) increased time spent in open arms, implying an anxiolytic effect. However, doses ranging from 10 to 30 mg/kg decreased time spent in open arms (~40%), without reaching statistical significance, which suggests a trend representative of an anxiogenic-like effect (Minkeviciene et al., 2008). Additionally, chronic antagonism of NMDAR with piperine18 exacerbated anxiogenic symptoms in C57BL/6 mice (Hanson et al., 2014). Indeed, it would appear that the antagonism of NMDAR does not follow a linear dose-response effect in terms of modulating anxiety-like behavior.

It has also been shown that memantine plays a role in controlling synaptic glutamate release. In fact, Lu et al. (2010) have shown that memantine suppresses glutamate release in cortical synaptosomes. In this study, however, we showed that long-term administration of memantine reduces glutamate uptake without affecting the glutamate transporters expression, GLT-1 and GLAST, in the frontoparietal cortex and hippocampus. Based on these findings, one could argue that memantine-induced reduction of glutamate uptake by astrocytes is a direct adaptive response to the reduced release of glutamate by neurons. This assumption reinforces a theoretical framework in which neurons and astrocytes are capable of sensing each other while regulating tripartite glutamatergic synapses (Wade et al., 2013; Karus et al., 2015). However, further studies using additional methodologies, such as immunostaining and electron microscopy, are necessary to better understand neuron-astrocyte coupling in the context of anxiety-like phenotypes.

Interestingly, a recent work demonstrated that blockade of GLT-1 in the central amygdala was also capable of inducing anxiety-like behavior, which reinforces the association between

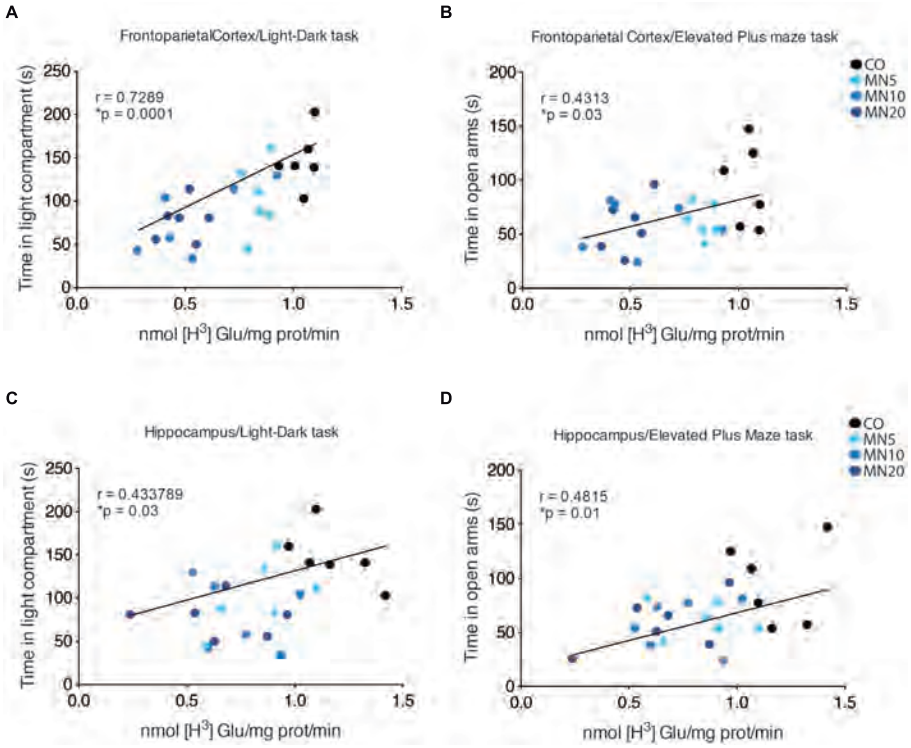

FIGURE 3 | Anxiety-like behavior correlates with glutamate uptake. **(A)** Linear correlation between time spent in light compartment during the light/dark task and glutamate uptake in slices of frontoparietal cortex. **(B)** Linear correlation between time spent in open arms and glutamate uptake in slices of frontoparietal cortex. **(C)** Linear correlation between time spent in light compartment during light/dark task and glutamate uptake in slices of hippocampus. **(D)** Linear correlation between time spent in open arms in elevated plus-maze test and glutamate uptake in slices of hippocampus. Groups: CO, memantine 5 mg (MN 5), memantine 10 mg (MN 10), and memantine 20 mg (MN 20); $n = 24$. Data presented by one animal per point. $^*p < 0.05$.

astrocytic glutamate uptake activity and the development of an anxiety phenotype (John et al., 2015). Remarkably, we were able to show through linear correlation that decreased glutamate uptake activity in the hippocampus and frontoparietal cortex was significantly correlated with an increased anxiety-like response.

Conclusion

Long-term NMDAR antagonism by memantine induces an anxiety phenotype that is associated with reduced glutamate uptake activity in healthy CF-1 mice, which suggests that interactions between neurons and astrocytes can shape anxiety-related behavior.

Author Contributions

EZ was responsible for the design, acquisition, analysis, interpretation, drafting, and approval of the final version of the manuscript. VT, EK, MA, KZ, RA, and GH were responsible for acquisition, analysis, interpretation, and approval of the final version of the manuscript. AM, DS, and RV were responsible for interpretation, drafting, critical revision, and approval of the final version of the manuscript. LV was responsible for the design, interpretation, drafting, critical revision, and approval of the final version of the manuscript.

Acknowledgments

This work was supported by the following Brazilian agencies and grants: National Counsel of Technological and Scientific Development (CNPq), CAPES, FAPERGS, Brazilian Institute of Neuroscience (IBNnet), FINEP, and National Institute of Science and Technology (INCT) – Excitotoxicity and Neuroprotection.

Supplementary Material

The Supplementary Material for this article can be found online at: http://journal.frontiersin.org/article/10.3389/fncel.2015.00219/abstract

References

Abramoff, M. D., Magalhaes, P. J., and Ram, S. J. (2004). Processing with ImageJ. *Biophotonics Intern.* 11, 36–42.

Anderson, C. M., and Swanson, R. A. (2000). Astrocyte glutamate transport: review of properties, regulation, and physiological functions. *Glia* 32, 1–14. doi: 10.1002/1098-1136(200010)32:1<1::AID-GLIA10>3.0.CO;2-W

Bechtholt-Gompf, A. J., Walther, H. V., Adams, M. A., Carlezon, W. A. Jr., Ongur, D., and Cohen, B. M. (2010). Blockade of astrocytic glutamate uptake in rats induces signs of anhedonia and impaired spatial memory. *Neuropsychopharmacology* 35, 2049–2059. doi: 10.1038/npp.2010.74

Clement, Y., and Chapouthier, G. (1998). Biological bases of anxiety. *Neurosci. Biobehav. Rev.* 22, 623–633. doi: 10.1016/S0149-7634(97)00058-4

Cortese, B. M., and Phan, K. L. (2005). The role of glutamate in anxiety and related disorders. *CNS Spectr.* 10, 820–830.

Crawley, J., and Goodwin, F. K. (1980). Preliminary report of a simple animal behavior model for the anxiolytic effects of benzodiazepines. *Pharmacol. Biochem. Behav.* 13, 167–170. doi: 10.1016/0091-3057(80)90067-2

Danbolt, N. C. (2001). Glutamate uptake. *Prog. Neurobiol.* 65, 1–105. doi: 10.1016/S0301-0082(00)00067-8

Danbolt, N. C., Storm-Mathisen, J., and Kanner, B. I. (1992). An [Na+ + K+]coupled L-glutamate transporter purified from rat brain is located in glial cell processes. *Neuroscience* 51, 295–310. doi: 10.1016/0306-4522(92)90316-T

Gross, C., and Hen, R. (2004). The developmental origins of anxiety. *Nat. Rev. Neurosci.* 5, 545–552. doi: 10.1038/nrn1429

Hanson, J. E., Meilandt, W. J., Gogineni, A., Reynen, P., Herrington, J., Weimer, R. M., et al. (2014). Chronic GluN2B antagonism disrupts behavior in wild-type mice without protecting against synapse loss or memory impairment in Alzheimer's disease mouse models. *J. Neurosci.* 34, 8277–8288. doi: 10.1523/JNEUROSCI.5106-13.2014

John, C. S., Sypek, E. I., Carlezon, W. A., Cohen, B. M., Ongur, D., and Bechtholt, A. J. (2015). Blockade of the GLT-1 transporter in the central nucleus of the amygdala induces both anxiety and depressive-like symptoms. *Neuropsychopharmacology* 40, 1700–1708. doi: 10.1038/npp.2015.16

Karus, C., Mondragao, M. A., Ziemens, D., and Rose, C. R. (2015). Astrocytes restrict discharge duration and neuronal sodium loads during recurrent network activity. *Glia* 63, 936–957. doi: 10.1002/glia.22793

Leasure, J. L., and Decker, L. (2009). Social isolation prevents exercise-induced proliferation of hippocampal progenitor cells in female rats. *Hippocampus* 19, 907–912. doi: 10.1002/hipo.20563

Lee, Y., Son, H., Kim, G., Kim, S., Lee, D. H., Roh, G. S., et al. (2013). Glutamine deficiency in the prefrontal cortex increases depressive-like behaviours in male mice. *J. Psychiatry Neurosci.* 38, 183–191. doi: 10.1503/jpn.120024

Lehre, K. P., and Danbolt, N. C. (1998). The number of glutamate transporter subtype molecules at glutamatergic synapses: chemical and stereological quantification in young adult rat brain. *J. Neurosci.* 18, 8751–8757.

Lu, C. W., Lin, T. Y., and Wang, S. J. (2010). Memantine depresses glutamate release through inhibition of voltage-dependent $Ca2^{+}$ entry and protein kinase C in rat cerebral cortex nerve terminals: an NMDA receptor-independent mechanism. *Neurochem. Int.* 57, 168–176. doi: 10.1016/j.neuint.2010.05.010

Machado-Vieira, R., Ibrahim, L., Henter, I. D., and Zarate, C. A. Jr. (2012). Novel glutamatergic agents for major depressive disorder and bipolar disorder. *Pharmacol. Biochem. Behav.* 100, 678–687. doi: 10.1016/j.pbb.2011.09.010

Machado-Vieira, R., Manji, H. K., and Zarate, C. A. (2009). The role of the tripartite glutamatergic synapse in the pathophysiology and therapeutics of mood disorders. *Neuroscientist* 15, 525–539. doi: 10.1177/1073858409336093

Minkeviciene, R., Banerjee, P., and Tanila, H. (2008). Cognition-enhancing and anxiolytic effects of memantine. *Neuropharmacology* 54, 1079–1085. doi: 10.1016/j.neuropharm.2008.02.014

Muller, A. P., Zimmer, E. R., Kalinine, E., Haas, C. B., Oses, J. P., Martimbianco De Assis, A., et al. (2012). Physical exercise exacerbates memory deficits induced by intracerebroventricular STZ but improves insulin regulation of H2O2 production in mice synaptosomes. *J. Alzheimers Dis.* 30, 889–898. doi: 10.3233/JAD-2012-112066

Nemeroff, C. B. (2003). The role of GABA in the pathophysiology and treatment of anxiety disorders. *Psychopharmacol. Bull.* 37, 133–146.

Nutt, D. J., and Malizia, A. L. (2001). New insights into the role of the GABA(A)-benzodiazepine receptor in psychiatric disorder. *Br. J. Psychiatry* 179, 390–396. doi: 10.1192/bjp.179.5.390

Pellow, S. (1986). Anxiolytic and anxiogenic drug effects in a novel test of anxiety: are exploratory models of anxiety in rodents valid? *Methods Find Exp. Clin. Pharmacol.* 8, 557–565.

Peterson, G. L. (1977). A simplification of the protein assay method of Lowry et al. which is more generally applicable. *Anal. Biochem.* 83, 346–356. doi: 10.1016/0003-2697(77)90043-4

Pilc, A., Wierońska, J. M., and Skolnick, P. (2013). Glutamate-based antidepressants: preclinical psychopharmacology. *Biol. Psychiatry* 73, 1125–1132. doi: 10.1016/j.biopsych.2013.01.021

Reus, G. Z., Stringari, R. B., Kirsch, T. R., Fries, G. R., Kapczinski, F., Roesler, R., et al. (2010). Neurochemical and behavioural effects of acute and chronic memantine administration in rats: further support for NMDA as a new pharmacological target for the treatment of depression? *Brain Res. Bull.* 81, 585–589. doi: 10.1016/j.brainresbull.2009.11.013

Riaza Bermudo-Soriano, C., Perez-Rodriguez, M. M., Vaquero-Lorenzo, C., and Baca-Garcia, E. (2012). New perspectives in glutamate and anxiety. *Pharmacol. Biochem. Behav.* 100, 752–774. doi: 10.1016/j.pbb.2011.04.010

Sani, G., Serra, G., Kotzalidis, G. D., Romano, S., Tamorri, S. M., Manfredi, G., et al. (2012). The role of memantine in the treatment of psychiatric disorders other than the dementias: a review of current preclinical and clinical evidence. *CNS Drugs* 26, 663–690. doi: 10.2165/11634390-000000000-00000

Schroeter, M. L., Abdul-Khaliq, H., Sacher, J., Steiner, J., Blasig, I. E., and Mueller, K. (2010). Mood disorders are glial disorders: evidence from in vivo studies. *Cardiovasc. Psychiatry Neurol.* 2010:780645. doi: 10.1155/2010/780645

Schwartz, T. L., Siddiqui, U. A., and Raza, S. (2012). Memantine as an augmentation therapy for anxiety disorders. *Case Rep. Psychiatry* 2012:749796. doi: 10.1155/2012/749796

Silvestre, J. S., Nadal, R., Pallares, M., and Ferre, N. (1997). Acute effects of ketamine in the holeboard, the elevated-plus maze, and the social interaction test in Wistar rats. *Depress. Anxiety* 5, 29–33. doi: 10.1002/(SICI)1520-6394(1997)5:1<29::AID-DA5>3.0.CO;2-0

Solati, J. (2011). Dorsal hippocampal N-methyl-d-aspartate glutamatergic and delta-opioidergic systems modulate anxiety behaviors in rats in a noninteractive manner. *Kaohsiung J. Med. Sci.* 27, 485–493. doi: 10.1016/j.kjms.2011.06.011

Szabo, S. T., Machado-Vieira, R., Yuan, P., Wang, Y., Wei, Y., Falke, C., et al. (2009). Glutamate receptors as targets of protein kinase C in the pathophysiology and treatment of animal models of mania. *Neuropharmacology* 56, 47–55. doi: 10.1016/j.neuropharm.2008.08.015

Tariot, P. N., Farlow, M. R., Grossberg, G. T., Graham, S. M., Mcdonald, S., and Gergel, I. (2004). Memantine treatment in patients with moderate to severe Alzheimer disease already receiving donepezil: a randomized controlled trial. *JAMA* 291, 317–324. doi: 10.1001/jama.291.3.317

Thomazi, A. P., Godinho, G. F., Rodrigues, J. M., Schwalm, F. D., Frizzo, M. E., Moriguchi, E., et al. (2004). Ontogenetic profile of glutamate uptake in brain structures slices from rats: sensitivity to guanosine. *Mech. Ageing Dev.* 125, 475–481. doi: 10.1016/j.mad.2004.04.005

Wade, J., Mcdaid, L., Harkin, J., Crunelli, V., and Kelso, S. (2013). Biophysically based computational models of astrocyte $\sim$ neuron coupling and their functional significance. *Front. Comput. Neurosci.* 7:44. doi: 10.3389/fncom.2013.00044

Zarate, C. Jr., Machado-Vieira, R., Henter, I., Ibrahim, L., Diazgranados, N., and Salvadore, G. (2010). Glutamatergic modulators: the future of treating mood disorders? *Harv. Rev. Psychiatry* 18, 293–303. doi: 10.3109/10673229.2010.511059

Zhou, Y., and Danbolt, N. C. (2014). Glutamate as a neurotransmitter in the healthy brain. *J. Neural. Transm.* 121, 799–817. doi: 10.1007/s00702-014-1180-8

Zimmer, E. R., Kalinine, E., Haas, C. B., Torrez, V. R., Souza, D. O., Muller, A. P., et al. (2012). Pretreatment with memantine prevents Alzheimer-like alterations induced by intrahippocampal okadaic acid administration in rats. *Curr. Alzheimer Res.* 9, 1182–1190. doi: 10.2174/156720512804142877

Conflict of Interest Statement: The authors declare that the research was conducted in the absence of any commercial or financial relationships that could be construed as a potential conflict of interest.

Copyright © 2015 Zimmer, Torrez, Kalinine, Augustin, Zenki, Almeida, Hansel, Muller, Souza, Machado-Vieira and Portela. This is an open-access article distributed under the terms of the Creative Commons Attribution License (CC BY). The use, distribution or reproduction in other forums is permitted, provided the original author(s) or licensor are credited and that the original publication in this journal is cited, in accordance with accepted academic practice. No use, distribution or reproduction is permitted which does not comply with these terms.

Capítulo V. *Imaging biomarkers for amyloid: a new generation of probes and what lies ahead.*

No **capítulo V** apresentamos o artigo publicado no periódico *International Psychogeriatrics.*

Muitos esforços têm sido feitos para o desenvolvimento de uma maneira efetiva de diagnosticar a DA precocemente. Neste sentido, os primeiros estudos com PET [^{11}C]PIB, que se liga em placas de β-amilóide, trouxerem avanços sem precedentes em termos de diagnóstico *in vivo* da DA. Neste capítulo, relembramos o critério de diagnóstico da DA de 1984 proposto pelo *National Institute of Neurological and Communicative Disorders and Stroke* (NINCDS) e pelo *Alzheimer's Disease and Related Disorders Association* (ADRDA), e avaliamos os novos critérios recentemente propostos que incluem o uso de imagem de PET β-amilóide. Também apresentamos as novas gerações de radiofármacos para β-amilóide desenvolvidos com o radioisótopo [^{18}F] (meia vida de ~110 minutos) e seu potencial uso para distribuição regional e uso generalizado a nível clínico.

International Psychogeriatrics: page 1 of 5 © International Psychogeriatric Association 2014
doi:10.1017/S1041610214000118

GUEST EDITORIAL

Imaging biomarkers for amyloid: a new generation of probes and what lies ahead

Introduction

Since the original 1984 criteria for Alzheimer's disease (AD), put forth by a work group jointly established by the National Institute of Neurological and Communicative Disorders and Stroke (NINCDS) and the Alzheimer's Disease and Related Disorders Association (ADRDA) (McKhann *et al.*, 1984), important advances have occurred in our ability to detect AD pathophysiology, with the incorporation of biomarkers – defined as anatomic, biochemical, or physiologic parameters that provide *in vivo* evidence of AD neuropathology (Cummings, 2011) – that can improve the certainty of AD diagnosis. Use of imaging biomarkers such as positron emission tomography (PET) with amyloid ligands, particularly in asymptomatic and pre-dementia stages of AD, however, has been the subject of debate (Dubois *et al.*, 2013), with arguments both for and against the biomarker driven diagnosis of AD.

Revised conceptualization of AD: the role of amyloid imaging

In contrast to the original 1984 criteria the recently proposed revisions put forth by the International Working Group (IWG; Dubois *et al.*, 2007) and the National Institute on Aging/Alzheimer's Association (NIA-AA; Sperling *et al.*, 2011a) redefine AD as a clinicobiological entity, comprising a semantic and conceptual distinction between AD neuropathology and resulting clinical phenomenology. Currently, AD is conceptualized as a progressive pathophysiological process in which β-amyloid pathology is thought to accumulate during a silent "preclinical" phase followed by a dynamic cascade of neurodegenerative events including tau pathology, which ultimately cause cognitive impairment and dementia. This amyloidocentric framework incorporates the use of imaging biomarkers for amyloid in the form of abnormal PET amyloid tracer retention. The slow progression of β-amyloid deposition in AD supports the idea that amyloid pathology occurs very early in the disease process and tends to reach a plateau by the onset of the first clinical signs of dementia.

As novel amyloid directed therapeutics enter clinical trials, the role of amyloid imaging is increasingly clear given that its ability to allow for accurate, reliable, and reproducible quantification of both regional and global amyloid burden, and the growing consensus emerging from longitudinal studies that disease-modifying therapies targeting amyloid must be administered early on in the disease course (Sperling *et al.*, 2011b). In addition to serving as a diagnostic biomarker to guide population enrichment strategies, amyloid imaging can be used to calculate sample size and to increase statistical power via population stratification or through use as baseline predictors (Wu *et al.*, 2011). In parallel, amyloid-imaging outcomes can serve as endpoint biomarkers to monitor the rate of disease progression, as well as response to therapy.

First generation of amyloid probes: ^{11}C Pittsburgh Compound B

The ^{11}C labeled thioflavin T derivative Pittsburgh Compound B (PIB) is the benchmark PET amyloid-imaging agent, demonstrating high sensitivity and specificity for *in vivo* quantification of fibrillar Aβ in both plaques and related Aβ containing lesions, such as diffuse plaques and cerebral amyloid angiopathy (Price *et al.*, 2005; Lockhart *et al.*, 2007; Cohen *et al.*, 2012). Importantly, on the basis of concentrations achieved during PET studies, cortical retention of ^{11}C-PIB has been shown to reflect Aβ load as opposed to Lewy bodies or tau pathology (Fodero-Tavoletti *et al.*, 2007; Lockhart *et al.*, 2007; Ikonomovic *et al.*, 2008). In addition to accelerating current understanding of cerebral amyloidosis and advancing detection of AD pathology to an earlier stage (Klunk *et al.*, 2004; Mintun *et al.*, 2006; Rowe *et al.*, 2007; Cohen *et al.*, 2012), ^{11}C-PIB has contributed to improvements in the differential diagnosis of neurodegenerative diseases (Ng *et al.*, 2007; Rabinovici *et al.*, 2007; Rowe *et al.*, 2007). However, the short 20-minute half-life of carbon-11 probes limits their use to imaging centers possessing an onsite cyclotron and

a radiochemistry department with expertise in the synthesis of ^{11}C; the cost of ^{11}C-PIB studies has precluded it's routine use in clinical settings.

Second and third generation amyloid probes: ^{18}F-labeled radiopharmaceuticals

In order to address short half-life limitations a number of ^{18}F labeled amyloid PET radiopharmaceuticals have been developed with a 110-minute half-life. Radiopharmaceuticals like [^{18}F]3′-F-PIB (flutemetamol; Wolk *et al.*, 2011), [^{18}F]AV-45 (florbetapir; Clark *et al.*, 2012), [^{18}F]-AV-1 or [^{18}F]-BAY94–9172 (florbetapen; Rowe *et al.*, 2008; Vallabhajosula, 2011), and [^{18}F]AZD4694 or NAV4694 (Jureus *et al.*, 2010; Cselenyi *et al.*, 2012; Rowe *et al.*, 2013) can facilitate the integration of PET into routine clinical use by allowing for centralized production and regional distribution (Rowe and Villemagne, 2013).

While ^{18}F-florbetapir, ^{18}F-florbetaben, and ^{18}F-flutemetamol allow for clear differentiation of AD patients from healthy controls, cortical retention of ^{18}F-florbetapir and ^{18}F-florbetaben are inferior to that of ^{11}C-PIB (Villemagne *et al.*, 2012) and are characterized by a more narrow dynamic range of standardized uptake value ratios (SUVRs), associated visually with elevated non-specific white matter (WM) binding (Vandenberghe *et al.*, 2010). Moreover, novel ^{18}F amyloid tracers are associated with the loss of gray-white matter demarcation (Rowe and Villemagne, 2011), in contrast to ^{11}C-PIB, where gray matter retention is visibly greater relative to subjacent WM uptake (Rowe and Villemagne, 2013). Though it has yet to pass through phase II trials, ^{18}F-AZD4694 (NAV4694) is similar to ^{11}C-PIB, possessing rapid kinetics, low non-specific WM binding, and a wider dynamic range when comparing AD to healthy control individuals (Cselenyi *et al.*, 2012; Zimmer *et al.*, 2013). In a head-to-head comparison study with ^{11}C-PIB among healthy controls and patients with AD and frontotemporal lobar degeneration (FTLD), ^{18}FNAV4694 showed an r of 0.98 and a slope of 0.95, indicating significant overlap with ^{11}C-PIB (Rowe *et al.*, 2013).

Criteria for appropriate use of amyloid PET imaging

Given that ^{18}F-florbetapir is now approved by the Food and Drug Administration (FDA) for the clinical assessment of individuals with cognitive impairment, with additional ^{18}F tracers likely to become available in the coming years, appropriate use criteria (AUC) are of chief importance owing to (1) the potential for harm if scans are performed for inappropriate reasons, are misinterpreted, and/or the information obtained incorrectly applied; and (2) the high cost associated with such investigations. Apropos the first instance, a suitable example is the disclosure of amyloid positivity in an individual without cognitive impairment. Given positive findings in close to 30% of cognitively normal individuals over the age of 70 – and the lack of sufficient longitudinal data to adequately characterize the potential risk of future cognitive decline – premature diagnosis of AD on the basis of a positive Aβ scan alone has been categorized as inappropriate given the potential for detrimental social, psychological, employment, lifestyle, and financial consequences (Rowe and Villemagne, 2013). In addition, among patients with cognitive complaints, precipitous conclusions could lead to lack of appropriate treatment for underlying alternative causes, such as depression. Moreover, from an economic perspective, the lack of established disease-modifying therapies necessitates a careful cost-benefit analysis, with the likelihood of improved diagnostic accuracy and altered treatment guiding a decision to opt for amyloid imaging. In short, amyloid findings must be situated within the context of a comprehensive investigatory framework, interpreted by a physician with requisite expertise, and, where possible, supported by additional markers suggestive of AD such as an amnestic syndrome of the hippocampal type (Dubois and Albert, 2004), hippocampal atrophy on magnetic resonance imaging (MRI), or a parietotemporal pattern of hypometabolism on ^{18}F-FDG PET.

Assembled in late 2012 by the Alzheimer's Association (AA) and the Society of Nuclear Medicine and Molecular Imaging (SNMMI), the Amyloid Imaging Taskforce (AIT) was charged with delineating AUC for amyloid PET imaging using available literature and a consensus-based approach among dementia experts. On the basis of this approach amyloid imaging was deemed appropriate in the following clinical contexts: (1) patients exhibiting unexplained mild cognitive impairment (MCI) that is persistent or progressive, (2) patients fulfilling core criteria for possible AD yet with a clinical course that is atypical or an etiologically mixed presentation, and (3) patients with rapidly progressive dementia and atypically young age at the onset. In a sister publication (Johnson *et al.*, 2013b), clarification and expansion of three topics were discussed in the original publication (Johnson *et al.*, 2013a), including the practical identification of physicians possessing the expertise required for appropriate integration of amyloid PET imaging; the importance of identifying

the specific subset of MCI individuals for whom amyloid PET imaging would prove appropriate; and the creation of developing education programs aiming to augment awareness of the amyloid PET AUC and how best to integrate this technique into clinical decision-making algorithms.

Potential ethical issues tied to disclosure of amyloid positivity

With the increasing paradigmatic shift toward the uncoupling of AD pathophysiology from resulting clinical phenomenology – with the attendant implication of a diagnosis of AD issued during the presymptomatic/minimally symptomatic phase – appropriate legal revisions must occur in parallel to guard against privacy and confidentiality infringements (Karlawish, 2011). Guidelines must also be put in place to address the well-established stigma tied to AD, and to guide assessment of the potential for negative psychological sequelae in a given individual following disclosure of biomarker information conferring an elevated risk of AD (e.g. amyloid positivity).

Although researchers are currently not under obligation to disclose biomarker findings to research participants owing to uncertainty regarding the clinical utility of this information – a case in point being the Alzheimer's Disease Neuroimaging Initiative's (ADNI) "no return policy" – a move toward clinical trials and increasing calls for disclosure of research results from the public (Shalowitz and Miller, 2008) makes clear the need to accelerate the development of appropriate guidelines. This reorientation toward disclosure has been, furthermore, strengthened by recent findings suggesting that ADNI investigators support disclosure of amyloid imaging results – as well as, more generally, other biomarker findings – to ADNI participants (Shulman *et al.*, 2013). In addition, despite a lack of evidence supporting the predictive value associated with imaging biomarkers, some clinicians have already begun incorporating IWG and NIA-AA research diagnostic criteria for asymptomatic at risk and MCI/prodromal into clinical practice (Gauthier and Rosa-Neto, 2013).

As the field of AD moves rapidly forward, a growing need exists in terms of the incorporation of procedures addressing disclosure of biomarker findings into large-scale studies and the encouragement of research addressing the impact of disclosure of biomarker findings (Gauthier and Rosa-Neto, 2013). Importantly, those ADNI investigators who endorsed disclosure likewise, in a majority of cases, highlighted the importance of developing standardized protocols and participant educational materials addressing disclosure, as well as longitudinal outcome studies to assess the effects of this information on the well-being of participants (Shulman *et al.*, 2013).

Future directions

In research, amyloid-imaging agents can serve to enrich clinical trial populations, monitor disease progression, or assess the effect of amyloid-targeted interventions. While PET amyloid probes have yet to find application in routine general clinical practice, FDA approval of ^{18}F florbetapir – with approval of additional ^{18}F compounds likely in the coming years – requires careful adherence to, and promulgation of, current AUC. Moreover, as new data are gathered, and, in particular, should new effective therapies emerge, these criteria will likely require re-evaluation and, possibly, redefinition. In the interim, special care must be paid to the potential consequences associated with inappropriate use of amyloid PET imaging. Further, given the increasing attitudinal shift toward disclosure of research results it is vital that psychosocial research keep apace with developments in the area of AD biomarkers.

ANTOINE LEUZY,[1,2,*]
EDUARDO RIGON ZIMMER,[1,2,3,*] VENKAT BHAT,[4]
PEDRO ROSA-NETO[1,2] AND SERGE GAUTHIER[2]

[1]Translational Neuroimaging Laboratory (TNL), McGill Center for Studies in Aging (MCSA), Douglas Mental Health Research Institute, Montreal, Canada
[2]Alzheimer's Disease and Related Disorders Research Unit, McGill Center for Studies in Aging (MCSA), Douglas Mental Health Research Institute, Montreal, Canada
[3]Department of Biochemistry, Federal University of Rio Grande do Sul (UFRGS), Porto Alegre, Brazil
[4]Department of Psychiatry, McGill University, Montreal, Canada
*Both authors contributed equally to this work.
Email: serge.gauthier@mcgill.ca

References

Clark, C. M. *et al.* (2012). Cerebral PET with florbetapir compared with neuropathology at autopsy for detection of neuritic amyloid-beta plaques: a prospective cohort study. *Lancet Neurology*, 11, 669–678. doi:10.1016/S1474-4422(12)70142-4.

Cohen, A. D., Rabinovici, G. D., Mathis, C. A., Jagust, W. J., Klunk, W. E. and Ikonomovic, M. D. (2012). Using Pittsburgh Compound B for in vivo PET imaging of fibrillar amyloid-beta. *Advances in Pharmacology*, 64, 27–81. doi:10.1016/B978-0-12-394816-8.00002-7.

Cselenyi, Z. *et al.* (2012). Clinical validation of 18F-AZD4694, an amyloid-beta-specific PET radioligand. *Journal of Nuclear Medicine*, 53, 415–424. doi:10.2967/jnumed.111.094029.

Cummings, J. L. (2011). Biomarkers in Alzheimer's disease drug development. *Alzheimer's & Dementia*, 7, e13–e44. doi:10.1016/j.jalz.2010.06.004.

Dubois, B. and Albert, M. L. (2004). Amnestic MCI or prodromal Alzheimer's disease? *Lancet Neurology*, 3, 246–248. doi: 10.1016/S1474-4422(04)00710-0.

Dubois, B. *et al.* (2007). Research criteria for the diagnosis of Alzheimer's disease: revising the NINCDS-ADRDA criteria. *Lancet Neurology*, 6, 734–746. doi:10.1016/S1474-4422(07)70178-3.

Dubois, B., Gauthier, S. and Cummings, J. (2013). The utility of the new research diagnostic criteria for Alzheimer's disease. *International Psychogeriatrics*, 25, 175–177. doi:10.1017/S1041610212002098.

Fodero-Tavoletti, M. T. *et al.* (2007). In vitro characterization of Pittsburgh compound-B binding to Lewy bodies. *The Journal of Neuroscience*, 27, 10365–10371. doi:10.1523/JNEUROSCI.0630-07.2007.

Gauthier, S. and Rosa-Neto, P. (2013). Dementia: disclosure of results to participants in dementia research. *Nature Reviews Neurology*, 9, 608–609. doi:10.1038/nrneurol.2013.213.

Ikonomovic, M. D. *et al.* (2008). Post-mortem correlates of in vivo PiB-PET amyloid imaging in a typical case of Alzheimer's disease. *Brain*, 131, 1630–1645. doi:10.1093/brain/awn016.

Johnson, K. A. *et al.* (2013a). Appropriate use criteria for amyloid PET: a report of the Amyloid Imaging Task Force, the Society of Nuclear Medicine and Molecular Imaging, and the Alzheimer's Association. *Alzheimer's & Dementia*, 9, e-1–e-16. doi:10.1016/j.jalz.2013.01.002.

Johnson, K. A. *et al.* (2013b). Update on appropriate use criteria for amyloid PET imaging: dementia experts, mild cognitive impairment, and education. *Journal of Nuclear Medicine*, 54, 1011–1013. doi:10.2967/jnumed.113.127068.

Jureus, A. *et al.* (2010). Characterization of AZD4694, a novel fluorinated Abeta plaque neuroimaging PET radioligand. *Journal of Neurochemistry*, 114, 784–794. doi:10.1111/j.1471-4159.2010.06812.x.

Karlawish, J. (2011). Addressing the ethical, policy, and social challenges of preclinical Alzheimer disease. *Neurology*, 77, 1487–1493. doi:10.1212/WNL.0b013e318232ac1a.

Klunk, W. E. *et al.* (2004). Imaging brain amyloid in Alzheimer's disease with Pittsburgh Compound-B. *Annals of Neurology*, 55, 306–319. doi:10.1002/ana.20009.

Lockhart, A. *et al.* (2007). PIB is a non-specific imaging marker of amyloid-beta (Abeta) peptide-related cerebral amyloidosis. *Brain*, 130, 2607–2615. doi:10.1093/brain/awm191.

McKhann, G., Drachman, D., Folstein, M., Katzman, R., Price, D. and Stadlan, E. M. (1984). Clinical diagnosis of Alzheimer's disease: report of the NINCDS-ADRDA work group under the auspices of Department of Health and Human Services Task Force on Alzheimer's Disease. *Neurology*, 34, 939–944.

Mintun, M. A. *et al.* (2006). [11C]PIB in a nondemented population: potential antecedent marker of Alzheimer disease. *Neurology*, 67, 446–452. doi:10.1212/01.wnl.0000228230.26044.a4.

Ng, S. Y., Villemagne, V. L., Masters, C. L. and Rowe, C. C. (2007). Evaluating atypical dementia syndromes using positron emission tomography with carbon 11 labeled Pittsburgh Compound B. *Archives of Neurology*, 64, 1140–1144. doi:10.1001/archneur.64.8.1140.

Price, J. C. *et al.* (2005). Kinetic modeling of amyloid binding in humans using PET imaging and Pittsburgh Compound-B. *Journal of Cerebral Blood Flow & Metabolism*, 25, 1528–1547. doi:10.1038/sj.jcbfm.9600146.

Rabinovici, G. D. *et al.* (2007). 11C-PIB PET imaging in Alzheimer disease and frontotemporal lobar degeneration. *Neurology*, 68, 1205–1212. doi:10.1212/01.wnl.0000259035.98480.ed.

Rowe, C. C. and Villemagne, V. L. (2011). Brain amyloid imaging. *Journal of Nuclear Medicine*, 52, 1733–1740. doi:10.2967/jnumed.110.076315.

Rowe, C. C. and Villemagne, V. L. (2013). Brain amyloid imaging. *Journal of Nuclear Medicine Technology*, 41, 11–18. doi:10.2967/jnumed.110.076315.

Rowe, C. C. *et al.* (2007). Imaging beta-amyloid burden in aging and dementia. *Neurology*, 68, 1718–1725. doi:10.1212/01.wnl.0000261919.22630.ea.

Rowe, C. C. *et al.* (2008). Imaging of amyloid beta in Alzheimer's disease with 18F-BAY94–9172, a novel PET tracer: proof of mechanism. *Lancet Neurology*, 7, 129–135. doi: 10.1016/S1474-4422(08)70001-2.

Rowe, C. C. *et al.* (2013). Head-to-head comparison of 11C-PiB and 18F-AZD4694 (NAV4694) for beta-amyloid imaging in aging and dementia. *Journal of Nuclear Medicine*, 54, 880–886. doi:10.2967/jnumed.112.114785.

Shalowitz, D. I. and Miller, F. G. (2008). Communicating the results of clinical research to participants: attitudes, practices, and future directions. *PLoS Medicine*, 5, e91. doi:10.1371/journal.pmed.0050091.

Shulman, M. B., Harkins, K., Green, R. C. and Karlawish, J. (2013). Using AD biomarker research results for clinical care: a survey of ADNI investigators. *Neurology*, 81, 1114–1121. doi:10.1212/WNL.0b013e3182a55f4a.

Sperling, R. A. *et al.* (2011a). Toward defining the preclinical stages of Alzheimer's disease: recommendations from the National Institute on Aging-Alzheimer's Association workgroups on diagnostic guidelines for Alzheimer's disease. *Alzheimer's & Dementia*, 7, 280–292. doi:10.1016/j.jalz.2011.03.003.

Sperling, R. A., Jack, C. R., Jr. and Aisen, P. S. (2011b). Testing the right target and right drug at the right stage. *Science Translational Medicine*, 3, 111cm133. doi:10.1126/scitranslmed.3002609.

Vallabhajosula, S. (2011). Positron emission tomography radiopharmaceuticals for imaging brain Beta-amyloid. *Seminars in Nuclear Medicine*, 41, 283–299. doi:10.1053/j.semnuclmed.2011.02.005.

Vandenberghe, R. *et al.* (2010). 18F-flutemetamol amyloid imaging in Alzheimer disease and mild cognitive impairment: a phase 2 trial. *Annals of Neurology*, 68, 319–329. doi:10.1002/ana.22068.

Villemagne, V. L. *et al.* (2012). Comparison of 11C-PiB and 18F-florbetaben for Abeta imaging in ageing and

Alzheimer's disease. *European Journal of Nuclear Medicine and Molecular Imaging*, 39, 983–989. doi:10.1007/s00259-012-2088-x.

Wolk, D. A. *et al.* (2011). Association between in vivo fluorine 18-labeled flutemetamol amyloid positron emission tomography imaging and in vivo cerebral cortical histopathology. *Archives of Neurology*, 68, 1398–1403. doi:10.1001/archneurol.2011.153.

Wu, L., Rosa-Neto, P. and Gauthier, S. (2011). Use of biomarkers in clinical trials of Alzheimer disease: from concept to application. *Molecular Diagnosis & Therapy*, 15, 313–325. doi:10.2165/11595090-000000000-00000.

Zimmer, E. *et al.* (2013). [18F]NAV4694 shows higher binding and wider dynamic range compared with [11C]PiB in Alzheimer's disease postmortem tissue. *Alzheimer's & Dementia*, 9, P22–P23. doi:10.1016/j.jalz.2013.05.1161.

Capítulo VI. *Use of amyloid PET across the spectrum of Alzheimer's disease: clinical utility and associated ethical issues.*

No **capítulo VI** apresentamos o artigo publicado no periódico *Amyloid: the Journal of Protein Folding Disorders.*

No capítulo anterior (capítulo V) avaliamos os radiofármacos disponíveis para visualização de placas de β-amilóide na clínica. Neste capítulo avaliamos o potencial uso dos radiofármacos de β-amilóide via PET para o monitoramento da progressão das diversas fases da DA. Além disso, discutimos as implicações éticas da divulgação dos resultados dos exames de PET β-amilóide associados com o potencial impacto psicossocial de ser amilóide positivo (do inglês *amyloid positivity*).

Amyloid
The Journal of Protein Folding Disorders

http://informahealthcare.com/amy
ISSN: 1350-6129 (print), 1744-2818 (electronic)

Amyloid, Early Online: 1–6
© 2014 Informa UK Ltd. DOI: 10.3109/13506129.2014.926267

informa
healthcare

REVIEW ARTICLE

Use of amyloid PET across the spectrum of Alzheimer's disease: clinical utility and associated ethical issues

Antoine Leuzy[1,2]*, Eduardo Rigon Zimmer[1,2,3]*, Kerstin Heurling[4], Pedro Rosa-Neto[1,2], and Serge Gauthier[2]

[1]*Translational Neuroimaging Laboratory (TNL), Douglas Mental Health University Institute, Montreal, Canada,* [2]*Alzheimer's Disease Research Unit, McGill Centre for Studies in Aging, McGill University, Montreal, Canada,* [3]*Department of Biochemistry, Federal University of Rio Grande do Sul (UFRGS), Porto Alegre, Brazil, and* [4]*Section of Nuclear Medicine and PET, Department of Radiology, Oncology and Radiation Science, Uppsala University, Uppsala, Sweden*

Amyloid
Downloaded from informahealthcare.com by 61.163.77.42 on 06/11/14. For personal use only.

Abstract

Recent advances have made possible the *in vivo* detection of beta-amyloid (Aβ) pathology using positron emission tomography. While the gold standard for amyloid imaging, carbon-11 labeled Pittsburgh compound B is increasingly being replaced by fluorine-18 labeled radiopharmaceuticals, with three already approved for clinical use by US and European regulatory bodies. Appropriate use criteria proposed by an amyloid imaging taskforce convened by the Alzheimer's Association and the Society of Nuclear Medicine and Molecular Imaging recommend restricting use of this technology to the evaluation of patients with mild cognitive impairment or atypical dementia syndromes. While use among asymptomatic individuals is currently viewed as inappropriate due prognostic uncertainty, elevated levels of brain Aβ among asymptomatic individuals may represent preclinical Alzheimer's disease. Amyloid imaging is likewise expected to play a role in the design of clinical trials. Though preliminary results suggest amyloid imaging to possess clinical utility and cost-effectiveness, both domains have yet to be assessed systematically. As the field moves toward adoption of a pro-disclosure stance for amyloid imaging findings, it is imperative that a broad range of stakeholders be involved to ensure the appropriateness of emerging policies and protocols.

Abbreviations: A4: Anti-Amyloid treatment of Asymptomatic Alzheimer's disease trial; Aβ: beta-amyloid; ADNI: Alzheimer's Disease Neuroimaging Initiative; AIT: Amyloid Imaging Taskforce; AUC: appropriate use criteria; CCCDTD4: Fourth Canadian Consensus Conference on the Diagnosis and Treatment of Dementia; [^{11}C]PIB: Pittsburgh Compound B; DIAN: Dominantly Inherited Alzheimer Network; DLB: dementia with Lewy bodies; Flutemetamol: [^{18}F]3′-F-PIB; Florbetapir: [^{18}F]AV-45; Florbetaben: [^{18}F]-AV-1 and [^{18}F]-BAY94-9172; FTD: frontotemporal dementia; FTLD: frontotemporal lobar degeneration; IWG: International Working Group; MCI: mild cognitive impairment; NIA-AA: National Institute on Aging-Alzheimer's Association; PET: positron emission tomography.

Keywords

[^{18}F]Florbetapir, [^{18}F]flutemetamol, appropriate use criteria, diagnosis, mild cognitive impairment, positron emission tomography

History

Received 7 March 2014
Revised 17 April 2014
Accepted 16 May 2014
Published online 9 June 2014

Introduction

Research progress during the past decade has made possible the *in vivo* detection of beta-amyloid (Aβ) pathology using positron emission tomography (PET). A neuropathological hallmark of Alzheimer's disease (AD), Aβ accumulates extracellularly in the form of neuritic plaques, with this process thought to precede clinical symptoms by more than a decade. To date, a majority of studies using PET amyloid imaging agents have focused on the validation of this technology and investigation of Aβ's role in the onset and progression of AD. As a result, few studies have examined the clinical utility of amyloid PET, limited so far to highly selected populations free of comorbidities, complex histories and atypical features [1].

Despite the paucity of clinical use data, the Alzheimer's Association and the Society of Nuclear Medicine and Molecular Imaging recently convened an Amyloid Imaging Taskforce (AIT), in recognition of the potential clinical utility of amyloid PET in the evaluation of patients with cognitive impairment (see Figure 1). On the basis of a review of current literature and expert opinion, the AIT defined a set of appropriate use criteria (AUC), restricting use of amyloid imaging to patients showing objective evidence of cognitive

*These authors contributed equally to this work.

Address for correspondence: Serge Gauthier, Alzheimer's Disease Research Unit, McGill Center for Studies in Aging, McGill University, 6825 LaSalle Blvd., Montreal, QC H4H 1R3, Canada. Tel: +1 514 761 6131 (ext. 6302). Fax: +1 514 888 4050. E-mail: serge.gauthier@mcgill.ca

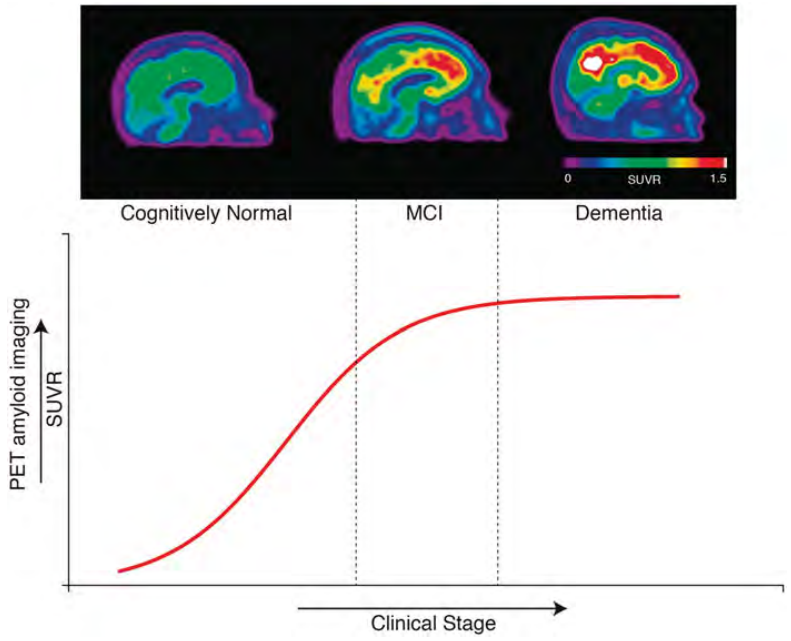

Figure 1. Potential clinical utility of amyloid PET imaging across the spectrum of AD. The potential for amyloid PET to prove of use in the evaluation of patients with cognitive impairment – or to aid in the identification of individuals at risk for future cognitive decline – rests on the assumption that brain amyloidosis precedes clinical change. Here, an idealized representation showing the absence of brain amyloid among cognitively normal individuals, with a signal appearing in the MCI phase.

Table 1. Appropriate use criteria for amyloid PET.

(A) Amyloid imaging is considered appropriate in situations 1 through 3 among individuals exhibiting the following characteristics:
(i) Subjective complaint about cognition corroborated by objective evidence.
(ii) Diagnosis is uncertainty following a comprehensive evaluation by a dementia expert, though Alzheimer's disease remains a possibility.
(iii) When knowledge of amyloid status is expected to augment diagnostic certainty and alter patient management.
(B) Appropriate situations:
(i) Patients exhibiting unexplained mild cognitive impairment that is persistent or progressive.
(ii) Patients exhibiting an atypical dementia syndrome in terms of clinical course or presentation.
(iii) Patients with a progressive dementia and early age at onset ($\leq$65 years).

Appropriate use criteria for amyloid PET, as defined by the Society of Nuclear Medicine and Molecular Imaging and the Alzheimer's Association joint Amyloid Imaging Task Force 2012. Section A addresses patient characteristics that must be present prior to consideration of amyloid PET. Section B describes clinical situations in which amyloid PET may prove of use (adapted from ref. [1]).

Amyloid
Downloaded from informahealthcare.com by 61.163.77.42 on 06/11/14. For personal use only.

impairment, uncertain etiology, and when knowledge of amyloid status is expected to augment diagnostic certainty and alter patient management (see Table 1, section A). This consensus paper is largely in line with recommendations elaborated during the Fourth Canadian Consensus Conference on the Diagnosis and Treatment of Dementia (CCCDTD4) [2] as well as with those put forth by Rowe and Villemagne [3]. We here aim to address the current status of amyloid imaging at the asymptomatic, pre-dementia and dementia stages of AD, and potential ethical issues tied to clinical utility, cost-effectiveness and disclosure.

Development of amyloid PET imaging agents

The ^{11}C labeled Pittsburgh compound B ([^{11}C]PIB) is the gold-standard amyloid PET agent, however its short half-life limits its use to centers possessing an onsite cyclotron and a specialized radiochemistry department [4]. To address this issue, several ^{18}F labeled agents have been developed, with a 110-min half-life allowing for centralized production and regional distribution. In this respect, ^{18}F-labelled radiopharmaceuticals such as [^{18}F]3′-F-PIB (flutemetamol) [5], [^{18}F]AV-45 (florbetapir) [6], [^{18}F]-AV-1 and [^{18}F]-BAY94-9172 (florbetaben) [7,8] can facilitate the integration of amyloid PET imaging into routine clinical practice [9], with florbetapir and florbetaben approved for clinical use by US and European regulatory bodies [10–13] and flutemetamol close behind [14]. A third generation probe, [^{18}F]AZD4694 – recently renamed NAV4694 [15,16] – likewise shows promise; exhibiting similar properties to [^{11}C]PIB – and lower non-specific white matter binding relative to other ^{18}F tracers [16] – preliminary *in vitro* data show that [^{18}F]NAV4694 is able to differentiate AD from healthy controls [15,17]. Similar head-to-head comparisons between [^{11}C]PIB and ^{18}F-labelled amyloid ligands have revealed significant overlap with respect to detection of amyloid plaques, linear regression slope and diagnostic performance [18–22].

Use of amyloid PET in patients with mild cognitive impairment

A period varying up to 5 years, mild cognitive impairment (MCI) is considered a transitional state between normal aging

Amyloid
Downloaded from informahealthcare.com by 61.163.77.42 on 06/11/14. For personal use only.

and dementia [23], most commonly of the Alzheimer's type [24]. Despite the continued evolution and debate over criteria for MCI, its core clinical features, by consensus, include a concern about a change in cognition, impairment in one or more cognitive domains, and the preservation of independence in functional activities. Thus, while impaired according to objective measures the patient with MCI does not meet criteria for dementia [23].

The recent AIT criteria include MCI associated with etiologic uncertainty as an appropriate indication for use of amyloid PET (see Table 1, section B), provided that greater certainty of the underlying pathology likely results in altered clinical management [1]. In the case of amyloid positivity, the level of certainty regarding AD as the underlying etiology would be increased due the close correspondence between amyloid PET and brain Aβ load. In contrast, amyloid negativity points to alternative, non-AD neurodegenerative processes; in practice, this scenario may be the most useful given the potential presence of age related Aβ. As such, amyloid PET may prove of use in ruling out AD pathology as the cause for the clinical phenotype in MCI patients whose clinical tableau may be complicated by potential traumatic, cerebrovascular or additional medical factors capable of causing cognitive impairment [1].

Though empirical evidence regarding the value of added certainty resulting from amyloid PET has not yet been reported, the AIT considered several situations in which the added certainty of amyloid PET could be useful to patients and caregivers. In the context of an individual with MCI, diagnostic delay frequently results in costly consecutive investigations, delayed forward planning – addressing issues such as finances, employment and future preferences – and delayed initiation of potentially effective therapies targeting amyloid [3]. Further, use of such medications in the absence of findings pointing to amyloid positivity would be inappropriate in the 50% of MCI patients who do not exhibit AD pathology [3]. Finally, earlier and more accurate diagnosis of AD may prove essential if future disease modifying therapies are to prove effective.

Use of amyloid PET in patients with AD

The second indication for use of amyloid PET identified by the AIT is among patients qualifying as having an atypical dementia syndrome, including those meeting criteria for possible AD. While fulfilling the core clinical criteria for AD dementia, doubt surrounds whether the syndrome is due to AD owing to either an atypical course (e.g. sudden onset of cognitive impairment or insufficient evidence to support progressive decline) [25] or due a non-amnestic presentation, such as in frontotemporal dementia (FTD), which can prove difficult to distinguish from early-onset AD, particularly early on in the disease course. Although Aβ imaging cannot contribute to the differential diagnosis between AD and dementia with Lewy bodies (DLB) it may have prognostic relevance in the latter population as Aβ burden has been shown to correlate inversely with duration of the prodromal phase [26], similar to that reported in Parkinson's disease dementia [27]. Lastly, amyloid PET is likewise appropriate for use in cases with a relatively early age at onset (e.g. 50–65 years old, though possibly younger) where the clinical portrait is characterized by progressive cognitive impairment and the presence of AD and non-AD dementia features [1]. Importantly, histopathologic examination completed during phase III trials for several second and third generation ^{18}F amyloid ligands confirm that amyloid imaging with PET is able to detect amyloid plaques, and that the likelihood of AD is low in patients who are ''amyloid negative'' [3].

Potential future use of amyloid PET in asymptomatic persons

Among cognitively normal older individuals elevated levels of brain amyloid have been reported in 25–35% of cases [28–30], a figure in line with findings from autopsy studies [31,32]. Among these individuals, Aβ deposition may represent preclinical AD [3]. While the validity of the recently proposed National Institute on Aging-Alzheimer's Association (NIA-AA) framework for preclinical AD [33] has yet to be determined, cross-sectional data from the Dominantly Inherited Alzheimer Network (DIAN) [34] – as well as longitudinal data from the Alzheimer's Disease Neuroimaging Initiative [35] and the Mayo Clinic [36] – provide support for this model. This notwithstanding, the clinical implications of amyloid positivity in this population remain uncertain, with no clinical indication for amyloid imaging in cognitively normal individuals at this time [1]. The availability of future disease modifying therapies – non-pharmacological or pharmacologic, particularly the latter if anti-amyloid drugs are used – as well as greater certainty *vis-à-vis* predictive validity, will, however, undoubtedly alter this position. In this respect, the Anti-Amyloid treatment of Asymptomatic Alzheimer's disease (A4) trial recently proposed by the Alzheimer's Disease Cooperative Study [37] – aiming to delay progression from normal cognition to MCI or dementia using monthly infusions of Aβ antibodies in amyloid positive individuals – will see the use of amyloid PET with regard to risk assessment and treatment response.

Potential ethical issues tied to use of amyloid PET

Disclosure of amyloid positivity

The Alzheimer's Disease Neuroimaging Initiative (ADNI) is an US cohort of individuals with normal cognition, MCI or mild dementia who are being followed over time in order to establish the link between various clinical and biological parameters, including brain amyloid load. Since its inception in 2004, ADNI has held a ''no return policy'' regarding the disclosure of research findings [38], a position motivated by the uncertain prognostic value of biomarker findings, including amyloid imaging. While at present standard practice, this stance of non-disclosure will become less tenable once the clinical value of amyloid imaging becomes more firmly established. Moreover, the A4 trial recently proposed by the Alzheimer's Disease Cooperative Study will, by its very design, result in asymptomatic participants being informed of their amyloid imaging results.

A shift away from this position of non-disclosure, however, is currently underway, with a majority of researchers from

Amyloid
Downloaded from informahealthcare.com by 61.163.77.42 on 06/11/14. For personal use only.

the ADNI endorsing disclosure of biomarker findings [38]. This, combined with increasing calls from the public for disclosure of research findings [39] and incorporation of International Working Group (IWG) and NIA-AA research diagnostic criteria for asymptomatic at risk and MCI/prodromal AD [40,41] into clinical practice by some physicians [42], highlight the importance of delineating the circumstances under which amyloid imaging results should be disclosed. While generally in agreement with AIT AUC, Canadian and Australian perspectives do not address the act of disclosure per se. While empirical data have yet to be evaluated, predisclosure counseling addressing the potential social and emotional implications tied to amyloid imaging results (i.e. positive or negative) have been proposed by the AIT in order to minimize the potential for psychological harm [1].

As data addressing the clinical utility of amyloid imaging continues to accumulate – increasingly, within a pro-disclosure framework – the need to accelerate the development of appropriate disclosure guidelines has emerged as a key area within the field. In this respect, research participants' own formulation of benefit, harm and acceptable risk [39,43] must be given increased recognition along with greater reliance on empiric evidence pointing to a low prevalence of negative consequence following disclosure of test results [44], with individuals tending to find disclosure beneficial irrespective of the actual result or secondary psychological distress [45–47]. Given that the implications of amyloid status apropos employability, insurability, and related stigmatization and discrimination [48] are not fully understood at present, a broad range of stakeholders – including regulators, investigators and research participants [49] – should be canvassed in order to ensure the appropriateness of emerging policies and protocols.

Clinical utility and cost effectiveness of amyloid PET

While a substantial body of research has been generated via amyloid imaging in a relatively short time span, systematic evidence addressing the clinical utility of amyloid PET – encompassing a change in diagnostic evaluation, patient management and/or a related improvement in clinical outcomes – has yet to be reported [1]. Preliminary results, however, indicate that amyloid imaging findings carry prognostic information. In the largest longitudinal study of patients with MCI conducted to date, the rate of progression to AD was 82% among those who were ''PIB-positive'', relative to only 7% among ''PIB-negative'' subjects [50]. Amyloid imaging likewise seems to carry treatment implications, chiefly in terms of affecting the initiation or discontinuation of acetylcholinesterase inhibitor therapy [51]. Though likely adding little to the diagnostic workup of patients with a classic amnestic AD phenotype, amyloid imaging is likely to prove of use in patients with atypical presentations or early age at onset [1–3]. In this respect, a study aiming to differentiate between AD and frontotemporal lobar degeneration (FTLD) showed greater accuracy and precision associated with [^{11}C]PIB, relative to [^{18}F]FDG [52]. Owing to its high sensitivity, amyloid PET will likely prove of greater use in terms of ruling out, rather than ruling in, AD as the underlying etiology, since amyloid positivity cannot per se exclude the presence of comorbid non-Aβ pathology [51,53].

Despite the recognition that amyloid PET could lead to significant savings tied to earlier accurate diagnosis and initiation of treatment [2], others point to substantially elevated costs associated with the incorporation of amyloid imaging into current assessment protocols [54]. Among the benefits of amyloid PET, the ''value of knowing'' allows for more effective medication management, engagement with support services, broaching of issues pertaining to driving and safety, and enrolment in clinical trials, among others [55]. Numerous unknowns exist, however, regarding the benefits of amyloid PET at the level of diagnostic utility [56]; among these, the incorporation of demographic factors, including age and genetic variables, into threshold adjustment for amyloid positivity, determining the optimal threshold for determining scan positivity using a quantitative approach, and the presence of false positives and false negatives [51]. In the case of computer aided image interpretation – an approach that will likely prove crucial to the widespread implementation of amyloid PET imaging outside of specialized centers – software is currently under development, with several computer-based training approaches having proven highly effective in training inexperienced readers [57,58]. Finally, systematic assessment of amyloid PET cost-effectiveness has yet to be carried out and should be implemented in the context of multicentric cohort studies [59] and in more representative clinical populations [51].

Future directions

The current evidence base suggests that amyloid imaging carries clinical utility when used in the context of MCI and atypical dementia syndromes. In addition, PET compounds for amyloid may prove of use in the context of subject selection and monitoring in clinical trials. Its widespread clinical use, however, will likely depend on the availability of treatments capable of arresting disease progression [60]. Regarding clinical utility and cost-effectiveness, comparisons are required between amyloid PET and serum, plasma or cerebrospinal fluid biomarkers for amyloid as, in addition to potentially being equally valid and possibly of greater clinical use, such techniques carry lower cost, invasiveness and radiation exposure [61]. As the field moves toward revising current policies surrounding disclosure of amyloid findings, careful attention must be paid to the A4 sub study addressing the impact of amyloid status disclosure on participant well being.

Declaration of interest

K.H. is an employee at GE Healthcare (Uppsala, Sweden) in addition to her association with Uppsala University. A.L., E.R.Z., S.G. and P.R.N. declare no competing interests. This work was supported by the Canadian institutes of Health Research (CIHR) [MOP-11-51-31], the Alzheimer's Association [NIRG-08-92090], the Nussia & André Aisenstadt Foundation and Fonds de la recherche en santé du Québec (Chercheur-boursier).

Amyloid
Downloaded from informahealthcare.com by 61.163.77.42 on 06/11/14. For personal use only.

References

1. Johnson KA, Minoshima S, Bohnen NI, Donohoe KJ, Foster NL, Herscovitch P, Karlawish JH, et al. Appropriate use criteria for amyloid PET: a report of the Amyloid Imaging Task Force, the Society of Nuclear Medicine and Molecular Imaging, and the Alzheimer's Association. Alzheimers Dement 2013;9:1–15.
2. Soucy JP, Bartha R, Bocti C, Borrie M, Burhan AM, Laforce Jr R, Rosa-Neto, P. Clinical applications of neuroimaging in patients with Alzheimer's disease: a review from the Fourth Canadian Consensus Conference on the Diagnosis and Treatment of Dementia 2012. Alzheimers Res Ther 2013;5:1–11.
3. Rowe CC, Villemagne VL. Amyloid imaging with PET in early Alzheimer disease diagnosis. Med Clin North Am 2013;97: 377–98.
4. Cohen AD, Rabinovici GD, Mathis CA, Jagust WJ, Klunk WE, Ikonomovic MD. Using Pittsburgh Compound B for in vivo PET imaging of fibrillar amyloid-beta. Adv Pharmacol 2012;64: 27–81.
5. Wolk DA, Grachev ID, Buckley C, Kazi H, Grady MS, Trojanowski JQ, Hamilton RH, et al. Association between in vivo fluorine 18-labeled flutemetamol amyloid positron emission tomography imaging and in vivo cerebral cortical histopathology. Arch Neurol 2011;68:1398–403.
6. Clark CM, Pontecorvo MJ, Beach TG, Bedell BJ, Coleman RE, Doraiswamy PM, Fleisher AS, et al. Cerebral PET with florbetapir compared with neuropathology at autopsy for detection of neuritic amyloid-beta plaques: a prospective cohort study. Lancet Neurol 2012;11:669–78.
7. Rowe CC, Ackerman U, Browne W, Mulligan R, Pike KL, O'Keefe G, Tochoy-Danguy H, et al. Imaging of amyloid beta in Alzheimer's disease with 18F-BAY94-9172, a novel PET tracer: proof of mechanism. Lancet Neurol 2008;7:129–35.
8. Vallabhajosula S. Positron emission tomography radiopharmaceuticals for imaging brain Beta-amyloid. Semin Nucl Med 2011;41: 283–99.
9. Rowe CC, Villemagne VL. Brain amyloid imaging. J Nucl Med Technol 2013;41:11–8.
10. U.S. Food and Drug Administration. FDA approves imaging drug Amyvid: estimates brain amyloid plaque content in patients with cognitive decline. 2012 Apr 10. Available from: http://www.fda.gov/newsevents/newsroom/pressannouncements/ucm299678.htm [last accessed 1 Dec 2013].
11. European Medicines Agency. Amyvid: florbetapir (^{18}F). 2013 Jan 23. Available from: http://www.ema.europa.eu/ema/index.jsp?curl=pages/medicines/human/medicines/002422/human_med_001611.jsp&mid=WC0b01ac058001d124 [last accessed 16 Apr 2014].
12. Piramal Group. FDA Approves Piramal Imaging's Neuraceq™ (florbetaben F18 injection) for PET Imaging of Beta-Amyloid Neuritic Plaques in the Brain. 2014 Mar 20. Available from: http://www.prnewswire.com/news-releases/fda-approves-piramal-imagings-neuraceq-florbetaben-f18-injection-for-pet-imaging-of-beta-amyloid-neuritic-plaques-in-the-brain-251216031.html [last accessed 16 Apr 2014].
13. European Medicines Agency. Neuraceq: florbetaben (^{18}F) Amyvid: florbetapir (^{18}F). 2014 Mar 11. Available from: http://www.ema.europa.eu/ema/index.jsp?curl=pages/medicines/human/medicines/002553/human_med_001716.jsp&mid=WC0b01ac058001d124 [last accessed 16 Apr 2014].
14. U.S. Food and Drug Administration. FDA Approves a Second Amyloid Imaging Agent. 2013 Nov 21. Available from: http://www.fda.gov/newsevents/newsroom/pressannouncements/ucm299678.htm [last accessed 16 Apr 2014].
15. Cselenyi Z, Jönhagen ME, Forsberg A, Halldin C, Julin P, Schou M, Johnström P, et al. Clinical validation of 18F-AZD4694, an amyloid-beta-specific PET radioligand. J Nucl Med 2012;53: 415–24.
16. Jureus A, Swahn BM, Sandell J, Jeppsson F, Johnson AE, Johnström P, Neelissen JA, et al. Characterization of AZD4694, a novel fluorinated Abeta plaque neuroimaging PET radioligand. J Neurochem 2010;114:784–94.
17. Zimmer E, Parent M, Leuzy A, Rowley J, Cheewakriengkrai L, Shin M, Wang S, et al. [18F]NAV4694 shows higher binding and wider dynamic range compared with [11C]PiB in Alzheimer's disease postmortem tissue. Alzheimers Dement 2013;9:P584.
18. Rowe CC, Pejoska S, Mulligan RS, Jones G, Chan JG, Svensson S, Cselényi Z, et al. Head-to-head comparison of 11C-PiB and 18F-AZD4694 (NAV4694) for beta-amyloid imaging in aging and dementia. J Nucl Med 2013;54:880–6.
19. Vandenberghe R, Van Laere K, Ivanoiu A, Salmon E, Bastin C, Triau E, Hasselbalch S, et al. 18F-flutemetamol amyloid imaging in Alzheimer disease and mild cognitive impairment: a phase 2 trial. Ann Neurol 2010;68:319–29.
20. Wolk DA, Zhang Z, Boudhar S, Clark CM, Pontecorvo MJ, Arnold SE. Amyloid imaging in Alzheimer's disease: comparison of florbetapir and Pittsburgh compound-S positron emission tomography. J Neurol Neurosurg Psychiatry 2012;83:923–6.
21. Villemagne VL, Mulligan RS, Pejoska S, Ong K, Jones G, O'Keefe G, Chan JG, et al. Comparison of 11C-PiB and 18F-Horbetaben for A beta imaging in ageing and Alzheimer's disease. Eur J Nucl Med Mol Imaging 2012;39:983–9.
22. Landau SM, Breault C, Joshi AD, Pontecorvo M, Mathis CA, Jagust WJ, Mintun MA, et al. Amyloid-beta imaging with Pittsburgh compound B and florbetapir: comparing radiotracers and quantification methods. J Nucl Med 2013;54:70–7.
23. Petersen RC, Smith GE, Waring SC, Ivnik RJ, Tangalos EG, Kokmen E. Mild cognitive impairment: clinical characterization and outcome. Arch Neurol 1999;56:303–8.
24. Petersen RC. Mild cognitive impairment: transition between aging and Alzheimer's disease. Neurologia 2000;15:93–101.
25. McKhann GM, Knopman DS, Chertkow H, Hyman BT, Jack Jr CR, Kawas CH, Klunk WE, et al. The diagnosis of dementia due to Alzheimer's disease: recommendations from the National Institute on Aging-Alzheimer's Association workgroups on diagnostic guidelines for Alzheimer's disease. Alzheimers Dement 2011;7: 263–9.
26. Rowe CC, Ng S, Ackermann U, Gong SJ, Pike K, Savage G, Cowie TF, et al. Imaging beta-amyloid burden in aging and dementia. Neurology 2007;68:1718–25.
27. Halliday G, Hely M, Reid W, Morris J. The progression of pathology in longitudinally followed patients with Parkinson's disease. Acta Neuropathol 2008;115:409–15.
28. Mintun MA, Larossa GN, Sheline YI, Dence CS, Lee SY, Mach RH, Klunk WE, et al. [11C]PIB in a nondemented population: potential antecedent marker of Alzheimer disease. Neurology 2006; 67:446–52.
29. Aizenstein HJ, Nebes RD, Saxton JA, Price JC, Mathis CA, Tsopelas ND, Kiolko SK, et al. Frequent amyloid deposition without significant cognitive impairment among the elderly. Arch Neurol 2008;65:1509–17.
30. Rowe CC, Ellis KA, Rimajova M, Bourgeat P, Pike KE, Jones G, Fripp J, et al. Amyloid imaging results from the Australian Imaging, Biomarkers and Lifestyle (AIBL) study of aging. Neurobiol Aging 2010;31:1275–83.
31. Bennett DA, Schneider JA, Arvanitakis Z, Kelly JF, Aggarwal NT, Shah RC, Wilson RS. Neuropathology of older persons without cognitive impairment from two community-based studies. Neurology 2006;66:1837–44.
32. Pike KE, Savage G, Villemagne VL, Ng S, Moss SA, Maruff P, Mathis CA, et al. Beta-amyloid imaging and memory in non-demented individuals: evidence for preclinical Alzheimer's disease. Brain 2007;130:2837–44.
33. Sperling RA, Aisen PS, Beckett LA, Bennett DA, Craft S, Fagan AM, Iwatsubo T, et al. Toward defining the preclinical stages of Alzheimer's disease: recommendations from the National Institute on Aging-Alzheimer's Association workgroups on diagnostic guidelines for Alzheimer's disease. Alzheimers Dement 2011;7: 280–92.
34. Bateman RJ, Xiong C, Benzinger TL, Fagan AM, Goate A, Fox NC, Marcus DS, et al. Clinical and biomarker changes in dominantly inherited Alzheimer's disease. N Engl J Med 2012; 367:795–804.
35. Desikan RS, McEvoy LK, Thompson WK, Holland D, Brewer JB, Aisen PS, Sperling RA, et al. Amyloid-beta-associated clinical decline occurs only in the presence of elevated P-tau. Arch Neurol 2012;69:709–13.
36. Knopman DS, Jack Jr CR, Wiste HJ, Weigand SD, Vemuri P, Lowe V, Kantarci K, et al. Short-term clinical outcomes for stages of

NIA-AA preclinical Alzheimer disease. Neurology 2012;78: 1576–82.
37. Alzheimer's Disease Cooperative Study. Anti-Amyloid treatment of Asymptomatic AD – The A4 Trial. Available from: http://www.adcs.org/Studies/A4.aspx [last accessed 4 Dec 2013].
38. Shulman MB, Harkins K, Green RC, Karlawish J. Using AD biomarker research results for clinical care: a survey of ADNI investigators. Neurology 2013;81:1114–21.
39. Bredenoord A, Kroes H, Cuppen E, Parker M, van Delden JJ. Disclosure of individual genetic data to research participants: the debate reconsidered. Trends Genet 2014;27:41–7.
40. Albert MS, DeKosky ST, Dickson D, Dubois B, Feldman HH, Fox NC, Gamst A, et al. The diagnosis of mild cognitive impairment due to Alzheimer's disease: recommendations from the National Institute on Aging-Alzheimer's Association workgroups on diagnostic guidelines for Alzheimer's disease. Alzheimers Dement 2011;7:270–9.
41. Dubois B, Feldman HH, Jacova C, Dekosky ST, Barberger-Gateau P, Cummings J, Delacourte A, et al. Research criteria for the diagnosis of Alzheimer's disease: revising the NINCDS-ADRDA criteria. Lancet Neurol 2007;6:734–46.
42. Gauthier S, Rosa-Neto P. Dementia: disclosure of results to participants in dementia research. Nat Rev Neurol 2013;9: 608–9.
43. Shalowitz DI, Miller FG. Communicating the results of clinical research to participants: attitudes, practices, and future directions. PLoS Med 2008;5:e91.
44. Broadstock M, Michie S, Marteau T. Psychological consequences of predictive genetic testing: a systematic review. Eur J Hum Genet 2000;8:731–8.
45. Partridge AH, Wong JS, Knudsen K, Gelman R, Sampson E, Gadd M, Bishop KL, et al. Offering participants results of a clinical trial: sharing results of a negative study. Lancet 2005;365: 963–4.
46. Smith CO, Lipe HP, Bird TD. Impact of presymptomatic genetic testing for hereditary ataxia and neuromuscular disorders. Arch Neurol 2004;61:875–80.
47. Steinbart EJ, Smith CO, Poorkaj P, Bird TD. Impact of DNA testing for early-onset familial Alzheimer disease and frontotemporal dementia. Arch Neurol 2001;58:1828–31.
48. Karlawish J. Addressing the ethical, policy, and social challenges of preclinical Alzheimer disease. Neurology 2011;77:1487–93.
49. Lingler JH, Klunk WE. Disclosure of amyloid imaging results to research participants: has the time come? Alzheimers Dement 2013;9:741–4 e2.
50. Okello A, Koivunen J, Edison P, Archer HA, Turkheimer FE, Någren K, Bullock R, et al. Conversion of amyloid positive and negative MCI to AD over 3 years: an 11C-PIB PET study. Neurology 2009;73:754–60.
51. Laforce Jr R, Rabinovici GD. Amyloid imaging in the differential diagnosis of dementia: review and potential clinical applications. Alzheimers Res Ther 2011;3:31.
52. Rabinovici GD, Rosen HJ, Alkalay A, Kornak J, Furst AJ, Agarwal N, Mormino EC, et al. Amyloid vs FDG-PET in the differential diagnosis of AD and FTLD. Neurology 2011;77: 2034–42.
53. Vandenberghe R, Adamczuk K, Dupont P, Laere KV, Chételat G. Amyloid PET in clinical practice: its place in the multidimensional space of Alzheimer's disease. Neuroimage Clin 2013;2:497–511.
54. Klein EP, Kaye J. Dementia specialists and early adoption of amyloid imaging. J Alzheimers Dis 2013;33:445–50.
55. Blendon RJ, Benson JM, Wikler EM, Weldon KJ, Georges J, Baumgart M, Kallmyer BA. The Impact of Experience with a Family Member with Alzheimer's Disease on Views about the Disease across Five Countries. Int J Alzheimers Dis 2012;2012:1–9.
56. Jagust WJ. Amyloid imaging: liberal or conservative? Let the data decide. Arch Neurol 2011;68:1377–8.
57. GE Healthcare. New [18F]Flutemetamol Data Presented by GE Healthcare at 7th Annual Human Amyloid Imaging Conference. 2013 Jan 28. Available from: http://www.businesswire.com/news/home/20130118005505/en/18F-Flutemetamol-Data-Presented-GE-Healthcare-7th#.U07NQ61dWxR [last accessed 16 Apr 2014].
58. Seibyl J, Barthel H, Stephens A, Reininger C, Sabri O. Reliability, reproducibility and efficacy of the 18F florbetaben β-amyloid PET scan visual assessment method as trained via a computer-based instructional tool. J Nucl Med [Internet]. 2013;54:300. Available from: http://jnumedmtg.snmjournals.org/cgi/content/meeting_abstract/54/2_MeetingAbstracts/300 [last accessed 16 Apr 2014].
59. Ishii K. PET Approaches for Diagnosis of Dementia. AJNR Am J Neuroradiol 2013. In press 2014.
60. Jagust WJ. Amyloid imaging: coming to a PET scanner near you. Ann Neurol 2010;68:277–8.
61. Lerner AJ. Amyloid imaging: the court of public opinion. Neurology 2013;81:1108–9.

Amyloid
Downloaded from informahealthcare.com by 61.163.77.42 on 06/11/14. For personal use only.

Capítulo VII. *Amyloid imaging in Alzheimer's disease: a potential new era of personalized medicine?*

No **capítulo VII** apresentamos o artigo publicado no periódico *Translacional Neuroscience.*

Nos capítulos anteriores (capítulo V e VI) discutimos o uso dos radiofármacos de β-amilóide e implicações éticas para o uso destes exames de imagem na clínica. Neste capítulo avaliamos o potencial uso dos exames de PET β-amilóide de maneira personalizada e chegamos a conclusão que diretrizes éticas e socioeconômicas ainda impedem o uso de exames de PET β-amilóide no contexto de medicina personalizada.

Communication • DOI: 10.2478/s13380-014-0205-y • Translational Neuroscience • 5(1) • 2014

Translational Neuroscience

VERSITA

Springer

AMYLOID IMAGING IN ALZHEIMER'S DISEASE: A POTENTIAL NEW ERA OF PERSONALIZED MEDICINE?

Antoine Leuzy[1,2,#],
Eduardo Rigon Zimmer[1,2,3,#],
Serge Gauthier[1],
Pedro Rosa-Neto[1,2*]

[1]*Translational Neuroimaging Laboratory (TNL), McGill Centre for Studies in Aging (MCSA), Douglas Mental Health University Institute, Montreal, H4H 1R3, Quebec, Canada*

[2]*Alzheimer's Disease Research Unit, MCSA, Douglas Mental Health University Institute, Montreal, H4H 1R3, Quebec, Canada*

[3]*Department of Biochemistry, Federal University of Rio Grande do Sul (UFRGS), Brazil*

[#]*both authors contributed equally to this work*

Received 25 February 2014
accepted 28 February 2014

Abstract

Recent advances along clinical and neuropathological lines, as well as in our ability to detect the deposition of β-amyloid (Aβ) *in vivo* using positron emission tomography (PET), have helped redefine Alzheimer's disease (AD) as a dynamic clinicobiological entity. On the basis of these advances, AD is now conceptualized as a continuum comprising asymptomatic, minimally symptomatic, and dementia phases, with detection of brain Aβ - in particular, via PET amyloid imaging - central to the diagnostic process. In this respect, [^{18}F]florbetapir (Amyvid™) and [^{18}F]flutemetamol (Vizamyl™) have recently received approval for clinical use from the Food and Drug Administration (FDA) and the European Medicines Agency (EMA), with additional radiofluorinated tracers for detection of Aβ in phase III trials. Recent initiatives such as the Alzheimer's Disease Neuroimaging Initiative (ADNI) suggest that Aβ production, oligomerization and aggregation begins many years, possibly decades, before detectable cognitive impairment, with Aβ shown to associate with cognitive decline and conversion to dementia. While personalized medicine has now emerged as a prospect for the field, the recent decision by the Centers for Medicare & Medicaid Services (CMS) - who declined to cover the cost of amyloid PET imaging citing insufficient evidence to support its clinical utility - highlights that such a move may be premature.

Keywords

• Alzheimer's disease • [^{11}C]PIB, [^{18}F]florbetapen • [^{18}F]florbetapir • [^{18}F]flutemetamol • [^{18}F]NAV4694 • Amyloid cascade hypothesis • Personalized medicine

© Versita Sp. z o.o.

Introduction

Historically, Alzheimer's disease (AD) has been conceptualized as a dual clinicopathological entity, comprising a progressive dementia syndrome - an amnestic core, followed by involvement of additional cognitive domains - and specific histologic features, including β-amyloid (Aβ) deposition. This framework assumed a static relationship between neuropathology and clinical phenotype, with the attendant implications of synonymity between AD pathology and the clinical symptoms of AD, and a binary framework in which one either did or did not have dementia due to AD. Embodied in the 1984 National Institute of Neurological and Communicative Disorders and Stroke and Alzheimer's Disease and Related Disorders Association (NINCDS-ADRDA) criteria [1], this conceptualization endured without modification for over a quarter of a century. In the intervening period, however, important advances have occurred in terms of the characterization of AD along clinical and neuropathological lines, as well as in our ability to detect Aβ deposition *in vivo*, in particular, via positron emission tomography (PET) (see Figure 1). On the basis of these advances, AD is now conceptualized as dynamic clinicobiological entity [2], comprising a continuum encompassing an asymptomatic 'preclinical' phase, a symptomatic, 'mild cognitive impairment' (MCI) pre-dementia phase, and a dementia phase, with levels of brain Aβ, as detected using PET amyloid imaging and cerebrospinal fluid (CSF) assays, integral to the diagnostic process [2-6]. As the field moves toward stage specific therapies, and, increasingly, toward the incorporation of amyloid imaging into clinical practice, personalized medicine in AD has emerged as a prospect for the not too distant future.

Revised conceptualization of AD: the IWG and NIA-AA diagnostic criteria

Though useful and widely adopted, the NINCDS-ADRDA criteria possessed several shortcomings, including insufficient diagnostic specificity [7,8] and the fact that they only allowed for the diagnosis of AD to be made late in the disease course, once the threshold for dementia had already been reached. As a result of such shortcomings, and in an attempt to incorporate the scientific gains made since the release of the NINCDS-ADRDA criteria, various revisions have been proposed. Those of the International Working Group (IWG) acknowledged the concept of cognitive impairment that did not reach the threshold for dementia, and suggested the incorporation of biological markers (biomarkers), parameters that can be measured *in vivo* and that are considered surrogate markers of normal biologic processes, pathological processes, or responses to a therapeutic intervention [2,3,9]. Similarly, National Institute of Aging - Alzheimer's Association (NIA-AA) working groups proposed revised criteria for asymptomatic and symptomatic pre-dementia stages, and incorporated advancements in PET amyloid imaging [4-6].

* *E-mail: pedro.rosa@mcgill.ca*

Though differing in approach and terminology, both sets of criteria subscribed to the amyloid cascade hypothesis [10], with the corresponding concept of differential risk of AD based on the combination of clinical markers and biomarkers of Aβ deposition. While it has been proposed that CSF Aβ abnormalities may precede fibrillary Aβ aggregation [11-13] findings have been conflicting [14,15] with recent work failing to support this association [16]. Although significant advances have been made in CSF amyloid biomarkers, several methodological constraints limit their application in clinical practice, including high inter-laboratory variation, which hinders comparison of data obtained in different settings [17]. By contrast, amyloid PET imaging is associated with superior test-retest reliability and between-center comparability of cut-offs and interpretation [18,19].

Imaging Aβ deposition in AD using PET

Carbon-11 [^{11}C] labeled 2-(4'-methylaminophenyl)-6-hydroxybenzothiazole ([^{11}C] Pittsburgh Compound B or [^{11}C]PIB) is the canonical PET tracer for amyloid imaging, exhibiting high sensitivity and specificity for fibrillary Aβ [20,21]. A derivative of thioflavin T, [^{11}C] PIB likewise exhibits affinity for other Aβ-containing lesions, including diffuse plaques, cerebrovascular amyloid [22] and Aβ-oligomers [23]. Showing robust retention in AD brain, [^{11}C] PIB is the most widely studied amyloid tracer to date [24,25]. High [^{11}C]PIB retention has also been observed in patients with MCI who later convert to AD [26,27] and also in cognitively normal older individuals [28-30]. In addition to accelerating current understanding of cerebral amyloidosis and advancing detection of AD pathology to an earlier stage [20,25,31,32], [^{11}C] PIB has contributed to improvements in the differential diagnosis of neurodegenerative diseases [32-34].

The short 20-minute half-life of ^{11}C however, limits use of [^{11}C]PIB to imaging centers possessing an onsite cyclotron and a radiochemistry department with expertise in the synthesis of ^{11}C, making the cost of studies prohibitive for routine clinical use. To overcome these limitations, several radiofluorinated Aβ tracers (half-life of 110 minutes) have been developed, including [^{18}F]florbetapen [35], [^{18}F] florbetapir [36], [^{18}F]flutemetamol [37] and [^{18}F] NAV4694 [38]. Similarly to [^{11}C]PIB, these tracers exhibit good *in vitro* / *in vivo* correlations and binding to fibrillary Aβ [37,39,40]. In contrast with [^{11}C]PIB, however, [^{18}F]flutemetamol, [^{18}F]florbetapir, and [^{18}F]florbetaben show significant nonspecific white matter retention; [^{18}F]NAV4694, however, seems to have less nonspecific binding and, in a manner similar to [^{11}C]PIB, shows rapid kinetics, and a wide dynamic range [38,41]. At present, [^{18}F] florbetapir (Amyvid™) and [^{18}F]flutemetamol (Vizamyl™) are approved for clinical use by the Food and Drug Administration (FDA) and the European Medicines Agency (EMA), with [^{18}F]florbetaben and [^{18}F]NAV4694 currently in phase III trials (see Table 1). Appropriate use criteria (AUC) recently issued by the Alzheimer's Association (AA) and the Society of Nuclear Medicine and Molecular Imaging (SNMMI) commissioned Amyloid Imaging Taskforce (AIT) deem use of amyloid PET appropriate

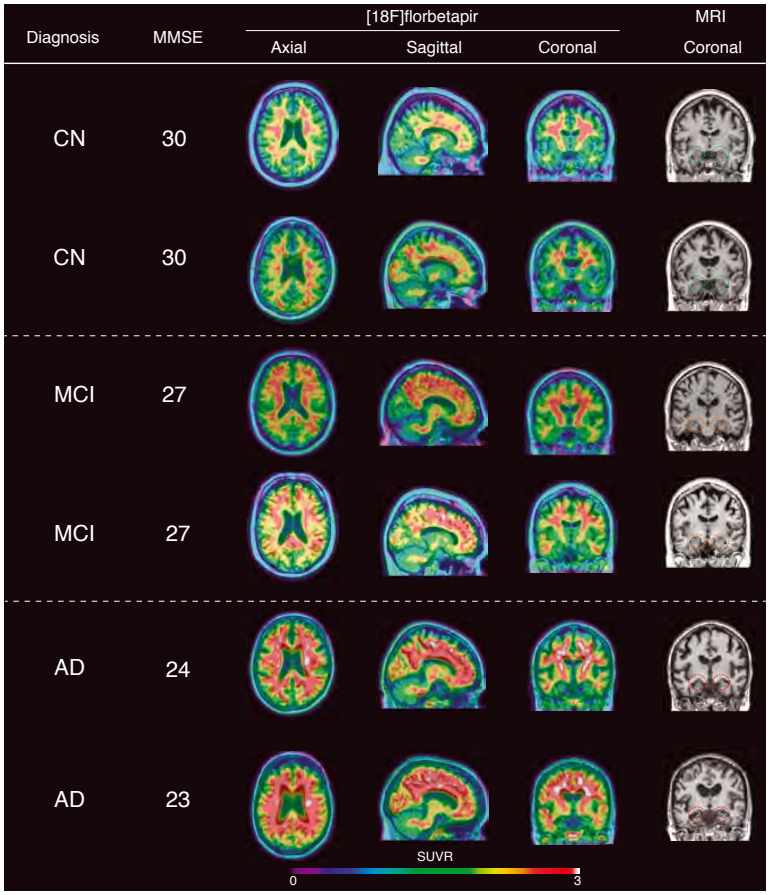

Figure 1. Representative [^{18}F]florbetapir PET images in cognitively normal, MCI and AD patients. In patients with MCI and AD, Aβ accumulation - as indexed by [^{18}F]florbetapir cortical to cerebellar (vermis excluded) standardized uptake value ratio (SUVR) - is seen in cortical regions expected to be high in amyloid deposition, such as the frontal cortex, temporal cortex and precuneus. In contrast, cognitively normal (CN) subjects exhibit tracer retention predominantly in white matter areas. T1-weighted MRI coronal images show hippocampal atrophy in both MCI (orange dashed circles) and AD (red dashed circles), as compared to controls (green dashed circles).

Table 1. FDA approved and phase III clinical trial amyloid PET imaging agents.

Radiopharmaceutical	Drug name	Clinical trials	Status	Clinical trial identifier	FDA application number	References
[^{18}F]Florbetapir	Amyvid™	FDA approved	Completed	-	(NDA) 202008	http://www.accessdata.fda.gov/drugsatfda_docs/nda/2012/202008_Florbetapir_Orig1s-000TOC.cfm
[^{18}F]Flutemetamol	Vizamyl™	FDA approved	Completed	-	(NDA) 203137	http://www.accessdata.fda.gov/drugsatfda_docs/nda/2013/203137_vizamyl_toc.cfm
[^{18}F]Florbetaben	-	Phase III	Active	NCT01020838	-	http://clinicaltrials.gov/show/NCT01886820
[^{18}F]NAV4694	-	Phase III	Recruiting	NCT01886820	-	http://clinicaltrials.gov/show/NCT01886820

in the clinical evaluation of patients with MCI associated with etiologic uncertainty and when knowledge of amyloid status is expected to augment diagnostic certainty and alter patient management [42,43].

Amyloid PET imaging and AD: the prospect of personalized medicine

While the phrase 'personalized medicine' is commonly used in relation to genomic medicine - defined as the "the use of information from genomes (from humans and other organisms) and their derivatives (RNA, proteins and metabolites) to guide medical decision-making" [44] - personalized medicine may be defined along broader lines, as a model of healthcare that is predictive, personalized, preventive and participatory ('P4 medicine') [45], one that applies technologies to achieve customized care delivery [46]. Though personalized medicine has, to date, flourished "below the neck," for instance, in the care of patients with cancer and cardiovascular disease, recent multicenter biomarker initiatives, including the Alzheimer's Disease Neuroimaging Initiative (ADNI) [47] and the Australian Imaging, Biomarkers and Lifestyle Flagship Study of Aging (AIBL) [48] have begun to reshape how we talk about the diagnosis and treatment of AD [http://www.rwjf.org/en/blogs/human-capital-blog/2013/09/is_the_brain_readyf.html].

Aiming to further our understanding of the biology and pathobiology of normal aging, MCI, and AD through integration of clinical and biomarker data, studies such as ADNI and AIBL suggest that the accumulation of Aβ begins years, if not decades, before detectable cognitive impairment (see Figure 2), providing preliminary support for the amyloid cascade hypothesis [10]. While cross-sectional results surrounding the relation between brain levels of Aβ and concurrent cognitive performance in cognitively normal older individuals have proven inconsistent [49-52], longitudinal studies using intraindividual comparison - as opposed to normative data - point to a slightly downward cognitive trajectory among those with elevated brain Aβ [53-55]. Moreover, in the context of conversion studies, amyloid positivity is associated with a greater rate of clinical conversion from MCI to AD, with faster converters having a higher amyloid load at baseline [27,56,57]. Further, amyloid imaging has been shown to possess high sensitivity and specificity, and, when combined with magnetic resonance imaging (MRI), led to improved accuracy *vis à vis* predicting conversion [58].

The evolving conceptual framework for AD, with its increasing emphasis on the integration of biomarker data at presymptomatic/minimally symptomatic phases, has led clinicians, ethicists, and policy-makers to ask how we should practice personalized medicine for those potentially at risk for AD. While findings from the Risk Evaluation and Education for Alzheimer's Disease (REVEAL) study - in which disclosure of apolipoprotein E ε4 (*APOE* ε4) homozygosity among middle-aged adults with a family history of AD was found to promote risk reducing behaviors in the absence of adverse psychological effects [59] - support the introduction of personalized medicine, the recent draft decision memo released by the Centers for Medicare & Medicaid Services (CMS) denies coverage of amyloid PET imaging in routine clinical practice, citing an insufficiency of data with which to evaluate its clinical utility [60]. Indeed, to date the majority of studies have

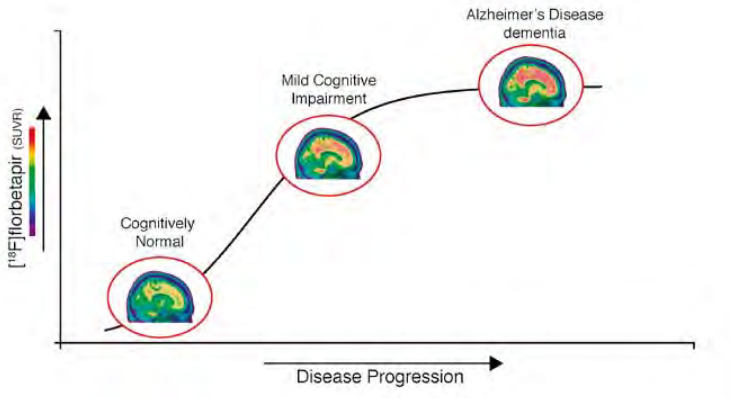

Figure 2. Hypothetical model of dynamic Aβ accumulation across the AD continuum. The potential of amyloid PET imaging rests on the assumption that Aβ accumulation is the initiating event in AD. Importantly, its accumulation is thought to occur in individuals who are still cognitively normal, preceding the emergence of symptoms by decades. Aβ accumulation is thought to accumulate through the MCI phase, reaching a plateau in AD dementia.

addressed diagnostic accuracy, with issues such as cost-effectiveness, and whether test results translate into improved clinical management or patient outcomes, unaddressed [61]. Further, the potential impact of amyloid PET imaging on the clinical management of patients with neurodegenerative diseases other than AD has not been assessed; likewise, the psychological impact of test results on patients and families - including the ability to make plans for the future - has not been addressed [61]. Finally, generalization from diagnostic performance studies is difficult given that study physicians were highly trained, with non-representative study populations due to enrichment with subjects characterized by high likelihood of AD [61].

Conclusion

At present, the literature offers only limited data with which to evaluate the clinical utility of amyloid PET. While there is data indicating that, when read by qualified interpreters, amyloid PET is highly accurate in terms of determining the presence of amyloid in the brain, the clinical utility of 'amyloid positivity' remains uncertain given that approximately 20 to 30% of cognitively normal older adults show evidence of amyloid in the brain following amyloid imaging [31,32,49,51]. Further, among individuals with MCI, a positive result does not accurately predict the risk or the time frame for progression to AD [62]. On the basis of available evidence, the clinical utility of amyloid PET may be greatest in negative cases, allowing AD to be effectively excluded from the list of possible diagnoses underlying a patient's cognitive impairment [63]. While potentially useful in terms of diagnosis and management, false positives could prove harmful given the well-established stigma tied to AD, and discrimination at the level of employability and insurability [64]. Moreover, recent findings suggest that knowledge of one's amyloid status may exert a deleterious effect on cognition [65,66]. Finally, much work remains if amyloid imaging is to become a widely used and clinically relevant biomarker for AD. While it is likely to play a pivotal role in advancing the field - in particular, to provide evidence of amyloid clearance in individuals receiving amyloid-lowering therapies - until the overall balance of merits and demerits of amyloid PET is determined in representative patient populations, the field does not seem ready to see personalized medicine migrate above the neck.

Acknowledgements

This work was supported by the Canadian institutes of Health Research (CIHR) [MOP-11-51-31], the Alzheimer's Association [NIRG-08-92090], the Nussia & André Aisenstadt Foundation, and Fonds de la recherche en santé du Québec (chercheur-boursier). AL and ERZ drafted the manuscript and designed the figures. SG and PRN guided and supervised the work. All authors read and approved the final manuscript. None of the authors have any conflict of interest to disclose.

References

[1] McKhann G., Drachman D., Folstein M., Katzman R., Price D.,Stadlan E.M., Clinical diagnosis of Alzheimer's disease: report of the NINCDS-ADRDA Work Group under the auspices of Department of Health and Human Services Task Force on Alzheimer's Disease, Neurology, 1984, 34, 939-944

[2] Dubois B., Feldman H.H., Jacova C., Cummings J.L., Dekosky S.T., Barberger-Gateau P., et al., Revising the definition of Alzheimer's disease: a new lexicon, Lancet Neurol., 2010, 9, 1118-1127

[3] Dubois B., Feldman H.H., Jacova C., Dekosky S.T., Barberger-Gateau P., Cummings J., et al., Research criteria for the diagnosis of Alzheimer's disease: revising the NINCDS-ADRDA criteria, Lancet Neurol., 2007, 6, 734-746

[4] Sperling R.A., Aisen P.S., Beckett L.A., Bennett D.A., Craft S., Fagan A.M., et al., Toward defining the preclinical stages of Alzheimer's disease: recommendations from the National Institute on Aging-Alzheimer's Association workgroups on diagnostic guidelines for Alzheimer's disease, Alzheimers Dement., 2011, 7, 280-292

[5] Albert M.S., DeKosky S.T., Dickson D., Dubois B., Feldman H.H., Fox N.C., et al., The diagnosis of mild cognitive impairment due to Alzheimer's disease: recommendations from the National Institute on Aging-Alzheimer's Association workgroups on diagnostic guidelines for Alzheimer's disease, Alzheimers Dement., 2011, 7, 270-279

[6] McKhann G.M., Knopman D.S., Chertkow H., Hyman B.T., Jack C.R., Jr., Kawas C.H., et al., The diagnosis of dementia due to Alzheimer's disease: recommendations from the National Institute on Aging-Alzheimer's Association workgroups on diagnostic guidelines for Alzheimer's disease, Alzheimers Dement., 2011, 7, 263-269

[7] Varma A.R., Snowden J.S., Lloyd J.J., Talbot P.R., Mann D.M.,Neary D., Evaluation of the NINCDS-ADRDA criteria in the differentiation of Alzheimer's disease and frontotemporal dementia, J. Neurol. Neurosurg. Psychiatry, 1999, 66, 184-188

[8] Kazee A.M., Eskin T.A., Lapham L.W., Gabriel K.R., McDaniel K.D.,Hamill R.W., Clinicopathologic correlates in Alzheimer disease: assessment of clinical and pathologic diagnostic criteria, Alzheimer Dis. Assoc. Disord., 1993, 7, 152-164

[9] Biomarkers Definitions Working G., Biomarkers and surrogate endpoints: preferred definitions and conceptual framework, Clin. Pharmacol. Ther., 2001, 69, 89-95

[10] Hardy J., Selkoe D.J., The amyloid hypothesis of Alzheimer's disease: progress and problems on the road to therapeutics, Science, 2002, 297, 353-356

[11] Fagan A.M., Mintun M.A., Shah A.R., Aldea P., Roe C.M., Mach R.H., et al., Cerebrospinal fluid tau and ptau(181) increase with cortical amyloid deposition in cognitively normal individuals: implications for future clinical trials of Alzheimer's disease, EMBO Mol. Med., 2009, 1, 371-380

[12] Morris J.C., Roe C.M., Xiong C., Fagan A.M., Goate A.M., Holtzman D.M., et al., APOE predicts amyloid-beta but not tau Alzheimer pathology

in cognitively normal aging, Ann. Neurol., 2010, 67, 122-131
[13] Fagan A.M., Mintun M.A., Mach R.H., Lee S.Y., Dence C.S., Shah A.R., et al., Inverse relation between in vivo amyloid imaging load and cerebrospinal fluid Abeta42 in humans, Ann. Neurol., 2006, 59, 512-519
[14] Koivunen J., Pirttila T., Kemppainen N., Aalto S., Herukka S.K., Jauhianen A.M., et al., PET amyloid ligand [11C]PIB uptake and cerebrospinal fluid beta-amyloid in mild cognitive impairment, Dement. Geriatr. Cogn. Disord., 2008, 26, 378-383
[15] Forsberg A., Almkvist O., Engler H., Wall A., Langstrom B.,Nordberg A., High PIB retention in Alzheimer's disease is an early event with complex relationship with CSF biomarkers and functional parameters, Curr. Alzheimer Res., 2010, 7, 56-66
[16] Landau S.M., Lu M., Joshi A.D., Pontecorvo M., Mintun M.A., Trojanowski J.Q., et al., Comparing positron emission tomography imaging and cerebrospinal fluid measurements of beta-amyloid, Ann. Neurol., 2013, 74, 826-836
[17] Mattsson N., Blennow K., Zetterberg H., Inter-laboratory variation in cerebrospinal fluid biomarkers for Alzheimer's disease: united we stand, divided we fall, Clin. Chem. Lab. Med., 2010, 48, 603-607
[18] Nordberg A., Carter S.F., Rinne J., Drzezga A., Brooks D.J., Vandenberghe R., et al., A European multicentre PET study of fibrillar amyloid in Alzheimer's disease, Eur. J. Nucl. Med. Mol. Imaging, 2013, 40, 104-114
[19] Vandenberghe R., Adamczuk K., Dupont P., Laere K.V., Chételat G., Amyloid PET in clinical practice: its place in the multidimensional space of Alzheimer's disease, Neuroimage. Clin., 2013, 2, 497-511
[20] Cohen A.D., Rabinovici G.D., Mathis C.A., Jagust W.J., Klunk W.E.,Ikonomovic M.D., Using Pittsburgh Compound B for in vivo PET imaging of fibrillar amyloid-beta, Adv. Pharmacol., 2012, 64, 27-81
[21] Price J.C., Klunk W.E., Lopresti B.J., Lu X., Hoge J.A., Ziolko S.K., et al., Kinetic modeling of amyloid binding in humans using PET imaging and Pittsburgh Compound-B, J. Cereb. Blood Flow Metab., 2005, 25, 1528-1547
[22] Lockhart A., Lamb J.R., Osredkar T., Sue L.I., Joyce J.N., Ye L., et al., PIB is a non-specific imaging marker of amyloid-beta (Abeta) peptide-related cerebral amyloidosis, Brain, 2007, 130, 2607-2615
[23] Maezawa I., Hong H.S., Liu R., Wu C.Y., Cheng R.H., Kung M.P., et al., Congo red and thioflavin-T analogs detect Abeta oligomers, J. Neurochem., 2008, 104, 457-468
[24] Kemppainen N.M., Aalto S., Wilson I.A., Nagren K., Helin S., Bruck A., et al., PET amyloid ligand [11C]PIB uptake is increased in mild cognitive impairment, Neurology, 2007, 68, 1603-1606
[25] Klunk W.E., Engler H., Nordberg A., Wang Y., Blomqvist G., Holt D.P., et al., Imaging brain amyloid in Alzheimer's disease with Pittsburgh Compound-B, Ann. Neurol., 2004, 55, 306-319
[26] Forsberg A., Engler H., Almkvist O., Blomquist G., Hagman G., Wall A., et al., PET imaging of amyloid deposition in patients with mild cognitive impairment, Neurobiol. Aging, 2008, 29, 1456-1465
[27] Okello A., Koivunen J., Edison P., Archer H.A., Turkheimer F.E., Nagren K., et al., Conversion of amyloid positive and negative MCI to AD over 3 years: an 11C-PIB PET study, Neurology, 2009, 73, 754-760
[28] Jagust W.J., Bandy D., Chen K., Foster N.L., Landau S.M., Mathis C.A., et al., The Alzheimer's Disease Neuroimaging Initiative positron emission tomography core, Alzheimers Dement., , 2010, 6, 221-229
[29] Resnick S.M.,Sojkova J., Amyloid imaging and memory change for prediction of cognitive impairment, Alzheimers Res.Ther., 2011, 3, 3
[30] Rowe C.C., Ellis K.A., Rimajova M., Bourgeat P., Pike K.E., Jones G., et al., Amyloid imaging results from the Australian Imaging, Biomarkers and Lifestyle (AIBL) study of aging, Neurobiol. Aging, 2010, 31, 1275-1283
[31] Mintun M.A., Larossa G.N., Sheline Y.I., Dence C.S., Lee S.Y., Mach R.H., et al., [11C]PIB in a nondemented population: potential antecedent marker of Alzheimer disease, Neurology, 2006, 67, 446-452
[32] Rowe C.C., Ng S., Ackermann U., Gong S.J., Pike K., Savage G., et al., Imaging beta-amyloid burden in aging and dementia, Neurology, 2007, 68, 1718-1725
[33] Ng S.Y., Villemagne V.L., Masters C.L.,Rowe C.C., Evaluating atypical dementia syndromes using positron emission tomography with carbon 11 labeled Pittsburgh Compound B, Arch. Neurol., 2007, 64, 1140-1144
[34] Rabinovici G.D., Furst A.J., O'Neil J.P., Racine C.A., Mormino E.C., Baker S.L., et al., 11C-PIB PET imaging in Alzheimer disease and frontotemporal lobar degeneration, Neurology, 2007, 68, 1205-1212
[35] Rowe C.C., Ackerman U., Browne W., Mulligan R., Pike K.L., O'Keefe G., et al., Imaging of amyloid beta in Alzheimer's disease with 18F-BAY94-9172, a novel PET tracer: proof of mechanism, Lancet Neurol., 2008, 7, 129-135
[36] Clark C.M., Pontecorvo M.J., Beach T.G., Bedell B.J., Coleman R.E., Doraiswamy P.M., et al., Cerebral PET with florbetapir compared with neuropathology at autopsy for detection of neuritic amyloid-beta plaques: a prospective cohort study, Lancet Neurol., 2012, 11, 669-678
[37] Wolk D.A., Grachev I.D., Buckley C., Kazi H., Grady M.S., Trojanowski J.Q., et al., Association between in vivo fluorine 18-labeled flutemetamol amyloid positron emission tomography imaging and in vivo cerebral cortical histopathology, Arch. Neurol., 2011, 68, 1398-1403
[38] Cselenyi Z., Jonhagen M.E., Forsberg A., Halldin C., Julin P., Schou M., et al., Clinical validation of 18F-AZD4694, an amyloid-beta-specific PET radioligand, J. Nucl. Med., 2012, 53, 415-424
[39] Ikonomovic M.D., Klunk W.E., Abrahamson E.E., Mathis C.A., Price J.C., Tsopelas N.D., et al., Post-mortem correlates of in vivo PiB-PET amyloid imaging in a typical case of Alzheimer's disease, Brain, 2008, 131, 1630-1645
[40] Clark C.M., Schneider J.A., Bedell B.J., Beach T.G., Bilker W.B., Mintun M.A., et al., Use of florbetapir-PET for imaging beta-amyloid pathology, JAMA, 2011, 305, 275-283
[41] Zimmer E., Parent M., Leuzy A., Rowley J., Cheewakriengkrai L., Shin M., et al., [18F]NAV4694 shows higher binding and wider dynamic range compared with [11C]PiB in Alzheimer's disease postmortem tissue, Alzheimers Dement., 2013, 9, P22-P23
[42] Johnson K.A., Minoshima S., Bohnen N.I., Donohoe K.J., Foster N.L., Herscovitch P., et al., Appropriate use criteria for amyloid PET: a report

of the Amyloid Imaging Task Force, the Society of Nuclear Medicine and Molecular Imaging, and the Alzheimer's Association, Alzheimers Dement., 2013, 9, e-1-16

[43] Johnson K.A., Fox N.C., Sperling R.A.,Klunk W.E., Brain imaging in Alzheimer disease, Cold Spring Harb. Perspect. Med., 2012, 2, a006213

[44] Olson S., Institute of Medicine (U.S.). Roundtable on translating genomic-based research for health., Institute of Medicine (U.S.). Board on Health Sciences Policy., Integrating large-scale genomic information into clinical practice: workshop summary, National Academies Press, Washington, D.C., 2012

[45] Hood L., Flores M., A personal view on systems medicine and the emergence of proactive P4 medicine: predictive, preventive, personalized and participatory, N. Biotechnol., 2012, 29, 613-624

[46] Snyderman R., Personalized health care: from theory to practice, Biotechnol. J., 2012, 7, 973-979

[47] Weiner M.W., Veitch D.P., Aisen P.S., Beckett L.A., Cairns N.J., Green R.C., et al., The Alzheimer's Disease Neuroimaging Initiative: a review of papers published since its inception, Alzheimers Dement., 2012, 8, S1-68

[48] Ellis K.A., Bush A.I., Darby D., De Fazio D., Foster J., Hudson P., et al., The Australian Imaging, Biomarkers and Lifestyle (AIBL) study of aging: methodology and baseline characteristics of 1112 individuals recruited for a longitudinal study of Alzheimer's disease, Int. Psychogeriatr., 2009, 21, 672-687

[49] Pike K.E., Savage G., Villemagne V.L., Ng S., Moss S.A., Maruff P., et al., Beta-amyloid imaging and memory in non-demented individuals: evidence for preclinical Alzheimer's disease, Brain, 2007, 130, 2837-2844

[50] Jack C.R., Jr., Lowe V.J., Senjem M.L., Weigand S.D., Kemp B.J., Shiung M.M., et al., 11C PiB and structural MRI provide complementary information in imaging of Alzheimer's disease and amnestic mild cognitive impairment, Brain, 2008, 131, 665-680

[51] Aizenstein H.J., Nebes R.D., Saxton J.A., Price J.C., Mathis C.A., Tsopelas N.D., et al., Frequent amyloid deposition without significant cognitive impairment among the elderly, Arch. Neurol., 2008, 65, 1509-1517

[52] Mormino E.C., Kluth J.T., Madison C.M., Rabinovici G.D., Baker S.L., Miller B.L., et al., Episodic memory loss is related to hippocampal-mediated beta-amyloid deposition in elderly subjects, Brain, 2009, 132, 1310-1323

[53] Storandt M., Mintun M.A., Head D.,Morris J.C., Cognitive decline and brain volume loss as signatures of cerebral amyloid-beta peptide deposition identified with Pittsburgh compound B: cognitive decline associated with Abeta deposition, Arch. Neurol., 2009, 66, 1476-1481

[54] Villemagne V.L., Pike K.E., Chetelat G., Ellis K.A., Mulligan R.S., Bourgeat P., et al., Longitudinal assessment of Abeta and cognition in aging and Alzheimer disease, Ann. Neurol., 2011, 69, 181-192

[55] Landau S.M., Mintun M.A., Joshi A.D., Koeppe R.A., Petersen R.C., Aisen P.S., et al., Amyloid deposition, hypometabolism, and longitudinal cognitive decline, Ann. Neurology, 2012, 72, 578-586

[56] Jack C.R., Jr., Wiste H.J., Vemuri P., Weigand S.D., Senjem M.L., Zeng G., et al., Brain beta-amyloid measures and magnetic resonance imaging atrophy both predict time-to-progression from mild cognitive impairment to Alzheimer's disease, Brain, 2010, 133, 3336-3348

[57] Wolk D.A., Price J.C., Saxton J.A., Snitz B.E., James J.A., Lopez O.L., et al., Amyloid imaging in mild cognitive impairment subtypes, Ann. Neurol., 2009, 65, 557-568

[58] Trzepacz P.T., Yu P., Sun J., Schuh K., Case M., Witte M.M., et al., Comparison of neuroimaging modalities for the prediction of conversion from mild cognitive impairment to Alzheimer's dementia, Neurobiol. Aging, 2014, 35, 143-151

[59] Green R.C., Roberts J.S., Cupples L.A., Relkin N.R., Whitehouse P.J., Brown T., et al., Disclosure of APOE genotype for risk of Alzheimer's disease, N. Engl. J. Med., 2009, 361, 245-254

[60] Steinbrook R., The Centers for Medicare & Medicaid Services and amyloid-beta positron emission tomography for Alzheimer disease, JAMA Intern. Med., 2014, 174, 135

[61] Pearson S.D., Ollendorf D.A.,Colby J.A., Amyloid-beta positron emission tomography in the diagnostic evaluation of Alzheimer disease: summary of primary findings and conclusions, JAMA Intern. Med., 2014, 174, 133-134

[62] Doraiswamy P.M., Sperling R.A., Coleman R.E., Johnson K.A., Reiman E.M., Davis M.D., et al., Amyloid-beta assessed by florbetapir F 18 PET and 18-month cognitive decline: a multicenter study, Neurology, 2012, 79, 1636-1644

[63] Garber K., First FDA-approved beta-amyloid diagnostic hits the market, Nat. Biotechnol., 2012, 30, 575

[64] Leuzy A., Gauthier S., Ethical issues in Alzheimer's disease: an overview, Expert Rev. Neurother., 2012, 12, 557-567

[65] Lineweaver T.T., Bondi M.W., Galasko D., Salmon D.P., Effect of knowledge of APOE genotype on subjective and objective memory performance in healthy older adults, Am. J. Psychiatry, 2014, 171, 201-208

[66] Karlawish J.,Green R.C., Minding the aging brain: are we ready for personalized medicine?, Am. J. Psychiatry, 2014, 171, 137-139

Capítulo VIII. *Developments in Tau PET Imaging.*

No **capítulo VIII** apresentamos o artigo publicado no periódico *Canadian Journal of Neurological Sciences.*

Nos capítulos anteriores (capítulos V-VII) avaliamos os radiofármacos de PET disponíveis para visualização de placas de β-amilóide. Neste capítulo, avaliamos os recentemente desenvolvidos radiofármacos com afinidade por agregados da proteína tau, os NFTs. Cabe relembrar, que os níveis de t-tau e p-tau no LCR são utilizados como biomarcadores de neurodegeneração na DA, porém eles não conseguem fornecer informações cerebrais a nível topográfico. Neste estudo, demonstramos que os PET radiofármacos para tau – [^{18}F]THK523, [^{18}F]THK5105, [^{18}F]THK5117, [^{18}F]T807, [^{18}F]T808, e [^{11}C]PBB3 – tem alta especificidade e boas propriedades farmacocinéticas, e com isso apresentam alto potencial para serem utilizados na clínica. Artigo escolhido como capa da edição de setembro do periódico *Canadian Journal of Neurological Sciences.*

VOLUME 41, NO. 5

CANADIAN NEUROLOGICAL SCIENCES FEDERATION
FÉDÉRATION DES SCIENCES NEUROLOGIQUES DU CANADA

The journal

Canadian Journal of Neurological Sciences

Volume 41 Number 5 September 2014

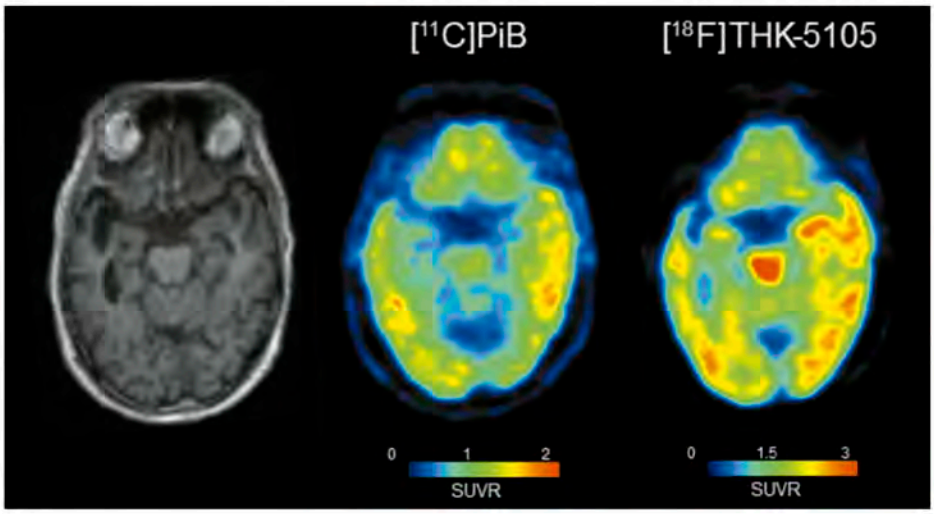

Developments in Tau PET Imaging

Eduardo Rigon Zimmer, Antoine Leuzy, Serge Gauthier, Pedro Rosa-Neto

Can J Neurol Sci. 2014; 41: 547

Figure: *Co-registered MRI, [11C]PiB and [18F]THK-5105 images in a patient with Alzheimer's disease (AD).*

THE CANADIAN JOURNAL OF NEUROLOGICAL SCIENCES

SEPTEMBER 2014 (545-676)

PM 40007777 R 9824

AN INTERNATIONAL JOURNAL PUBLISHED BY THE CANADIAN NEUROLOGICAL SCIENCES FEDERATION

The official Journal of: The Canadian Neurological Society, The Canadian Neurosurgical Society, The Canadian Society of Clinical Neurophysiologists, The Canadian Association of Child Neurology

REVIEW ARTICLE

COPYRIGHT © 2014 THE CANADIAN JOURNAL OF NEUROLOGICAL SCIENCES INC.

Developments in Tau PET Imaging

Eduardo Rigon Zimmer, Antoine Leuzy, Serge Gauthier, Pedro Rosa-Neto

ABSTRACT: The presence of neurofibrillary tangles in the brain is a hallmark feature of several neurodegenerative diseases termed "tauopathies," including Alzheimer's disease (AD) and the tau molecular subgroup of frontotemporal lobar degeneration (FTLD-tau). Recently, several positron emission tomography (PET) radiopharmaceuticals targeting abnormal conformations of the tau protein have been developed. To date, six novel tau imaging agents—[^{18}F]THK523, [^{18}F]THK5105, [^{18}F]THK5117, [^{18}F]T807, [^{18}F]T808, and [^{11}C]PBB3—have been described and are considered promising as potential tau radioligands. Tau imaging agents offer the opportunity of in vivo topographical mapping and quantification of tau aggregates in parallel with clinical and cognitive assessments. As such, tau imaging is considered of key importance for progress toward earlier and more accurate diagnosis of tauopathies as well as for the monitoring of therapeutic interventions and drug development. Here, we shed light on the most important developments in tau radiopharmaceuticals, highlighting challenges, possibilities and future directions.

RÉSUMÉ: La présence d'enchevêtrements neurofibrillaires dans le cerveau est une des caractéristiques dans plusieurs maladies neurodégénératives appelées «tauopathies» dont font partie la maladie d'Alzheimer (MA) et le sous-moléculaire de la protéine tau de la dégénérescence fronto-temporale lobaire (DFTL-tau). Récemment, plusieurs tomographies par émission de positons (TEP) radiopharmaceutiques ont été mises au point afin de cibler avec précision les conformations anormales de la protéine tau. Six nouveaux agents d'imagerie tau [^{18}F]THK523, [^{18}F]THK5105, [^{18}F]THK5117, [^{18}F] T807, [^{18}F]T808, et [^{11}C]PBB3 ont été décrits à ce jour et sont considérés très prometteurs en tant que radioligands tau potentiels. Les agents d'imagerie tau ouvrent de nouvelles voies à la cartographie topographique et à la quantification in vivo des agrégats de la protéine tau en parallèle avec les évaluations cliniques et cognitives en cours. L'imagerie de la protéine tau est considérée en tant que telle comme ayant une importance capitale pour faire progresser les diagnostics actuels vers des diagnostics plus précoces et plus précis de tauopathies, ainsi que pour le suivi des interventions thérapeutiques et le développement de médicaments. La suite de cet article permettra, nous l'espérons, d'apporter plus de lumière sur les développements radiopharmaceutiques les plus importants de la protéine tau, les défis et possibilités, tout en mettant en évidence les orientations futures de cette imagerie.

Keywords: Dementia, positron emission tomography (PET), radiopharmaceuticals, tau, tauopathy

doi:10.1017/cjn.2014.15

Can J Neurol Sci. 2014; 41: 547-553

INTRODUCTION

Tau is a phosphoprotein that belongs to the microtubule-associated family (MAP). In the human brain, tau proteins can assume six different isoforms, with each variant containing a microtubule-binding domain comprising three repeat (3R) or four repeat (4R) regions in the protein carboxy-terminal (C-terminal) as well as one or two amino acid terminal (N-terminal) inserts.[1] Importantly, the expression of tau isoforms may not be equal across neurons. For instance, tau messenger RNAs containing exon 10—which encodes the fourth microtubule-binding domain—are not found in granular cells within the dentate gyrus.[2] As such, tau isoforms are thought to be differentially distributed within neuronal subpopulations.

A key mediator of microtubule assembly and stability,[3-5] tau functionality is regulated by a wide range of serine and threonine phosphorylation sites. In addition to reducing tau's affinity for microtubules, abnormal phosphorylation of these sites results in a complementary toxic gain of function—in the form of an increased propensity for misfolding and subsequent polymerization—with this mechanism believed to occupy a central role in various neurodegenerative conditions,[6,7] including Alzheimer's disease (AD), and the tau molecular subgroup of frontotemporal lobar degeneration (FLTD-tau) (Table 1). In the case of AD, the accumulation of abnormally phosphorylated tau is known to proceed hierarchically—affecting first the transentorhinal pre-α layer (Braak stage I–II), before progressing toward limbic (Braak stage III/IV) and isocortical areas (Braak stage V/VI)—with its spread thought to occur following a shift toward prion-like self-propagation.[8,9]

Though quantitative assessment of cerebrospinal fluid (CSF) levels of tau and phosphorylated tau (p-tau) are currently acknowledged as biomarkers of neurodegeneration,[10] with levels shown to correlate with cognitive impairment in AD,[11-13] the collection of

From the Translational Neuroimaging Laboratory (ERZ, AL, PR-N); Alzheimer's Disease Research Unit (ERZ, AL, SG, PR-N), McGill Centre for Studies in Aging, Douglas Mental Health University Institute, Montreal, Quebec, Canada; Department of Biochemistry (ERZ), Federal University of Rio Grande do Sul, Brazil.

RECEIVED FEBRUARY 10, 2014. FINAL REVISIONS SUBMITTED APRIL 11, 2014.

Correspondence to: Pedro Rosa-Neto, McGill Center for Studies in Aging, 6825 LaSalle Blvd., Montreal, Canada H4H 1R3. Email: pedro.rosa@mcgill.ca

Table 1: Tau isoforms in AD and various non-AD tauopathies

Pathology	Tau isoform
AD	3R + 4R
Diffuse neurofibrillary tangle dementia with calcifications	3R + 4R
Pick's disease	3R
Cortical basal degeneration	4R
Progressive supranuclear palsy	4R
Argyrophilic grain disease	4R
Multisystem tauopathy with globular inclusions	4R

3R = three repeat tau microtubule binding domains; 4R = four repeat tau microtubule binding domains; AD = Alzheimer's disease.

CSF via lumbar puncture is invasive in nature and is associated with high inter-laboratory variability, hampering comparison of data across centers.[14] In addition, levels of tau and p-tau are unable to provide information regarding the topography of tau pathology in the brain, which is critical to the differential diagnosis of certain tauopathies.[15,16] The concept of misfolded tau as a central process underlying neurodegeneration[17-20] has led to the development of tau-focused therapeutics aiming to reduce tau-mediated neurodegeneration, with approaches including microtubule stabilizing agents, reduction of tau hyperphosphorylation, inhibition of tau fibril aggregation, and promotion of microtubule stability.[21] As such, the development of noninvasive methodologies has a high priority for determining tau pathology propagation and monitoring treatment effects in clinical trials.

Positron emission tomography (PET), a noninvasive molecular imaging method, allows for quantitative analysis of a wide array of biological processes in the living human brain. Recently, three new classes of radiopharmaceuticals with a high affinity for tau tangles have been described (Table 2). PET using tau radiopharmaceuticals holds the promise of accurate, reliable, and reproducible quantification of both regional and global tau burden, which could translate into earlier and more accurate differential diagnosis, as well as aid in monitoring disease progression and therapeutic efficacy in clinical trials.

In a recent review, we underscored the opportunity for improved modeling using tau radiopharmaceuticals and animals models.[26] Here, we shed light on the most promising tau radiopharmaceuticals and highlight future directions for tracking tau pathology using PET molecular imaging.

Tau Radiopharmaceuticals

Until recently, the main focus of PET molecular imaging has been the development of highly specific ligands for early detection of amyloid deposition. A variety of such tracers, including Pittsburgh compound B ([^{11}C]PiB) and several [^{18}F]-labeled tracers, have been developed and have provided important new insights into the role played by amyloid deposition in neurodegenerative disorders.[27] Though one tracer among these [^{18}F]FDDNP, appeared to bind both amyloid plaques and tau tangles,[28] a subsequent study using [^{3}H]FDDNP autoradiography in sections containing neurofibrillary tangles (NFTs) failed to demonstrate overt labeling of tau pathology because of a low affinity for NFTs.[29] In fact, low levels of tau aggregates in the brain (relative to β-amyloid), as well as the multiple structural conformations it can assume, make tau tracking a more complicated task when compared with detection of β-amyloid deposition.[30]

Recently, three new classes of compounds have been developed aiming to bind tau fibrils and stand as potential tau imaging biomarkers. These include: (1) quinoline derivatives, (2) benzimidazole pyrimidine derivatives, and (3) benzothiazole derivatives.[15,23,25] In the following paragraphs, we describe the most important insights generated from in vitro and in vivo studies using these novel tracers (for detailed information, see Table 3).

Quinoline Derivatives

The first quinoline derived tau ligand was [^{18}F]THK523. Following optimization in the form of improved specificity, second-generation tracers were released in the form of [^{18}F]THK5105 and [^{18}F]THK5117. In vitro binding assays involving such tracers were performed using synthetic truncated tau (K18ΔK280) fibrils, comprising four repeat regions (244-372) in the absence of lysine 280 (ΔK280). K18ΔK280 tau aggregates form rapidly without cofactors and exhibit similar characteristics to paired helical filamentous (PHF) tau.[34,35] These studies demonstrated that [^{18}F]THK5105 and [^{18}F]THK5117 are associated with higher binding for K18ΔK280 tau aggregates, relative to [^{18}F]THK523.[22] Using histofluorescence analysis, Fodero-Tavoletti and colleagues[15] showed that [^{18}F]THK523 colocalizes with tau tangles and presents negligible binding to β-amyloid plaques in hippocampal tissue obtained from AD patients. Furthermore, they showed colocalization of [^{18}F]THK523 and tau tangles in mouse (Tg4510, tau model) tissue immunostained with tau antibodies. In contrast, there was no colocalization in a mouse model harboring human amyloid precursor protein (APP) and presenilin 1 (PS1)

Table 2: Tau Radiopharmaceuticals

Tracer	Biological target	K_D (High-affinity binding site)	References
[^{18}F]THK523	Tau fibrils	1.67 nM	15
[^{18}F]THK5105	Tau fibrils	1.45 nM	22
[^{18}F]THK5117	Tau fibrils	5.19 nM	22
[^{18}F]T807	Tau fibrils	14.6 nM	23
[^{18}F]T808	Tau fibrils	22 nM	24
[^{11}C]PBB3	Tau fibrils	2.5 nM	25

K_D = ligand property equal to the inverse of affinity

Table 3: Most relevant in vitro and in vivo studies conducted with tau radiopharmaceuticals

Binding studies				
Radiopharmaceutical	**Binding target**	**Expected findings**	**Results**	**References**
[^{18}F]THK523	Synthetic tau fibrils	Binding to tau fibrils	Two binding sites on tau fibrils (high- and low-affinity sites)	15,31
[^{18}F]THK5105	Synthetic tau fibrils	Binding to tau fibrils	Two binding sites on tau fibrils (high- and low-affinity sites)	22
Immunohistochemistry				
Fluorescence probes	**Tissue**	**Expected findings**	**Results**	**References**
THK523	Tau Tg mice (rTg4510 model)	Colocalization	THK523 colocalized with tau staining	15
THK523	AD	Colocalization	THK523 colocalized with tau tangles staining	15
THK5105	AD	Colocalization	THK5105 colocalized with tau staining	22
THK5117	AD	Colocalization	THK5117 colocalized with tau staining	22
T726 (T807 analogue)	AD	Colocalization	T726 colocalized with tau staining	23
PBB3	Tau Tg mice (PS19 mice)	Colocalization	PBB3 colocalized with tau staining	25
PBB3	AD, PID, PSP, CDB	Colocalization	PBB3 colocalized with tau staining	25
Autoradiography				
Radiopharmaceutical	**Tissue**	**Expected findings**	**Results**	**References**
[^{18}F]THK523	AD	Binding to tau tangles	High binding to tau fibrils	15,31
[^{18}F]THK5105	AD	Binding to tau tangles	High binding to tau fibrils	22
[^{18}F]THK5117	AD	Binding to tau tangles	High binding to tau fibrils	22
[^{18}F]T807	AD	Binding to tau tangles	High binding to tau fibrils	23,32
[^{18}F]T808	AD	Binding to tau tangles	High binding to tau fibrils	24
[^{11}C]PBB3	Tau Tg mice (PS19 mice)	Binding to tau tangles	High binding to tau fibrils	25
[^{11}C]PBB3	AD	Binding to tau tangles	High binding to tau fibrils	25
PET				
Radiopharmaceutical	**Model/disease**	**Expected findings**	**Results**	**References**
[^{18}F]THK523	Tau Tg mice (rTg4510)	High binding	Tg > Wt	15
[^{18}F]THK523	Amyloid Tg mice (APP/PS1 mice)	No binding	Tg = Wt	15
[^{18}F]THK523	AD patients	High binding	AD > HC	33
[^{18}F]T807	Tau/amyloid Tg mice (APPswe-Tau mice)	High binding	Tg = Wt	23
[^{11}C]PBB3	Tau mice (PS19)	High binding	Tg > Wt	25
[^{18}F]T807	AD patients	High binding	AD > MCI > HC	32
[^{18}F]T808	AD patients	High binding	AD > HC	37
[^{11}C]PBB3	AD patients	High binding	AD > HC	25
[^{11}C]PBB3	CBS patient	High binding	CBS > HC	25

AD = Alzheimer's disease; HC = healthy control; CBS = corticobasal syndrome; MCI = mild cognitive impairment; PID = Pick's disease; PSP = progressive supranuclear palsy; Tg = transgenic; Wt = wild-type.

mutations, a model that displays amyloidosis, but not tau tangles. [^{18}F]THK523 bound to tau aggregates in AD hippocampal sections and not to amyloid pathology confirmed using anti-β-amyloid and anti-tau antibodies.[15] Furthermore, [^{18}F]THK523 was found to accumulate in Sommer's sector (CA1) as well in layers pre- and pri-α of the entorhinal cortex in AD brain sections. These findings were consistent with the density of PHF-tau deposition, as confirmed via immunohistochemistry.[31] However, a recent autoradiography study showed that [^{18}F]THK523 has affinity only for tau filaments present in AD brains, but not for tau lesions present in non-AD tauopathies.[36] Immunostaining with fluorescent THK5105 and THK5117 indicated colocalization with tau (AT8 antibody) in human hippocampal brain sections.[22] In addition, autoradiography using [^{18}F]THK5117 showed strong accumulation in regions displaying high amounts of tau deposition, such as the subiculum, parahippocampus, CA1 subfield, insula, inferior and middle temporal gyri, and the cingulate gyrus.[22] Importantly, in vitro validation using binding assays and autoradiography combined with immunohistochemistry is sine qua non for the development of novel radiopharmaceuticals. In fact, these parameters are used to define which radiopharmaceuticals should be further investigated in in vivo studies.

In vivo studies showed that [^{18}F]THK523, [^{18}F]THK5105, and [^{18}F]THK5117 exhibited sufficient amounts of tracer uptake in the mouse brain after intravenous infusion, although [^{18}F]THK5105 and [^{18}F]THK5117 showed higher brain uptake and

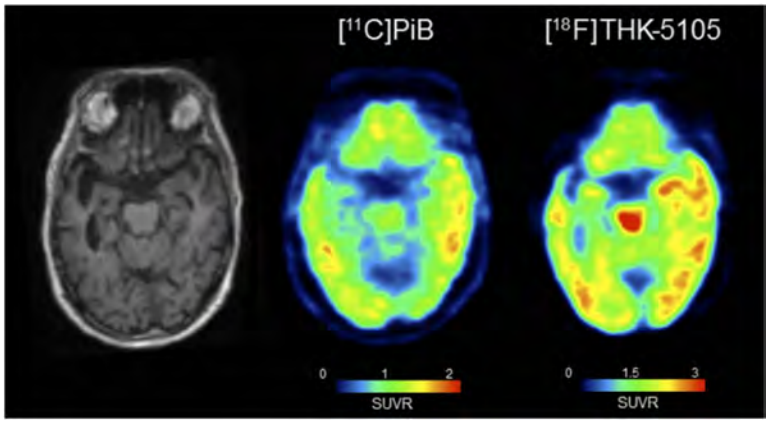

Figure 1: *Co-registered MRI, [^{11}C]PiB and [^{18}F]THK-5105 images in a patient with Alzheimer's disease (AD). Figure depicts a structural MRI (left), [^{11}C]PIB (center), and [^{18}F]THK-5105 PET images (right), from a patient with dementia resulting from AD (images courtesy of Profs. V. Villemagne and N. Okamura). Images were co-registered in the plane encompassing the temporal lobe, hippocampus, orbitofrontal cortex, amygdala, midbrain, and cerebellum. MRI shows bilateral hippocampal atrophy (right > left). [^{11}C]PIB images show high uptake (yellow-red spots) in the temporal neocortex. [^{18}F]THK-5105 shows high uptake (yellow-red spots) in the mesial temporal as well as the temporal neocortex. The high [^{18}F]THK-5105 uptake in the midbrain possibly represents high nonspecific binding, a finding that would prove consistent with the vast literature addressing AD imaging and neuropathology. Of note, low uptake of both [^{11}C]PIB and [^{18}F]THK-5105 can be seen in the cerebellum, an important finding because the cerebellum serves as the reference region when determining the standardized uptake value ratio (SUVR). A semiquantitative approach, SUVR is defined as the ratio of cortical to reference region radioactivity (i.e. tracer retention). In the case of [^{11}C]PiB and [^{18}F]THK-51505 here shown, the reference regions are the cerebellum (vermis excluded) and the pons, respectively.*

faster clearance than [^{18}F]THK523.[22] Though microPET assessment using [^{18}F]THK523 showed higher retention in rTg4510 mice relative to APP/PS1 mice and wild-type littermates, the first clinical PET study revealed elevated white matter (WM) retention, precluding future use of [^{18}F]THK523 in research or clinical settings.[33] In the case of [^{18}F]THK5105, however, unpublished preliminary data (courtesy of professors Okamura and Villemagne) revealed labeling of tau pathology in a subject with AD, with delineated areas (e.g. hippocampus) differing from those identified using [^{11}C]PiB (Figure 1).

Benzimidazole Pyrimidines

After screening more than 900 compounds, benzimidazole pyrimidines derivatives [^{18}F]T807 and [^{18}F]T808 were developed. For characterization, a T807 analogue (T726) was used by Xia and colleagues[23] and showed a high degree of colocalization with PHF-tau but not with A$\beta_{1\text{-}42}$ in frontal lobe postmortem tissue exhibiting AD pathology.

Autoradiography using [^{18}F]T807 was conducted on frontal brain sections in three different groups classified as high PHF-tau and β-amyloid (group A); low PHF-tau, high β-amyloid (group B); and negative PHF-tau/β-amyloid (group C). Although strong gray matter signals were detected in group A, cortical regions from group B emitted only weak signals, and group C emitted only background signal. Comparison between double immunostained adjoining brain sections and [^{18}F]T807 autoradiography revealed that [^{18}F]T807 signals colocalized with immunostaining for PHF-tau but not with A$\beta_{1\text{-}42}$ plaques.[23] [^{18}F]T807 autoradiographic analysis using frontal lobe sections provided a selectivity estimate of 29-fold for tau relative to β-amyloid, confirmed by immunohistochemistry.[32] In agreement, autoradiography with [^{18}F]T808 also showed increased binding in "tau-rich" regions in AD brains, and a significant overlap in areas stained with anti-tau antibodies.[24] Further, [^{18}F]T807 and [^{18}F]T808 tracers showed fast brain uptake followed by a rapid washout in normal mice, suggesting low nonspecific binding.[23,24] However, [^{18}F]T807 was insensitive to differences between APPswe-Tau and wild-type background mice.[15]

The first [^{18}F]T807 PET imaging results obtained in healthy controls (HCs), mild cognitive impairment (MCI), and AD subjects showed favourable kinetics—with both rapid brain delivery and WM clearance—as well as low nonspecific WM and cortical binding in HCs. In patients with MCI and AD, a distinct pattern of tracer uptake was observed, relative to the cerebellum—comprising lateral temporal, mesial temporal, parietal, occipital, and frontal cortices—mirroring the current understanding of tau deposition, as described by Braak and Braak.[32] Similar findings were obtained using [^{18}F]T808, with increasing signal intensity within these regions noted as a function of clinical severity. Although difficult to determine because of the small sample size, these results suggest that a 30- to 50-minute imaging time point may prove sufficient with respect to differentiating HCs from subjects with AD, with a time frame of 80 to 100 minutes optimal for detection of smaller amounts of tau deposits.[37]

Benzothiazole Derivative: [^{11}C]PBB3

Following a screening of several fluorescent chemicals with affinity for β-sheet conformations, a PBB class of ligands was

recently developed for visualization of diverse structural forms of tau inclusions. The most promising of these tracers is [^{11}C]PBB3, which shows good pharmacokinetic properties and robust binding to tau inclusions in small animals and humans.[25]

In vitro and ex vivo fluorescence microscopy showed that PBB3 clearly identified tau inclusions in tau transgenic mice (PS19 line, harbouring P301S FTDP-17 mutation). Additionally, in vitro autoradiography studies showed that [^{11}C]PBB3 produced high-contrast signals in the tissue of PS19 mice and AD patients with low nonspecific binding. Ex vivo autoradiography likewise demonstrated selectivity for tau inclusions in the PS19 mouse model.[25] These findings were supported by preclinical in vivo assessment showing that [^{11}C]PBB3 identified tau inclusions in the PS19 mouse model.

The first exploratory clinical [^{11}C]PBB3 PET study for patients with probable AD showed minimal nonspecific WM binding and rapid brain delivery. [^{11}C]PBB3 signal was found to accumulate in the limbic system in mild AD, with expansion to most cortical areas with progression through moderate AD, consistent with Braak stage V/VI. Interestingly, a slight retention of [^{11}C]PBB3 was noted around the hippocampus in a normal control subject who had shown a decline of several points on the Mini-Mental Status Examination (MMSE), similar to early Braak stages. Finally, elevated [^{11}C]PPB3 binding was noted in the basal ganglia of a patient diagnosed with corticobasal syndrome, supporting the use of [^{11}C]PPB3 to detect tau lesions in both AD and non-AD tauopathies.[25]

Summary of General Properties of Tau Radiopharmaceuticals

The association between autoradiographic and immunohistochemical findings across multiple brain regions in both human and transgenic mouse brain tissue revealed the colocalization of all tracers with immunoreactive tau antibodies, indicating high selectivity for tau aggregates. Furthermore, autoradiography studies have provided specific and nonspecific binding, number of available binding sites, and affinity, parameters crucial for the interpretation of PET studies (for review, see (39); Table 2). Additionally, the tau tracers here reviewed possess desirable properties for consideration as potential neuroimaging probes, including high lipophilicity, low molecular weight, high selectivity/affinity, and rapid plasma clearance.[39,40]

Possibilities and Challenges for in vivo Tracking of Tau Pathology

Clinical PET using such tau radiopharmaceuticals should be viewed as a work in progress. Initial PET studies using [^{18}F]THK523 ruled out its use in clinical settings because of elevated WM binding. However, optimized second-generation compounds remain under investigation and carry promise for future use because of their expected specificity for AD forms of tau. In the case of [^{18}F]T807 and [^{18}F]T808, clinical studies conducted thus far indicate their ability to track cognitive decline—as indexed by MMSE scores—as well as the propagation of tau pathology, according to Braak staging. In the case of [^{11}C]PBB3, despite findings highlighting its potential to detect tau pathology in both AD and non-AD tauopathies, its short half-life (20 minutes) limits its use to imaging centers possessing an onsite cyclotron and specialized radiochemistry, making it unsuitable for widespread clinical use.

Based on these early clinical studies, tau tracers may facilitate the differential diagnosis of AD—where tau tangles are composed of equimolar 3R and 4R isoforms[41]—and non-AD tauopathies, where tau tangles contain predominantly 3R or 4R isoforms. When combined with complementary structural and functional imaging approaches, the use of tau tracers may allow for improved detection and characterization of mixed pathology and refine our current understanding of the link between tau deposition, metabolic change, and brain atrophy. At the same time, tau tracers may provide further insight into the link between alterations in tau protein distribution that accompany normal aging and performance decrements on neuropsychological measures in non-demented elderly individuals.[42] In the context of clinical trials involving tau-directed therapeutics, tau PET ligands may serve as diagnostic biomarkers to guide population enrichment strategies, to calculate sample size, and to increase the statistical power via population stratification or through use as baseline predictors.[43] In parallel, tau-ligands can serve as endpoint biomarkers to monitor the rate of disease progression as well as response to therapy. Finally, tau ligands may aid in the testing of new hypotheses, including the hypothesis that β-amyloid and tau pathology arise independently in sporadic AD, with incident β-amyloid pathophysiology interacting synergistically with an antecedent limbic/brainstem tauopathy.[10,44]

Despite the promise held by the tracers discussed here, a number of challenges remain. Given that structural polymorphisms are the rule rather than the exception,[45] with a given tau isoform assuming various conformations, and different isoforms assuming similar forms ultrastructurally,[46] the distribution of such tau aggregates within the brain varies by phenotype.[45] Though an advantage in terms of differential diagnosis, the underlying assumption—namely, that binding of tau ligands will be comparable across the spectrum of tau polymorphisms—is unlikely.[45] In addition, the ability of tracers to bind tau may be affected by different posttranslational modifications[47] such that a given radiotracer may be able to bind PHF-tau but not other ultrastructural tau conformations, such as straight filaments or randomly coiled filaments. Additionally, tau deposition from normal aging must be addressed to provide a reliable threshold and avoid false positives given the presence of tau pathology in a certain percentage of cognitively normal individuals.[48,49] Finally, additional PET studies incorporating increased subject numbers and a wider range of tauopathies are necessary to further validate the use of tau ligands in clinical settings.

Conclusion

The growing interest in tau radiopharmaceutical will surely contribute to significant advancements in the field. Indeed, it is expected that many additional tau-focused radiopharmaceuticals will soon be examined. Current tau tracers hold translational value in terms of characterizing the link between the progression of tau pathology and cognitive impairment as well as in terms of monitoring treatment effects in clinical trials using tau-focused therapeutics. Finally, tau tracers hold the potential for inclusion as biomarkers of neurodegeneration, to be used alone or in parallel with CSF tau measurements in order to achieve an improved understanding of tauopathies.

ACKNOWLEDGEMENTS AND FUNDING

The authors thank Professors Victor Villemagne and Noboyuki Okamura for providing Figure 1.

This work was supported by the Canadian Institutes of Health Research (CIHR; MOP-11-51-31), Alzheimer's Association (NIRG-12-259245), Fonds de Recherche du Québec - Santé (FRQS; Chercheur Boursier), the Allan Tiffin Trust (Infrastructure), the Conselho Nacional de Desenvolvimento Cientifico e Tecnológico (CNPq, Brazil), Fundação de Amparo à Pesquisa do Rio Grande do Sul (Fapergs, Brazil), and INCT for Excitotoxicity and Neuroprotection/CNPq.

STATEMENT OF AUTHORSHIP

ERZ and AL contributed equally to this work. ERZ and AL were responsible for the conception and design of the review and for drafting and revising the manuscript. SG and PRN were responsible for revising the manuscript.

REFERENCES

1. Buee L, Bussiere T, Buee-Scherrer V, Delacourte A, Hof PR. Tau protein isoforms, phosphorylation and role in neurodegenerative disorders. Brain Res Brain Res Rev. 2000;33(1):95-130.
2. Goedert M, Spillantini MG, Jakes R, Rutherford D, Crowther RA. Multiple isoforms of human microtubule-associated protein tau: sequences and localization in neurofibrillary tangles of Alzheimer's disease. Neuron. 1989;3(4):519-26.
3. Weingarten MD, Lockwood AH, Hwo SY, Kirschner MW. A protein factor essential for microtubule assembly. Proc Natl Acad Sci U S A. 1975;72(5):1858-62.
4. Cleveland DW, Hwo SY, Kirschner MW. Physical and chemical properties of purified tau factor and the role of tau in microtubule assembly. J Mol Biol. 1977;116(2):227-47.
5. Horio T, Hotani H. Visualization of the dynamic instability of individual microtubules by dark-field microscopy. Nature. 1986; 321(6070):605-7.
6. Jucker M, Walker LC. Pathogenic protein seeding in Alzheimer disease and other neurodegenerative disorders. Ann Neurol. 2011;70(4):532-40.
7. Spires-Jones TL, Stoothoff WH, de Calignon A, Jones PB, Hyman BT. Tau pathophysiology in neurodegeneration: a tangled issue. Trends Neurosci. 2009;32(3):150-9.
8. de Calignon A, Polydoro M, Suarez-Calvet M, et al. Propagation of tau pathology in a model of early Alzheimer's disease. Neuron. 2012;73(4):685-97.
9. Braak H, Braak E. Neuropathological stageing of Alzheimer-related changes. Acta Neuropathol. 1991;82(4):239-59.
10. Jack CR Jr., Knopman DS, Jagust WJ, et al. Tracking pathophysiological processes in Alzheimer's disease: an updated hypothetical model of dynamic biomarkers. Lancet Neurol. 2013;12(2):207-16.
11. Shaw LM, Vanderstichele H, Knapik-Czajka M, et al. Cerebrospinal fluid biomarker signature in Alzheimer's disease neuroimaging initiative subjects. Ann Neurol. 2009;65(4):403-13.
12. Buerger K, Teipel SJ, Zinkowski R, et al. CSF tau protein phosphorylated at threonine 231 correlates with cognitive decline in MCI subjects. Neurology. 2002;59(4):627-9.
13. Augustinack JC, Schneider A, Mandelkow EM, Hyman BT. Specific tau phosphorylation sites correlate with severity of neuronal cytopathology in Alzheimer's disease. Acta Neuropathol. 2002; 103(1):26-35.
14. Mattsson N, Blennow K, Zetterberg H. Inter-laboratory variation in cerebrospinal fluid biomarkers for Alzheimer's disease: united we stand, divided we fall. Clin Chem Lab Med. 2010;48(5):603-7.
15. Fodero-Tavoletti MT, Okamura N, Furumoto S, et al. 18F-THK523: a novel in vivo tau imaging ligand for Alzheimer's disease. Brain. 2011;134(Pt 4):1089-100.
16. Spies PE, Claassen JAHR, Slats D, Olde Rikkert MGM, Verbeek MMK, Kessels RPC. Cerebrospinal fluid tau and amyloid beta proteins do not correlate with cognitive functioning in cognitively impaired memory clinic patients. CNS Spectrum. 2010;15(9):588-93.
17. Goedert M, Jakes R. Mutations causing neurodegenerative tauopathies. Biochim Biophys Acta. 2005;1739(2-3):240-50.
18. von Bergen M, Barghorn S, Li L, et al. Mutations of tau protein in frontotemporal dementia promote aggregation of paired helical filaments by enhancing local beta-structure. J Biol Chem. 2001;276(51):48165-74.
19. Gotz J, Gladbach A, Pennanen L, et al. Animal models reveal role for tau phosphorylation in human disease. Biochim Biophys Acta. 2010;1802(10):860-71.
20. Roberson ED, Scearce-Levie K, Palop JJ, et al. Reducing endogenous tau ameliorates amyloid beta-induced deficits in an Alzheimer's disease mouse model. Science. 2007;316 (5825):750-4.
21. Giacobini E, Gold G. Alzheimer disease therapy-moving from amyloid-beta to tau. Nat Rev Neurol. 2013;9(12):677-86.
22. Okamura N, Furumoto S, Harada R, et al. Novel 18F-labeled arylquinoline derivatives for noninvasive imaging of tau pathology in Alzheimer disease. J Nucl Med. 2013;54(8):1420-7.
23. Xia CF, Arteaga J, Chen G, et al. [(18)F]T807, a novel tau positron emission tomography imaging agent for Alzheimer's disease. Alzheimers Dement. 2013;9(6):666-76.
24. Zhang W, Arteaga J, Cashion DK, et al. A highly selective and specific PET tracer for imaging of tau pathologies. J Alzheimers Dis. 2012;31(3):601-12.
25. Maruyama M, Shimada H, Suhara T, et al. Imaging of tau pathology in a tauopathy mouse model and in Alzheimer patients compared to normal controls. Neuron. 2013;79(6): 1094-1108.
26. Zimmer ER, Leuzy A, Bhat V, Gauthier S, Rosa-Neto P. In vivo tracking of tau pathology using positron emission tomography (PET) molecular imaging in small animals. Transl Neurodegener. 2014;3(1):6.
27. Rowe CC, Ng S, Ackermann U, et al. Imaging beta-amyloid burden in aging and dementia. Neurology. 2007;68(20):1718-25.
28. Agdeppa ED, Kepe V, Liu J, et al. Binding characteristics of radiofluorinated 6-dialkylamino-2-naphthylethylidene derivatives as positron emission tomography imaging probes for beta-amyloid plaques in Alzheimer's disease. J Neurosci. 2001; 21(24):RC189.
29. Thompson PW, Ye L, Morgenstern JL, et al. Interaction of the amyloid imaging tracer FDDNP with hallmark Alzheimer's disease pathologies. J Neurochem. 2009;109(2):623-30.
30. Mukaetova-Ladinska EB, Harrington CR, Roth M, Wischik CM. Biochemical and anatomical redistribution of tau protein in Alzheimer's disease. Am J Pathol. 1993;143(2):565-78.
31. Harada R, Okamura N, Furumoto S, et al. Comparison of the binding characteristics of [18F]THK-523 and other amyloid imaging tracers to Alzheimer's disease pathology. Eur J Nucl Med Mol Imaging. 2013;40(1):125-32.
32. Chien DT, Bahri S, Szardenings AK, et al. Early clinical PET imaging results with the novel PHF-tau radioligand [F-18]-T807. J Alzheimers Dis. 2013;34(2):457-68.
33. Villemagne VL, Furumoto S, Fodero-Tavoletti MT, et al. In vivo evaluation of a novel tau imaging tracer for Alzheimer's disease. Eur J Nucl Med Mol Imaging. 2014;41(5):816-26.
34. Barghorn S, Davies P, Mandelkow E. Tau paired helical filaments from Alzheimer's disease brain and assembled in vitro are based on beta-structure in the core domain. Biochemistry. 2004;43 (6):1694-703.
35. von Bergen M, Barghorn S, Muller SA, et al. The core of tau-paired helical filaments studied by scanning transmission electron microscopy and limited proteolysis. Biochemistry. 2006;45(20): 6446-57.
36. Fodero-Tavoletti MT, Furumoto S, Taylor L, et al. Assessing THK523 selectivity for tau deposits in Alzheimer's disease and non Alzheimer's disease tauopathies. Alzheimers Res Ther. 2014;6(1):11.
37. Chien DT, Szardenings AK, Bahri S, et al. Early clinical PET imaging results with the novel PHF-tau radioligand [F18]-T808. J Alzheimers Dis. 2014;38(1):171-84.

38. Langstrom B, Andren PE, Lindhe O, Svedberg M, Hall H. In vitro imaging techniques in neurodegenerative diseases. Mol Imaging Biol. 2007;9(4):161-75.
39. Laruelle M, Slifstein M, Huang Y. Relationships between radiotracer properties and image quality in molecular imaging of the brain with positron emission tomography. Mol Imaging Biol. 2003;5(6):363-75.
40. Pike VW. PET radiotracers: crossing the blood-brain barrier and surviving metabolism. Trends Pharmacol Sci. 2009;30(8):431-40.
41. Kouri N, Whitwell JL, Josephs KA, Rademakers R, Dickson DW. Corticobasal degeneration: a pathologically distinct 4R tauopathy. Nat Rev Neurol. 2011;7(5):263-72.
42. Mukaetova-Ladinska EB, Harrington CR, Roth M, Wischik CM. Alterations in tau protein metabolism during normal aging. Dementia. 1996;7(2):95-103.
43. Wu L, Rosa-Neto P, Gauthier S. Use of biomarkers in clinical trials of Alzheimer disease: from concept to application. Mol Diagn Ther. 2011;15(6):313-25.
44. Braak H, Del Tredici K. The pathological process underlying Alzheimer's disease in individuals under thirty. Acta Neuropathol. 2011;121(2):171-81.
45. Villemagne VL. The challenges of tau imaging. Future Neurol. 2012;7(4):409-21.
46. Wegmann S, Jung YJ, Chinnathambi S, Mandelkow EM, Mandelkow E, Muller DJ. Human tau isoforms assemble into ribbon-like fibrils that display polymorphic structure and stability. J Biol Chem. 2010;285(35):27302-13.
47. Martin L, Latypova X, Terro F. Post-translational modifications of tau protein: implications for Alzheimer's disease. Neurochem Int. 2011;58(4):458-71.
48. Braak H, Braak E. Frequency of stages of Alzheimer-related lesions in different age categories. Neurobiol Aging. 1997;18(4):351-7.
49. Knopman DS, Parisi JE, Salviati A, et al. Neuropathology of cognitively normal elderly. J Neuropathol Exp Neurol. 2003; 62(11):1087-95.

Capítulo IX. *Tracking neuroinflammation in Alzheimer's disease: the role of positron emission tomography imaging.*

No **capítulo IX** apresentamos o artigo publicado no periódico *Journal of Neuroinflammation.*

Além dos biomarcadores de PET β-amilóide (capítulos V-VII) e tau (capítulo VIII), outros PET radiofármacos para eventos fisiopatológicos não específicos da DA, podem fornecer assinaturas topográficas da doença. A neuroinflamação é um processo contínuo ao longo da progressão da DA. Neste capítulo revisamos os mecanismos envolvidos em processos neuroinflamatórios, os radiofármacos de PET atualmente disponíveis para a visualização de neuroinflamação e as estratégias terapêuticas envolvendo anti-inflamatórios não esteroides (NSAIDs, do inglês *Nonsteroidal anti-inflammatory drugs*) no contexto da DA. Além disso, discutimos o uso destes radiofármacos para acompanhamento da progressão da DA em função das alterações neuroinflamatórias.

Zimmer et al. Journal of Neuroinflammation 2014, 11:120
http://www.jneuroinflammation.com/content/11/1/120

JOURNAL OF NEUROINFLAMMATION

REVIEW Open Access

Tracking neuroinflammation in Alzheimer's disease: the role of positron emission tomography imaging

Eduardo Rigon Zimmer[1,2,3†], Antoine Leuzy[1,2†], Andréa Lessa Benedet[1,2,4], John Breitner[5], Serge Gauthier[2] and Pedro Rosa-Neto[1,2*]

Abstract

Alzheimer's disease (AD) has been reconceptualized as a dynamic pathophysiological process, where the accumulation of amyloid-beta (Aβ) is thought to trigger a cascade of neurodegenerative events resulting in cognitive impairment and, eventually, dementia. In addition to Aβ pathology, various lines of research have implicated neuroinflammation as an important participant in AD pathophysiology. Currently, neuroinflammation can be measured *in vivo* using positron emission tomography (PET) with ligands targeting diverse biological processes such as microglial activation, reactive astrocytes and phospholipase A2 activity. In terms of therapeutic strategies, despite a strong rationale and epidemiological studies suggesting that the use of non-steroidal anti-inflammatory drugs (NSAIDs) may reduce the prevalence of AD, clinical trials conducted to date have proven inconclusive. In this respect, it has been hypothesized that NSAIDs may only prove protective if administered early on in the disease course, prior to the accumulation of significant AD pathology. In order to test various hypotheses pertaining to the exact role of neuroinflammation in AD, studies in asymptomatic carriers of mutations deterministic for early-onset familial AD may prove of use. In this respect, PET ligands for neuroinflammation may act as surrogate markers of disease progression, allowing for the development of more integrative models of AD, as well as for the measuring of target engagement in the context of clinical trials using NSAIDs. In this review, we address the biological basis of neuroinflammatory changes in AD, underscore therapeutic strategies using anti-inflammatory compounds, and shed light on the possibility of tracking neuroinflammation *in vivo* using PET imaging ligands.

Keywords: Alzheimer's disease, Positron emission tomography, Neuroinflammation, Microglia, Astrocytes, Phospholipase A2, Amyloid-β, Hyperphosphorylated tau, Non-steroidal anti-inflammatory drugs, 18 kDa translocator protein

Background

Research advances over the past decade have led to the reconceptualization of Alzheimer's disease (AD) as a progressive pathophysiological process in which the accumulation of amyloid-beta (Aβ) is thought to trigger a cascade of neurodegenerative events, including the intracellular accumulation of hyperphosphorylated tau [1,2]. From a clinical standpoint, AD is viewed as a continuum, comprising a clinically silent phase [3] (characterized by cognitive normality in the presence of AD pathology), a prodromal mild cognitive impairment (MCI) phase [4]—during which individuals exhibit cognitive dysfunction, but of insufficient severity to meet criteria for dementia—and, finally, a dementia phase [5].

In addition to the pathological hallmarks of AD, Aβ and hyperphosphorylated tau, a growing body of literature points to neuroinflammation as an important player in the pathogenesis of AD. Following a set of classic studies implicating the complement factors C1q, C4 and C3 in the formation of amyloid plaques [6,7], activated microglia and the inflammatory cytokine IL-1 were found to be

* Correspondence: pedro.rosa@mcgill.ca
†Equal contributors
[1]Translational Neuroimaging Laboratory (TNL), McGill Center for Studies in Aging (MCSA), Douglas Mental Health University Institute, Montreal, QC H4H 1R3, Canada
[2]Alzheimer's Disease Research Unit, MCSA, Douglas Mental Health University Institute, Montreal, QC H4H 1R3, Canada
Full list of author information is available at the end of the article

BioMed Central

© 2014 Zimmer et al.; licensee BioMed Central Ltd. This is an Open Access article distributed under the terms of the Creative Commons Attribution License (http://creativecommons.org/licenses/by/4.0), which permits unrestricted use, distribution, and reproduction in any medium, provided the original work is properly credited. The Creative Commons Public Domain Dedication waiver (http://creativecommons.org/publicdomain/zero/1.0/) applies to the data made available in this article, unless otherwise stated.

elevated in AD patients [8,9]. In addition to its role in the promotion of astrogliosis [10,11], IL-1 is known to induce marked expression of the amyloid precursor protein (APP) gene [12] and α1-antichymotrypsin [13], both known components of amyloid plaques [14,15]. Further exploration of complement activation showed that while the opsonizing components were in proximity to amyloid plaques, the terminal components were associated with dystrophic neurites [16,17]. The importance of the complement system in AD was established shortly after, following the discovery that C1q possessed the ability to bind Aβ and its N-terminal fragments and thus to initiate neuroinflammation via activation of the classical complement pathway [18]. Since this early work, numerous post-mortem immunohistochemical, biochemical, and molecular studies have confirmed the presence of neuroinflammation in the brain of AD subjects (for review, see [19]).

A key issue regarding neuroinflammation in AD is whether this response is beneficial or detrimental in nature. While acute neuroinflammation seems to be an adaptive reaction aiming to restore brain integrity [20], chronic inflammation appears to be an injurious process, resulting in progressive neurodegeneration [21,22]. Clinical trials using non-steroidal anti-inflammatory drugs (NSAIDs) - initiated on the basis of numerous epidemiological studies suggesting that systemic use of NSAIDs can prevent or delay the onset of AD [23,24] - have yielded mixed or inconclusive results [25]. However, preliminary results from the Alzheimer's Disease Anti-inflammatory Prevention Trial (ADAPT) may suggest that NSAIDs can be beneficial only if administered early in the disease course, before any symptoms are evident [22]. While this *Janus face* of neuroinflammation in AD has yet to be fully understood, it is clear that neuroinflammation is an early and continuous process, present from preclinical through late stage AD [26-28].

Recently, positron emission tomography (PET) imaging agents targeting neuroinflammatory processes have been developed and offer the opportunity for non-invasive *in vivo* tracking of diverse brain inflammatory events (Table 1). Specifically, microglial activation, reactive astrocytosis and increased phospholipase activity are neuroinflammatory events amenable of quantification using PET imaging agents [29-31]. In addition to tracking the progression of AD as a function of neuroinflammatory response, the use of PET imaging agents may help shed light on the interplay between Aβ, hyperphosphorylated tau, and neuroinflammation, possibly leading to improved modeling of AD pathophysiology.

In this review, we describe some of the most important insights provided by PET imaging agents targeting neuroinflammation in AD, revise the evidence provided by preclinical and clinical trials using NSAIDs, and underscore the role that PET biomarkers may play in terms of the development of novel therapeutic strategies, monitoring of disease progression, as well as biomarkers of target engagement.

Imaging microglial activation using PET

Comprising approximately 10% of the cells within the central nervous system [46], microglia constitute the first line

Table 1 Positron emission tomography imaging agents for neuroinflammation

Process of interest	Biological target	Radiopharmaceutical	Reference
Microglial activation	18-kDa translocator protein	[^{11}C]PK11195	[32]
		[^{11}C]AC5216	[33]
		[^{11}C]PBR2806	[34]
		[^{11}C]DPA-713	[35]
		[^{11}C] DPA-714	[36]
		[^{11}C]MBMP	[37]
		[^{11}C]DAC	[38]
		[^{11}C]DAA1106	[39]
		[^{11}C]vinpocetine	[40]
		[^{18} F]PBR06	[41]
		[^{18} F]FEAC	[42]
		[^{18} F]FEDAC	[42]
		[^{18} F]DAA1106	[43]
Reactive astrocytes	Monoamine oxidase B	[^{11}C]-DED	[30]
		[^{11}C]Sch225336	[44]
Phospholipase A2 activity	Metabolism of arachidonic acid	1-[^{11}C]-AA	[31]
		[^{18} F]FAA	[45]

of defense against invading pathogens and other harmful agents. Under pathological conditions, microglial cells proliferate and migrate to the site of injury, acquiring phagocytic abilities and releasing various pro-inflammatory mediators [47-50]. In AD, reactive microglia in the vicinity of Aβ plaques have been repeatedly observed in both clinical [51,52] and experimental studies [53,54], with experimental models confirming Aβ-mediated release of various neurotoxic molecules by microglia [55-58]. In keeping with the biphasic hypothesis of neuroinflammation, however, additional studies have shown activated microglia to release neuroprotective cytokines such as transforming growth factor-β1, and there may be worsening of AD pathology following microglial inhibition [59].

Currently, PET imaging of microglial activation is possible using molecular agents targeting the 18 kDa translocator protein (TSPO), formerly named the peripheral benzodiazepine receptor (PBR) [60,61]. Located mainly in parenchymal glial cells, TSPO is present at low concentrations under normal physiological conditions [62], save for the ependyma, choroid plexus, and olfactory nerve layer of the olfactory bulb, which display high densities of TSPO receptors [63,64]. In response to neuroinflammation, however, TSPO levels undergo a dramatic increase, making it well-suited for assessment of microglial activation [62]. Indeed, numerous studies indicate TSPO to be a sensitive marker of reactive microglia and inflammation secondary to neurodegeneration, including of the AD type (for review see [65,66]).

Preclinical studies using PET ligands binding TSPO have been performed in transgenic (Tg) rodent models harboring human APP or tau pathogenic mutations. In the case of [^{11}C]PK11195 - the prototypical TSPO ligand - the number of available binding sites (B_{max}) was found to be significantly increased in the frontal cortex of AD post-mortem tissue, as compared to controls, while [^{3}H](R)-PK11195 binding correlated significantly with immunohistochemically labeled activated microglia [67]. Likewise, an age-dependent increase in [^{3}H](R)-PK11195 was noted in APP/PS1 Tg mice, in keeping with increased retention of [^{11}C](R)-PK11195 assessed using microPET, which was again correlated with the presence of activated microglia, as determined via histopathological assessment [67]. Similar work conducted using [^{11}C]AC-5216 [33], and [^{18}F]FEDAA1106 [68] - TSPO ligands which are optimized for improved blood-brain barrier permeability, affinity and, in the case of [^{11}C]AC-5216, kinetics - revealed increased TSPO signals in living Tg mice overexpressing human APP ($APP_{E6993\Delta}$) [69]. Importantly, the $APP_{E6993\Delta}$ model displays high levels of Aβ in the absence of fibrillary amyloid plaques [70], suggesting that amyloid dysmetabolism *per se* is sufficient to induce upregulation of TSPO-positive microglia.

Clinical studies using [^{11}C](R)-PK11195 in patients with mild-to-moderate AD have shown increased retention in the entorhinal, temporoparietal and posterior cingulate cortices, areas that show decreased glucose use, as measured with [^{18}F]DG-PET [71]. Furthermore, elevated microglial activation, as indexed by high [^{11}C](R)-PK11195 binding within cortical association and striatal regions (see Figure 1), was noted in a group of AD subjects with high Pittsburgh compound B ([^{11}C]PIB) retention, whose mini mental state examination (MMSE) scores were correlated negatively with microglial activation, but not with [^{11}C]PIB binding [29]. Additional studies have provided conflicting results [72]; however, it is possible that [^{11}C](R)-PK11195 sensitivity might be insufficient for detecting microglial activation present in mild-to-moderate AD [73]. In MCI, findings with [^{11}C](R)-PK11195 are inconclusive, with one study showing a small increase in PIB-positive patients relative to controls [74], but others studies reporting no increase, even among patients who subsequently converted to AD [72,73].

Among second generation TSPO radioligands, increased binding of [^{11}C]DAA1106 has been observed in AD, as compared to controls, though no correlation was found with respect to disease severity [75]. In a follow-up study among patients with MCI, the increased binding was associated with progression to AD over a 5-year follow-up period [39]. In the case of [^{11}C]PBR28, increased binding was noted in AD, but not MCI, despite the latter displaying cerebral amyloidosis and hippocampal atrophy using PIB-PET and magnetic resonance imaging (MRI) volumetry [76]. Furthermore, [^{11}C]PBR28 binding was shown to correlate with clinical severity and gray matter loss, particularly within regions exhibiting the highest density of TSPO [76] (see Figure 2). Finally, [^{11}C]PBR28 binding was found to be higher among patients with early-onset AD (<65 years), particularly within frontal and parietal regions, in keeping with studies showing greater frontoparietal atrophy in patients with early-onset AD [77-80]. Collectively, these findings with [^{11}C]PBR28 suggest that the increased expression of TSPO by activated microglia occurs after progression to AD, and continues as a function of disease progression, in those who develop disease symptoms at an early age.

Second-generation 18-kDa translocator protein ligands and the rs6971 polymorphism

In contrast to PET studies using [^{11}C]PK11195 - which binds with similar affinity across subjects [81] - interpretation of studies using second-generation ligands for the TSPO has been rendered difficult by substantial inter-individual variability in binding affinity, ranging from 4- to 50-fold [82]. Recently, a common single-nucleotide polymorphism (rs6971) in exon 4 of the

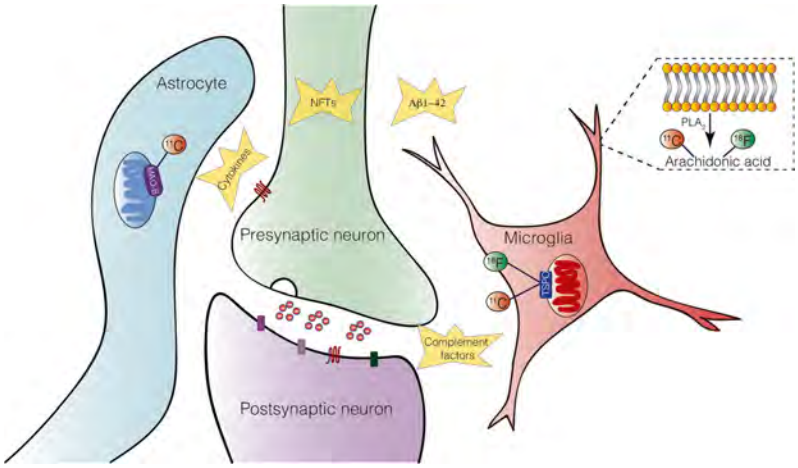

Figure 1 PET biological targets for measuring neuroinflammation in AD. Amyloid-beta $(Aβ)_{1–42}$ and neurofibrillary tangles (NFTs) - the classic hallmarks of Alzheimer's disease (AD) - can trigger neuroinflammatory changes, which induces the release of complement factors, cytokines and others inflammatory factors. Positron emission tomography (PET) uses biological surrogates for measuring neuroinflammation. Microglial activation is estimated by the expression of the 18-kDa translocator protein (TSPO), which is mainly found on the outer mitochondrial membrane of the microglial cells under inflammatory conditions. Monoamine oxidase-B (MAO-B), an enzyme usually located on the outer mitochondrial membrane of astrocytes, is proposed as an index of reactive astrocytosis. Radiolabeled arachidonic acid (AA), a phospholipid present in the cell membrane and cleaved by phospholipase A2 (PLA_2), can estimate the AA metabolism. AA is the precursor of eicosanoids - prostaglandins and leukotrienes - which are potent mediators of the inflammatory response.

TSPO gene has been identified as the key determinant of TSPO ligand affinity [83,84]. Based on the rs6971 polymorphism, subjects are currently divided in three groups: high-affinity binders (HAb), mixed-affinity binders (MAb) and low-affinity binders (LAb), with binding class determined on the basis of the number of high- versus low-affinity sites [81,82]. While the binding variation between HAb and MAb is around 30% [85], a difference approaching 80% has been observed between between HAb and LAb [76]. Adjusting for the rs6971 polymorphism - either via genotyping or by leucocyte binding assay - has been shown to result in more accurate quantitation of TSPO availability [76], as well as offering potential benefits of increased statistical power and smaller required sample size in the case of clinical studies (see Figure 3).

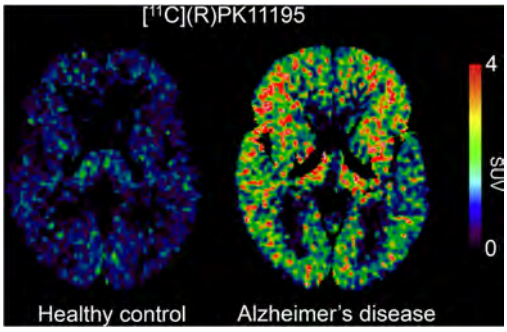

Figure 2 Illustrative [^{11}C](R)PK11195 PET imaging. Representative [^{11}C](R)PK11195 images in a healthy control (age 65 years) and in a patient with Alzheimer's disease (AD) dementia (age 68 years). The brain axial view shows increased [^{11}C](R)PK11195 binding in the AD subject (yellow-red spots) in comparison to the healthy control subject. Standardized uptake value (SUV) defined by the ratio of brain to reference region (supervised reference tissue extraction) radioactivity was used for estimating [^{11}C](R)PK11195 binding. Image provided by Dr Paul Edison of the Division of Brain Sciences, Department of Medicine, Imperial College London, UK.

Cannabinoid receptor type 2: a potential target for imaging microglial activation using PET

Under physiological conditions, the cannabinoid receptor type 2 (CB_2) is expressed in very low concentrations in the brain [86,87]. Recent studies, however, have demonstrated microglial overexpression of CB_2 in AD following Aβ deposition [88,89]. An attractive alternative to TSPO ligands, CB_2 radiopharmaceuticals, such as [^{11}C] Sch225336 [44] and [^{11}C]A-836339 [90], are potential imaging biomarkers for estimating activated microglia in the brain. Indeed, work using [^{11}C]A-836339 has provided the first *in vivo* evidence of CB_2 upregulation in APPswe/PS1dE9 mice [90], an animal model presenting Aβ deposition similar to that seen in AD. Moreover, preliminary findings highlight the CB_2 receptor as a potential therapeutic target, with use of selective CB_2 agonist

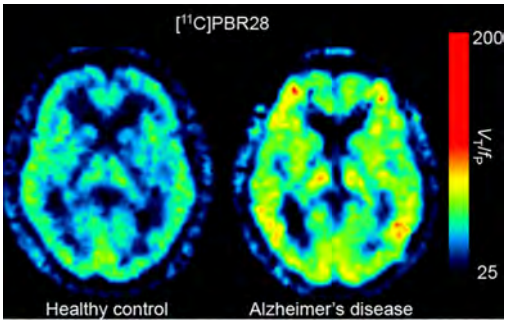

Figure 3 Illustrative [^{11}C]PBR28 PET imaging. Representative [^{11}C]PBR28 images in a healthy control (age 61 years) and in a patient with Alzheimer's disease (AD) dementia (age 57 years). The brain axial view show increased [^{11}C]PBR28 binding in the AD subject (yellow-red spots) in comparison to the healthy control subject. Of note, both subjects are high-affinity binders. Distribution volume corrected for free fraction of the radioligand in plasma (V_T/f_P) was used for estimating [^{11}C]PBR28 binding values. Image provided by Drs William Kreisl and Robert Innis of the Molecular Imaging Branch, National Institute of Mental Health-NIMH, USA.

shown to reduce microgliosis, promote Aβ clearance, and improve cognitive performance in both Tg APP 2576 mice [91] and in rats with cognitive impairment following bilateral microinjections of Aβ at the level of the hippocampus [92]. In addition, Tg amyloid mice lacking the CB_2 receptor have been shown to exhibit significantly increased levels of soluble $A\beta_{1-42}$ and plaque deposition [93]. Though the use CB_2 imaging agents may play a role in monitoring the effectiveness of CB_2-specific interventions, more studies are needed. The link between TSPO and CB_2 expression, however, remains elusive.

Imaging reactive astrocytes using PET

Astrocytes are the most prevalent cells in the central nervous system, outnumbering neurons by at least five-fold [94]. These specialized glial cells dynamically interact with neurons modulating diverse signaling pathways as well as synapse formation [95-97]. Similar to microglia, astrocytes become reactive in response to a variety of detrimental stimuli [98]. In AD, increased expression of glial fibrillary acidic protein (GFAP) is typically observed in immunohistochemical studies of post-mortem brain tissue, indicating an increased number of reactive astrocytes [99], with GFAP-positive astrocytes noted at the margins of amyloid deposits [100]. Though the astrocytic network is thought to exert a neuroprotective role via the sequestration/degradation of Aβ [101-105], its involvement is likewise believed to extend in deleterious directions, including the amplification of cortical amyloid deposition via propagation of intercellular calcium waves [106].

In PET imaging, the enzyme monoamine oxidase B (MAO-B) has been proposed as a biomarker for *in vivo* quantification of astrocytosis in AD [107]. Located on the outer mitochondrial membrane, MAO-B occurs predominantly in astrocytes [108,109], and can be imaged using 11C-deuterium-L-deprenyl ([^{11}C]-DED), a radiopharmaceutical exhibiting high affinity and specificity for MAO-B [110,111]. Catalyzing the oxidative deamination of catecholamines, MAO-B density has been shown to be highly expressed in astrocytes surrounding amyloid plaques [112] and seems to contribute to neurodegeneration by disrupting oxidative homeostasis [113].

Clinical studies using [^{11}C]DED have demonstrated increased tracer retention in MCI and AD, with binding highest among PIB + MCI individuals [30]. These findings suggest that reactive astrocytosis may be present early on in the course of AD, in keeping with previous hypotheses [99,114], as well as with findings of increased [^{11}C]DED binding in the earliest Braak stages of AD post-mortem tissue [115]. Several important factors remain unanswered with respect to this study, however. First, [^{11}C]DED binding may be underestimated since it is highly dependent on cerebral blood flow [111,116,117], a parameter known to be reduced in AD [118-121]. Moreover, it is unclear the degree to which the [^{11}C]DED signal represents reactive astrocytosis, since MAO-B is also found within serotonergic neurons and non-reactive astrocytes [108,109]. Another confounder that needs to be addressed is the fact that MAO-B seems to increase with age in almost all brain regions (with the exception of the cingulate gyrus) in healthy human subjects [111].

Imaging phospholipase A2 using PET

Microglia derived inflammatory cytokines are capable of binding astrocytic cytokine receptors that are coupled to cytosolic phospholipase A2 ($cPLA_2$), and secretory phospholipase A2 ($sPLA_2$) [122]. Activation of these Ca^{2+}-dependent enzymes results in the hydrolysis of membrane phospholipids, liberating arachidonic acid (AA) [123,124], itself a precursor of pro-inflammatory eicosanoids including prostaglandins and leukotrienes [125,126]. Moreover, nitric oxide, released as part of this reaction, can likewise promote AA hydrolysis via $cPLA_2$ via postsynaptic ionotropic N-methyl-D-aspartate glutamate receptors [127,128], as can Aβ [129,130]. Such mechanisms have been noted in AD, including increased expression of $cPLA_2$ and $sPLA_2$, elevated cytokine levels, increased glutamatergic markers and different forms of accumulated Aβ [129-131], as well as increased cerebrospinal fluid (CSF) levels of AA metabolites [132]. On the basis of these markers, AA metabolism has been hypothesized to be elevated in AD [31].

Preliminary results obtained using radiolabeled AA (1-[^{11}C]-AA) support this hypothesis, with elevated incorporation coefficients noted in neocortical areas shown to have high densities of neuritic plaques with activated

microglia [31]. To the extent that the elevated binding of 1-[^{11}C]-AA represents the upregulation of AA metabolism, PET with 1-[^{11}C]-AA may prove of use in the assessment of investigations in patients with AD.

Neuroinflammation as a therapeutic target in AD

Following an initial report of unexpectedly low prevalence of AD among patients with rheumatoid arthritis [133], numerous epidemiological studies have indicated a reduced incidence of AD among users of NSAIDs (for a review, see [134]). A systematic review suggests that duration of NSAID use of at least 2 years is required to reduce risk estimates [135], while the apparent protective effects of NSAIDs is diminished among older individuals, even to the point of disappearance [136,137] or, in one study, reversal [138]. The apparent protective effect may also be more pronounced among carriers of the apolipoprotein E (*APOE*) ε4 allele [24,137,139,140]. In general, non-aspirin compounds have been associated with greater protective effects, relative to aspirin compounds [134], and no protective effects have been suggested among users of acetaminophen [141].

Several mechanisms have been proposed to explain the possible protective effects of NSAIDs in AD, including the reduction of brain inflammation by inhibition of cyclooxygenase (COX)-mediated synthesis of pro-inflammatory prostaglandins [101]. Indeed, the beneficial effects of NSAIDs on memory performance in transgenic mouse models of AD have been proposed to relate directly to their blockade of COX activity [102-105,142,143], and not to their ability to lower levels of inflammatory cytokines, TNF-α or IL-1β [144]. A second proposed mechanistic hypothesis pertains to the ability of NSAIDs to inhibit processing of the APP or the production or aggregation of Aβ. A subset of NSAIDs (including ibuprofen and indomethacin) have been shown *in vitro* and in APP-Tg mouse models to preferentially lower levels of amyloidogenic $A\beta_{1-42}$, independently of their COX-inhibiting activity [145]. These NSAIDs are thought to stimulate non-amyloidogenic processing of APP via enhancement of α-secretase activity [146], to decrease secretion of Aβ in cell lines stimulated with pro-inflammatory cytokines [147], and to decrease the expression of α1-antichymotrypsin, an acute phase protein known to accelerate the development of amyloid pathology in APP-Tg mice [148]. It is noteworthy, however, that a large meta-analysis of NSAID use in human samples has failed to show a distinction between those NSAIDs that modulate γ-secretase activity *in v*itro and others, and between ibuprofen and naproxen in particular [149]. Finally, NSAIDs that are known to inhibit the multimerization of Aβ *in vitro* [150] may also inhibit the aggregation of Aβ via direct interaction [151], although human neuropathological studies have failed to show this [152,153].

The hypothesis that neuroinflammation plays a role in the pathogenesis of AD - and that its suppression via the use of anti-inflammatory compounds may prevent or delay the onset of AD - provided the rationale for a series of clinical trials utilizing various anti-inflammatory drugs [154]. While initial pilot studies using indomethacin (a COX-1 preferential inhibitor) and diclofenac (a non-selective COX inhibitor) combined with the gastroprotective agent misoprostol, suggested benefits in mild-to-moderate AD [155,156], gastrointestinal problems (a side effect commonly associated with inhibition of COX1) resulted in a high drop-out rate. Follow-up studies with nimesulide [157], celecoxib [158] or rofecoxib [159,160] - selective COX-2 inhibitors - showed no therapeutic effect [157-160]. Likewise, despite encouraging results in animal models, a 1-year clinical trial using the non-selective COX inhibitor ibuprofen showed no significant overall effects on cognitive and clinical outcomes in patients with mild-to-moderate AD (although positive results were seen in *APOE* ε4 carriers, with the opposite pattern observed in non-carriers) [161]. A primary prevention trial (ADAPT) using naproxen (mixed COX-1/COX-2 inhibitor) and celecoxib (selective COX-2 inhibitor) in individuals at risk for AD was terminated early due to perceived cardiovascular side effects [162], but with results that suggested that these NSAIDs may in fact accelerate disease progression if initiated in individuals already displaying MCI or substantial AD pathophysiology without symptoms. Their use among individuals without AD pathophysiology may prove beneficial, however; a hypothesis supported by CSF biomarker values obtained at 21 to 42 months follow-up [134].

Though the failure of clinical trials using NSAIDs has been ascribed to timing of intervention, duration of treatment, dosage, and drug class, the underlying problem remains the lack of consensus surrounding whether neuroinflammation causes neurodegeneration in AD, or is simply a protective response to primary pathological processes. At present, these findings offer only limited data making it difficult to evaluate the therapeutic utility of NSAIDs in AD. However, piecing together findings from preclinical work in AD-like Tg models, the finding of protective effects in *APOE* ε4 carriers and the overall results of the ADAPT trial, it seems likely that NSAIDs may exert a protective effect but only if administered early on in the disease course. Further studies are required to provide support for this idea.

Potential role of PET in monitoring responsivity to anti-inflammatory therapies in AD

The literature suggests that neuroinflammation occurs early in the course of AD, likely as a response to Aβ and pathologically phosphorylated forms of tau, and that early use of NSAIDs may prove effective in individuals

with minimal AD pathology and/or carriers of the *APOE* ε4 allele. Indeed, results from a masked long-term follow-up of the ADAPT cohort seemed to confirm this idea. The difficulty with early initiation of treatment, however, lies in recognizing those who have already experienced pre-symptomatic disease onset. In this respect, studies in asymptomatic carriers of mutations deterministic for early-onset familial AD may prove helpful, given the recent suggestion of the order in which biomarkers reach abnormal levels in this population [163], and that the clinical evolution of early-onset familial AD is highly predictable within a kindred, especially for age at onset [164]. Imaging of neuroinflammation in this population using PET, alongside CSF and plasma markers, may allow for a more integrative AD biomarker model [2,165], particularly with respect to the interplay between glial activation, seeding of Aβ and hyperphosphorylated tau species, and cognitive decline. Moreover, TSPO ligands may prove sensitive to early AD pathophysiological changes in the form of toxic Aβ oligomers [166], changes that lie below the detection threshold of current *in vivo* AD biomarkers [2]. In the context of clinical trials using NSAIDs (compounds that retain therapeutic potential despite the general failure of trials conducted to date, particularly since they are relatively safe and highly available), PET could serve to demonstrate target engagement in addition to proving topographical information, critical information lacking from fluid- and plasma-based biomarkers. The reproducibility of TSPO binding, however, remains under debate [167,168]. In this respect, clinical trials addressing this issue are currently underway, and will hopefully provide results clarifying the test-retest reliability of TSPO ligands [169,170].

Concluding remarks and future directions

In general, the continued study of inflammatory mechanisms, including in particular the use of PET imaging for tracking neuroinflammatory changes, seems to have a promising role in AD. To date, radioisotopic probes targeting neuroinflammation have demonstrated encouraging results in preclinical and clinical studies, with these radiopharmaceuticals holding promise for inclusion as surrogate markers of disease progression in the next generation of clinical trials using anti-inflammatory therapies. Importantly, novel approaches aiming to augment the sensitivity of these PET imaging agents may be required, with inclusion of vascular [171] and genetic [172,173] covariates likely to strengthen the value of PET outcomes.

Abbreviations

[^{11}C]-DED: 11C-deuterium-L-deprenyl; [^{11}C]PIB: Pittsburgh compound B; Aβ: amyloid-beta; AA: arachidonic acid; AD: Alzheimer's disease; ADAPT: Alzheimer's Disease Anti-inflammatory Prevention Trial; *APOE*: apolipoprotein E; APP: amyloid precursor protein; CB_2: cannabinoid receptor type 2; COX: cyclooxygenase; $cPLA_2$: cytosolic phospholipase A2; CSF: cerebrospinal fluid; GFAP: glial fibrillary acidic protein; HAb: high-affinity binders; IL: interleukin; LAb: low-affinity binders; MAb: mixed-affinity binders; MAO-B: monoamine oxidase B; MCI: mild cognitive impairment; NSAID: non-steroidal anti-inflammatory drug; PBR: peripheral benzodiazepine receptor; PET: positron emission tomography; $sPLA_2$: secretory phospholipase A2; Tg: transgenic; TNF: tumor necrosis factor; TSPO: 18 kDa translocator protein.

Competing interests

The authors declare that they have no competing interests.

Authors' contributions

ERZ and AL were responsible for the conception and design of the review, and for drafting and revising the manuscript. ALB, JB, SG and PRN were responsible for revising the manuscript. All authors read and approved the final manuscript.

Acknowledgments

This work was supported by the Canadian Institutes of Health Research (CIHR; MOP-11-51-31), Alzheimer's Association (NIRG-08-92090), Fonds de Recherche du Québec - Santé (FRSQ; Chercheur Boursier), the Allan Tiffin Trust (Infrastructure), the Conselho Nacional de Desenvolvimento Científico e Tecnológico (CNPq, Brazil), Fundação de Amparo à Pesquisa do Rio Grande do Sul (Fapergs, Brazil), and INCT for Excitotoxicity and Neuroprotection/CNPq. The authors wish to thank Dr Paul Edison and Drs William Kreisl and Robert Innis for providing Figures 2 and 3, respectively.

Author details

[1]Translational Neuroimaging Laboratory (TNL), McGill Center for Studies in Aging (MCSA), Douglas Mental Health University Institute, Montreal, QC H4H 1R3, Canada. [2]Alzheimer's Disease Research Unit, MCSA, Douglas Mental Health University Institute, Montreal, QC H4H 1R3, Canada. [3]Department of Biochemistry, Federal University of Rio Grande do Sul (UFRGS), Porto Alegre, Brazil. [4]CAPES Foundation, Ministry of Education of Brazil, Brasília, Brazil. [5]Centre for Studies on Prevention of Alzheimer's Disease, Douglas Mental Health University Institute, Montreal, QC H4H 1R3, Canada.

Received: 13 May 2014 Accepted: 20 June 2014
Published: 8 July 2014

References

1. Hardy J, Selkoe DJ: **The amyloid hypothesis of Alzheimer's disease: progress and problems on the road to therapeutics.** *Science* 2002, **297:**353–356.
2. Jack CR Jr, Knopman DS, Jagust WJ, Petersen RC, Weiner MW, Aisen PS, Shaw LM, Vemuri P, Wiste HJ, Weigand SD, Lesnick TG, Pankratz VS, Donohue MC, Trojanowski JQ: **Tracking pathophysiological processes in Alzheimer's disease: an updated hypothetical model of dynamic biomarkers.** *Lancet Neurol* 2013, **12:**207–216.
3. Sperling RA, Aisen PS, Beckett LA, Bennett DA, Craft S, Fagan AM, Iwatsubo T, Jack CR Jr, Kaye J, Montine TJ, Park DC, Reiman EM, Rowe CC, Siemers E, Stern Y, Yaffe K, Carrillo MC, Thies B, Morrison-Bogorad M, Wagster MV, Phelps CH: **Toward defining the preclinical stages of Alzheimer's disease: recommendations from the National Institute on Aging-Alzheimer's Association workgroups on diagnostic guidelines for Alzheimer's disease.** *Alzheimers Dement* 2011, **7:**280–292.
4. Albert MS, DeKosky ST, Dickson D, Dubois B, Feldman HH, Fox NC, Gamst A, Holtzman DM, Jagust WJ, Petersen RC, Snyder PJ, Carrillo MC, Thies B, Phelps CH: **The diagnosis of mild cognitive impairment due to Alzheimer's disease: recommendations from the National Institute on Aging-Alzheimer's Association workgroups on diagnostic guidelines for Alzheimer's disease.** *Alzheimers Dement* 2011, **7:**270–279.
5. McKhann GM, Knopman DS, Chertkow H, Hyman BT, Jack CR Jr, Kawas CH, Klunk WE, Koroshetz WJ, Manly JJ, Mayeux R, Mohs RC, Morris JC, Rossor MN, Scheltens P, Carrillo MC, Thies B, Weintraub S, Phelps CH: **The diagnosis of dementia due to Alzheimer's disease: recommendations from the National Institute on Aging-Alzheimer's Association workgroups on diagnostic guidelines for Alzheimer's disease.** *Alzheimers Dement* 2011, **7:**263–269.

6. Eikelenboom P, Stam FC: **Immunoglobulins and complement factors in senile plaques. An immunoperoxidase study.** *Acta Neuropathol* 1982, **57:**239–242.
7. Eikelenboom P, Hack CE, Rozemuller JM, Stam FC: **Complement activation in amyloid plaques in Alzheimer's dementia.** *Virchows Arch B Cell Pathol Incl Mol Pathol* 1989, **56:**259–262.
8. Griffin WS, Stanley LC, Ling C, White L, MacLeod V, Perrot LJ, White CL 3rd, Araoz C: **Brain interleukin 1 and S-100 immunoreactivity are elevated in Down syndrome and Alzheimer disease.** *Proc Natl Acad Sci U S A* 1989, **86:**7611–7615.
9. Eikelenboom P, van Gool WA: **Neuroinflammatory perspectives on the two faces of Alzheimer's disease.** *J Neural Transm* 2004, **111:**281–294.
10. Giulian D, Lachman LB: **Interleukin-1 stimulation of astroglial proliferation after brain injury.** *Science* 1985, **228:**497–499.
11. Giulian D, Woodward J, Young DG, Krebs JF, Lachman LB: **Interleukin-1 injected into mammalian brain stimulates astrogliosis and neovascularization.** *J Neurosci* 1988, **8:**2485–2490.
12. Goldgaber D, Harris HW, Hla T, Maciag T, Donnelly RJ, Jacobsen JS, Vitek MP, Gajdusek DC: **Interleukin 1 regulates synthesis of amyloid beta-protein precursor mRNA in human endothelial cells.** *Proc Natl Acad Sci U S A* 1989, **86:**7606–7610.
13. Perlmutter DH, Dinarello CA, Punsal PI, Colten HR: **Cachectin/tumor necrosis factor regulates hepatic acute-phase gene expression.** *J Clin Invest* 1986, **78:**1349–1354.
14. Masters CL, Simms G, Weinman NA, Multhaup G, McDonald BL, Beyreuther K: **Amyloid plaque core protein in Alzheimer disease and Down syndrome.** *Proc Natl Acad Sci U S A* 1985, **82:**4245–4249.
15. Abraham CR, Selkoe DJ, Potter H: **Immunochemical identification of the serine protease inhibitor alpha 1-antichymotrypsin in the brain amyloid deposits of Alzheimer's disease.** *Cell* 1988, **52:**487–501.
16. McGeer PL, Akiyama H, Itagaki S, McGeer EG: **Immune system response in Alzheimer's disease.** *Can J Neurol Sci* 1989, **16:**516–527.
17. McGeer PL, Akiyama H, Itagaki S, McGeer EG: **Activation of the classical complement pathway in brain tissue of Alzheimer patients.** *Neurosci Lett* 1989, **107:**341–346.
18. Rogers J, Cooper NR, Webster S, Schultz J, McGeer PL, Styren SD, Civin WH, Brachova L, Bradt B, Ward P: **Complement activation by beta-amyloid in Alzheimer disease.** *Proc Natl Acad Sci U S A* 1992, **89:**10016–10020.
19. Akiyama H, Barger S, Barnum S, Bradt B, Bauer J, Cole GM, Cooper NR, Eikelenboom P, Emmerling M, Fiebich BL, Finch CE, Frautschy S, Griffin WS, Hampel H, Hull M, Landreth G, Lue L, Mrak R, Mackenzie IR, McGeer PL, O'Banion MK, Pachter J, Pasinetti G, Plata-Salaman C, Rogers J, Rydel R, Shen Y, Streit W, Strohmeyer R, Tooyoma I, Van Muiswinkel FL, Veerhuis R, Walker D, Webster S, Wegrzyniak B, Wenk G, Wyss-Coray T: **Inflammation and Alzheimer's disease.** *Neurobiol Aging* 2000, **21:**383–421.
20. Wyss-Coray T, Mucke L: **Inflammation in neurodegenerative disease - a double-edged sword.** *Neuron* 2002, **35:**419–432.
21. Mrak RE, Griffin WS: **Glia and their cytokines in progression of neurodegeneration.** *Neurobiol Aging* 2005, **26:**349–354.
22. Hoozemans JJ, Veerhuis R, Rozemuller JM, Eikelenboom P: **Soothing the inflamed brain: effect of non-steroidal anti-inflammatory drugs on Alzheimer's disease pathology.** *CNS Neurol Disord Drug Targets* 2011, **10:**57–67.
23. McGeer PL, Schulzer M, McGeer EG: **Arthritis and anti-inflammatory agents as possible protective factors for Alzheimer's disease: a review of 17 epidemiologic studies.** *Neurology* 1996, **47:**425–432.
24. in t' Veld BA, Ruitenberg A, Hofman A, Launer LJ, van Duijn CM, Stijnen T, Breteler MM, Stricker BH: **Nonsteroidal antiinflammatory drugs and the risk of Alzheimer's disease.** *N Engl J Med* 2001, **345:**1515–1521.
25. Hoozemans JJ, Veerhuis R, Rozemuller AJ, Eikelenboom P: **Non-steroidal anti-inflammatory drugs and cyclooxygenase in Alzheimer's disease.** *Curr Drug Targets* 2003, **4:**461–468.
26. Arends YM, Duyckaerts C, Rozemuller JM, Eikelenboom P, Hauw JJ: **Microglia, amyloid and dementia in alzheimer disease. A correlative study.** *Neurobiol Aging* 2000, **21:**39–47.
27. Vehmas AK, Kawas CH, Stewart WF, Troncoso JC: **Immune reactive cells in senile plaques and cognitive decline in Alzheimer's disease.** *Neurobiol Aging* 2003, **24:**321–331.
28. Hoozemans JJ, van Haastert ES, Veerhuis R, Arendt T, Scheper W, Eikelenboom P, Rozemuller AJ: **Maximal COX-2 and ppRb expression in neurons occurs during early Braak stages prior to the maximal activation of astrocytes and microglia in Alzheimer's disease.** *J Neuroinflammation* 2005, **2:**27.
29. Edison P, Archer HA, Gerhard A, Hinz R, Pavese N, Turkheimer FE, Hammers A, Tai YF, Fox N, Kennedy A, Rossor M, Brooks DJ: **Microglia, amyloid, and cognition in Alzheimer's disease: An [11C](R)PK11195-PET and [11C]PIB-PET study.** *Neurobiol Dis* 2008, **32:**412–419.
30. Carter SF, Scholl M, Almkvist O, Wall A, Engler H, Langstrom B, Nordberg A: **Evidence for astrocytosis in prodromal Alzheimer disease provided by 11C-deuterium-L-deprenyl: a multitracer PET paradigm combining 11C-Pittsburgh compound B and 18F-FDG.** *J Nucl Med* 2012, **53:**37–46.
31. Esposito G, Giovacchini G, Liow JS, Bhattacharjee AK, Greenstein D, Schapiro M, Hallett M, Herscovitch P, Eckelman WC, Carson RE, Rapoport SI: **Imaging neuroinflammation in Alzheimer's disease with radiolabeled arachidonic acid and PET.** *J Nucl Med* 2008, **49:**1414–1421.
32. Hashimoto K, Inoue O, Suzuki K, Yamasaki T, Kojima M: **Synthesis and evaluation of 11C-PK 11195 for in vivo study of peripheral-type benzodiazepine receptors using positron emission tomography.** *Ann Nucl Med* 1989, **3:**63–71.
33. Zhang MR, Kumata K, Maeda J, Yanamoto K, Hatori A, Okada M, Higuchi M, Obayashi S, Suhara T, Suzuki K: **11C-AC-5216: a novel PET ligand for peripheral benzodiazepine receptors in the primate brain.** *J Nucl Med* 2007, **48:**1853–1861.
34. Brown AK, Fujita M, Fujimura Y, Liow JS, Stabin M, Ryu YH, Imaizumi M, Hong J, Pike VW, Innis RB: **Radiation dosimetry and biodistribution in monkey and man of 11C-PBR28: a PET radioligand to image inflammation.** *J Nucl Med* 2007, **48:**2072–2079.
35. Chauveau F, Van Camp N, Dolle F, Kuhnast B, Hinnen F, Damont A, Boutin H, James M, Kassiou M, Tavitian B: **Comparative evaluation of the translocator protein radioligands 11C-DPA-713, 18F-DPA-714, and 11C-PK11195 in a rat model of acute neuroinflammation.** *J Nucl Med* 2009, **50:**468–476.
36. Doorduin J, Klein HC, Dierckx RA, James M, Kassiou M, de Vries EF: **[11C]-DPA-713 and [18F]-DPA-714 as new PET tracers for TSPO: a comparison with [11C]-(R)-PK11195 in a rat model of herpes encephalitis.** *Mol Imaging Biol* 2009, **11:**386–398.
37. Tiwari AK, Yui J, Fujinaga M, Kumata K, Shimoda Y, Yamasaki T, Xie L, Hatori A, Maeda J, Nengaki N, Zhang MR: **Characterization of a novel acetamidobenzoxazolone-based PET ligand for translocator protein (18 kDa) imaging of neuroinflammation in the brain.** *J Neurochem* 2014, **129:**712–720.
38. Yanamoto K, Yamasaki T, Kumata K, Yui J, Odawara C, Kawamura K, Hatori A, Inoue O, Yamaguchi M, Suzuki K, Zhang MR: **Evaluation of N-benzyl-N-[11C] methyl-2-(7-methyl-8-oxo-2-phenyl-7,8-dihydro-9H-purin-9-yl)acetamide ([11C]DAC) as a novel translocator protein (18 kDa) radioligand in kainic acid-lesioned rat.** *Synapse* 2009, **63:**961–971.
39. Yasuno F, Kosaka J, Ota M, Higuchi M, Ito H, Fujimura Y, Nozaki S, Takahashi S, Mizukami K, Asada T, Suhara T: **Increased binding of peripheral benzodiazepine receptor in mild cognitive impairment-dementia converters measured by positron emission tomography with [11C]DAA1106.** *Psychiatry Res* 2012, **203:**67–74.
40. Gulyas B, Halldin C, Vas A, Banati RB, Shchukin E, Finnema S, Tarkainen J, Tihanyi K, Szilagyi G, Farde L: **[11C]vinpocetine: a prospective peripheral benzodiazepine receptor ligand for primate PET studies.** *J Neurol Sci* 2005, **229–230:**219–223.
41. Fujimura Y, Zoghbi SS, Simeon FG, Taku A, Pike VW, Innis RB, Fujita M: **Quantification of translocator protein (18 kDa) in the human brain with PET and a novel radioligand, (18)F-PBR06.** *J Nucl Med* 2009, **50:**1047–1053.
42. Yui J, Maeda J, Kumata K, Kawamura K, Yanamoto K, Hatori A, Yamasaki T, Nengaki N, Higuchi M, Zhang MR: **18F-FEAC and 18F-FEDAC: PET of the monkey brain and imaging of translocator protein (18 kDa) in the infarcted rat brain.** *J Nucl Med* 2010, **51:**1301–1309.
43. Varrone A, Mattsson P, Forsberg A, Takano A, Nag S, Gulyas B, Borg J, Boellaard R, Al-Tawil N, Eriksdotter M, Zimmermann T, Schultze-Mosgau M, Thiele A, Hoffmann A, Lammertsma AA, Halldin C: **In vivo imaging of the 18-kDa translocator protein (TSPO) with [18F]FEDAA1106 and PET does not show increased binding in Alzheimer's disease patients.** *Eur J Nucl Med Mol Imaging* 2013, **40:**921–931.
44. Evens N, Bosier B, Lavey BJ, Kozlowski JA, Vermaelen P, Baudemprez L, Busson R, Lambert DM, Van Laere K, Verbruggen AM, Bormans GM: **Labelling and biological evaluation of [(11)C]methoxy-Sch225336: a radioligand for the cannabinoid-type 2 receptor.** *Nucl Med Biol* 2008, **35:**793–800.

45. Nagatsugi F, Hokazono J, Sasaki S, Maeda M: **20-[18F]fluoroarachidonic acid: tissue biodistribution and incorporation into phospholipids.** *Biol Pharm Bull* 1996, **19:**1316–1321.
46. Solito E, Sastre M: **Microglia function in Alzheimer's disease.** *Front Pharmacol* 2012, **3:**14.
47. Chan WY, Kohsaka S, Rezaie P: **The origin and cell lineage of microglia: new concepts.** *Brain Res Rev* 2007, **53:**344–354.
48. Nimmerjahn A, Kirchhoff F, Helmchen F: **Resting microglial cells are highly dynamic surveillants of brain parenchyma in vivo.** *Science* 2005, **308:**1314–1318.
49. Ransohoff RM, Perry VH: **Microglial physiology: unique stimuli, specialized responses.** *Annu Rev Immunol* 2009, **27:**119–145.
50. Fetler L, Amigorena S: **Neuroscience: Brain under surveillance: the microglia patrol.** *Science* 2005, **309:**392–393.
51. Rogers J, Luber-Narod J, Styren SD, Civin WH: **Expression of immune system-associated antigens by cells of the human central nervous system: relationship to the pathology of Alzheimer's disease.** *Neurobiol Aging* 1988, **9:**339–349.
52. Styren SD, Civin WH, Rogers J: **Molecular, cellular, and pathologic characterization of HLA-DR immunoreactivity in normal elderly and Alzheimer's disease brain.** *Exp Neurol* 1990, **110:**93–104.
53. Frautschy SA, Yang F, Irrizarry M, Hyman B, Saido TC, Hsiao K, Cole GM: **Microglial response to amyloid plaques in APPsw transgenic mice.** *Am J Pathol* 1998, **152:**307–317.
54. Stalder M, Phinney A, Probst A, Sommer B, Staufenbiel M, Jucker M: **Association of microglia with amyloid plaques in brains of APP23 transgenic mice.** *Am J Pathol* 1999, **154:**1673–1684.
55. Combs CK, Johnson DE, Cannady SB, Lehman TM, Landreth GE: **Identification of microglial signal transduction pathways mediating a neurotoxic response to amyloidogenic fragments of beta-amyloid and prion proteins.** *J Neurosci* 1999, **19:**928–939.
56. Combs CK, Johnson DE, Karlo JC, Cannady SB, Landreth GE: **Inflammatory mechanisms in Alzheimer's disease: inhibition of beta-amyloid-stimulated proinflammatory responses and neurotoxicity by PPARgamma agonists.** *J Neurosci* 2000, **20:**558–567.
57. Klegeris A, McGeer PL: **Beta-amyloid protein enhances macrophage production of oxygen free radicals and glutamate.** *J Neurosci Res* 1997, **49:**229–235.
58. McDonald DR, Brunden KR, Landreth GE: **Amyloid fibrils activate tyrosine kinase-dependent signaling and superoxide production in microglia.** *J Neurosci* 1997, **17:**2284–2294.
59. Prokop S, Miller KR, Heppner FL: **Microglia actions in Alzheimer's disease.** *Acta Neuropathol* 2013, **126:**461–477.
60. Papadopoulos V, Baraldi M, Guilarte TR, Knudsen TB, Lacapere JJ, Lindemann P, Norenberg MD, Nutt D, Weizman A, Zhang MR, Gavish M: **Translocator protein (18 kDa): new nomenclature for the peripheral-type benzodiazepine receptor based on its structure and molecular function.** *Trends Pharmacol Sci* 2006, **27:**402–409.
61. Venneti S, Lopresti BJ, Wiley CA: **The peripheral benzodiazepine receptor (Translocator protein 18 kDa) in microglia: from pathology to imaging.** *Prog Neurobiol* 2006, **80:**308–322.
62. Chen MK, Guilarte TR: **Translocator protein 18 kDa (TSPO): molecular sensor of brain injury and repair.** *Pharmacol Ther* 2008, **118:**1–17.
63. Anholt RR, Pedersen PL, De Souza EB, Snyder SH: **The peripheral-type benzodiazepine receptor: localization to the mitochondrial outer membrane.** *J Biol Chem* 1986, **261:**576–583.
64. Cymerman U, Pazos A, Palacios JM: **Evidence for species differences in 'peripheral' benzodiazepine receptors: an autoradiographic study.** *Neurosci Lett* 1986, **66:**153–158.
65. Ching AS, Kuhnast B, Damont A, Roeda D, Tavitian B, Dolle F: **Current paradigm of the 18-kDa translocator protein (TSPO) as a molecular target for PET imaging in neuroinflammation and neurodegenerative diseases.** *Insights Imaging* 2012, **3:**111–119.
66. Jacobs AH, Tavitian B, INMiND consortium: **Noninvasive molecular imaging of neuroinflammation.** *J Cereb Blood Flow Metab* 2012, **32:**1393–1415.
67. Venneti S, Lopresti BJ, Wang G, Hamilton RL, Mathis CA, Klunk WE, Apte UM, Wiley CA: **PK11195 labels activated microglia in Alzheimer's disease and in vivo in a mouse model using PET.** *Neurobiol Aging* 2009, **30:**1217–1226.
68. Zhang MR, Maeda J, Ogawa M, Noguchi J, Ito T, Yoshida Y, Okauchi T, Obayashi S, Suhara T, Suzuki K: **Development of a new radioligand, N-(5-fluoro-2-phenoxyphenyl)-N-(2-[18F]fluoroethyl-5-methoxybenzyl) acetamide, for pet imaging of peripheral benzodiazepine receptor in primate brain.** *J Med Chem* 2004, **47:**2228–2235.
69. Maeda J, Zhang MR, Okauchi T, Ji B, Ono M, Hattori S, Kumata K, Iwata N, Saido TC, Trojanowski JQ, Lee VM, Staufenbiel M, Tomiyama T, Mori H, Fukumura T, Suhara T, Higuchi M: **In vivo positron emission tomographic imaging of glial responses to amyloid-beta and tau pathologies in mouse models of Alzheimer's disease and related disorders.** *J Neurosci* 2011, **31:**4720–4730.
70. Sturchler-Pierrat C, Abramowski D, Duke M, Wiederhold KH, Mistl C, Rothacher S, Ledermann B, Burki K, Frey P, Paganetti PA, Waridel C, Calhoun ME, Jucker M, Probst A, Staufenbiel M, Sommer B: **Two amyloid precursor protein transgenic mouse models with Alzheimer disease-like pathology.** *Proc Natl Acad Sci U S A* 1997, **94:**13287–13292.
71. Cagnin A, Brooks DJ, Kennedy AM, Gunn RN, Myers R, Turkheimer FE, Jones T, Banati RB: **In-vivo measurement of activated microglia in dementia.** *Lancet* 2001, **358:**461–467.
72. Schuitemaker A, Kropholler MA, Boellaard R, van der Flier WM, Kloet RW, van der Doef TF, Knol DL, Windhorst AD, Luurtsema G, Barkhof F, Jonker C, Lammertsma AA, Scheltens P, van Berckel BN: **Microglial activation in Alzheimer's disease: an (R)-[^{11}C]PK11195 positron emission tomography study.** *Neurobiol Aging* 2013, **34:**128–136.
73. Wiley CA, Lopresti BJ, Venneti S, Price J, Klunk WE, DeKosky ST, Mathis CA: **Carbon 11-labeled Pittsburgh Compound B and carbon 11-labeled (R)-PK11195 positron emission tomographic imaging in Alzheimer disease.** *Arch Neurol* 2009, **66:**60–67.
74. Okello A, Edison P, Archer HA, Turkheimer FE, Kennedy J, Bullock R, Walker Z, Kennedy A, Fox N, Rossor M, Brooks DJ: **Microglial activation and amyloid deposition in mild cognitive impairment: a PET study.** *Neurology* 2009, **72:**56–62.
75. Yasuno F, Ota M, Kosaka J, Ito H, Higuchi M, Doronbekov TK, Nozaki S, Fujimura Y, Koeda M, Asada T, Suhara T: **Increased binding of peripheral benzodiazepine receptor in Alzheimer's disease measured by positron emission tomography with [11C]DAA1106.** *Biol Psychiatry* 2008, **64:**835–841.
76. Kreisl WC, Jenko KJ, Hines CS, Lyoo CH, Corona W, Morse CL, Zoghbi SS, Hyde T, Kleinman JE, Pike VW, *et al*: **A genetic polymorphism for translocator protein 18 kDa affects both in vitro and in vivo radioligand binding in human brain to this putative biomarker of neuroinflammation.** *J Cereb Blood Flow Metab* 2013, **33:**53–58.
77. Suribhatla S, Baillon S, Dennis M, Marudkar M, Muhammad S, Munro D, Spreadbury C, Lindesay J: **Neuropsychological performance in early and late onset Alzheimer's disease: comparisons in a memory clinic population.** *Int J Geriatr Psychiatry* 2004, **19:**1140–1147.
78. Shiino A, Watanabe T, Maeda K, Kotani E, Akiguchi I, Matsuda M: **Four subgroups of Alzheimer's disease based on patterns of atrophy using VBM and a unique pattern for early onset disease.** *Neuroimage* 2006, **33:**17–26.
79. Karas G, Scheltens P, Rombouts S, van Schijndel R, Klein M, Jones B, van der Flier W, Vrenken H, Barkhof F: **Precuneus atrophy in early-onset Alzheimer's disease: a morphometric structural MRI study.** *Neuroradiology* 2007, **49:**967–976.
80. Licht EA, McMurtray AM, Saul RE, Mendez MF: **Cognitive differences between early- and late-onset Alzheimer's disease.** *Am J Alzheimers Dis Other Demen* 2007, **22:**218–222.
81. Owen DR, Howell OW, Tang SP, Wells LA, Bennacef I, Bergstrom M, Gunn RN, Rabiner EA, Wilkins MR, Reynolds R, Matthews PM, Parker CA: **Two binding sites for [3H]PBR28 in human brain: implications for TSPO PET imaging of neuroinflammation.** *J Cereb Blood Flow Metab* 2010, **30:**1608–1618.
82. Owen DR, Gunn RN, Rabiner EA, Bennacef I, Fujita M, Kreisl WC, Innis RB, Pike VW, Reynolds R, Matthews PM, Parker CA: **Mixed-affinity binding in humans with 18-kDa translocator protein ligands.** *J Nucl Med* 2011, **52:**24–32.
83. Owen DR, Yeo AJ, Gunn RN, Song K, Wadsworth G, Lewis A, Rhodes C, Pulford DJ, Bennacef I, Parker CA, StJean PL, Cardon LR, Mooser VE, Matthews PM, Rabiner EA, Rubio JP: **An 18-kDa translocator protein (TSPO) polymorphism explains differences in binding affinity of the PET radioligand PBR28.** *J Cereb Blood Flow Metab* 2012, **32:**1–5.
84. Mizrahi R, Rusjan PM, Kennedy J, Pollock B, Mulsant B, Suridjan I, De Luca V, Wilson AA, Houle S: **Translocator protein (18 kDa) polymorphism (rs6971) explains in-vivo brain binding affinity of the PET radioligand [18F]-FEPPA.** *J Cereb Blood Flow Metab* 2012, **32:**968–972.

85. Yoder KK, Nho K, Risacher SL, Kim S, Shen L, Saykin AJ: **Influence of TSPO genotype on 11C-PBR28 standardized uptake values.** *J Nucl Med* 2013, **54:**1320–1322.
86. Gong JP, Onaivi ES, Ishiguro H, Liu QR, Tagliaferro PA, Brusco A, Uhl GR: **Cannabinoid CB2 receptors: immunohistochemical localization in rat brain.** *Brain Res* 2006, **1071:**10–23.
87. Van Sickle MD, Duncan M, Kingsley PJ, Mouihate A, Urbani P, Mackie K, Stella N, Makriyannis A, Piomelli D, Davison JS, Marnett LJ, Di Marzo V, Pittman QJ, Patel KD, Sharkey KA: **Identification and functional characterization of brainstem cannabinoid CB2 receptors.** *Science* 2005, **310:**329–332.
88. Esposito G, Iuvone T, Savani C, Scuderi C, De Filippis D, Papa M, Di Marzo V, Steardo L: **Opposing control of cannabinoid receptor stimulation on amyloid-beta-induced reactive gliosis: in vitro and in vivo evidence.** *J Pharmacol Exp Ther* 2007, **322:**1144–1152.
89. Benito C, Tolon RM, Pazos MR, Nunez E, Castillo AI, Romero J: **Cannabinoid CB2 receptors in human brain inflammation.** *Br J Pharmacol* 2008, **153:**277–285.
90. Horti AG, Gao Y, Ravert HT, Finley P, Valentine H, Wong DF, Endres CJ, Savonenko AV, Dannals RF: **Synthesis and biodistribution of [11C]A-836339, a new potential radioligand for PET imaging of cannabinoid type 2 receptors (CB2).** *Bioorg Med Chem* 2010, **18:**5202–5207.
91. Martin-Moreno AM, Brera B, Spuch C, Carro E, Garcia-Garcia L, Delgado M, Pozo MA, Innamorato NG, Cuadrado A, de Ceballos ML: **Prolonged oral cannabinoid administration prevents neuroinflammation, lowers beta-amyloid levels and improves cognitive performance in Tg APP 2576 mice.** *J Neuroinflammation* 2012, **9:**8.
92. Wu J, Bie B, Yang H, Xu JJ, Brown DL, Naguib M: **Activation of the CB2 receptor system reverses amyloid-induced memory deficiency.** *Neurobiol Aging* 2013, **34:**791–804.
93. Koppel J, Vingtdeux V, Marambaud P, d'Abramo C, Jimenez H, Stauber M, Friedman R, Davies P: **CB2 receptor deficiency increases amyloid pathology and alters tau processing in a transgenic mouse model of Alzheimer's disease.** *Mol Med* 2014, **20:**29–36.
94. Sofroniew MV, Vinters HV: **Astrocytes: biology and pathology.** *Acta Neuropathol* 2010, **119:**7–35.
95. Allen NJ, Bennett ML, Foo LC, Wang GX, Chakraborty C, Smith SJ, Barres BA: **Astrocyte glypicans 4 and 6 promote formation of excitatory synapses via GluA1 AMPA receptors.** *Nature* 2012, **486:**410–414.
96. Hughes EG, Elmariah SB, Balice-Gordon RJ: **Astrocyte secreted proteins selectively increase hippocampal GABAergic axon length, branching, and synaptogenesis.** *Mol Cell Neurosci* 2010, **43:**136–145.
97. Ullian EM, Sapperstein SK, Christopherson KS, Barres BA: **Control of synapse number by glia.** *Science* 2001, **291:**657–661.
98. Sofroniew MV: **Molecular dissection of reactive astrogliosis and glial scar formation.** *Trends Neurosci* 2009, **32:**638–647.
99. Verkhratsky A, Olabarria M, Noristani HN, Yeh CY, Rodriguez JJ: **Astrocytes in Alzheimer's disease.** *Neurotherapeutics* 2010, **7:**399–412.
100. Itagaki S, McGeer PL, Akiyama H, Zhu S, Selkoe D: **Relationship of microglia and astrocytes to amyloid deposits of Alzheimer disease.** *J Neuroimmunol* 1989, **24:**173–182.
101. Hoozemans JJ, Rozemuller JM, van Haastert ES, Veerhuis R, Eikelenboom P: **Cyclooxygenase-1 and −2 in the different stages of Alzheimer's disease pathology.** *Curr Pharm Des* 2008, **14:**1419–1427.
102. Jantzen PT, Connor KE, DiCarlo G, Wenk GL, Wallace JL, Rojiani AM, Coppola D, Morgan D, Gordon MN: **Microglial activation and beta-amyloid deposit reduction caused by a nitric oxide-releasing nonsteroidal anti-inflammatory drug in amyloid precursor protein plus presenilin-1 transgenic mice.** *J Nucl Med* 2002, **22:**2246–2254.
103. Lim GP, Yang F, Chu T, Chen P, Beech W, Teter B, Tran T, Ubeda O, Ashe KH, Frautschy SA, Cole GM: **Ibuprofen suppresses plaque pathology and inflammation in a mouse model for Alzheimer's disease.** *J Nucl Med* 2000, **20:**5709–5714.
104. Lim GP, Yang F, Chu T, Gahtan E, Ubeda O, Beech W, Overmier JB, Hsiao-Ashec K, Frautschy SA, Cole GM: **Ibuprofen effects on Alzheimer pathology and open field activity in APPsw transgenic mice.** *Neurobiol Aging* 2001, **22:**983–991.
105. Yan Q, Zhang J, Liu H, Babu-Khan S, Vassar R, Biere AL, Citron M, Landreth G: **Anti-inflammatory drug therapy alters beta-amyloid processing and deposition in an animal model of Alzheimer's disease.** *J Nucl Med* 2003, **23:**7504–7509.
106. Kuchibhotla KV, Lattarulo CR, Hyman BT, Bacskai BJ: **Synchronous hyperactivity and intercellular calcium waves in astrocytes in Alzheimer mice.** *Science* 2009, **323:**1211–1215.
107. Santillo AF, Gambini JP, Lannfelt L, Langstrom B, Ulla-Marja L, Kilander L, Engler H: **In vivo imaging of astrocytosis in Alzheimer's disease: an ^{11}C-L-deuteriodeprenyl and PIB PET study.** *Eur J Nucl Med Mol Imaging* 2011, **38:**2202–2208.
108. Fowler JS, Logan J, Volkow ND, Wang GJ: **Translational neuroimaging: positron emission tomography studies of monoamine oxidase.** *Mol Imaging Biol* 2005, **7:**377–387.
109. Saura J, Bleuel Z, Ulrich J, Mendelowitsch A, Chen K, Shih JC, Malherbe P, Da Prada M, Richards JG: **Molecular neuroanatomy of human monoamine oxidases A and B revealed by quantitative enzyme radioautography and in situ hybridization histochemistry.** *Neuroscience* 1996, **70:**755–774.
110. Fowler JS, MacGregor RR, Wolf AP, Arnett CD, Dewey SL, Schlyer D, Christman D, Logan J, Smith M, Sachs H, Aquilonius SM, Bjurling P, Halldin C, Hartvig P, Leenders KL, Lundqvist H, Oreland L, Stalnacke CG, Langstrom B: **Mapping human brain monoamine oxidase A and B with 11C-labeled suicide inactivators and PET.** *Science* 1987, **235:**481–485.
111. Fowler JS, Volkow ND, Wang GJ, Logan J, Pappas N, Shea C, MacGregor R: **Age-related increases in brain monoamine oxidase B in living healthy human subjects.** *Neurobiol Aging* 1997, **18:**431–435.
112. Saura J, Luque JM, Cesura AM, Da Prada M, Chan-Palay V, Huber G, Loffler J, Richards JG: **Increased monoamine oxidase B activity in plaque-associated astrocytes of Alzheimer brains revealed by quantitative enzyme radioautography.** *Neuroscience* 1994, **62:**15–30.
113. Smith MA, Rottkamp CA, Nunomura A, Raina AK, Perry G: **Oxidative stress in Alzheimer's disease.** *Biochim Biophys Acta* 2000, **1502:**139–144.
114. Lichtenstein MP, Carriba P, Masgrau R, Pujol A, Galea E: **Staging anti-inflammatory therapy in Alzheimer's disease.** *Front Aging Neurosci* 2010, **2:**142.
115. Gulyas B, Pavlova E, Kasa P, Gulya K, Bakota L, Varszegi S, Keller E, Horvath MC, Nag S, Hermecz I, Magyar K, Halldin C: **Activated MAO-B in the brain of Alzheimer patients, demonstrated by [11C]-L-deprenyl using whole hemisphere autoradiography.** *Neurochem Int* 2011, **58:**60–68.
116. Engler H, Lundberg PO, Ekbom K, Nennesmo I, Nilsson A, Bergstrom M, Tsukada H, Hartvig P, Langstrom B: **Multitracer study with positron emission tomography in Creutzfeldt-Jakob disease.** *Eur J Nucl Med Mol Imaging* 2003, **30:**85–95.
117. Fowler JS, Volkow ND, Logan J, Schlyer DJ, MacGregor RR, Wang GJ, Wolf AP, Pappas N, Alexoff D, Shea C, Gatley SJ, Dorflinger E, Yoo K, Morawsky L, Fazzini E: **Monoamine oxidase B (MAO B) inhibitor therapy in Parkinson's disease: the degree and reversibility of human brain MAO B inhibition by Ro 19 6327.** *Neurology* 1993, **43:**1984–1992.
118. Johnson KA, Mueller ST, Walshe TM, English RJ, Holman BL: **Cerebral perfusion imaging in Alzheimer's disease. Use of single photon emission computed tomography and iofetamine hydrochloride I 123.** *Arch Neurol* 1987, **44:**165–168.
119. Powers WJ, Perlmutter JS, Videen TO, Herscovitch P, Griffeth LK, Royal HD, Siegel BA, Morris JC, Berg L: **Blinded clinical evaluation of positron emission tomography for diagnosis of probable Alzheimer's disease.** *Neurology* 1992, **42:**765–770.
120. Yoshiura T, Hiwatashi A, Noguchi T, Yamashita K, Ohyagi Y, Monji A, Nagao E, Kamano H, Togao O, Honda H: **Arterial spin labelling at 3-T MR imaging for detection of individuals with Alzheimer's disease.** *Eur Radiol* 2009, **19:**2819–2825.
121. Bartenstein P, Minoshima S, Hirsch C, Buch K, Willoch F, Mosch D, Schad D, Schwaiger M, Kurz A: **Quantitative assessment of cerebral blood flow in patients with Alzheimer's disease by SPECT.** *J Nucl Med* 1997, **38:**1095–1101.
122. Sun GY, Horrocks LA, Farooqui AA: **The roles of NADPH oxidase and phospholipases A2 in oxidative and inflammatory responses in neurodegenerative diseases.** *J Neurochem* 2007, **103:**1–16.
123. Shimizu T, Wolfe LS: **Arachidonic acid cascade and signal transduction.** *J Neurochem* 1990, **55:**1–15.
124. Balsinde J, Winstead MV, Dennis EA: **Phospholipase A(2) regulation of arachidonic acid mobilization.** *FEBS Lett* 2002, **531:**2–6.
125. Ricciotti E, FitzGerald GA: **Prostaglandins and inflammation.** *Arterioscler Thromb Vasc Biol* 2011, **31:**986–1000.
126. Park JY, Pillinger MH, Abramson SB: **Prostaglandin E2 synthesis and secretion: the role of PGE2 synthases.** *Clin Immunol* 2006, **119:**229–240.

127. Dennis EA: **Diversity of group types, regulation, and function of phospholipase A2.** *J Biol Chem* 1994, **269:**13057–13060.
128. Weichel O, Hilgert M, Chatterjee SS, Lehr M, Klein J: **Bilobalide, a constituent of Ginkgo biloba, inhibits NMDA-induced phospholipase A2 activation and phospholipid breakdown in rat hippocampus.** *Naunyn Schmiedebergs Arch Pharmacol* 1999, **360:**609–615.
129. Mattson MP, Chan SL: **Neuronal and glial calcium signaling in Alzheimer's disease.** *Cell Calcium* 2003, **34:**385–397.
130. Lehtonen JY, Holopainen JM, Kinnunen PK: **Activation of phospholipase A2 by amyloid beta-peptides in vitro.** *Biochemistry* 1996, **35:**9407–9414.
131. Greenamyre JT, Maragos WF, Albin RL, Penney JB, Young AB: **Glutamate transmission and toxicity in Alzheimer's disease.** *Prog Neuropsychopharmacol Biol Psychiatry* 1988, **12:**421–430.
132. Montine KS, Quinn JF, Zhang J, Fessel JP, Roberts LJ 2nd, Morrow JD, Montine TJ: **Isoprostanes and related products of lipid peroxidation in neurodegenerative diseases.** *Chem Phys Lipids* 2004, **128:**117–124.
133. McGeer PL, McGeer E, Rogers J, Sibley J: **Anti-inflammatory drugs and Alzheimer disease.** *Lancet* 1990, **335:**1037.
134. Imbimbo BP, Solfrizzi V, Panza F: **Are NSAIDs useful to treat Alzheimer's disease or mild cognitive impairment?** *Front Aging Neurosci* 2010, **2.** doi:10.3389/fnagi.2010.00019.
135. Szekely CA, Thorne JE, Zandi PP, Ek M, Messias E, Breitner JC, Goodman SN: **Nonsteroidal anti-inflammatory drugs for the prevention of Alzheimer's disease: a systematic review.** *Neuroepidemiology* 2004, **23:**159–169.
136. Zandi PP, Anthony JC, Hayden KM, Mehta K, Mayer L, Breitner JC, Cache County Study I: **Reduced incidence of AD with NSAID but not H2 receptor antagonists: the Cache County Study.** *Neurology* 2002, **59:**880–886.
137. Szekely CA, Breitner JC, Fitzpatrick AL, Rea TD, Psaty BM, Kuller LH, Zandi PP: **NSAID use and dementia risk in the Cardiovascular Health Study: role of APOE and NSAID type.** *Neurology* 2008, **70:**17–24.
138. Breitner JC, Haneuse SJ, Walker R, Dublin S, Crane PK, Gray SL, Larson EB: **Risk of dementia and AD with prior exposure to NSAIDs in an elderly community-based cohort.** *Neurology* 2009, **72:**1899–1905.
139. Hayden KM, Zandi PP, Khachaturian AS, Szekely CA, Fotuhi M, Norton MC, Tschanz JT, Pieper CF, Corcoran C, Lyketsos CG, Breitner JC, Welsh-Bohmer KA: **Does NSAID use modify cognitive trajectories in the elderly? The Cache County study.** *Neurology* 2007, **69:**275–282.
140. Cornelius C, Fastbom J, Winblad B, Viitanen M: **Aspirin, NSAIDs, risk of dementia, and influence of the apolipoprotein E epsilon 4 allele in an elderly population.** *Neuroepidemiology* 2004, **23:**135–143.
141. Stewart WF, Kawas C, Corrada M, Metter EJ: **Risk of Alzheimer's disease and duration of NSAID use.** *Neurology* 1997, **48:**626–632.
142. Van Dam D, Coen K, De Deyn PP: **Ibuprofen modifies cognitive disease progression in an Alzheimer's mouse model.** *J Psychopharmacol* 2010, **24:**383–388.
143. McKee AC, Carreras I, Hossain L, Ryu H, Klein WL, Oddo S, LaFerla FM, Jenkins BG, Kowall NW, Dedeoglu A: **Ibuprofen reduces Abeta, hyperphosphorylated tau and memory deficits in Alzheimer mice.** *Brain Res* 2008, **1207:**225–236.
144. Kotilinek LA, Westerman MA, Wang Q, Panizzon K, Lim GP, Simonyi A, Lesne S, Falinska A, Younkin LH, Younkin SG, Rowan M, Cleary J, Wallis RA, Sun GY, Cole G, Frautschy S, Anwyl R, Ashe KH: **Cyclooxygenase-2 inhibition improves amyloid-beta-mediated suppression of memory and synaptic plasticity.** *Brain* 2008, **131:**651–664.
145. Weggen S, Eriksen JL, Das P, Sagi SA, Wang R, Pietrzik CU, Findlay KA, Smith TE, Murphy MP, Bulter T, Bulter T, Kang DE, Marquez-Sterling N, Golde TE, Koo EH: **A subset of NSAIDs lower amyloidogenic Abeta42 independently of cyclooxygenase activity.** *Nature* 2001, **414:**212–216.
146. Avramovich Y, Amit T, Youdim MB: **Non-steroidal anti-inflammatory drugs stimulate secretion of non-amyloidogenic precursor protein.** *J Biol Chem* 2002, **277:**31466–31473.
147. Sastre M, Dewachter I, Rossner S, Bogdanovic N, Rosen E, Borghgraef P, Evert BO, Dumitrescu-Ozimek L, Thal DR, Landreth G, Walter J, Klockgether T, van Leuven F, Heneka MT: **Nonsteroidal anti-inflammatory drugs repress beta-secretase gene promoter activity by the activation of PPARgamma.** *Proc Natl Acad Sci U S A* 2006, **103:**443–448.
148. Morihara T, Teter B, Yang F, Lim GP, Boudinot S, Boudinot FD, Frautschy SA, Cole GM: **Ibuprofen suppresses interleukin-1beta induction of pro-amyloidogenic alpha1-antichymotrypsin to ameliorate beta-amyloid (Abeta) pathology in Alzheimer's models.** *Neuropsychopharmacology* 2005, **30:**1111–1120.
149. Szekely CA, Green RC, Breitner JC, Ostbye T, Beiser AS, Corrada MM, Dodge HH, Ganguli M, Kawas CH, Kuller LH, Psaty BM, Resnick SM, Wolf PA, Zonderman AB, Welsh-Bohmer KA, Zandi PP: **No advantage of A beta 42-lowering NSAIDs for prevention of Alzheimer dementia in six pooled cohort studies.** *Neurology* 2008, **70:**2291–2298.
150. Thomas T, Nadackal TG, Thomas K: **Aspirin and non-steroidal anti-inflammatory drugs inhibit amyloid-beta aggregation.** *Neuroreport* 2001, **12:**3263–3267.
151. Kukar TL, Ladd TB, Bann MA, Fraering PC, Narlawar R, Maharvi GM, Healy B, Chapman R, Welzel AT, Price RW, Moore B, Rangachari V, Cusack B, Eriksen J, Jansen-West K, Verbeeck C, Yager D, Eckman C, Ye W, Sagi S, Cottrell BA, Torpey J, Rosenberry TL, Fauq A, Wolfe MS, Schmidt B, Walsh DM, Koo EH, Golde TE: **Substrate-targeting gamma-secretase modulators.** *Nature* 2008, **453:**925–929.
152. Alafuzoff I, Overmyer M, Helisalmi S, Soininen H: **Lower counts of astroglia and activated microglia in patients with Alzheimer's disease with regular use of non-steroidal anti-inflammatory drugs.** *J Alzheimers Dis* 2000, **2:**37–46.
153. Halliday GM, Shepherd CE, McCann H, Reid WG, Grayson DA, Broe GA, Kril JJ: **Effect of anti-inflammatory medications on neuropathological findings in Alzheimer disease.** *Arch Neurol* 2000, **57:**831–836.
154. Aisen PS, Davis KL: **Inflammatory mechanisms in Alzheimer's disease: implications for therapy.** *Am J Psychiatry* 1994, **151:**1105–1113.
155. Rogers J, Kirby LC, Hempelman SR, Berry DL, McGeer PL, Kaszniak AW, Zalinski J, Cofield M, Mansukhani L, Willson P, Kogan F: **Clinical trial of indomethacin in Alzheimer's disease.** *Neurology* 1993, **43:**1609–1611.
156. Scharf S, Mander A, Ugoni A, Vajda F, Christophidis N: **A double-blind, placebo-controlled trial of diclofenac/misoprostol in Alzheimer's disease.** *Neurology* 1999, **53:**197–201.
157. Aisen PS, Schmeidler J, Pasinetti GM: **Randomized pilot study of nimesulide treatment in Alzheimer's disease.** *Neurology* 2002, **58:**1050–1054.
158. Soininen H, West C, Robbins J, Niculescu L: **Long-term efficacy and safety of celecoxib in Alzheimer's disease.** *Dement Geriatr Cogn Disord* 2007, **23:**8–21.
159. Aisen PS, Schafer KA, Grundman M, Pfeiffer E, Sano M, Davis KL, Farlow MR, Jin S, Thomas RG, Thal LJ, Alzheimer's Disease Cooperative Study: **Effects of rofecoxib or naproxen vs placebo on Alzheimer disease progression: a randomized controlled trial.** *JAMA* 2003, **289:**2819–2826.
160. Reines SA, Block GA, Morris JC, Liu G, Nessly ML, Lines CR, Norman BA, Baranak CC, Rofecoxib Protocol 091 Study Group: **Rofecoxib: no effect on Alzheimer's disease in a 1-year, randomized, blinded, controlled study.** *Neurology* 2004, **62:**66–71.
161. Pasqualetti P, Bonomini C, Dal Forno G, Paulon L, Sinforiani E, Marra C, Rossini PM, Zanetti O: **A randomized controlled study on effects of ibuprofen on cognitive progression of Alzheimer's disease.** *Aging Clin Exp Res* 2009, **21:**102–110.
162. ADAPT Research Group: **Cardiovascular and cerebrovascular events in the randomized, controlled Alzheimer's Disease Anti-Inflammatory Prevention Trial (ADAPT).** *PLoS Clin Trials* 2006, **1:**e33.
163. Bateman RJ, Xiong C, Benzinger TL, Fagan AM, Goate A, Fox NC, Marcus DS, Cairns NJ, Xie X, Blazey TM, Holtzman DM, Santacruz A, Buckles V, Oliver A, Moulder K, Aisen PS, Ghetti B, Klunk WE, McDade E, Martins RN, Masters CL, Mayeux R, Ringman JM, Rossor MN, Schofield PR, Sperling RA, Salloway S, Morris JC, Dominantly Inherited Alzheimer Network: **Clinical and biomarker changes in dominantly inherited Alzheimer's disease.** *N Engl J Med* 2012, **367:**795–804.
164. Wu L, Rosa-Neto P, Hsiung GY, Sadovnick AD, Masellis M, Black SE, Jia J, Gauthier S: **Early-onset familial Alzheimer's disease (EOFAD).** *Can J Neurol Sci* 2012, **39:**436–445.
165. Jack CR Jr, Knopman DS, Jagust WJ, Shaw LM, Aisen PS, Weiner MW, Petersen RC, Trojanowski JQ: **Hypothetical model of dynamic biomarkers of the Alzheimer's pathological cascade.** *Lancet Neurol* 2010, **9:**119–128.
166. Lambert MP, Barlow AK, Chromy BA, Edwards C, Freed R, Liosatos M, Morgan TE, Rozovsky I, Trommer B, Viola KL, Wals P, Zhang C, Finch CE, Krafft GA, Klein WL: **Diffusible, nonfibrillar ligands derived from Abeta1-42 are potent central nervous system neurotoxins.** *Proc Natl Acad Sci U S A* 1998, **95:**6448–6453.
167. Jucaite A, Cselenyi Z, Arvidsson A, Ahlberg G, Julin P, Varnas K, Stenkrona P, Andersson J, Halldin C, Farde L: **Kinetic analysis and test-retest variability of the radioligand [11C](R)-PK11195 binding to TSPO in the human brain - a PET study in control subjects.** *EJNMMI Res* 2012, **2:**15.

168. Turkheimer FE, Edison P, Pavese N, Roncaroli F, Anderson AN, Hammers A, Gerhard A, Hinz R, Tai YF, Brooks DJ: **Reference and target region modeling of [11C]-(R)-PK11195 brain studies.** *J Nucl Med* 2007, **48:**158–167.
169. **Reproducibility of the 11C-PBR28 PET Signal.** [http://www.clinicaltrials.gov/ct2/show/NCT02086240]
170. **Study of [11C]PBR28 TSPO PET as a disease marker in MS patients.** [http://public.ukcrn.org.uk/search/StudyDetail.aspx?StudyID=16651]
171. Tomasi G, Edison P, Bertoldo A, Roncaroli F, Singh P, Gerhard A, Cobelli C, Brooks DJ, Turkheimer FE: **Novel reference region model reveals increased microglial and reduced vascular binding of 11C-(R)-PK11195 in patients with Alzheimer's disease.** *J Nucl Med* 2008, **49:**1249–1256.
172. Lambert JC, Heath S, Even G, Campion D, Sleegers K, Hiltunen M, Combarros O, Zelenika D, Bullido MJ, Tavernier B, Letenneur L, Bettens K, Berr C, Pasquier F, Fiévet N, Barberger-Gateau P, Engelborghs S, De Deyn P, Mateo I, Franck A, Helisalmi S, Porcellini E, Hanon O, European Alzheimer's Disease Initiative Investigators, de Pancorbo MM, Lendon C, Dufouil C, Jaillard C, Leveillard T, Alvarez V, Bosco P, *et al*: **Genome-wide association study identifies variants at CLU and CR1 associated with Alzheimer's disease.** *Nat Genet* 2009, **41:**1094–1099.
173. Kamboh MI, Demirci FY, Wang X, Minster RL, Carrasquillo MM, Pankratz VS, Younkin SG, Saykin AJ, Alzheimer's Disease Neuroimaging Initiative, Jun G, Baldwin C, Logue MW, Buros J, Farrer L, Pericak-Vance MA, Haines JL, Sweet RA, Ganguli M, Feingold E, Dekosky ST, Lopez OL, Barmada MM: **Genome-wide association study of Alzheimer's disease.** *Transl Psychiatry* 2012, **2:**e117.

doi:10.1186/1742-2094-11-120
Cite this article as: Zimmer *et al.*: Tracking neuroinflammation in Alzheimer's disease: the role of positron emission tomography imaging. *Journal of Neuroinflammation* 2014 **11**:120.

Submit your next manuscript to BioMed Central and take full advantage of:

- **Convenient online submission**
- **Thorough peer review**
- **No space constraints or color figure charges**
- **Immediate publication on acceptance**
- **Inclusion in PubMed, CAS, Scopus and Google Scholar**
- **Research which is freely available for redistribution**

Submit your manuscript at
www.biomedcentral.com/submit

BioMed Central

Capítulo X. *MicroPET imaging and transgenic models: a blueprint for Alzheimer's disease clinical research.*

No **capítulo X** apresentamos o artigo publicado no periódico *Trends in Neurosciences*.

O diagnóstico precoce parece ser a chave para a otimização das estratégias terapêuticas na DA. Neste capítulo, revisamos os estudos envolvendo a versão miniaturizada do PET (microPET) e modelos transgênicos de β-amilóide e tau. Chegamos a conclusão que o uso desta tecnologia em modelos animais ainda está em seus primórdios e propusemos aplicações avançadas do microPET para o entendimento da progressão dos efeitos das patologias de β-amilóide e tau, como estudos longitudinais e análise de redes metabólicas. Artigo escolhido como “artigo do mês” da edição de novembro do periódico *Trends in Neurosciences*.

Trends in Neurosciences November 2014 Vol. 37 No. 11, pp. 615–682 ISSN 0166-2236

Trends in Neurosciences

Feature Review

CellPress

MicroPET imaging and transgenic models: a blueprint for Alzheimer's disease clinical research

Eduardo R. Zimmer[1,2,3], Maxime J. Parent[1,2], A. Claudio Cuello[4], Serge Gauthier[1,2], and Pedro Rosa-Neto[1,2]

[1] Translational Neuroimaging Laboratory (TNL), McGill Center for Studies in Aging, Douglas Mental Health University Institute, Montreal, Quebec, Canada
[2] PET unit, Montreal Neurological Institute (MNI), Montreal, Quebec, Canada
[3] Department of Biochemistry, Federal University of Rio Grande do Sul, Porto Alegre, Rio Grande do Sul, Brazil
[4] Department of Pharmacology and Therapeutics, McGill University, Montreal, Quebec, Canada

Over the past decades, developments in neuroimaging have significantly contributed to the understanding of Alzheimer's disease (AD) pathophysiology. Specifically, positron emission tomography (PET) imaging agents targeting amyloid deposition have provided unprecedented opportunities for refining *in vivo* diagnosis, monitoring disease propagation, and advancing AD clinical trials. Furthermore, the use of a miniaturized version of PET (microPET) in transgenic (Tg) animals has been a successful strategy for accelerating the development of novel radiopharmaceuticals. However, advanced applications of microPET focusing on the longitudinal propagation of AD pathophysiology or therapeutic strategies remain in their infancy. This review highlights what we have learned from microPET imaging in Tg models displaying amyloid and tau pathology, and anticipates cutting-edge applications with high translational value to clinical research.

AD: current conceptualization and the role of PET imaging

AD is currently conceptualized as a progressive pathophysiological process, initially characterized by amyloidosis (extracellular Aβ accumulation; see Glossary), followed by a cascade of neurodegenerative events, including the formation of neurofibrillary tangles (NFTs, intracellular tau protein aggregates), neuroinflammation, and neurotransmission abnormalities, ultimately leading to cognitive decline and dementia [1–3]. In the past decade, developments in radiopharmaceutical research have allowed the synthesis of highly specific PET imaging agents, which have allowed the *in vivo* quantification of amyloid deposition in AD patients [4].

PET permits the quantification of numerous biological and pharmacological processes via the pharmacokinetic analysis of imaging agents labeled with positron-emitting radioisotopes (radiopharmaceuticals) administered in living individuals. The high sensitivity of PET (nanomolar to picomolar) is ideal for the non-invasive quantification of receptor availability, transporter systems, gene expression, signal transduction, protein binding, and transcriptional regulation [5]. As such, PET imaging has numerous research and clinical applications in the field of neurodegenerative diseases. In fact, PET imaging has been

Corresponding author: Rosa-Neto, P. (pedro.rosa@mcgill.ca).
Keywords: Alzheimer's disease; amyloid; microPET; neurodegeneration; positron emission tomography; radiopharmaceuticals.

0166-2236/
© 2014 Elsevier Ltd. All rights reserved. http://dx.doi.org/10.1016/j.tins.2014.07.002

Glossary

Amyloid load: the density of amyloid deposits estimated by the magnitude of amyloid imaging agents binding.
Amyloid precursor protein (APP): an integral membrane protein expressed in many tissues and concentrated in the synapses of neurons.
Biomarker: an indicator of biological processes, pathogenic processes, or pharmacologic responses.
Binding potential (BP_{ND}): imaging outcome measure expressing the availability of binding sites to the radiopharmaceutical at a given tracer concentration. This value is proportional to the ratio between Bmax and Kd.
Bmax: the maximum number of receptor binding sites.
Consortium to Establish a Registry for Alzheimer's disease (CERAD): standardized procedures for the evaluation and diagnosis of patients with Alzheimer's disease.
Dissociation constant (Kd): a ligand property equal to the inverse of affinity; the half-saturation constant of the ligand.
Frontotemporal dementias (FTDs): subgroup of overlapping non-Alzheimer clinical syndromes characterized by behavioral changes, impairment of semantic memory, and aphasia.
Frontotemporal lobar degeneration (FTLD): a term utilized for the spectrum of FTD-related neuropathologies that are subdivided into five groups: FTLD-tau, FTLD-TDP, FTLD-UPS, FTLD-FUS, and FTLD-ni.
Half-life: the time required for the radioactivity of a compound to decrease to half its initial value.
Positron emission tomography (PET): imaging technique based on molecular agents labeled with positron-emitting radioisotopes. PET data can produce 2D, 3D, or 4D (volume and time) images of biological processes (10 $^{-3}$–10 $^{-12}$ M sensitivity).
Radiopharmaceutical: compound labeled with a radioactive molecule.
Specific activity (SA): the ratio between radiolabeled and unlabeled molecules, expressed as radioactivity per unit mass (or volume).
Standardized uptake value (SUV): the ratio between the tissue radioactivity and the normalized dose injected. This value represents the fraction of radioactivity trapped in a target region.
Standardized uptake value ratio (SUVR): the ratio between target and reference SUVs.
Target engagement biomarker: a parameter expressing the interaction between small molecules and their target proteins in a living system.
Transgenic (Tg) models: animals whose genomes have been altered by the insertion of one or more foreign genes.

Neural mechanisms of social hierarchy

CellPress

Trends in Neurosciences

November 2014 Volume 37, Number 11 pp. 615–682

Editor
Andrew M. Clark

Executive Editor, Neuroscience
Katja Brose

Journal Manager
Olaf Meesters

Journal Administrators
Ria Otten
Patrick Scheffmann

Advisory Editorial Board
Silvia Arber, *Basel, Switzerland*
Anders Björklund, *Lund, Sweden*
J. Paul Bolam, *Oxford, UK*
Sarah W. Bottjer, *Los Angeles, CA, USA*
Barry J. Dickson, *Vienna, Austria*
Chris Q. Doe, *Eugene, OR, USA*
Craig C. Garner, *Stanford, CA, USA*
Yukiko Goda, *Wako, Japan*
Kenneth D. Harris, *London, UK*
Nancy Ip, *Kowloon, Hong Kong*
Meyer Jackson, *Madison, WI, USA*
Maria Karayiorgou, *New York, NY, USA*
Robert C. Malenka, *Stanford, CA, USA*
Mark P. Mattson, *Baltimore, MD, USA*
Freda D. Miller, *Toronto, Canada*
Richard G.M. Morris, *Edinburgh, UK*
Maiken Nedergaard, *Valhalla, NY, USA*
Eric Nestler, *New York, NY, USA*
Hitoshi Sakano, *Tokyo, Japan*
Greg Stuart, *Canberra, Australia*
Wolf Singer, *Frankfurt, Germany*
Marc Tessier-Lavigne, *New York, NY, USA*
Chris A. Walsh, *Boston, MA, USA*

Editorial Enquiries
Trends in Neurosciences
Cell Press
600 Technology Square
Cambridge, MA 02139, USA
Tel: +1 617 386 2133
Fax: +1 617 3972810
E-mail: tins@cell.com

Cover: Numerous brain regions are active during the formation of social hierarchies, which greatly influence behavior and health. On pages 674–682 of this issue, Wang, Kessels, and Hu review recent work examining social hierarchies in mice, and discuss the putative neural circuitry controlling social status. As an example, the cover image shows a hierarchy formed between two mice as determined by a tube test, a common laboratory assay of social status. Cover art by Jiafeng Zhao and Yefei Li.

Feature Review

CellPress

MicroPET imaging and transgenic models: a blueprint for Alzheimer's disease clinical research

Eduardo R. Zimmer[1,2,3], Maxime J. Parent[1,2], A. Claudio Cuello[4], Serge Gauthier[1,2], and Pedro Rosa-Neto[1,2]

[1] Translational Neuroimaging Laboratory (TNL), McGill Center for Studies in Aging, Douglas Mental Health University Institute, Montreal, Quebec, Canada
[2] PET unit, Montreal Neurological Institute (MNI), Montreal, Quebec, Canada
[3] Department of Biochemistry, Federal University of Rio Grande do Sul, Porto Alegre, Rio Grande do Sul, Brazil
[4] Department of Pharmacology and Therapeutics, McGill University, Montreal, Quebec, Canada

Over the past decades, developments in neuroimaging have significantly contributed to the understanding of Alzheimer's disease (AD) pathophysiology. Specifically, positron emission tomography (PET) imaging agents targeting amyloid deposition have provided unprecedented opportunities for refining *in vivo* diagnosis, monitoring disease propagation, and advancing AD clinical trials. Furthermore, the use of a miniaturized version of PET (microPET) in transgenic (Tg) animals has been a successful strategy for accelerating the development of novel radiopharmaceuticals. However, advanced applications of microPET focusing on the longitudinal propagation of AD pathophysiology or therapeutic strategies remain in their infancy. This review highlights what we have learned from microPET imaging in Tg models displaying amyloid and tau pathology, and anticipates cutting-edge applications with high translational value to clinical research.

AD: current conceptualization and the role of PET imaging

AD is currently conceptualized as a progressive pathophysiological process, initially characterized by amyloidosis (extracellular Aβ accumulation; see Glossary), followed by a cascade of neurodegenerative events, including the formation of neurofibrillary tangles (NFTs, intracellular tau protein aggregates), neuroinflammation, and neurotransmission abnormalities, ultimately leading to cognitive decline and dementia [1–3]. In the past decade, developments in radiopharmaceutical research have allowed the synthesis of highly specific PET imaging agents, which have allowed the *in vivo* quantification of amyloid deposition in AD patients [4].

PET permits the quantification of numerous biological and pharmacological processes via the pharmacokinetic analysis of imaging agents labeled with positron-emitting radioisotopes (radiopharmaceuticals) administered in living individuals. The high sensitivity of PET (nanomolar to picomolar) is ideal for the non-invasive quantification of receptor availability, transporter systems, gene expression, signal transduction, protein binding, and transcriptional regulation [5]. As such, PET imaging has numerous research and clinical applications in the field of neurodegenerative diseases. In fact, PET imaging has been

Glossary

Amyloid load: the density of amyloid deposits estimated by the magnitude of amyloid imaging agents binding.
Amyloid precursor protein (APP): an integral membrane protein expressed in many tissues and concentrated in the synapses of neurons.
Biomarker: an indicator of biological processes, pathogenic processes, or pharmacologic responses.
Binding potential (BP_{ND}): imaging outcome measure expressing the availability of binding sites to the radiopharmaceutical at a given tracer concentration. This value is proportional to the ratio between Bmax and Kd.
Bmax: the maximum number of receptor binding sites.
Consortium to Establish a Registry for Alzheimer's disease (CERAD): standardized procedures for the evaluation and diagnosis of patients with Alzheimer's disease.
Dissociation constant (Kd): a ligand property equal to the inverse of affinity: the half-saturation constant of the ligand.
Frontotemporal dementias (FTDs): subgroup of overlapping non-Alzheimer clinical syndromes characterized by behavioral changes, impairment of semantic memory, and aphasia.
Frontotemporal lobar degeneration (FTLD): a term utilized for the spectrum of FTD-related neuropathologies that are subdivided into five groups: FTLD-tau, FTLD-TDP, FTLD-UPS, FTLD-FUS, and FTLD-ni.
Half-life: the time required for the radioactivity of a compound to decrease to half its initial value.
Positron emission tomography (PET): imaging technique based on molecular agents labeled with positron-emitting radioisotopes. PET data can produce 2D, 3D, or 4D (volume and time) images of biological processes (10^{-9}–10^{-12} M sensitivity).
Radiopharmaceutical: compound labeled with a radioactive molecule.
Specific activity (SA): the ratio between radiolabeled and unlabeled molecules, expressed as radioactivity per unit mass (or volume).
Standardized uptake value (SUV): the ratio between the tissue radioactivity and the normalized dose injected. This value represents the fraction of radioactivity trapped in a target region.
Standardized uptake value ratio (SUVR): the ratio between target and reference SUVs.
Target engagement biomarker: a parameter expressing the interaction between small molecules and their target proteins in a living system.
Transgenic (Tg) models: animals whose genomes have been altered by the insertion of one or more foreign genes.

Corresponding author: Rosa-Neto, P. (pedro.rosa@mcgill.ca).
Keywords: Alzheimer's disease; amyloid; microPET; neurodegeneration; positron emission tomography; radiopharmaceuticals.

0166-2236/
© 2014 Published by Elsevier Ltd. http://dx.doi.org/10.1016/j.tins.2014.07.002

recently incorporated into the diagnostic criteria for the spectrum of clinical manifestations of AD [6,7]. Moreover, PET has the potential to further contribute to AD research by determining disease staging and monitoring the efficacy of disease-modifying interventions [8].

Several PET radiopharmaceuticals have been used for estimating the pathophysiological features of AD. Amyloid load has been successfully quantified using [^{11}C]PIB, [^{18}F]florbetapir, [^{18}F]florbetaben, [^{18}F]flutemetamol, and [^{18}F]NAV4694. The imaging outcomes of several amyloid agents accurately reflect neuropathological post-mortem staging in AD brains [9–12]. Neurodegeneration has been quantified by estimating declines in cerebral blood flow ([^{15}O]H_2O), oxygen consumption ([^{15}O]O_2) and glucose metabolism ([^{18}F]fluorodeoxyglucose, FDG) [13–16]. Recently developed imaging agents for tau pathology, such as [^{18}F]THK523, [^{18}F]THK5105, [^{18}F]THK5117, [^{18}F]T807, [^{18}F]T808, and [^{11}C]PBB3, have reinforced the imaging armamentarium for tracking neurodegeneration in AD [17–19]. Molecular imaging agents targeting microglial activation, such as [^{11}C]-PK11195, have been used for the quantification of neuroinflammatory changes in AD [20] (Figure 1). In addition, PET technologies can be applied in clinical trials for population enrichment, target engagement, or monitoring therapeutic response. Aside from their clinical use, PET imaging technologies can be ported to preclinical settings, allowing *in vivo* studies in animal models.

Miniaturized PET imaging provides an optimal interface between animal models and human research, owing to similarities in acquisition and outcome measures. Radiopharmaceutical profiles, such as brain permeability and binding properties, are frequently comparable across species. Such translational power is boosted by the unparalleled opportunity for imaging human pathology phenotypes in genetically engineered animal models. Indeed, a body of literature dominated by radiopharmaceutical research has propelled the use of Tg animals expressing human mutations as platforms for radiopharmaceutical development using microPET. In fact, microPET imaging using Tg models has significantly advanced the development of radiopharmaceuticals, providing measures of brain permeability, pharmacological stability, and metabolite profiles [19,21].

Apart from its use in the development of imaging agents, the association of microPET with Tg models has tremendous potential for providing new insights into AD pathophysiology. In fact, given the diversity of imaging agents (see http://www.ncbi.nlm.nih.gov/books/NBK5330/) and numerous Tg models displaying amyloidosis and tau pathology ([22] for review), one can easily conclude that methods combining radiopharmaceuticals and Tg models for exploring disease processes remain in their early stages (Table 1, and Table S1 in the supplementary material online). However, critical analyses of such combinations in the literature reveal numerous discrepancies across studies, which overshadow their potential applications.

In the following paragraphs, we discuss potential sources of variability across these studies, including the properties of radiopharmaceuticals, Tg models, and microPET methodologies. Finally, we explore future directions of microPET imaging in AD experimental research, including a discussion of longitudinal multiparametric studies, refined statistical analyses, and the recent development of hybrid cutting-edge systems.

Imaging AD pathophysiology in Tg models

The coexistence of multiple pathological features in AD patients (e.g., amyloidosis, tau pathology, synaptic depletion, and neuroinflammation) makes it difficult to attribute particular aspects of AD pathophysiology to a single pathogenic mechanism. As such, microPET imaging combined with genetically engineered models constitutes an attractive strategy to test predictions regarding the progression of AD pathophysiological events following the overexpression of a specific mutant gene. For example, models with human amyloid precursor protein (APP) mutations are highly desirable for developing imaging biomarkers for amyloidosis because strains with APP mutations display a pattern of amyloid deposition similar to that observed in humans [23]. Similarly, models harboring human tau mutations display a phenotype dominated by tau hyperphosphorylation and the production of NFTs, yielding a pattern of tau pathology propagation similar to that described by Braak and Braak [24,25]. Interestingly, the topology of amyloidosis and tauopathy described above appears to be associated with connectivity patterns rather than reflecting direct homologies between areas of rodent and human brains [26,27]. Although these models did not fully mimic the anatomical distribution of the amyloid and tau lesions in the human brain, they share neurochemical features, such as protein conformational changes and molecular aggregation [22]. Thus, similarities between the AD pathophysiology observed in humans and Tg models make microPET an optimal *in vivo* method for proof-of-concept studies.

Imaging biomarkers for quantification of amyloid load

Amyloid imaging with [^{11}C]PiB and [^{18}F]FDNNP has been used in AD research for nearly a decade. To date, [^{11}C]PiB has been the best-studied tracer for quantifying amyloid load in both humans and experimental models. This thioflavin-T derivative has a high affinity and specificity for fibrillar Aβ depositions [28]. By contrast, the naphthalene derivative [^{18}F]FDNNP has a lower affinity and specificity for revealing amyloid plaques [29].

The new generation of ^{18}F-labeled imaging agents, including [^{18}F]AV45 (florbetapir), [^{18}F]florbetaben, and [^{18}F]flutemetamol, bind to fibrillary amyloid plaques with a higher affinity than [^{18}F]FDDNP. [^{18}F]florbetapir and [^{18}F]flutemetamol have been rapidly translated to clinical settings as FDA-approved diagnostic agents for brain amyloidosis [30,31]. Several studies have demonstrated optimal correspondence between *in vivo* amyloid imaging and post-mortem Congo red, thioflavin-T, or silver staining, which identify fibrillary Aβ deposition [32–34]. In fact, [^{18}F]florbetapir images obtained ante-mortem correspond to Consortium to Establish a Registry for Alzheimer's Disease (CERAD) pathological scores obtained from biopsies or the post-mortem brain in the same individuals [32]. One drawback is that the entire second generation of amyloid agents show an undesirably high level of white-matter (WM) retention [35]. Novel amyloid imaging

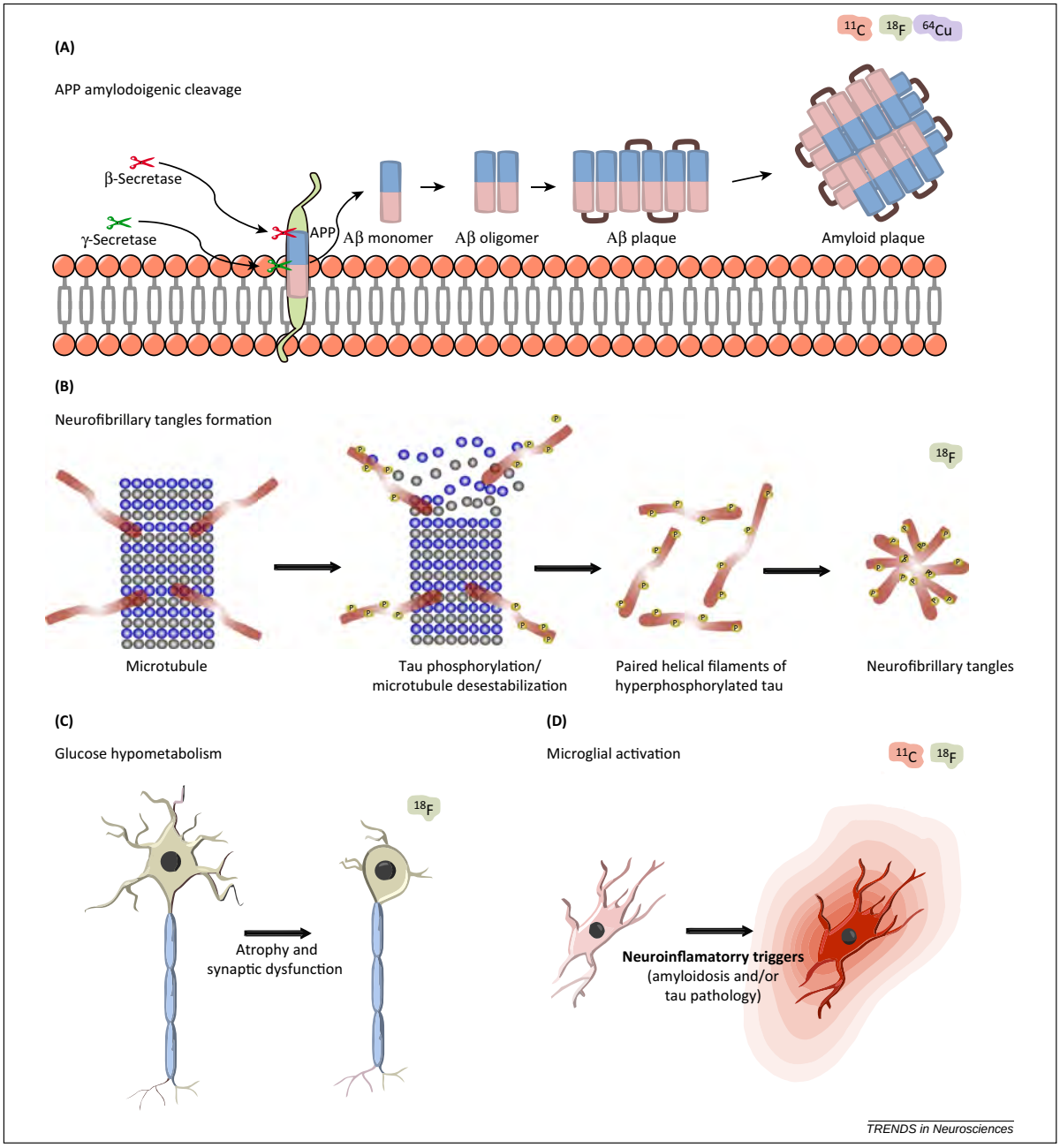

Figure 1. Alzheimer's disease (AD) pathophysiological events and PET biological target possibilities. **(A)** Amyloid pathology: amyloid precursor protein (APP) is cleaved by β-secretase and γ-secretase (transmembrane proteases), yielding an Aβ monomer. Monomer aggregation produces toxic Aβ oligomers, which further aggregate as insoluble Aβ plaques. Amyloid plaques are mature Aβ aggregates with a β-pleated sheet conformation. **(B)** Formation of neurofibrillary tangles (NFT): hyperphosphorylation of tau proteins induces microtubule instability leading to massive detachment of tau protein from microtubules, generating paired helical filaments. The aggregation of hyperphosphorylated tau produces a filamentous conformation, termed NFTs. **(C)** Glucose hypometabolism: [^{18}F]FDG has been used to measure rates of glucose metabolism in the cerebrum. [^{18}F]FDG can be used to follow the decrease in metabolic activity due to AD progression. **(D)** Microglial activation: neuroinflammation due to amyloid deposition or NFTs can accelerate AD progression. Radiopharmaceuticals can track the neuroinflammation by allowing the assessment of the binding site of translocator protein-18 kDa (TSPO, formerly known as the peripheral benzodiazepine receptor, PBR).

agents, such as benzoxazole derivatives (e.g., [^{18}F]24), imidazo-benzothiazoles (IBTs, such as [^{11}C]5), barbiturates (e.g., [^{18}F]1a), and [^{18}F]NAV4694, constitute alternatives that demonstrate fast brain penetration, high affinity for fibrillary amyloids, reduced WM retention, and rapid non-specific clearance [12,36–39]. Copper (Cu) radiopharmaceuticals, such as [^{64}Cu^{II}]L1, have interesting properties, including stability, a long half-life (12.7 h), and

Table 1. Radiopharmaceuticals currently used in microPET research involving transgenic models of amyloid and tau pathology

Biological target	Radiopharmaceutical	Refs
Amyloid plaques	[^{11}C]PiB	[28]
	[^{18}F]FDDNP	[123]
	[^{18}F]AV-45	[35]
	[^{11}C]5	[37]
	[^{18}F]24	[124]
	[^{18}F]1a	[38]
	[^{64}Cu^{II}](L1)	[40]
Glucose metabolism	[^{18}F]FDG	[125]
Tau fibrils	[^{18}F]THK523	[46]
	[^{18}F]T807	[93]
	[^{11}C]PBB3	[19]
Microglial activation	[^{11}C]AC-5216	[53]
	[^{18}F]FEDAA1106	[52]
	[^{11}C]PK11195	[119]
	[^{11}C]A-836339	[56]
$GABA_A$ receptor	[^{11}C]FMZ	[60]
Acetylcholinesterase activity	[^{11}C]MP4A	[121]

the ability to cross the blood–brain barrier (BBB) [40]. However, these imaging agents have been minimally explored in animal models and humans and still need to be validated fully.

Imaging biomarkers for the quantification of neurodegeneration, neuroinflammation, and altered neurotransmission

Hypometabolism and a high concentration of NFTs in the brain are considered biomarkers of neurodegeneration [41]. Glucose hypometabolism indicates reduced tissue hexokinase activity, a rate-limiting step of glucose metabolism [42]. For many years [^{18}F]FDG has served as the major PET tracer for mapping hypometabolic areas in experimental and clinical settings [43]. Although not specific to AD, hypometabolism in the parietal, temporal, and posterior cingulate cortices is considered an AD signature that increases diagnostic accuracy [44,45].

Recently, novel imaging agents targeting tau pathology have been developed. Tau radiopharmaceuticals may provide better diagnostic accuracy, which is crucial for patients with atypical dementia syndromes. [^{18}F]THK5105, [^{18}F]THK5117, [^{18}F]T808, [^{18}F]T807, and [^{11}C]PBB3 are particularly promising owing to their high affinity and selectivity for tau fibrils [17,18,46,47].

Increased phospholipid production [48], activated microglia [49], and astrogliosis [50] are neuroinflammatory processes that are amenable to quantification using PET. However, to date, only microglial activation has been reported in Tg models expressing amyloid or tau pathology phenotypes. [^{11}C]PK11195 was the first imaging agent targeting microglial activation. In fact, [^{11}C]PK11195 binds to the peripheral benzodiazepine receptor (PBR), recently renamed as the 18-kDa translocator protein (TSPO). Its high non-specific binding and poor signal-to-noise ratio limit its capacity to quantify low TSPO concentrations [51]. [^{18}F]FEDAA1106 was designed for improved BBB permeability and has a high affinity for TSPO [52]. [^{11}C]AC5216 exhibits better kinetics in the brain than any other TSPO molecular agent and produces high-contrast images, allowing the measurement of early neuroinflammatory signs [53]. However, the clinical utilization of numerous novel TSPO radiopharmaceuticals is limited by the rs6971 single-nucleotide polymorphism in the *TSPO* gene, which is responsible for 30% of the difference in the standardized uptake value (SUV) between carriers and non-carriers [54]. Cannabinoid receptor type 2 (CB2) constitutes a new molecular target for detecting activated microglia. In fact, the CB2 agonist [^{11}C]A836339 binds to CB2 receptors surrounding amyloid plaques [55], supporting the concept that the microglial upregulation of CB2 is associated with amyloidosis [56].

Dopamine, serotonin, acetylcholine, and GABA abnormalities have been quantified in AD patients by PET [57]. However, *in vivo* quantification of neurotransmission abnormalities has been largely neglected in Tg models of amyloid and tau pathology. At present, only GABAergic and cholinergic systems have been assessed in AD microPET research. [^{11}C]FMZ is a ligand that binds to α subunits of GABA-A receptor and presents fast kinetics and low non-specific binding in the brain [58,59]. [^{11}C]FMZ precisely revealed decreases in regions showing the greatest degree of neuronal loss in post-mortem studies and is suggested to serve as an imaging index of neuronal loss [60]. [^{11}C]MP4A targets acetylcholinesterase (AChE), and its rate of hydrolysis is used as a highly specific marker of AChE activity [61].

Genetic basis of Tg models displaying amyloidosis and tau pathology

Genetic mutations that underlie familial forms of AD (FAD) and frontotemporal lobar degeneration (FTLD) provided the basis for the development of genetically engineered models overexpressing human genes encoding key proteins involved in the aggregation of amyloid plaques and the formation of tau aggregates, respectively [22,24]. Animal phenotypes derived from genetic manipulations are crucial for the design and interpretation of microPET studies because the concentration of abnormal proteins in brain tissue changes dramatically across different models. As such, models with high concentrations of brain pathology (e.g., amyloid plaques) provide an improved signal-to-noise ratio. We briefly review Tg models of amyloidosis and tau pathology that have previously been studied with microPET. These models typically use combinatorial approaches involving the expression of APP, presenilin-1 (PS1), and mutant tau (Figure 2, Table S2 in the supplementary material online; for a complete description of the models see http://www.alzforum.org/research-models).

APP models

The overexpression of the mutant human APP gene is the key concept underlying the majority of amyloid models. Several APP mutations produce a wide range of phenotypes with various degrees of amyloidosis, neuroinflammation, and neurodegeneration. The Tg2576 mouse model presents elevated Aβ levels at 6–9 months and amyloid deposits starting at 9–12 months; however, there is no neuronal loss or NFT formation [62]. The APP23 mouse model presents amyloid plaques as early as 6 months,

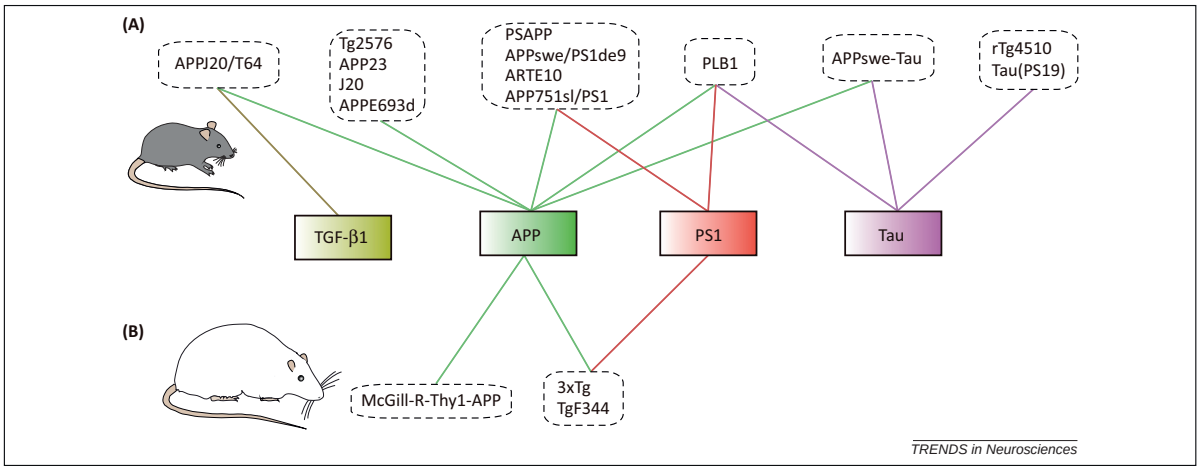

Figure 2. Transgenic (Tg) models displaying amyloidosis and tau pathology. Tg models of amyloidosis and tau pathology are produced by the overexpression of mutant human genes, such as amyloid precursor protein (*APP*), presenilin-1/PS1 (*PSEN1*), or microtubule-associated protein tau (*MAPT*). Genetic advances have provided the opportunity to combine these mutations and build models displaying phenotypes that closely resemble human AD neuropathology. Although more studies have been conducted with Tg mice models **(A)**, rat models **(B)** offer advantages for imaging procedures, mainly owing to their larger brain volumes and closer phylogenetic similarity to humans.

together with cell loss and tau hyperphosphorylation, although there is no NFT aggregation [63]. The APPE693d mouse model shows elevated Aβ production and abnormal tau phosphorylation at 8 months, and it develops increased microglial activation at 12 months; however, there is no plaque deposition, even at 24 months [64]. Finally, the J20 mouse model shows an early decline in synaptophysin immunoreactivity, a measure of synaptic density, at 2–4 months and amyloid plaques at approximately 5–7 months [65].

APP/PS1 models

The addition of a PS1 mutation in models overexpressing APP yields a more severe brain amyloidosis phenotype. Compared with APP models, PSAPP mice have higher $A\beta_{1-42}$ brain concentrations, although amyloid plaques are detectable only at 6 months of age [66]. The APPswe/PS1d9 mutations produce a combination of brain amyloidosis and decreases in cholinergic activity at 6 months [67,68]. The Arte10 mouse model shows early (3–5 months) amyloidosis and microglial activation [69]. Similarly, APP751sl/PS1 mice show amyloidosis at 3–4 months and microglial activation surrounding Aβ plaques at 6 months [70,71]. Interestingly, APP/PS1-21 mice exhibit aggressive cerebral amyloidosis starting at 1.5–2 months of age, which is accompanied by microglial activation and neuronal loss [72]. In addition to mouse models, there are recently developed rat models carrying APP/PS1 mutations. The 3×Tg rat model exhibits brain amyloidosis, microglial activation, and hyperphosphorylated tau at 7 months of age [73]. The TgF344 rat model displays age-dependent amyloidosis and phosphorylated tau starting at 6 months, accompanied by astrogliosis and neuronal loss at 16 months [74].

APP/TGF-β1 model

TGF-β1 and APP mutations combine in the mouse model J20/T64, which was designed to investigate vascular and tissue aspects of amyloidosis [75]. This model shows an early dysfunctional cerebrovascular response and strong microglial activation at 5 months, followed by an increase in Aβ levels at 6–8 months, reaching a plateau in the amount of plaques between 12 and 18 months [76,77].

Tau models

It is expected that ligands for NFTs will play an important role in the differential diagnosis of early-onset dementia, atypical presentations of dementia (e.g., frontal variants of AD), and mixed dementia. Although tau Tg models are typically based on human FTLD mutations (mainly frontotemporal dementia with parkinsonism-17, or FTDP-17), they were crucial for the validation of tau imaging agents. For example, the rTg4510 model, which carries an FTDP-17 tau mutation, exhibits NFTs, neuronal loss, and brain atrophy starting at 4 months [78]. In the PS19 model, which also carries an FTDP-17 tau mutation, microglial activation and synaptic loss (3 months) precede filamentous tau lesions at 6 months of age [79].

APP/Tau

The presence of both APPswe and FTDP-17 tau mutations in the TAPP mice model produces a phenotype of amyloidosis and NFTs that is detectable at 9–10 months [80]. As expected, this model shows that amyloidosis and NFTs arise in distinct brain regions.

APP/PS1 and tau model

Although it is expected that APP, PS1, and FTDP-17 tau mutations induce an aggressive pathological phenotype in mouse models, the PLB1 mouse model exhibits a mild phenotype owing to a single-copy knock-in of a dual Tg construct expressing mutant human APP and tau. Indeed, this model presents lower brain human APP/Aβ concentrations and low tau immunoreactivity at 6 months [81].

In summary, there is a wide range of phenotypic expression among Tg models of amyloidosis and tau pathology.

Variability due to different expression levels, mutant isoforms, background strains, or promoters ultimately has an impact on microPET outcome measures. Such substantial phenotypic heterogeneity makes the choice of Tg strains a key step in designing a successful microPET experiment. Although some models display amyloidosis associated with a degree of neuroinflammation or neurodegeneration, none of the available Tg models can reproduce the full complexity of human sporadic or genetic AD pathophysiology.

The pathology phenotype dictates the *in vivo* amyloid load

The ability to image brain amyloidosis with microPET depends on the brain degree of amyloid pathology (amyloid plaques), properties of the radiopharmaceutical [specific activity (SA), K_D, radiometabolites], scanner resolution, acquisition parameters, and analytical methods (Box 1). The age of the animals also becomes an important variable because amyloid pathology accumulates as a function of time in models harboring APP mutations. APP Tg strains usually fail to retain amyloid imaging agents owing to their modest concentrations of brain fibrillary amyloid, particularly in young animals. For example, [^{18}F]24 was the only compound reported to accumulate in Tg2576 mice aged 31 months, whereas [^{11}C]PiB and [^{18}F]FDDNP were not retained even in mice aged 22–23 months [36,82,83]. Outstanding radiochemistry contributed to the detection of [^{11}C]PiB retention in the APP23 mouse model (17–29 months) [21,84,85].

Animals harboring mutant *APP* and *PS1* genes display more aggressive amyloidosis than APP strains. As a consequence, the Arte10 mouse model exhibits [^{11}C]PiB retention with a radiochemistry preparation similar to those administered to human subjects [86,87]. As expected, Arte10 mice aged 22 months also showed retention of the new amyloid agent [^{11}C]5 [37]. Age-dependent [^{18}F]florbetapir retention has been demonstrated in the APP/PS1-21 mouse model [88]. Finally, [^{64}Cu^{II}]L1 and [^{18}F]1 could be used to detect the amyloid load in APPswe/PS1 mice aged 9 months [38,40]. By contrast, PS1/APP mice failed to retain [^{11}C]PIB at 6, 9, or 12 months. This unexpected negative result could be attributed to study design issues, such as the small sample size for each time-point and the large brain volumes of interest (VOIs) [89]. Rat models displaying amyloidosis are more suitable for the resolution of microPET scanners. In fact, a 3×Tg rat model showed an age-dependent increase in [^{18}F]FDDNP retention in cross-sectional (9, 14, and 22 months) and longitudinal (10, 13, 15, and 18 months) studies [90]. Furthermore, the TgF344 rat model showed high [^{18}F]FDDNP retention at 15 months [74]. Additionally, an early [11C]PiB microPET study with the McGill-R-Thy1-APP model (APPswe/ind) have shown promising results [134,135]. These results underscore the advantages of models with larger brain volumes in microPET experiments.

In summary, it is intuitive that Tg models displaying significant amounts of brain amyloidosis exhibit better retention of amyloid imaging agents. More elaborate research focusing on *in vivo* brain amyloid gold-standard quantification using microPET is a complex task in mice owing to the need for repeated blood sampling for estimation of plasma concentrations of radiopharmaceuticals. In rats, the larger body mass, brain size, and blood volume permit the proper estimation of the plasma input necessary to carry out gold-standard binding experiments using kinetic modeling (Figure 3). Such kinetic modeling experiments are necessary for validating simplified methods such as the standardized uptake value ratio (SUVR). For the same reasons, Tg rats are advantageous for longitudinal studies focusing on modeling pathophysiology as a function of amyloid progression or monitoring novel therapeutic interventions. One of the best examples illustrating the translational power of Tg models is the development of diverse $A\beta_{1-42}$ vaccines, which are currently being tested in clinical trials [91,92]. However, to date, the combination of microPET amyloid agents with Tg models has only contributed to the development of new molecular agents.

Imaging AD biomarkers of neurodegeneration

Tau imaging agents and [^{18}F]FDG are defined as biomarkers of neurodegeneration. Although initial PET results using tau ligands are promising, they still must be validated and utilized in a wider range of animal models and human tauopathies. [^{18}F]THK523 (K_D = 1.67 nM) and [^{11}C]PBB3 (K_D = 2.5 nM) were used successfully to identify tau fibrils in rTg4510 and PS19 mice models, respectively [19,46]. By contrast, [^{18}F]T807 binding was negative in the TAPP mouse model, possibly owing to the reduced signal-to-noise ratio caused by its inferior affinity (K_D=14.6 nM) [93]. It is expected that novel radiopharmaceuticals targeting NFTs will soon be developed and examined. Such radiopharmaceuticals will have multiple applications in translational neuroscience by enabling the assessment of tauopathy propagation in parallel with cognitive decline [94].

Glucose hypometabolism is a well-known feature in the AD brain. Although hypometabolism is an early abnormality in AD, the link between amyloidosis, tau pathology, and metabolic decline remains elusive [16]. Although glucose hypometabolism correlates with cognitive decline in humans [95], such associations remain unclear in animal models. Glucose metabolism abnormalities indexed by [^{18}F]FDG uptake have been reported either during the resting state or as a result of sensory or motor activation. During prolonged whisker stimulation, higher metabolism in the contralateral, compared with the ipsilateral, barrel cortex is expected. Experiments conducted on J20 (9, 12, and 19 months of age) and J20/T64 (18 months of age) mouse models showed reduced glucose uptake in the barrel cortex contralateral to whisker stimulation [77,96,97]. These results are consistent with the hypothesis that models overexpressing APP show abnormal coupling between brain activation and metabolism.

In contrast to activation studies, resting acquisitions have provided variable results. In APP strains, such as the Tg2576 model, hypermetabolism was observed at 7 months of age, whereas normal metabolism was observed at 9, 13, and 15 months [98–100]. The only study conducted in the APP23 mouse revealed normal glucose metabolism at 13 months, despite the neuronal depletion that is characteristic of this model [101,102]. In fact, these findings might

Box 1. Key points for microPET

The procedures employed determine the success of microPET experiments using small animal models, particularly mice, which are at least fivefold smaller than rats [126]. The logistics involved in these experiments are substantially more complex than those involved in clinical PET experiments. Importantly, microPET experiments must be carried out by an experienced team.

(i) **Cyclotron:** refined hot-atom chemistry within a target is necessary to produce radionuclides with high specific activity (SA; see Glossary). These radionuclides are used for the radiolabeling of molecules [127].

(ii) **Radiochemistry:** radiopharmaceutical doses should be stable in the appropriate excipient and prepared at concentrations sufficiently high to permit the administration of small volumes (<10% of total blood volume) with high SA (the mass injected should be ≤5% of the radiopharmaceutical K_M or K_D) [128]. Compounds labeled with [^{18}F] are preferable over [^{11}C]-labeled compounds owing to the less complex radiochemistry and longer half-life [129].

(iii) **MicroPET procedures:** list-mode acquisitions are preferable because they provide greater flexibility for data reanalysis. Anesthesia should be avoided whenever possible; however, when unavoidable, the choice of anesthetic should be carefully considered. For example, gas anesthetics are easier to adjust during the course of a microPET experiment. The monitoring of anesthetized animals is crucial to avoid undesirable physiological states such as cardiovascular instability, low central temperature, and brain hyperperfusion or hypoperfusion [110–113]. Radiopharmaceuticals should be administered in the venous system to secure easy access to the central circulation, to ensure equal distribution to the tissues, and to avoid first-pass effects [130]. In terms of acquisition, the brain should be placed in the center of the scanner's field of view (FOV) to maximize resolution. The dose injected should respect the limits imposed by the scanner hardware. Arterial or venous blood samples should account for less than 10% of the total blood volume of the animal. A transmission scan or CT (anatomical structural image) should be conducted to allow data reconstruction [131] (Figure I).

(iv) **Data processing:** optimized reconstruction algorithms such as ordered-subset expectation maximization (OSEM) or maximum *a posteriori* (MAP) are desirable because they generate images with better signal-to-noise ratios and resolution. Every voxel of an image expresses the tissue-radioactivity concentration over time (time–activity curves; TACs), which can be arranged as single or multiple time-frames. The choice of analytical model for the TACs is crucial for interpreting microPET results. Although simplified models that do not require blood sampling are usually preferred owing to their simplicity, they rely on several assumptions that must be substantiated. Indeed, those models need to be validated beforehand using the full kinetic models to identify an appropriate reference region that is both stable and devoid of any specific binding. Biologically relevant outcome measures such as binding potentials (BP_{ND}), total volume of distribution (VT), and distribution volumes (DV) can be derived from the TACs and an arterial input function. The biological validity of outcome measures such as the distribution volume ratios (DVRs), the percentage of brain uptake normalized by the total body weight (SUV), and the ratio between a brain region and a reference region (SUVR) require validation with gold-standard kinetic methods [131].

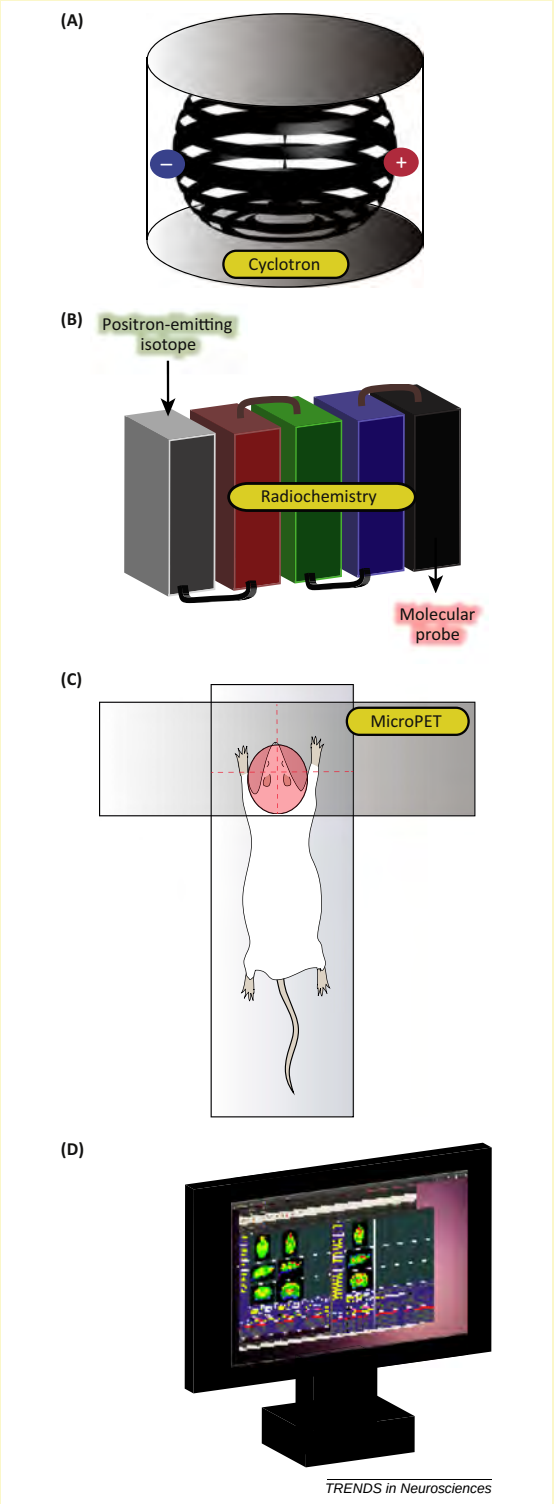

Figure I. Outline of a microPET acquisition.

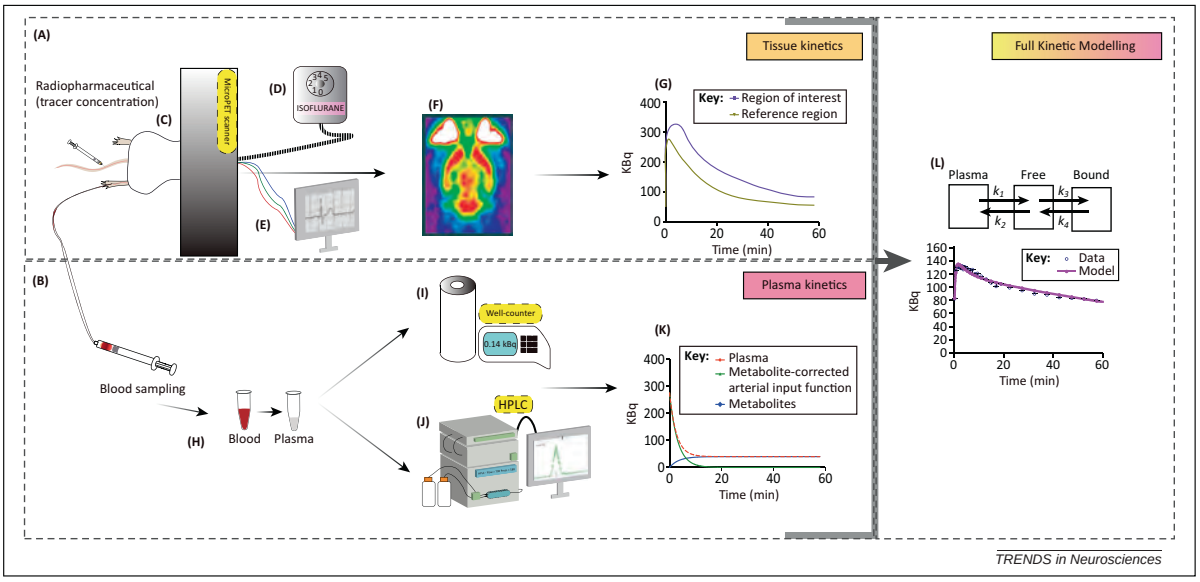

Figure 3. Full kinetic modeling. Pharmacokinetic modeling requires dynamic acquisitions (multiple time-frames) obtained from tissue kinetics **(A)** and plasma input function **(B)**. The setup for these experiments includes a dose calibrator for dose surveillance. Tissue kinetics information is obtained via a microPET camera **(C)** which is equipped with an anesthetics system **(D)** and a monitoring system **(E)** to maintain the animal in a physiological steady-state during the experiment. Imaging analysis **(F)** provides PET time–activity curves of the region of interest and the reference region **(G)**. The measurement of plasma kinetics involves the implantation of femoral artery catheter, a precise sampling system for small volumes of arterial blood **(H)**, a well-counter **(I)**, a gradient HPLC **(J)** for metabolite measurements, and a high-resolution balance. The plasma input function is the plasma time–activity curve adjusted for the fraction of radioactivity that remains attached to the radiopharmaceutical. The plasma time–activity curves **(K)** illustrate plasma radioactivity concentrations from a series of blood samples obtained during the microPET acquisition. Metabolite correction is needed because a fraction of the radioactivity present in the plasma detaches from the radiopharmaceutical (drug metabolism): radio-HPLC analysis of a series of plasma samples reveals the fraction of radioactivity remaining attached to the radiopharmaceutical through the plasma activity curve. **(L)** Kinetic models are used to estimate volumes of distribution, binding potentials or rate constants (K1, k2, k3 and k4). by using the tissue input function and the tissue time-activity curves. The presence of an appropriate reference region is important for the determination of binding potentials as well as for the determination of simplified methods, which bypasses the need for an arterial input function. KBq, kilobecquerel.

suggest the coexistence of temporary compensatory mechanisms due to amyloid deposition. Indeed, patterns of temporarily altered glucose metabolism have already been identified in patients with mild cognitive impairment (MCI) and AD [103].

In APP/PS1 strains, such as APP751sl/PS1 and APPswe/PS1de9 mice, PET [^{18}F]FDG shows brain hypometabolism at the beginning of the plaque formation phase, which occurs at 3 and 6 months, respectively, for these two models [104,105]. Hypometabolism may be associated with the neurodegeneration present in these models. By contrast, aged APPswe/PS1d9 animals (13–15 months) show normal [^{18}F]FDG uptake, whereas the APP751sl/PS1 model showed hypermetabolism despite its higher degree of neuronal depletion [105,106]. The hypermetabolism exhibited by the aged APP751sl/PS1 animals may be linked to the significant inflammatory reaction present in this model. PLB1 mice showed normal metabolism at 9 and 17 months of age, likely owing to the less-aggressive phenotype observed in these animals [81].

In contrast to studies using amyloid imaging agents, [^{18}F]FDG research in Tg models has advanced our knowledge regarding AD pathophysiology. First, the current data support the hypothesis that amyloidosis imposes reorganization of brain metabolic activity. In addition, [^{18}F]FDG was used successfully to measure the effects of effective pharmacological interventions in Tg models [107]. The data presented in our review suggest that [^{18}F]FDG uptake is might be responsive to inflammatory reactions and compensatory mechanisms during the progression of amyloidosis and tau pathology. Because human AD pathophysiological events are thought to begin at least a decade before symptom onset [41], the insights provided by Tg animals can aid the interpretation of metabolic changes observed during the early stages of human disease.

Sources of bias and variance in [^{18}F]FDG uptake

Brain metabolic changes assessed with microPET [^{18}F]FDG do not appear to follow a linear association with the model phenotype. Overall, the [^{18}F]FDG data obtained in Tg models refute a simple disease model where hypometabolism progresses as a function of amyloidosis or tau pathology. Alternatively, one could argue that variability in acquisition parameters or analytical issues, rather than phenotypic heterogeneity across Tg models, might explain the discrepancies between the reported results and predictions derived from the dynamic biomarkers of the AD pathological cascade hypothesis [3]. In addition, differences in scanner resolution can reduce the sensitivity of [^{18}F]FDG PET owing to the small volume of the mouse brain (Figure 4). Particularly, spillover effects from the harderian glands and partial volume effects constitute a significant issue that is present even in cutting-edge microPET systems [108]. Counting rate performance, scatter fraction, sensitivity, and image quality ([109] for review) might also introduce variability across microPET studies.

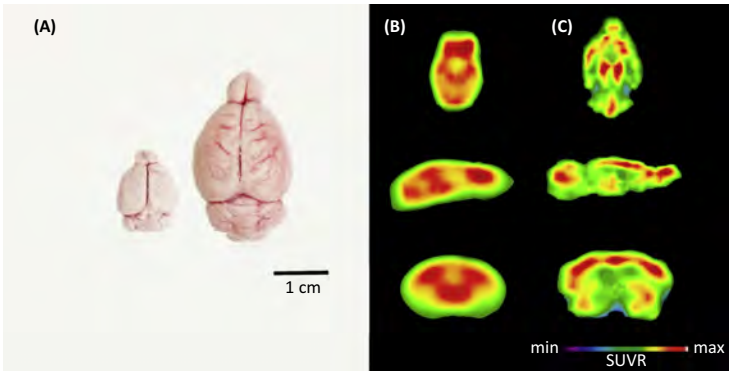

Figure 4. Comparison between microPET in rats and mice. The larger rat brain allows for the differentiation of several brain regions (e.g., the prefrontal cortex and cerebellum), allowing a more reliable analysis and providing more robust data. **(A)** Rat (wistar) and mouse (C57BL/6) brain specimens. [^{18}F]FDG scan in mice **(B)** and **(C)** rat. For further details see [132].

Handling, anesthesia, and maintenance of physiological conditions during PET [^{18}F]FDG acquisition are crucial. Variations in dietary conditions, ambient temperature, and circadian cycle have an impact on [^{18}F]FDG biodistribution in mice [110,111]. Furthermore, stressful handling or immobilization can cause the release of corticosteroids and consequently interfere with the global and regional rate of glucose consumption [112]. In addition, the suppression of brain activity imposed by anesthetics has a direct impact on glucose metabolism. For example, animals anesthetized with isoflurane show reduced global and regional [^{18}F]FDG uptake compared to awake animals [113]. In summary, the interpretation of [^{18}F]FDG microPET studies is complex and should take into consideration the imaging acquisition methodology and the physiological conditions during the [^{18}F]FDG uptake phase. Based on the present literature on microPET and [^{18}F]FDG, simple steps can significantly increase the reproducibility across studies. For example, the [^{18}F]FDG uptake phase should be performed systematically in fasting awake animals, and the scanning phase should be conducted under light anesthesia with constant monitoring of physiological conditions. In addition, documenting physiological conditions such as temperature, heart rate, and blood pressure during acquisitions may aid in analyzing discordances across studies.

Imaging neuroinflammation and neurotransmission

Aβ peptides and tau pathology independently trigger neuroinflammatory responses such as reactive astrogliosis and microglial activation [114,115]. Activated astrocytes and/or microglia serve as surrogates for neuroinflammation and can be quantified using PET technologies [116]. Although astrocyte activation in Tg models of amyloid and tau pathology has not yet been assessed using microPET, microglial activation has been described in several studies.

[^{11}C]PK11195 was capable of detecting higher TSPO expression in APPswe/PS1 from 9 to 16 months [117]. In models expressing a milder amyloid pathology, whereas [^{18}F]FEDAA1106 provided negative results even in APP23 mice aged 24 months [21], [^{11}C]AC5216 detected TSPO expression in animals with (APP23) and without (APPE693d) amyloid plaque deposition [21]. The higher sensitivity of [^{11}C]AC5216 for microgliosis is attributable to its better kinetics and affinity. TSPO imaging agents such as [^{11}C]AC5216 or [^{18}F]FEDAA1106 captured microglial activation in tau-PS19 aged 7 months mice [21,85]. The CB_2 receptor is a novel target for quantifying microglial activation [118]. In fact, [^{11}C]A836339 was capable of detecting brain CB_2 receptor upregulation in the APPswe/PS1de9 mouse model at 18 months of age [56].

Together, these data support the feasibility of quantifying the brain concentrations of activated microglia in response to amyloidosis and tau pathology in Tg models. The sensitivity of these studies relies on tracers with better affinity and higher specific binding than [^{11}C]PK11195, such as [^{11}C]AC5216 [53]. These experimental studies support human PET findings demonstrating that microglial activation precedes AD dementia symptoms [119,120]. Thus, *in vivo* tracking of neuroinflammation in animals displaying amyloidosis or tau pathology can be used as a marker of therapeutic effectiveness. In this context, AD clinical trials using anti-inflammatory drugs can incorporate PET imaging agents as biomarkers for target engagement.

Alterations in neurotransmission were minimally explored using microPET. Although neuronal integrity and AChE activity are reduced in the early stages of AD [121,122], [^{11}C]FMZ and [^{11}C]MP4A were unable to detect differences between the APP23 mouse model and wild type mice [102]. In this context, subtle fluctuations in neurotransmission may not be detected owing to the small brain size and the spatial resolution limitations of microPET.

Concluding remarks and future directions

Despite being technically challenging, the combination of microPET with Tg models has advanced our understanding of AD pathophysiology, assisted in the development of AD biomarkers and opened new frontiers for disease-modifying therapies (a summary overview of microPET experiments is given in Table S3 in the supplementary material online). Animal models constructed via advanced genetic combinatorial techniques associated with the growing number of PET radiopharmaceuticals are likely to play

a major role in AD research. Importantly, our review emphasizes that pharmacokinetic properties and the animal model phenotypes should be carefully considered when designing microPET studies. In addition, the accuracy and sensitivity of these methods are dependent on the radiochemistry quality (particularly the SA), animal physiological conditions, scanner resolution, and acquisition protocols. Furthermore, full kinetic models (e.g., one- or two-tissue compartment models) should be used whenever possible; failing that, simplified models can be used if they have been previously validated for the radiopharmaceutical of interest. Finally, recent advances in the generation of genetically engineered rats have provided a better animal model for microPET given their larger brain and body size, homeostatic stability during anesthesia, and larger blood volume, which translate into robust longitudinal assessments.

Box 2. The [^{18}F]FDG metabolic network in small animals: what lies ahead?

Network analysis of PET [^{18}F]FDG data can reveal brain functional connectivity by means of correlation coefficient maps of glucose metabolism across all brain regions. Abnormalities in large-scale brain organization revealed by this advanced PET analysis showed progressive reduction of the whole-brain metabolic network as a result of AD pathology [133]. Because of spatial limitations, this approach is limited for mice owing to microPET present resolution; however, Tg rats are more suited to network analysis given their larger brain size. Although unexplored in Tg models, this technique has the potential to reveal the time-course of neurodegeneration propagation and compensatory mechanisms underlying metabolic network architecture. Furthermore, network architecture elements such as hubs (network nodes with the highest connectivity) may deliver information regarding brain metabolic plasticity in response to the deleterious effects of amyloidosis, neurodegeneration, neuroinflammation, and neurotransmission dysfunction. In summary, microPET [^{18}F]FDG metabolic networks might play an interesting role in AD research by providing new insights regarding glucose metabolism decline. Nodes obtained from [^{18}F]FDG SUVR values can be extracted using a rat brain atlas, and (provide data to generate large-scale and regional cross-correlation metabolic maps (Figure I) [132] for further details.

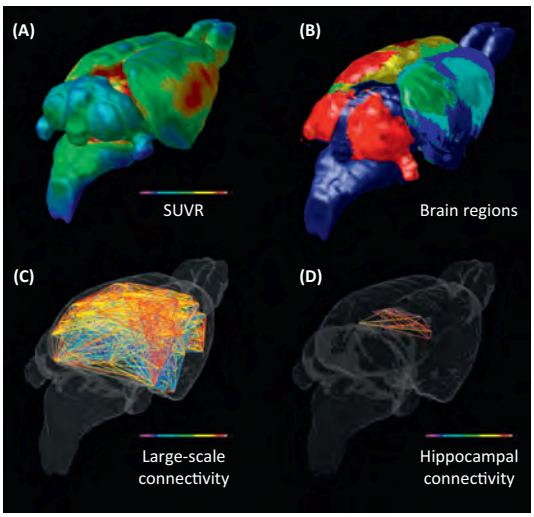

Figure I. Brain metabolic network inferred from microPET [^{18}F]FDG imaging.

In the near future it seems reasonable to expect that Tg mice models will continue to play a significant role in the development of radiopharmaceuticals. Refined statistical analyses offer the opportunity to explore pathophysiological mechanisms needed to interpret downstream outcome measures such as large- or small-scale brain architecture (Box 2). The future also promises exciting advances in multi-modality imaging approaches. The combination of microPET acquisition with cutting-edge technologies such as optogenetics (optoPET) and hybrid functional magnetic resonance imaging (PET-fMRI) will dissect the role of AD pathophysiology in the context of specific neural populations or large-scale brain connectivity, respectively. Novel radiopharmaceuticals will expand microPET possibilities of monitoring neurotransmission fluctuations, target engagement, and drug efficacy. Finally, longitudinal studies using microPET in rats (i.e., McGill-R-Thy1-APP, TgF3443, and 3×Tg) are ideally suited for accelerating the delivery of better biomarkers and pharmacotherapies, which ultimately translates into earlier diagnosis and more effective treatments for human AD.

Acknowledgments

This work was supported by the Canadian Institutes of Health Research (CIHR; MOP-11-51-31 and MOP 10-27-52), Alzheimer's Association (NIRG-12-259245), Fonds de Recherche du Québec - Santé (FRQS; Chercheur Boursier), the Allan Tiffin Trust (Infrastructure), the Conselho Nacional de Desenvolvimento Científico e Tecnológico (CNPq, Brazil), Fundação de Amparo à Pesquisa do Rio Grande do Sul (Fapergs, Brazil), and INCT for Excitotoxicity and Neuroprotection/CNPq. This research was also partially supported by Fonds d'innovation Pfizer-FRQS sur la maladie d'Alzheimer et les maladies apparentées - Volet 2 to A.C.C. and P.R.-N. A.C.C., S.G. and P.R.-N. are members of the CIHR Canadian Consortium of Neurodegeneration in Aging. We wish to thank Mr. Antoine Leuzy (McGill University) and Dr. Marcelo Dietrich (Yale University) for their insightful comments.

Appendix A. Supplementary data

Supplementary data associated with this article can be found, in the online version, at http://dx.doi.org/10.1016/j.tins.2014.07.002.

References

1 Selkoe, D.J. (2002) Alzheimer's disease is a synaptic failure. *Science* 298, 789–791
2 McGeer, P.L. and McGeer, E.G. (2013) The amyloid cascade-inflammatory hypothesis of Alzheimer disease: implications for therapy. *Acta Neuropathol.* 126, 479–497
3 Jack, C.R., Jr *et al.* (2013) Tracking pathophysiological processes in Alzheimer's disease: an updated hypothetical model of dynamic biomarkers. *Lancet Neurol.* 12, 207–216
4 Rowe, C.C. *et al.* (2007) Imaging beta-amyloid burden in aging and dementia. *Neurology* 68, 1718–1725
5 Jacobs, A.H. *et al.* (2003) PET-based molecular imaging in neuroscience. *Eur. J. Nucl. Med. Mol. Imaging* 30, 1051–1065
6 McKhann, G.M. *et al.* (2011) The diagnosis of dementia due to Alzheimer's disease: recommendations from the National Institute on Aging – Alzheimer's Association workgroups on diagnostic guidelines for Alzheimer's disease. *Alzheimers Dement.* 7, 263–269
7 Dubois, B. *et al.* (2007) Research criteria for the diagnosis of Alzheimer's disease: revising the NINCDS–ADRDA criteria. *Lancet Neurol.* 6, 734–746
8 Roman, G. and Pascual, B. (2012) Contribution of neuroimaging to the diagnosis of Alzheimer's disease and vascular dementia. *Arch. Med. Res.* 43, 671–676
9 Nichols, L. *et al.* (2006) Imaging and in vivo quantitation of beta-amyloid: an exemplary biomarker for Alzheimer's disease? *Biol. Psychiatry* 59, 940–947

10 Herholz, K. and Ebmeier, K. (2011) Clinical amyloid imaging in Alzheimer's disease. *Lancet Neurol.* 10, 667–670
11 Rowe, C.C. and Villemagne, V.L. (2011) Brain amyloid imaging. *J. Nucl. Med.* 52, 1733–1740
12 Rowe, C.C. *et al.* (2013) Head-to-head comparison of ^{11}C-PiB and ^{18}F-AZD4694 (NAV4694) for beta-amyloid imaging in aging and dementia. *J. Nucl. Med.* 54, 880–886
13 Scarmeas, N. *et al.* (2004) APOE-dependent PET patterns of brain activation in Alzheimer disease. *Neurology* 63, 913–915
14 Ishii, K. *et al.* (1996) Decreased medial temporal oxygen metabolism in Alzheimer's disease shown by PET. *J. Nucl. Med.* 37, 1159–1165
15 Foster, N.L. *et al.* (2007) FDG-PET improves accuracy in distinguishing frontotemporal dementia and Alzheimer's disease. *Brain* 130, 2616–2635
16 Mosconi, L. *et al.* (2010) Pre-clinical detection of Alzheimer's disease using FDG-PET, with or without amyloid imaging. *J. Alzheimers Dis.* 20, 843–854
17 Okamura, N. *et al.* (2013) Novel ^{18}F-labeled arylquinoline derivatives for noninvasive imaging of tau pathology in Alzheimer disease. *J. Nucl. Med.* 54, 1420–1427
18 Chien, D.T. *et al.* (2013) Early clinical PET imaging results with the novel PHF-tau radioligand [^{18}F]-T807. *J. Alzheimers Dis.* 34, 457–468
19 Maruyama, M. *et al.* (2013) Imaging of tau pathology in a tauopathy mouse model and in Alzheimer patients compared to normal controls. *Neuron* 79, 1094–1108
20 Politis, M. *et al.* (2012) Imaging of microglia in patients with neurodegenerative disorders. *Front. Pharmacol.* 3, 96
21 Maeda, J. *et al.* (2011) In vivo positron emission tomographic imaging of glial responses to amyloid-beta and tau pathologies in mouse models of Alzheimer's disease and related disorders. *J. Neurosci.* 31, 4720–4730
22 Gotz, J. and Ittner, L.M. (2008) Animal models of Alzheimer's disease and frontotemporal dementia. *Nat. Rev. Neurosci.* 9, 532–544
23 McGowan, E. *et al.* (1999) Amyloid phenotype characterization of transgenic mice overexpressing both mutant amyloid precursor protein and mutant presenilin 1 transgenes. *Neurobiol. Dis.* 6, 231–244
24 de Calignon, A. *et al.* (2012) Propagation of tau pathology in a model of early Alzheimer's disease. *Neuron* 73, 685–697
25 Braak, H. and Braak, E. (1991) Neuropathological stageing of Alzheimer-related changes. *Acta Neuropathol.* 82, 239–259
26 Vogt, B.A. and Paxinos, G. (2014) Cytoarchitecture of mouse and rat cingulate cortex with human homologies. *Brain Struct. Funct.* 219, 185–192
27 Lu, H. *et al.* (2012) Rat brains also have a default mode network. *Proc. Natl. Acad. Sci. U.S.A.* 109, 3979–3984
28 Mathis, C.A. *et al.* (2002) A lipophilic thioflavin-T derivative for positron emission tomography (PET) imaging of amyloid in brain. *Bioorg. Med. Chem. Lett.* 12, 295–298
29 Tolboom, N. *et al.* (2009) Relationship of cerebrospinal fluid markers to ^{11}C-PiB and ^{18}F-FDDNP binding. *J. Nucl. Med.* 50, 1464–1470
30 Yang, L. *et al.* (2012) Brain amyloid imaging–FDA approval of florbetapir F18 injection. *N. Engl. J. Med.* 367, 885–887
31 US Food and Drug Administration (2013) GE beta-amyloid agent approved. *J. Nucl. Med.* 54, 10N
32 Clark, C.M. *et al.* (2011) Use of florbetapir-PET for imaging beta-amyloid pathology. *J. Am. Med. Assoc.* 305, 275–283
33 Ikonomovic, M.D. *et al.* (2008) Post-mortem correlates of in vivo PiB-PET amyloid imaging in a typical case of Alzheimer's disease. *Brain* 131, 1630–1645
34 Maia, L.F. *et al.* (2013) Changes in amyloid-beta and Tau in the cerebrospinal fluid of transgenic mice overexpressing amyloid precursor protein. *Sci. Transl. Med.* 5, 194re192
35 Wong, D.F. *et al.* (2010) In vivo imaging of amyloid deposition in Alzheimer disease using the radioligand ^{18}F-AV-45 (Florbetapir F 18). *J. Nucl. Med.* 51, 913–920
36 Cui, M. *et al.* (2012) Novel ^{18}F-labeled benzoxazole derivatives as potential positron emission tomography probes for imaging of cerebral beta-amyloid plaques in Alzheimer's disease. *J. Med. Chem.* 55, 9136–9145
37 Yousefi, B.H. *et al.* (2011) Synthesis and evaluation of ^{11}C-labeled imidazo[2,1-b]benzothiazoles (IBTs) as PET tracers for imaging beta-amyloid plaques in Alzheimer's disease. *J. Med. Chem.* 54, 949–956
38 Calamai, E. *et al.* (2013) ^{18}F-barbiturates are PET tracers with diagnostic potential in Alzheimer's disease. *Chem. Commun. (Camb.)* 49, 792–794
39 Zimmer, E. *et al.* (2013) [^{18}F]NAV4694 shows higher binding and wider dynamic range compared with [^{11}C]PiB in Alzheimer's disease postmortem tissue. *Alzheimers Dement.* 9, P22–P23
40 Lim, S. *et al.* (2010) A copper radiopharmaceutical for diagnostic imaging of Alzheimer's disease: a bis(thiosemicarbazonato)copper(II) complex that binds to amyloid-beta plaques. *Chem. Commun.* 46, 5437–5439
41 Jack, C.R., Jr *et al.* (2010) Hypothetical model of dynamic biomarkers of the Alzheimer's pathological cascade. *Lancet Neurol.* 9, 119–128
42 Hattori, N. *et al.* (2004) Acute changes in regional cerebral ^{18}F-FDG kinetics in patients with traumatic brain injury. *J. Nucl. Med.* 45, 775–783
43 Silverman, D.H. (2004) Brain ^{18}F-FDG PET in the diagnosis of neurodegenerative dementias: comparison with perfusion SPECT and with clinical evaluations lacking nuclear imaging. *J. Nucl. Med.* 45, 594–607
44 Bohnen, N.I. *et al.* (2012) Effectiveness and safety of ^{18}F-FDG PET in the evaluation of dementia: a review of the recent literature. *J. Nucl. Med.* 53, 59–71
45 Mosconi, L. *et al.* (2008) Multicenter standardized ^{18}F-FDG PET diagnosis of mild cognitive impairment, Alzheimer's disease, and other dementias. *J. Nucl. Med.* 49, 390–398
46 Fodero-Tavoletti, M.T. *et al.* (2011) ^{18}F-THK523: a novel in vivo tau imaging ligand for Alzheimer's disease. *Brain* 134, 1089–1100
47 Zhang, W. *et al.* (2012) A highly selective and specific PET tracer for imaging of tau pathologies. *J. Alzheimers Dis.* 31, 601–612
48 Belhocine, T.Z. and Prato, F.S. (2011) Transbilayer phospholipids molecular imaging. *EJNMMI Res.* 1, 17
49 Edison, P. *et al.* (2008) Microglia, amyloid, and cognition in Alzheimer's disease: an [^{11}C](R)PK11195-PET and [^{11}C]PIB-PET study. *Neurobiol. Dis.* 32, 412–419
50 Carter, S.F. *et al.* (2012) Evidence for astrocytosis in prodromal Alzheimer disease provided by ^{11}C-deuterium-L-deprenyl: a multitracer PET paradigm combining ^{11}C-Pittsburgh compound B and ^{18}F-FDG. *J. Nucl. Med.* 53, 37–46
51 Shah, F. *et al.* (1994) Synthesis of the enantiomers of [N-methyl-^{11}C]PK 11195 and comparison of their behaviours as radioligands for PK binding sites in rats. *Nucl. Med. Biol.* 21, 573–581
52 Zhang, M.R. *et al.* (2004) Development of a new radioligand, N-(5-fluoro-2-phenoxyphenyl)-N-(2-[^{18}F]fluoroethyl-5-methoxybenzyl)acetamide, for pet imaging of peripheral benzodiazepine receptor in primate brain. *J. Med. Chem.* 47, 2228–2235
53 Zhang, M.R. *et al.* (2007) ^{11}C-AC-5216: a novel PET ligand for peripheral benzodiazepine receptors in the primate brain. *J. Nucl. Med.* 48, 1853–1861
54 Yoder, K.K. *et al.* (2013) Influence of TSPO genotype on ^{11}C-PBR28 standardized uptake values. *J. Nucl. Med.* 54, 1320–1322
55 Pazos, M.R. *et al.* (2004) Role of the endocannabinoid system in Alzheimer's disease: new perspectives. *Life Sci.* 75, 1907–1915
56 Horti, A.G. *et al.* (2010) Synthesis and biodistribution of [^{11}C]A-836339, a new potential radioligand for PET imaging of cannabinoid type 2 receptors (CB2). *Bioorg. Med. Chem.* 18, 5202–5207
57 Pappata, S. *et al.* (2008) In vivo imaging of neurotransmission and brain receptors in dementia. *J. Neuroimaging* 18, 111–124
58 Debruyne, D. *et al.* (1991) Plasma pharmacokinetics and metabolism of the benzodiazepine antagonist [^{11}C] Ro 15-1788 (flumazenil) in baboon and human during positron emission tomography studies. *Eur. J. Drug Metab. Pharmacokinet.* 16, 141–152
59 Hansen, T.D. *et al.* (1991) The influence of inhalational anesthetics on in vivo and in vitro benzodiazepine receptor binding in the rat cerebral cortex. *Anesthesiology* 74, 97–104
60 Pascual, B. *et al.* (2012) Decreased carbon-11-flumazenil binding in early Alzheimer's disease. *Brain* 135, 2817–2825
61 Sato, K. *et al.* (2004) Evaluation of simplified kinetic analyses for measurement of brain acetylcholinesterase activity using N-[^{11}C]Methylpiperidin-4-yl propionate and positron emission tomography. *J. Cereb. Blood Flow Metab.* 24, 600–611
62 Hsiao, K. *et al.* (1996) Correlative memory deficits, Abeta elevation, and amyloid plaques in transgenic mice. *Science* 274, 99–102

63 Sturchler-Pierrat, C. *et al.* (1997) Two amyloid precursor protein transgenic mouse models with Alzheimer disease-like pathology. *Proc. Natl. Acad. Sci. U.S.A.* 94, 13287–13292
64 Tomiyama, T. *et al.* (2010) A mouse model of amyloid beta oligomers: their contribution to synaptic alteration, abnormal tau phosphorylation, glial activation, and neuronal loss in vivo. *J. Neurosci.* 30, 4845–4856
65 Mucke, L. *et al.* (2000) High-level neuronal expression of Abeta 1-42 in wild-type human amyloid protein precursor transgenic mice: synaptotoxicity without plaque formation. *J. Neurosci.* 20, 4050–4058
66 Holcomb, L. *et al.* (1998) Accelerated Alzheimer-type phenotype in transgenic mice carrying both mutant amyloid precursor protein and presenilin 1 transgenes. *Nat. Med.* 4, 97–100
67 Savonenko, A. *et al.* (2005) Episodic-like memory deficits in the APPswe/PS1dE9 mouse model of Alzheimer's disease: relationships to beta-amyloid deposition and neurotransmitter abnormalities. *Neurobiol. Dis.* 18, 602–617
68 Jankowsky, J.L. *et al.* (2004) Mutant presenilins specifically elevate the levels of the 42 residue beta-amyloid peptide in vivo: evidence for augmentation of a 42-specific gamma secretase. *Hum. Mol. Genet.* 13, 159–170
69 Willuweit, A. *et al.* (2009) Early-onset and robust amyloid pathology in a new homozygous mouse model of Alzheimer's disease. *PLoS ONE* 4, e7931
70 Jimenez, S. *et al.* (2008) Inflammatory response in the hippocampus of PS1M146L/APP751SL mouse model of Alzheimer's disease: age-dependent switch in the microglial phenotype from alternative to classic. *J. Neurosci.* 28, 11650–11661
71 Blanchard, V. *et al.* (2003) Time sequence of maturation of dystrophic neurites associated with Abeta deposits in APP/PS1 transgenic mice. *Exp. Neurol.* 184, 247–263
72 Radde, R. *et al.* (2006) Abeta42-driven cerebral amyloidosis in transgenic mice reveals early and robust pathology. *EMBO Rep.* 7, 940–946
73 Flood, D.G. *et al.* (2009) A transgenic rat model of Alzheimer's disease with extracellular Abeta deposition. *Neurobiol. Aging* 30, 1078–1090
74 Cohen, R.M. *et al.* (2013) A transgenic Alzheimer rat with plaques, tau pathology, behavioral impairment, oligomeric abeta, and frank neuronal loss. *J. Neurosci.* 33, 6245–6256
75 Wyss-Coray, T. *et al.* (1997) Amyloidogenic role of cytokine TGF-beta1 in transgenic mice and in Alzheimer's disease. *Nature* 389, 603–606
76 Wyss-Coray, T. *et al.* (2001) TGF-beta1 promotes microglial amyloid-beta clearance and reduces plaque burden in transgenic mice. *Nat. Med.* 7, 612–618
77 Ongali, B. *et al.* (2010) Transgenic mice overexpressing APP and transforming growth factor-beta1 feature cognitive and vascular hallmarks of Alzheimer's disease. *Am. J. Pathol.* 177, 3071–3080
78 Santacruz, K. *et al.* (2005) Tau suppression in a neurodegenerative mouse model improves memory function. *Science* 309, 476–481
79 Yoshiyama, Y. *et al.* (2007) Synapse loss and microglial activation precede tangles in a P301S tauopathy mouse model. *Neuron* 53, 337–351
80 Lewis, J. *et al.* (2001) Enhanced neurofibrillary degeneration in transgenic mice expressing mutant tau and APP. *Science* 293, 1487–1491
81 Platt, B. *et al.* (2011) Abnormal cognition, sleep, EEG and brain metabolism in a novel knock-in Alzheimer mouse, PLB1. *PLoS ONE* 6, e27068
82 Toyama, H. *et al.* (2005) PET imaging of brain with the beta-amyloid probe, [^{11}C]6-OH-BTA-1, in a transgenic mouse model of Alzheimer's disease. *Eur. J. Nucl. Med. Mol. Imaging* 32, 593–600
83 Kawarabayashi, T. *et al.* (2001) Age-dependent changes in brain, CSF, and plasma amyloid (beta) protein in the Tg2576 transgenic mouse model of Alzheimer's disease. *J. Neurosci.* 21, 372–381
84 Maeda, J. *et al.* (2007) Longitudinal, quantitative assessment of amyloid, neuroinflammation, and anti-amyloid treatment in a living mouse model of Alzheimer's disease enabled by positron emission tomography. *J. Neurosci.* 27, 10957–10968
85 Higuchi, M. (2009) Visualization of brain amyloid and microglial activation in mouse models of Alzheimer's disease. *Curr. Alzheimer Res.* 6, 137–143
86 Klunk, W.E. *et al.* (2004) Imaging brain amyloid in Alzheimer's disease with Pittsburgh Compound-B. *Ann. Neurol.* 55, 306–319
87 Manook, A. *et al.* (2012) Small-animal PET imaging of amyloid-beta plaques with [^{11}C]PiB and its multi-modal validation in an APP/PS1 mouse model of Alzheimer's disease. *PLoS ONE* 7, e31310
88 Poisnel, G. *et al.* (2012) PET imaging with [^{18}F]AV-45 in an APP/PS1-21 murine model of amyloid plaque deposition. *Neurobiol. Aging* 33, 2561–2571
89 Klunk, W.E. *et al.* (2005) Binding of the positron emission tomography tracer Pittsburgh compound-B reflects the amount of amyloid-beta in Alzheimer's disease brain but not in transgenic mouse brain. *J. Neurosci.* 25, 10598–10606
90 Teng, E. *et al.* (2011) [^{18}F]FDDNP microPET imaging correlates with brain Abeta burden in a transgenic rat model of Alzheimer disease: effects of aging, in vivo blockade, and anti-Abeta antibody treatment. *Neurobiol. Dis.* 43, 565–575
91 Schenk, D. *et al.* (1999) Immunization with amyloid-beta attenuates Alzheimer-disease-like pathology in the PDAPP mouse. *Nature* 400, 173–177
92 Wang, Y.J. (2014) Alzheimer disease: lessons from immunotherapy for Alzheimer disease. *Nat. Rev. Neurol.* 10, 188–189
93 Xia, C.F. *et al.* (2013) [^{18}F]T807, a novel tau positron emission tomography imaging agent for Alzheimer's disease. *Alzheimers Dement.* 9, 666–676
94 Zimmer, E.R. *et al.* (2014) In vivo tracking of tau pathology using positron emission tomography (PET) molecular imaging in small animals. *Transl. Neurodegener.* 3, 6
95 Shokouhi, S. *et al.* (2013) Longitudinal progression of cognitive decline correlates with changes in the spatial pattern of brain ^{18}F-FDG PET. *J. Nucl. Med.* 54, 1564–1569
96 Nicolakakis, N. *et al.* (2008) Complete rescue of cerebrovascular function in aged Alzheimer's disease transgenic mice by antioxidants and pioglitazone, a peroxisome proliferator-activated receptor gamma agonist. *J. Neurosci.* 28, 9287–9296
97 Tong, X.K. *et al.* (2012) Age-dependent rescue by simvastatin of Alzheimer's disease cerebrovascular and memory deficits. *J. Neurosci.* 32, 4705–4715
98 Luo, F. *et al.* (2012) Characterization of 7- and 19-month-old Tg2576 mice using multimodal in vivo imaging: limitations as a translatable model of Alzheimer's disease. *Neurobiol. Aging* 33, 933–944
99 Kuntner, C. *et al.* (2009) Limitations of small animal PET imaging with [^{18}F]FDDNP and FDG for quantitative studies in a transgenic mouse model of Alzheimer's disease. *Mol. Imaging Biol.* 11, 236–240
100 Martin-Moreno, A.M. *et al.* (2012) Prolonged oral cannabinoid administration prevents neuroinflammation, lowers beta-amyloid levels and improves cognitive performance in Tg APP 2576 mice. *J. Neuroinflammation* 9, 8
101 Bondolfi, L. *et al.* (2002) Amyloid-associated neuron loss and gliogenesis in the neocortex of amyloid precursor protein transgenic mice. *J. Neurosci.* 22, 515–522
102 Heneka, M.T. *et al.* (2006) Locus ceruleus degeneration promotes Alzheimer pathogenesis in amyloid precursor protein 23 transgenic mice. *J. Neurosci.* 26, 1343–1354
103 Sanabria-Diaz, G. *et al.* (2013) Glucose metabolism during resting state reveals abnormal brain networks organization in the Alzheimer's disease and mild cognitive impairment. *PLoS ONE* 8, e68860
104 Yuan, S.M. *et al.* (2011) Evodiamine improves congnitive abilities in SAMP8 and APP(swe)/PS1(DeltaE9) transgenic mouse models of Alzheimer's disease. *Acta Pharmacol. Sin.* 32, 295–302
105 Poisnel, G. *et al.* (2012) Increased regional cerebral glucose uptake in an APP/PS1 model of Alzheimer's disease. *Neurobiol. Aging* 33, 1995–2005
106 Rapic, S. *et al.* (2013) Imaging microglial activation and glucose consumption in a mouse model of Alzheimer's disease. *Neurobiol. Aging* 34, 351–354
107 Papadopoulos, P. *et al.* (2013) Pioglitazone improves reversal learning and exerts mixed cerebrovascular effects in a mouse model of Alzheimer's disease with combined amyloid-beta and cerebrovascular pathology. *PLoS ONE* 8, e68612
108 Mirrione, M.M. *et al.* (2007) A novel approach for imaging brain-behavior relationships in mice reveals unexpected metabolic patterns during seizures in the absence of tissue plasminogen activator. *Neuroimage* 38, 34–42
109 Goertzen, A.L. *et al.* (2012) NEMA NU 4-2008 comparison of preclinical PET imaging systems. *J. Nucl. Med.* 53, 1300–1309

110 Fueger, B.J. *et al.* (2006) Impact of animal handling on the results of ^{18}F-FDG PET studies in mice. *J. Nucl. Med.* 47, 999–1006
111 Hildebrandt, I.J. *et al.* (2008) Anesthesia and other considerations for in vivo imaging of small animals. *ILAR J.* 49, 17–26
112 Sung, K.K. *et al.* (2009) Neural responses in rat brain during acute immobilization stress: a [^{18}F]FDG micro PET imaging study. *Neuroimage* 44, 1074–1080
113 Toyama, H. *et al.* (2004) Evaluation of anesthesia effects on [^{18}F]FDG uptake in mouse brain and heart using small animal PET. *Nucl. Med. Biol.* 31, 251–256
114 Qin, L. *et al.* (2002) Microglia enhance beta-amyloid peptide-induced toxicity in cortical and mesencephalic neurons by producing reactive oxygen species. *J. Neurochem.* 83, 973–983
115 Xie, Z. *et al.* (2002) Peroxynitrite mediates neurotoxicity of amyloid beta-peptide1-42- and lipopolysaccharide-activated microglia. *J. Neurosci.* 22, 3484–3492
116 Liu, B. and Hong, J.S. (2003) Role of microglia in inflammation-mediated neurodegenerative diseases: mechanisms and strategies for therapeutic intervention. *J. Pharmacol. Exp. Ther.* 304, 1–7
117 Venneti, S. *et al.* (2009) PK11195 labels activated microglia in Alzheimer's disease and in vivo in a mouse model using PET. *Neurobiol. Aging* 30, 1217–1226
118 Benito, C. *et al.* (2008) Cannabinoid CB2 receptors in human brain inflammation. *Br. J. Pharmacol.* 153, 277–285
119 Cagnin, A. *et al.* (2001) In-vivo measurement of activated microglia in dementia. *Lancet* 358, 461–467
120 Yasuno, F. *et al.* (2012) Increased binding of peripheral benzodiazepine receptor in mild cognitive impairment-dementia converters measured by positron emission tomography with [^{11}C]DAA1106. *Psychiatry Res.* 203, 67–74
121 Iyo, M. *et al.* (1997) Measurement of acetylcholinesterase by positron emission tomography in the brains of healthy controls and patients with Alzheimer's disease. *Lancet* 349, 1805–1809
122 Hanyu, H. *et al.* (2012) Regional differences in cortical benzodiazepine receptors of Alzheimer, vascular, and mixed dementia patients. *J. Neurol. Sci.* 323, 71–76
123 Small, G.W. *et al.* (2006) PET of brain amyloid and tau in mild cognitive impairment. *N. Engl. J. Med.* 355, 2652–2663
124 Cui, M. *et al.* (2012) Novel ^{18}F-Labeled benzoxazole derivatives as potential positron emission tomography probes for imaging of cerebral beta-amyloid plaques in Alzheimer's disease. *J. Med. Chem.* 55, 9136–9145
125 Mosconi, L. *et al.* (2005) Reduced hippocampal metabolism in MCI and AD: automated FDG-PET image analysis. *Neurology* 64, 1860–1867
126 Bishop, K.M. and Wahlsten, D. (1999) Sex and species differences in mouse and rat forebrain commissures depend on the method of adjusting for brain size. *Brain Res.* 815, 358–366
127 Jones, T. and Rabiner, E.A. (2012) The development, past achievements, and future directions of brain PET. *J. Cereb. Blood Flow Metab.* 32, 1426–1454
128 Hume, S.P. *et al.* (1998) Pharmacological constraints associated with positron emission tomographic scanning of small laboratory animals. *Eur. J. Nucl. Med.* 25, 173–176
129 Johnson, G. (2003) Neuropsychopharmacology: the fifth generation of progress, 5th edn. *Aust. N. Z. J. Psychiatry* 37, 247–249
130 Pike, V.W. (2009) PET radiotracers: crossing the blood–brain barrier and surviving metabolism. *Trends Pharmacol. Sci.* 30, 431–440
131 Kiessling, F. and Pichler, B.J., eds (2011) *Small Animal Imaging – Basics and Practical Guide*, Springer-Verlag
132 Kim, H.S. *et al.* (2014) A rat model of photothrombotic capsular infarct with marked motor deficit: a behavioral, histologic, and microPET study. *J. Cereb. Blood Flow Metab.* 34, 683–689
133 Seo, E.H. *et al.* (2013) Whole-brain functional networks in cognitively normal, mild cognitive impairment, and Alzheimer's disease. *PLoS ONE* 8, e53922
134 Parent, M., *et al*. Resting-state connectivity impairment in a rat model of Alzheimer's disease. *Alzheimer's & Dementia: The Journal of the Alzheimer's Association* 9, P29–P30
135 Leon, W.C. *et al.* (2010) A novel transgenic rat model with a full Alzheimer's-like amyloid pathology displays pre-plaque intracellular amyloid-beta-associated cognitive impairment. *Journal of Alzheimer's disease: JAD* 20, 113–126

Capítulo XI. *In vivo tracking of tau pathology using positron emission tomography (PET) molecular imaging in small animals.*

No **capítulo XI** apresentamos o artigo publicado no periódico no periódico *Translational Neurodegeneration*.

No capítulo anterior (capítulo X) avaliamos os estudos com PET em modelos transgênicos de β-amilóide e tau. A propagação da patologia de tau parece correlacionar com a severidade do declínio cognitivo e da disfunção sináptica. Porém este pressuposto se baseia em dados *post-mortem* e análises de LCR, pouco sabe-se da propagação *in vivo* da patologia de tau e sua relação com o declínio cognitivo. Neste estudo, propusemos o uso de PET com radiofármacos para tau acoplados a estudos multimodais e longitudinais em animais transgênicos portadores de mutações humanas da proteína tau, para avançar no entendimento da progressão da patologia de tau.

Zimmer et al. Translational Neurodegeneration 2014, 3:6
http://www.translationalneurodegeneration.com/content/3/1/6

Translational Neurodegeneration

REVIEW Open Access

In vivo tracking of tau pathology using positron emission tomography (PET) molecular imaging in small animals

Eduardo Rigon Zimmer[1,2,3†], Antoine Leuzy[1,2†], Venkat Bhat[4], Serge Gauthier[1] and Pedro Rosa-Neto[1,2*]

Abstract

Hyperphosphorylation of the tau protein leading to the formation of neurofibrillary tangles (NFTs) is a common feature in a wide range of neurodegenerative diseases known as tauopathies, which include Alzheimer's disease (AD) and the frontotemporal dementias (FTDs). Although heavily investigated, the mechanisms underlying the pathogenesis and progression of tauopathies have yet to be fully understood. In this context, several rodent models have been developed that successfully recapitulate the behavioral and neurochemical features of tau pathology, aiming to achieve a better understanding of the link between tau and neurodegeneration. To date, behavioral and biochemical parameters assessed using these models have been conducted using a combination of memory tasks and invasive methods such as cerebrospinal fluid (CSF) sampling or post-mortem analysis. Recently, several novel positron emission tomography (PET) radiopharmaceuticals targeting tau tangles have been developed, allowing for non-invasive *in vivo* quantification of tau pathology. Combined with tau transgenic models and micro-PET, these tracers hold the promise of advancing the development of theoretical models and advancing our understanding of the natural history of AD and non-AD tauopathies. In this review, we briefly describe some of the most important insights for understanding the biological basis of tau pathology, and shed light on the opportunity for improved modeling of tau pathology using a combination of tau-radiopharmaceuticals and animal models.

Keywords: Positron emission tomography, Tau molecular agents, Tau rodent models, Tauopathies

Introduction

Tau is a microtubule-associated protein (MAP) responsible for the maintenance and promotion of cell microtubule stability. In the human brain there are six tau isoforms generated by in or out exons splicing and expressed as three repeat (3R) and four repeat (4R) isoforms. In the normal human brain these isoforms are present at similar levels [1]. Several serine (Ser) and threonine (Thr) phosphate acceptor residues (almost 90 sites in the longest form of human tau) are the main regulators of tau functioning and are a target for a wide range of brain kinases involved in crucial signaling pathways owing to the high availability of these phosphorylation sites [2].

There are at least four key kinases regulating tau phosphorylation states: glycogen synthase kinase-3B (GSK3-B), cyclin-dependent kinase 5 (CDK5), cAMP-dependent protein kinase (PKA) and microtubule-associated regulatory kinase (MARK). In addition to mediating axonal cytoskeletal stability, tau is involved in axonal development—including axonogenesis, polarization, outgrowth and myelination [3]—as well as in neuronal plasticity and the integration of microtubule functions with interneuronal signaling pathways [3,4].

The fine-tuning of tau phosphorylation also depends on protein phosphatase activities, in particular protein phosphatase 2A (PP2A). The major phosphatase in the human brain [5], PP2A accounts for the overwhelming majority of tau dephosphorylation. In fact, tau homeostasis depends on kinase/phosphatase activities and is of vital importance for the maintenance of microtubule stability, dynamics, as well as neuronal viability (Figure 1a).

* Correspondence: pedro.rosa@mcgill.ca
†Equal contributors
[1]Translational Neuroimaging Laboratory (TNL), McGill Center for Studies in Aging, Douglas Mental Health University Institute, McGill University, 6875 La Salle Blv - FBC room 3149, Montreal, QC, H4H 1R3, Canada
[2]Montreal Neurological Institute (MNI), Montreal, Canada
Full list of author information is available at the end of the article

BioMed Central

© 2014 Zimmer et al.; licensee BioMed Central Ltd. This is an Open Access article distributed under the terms of the Creative Commons Attribution License (http://creativecommons.org/licenses/by/2.0), which permits unrestricted use, distribution, and reproduction in any medium, provided the original work is properly credited. The Creative Commons Public Domain Dedication waiver (http://creativecommons.org/publicdomain/zero/1.0/) applies to the data made available in this article, unless otherwise stated.

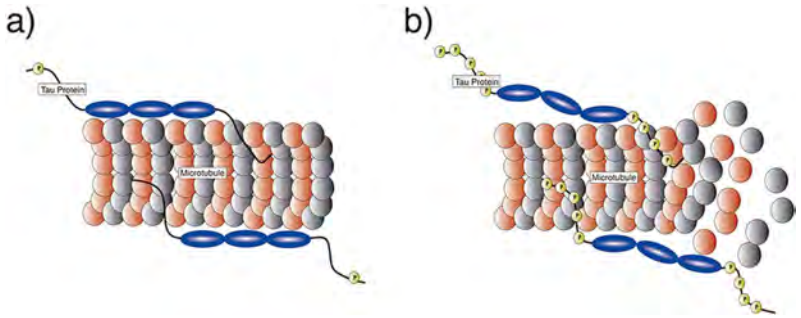

Figure 1 Tau protein physiological functions and pathological role. a) Physiological function: Tau protein promotes assembly and stabilization of microtubule architecture. Tau phosphorylation sites and isoforms are in charge of regulating tau function; **b)** Pathological role: Aberrant phosphorylation at various serine/threonine sites attenuates tau binding, which results in microtubule destabilization followed by accumulation in paired helical filaments (PHFs) and formation of insoluble aggregates (neurofibrillary tangles; NFTs).

Seeding and spreading of tau pathology

Aberrant phosphorylation of tau leads to disruption of microtubule stability and neurodegeneration. Phosphorylation in the residues Ser199/Ser202/Thr205 (AT8), Thr212/Ser214/Thr217 (AT100), Thr231/235 (AT180) and Ser396/Ser404 (PHF-1) are invariably abnormal in pathological processes involving tau [6] (Figure 1b). Abnormally phosphorylated tau undergoes misfolding and aggregation, which constitutes a widespread feature among neurodegenerative diseases, including Alzheimer's disease (AD) and Frontotemporal dementias (FTDs) [7,8].

In these diseases, the so-called tauopathies, tau deposits are commonly found in the cell bodies and neuronal dendrites, assuming a fibrillar conformation known as neurofibrillary tangles (NFTs) [9] (Figure 2a). In AD, NFT formation follows a well-characterized pattern of propagation, first described by Braak and Braak. The Braak staging follows the topographical evolution of the disease by means of six stages, which demonstrate the spread of tau pathology from the transentorhinal layer (I-II) toward limbic (III-IV) and isocortical areas (V-VI) [10]. Additionally, several studies have shown the degree of tau pathology to correlate with synaptic dysfunction and brain atrophy, as well as the severity of cognitive decline [11-13]. Importantly, while in AD tangles are constituted of equimolar 3R and 4R isoforms, FTD variants express predominantly 3R or 4R isoforms [14].

The main challenge with respect to defining the role of tau pathology in human neurodegenerative conditions is the co-existence of multiple pathology types. For example, in AD it is hard to develop theoretical models that allow for predictions regarding the evolution of tau pathology since amyloidosis is also present to an important degree. To overcome the effect of multiple pathologies, animal models expressing a single human tau mutation or displaying aberrant tau phosphorylation can be used as a method of choice to achieve an improved understanding of tau biology, pathology and the mechanisms underlying its spread throughout the brain.

Genetic and chemical models of tau pathology

The use of rodents for recapitulating human neurodegenerative diseases has been unquestionable in providing new insights at a mechanistic level, with various genetic and chemical models capable of mimicking different features of tau pathology [15]. More specifically, the majority of transgenic models are constructed based on tau pathogenic mutations from frontotemporal dementia with parkinsonism-17 (FTDP-17), producing 4R pathology [16-18]. In addition, transgenic models using non-mutated human truncated tau are able to recapitulate neurofibrillary degeneration [19]. Recent advances, aiming to better model neurodegenerative changes seen in AD, pieced together mutated human amyloid precursor protein (hAPP) and wild-type human tau (without pathogenic mutation), producing a model displaying amyloid plaques and NFTs containing both 3R and 4R isoforms [20].

Importantly, transgenic models expressing human tau are capable of reproducing NFT formation [21,22]. In contrast, genetic models lacking human tau expression such as p25-transgenic mice, which overexpress the human activator of CDK5 kinase, [23,24] and chemical-induced models [25,26] lead to hyperphosphorylated tau in brain regions rich in tau expression, but not to NFT formation (for review of tau rodent models see http://www.alzforum.org/research-models).

Tau models have been employed for analyzing mechanisms, pathophysiology, behavior, and also for testing novel therapeutic strategies. Currently, behavioral tasks, analyzed by several memory paradigms, such as the Morris water maze (spatial memory), object recognition task (recognition memory) and Y or T-maze (working

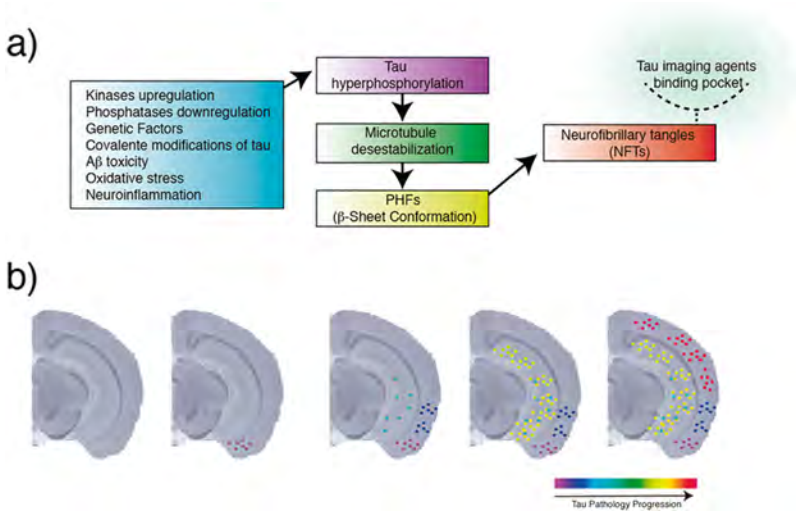

Figure 2 Neuropathological mechanisms possibly involved in tauopathies and expected tracking of tau spreading by imaging agents in rodent models. a) Pathological events (blue box) that contribute to tau hypherphosphorylation (purple box), microtubule detachment (green box), aggregation of paired helical filaments (PHFs) containing β-sheet structures (yellow box) and formation of neurofibrillary tangles (NFTs) containing the binding pocket for tau tracers (red box); **b)** Expected progression of tau pathology as shown by tau imaging agents based on previous findings in AD-like mouse models using immunohistochemistry. The image represents a coronal view of a T1-weighted mouse brain structural magnetic resonance imaging (MRI) image at bregma −2.88 mm.

memory), have been correlated with cerebrospinal fluid levels of tau and phospho-tau. Similar to humans, animal cognition correlates with tau pathology quantified in post-mortem tissue [25,27-29]. However, in terms of assessing the role of tau burden on cognition, classic behavior-pathology correlation methods are of limited use due their invasiveness and intrinsic cross-sectional study designs. In contrast, Positron Emission Tomography (PET) using tau-imaging agents provides a unique opportunity to observe the progression of tau pathology non-invasively and longitudinally.

Tau imaging agents

Advances in radiopharmaceuticals have recently led to novel tau-imaging agents, including [^{18}F]T807, [^{18}F]T808, [^{18}F]THK523, [^{18}F]THK5105, [^{18}F]THK5115 and [^{11}C]PBB3. In the following paragraphs, we briefly discuss the state-of-the-art of these compounds and what lies ahead.

[^{18}F]T807 and [^{18}F]T808 probes show promising results for tracking tau pathology in early clinical studies. In addition, post-mortem autoradiography followed by immunohistochemistry shows co-localization between these radiopharmaceuticals and phospo-tau antibodies [30,31].

Similar autoradiography studies with fluorine-tagged ligands THK523 (first-generation), THK5105 and THK5117 (second-generation) show high affinity for tau fibrils [32]. [^{18}F]THK523 shows specificity for tangles in studies conducted in transgenic mice models harboring only amyloid plaques or NFTs [33]. However, similarly to several [^{18}F] tracers, [^{18}F]THK523 shows an undesired high non-specific retention in white matter (WM) that may obscure cortical uptake. WM non-specific uptake reduces the diagnostic sensitivity of numerous imaging agents. To overcome this limitation, the second-generation of THK tracers, [^{18}F]THK5105 and [^{18}F]THK5117, were optimized for higher NFT cortical uptake and less WM retention [34].

The only tau radioligand labeled with carbon-11, [^{11}C]PBB3, shows striking specificity for NFT detection in transgenic models overexpressing human tau mutation. Despite its structural similarities with [^{11}C]PiB, the [^{11}C]PBB3 data obtained in transgenic mice support specificity for tau pathology. In humans, [^{11}C]PBB3 shows cortical uptake consistent with Braak staging. Indeed, positive [^{11}C]PBB3 and negative [^{11}C]PiB characterized a cortico-basal syndrome patient [35]. These tracers hold the promise of allowing for the *in vivo* detection and tracking of tau pathology, and may prove of use in differentiating AD and non-AD tauopathies. However, it is not entirely clear whether a single tau-imaging agent will be useful to quantify pathology underlying the entire spectrum of tauopathies given the presence of molecular heterogeneity. For example, it is commonly known in PET literature that the interaction between an imaging agent and a molecular target (e.g. a protein) occurs only if the binding pocket is accessible to the imaging agent. Binding pocket availability

is highly dependent on the protein structural conformation, which can be absent if the protein assumes an unusual conformation. Consequently, the ability of tracers to bind to NFTs may be affected by different post-translational modifications such that a given radiotracer may be able to bind NFTs but not to other ultrastructural tau conformations, such as straight (SF) or randomly coiled filaments (RCFs). Additionally, tau expression as 3R and 4R isoforms can strongly modulate the availability of binding pockets, since these different isoforms can assume distinct structural conformations.

In this context, the combination of tau tracers and genetic manipulation to achieve transgenic rodent models expressing human tau with a given conformation/isoform may accelerate our understanding of the mechanisms subserving tau-mediated neurodegeneration and clinical progression across the spectrum of tauopathies.

Tracking tau pathology in small animals

Since only human tau protein assumes the structural conformation rendering NFTs, transgenic models expressing human tau are *sine-qua-non* for testing new imaging agents with high translation value for human diseases [9]. Further, a high degree of homology and functional similarity is observed between humans and rodents in brain areas recognized as predilection sites for tau pathology, including the hippocampus [36-38].

Tau transgenic models, combined with behavioral assessment and *in vivo* imaging using microPET stands as a unique strategy for establishing the clinico-pathological correlations needed for testing the efficacy of novel disease-modifying drugs. Additionally, *in vivo* tracking of tau pathology in transgenic rodent models will provide new insights with high translational value owing to the spatiotemporal pattern of propagation similar to that observed in human tauopathies [37] (Figure 2b). In addition to occupying an important role in the full validation of tau-imaging tracers, microPET has the potential to provide high-resolution dynamic images that will estimate the content of tau aggregates via pharmacokinetic analysis. Finally, microPET can deliver crucial information regarding tracer kinetics, requisite for both the development of novel tau radiopharmaceuticals and in the context of imaging analysis.

Clinical utility

It is expected that tau-imaging agents will contribute to the early diagnosis of tauopathies. In addition, these imaging agents will significantly expand our knowledge regarding the propagation of tau protein in the human brain as well as its relationships with clinical features of the various tauopathies. Given the numerous drugs aiming to halt the progression of tau pathology, it is also expected that these ligands will allow for the monitoring of treatment effects of novel anti-tau therapies (see review Giacobini et al. [39]). Yet, there remains a significant amount of research to be conducted in order to establish the advantages and limitations of tau-imaging agents. Indeed, well-controlled microPET studies in animal models are necessary for the validation and development of tau specific PET agents with less non-specific binding and favorable kinetics (Table 1).

Table 1 Tau imaging agents: from basic to clinical applications

Basic research	The combination of Tau imaging agents and transgenic models can allow for:
	a) Non-invasive longitudinal tracking of tau pathology
	b) Longitudinal assessment of behavior as a function of tau pathology
	c) Determination of pharmacokinetic properties
	d) Development of novel radiopharmaceuticals
	e) Development of theoretical models regarding progression of tau pathology
Clinical applications	The use of Tau imaging agents in the clinical approach can allow for:
	a) Early diagnosis
	b) Differential diagnosis
	c) Follow-up of cognitive decline as function of tau pathology progression
	d) Monitoring of treatment effectiveness of novel anti-tau and associated therapies
	e) Development of theoretical models regarding tau pathology progression
	f) Estimation of sample size and endpoints in the context of clinical trials

Concluding remarks

PET in tau transgenic models allows for longitudinal assessment and thus is ideally suited for following tau pathology progression and/or response to disease-modifying drugs. Simultaneously, the use of the same animal for PET imaging and behavioral assessments eliminates the between-subject variability and will provide key insights on the role of tau in neurodegeneration and associated cognitive decline. Finally, these results can rapidly be translated to human research, delivering novel therapeutic strategies, mechanistic insights, predictive models and biomarkers.

Competing interest

The authors declare that they have no competing interest.

Authors' contribution

ERZ and AL drafted the manuscript and designed the figures. VB critically revised the manuscript. SG and PRN guided and supervised the work. All authors read and approved the final manuscript.

Acknowledgements
This work was supported by Canadian institutes of Health Research (CIHR) [MOP-11-51-31], Alzheimer's Association [NIRG-08-92090], Nussia & André Aisenstadt Foundation, and Fonds de la recherche en santé du Québec (chercheur boursier).

Author details
[1]Translational Neuroimaging Laboratory (TNL), McGill Center for Studies in Aging, Douglas Mental Health University Institute, McGill University, 6875 La Salle Blv - FBC room 3149, Montreal, QC, H4H 1R3, Canada. [2]Montreal Neurological Institute (MNI), Montreal, Canada. [3]Department of Biochemistry, Federal University of Rio Grande do Sul (UFRGS), Porto Alegre, Brazil. [4]Department of Psychiatry, McGill University, Montreal, Brazil.

Received: 9 December 2013 Accepted: 7 March 2014
Published: 15 March 2014

References

1. Williams DR: **Tauopathies: classification and clinical update on neurodegenerative diseases associated with microtubule-associated protein tau.** *Int Med J* 2006, **36:**652–660.
2. Buee L, Bussiere T, Buee-Scherrer V, Delacourte A, Hof PR: **Tau protein isoforms, phosphorylation and role in neurodegenerative disorders.** *Brain Res Brain Res Rev* 2000, **33:**95–130.
3. Gendreau KL, Hall GF: **Tangles, toxicity, and tau secretion in AD - New approaches to a vexing problem.** *Frontiers in Neurol* 2013, **4:**160.
4. Johnson GV, Stoothoff WH: **Tau phosphorylation in neuronal cell function and dysfunction.** *J of cell Sci* 2004, **117:**5721–5729.
5. Gong CX, Iqbal K: **Hyperphosphorylation of microtubule-associated protein tau: a promising therapeutic target for Alzheimer disease.** *Current Med Chem* 2008, **15:**2321–2328.
6. Augustinack JC, Schneider A, Mandelkow EM, Hyman BT: **Specific tau phosphorylation sites correlate with severity of neuronal cytopathology in Alzheimer's disease.** *Acta Neuropathologica* 2002, **103:**26–35.
7. Spires-Jones TL, Stoothoff WH, de Calignon A, Jones PB, Hyman BT: **Tau pathophysiology in neurodegeneration: a tangled issue.** *Trends in Neurosci* 2009, **32:**150–159.
8. Mackenzie IR, Neumann M, Bigio EH, Cairns NJ, Alafuzoff I, Kril J, Kovacs GG, Ghetti B, Halliday G, Holm IE, Ince PG, Kamphorst W, Revesz T, Rozemuller AJ, Kumar-Singh S, Akiyama H, Baborie A, Spina S, Dickson DW, Trojanowski JQ, Mann DM: **Nomenclature and nosology for neuropathologic subtypes of frontotemporal lobar degeneration: an update.** *Acta Neuropathologica* 2010, **119:**1–4.
9. Ballatore C, Lee VM, Trojanowski JQ: **Tau-mediated neurodegeneration in Alzheimer's disease and related disorders.** *Nat Rev Neurosci* 2007, **8:**663–672.
10. Braak H, Braak E: **Neuropathological stageing of Alzheimer-related changes.** *Acta Neuropathologica* 1991, **82:**239–259.
11. Arriagada PV, Growdon JH, Hedley-Whyte ET, Hyman BT: **Neurofibrillary tangles but not senile plaques parallel duration and severity of Alzheimer's disease.** *Neurology* 1992, **42:**631–639.
12. Hampel H, Burger K, Pruessner JC, Zinkowski R, DeBernardis J, Kerkman D, Leinsinger G, Evans AC, Davies P, Moller HJ, Teipel SJ: **Correlation of cerebrospinal fluid levels of tau protein phosphorylated at threonine 231 with rates of hippocampal atrophy in Alzheimer disease.** *Archives of Neurol* 2005, **62:**770–773.
13. Guillozet AL, Weintraub S, Mash DC, Mesulam MM: **Neurofibrillary tangles, amyloid, and memory in aging and mild cognitive impairment.** *Archives of Neurol* 2003, **60:**729–736.
14. Kouri N, Whitwell JL, Josephs KA, Rademakers R, Dickson DW: **Corticobasal degeneration: a pathologically distinct 4R tauopathy.** *Nat Rev Neurol* 2011, **7:**263–272.
15. Gotz J, Deters N, Doldissen A, Bokhari L, Ke Y, Wiesner A, Schonrock N, Ittner LM: **A decade of tau transgenic animal models and beyond.** *Brain Pathol* 2007, **17:**91–103.
16. Goedert M, Spillantini MG: **A century of Alzheimer's disease.** *Science* 2006, **314:**777–781.
17. Platt TL, Reeves VL, Murphy MP: **Transgenic models of Alzheimer's disease: better utilization of existing models through viral transgenesis.** *Biochimica et biophysica Acta* 1832, **2013:**1437–1448.
18. Nasreddine ZS, Loginov M, Clark LN, Lamarche J, Miller BL, Lamontagne A, Zhukareva V, Lee VM, Wilhelmsen KC, Geschwind DH: **From genotype to phenotype: a clinical pathological, and biochemical investigation of frontotemporal dementia and parkinsonism (FTDP-17) caused by the P301L tau mutation.** *Annals of Neurol* 1999, **45:**704–715.
19. Zilka N, Filipcik P, Koson P, Fialova L, Skrabana R, Zilkova M, Rolkova G, Kontsekova E, Novak M: **Truncated tau from sporadic Alzheimer's disease suffices to drive neurofibrillary degeneration in vivo.** *FEBS Lett* 2006, **580:**3582–3588.
20. Umeda T, Maekawa S, Kimura T, Takashima A, Tomiyama T, Mori H: **Neurofibrillary tangle formation by introducing wild-type human tau into APP transgenic mice.** *Acta Neuropathol* 2014. In press.
21. de Calignon A, Polydoro M, Suarez-Calvet M, William C, Adamowicz DH, Kopeikina KJ, Pitstick R, Sahara N, Ashe KH, Carlson GA, Spires-Jones TL, Hyman BT: **Propagation of tau pathology in a model of early Alzheimer's disease.** *Neuron* 2012, **73:**685–697.
22. Iba M, Guo JL, McBride JD, Zhang B, Trojanowski JQ, Lee VM: **Synthetic tau fibrils mediate transmission of neurofibrillary tangles in a transgenic mouse model of Alzheimer's-like tauopathy.** *The J of Neurosci: the Off J of the Soc for Neurosci* 2013, **33:**1024–1037.
23. Ahlijanian MK, Barrezueta NX, Williams RD, Jakowski A, Kowsz KP, McCarthy S, Coskran T, Carlo A, Seymour PA, Burkhardt JE, Nelson RB, McNeish JD: **Hyperphosphorylated tau and neurofilament and cytoskeletal disruptions in mice overexpressing human p25, an activator of cdk5.** *Proc Natl Acad Sci U S A* 2000, **97:**2910–2915.
24. Bian F, Nath R, Sobocinski G, Booher RN, Lipinski WJ, Callahan MJ, Pack A, Wang KK, Walker LC: **Axonopathy, tau abnormalities, and dyskinesia, but no neurofibrillary tangles in p25-transgenic mice.** *The J of comparative Neurol* 2002, **446:**257–266.
25. Zimmer ER, Kalinine E, Haas CB, Torrez VR, Souza DO, Muller AP, Portela LV: **Pretreatment with memantine prevents Alzheimer-like alterations induced by intrahippocampal okadaic acid administration in rats.** *Curr Alzheimer Res* 2012, **9:**1182–1190.
26. Grunblatt E, Salkovic-Petrisic M, Osmanovic J, Riederer P, Hoyer S: **Brain insulin system dysfunction in streptozotocin intracerebroventricularly treated rats generates hyperphosphorylated tau protein.** *J of Neurochem* 2007, **101:**757–770.
27. Van der Jeugd A, Vermaercke B, Derisbourg M, Lo AC, Hamdane M, Blum D, Buee L, D'Hooge R: **Progressive age-related cognitive decline in tau mice.** *J of Alzheimer's Dis: JAD* 2013, **37:**777–788.
28. Boutajangout A, Quartermain D, Sigurdsson EM: **Immunotherapy targeting pathological tau prevents cognitive decline in a new tangle mouse model.** *The J of Neurosci: the Off J of the Soc for Neurosci* 2010, **30:**16559–16566.
29. Carreras I, McKee AC, Choi JK, Aytan N, Kowall NW, Jenkins BG, Dedeoglu A: **R-flurbiprofen improves tau, but not Ass pathology in a triple transgenic model of Alzheimer's disease.** *Brain Res* 2013, **1541:**115–127.
30. Chien DT, Bahri S, Szardenings AK, Walsh JC, Mu F, Su MY, Shankle WR, Elizarov A, Kolb HC: **Early clinical PET imaging results with the novel PHF-tau radioligand [F-18]-T807.** *J of Alzheimer's Dis: JAD* 2013, **34:**457–468.
31. Chien DT, Szardenings AK, Bahri S, Walsh JC, Mu F, Xia C, Shankle WR, Lerner AJ, Su MY, Elizarov A, Kolb HC: **Early clinical PET imaging results with the novel PHF-Tau radioligand [F18]-T808.** *J of Alzheimer's Dis: JAD* 2014, **38:**171–184.
32. Harada R, Okamura N, Furumoto S, Tago T, Maruyama M, Higuchi M, Yoshikawa T, Arai H, Iwata R, Kudo Y, Yanai K: **Comparison of the binding characteristics of [18 F]THK-523 and other amyloid imaging tracers to Alzheimer's disease pathology.** *European J of nuclear Med and Mole imaging* 2013, **40:**125–132.
33. Fodero-Tavoletti MT, Okamura N, Furumoto S, Mulligan RS, Connor AR, McLean CA, Cao D, Rigopoulos A, Cartwright GA, O'Keefe G, Gong S, Adlard PA, Barnham KJ, Rowe CC, Masters CL, Kudo Y, Cappai R, Yanai K, Villemagne VL: **18 F-THK523: a novel in vivo tau imaging ligand for Alzheimer's disease.** *Brain J Neurol* 2011, **134:**1089–1100.
34. Okamura N, Furumoto S, Harada R, Tago T, Yoshikawa T, Fodero-Tavoletti M, Mulligan RS, Villemagne VL, Akatsu H, Yamamoto T, Arai H, Iwata R, Yanai K, Kudo Y: **Novel 18 F-labeled arylquinoline derivatives for noninvasive imaging of tau pathology in Alzheimer disease.** *J Nuclear Med* 2013, **54:**1420–1427.

35. Maruyama M, Shimada H, Suhara T, Shinotoh H, Ji B, Maeda J, Zhang MR, Trojanowski JQ, Lee VM, Ono M, Masamoto K, Takano H, Sahara N, Iwata N, Okamura N, Furumoto S, Kudo Y, Chang Q, Saido TC, Takashima A, Lewis J, Jang MK, Aoki I, Ito H, Higuchi M: **Imaging of tau pathology in a tauopathy mouse model and in Alzheimer patients compared to normal controls.** *Neuron* 2013, **79:**1094–1108.
36. Bunsey M, Eichenbaum H: **Conservation of hippocampal memory function in rats and humans.** *Nature* 1996, **379:**255–257.
37. Hurtado DE, Molina-Porcel L, Iba M, Aboagye AK, Paul SM, Trojanowski JQ, Lee VM: **A{beta} accelerates the spatiotemporal progression of tau pathology and augments tau amyloidosis in an Alzheimer mouse model.** *The Am J of Pathol* 1977–1988, **2010:**177.
38. Vogt BA, Paxinos G: **Cytoarchitecture of mouse and rat cingulate cortex with human homologies.** *Brain Struct Funct* 2014, **219:**185–192.
39. Giacobini E, Gold G: **Alzheimer disease therapy-moving from amyloid-beta to tau.** *Nature Rev Neurol* 2013, **9:**677–686.

doi:10.1186/2047-9158-3-6
Cite this article as: Zimmer *et al.*: In vivo tracking of tau pathology using positron emission tomography (PET) molecular imaging in small animals. *Translational Neurodegeneration* 2014 **3**:6.

Submit your next manuscript to BioMed Central and take full advantage of:

- **Convenient online submission**
- **Thorough peer review**
- **No space constraints or color figure charges**
- **Immediate publication on acceptance**
- **Inclusion in PubMed, CAS, Scopus and Google Scholar**
- **Research which is freely available for redistribution**

Submit your manuscript at
www.biomedcentral.com/submit

BioMed Central

Capítulo XII. *Imaging in vivo glutamate fluctuations with [11C]ABP688: a GLT-1 challenge with ceftriaxone.*

No **capítulo XII** apresentamos o artigo publicado no periódico *Journal of Cerebral Blood Flow & Metabolism.*

A excitotoxicidade glutamatérgica é um dos mecanismos envolvidos na fisiopatologia da DA. Neste capítulo, avaliamos a sensibilidade aos níveis de glutamato do radiofármaco de PET [^{11}C]ABP688, que se liga no sítio alostérico do mGluR5, em um estudo experimental de microPET. Para isso, utilizamos a ceftriaxona, um potente ativador do transportador astrocitário GLT-1, para modular os níveis extracelulares de glutamato. A redução dos níveis extracelulares de glutamato parece aumentar a disponibilidade do sítio alostérico do mGluR5. Estes dados apontam para o [^{11}C]ABP688 como um radiofármaco capaz de identificar flutuações glutamatérgicas. Desta maneira, o [^{11}C]ABP688 se torna potencialmente interessante para o reconhecimento de cenários de excitotoxicidade cerebral *in vivo* e não-invasivamente.

OPEN

Journal of Cerebral Blood Flow & Metabolism (2015) 35, 1169–1174
© 2015 ISCBFM All rights reserved 0271-678X/15 $32.00
www.jcbfm.com

ORIGINAL ARTICLE

Imaging *in vivo* glutamate fluctuations with [^{11}C]ABP688: a GLT-1 challenge with ceftriaxone

Eduardo R Zimmer[1,2,3], Maxime J Parent[1,2], Antoine Leuzy[1,2], Antonio Aliaga[4], Arturo Aliaga[1], Luc Moquin[5], Esther S Schirrmacher[4], Jean-Paul Soucy[4], Ivan Skelin[4], Alain Gratton[5], Serge Gauthier[2] and Pedro Rosa-Neto[1,2,4]

Molecular imaging offers unprecedented opportunities for investigating dynamic changes underlying neuropsychiatric conditions. Here, we evaluated whether [^{11}C]ABP688, a positron emission tomography (PET) ligand that binds to the allosteric site of the metabotropic glutamate receptor type 5 (mGluR5), is sensitive to glutamate fluctuations after a pharmacological challenge. For this, we used ceftriaxone (CEF) administration in rats, an activator of the GLT-1 transporter (EAAT2), which is known to decrease extracellular levels of glutamate. MicroPET [^{11}C]ABP688 dynamic acquisitions were conducted in rats after a venous injection of either saline (baseline) or CEF 200 mg/kg (challenge). Binding potentials (BP_{ND}) were obtained using the simplified reference tissue method. Between-condition statistical parametric maps indicating brain regions showing the highest CEF effects guided placement of microdialysis probes for subsequent assessment of extracellular levels of glutamate. The CEF administration increased [^{11}C]ABP688 BP_{ND} in the thalamic ventral anterior (VA) nucleus bilaterally. Subsequent microdialysis assessment revealed declines in extracellular glutamate concentrations in the VA. The present results support the concept that availability of mGluR5 allosteric binding sites is sensitive to extracellular concentrations of glutamate. This interesting property of mGluR5 allosteric binding sites has potential applications for assessing the role of glutamate in the pathogenesis of neuropsychiatric conditions.

Journal of Cerebral Blood Flow & Metabolism (2015) **35,** 1169–1174; doi:10.1038/jcbfm.2015.35; published online 25 March 2015

Keywords: [^{11}C]ABP688; ceftriaxone; glutamate; GLT-1; mGluR5; positron emission tomography

INTRODUCTION

Glutamate is the major excitatory neurotransmitter in the mammalian brain, acting on ionotropic (AMPAr, KAr and NMDAr) and metabotropic (mGluRs) receptors. The ionotropic receptors produce fast-acting excitatory effects, while mGluRs (G protein-coupled receptors) have a crucial role in the modulation of glutamatergic neurotransmission.[1] Since glutamate is not degraded in the extracellular compartment, two major astrocytic transporters, GLT-1 (EAAT2) and GLAST (EAAT1), remove glutamate from the synapses and provide the regulation necessary to orchestrate receptor excitability.[2] The disruption of this fine-tuning mechanism causes hyperactivation of glutamatergic receptors, a well-established detrimental scenario termed excitotoxicity, which is described as a fundamental player in the pathophysiology of several neurologic and psychiatric disorders.[3,4] Due to the glutamatergic system's involvement in a large array of neuropsychiatric conditions, techniques allowing for noninvasive *in vivo* estimation of glutamatergic neurotransmission are highly desirable.

Positron emission tomography (PET) is an imaging technique that allows for the *in vivo* measurement of biologic processes such as receptor availability or fluctuations of endogenous neurotransmitters.[5] Advances in pharmacology have allowed for the development of PET radiopharmaceuticals targeting allosteric binding sites of the metabotropic glutamate receptor type 5 (mGluR5).[6] Previous PET studies showed that pharmacological challenges with *N*-acetylcysteine, a facilitator of the cysteine-glutamate antiporter that increases the release of nonsynaptic glutamate, produced a decrease in the binding of the PET radiopharmaceutical [^{11}C]ABP688, an allosteric and highly selective mGluR5 antagonist, in baboons[7] and in rhesus monkeys.[8] In contrast, a recent study showed no effect of *N*-acetylcysteine on [^{11}C]ABP688 binding in rats.[9] In fact, little is known regarding noncompetitive interactions between glutamate and the availability of mGluR5 allosteric binding sites. Although important, none of the previous studies tested whether pharmacologically induced declines of extracellular glutamate concentrations increased the availability of mGluR5 allosteric binding sites.

With this in mind, we used ceftriaxone (CEF)—a potent GLT-1 activator, which decreases extracellular levels of glutamate[10–12]—to investigate whether the PET radiopharmaceutical [^{11}C]ABP688 is sensitive to declines in extracellular glutamate concentrations.

MATERIALS AND METHODS

Animals

Sprague-Dawley rats ($n = 5$, 392.10 ± 58.69 g) were scanned twice within 2 to 7 days (baseline and challenge). The scanning was conducted between

[1]Translational Neuroimaging Laboratory (TNL), McGill Center for Studies in Aging, Douglas Mental Health University Institute, Verdun, Quebec, Canada; [2]Alzheimer's Disease Research Unit, McGill Centre for Studies in Aging, McGill University, Montreal, Quebec, Canada; [3]Department of Biochemistry, Federal University of Rio Grande do Sul (UFRGS), Porto Alegre, RS, Brazil; [4]Montreal Neurological Institute (MNI), Montreal, Quebec, Canada and [5]Department of Psychiatry, Douglas Hospital Research Centre, McGill University, Montreal, Quebec, Canada. Correspondence: Dr P Rosa-Neto, McGill Center for Studies in Aging, 6825 LaSalle Boulevad, Montreal, H4H 1R3 Quebec, Canada.
E-mail: pedro.rosa@mcgill.ca
This work was supported by the Canadian Institutes of Health Research (CIHR) [MOP-11-51-31], the Allan Tiffin Foundation, the Alzheimer's Association [NIRG-08-92090], the Fonds de recherche du Québec – Santé (FRSQ; chercheur boursier), the Conselho Nacional de Desenvolvimento Científico e Tecnológico (CNPq, Brazil), fundação de Amparo à Pesquisa do Rio Grande do Sul (Fapergs, Brazil), and INCT for Excitotoxicity and Neuroprotection/CNPq.
Received 20 August 2014; revised 16 December 2014; accepted 30 December 2014; published online 25 March 2015

1030 h and 1330 h. Additional Sprague-Dawley rats ($n = 6$, 452.10 ± 68.69 g) were used for microdialysis. The microdialysis was conducted between 1030 h and 1530 h. Animals were kept in a room with controlled temperature (21°C) under a 12-hour light/12-hour dark cycle (lights on 0800 h), with *ad libitum* access to food and water. All procedures were performed according the Guide to the Care and Use of Experimental Animals (Ed2) of the Canadian Council on Animal Care. The protocols for PET imaging, surgery, and microdialysis were approved by the Animal Care Committee of McGill University (Montreal, QC, Canada).

Radiosynthesis, Pharmaceuticals, and Imaging Procedures

[11C]ABP688 was synthesized as described previously.[13] The mean specific radioactivity for the baseline was 12.35 ± 5.75 TBq/mmol and for the challenge 12.74 ± 2.49 TBq/mmol (mean ± s.d.). The PET acquisitions were performed using a Concorde MicroPET R4 scanner (Siemens-CTI, Knoxville, TN, USA), as previously described by Elmenhorst.[13] Rats were placed in a prone position with the head immobilized by both the body holder and the nose cone of the anesthesia system (2% isoflurane at 0.5 L/min oxygen flow). The brain was positioned in the center of the field of view. A 10-min transmission scan with a rotating [57Co] point source was acquired to correct for attenuation followed by the 60-minute emission scan. For the baseline, they received a tail vein injection of saline 30 minutes before the scan (Figure 1A). For the challenge, they received a tail vein injection of CEF 200 mg/kg 30 minutes before the scan (Figure 1B). Subsequently, [11C] ABP688 was administered as a bolus injection (0.2 mL) into the tail vein. Respiratory rate, heart rate, and body temperature were monitored throughout the scan (Biopac Systems MP150, Goleta, CA, USA). Mean injected radioactivity was 17.02 ± 2.89 MBq for baseline and 16.62 ± 4.31 MBq for challenge (mean ± s.d.). Ceftriaxone was dissolved in saline (200 mg/kg).

Image Reconstruction, Analysis, Processing, and Estimation of Binding Parameters

Images were reconstructed using an MAP (maximum *a posteriori*) algorithm, normalized and corrected for scatter, dead time, and decay. Imaging analysis was conducted using minctools (http://www.bic.mni.mcgill.ca/ServicesSoftware/). Time-averaged tissue-radioactivity images were manually coregistered to a standard rat histologic template.[14] The image outcome measure, nondisplaceable binding potential (BP_{ND}), was estimated using the simplified reference tissue model,[15] with the cerebellum as a reference region due to its low [11C]ABP688 binding.[13] [11C]ABP688 BP_{ND} was estimated for every dynamic scan, with resulting images convolved using a 2.4-mm Gaussian kernel. The PET images were corrected for motion by realigning each frame to a reference frame using mutual information as the cost function.[16] For detailed information regarding PET methodology (including error analysis, parameter sensitivity analysis, and scan duration) and simplified reference tissue model analytical details, see Elmenhorst.[13]

Microdialysis Surgery, Procedure, and Histology

Rats were anesthetized with sodium isoflurane (2% isoflurane at 0.5 L/min oxygen flow), and stereotaxically implanted with 22 gauge stainless steel guides into the left frontal cortex (FC), anteroposterior (AP): 4.20 mm, mediolateral (ML): 1.0 mm, dorsoventral (DV): 5.0 mm) and into the right thalamic ventral anterior (VA) (AP:− 1.88 mm, ML: 2.0 mm, DV: 6.5 mm) following Paxinos coordinates.[17] These cannulas were used to insert the microdialysis probes into the target sites. Cannulas were secured with acrylic dental cement and a single anchor screw threaded into the cranium. Carprofen (5 mg/kg, subcutaneously) was used for postoperative analgesia (once daily for 2 days). Animals were allowed 1 week for recovery (housed one per cage) before testing. Microdialysis was performed as previously described by Lupinsky.[18] Probes were calibrated in artificial cerebrospinal fluid (26 mmol/L $NaHCO_3$, 3 mmol/L NaH_2PO_4, 1.3 mmol/L $MgCl_2$, 2.3 mmol/L $CaCl_2$, 3.0 mmol/L KCl, 126 mmol/L NaCl, 0.2 mmol/L L-ascorbic acid) containing 100 ng/ml aspartate, GLU, and GABA. *In vitro* probe recovery ranged from 14% to 19% at a flow rate of 2 μL/min. Computer-controlled microinfusion pumps were used to deliver perfusate to the probes, and the dialysate was collected from the fused silica outlet line (dead volume: 0.79 μL).

Microdialysis was performed under isoflurane anesthesia (2% isoflurane at 0.5 L/min oxygen flow). Two microdialysis probes (see Figures 4A and 4B) were inserted into the animals' indwelling guide cannula and perfused with sterile artificial cerebrospinal fluid (flow rate set at 1 μL/min). Samples were then taken at 20-minute intervals for 1 hour (baseline), followed by CEF (200 mg/kg) injection in the tail vein, while still collecting samples for 4 hours (challenge, Figure 1C). Each 20-μL dialysate sample was collected in a fraction vial preloaded with 1 μL of 0.25 mol/L perchloric acid to prevent analyte degradation and immediately stored at 4°C for subsequent analysis. After microdialysis, animal brains were dissected and stored in 4% paraformaldehyde and subsequently cryoprotected in a 30% sucrose solution. Brains were sliced in 20-μm-thick samples (coronal) and stained with cresyl violet (Nissl staining) for confirmation of probes placement.

Lysate High-Performance Liquid Chromatography Analysis

Glutamate levels were determined as previously described by Lupinsky.[18] A high-performance liquid chromatography precolumn derivatization with electrochemical detection was used to determine glutamate levels. The chromatographic system consisted of an ESA pump (model 582) and an ESA injector (model 542) coupled to a Waters Xterra MS C18 3.0 × 50 mm 5 μm analytical column. The mobile phase was prepared as needed and consisted of 3.5% acetonitrile, 20% methanol, and 100 mmol/L sodium

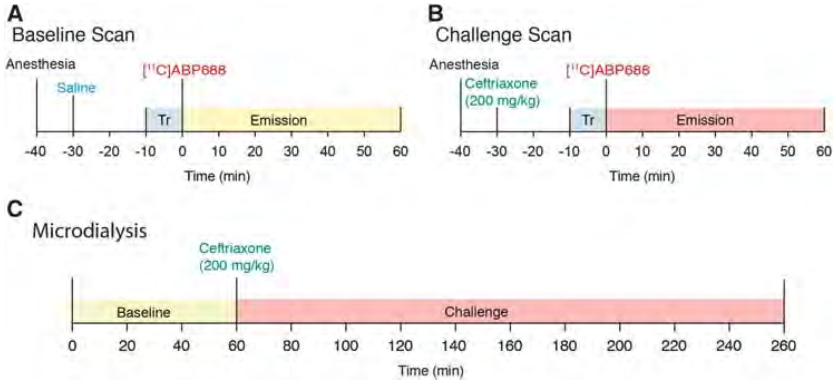

Figure 1. [11C]ABP688 and ceftriaxone (CEF) challenge study design. (**A**) MicroPET baseline: rats received a saline tail vein injection 30 minutes before the scan, a 10-minute transmission (Tr) scan preceded the 60-minute emission scan; (**B**) MicroPET challenge: the same rats used for baseline, received a CEF tail vein injection (200 mg/kg) 30 minutes before the scan, a 10-minute Tr scan preceded the 60-minute emission scan; (**C**) Microdialysis: additional rats are used for microdialysis, a baseline microdialysis was performed during 60 minutes (three samples) followed by a CEF tail vein injection (200 mg/kg) and microdialysis challenge sampling during 200 minutes (10 samples). PET, positron emission tomography.

© 2015 ISCBFM

phosphate dibasic (Na_2HPO_4) adjusted to pH 6.7 with 85% phosphoric acid. The flow rate was set at 0.5 mL/min, and the electrochemical detector ESA Coularray 5600 A, Chelmsford, MA, USA) was set at potentials of +150 mV and +550 mV. Working standards (100 ng/mL) and derivatization reagents were prepared fresh daily from stock solutions and loaded with samples into a refrigerated (10°C) ESA autosampler (model 542, Chelmsford, MA, USA). Before injection onto the analytical column, each fraction was sequentially mixed with 20 μL of o-phthaldehyde (0.0143 mol/L) diluted with 0.1 mol/L sodium tetraborate and 20 μL of 3-mercaptopropionic acid (0.071 mol/L) diluted with H_2O and allowed to react for 5 minutes. After each injection, the injection loop was flushed with 20% methanol to prevent contamination of subsequent samples. Under these conditions, the retention time for GLU was 2.4 minutes with a total run time of 30 minutes/sample. Chromatographic peak analysis was accomplished by

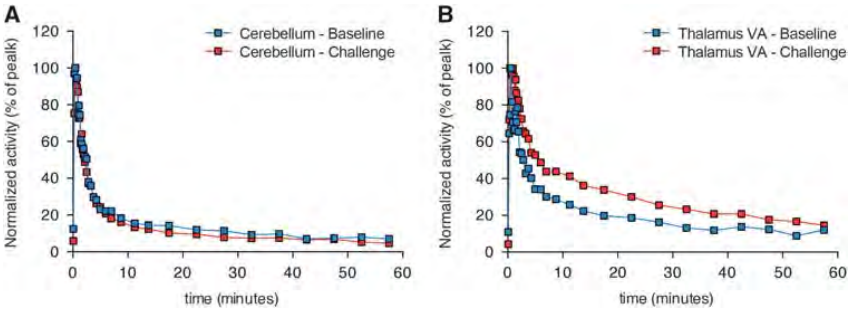

Figure 2. [^{11}C]ABP688 time-activity curves (TACs) obtained from baseline and challenge conditions. (**A**) Baseline and post ceftriaxone TACs from the cerebellum (reference region) and (**B**) the thalamic VA nucleus (high-binding region) of a single rat. Blue squares represent baseline condition and red squares the challenge condition.

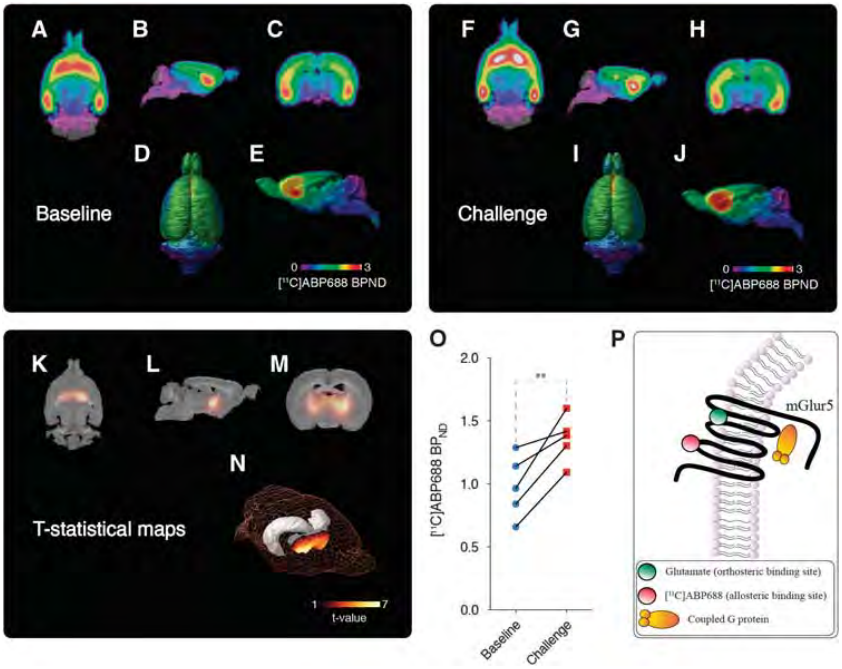

Figure 3. Baseline and ceftriaxone (CEF) challenge averaged [^{11}C]ABP688 nondisplaceable binding potential (BP_{ND}). Averaged [^{11}C]ABP688 BP_{ND} images obtained during the baseline overlaid on a histologic template are shown in axial (**A**), sagittal (**B**), coronal (**C**), as well as dorsal (**D**) and mid-sagittal surface projections (**E**). Averaged [^{11}C]ABP688 BP_{ND} images obtained after CEF challenge overlaid on a histologic template are shown in axial (**F**), sagittal (**G**), coronal (**H**), as well as dorsal (**I**) and mid-sagittal surface projections (**J**). Statistical parametric images (t-stats contrast (CEF challenge > baseline)) overlaid on a histologic template are shown on axial view (**K**); sagittal view (**L**); coronal view (**M**); and rat brain 3D surface showing (**N**) peak t-stat region (the gray object represents hippocampal position in the 3D surface). Note group differences showing a symmetric cluster in the anterior thalamus, encompassing basal forebrain and posterior striatum with the local maxima at the thalamic VA. [^{11}C]ABP688 BP_{ND} in the local maxima, during baseline and challenge microPET scans (**O**). Schematic representation of [^{11}C]ABP688 BP_{ND} binding in the metabotropic glutamate receptor type 5 (mGlur5) allosteric site (**P**). Images represented as [^{11}C]ABP688 BP_{ND} and *t*-value. Graph represented as mean ± s.d., $n = 5$. $^{**}P < 0.01$. PET, positron emission tomography.

© 2015 ISCBFM

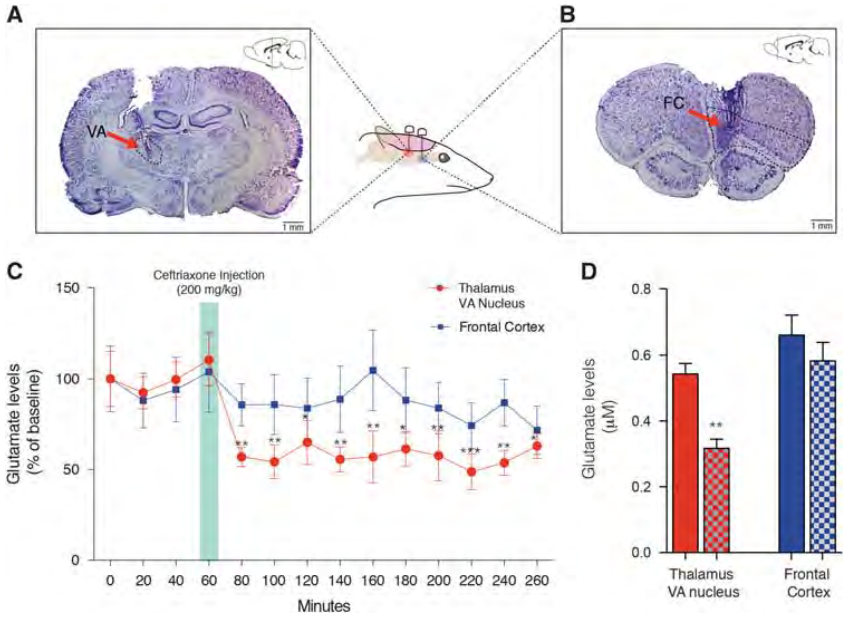

Figure 4. Ceftriaxone reduced levels of glutamate in the thalamic ventral nucleus but not in the frontal cortex (FC). (**A**) Histologic verification (cresyl violet) at VA (anteroposterior (AP): -1.88 mm, mediolateral (ML): 2.0 mm, dorsoventral (DV): 6.5 mm) microdialysis probes; (**B**) Histologic verification (cresyl violet) at FC (AP: 4.20 mm, ML: 1.0 mm, DV: 5.0 mm) microdialysis probes; (**C**) Levels of glutamate measured by microdialysis in the VA and in the FC during baseline (60 minutes) and challenge (200 minutes) conditions; (**D**) Comparison between levels of glutamate during baseline (solid bars) and challenge (checkered bars) at 60 minutes (the same duration as the PET scanning period). Data presented as mean ± s.e.m, $N = 6$. $^{*}P < 0.05$, $^{**}P < 0.01$, $^{***}P < 0.001$.

identification of unknown peaks in a sample matched according to retention times from known standards using ESA's CoulArray software.

Statistical Analysis

A paired Student's *t*-test was used to calculate differences in the [11C]ABP688 BP_{ND} between challenge and baseline. Comparisons between baseline and challenge were conducted at the voxel level using t-statistic analyses (RMINC, https://launchpad.net/rminc). Regions showing high specific binding were adjusted for a statistical cluster-wise threshold of $P < 0.05$, and corrected for multiple comparisons using random field theory.[19] For microdialysis, two-way ANOVA with repeated measures followed by Bonferroni correction was used. Differences were considered statistically significant at $P < 0.05$.

RESULTS

Ceftriaxone Challenge Increased [11C]ABP688 BP_{ND} with Peak Effect in the Thalamic Ventral Anterior Nucleus

Figure 2 shows the representative time-activity curves of reference region (cerebellum, Figure 2A) and of a high-binding region (thalamic VA nucleus, Figure 2B). Averaged BP_{ND} images showed consistent brain uptake of [11C]ABP688, and no global differences between baseline and challenge (baseline: 1.06 ± 0.24; challenge: 1.14 ± 0.26; $t_{(4)} = 0.5135$, $P = 0.6347$; Figures 3A and 3J). Voxel-based analysis showed a large bilateral symmetric cluster with increased [11C]ABP688 BP_{ND} in the thalamus, with peak effect in the thalamic ventral nucleus (VA) (peak $t_{(4)} = 6.78$, $P = 0.0025$, Figures 3K–3N) after the challenge with CEF. Paired *t*-test showed a significant increase in the [11C]ABP688 BP_{ND} in the VA (local maxima) after challenge with CEF ($t_{(4)} = 5.295$, $P = 0.0061$, baseline: 0.9781 ± 0.24; challenge: 1.379 ± 0.08 Figure 3O).

Ceftriaxone Evoked Glutamate Reductions in the Thalamic Ventral Nucleus

Repeated measures two-way ANOVA revealed an effect of drug ($F_{(13,130)} = 5.379$, $P = 0.0001$) but not of region ($F_{(1,10)} = 1.373$, $P = 0.2685$). A significant interaction between drug and region ($F_{(13,130)} = 2.109$, $P = 0.0175$) was observed. Bonferroni *post hoc* analysis revealed decreased glutamate concentrations after challenge in the VA ($P_{(range)} = 0.0004$ to 0.0314) but not in the FC ($P_{(range)} = 0.2526$ to 0.999; Figure 4C). Comparison between averages of baseline and CEF challenge during the scan period also showed decreased extracellular levels of glutamate in the VA ($t_{(5)} = 4.183$, $P = 0.0086$), but not in the FC ($t_{(5)} = 1.482$, $P = 0.20$; Figure 4D).

DISCUSSION

The present study showed for the first time the effect of the reduction of extracellular glutamate levels, using a GLT-1 pharmacological challenge with CEF, on PET [11C]ABP688 binding.

In a previous study, we validated the cerebellum as a suitable reference region for the quantification of mGluR5 availability using [11C]ABP688 in rats, via *in vivo* (microPET) and *in vitro* (autoradiography) techniques. Additionally, we performed a blood-based pharmacokinetics analysis and a blocking study with 1,2-methyl-6-(phenylethynyl)-pyridine, an antagonist of mGluR5 allosteric binding site and a competitor of [11C]ABP688.[13] Furthermore, we evaluated the reproducibility of [11C]ABP688 binding in a test-retest study and examined several pharmacokinetic models for determination of binding potential (BP_{ND}), showing that the simplified reference tissue model is the pharmacokinetic model that presents lowest variability.[20]

These validation studies allowed us to proceed with a pharmacological challenge aiming to identify the impact of reduced

© 2015 ISCBFM

glutamate concentrations on [11C]ABP688 binding in rats. Here, we show that the acute CEF challenge increased [11C]ABP688 binding in the thalamic VA. Beyond the considerable expression levels of GLT-1,[21] the thalamic VA receives massive glutamatergic afferents from the cerebellum and basal ganglia[22] and drives several connections with prefrontal, premotor, and motor cortices, a piece of the so-called thalamocortical network.[23,24]

Interestingly, [11C]ABP688 binding to the transmembrane allosteric site instead of orthosteric binding site of glutamate (Figure 3P) is highly dependent on the tertiary and quaternary receptor conformations.[25] Additionally, mGluR5 can assume oligomeric or heteromeric forms,[26–28] which may have an impact on the availability of the allosteric site. One could also argue that glutamate levels alter mGluR5 conformational states. In fact, affinity shift in the receptor–radioligand interactions is a phenomenon already described in the case of dopamine D2 receptors, where an amphetamine challenge altered the affinity of a D2 PET radiopharmaceutical.[29–31]

Guided by [11C]ABP688 microPET data, a microdialysis study was performed to confirm the reduction of glutamate levels in the VA. As expected, since [11C]ABP668 binding was not altered in the cerebral cortex, levels of glutamate in the FC (used as a control region) remained stable after CEF injection. In contrast, 20 minutes after CEF injection glutamate levels were reduced in the VA. However, the reason why this thalamic region is the first to be affected by CEF since GLT-1 and mGluR5 are expressed in almost all brain regions remains unknown and requires further investigation. One could argue that the differential expression and splice variants of GLT-1 in diverse brain regions may yield distinct activation by CEF.[32,33] Further studies are necessary to validate this observation; however, it seems unlikely that the changes in [11C]ABP688 binding are the result of a direct displacement by CEF, since CEF does not bind to the mGluR5 allosteric site. In fact, further methodological developments are necessary to better understand noncompetitive interactions using PET. Altogether, our results support a theoretical framework in which synaptic glutamate concentrations anticorrelate with [11C]ABP688 binding (i.e., low levels of glutamate will produce increased [11C]ABP688 binding and high levels of glutamate decreased [11C]ABP688 binding). Interestingly, two recent studies showed that [11C]ABP688 PET was capable of identifying reductions in mGluR5 availability in patients with major depressive disorder,[34] and in an epilepsy rat model.[35] On the basis of our assumptions, reduced [11C]ABP688 PET binding in this study may indicate increased glutamate levels, a possible sign of early excitotoxicity. This seems reasonable since excitotoxicity is an important pathological entity in both major depression[36] and epilepsy.[37]

In summary, molecular imaging using [11C]ABP688 seems to constitute a valuable tool for noninvasive and *in vivo* assessment of glutamatergic neurotransmission. Studies encompassing a wide range of clinical populations displaying glutamate-related neurologic and neuropsychiatric conditions are necessary to fully evaluate the feasibility and potential of [11C]ABP688 for measuring clinically-relevant glutamatergic fluctuations. If these clinical studies succeed, then [11C]ABP688 PET imaging will offer the opportunity of identifying glutamate abnormalities (e.g., brain excitotoxicity), which may allow for the development of glutamate-based disease signatures and for the evaluation of glutamate focused therapies.

AUTHOR CONTRIBUTIONS

ERZ and PRN were responsible for the design, drafting and revising the manuscript. ERZ and MJP were responsible for imaging processing and analysis. AL was responsible for drafting and revising the manuscript. ERZ, Arturo A and AA were responsible for microPET procedures and histology. ERZ, Arturo A and LM were responsible for microdialysis procedures. ESS and JPS were responsible for the radiochemistry. AG, SG and PRN critically revised the final version of the manuscript. PRN and AG were responsible for overseeing the entire PET and microdialysis procedures, respectively.

DISCLOSURE/CONFLICT OF INTEREST

The authors declare no conflict of interest.

REFERENCES

1 Schaeffer E, Duplantier A. Glutamate and neurodegenerative fisease. In: Dominguez C (ed.) *Neurodegenerative diseases* vol. 6. Springer: Berlin, Heidelberg, 2010 pp 91–147.
2 Danbolt NC. Glutamate uptake. *Prog Neurobiol* 2001; **65**: 1–105.
3 Mark LP, Prost RW, Ulmer JL, Smith MM, Daniels DL, Strottmann JM *et al.* Pictorial review of glutamate excitotoxicity: fundamental concepts for neuroimaging. *AJNR Am J Neuroradiol* 2001; **22**: 1813–1824.
4 Mehta A, Prabhakar M, Kumar P, Deshmukh R, Sharma PL. Excitotoxicity: bridge to various triggers in neurodegenerative disorders. *Eur J Pharmacol* 2013; **698**: 6–18.
5 Jacobs AH, Li H, Winkeler A, Hilker R, Knoess C, Ruger A *et al.* PET-based molecular imaging in neuroscience. *Eur J Nucl Med Mol Imaging* 2003; **30**: 1051–1065.
6 Ametamey SM, Kessler LJ, Honer M, Wyss MT, Buck A, Hintermann S *et al.* Radiosynthesis and preclinical evaluation of 11C-ABP688 as a probe for imaging the metabotropic glutamate receptor subtype 5. *J Nucl Med* 2006; **47**: 698–705.
7 Miyake N, Skinbjerg M, Easwaramoorthy B, Kumar D, Girgis RR, Xu X *et al.* Imaging changes in glutamate transmission in vivo with the metabotropic glutamate receptor 5 tracer [11C] ABP688 and N-acetylcysteine challenge. *Biol Psychiatry* 2011; **69**: 822–824.
8 Sandiego CM, Nabulsi N, Lin SF, Labaree D, Najafzadeh S, Huang Y *et al.* Studies of the metabotropic glutamate receptor 5 radioligand [(1)(1)C]ABP688 with N-acetylcysteine challenge in rhesus monkeys. *Synapse* 2013; **67**: 489–501.
9 Wyckhuys T, Verhaeghe J, Wyffels L, Langlois X, Schmidt M, Stroobants S *et al.* N-acetylcysteine- and MK-801-induced changes in glutamate levels do not affect in vivo binding of metabotropic glutamate 5 receptor radioligand 11C-ABP688 in rat brain. *J Nucl Med* 2013; **54**: 1954–1961.
10 Rothstein JD, Patel S, Regan MR, Haenggeli C, Huang YH, Bergles DE *et al.* Beta-lactam antibiotics offer neuroprotection by increasing glutamate transporter expression. *Nature* 2005; **433**: 73–77.
11 Rasmussen BA, Baron DA, Kim JK, Unterwald EM, Rawls SM. beta-Lactam antibiotic produces a sustained reduction in extracellular glutamate in the nucleus accumbens of rats. *Amino Acids* 2011; **40**: 761–764.
12 Thone-Reineke C, Neumann C, Namsolleck P, Schmerbach K, Krikov M, Schefe JH *et al.* The beta-lactam antibiotic, ceftriaxone, dramatically improves survival, increases glutamate uptake and induces neurotrophins in stroke. *J Hypertens* 2008; **26**: 2426–2435.
13 Elmenhorst D, Minuzzi L, Aliaga A, Rowley J, Massarweh G, Diksic M *et al.* In vivo and in vitro validation of reference tissue models for the mGluR(5) ligand [(11)C] ABP688. *J Cereb Blood Flow Metab* 2010; **30**: 1538–1549.
14 Rubins DJ, Melega WP, Lacan G, Way B, Plenevaux A, Luxen A *et al.* Development and evaluation of an automated atlas-based image analysis method for microPET studies of the rat brain. *Neuroimage* 2003; **20**: 2100–2118.
15 Lammertsma AA, Hume SP. Simplified reference tissue model for PET receptor studies. *Neuroimage* 1996; **4**(3 Pt 1): 153–158.
16 Gunn RN, Lammertsma AA, Hume SP, Cunningham VJ. Parametric imaging of ligand-receptor binding in PET using a simplified reference region model. *NeuroImage* 1997; **6**: 279–287.
17 Paxinos G, Watson C. *The rat brain in stereotaxic coordinates*, 4th ed. Academic Press: San Diego, 1998.
18 Lupinsky D, Moquin L, Gratton A. Interhemispheric regulation of the medial prefrontal cortical glutamate stress response in rats. *J Neurosci* 2010; **30**: 7624–7633.
19 Worsley KJ, Marrett S, Neelin P, Vandal AC, Friston KJ, Evans AC. A unified statistical approach for determining significant signals in images of cerebral activation. *Hum Brain Mapp* 1996; **4**: 58–73.
20 Elmenhorst D, Aliaga A, Bauer A, Rosa-Neto P. Test-retest stability of cerebral mGluR(5) quantification using [(1)(1)C]ABP688 and positron emission tomography in rats. *Synapse* 2012; **66**: 552–560.
21 Ozawa T, Nakagawa T, Shige K, Minami M, Satoh M. Changes in the expression of glial glutamate transporters in the rat brain accompanied with morphine dependence and naloxone-precipitated withdrawal. *Brain research* 2001; **905**: 254–258.
22 Kuramoto E, Fujiyama F, Nakamura KC, Tanaka Y, Hioki H, Kaneko T. Complementary distribution of glutamatergic cerebellar and GABAergic basal ganglia afferents to the rat motor thalamic nuclei. *Eur J Neurosci* 2011; **33**: 95–109.

© 2015 ISCBFM

23 Zikopoulos B, Barbas H. Parallel driving and modulatory pathways link the prefrontal cortex and thalamus. *PLoS One* 2007; **2**: e848.
24 Ngomba RT, Santolini I, Salt TE, Ferraguti F, Battaglia G, Nicoletti F *et al.* Metabotropic glutamate receptors in the thalamocortical network: strategic targets for the treatment of absence epilepsy. *Epilepsia* 2011; **52**: 1211–1222.
25 Changeux J-P, Edelstein SJ. Allosteric mechanisms of signal transduction. *Science* 2005; **308**: 1424–1428.
26 Canela L, Fernandez-Duenas V, Albergaria C, Watanabe M, Lluis C, Mallol J *et al.* The association of metabotropic glutamate receptor type 5 with the neuronal Ca2+-binding protein 2 modulates receptor function. *Journal of neurochemistry* 2009; **111**: 555–567.
27 Cabello N, Gandia J, Bertarelli DC, Watanabe M, Lluis C, Franco R *et al.* Metabotropic glutamate type 5, dopamine D2 and adenosine A2a receptors form higher-order oligomers in living cells. *Journal of neurochemistry* 2009; **109**: 1497–1507.
28 Romano C, Yang WL, O'Malley KL. Metabotropic glutamate receptor 5 is a disulfide-linked dimer. *J Biol Chem* 1996; **271**: 28612–28616.
29 Narendran R, Hwang DR, Slifstein M, Talbot PS, Erritzoe D, Huang Y *et al.* In vivo vulnerability to competition by endogenous dopamine: comparison of the D2 receptor agonist radiotracer (-)-N-[11C]propyl-norapomorphine ([11C]NPA) with the D2 receptor antagonist radiotracer [11C]-raclopride. *Synapse* 2004; **52**: 188–208.
30 Seneca N, Finnema SJ, Farde L, Gulyas B, Wikstrom HV, Halldin C *et al.* Effect of amphetamine on dopamine D2 receptor binding in nonhuman primate brain: a comparison of the agonist radioligand [11C]MNPA and antagonist [11C]raclopride. *Synapse* 2006; **59**: 260–269.
31 Wilson AA, McCormick P, Kapur S, Willeit M, Garcia A, Hussey D *et al.* Radiosynthesis and evaluation of [11C]-(+)-4-propyl-3,4,4a,5,6,10b-hexahydro-2H-naphtho[1,2-b][1,4]oxazin-9-ol as a potential radiotracer for in vivo imaging of the dopamine D2 high-affinity state with positron emission tomography. *Journal of medicinal chemistry* 2005; **48**: 4153–4160.
32 Reye P, Sullivan R, Scott H, Pow DV. Distribution of two splice variants of the glutamate transporter GLT-1 in rat brain and pituitary. *Glia* 2002; **38**: 246–255.
33 Torp R, Hoover F, Danbolt NC, Storm-Mathisen J, Ottersen OP. Differential distribution of the glutamate transporters GLT1 and rEAAC1 in rat cerebral cortex and thalamus: an in situ hybridization analysis. *Anat Embryol (Berl)* 1997; **195**: 317–326.
34 Deschwanden A, Karolewicz B, Feyissa AM, Treyer V, Ametamey SM, Johayem A *et al.* Reduced metabotropic glutamate receptor 5 density in major depression determined by [(11)C]ABP688 PET and postmortem study. *Am J Psychiatry* 2011; **168**: 727–734.
35 Choi H, Kim YK, Oh SW, Im HJ, Hwang do W, Kang H *et al.* In Vivo Imaging of mGluR5 Changes during Epileptogenesis Using [11C]ABP688 PET in Pilocarpine-Induced Epilepsy Rat Model. *PLoS One* 2014; **9**: e92765.
36 Hashimoto K. Emerging role of glutamate in the pathophysiology of major depressive disorder. *Brain Res Rev* 2009; **61**: 105–123.
37 Meldrum BS. The role of glutamate in epilepsy and other CNS disorders. *Neurology* 1994; **44**(11 Suppl 8): S14–S23.

This work is licensed under a Creative Commons Attribution-NonCommercial-NoDerivs 4.0 International License. The images or other third party material in this article are included in the article's Creative Commons license, unless indicated otherwise in the credit line; if the material is not included under the Creative Commons license, users will need to obtain permission from the license holder to reproduce the material. To view a copy of this license, visit http://creativecommons.org/licenses/by-nc-nd/4.0/

© 2015 ISCBFM

PARTE III

Discussão

Nesta tese investigamos diversos mecanismos envolvidos em processos neurodegenerativos relacionados com a atividade reduzida da PP2A, uma característica fisiopatológica da DA e de outras taupatias, com ênfase particular em vias de sinalização intracelular e no sistema glutamatérgico. Além disso, revisamos a situação atual do uso de biomarcadores de PET para β-amilóide, tau e neuroinflamacão em pacientes portadores da DA. Ademais, em estudos experimentais, investigamos flutuações no sistema glutamatérgico *in vivo* com o radiofármaco [^{11}C]ABP688 e demonstramos uma contribuição dos astrócitos no sinal do PET [^{18}F]FDG, ambos estudos com alto potencial translacional e aplicação direta na clínica em doenças neurodegenerativas. Nos próximos parágrafos discutiremos as principais implicações e avanços provenientes destes estudos.

Nesta tese estabelecemos dois modelos de taupatia com a infusão de OKA em roedores. O OKA é um inibidor de proteínas fosfatases cerebrais com relativa especificidade para PP2A e com alta afinidade (IC_{50} = 0.5 nM), que causa hiperfosforilação da proteína tau, e consequentes anormalidades similares aos processos degenerativos encontrados na DA e em outras taupatias (Cohen *et al.*, 1989; Gong *et al.*, 2000). Este modelo se torna atrativo para estudar alterações similares da DA, se levarmos em conta que até hoje não foram desvendadas mutações patológicas no gene da proteína tau em pacientes portadores da DA. As mutações patológicas atualmente conhecidas são provenientes das demências frontotemporais com parkinsonismo ligadas ao cromossomo 17 (FTDP-17, do inglês *frontotemporal dementia with parkinsonism-17*) (Gotz *et al.*, 2007). Desta maneira, um modelo químico parece ser a melhor estratégia para entender a

disfunção da tau na DA evitando modificações genéticas encontradas nas demências do tipo FTDP-17.

Primeiramente, mostramos que as anormalidades induzidas por OKA seguem um modelo dose-dependente, ou seja, infusões cerebrais de doses maiores de OKA – maior inibição da PP2A — causam danos neuroquímicos e comportamentais mais evidentes em um modelo ICV em camundongos CF1 (ver parte II, capítulo I, *"Inhibition of Protein phosphatase 2A links tau phosphorylation, oxidative stress and spatial memory"*). Mais especificamente, mostramos que OKA causa déficit cognitivo, alterações no sistema oxidativo cerebral e hiperfosforilação da proteína tau. No sistema redox, OKA aumentou o dano oxidativo em lipídios (níveis de peroxidação lipídica) e em proteínas (níveis de proteína carbonilada), e remodela a atividade das enzimas antioxidantes, como a peróxido dismutase (SOD), a catalase (CAT) e a glutationa peroxidase (GSH-Px). Neste sentido, cabe ressaltar que o aumento nos níveis cerebrais de peroxidação lipídica induzido por OKA se correlacionou linearmente e positivamente com o déficit cognitivo. Os nossos resultados estão de acordo com estudos em humanos demonstrando que existe um aumento de marcadores de peroxidação lipídica no LCR e no sangue de pacientes MCI, ou seja, no estágio pré-demência (Pratico *et al.,* 2002; Schrag *et al.,* 2013). Além disso, evidências de estudos com cérebros de pacientes com DA apontam para essa quebra da homeostasia no sistema redox em pacientes MCI e DA (Shmakov e Abrosimova, 1989).

O mesmo perfil se repetiu na fosforilação da proteína tau, ou seja, o grau de fosforilação de tau nos sítios Ser^{396} e $Ser^{199/202}$ se correlacionou linearmente com o déficit cognitivo. Nossos resultados fornecem mais uma evidência científica da associação entre tau hiperfosforilada e redução da performance cognitiva, e além disso, reforçam o papel

chave da PP2A mediando esse fenômeno. Neste sentido, nossos resultados replicaram estudos anteriores que sugerem que o grau de inibição da PP2A determina o estado de hiperfosforilação da proteína tau (Harris *et al.*, 1993; Gong *et al.*, 2000).

Entretanto a associação entre as anormalidades induzidas pela inibição da PP2A ainda não está bem definida. Resolvemos então usar os dados de estresse oxidativo cerebral e fosforilação de tau para uma análise de rede utilizando a técnica de matrizes simétricas de correlação. Com estes dados desenvolvemos o que denominamos "rede de eventos bioquímicos" relacionados com a inibição da PP2A via OKA. Identificamos três principais reguladores que parecem orquestrar as ações neurotóxicas do OKA: I) p-tau $ser^{199/202}$, um marcador de neurodegeneração; II) GSH-Px, uma marcador de atividade glial antioxidante; III) proteína carbonilada, um marcador de dano a proteínas. Baseado nestas análises, pode-se dizer então que estes três fenômenos estão acoplados, ou seja, a neurodegeneração (p-tau) está associada ao dano protéico (carbonilação) e parece ativar vias de neuroproteção gliais (GSH-Px). Além disso, desenvolvemos um modelo não-linear com os dados bioquímicos que se correlacionaram com o déficit cognitivo. Neste modelo, peroxidação lipídica e fosforilação de tau parecem ser os iniciadores do dano cognitivo induzido por OKA. Em resumo, nossos resultados indicam que o grau de inibição da PP2A estaria intimamente relacionado com o início e a progressão do declínio cognitivo, e que existe um acoplamento entre dano oxidativo e hiperfosforilação de tau. Sendo assim, podemos sugerir que a atividade reduzida da PP2A possa ser um dos eventos iniciais na fase assintomáticas da DA e de outras taupatias.

Utilizando um modelo similar (infusão unilateral intrahipocampal de OKA em ratos wistar) demonstramos o envolvimento do sistema glutamatérgico nos efeitos

neurotóxicos da inibição da PP2A (parte II, capítulo II, *"Pretreatment with Memantine Prevents Alzheimer-Like Alterations Induced by Intrahippocampal Okadaic Acid Administration in Rats"*). A infusão de OKA induziu déficit cognitivo e causou um aumento nos níveis liquóricos de glutamato e no imunoconteúdo hipocampal de CDK5, p25 e p-tau ser$^{199/202}$. Cabe relembrar que o p25 é um ativador aberrante da CDK5. Um pré-tratamento com memantina foi capaz de prevenir todas as alterações comportamentais e neuroquímicas induzidas pelo OKA (Zimmer *et al.*, 2012). Estes nossos resultados apontam para uma ação crucial do receptor NMDA mediando os efeitos neurotóxicos de OKA. Um achado importante aqui é o fato de que a inibição da PP2A intracelular, por algum mecanismo ainda não precisamente elucidado, induz um aumento nos níveis extracelulares de glutamato, e este aumento se correlaciona linearmente com o grau de déficit cognitivo. Estes resultados se tornam ainda mais atrativos devido as diversas maneiras em que as frações de β-amilóide são capazes de quebrar a homeostasia do sistema glutamatérgico (para revisão ver (Danysz e Parsons, 2012)), ou seja, pode haver um efeito colaborativo entre β-amilóide e tau mediando excitotoxicidade glutamatérgica. Em linha com os nossos resultados, um estudo recente demonstrou que MK-801, outro bloqueador do canal iônico do receptor NMDA, conseguiu proteger contra os efeitos neurotóxicos da infusão cerebral de OKA (Kamat *et al.*, 2014).

Baseado no exposto acima, propomos uma via de sinalização envolvendo a atividade reduzida da PP2A e o sistema glutamatérgico (ver parte II, capítulo III, *"Inhibition of Protein Phosphatase 2A: Focus on the Glutamatergic System"*). Mais especificamente, postulamos que o aumento nos níveis de glutamato induzido por OKA parecem hiperativar o receptor ionotrópico NMDA, o que desencadeia um aumento no

influxo de cálcio. A calpaína-2, enzima responsável pela clivagem de p35 em p25, é sensível aos níveis de cálcio e leva a uma ativação aberrante da CDK5. A atividade exacerbada da CDK5 induz hiperfosforilação da proteína tau e subsequente neurodegeneração associada a disfunção sináptica, e finalmente ao déficit cognitivo. Neste sentido, bloqueadores do canal do receptor NMDA, como a memantina e o MK-801, conseguem impedir o aumento nos níveis intracelulares de cálcio e assim evitar os efeitos excitotóxicos da inibição da PP2A via OKA (Zimmer *et al.*, 2015a). De fato, o pré-tratamento com bloqueadores do NMDA parece ter um efeito preventivo na disfunção das vias das sinalização acima descritas, e que possivelmente reflete em uma melhora no desempenho cognitivo dos animais tratados com OKA. Este potencial efeito profilático dos inibidores do NMDA, nos levou a tratar animais por um longo prazo para analisar possíveis efeitos adversos do tratamento com memantina (ver parte II, capítulo IV, *"Long-term NMDAR antagonism correlates reduced astrocytic glutamate uptake with anxiety-like phenotype"*) .

O tratamento de longo prazo (25 dias) com memantina em camundongos CF1 induziu um perfil ansiogênico em dois testes clássicos para se avaliar comportamentos ansiosos, o labirinto em cruz elevado (EPM, do inglês *elevated plus-maze*) e o teste do claro-escuro (LDB, do inglês *light-dark box*). Além disso, nossos resultados demostraram que a memantina resultou numa diminuição na captação astrocitária de glutamato no hipocampo e no córtex temporo-parietal destes animais, porém sem alterar o imunoconteúdo dos transportadores astrocitários GLT-1 e GLAST. Notavelmente, a diminuição da captação de glutamato se correlacionou com um maior perfil ansiogênico em ambos os testes (EPM e LDB). Interessantemente, uma publicação recente

demonstrou que a inibição do GLT-1 com ácido diidrocaínico (DHK, do inglês *dihydrokainic acid*) foi capaz de induzir ansiedade em camundongos, o que reforça o papel do transporte de glutamato astrocitário como modulador do perfil de ansiedade (John *et al.*, 2015). Além de bloquear o canal iônico do receptor NMDA, a memantina inibe a liberação pré-sináptica de glutamato resultando na diminuição do transporte de glutamato a nível astrocitários (Lu *et al.*, 2010). Este pressuposto está em linha com diversos modelos teóricos onde neurônios e astrócitos são capazes de regular um ao outro (Wade *et al.*, 2013; Karus *et al.*, 2015). Nosso estudo sugere que este acoplamento funcional neurônio-astrócito esteja envolvido no controle da sinapse glutamatérgica tripartite, e assim, tenha um impacto significante no controle do perfil de ansiedade (Zimmer *et al.*, 2015c).

Desta maneira, estratégias terapêuticas focando no sistema glutamatérgico para o tratamento da DA parecem depender primeiramente de um diagnóstico precoce e acurado. Neste sentido, diversas estratégias têm sido investigadas com a finalidade de proporcionar um diagnóstico precoce da DA, e o uso de biomarcadores para detectar as características clássicas da DA, como o β-amilóide e os NFTs, é considerado a estratégia mais promissora. Como discutido anteriormente, o acúmulo de β-amilóide pode ser detectado de maneira não invasiva com o uso de radiofármacos para PET. É importante ressaltar que a disfunção do metabolismo cerebral de β-amilóide começa até 30 anos antes dos primeiros sintomas da DA, o que oferece um lacuna temporal considerável para o tratamento da DA antes do aparecimento dos sintomas (Jansen *et al.*, 2015; Ossenkoppele *et al.*, 2015). Cabe salientar que o critério para diagnóstico da DA de 1984 (Mckhann *et al.*, 1984), foi recentemente atualizado com a inclusão dos biomarcadores –

definidos como parâmetros anatômicos, bioquímicos e fisiológicos que podem fornecer evidências *in vivo* da DA – como coadjuvantes no diagnóstico da DA (Dubois *et al.*, 2007; Sperling *et al.*, 2011).

Nesta tese revisamos os principais radiofármacos disponíveis para a visualização de placas de β-amilóide *in vivo* via PET, e os prós e contras para sua utilização em larga escala em centros clínicos (ver parte II, capítulo V, "*Imaging biomarkers for amyloid: a new generation of probes and what lies ahead*"). O [^{11}C]PIB é o radiofármaco de referência para visualização de placas de β-amilóide e demonstra alta sensibilidade e especificidade por agregados fibrilares de β-amilóide (placas maduras) (Klunk *et al.*, 2004; Price *et al.*, 2005). O [^{11}C]PIB tem sido amplamente utilizado para o diagnóstico diferencial de doenças neurodegenerativas com sintomatologia similar, como por exemplo a diferenciação entre a DA (amilóide positivo) e as FTDs (amilóide negativo) (Rabinovici *et al.*, 2007). Porém, a curta meia-vida (~20 minutos) do carbono-11 limita seu uso a centros que possuem um cíclotron, e inviabiliza sua distribuição regional.

Uma série de radiofármacos marcados com flúor-18 (meia-vida de ~110 minutos) foram desenvolvidos, entre eles o [^{18}F]flutemetamol, [^{18}F] florbetapir, [^{18}F]florbetapen e [^{18}F]NAV4694, com a finalidade de facilitar a produção centralizada e distribuição regional, e assim integrar os exames de PET na rotina clínica. Apesar de diferenciarem indivíduos com DA de indivíduos cognitivamente normais (CN), o [^{18}F]flutemetamol, [^{18}F]florbetapir e o [^{18}F]florbetapen apresentam alto grau de ligação não especifica na substância branca (WM, do inglês *White matter*), e desta maneira sua performance para marcar placas de β-amilóide em regiões corticais da substância cinzenta (GM, do inglês *grey matter*) é inferior a do [^{11}C]PIB (Leuzy *et al.*, 2014b). Em contraste, uma publicação

recente demonstrou que o [^{18}F]NAV4694 tem performance similar ao [^{11}C]PIB (Rowe *et al.*, 2013). Além disso, em estudos preliminares apresentados na *Alzheimer's Association International Conference* em 2013 e 2014 nós sugerimos que *in vitro* o [^{18}F]NAV4694 tem performance superior que o [^{11}C]PIB em estudos de autoradiografia com tecidos *post-mortem* de indivíduos com a DA (Zimmer *et al.*, 2013; Zimmer *et al.*, 2014a).

Atualmente o [^{18}F]flutemetamol, o [^{18}F] florbetapir e o [^{18}F]florbetapen já estão aprovados para uso clínico pelo FDA (referências do FDA número(s): 3667868, 3421114 e 3473704, respectivamente) e o [^{11}C]NAV4694: está em estudo clínico de fase III (referência do estudo clínico: NCT01886820). Devido a isto, o uso apropriado destes radiofármacos de PET é uma questão importante que está sendo muito debatida (ver parte II, capítulo VI, "*Use of amyloid PET across the spectrum of Alzheimer's disease: clinical utility and associated ethical issues*"). Por exemplo, cerca de 30% dos indivíduos CN com mais de 70 anos tem depósitos de placas de β-amilóide, ou seja, são amilóide positivos (Rowe e Villemagne, 2013). Um erro na interpretação destas imagens, pode levar a um fardo psicossocial, no estilo de vida e financeiro, e potencialmente o início de um tratamento inadequado. Além disso, o tratamento inadequado pode favorecer ao surgimento de sintomas neuropsiquiátricos, como sugerido preliminarmente pelos nossos resultados experimentais com memantina e em outros estudos (Menendez-Gonzalez *et al.*, 2005; Gaugler *et al.*, 2013; Safer *et al.*, 2015).

Baseado neste exemplo, fica claro que as imagens de PET β-amilóide para um diagnóstico precoce da DA devem ser acompanhadas de outros biomarcadores, como atrofia hipocampal por imagens de MRI e hipometabolismo no córtex parieto-temporal por PET [^{18}F]FDG (Schuff *et al.*, 2009; Mosconi *et al.*, 2010). Em 2012, um força tarefa,

denominada *Amyloid Imaging Taskforce* (AIT), estabeleceu três principais critérios para o uso de exames de PET β-amilóide nos seguintes indivíduos: I) indivíduos exibindo declínio cognitivo leve persistente e progressivo de etiologia não explicada; II) indivíduos com características clínicas da DA com um curso clínico atípico ou sugestivo de demência mista; e III) indivíduos jovens com rápida conversão a quadro de demência (< 65 anos) (Johnson *et al.*, 2013a; Johnson *et al.*, 2013b). Pode-se dizer então que o uso de exames de PET β-amilóide estaria restrito a pacientes apresentando declínio cognitivo, de etiologia não explicada, com finalidade de aumentar a acurácia do diagnóstico ou até mesmo para alterar o tratamento do paciente. Neste sentido, o uso de exames de PET β-amilóide durante a progressão temporal da DA, incluindo pacientes assintomáticos, ainda segue em debate, pois ainda não se sabe exatamente o significado do acúmulo de β-amilóide em indivíduos CN (Leuzy *et al.*, 2014c). A propósito, um estudo de larga escala denominado *Anti-Amyloid treatment of Asymptomatic Alzheimer's disease trial* (A4), que visa atrasar ou até mesmo impedir a progressão de CN para MCI e subsequente DA com o uso de infusões mensais de anticorpos de β-amilóide, está utilizando PET β-amilóide como marcador da progressão da doença longitudinalmente, e provavelmente vai revelar respostas mais contundentes para o significado do β-amilóide positivo em pacientes CN (http://www.adcs.org/Studies/A4.aspx).

Outro ponto importante em debate é a divulgação dos resultados dos exames de PET β-amilóide para os participantes destes estudos clínicos, pois os resultados podem ter um impacto psicossocial negativo na vida dos indivíduos amilóide positivo. Cabe salientar, que a maioria dos estudos de larga escala – em especial o ADNI – ainda não divulgam os resultados dos exames por PET β-amilóide para os indivíduos participantes.

Porém, o estudo A4 segue uma política diferente e revela o resultado dos seus exames de imagens com PET β-amilóide para os indivíduos participantes. Neste sentido, existe uma pressão da comunidade científica em favor da divulgação dos resultados, o que enfatiza a necessidade do desenvolvimento de um guia de orientações que possa minimizar danos psicossociais e estigmas discriminatórios aos indivíduos com o status de amilóide positivo (Shulman *et al.*, 2013). Em meio a tantas variáveis que ainda necessitam ser devidamente estudadas, a que se torna mais evidente é a necessidade do uso da imagem de PET β-amilóide em pacientes assintomáticos associado a outros biomarcadores, ou seja, o uso dessa tecnologia para um diagnóstico precoce individualizado (ver parte II, capítulo VII, *"Amyloid imaging in Alzheimer's disease: a potential new era of personalized medicine?"*). Entretanto, este conceito de medicina personalizada para o uso dos exames de PET β-amilóide ainda não parece pronto para tornar-se rotina em centros clínicos, devido a necessidade de mais estudos e respostas a estas variáveis (Leuzy *et al.*, 2014a).

Além dos radiofármacos para β-amilóide, foram recentemente desenvolvidos radioligantes capazes de identificar agregados da proteína tau (parte II, capítulo VIII, *"Developments in Tau PET Imaging"*). É importante ressaltar que a concentração de NFTs no cérebro é muito inferior aos níveis de placas de β-amilóide, e além disso, os NFTs podem assumir diversas conformações, o que torna a sua visualização uma tarefa complicada (Mukaetova-Ladinska *et al.*, 1993). Recentemente, seis (6) radiofármacos com afinidade por agregados da proteína tau foram desenvolvidos: [^{18}F]THK523, [^{18}F]THK5105, [^{18}F]THK5117, [^{18}F]T807, [^{18}F]T808 e [^{11}C]PBB3 (Fodero-Tavoletti *et al.*, 2011; Maruyama *et al.*, 2013; Xia *et al.*, 2013). Todos estes radiofármacos mostraram

alta especificidade e co-localizaram com NFTs em estudos *post-mortem*. Além disso, todos eles possuem características farmacocinéticas desejadas, como lipofilicidade, volume de distribuição, baixo peso molecular, alta seletividade/afinidade e rápido *clearence* do plasma (Zimmer *et al.*, 2014c).

Com exceção do [^{18}F]THK523, que recentemente demonstrou altos valores de ligação não específica na WM, os outros radiofármacos parecem promissores para uso clínico e oferecem uma oportunidade sem precedentes para análise longitudinal e topográfica da propagação dos NFTs na DA e em outras taupatias, porém muitas etapas de validação ainda necessitam ser conduzidas (Villemagne *et al.*, 2014). As etapas mais desafiadores são: I) o entendimento do acúmulo de agregados de tau devido ao envelhecimento para que com isto se evite falsos positivos em pacientes CN; e II) identificação da afinidade destes ligantes por diferentes conformações de tau.

Além disso, outros radiofármacos menos específicos para a DA têm sido propostos, como é o caso dos biomarcadores de PET para neuroinflamação (ver parte II, capítulo IX, *"Tracking neuroinflammation in Alzheimer's disease: the role of positron emission tomography imaging"*). Diversos estudos têm indicado que processos inflamatórios estão presentes durante toda a progressão da DA, ou seja, durante todas as fases da doença (Mcgeer e Mcgeer, 2013). O alvo da maioria dos radiofármacos de PET para neuroinflamação é a ativação microglial via afinidade pelo receptor TSPO (Zimmer *et al.*, 2014b). O TSPO é um receptor de membrana mitocondrial da microglia que somente é expresso quando a microglia está ativada (Venneti *et al.*, 2006). De fato diversos estudos com o [^{11}C]PK11195 (o radiofármaco de referência para TSPO) conseguiram identificar aumento na ativação microglial em pacientes com MCI e DA, e

estudos *in vitro* confirmam a co-localização entre microglia ativada e o PK11195 (Edison *et al.*, 2008; Tomasi *et al.*, 2008; Okello *et al.*, 2009; Venneti *et al.*, 2009). Além do [^{11}C]PK11195, outros radiofármacos com afinidade pelo TSPO também conseguem identificar sinais de neuroinflamação em estudos experimentais e em pacientes com MCI e DA (Yasuno *et al.*, 2012; James *et al.*, 2015).

Uma nova classe de radiofármacos tem se baseado na expressão cerebral do receptor canabinóide do tipo 2 (CB_2) para identificar ativação microglial. Em condições fisiológicas a concentração cerebral do receptor CB2 é muito baixa, porém em situações neurotóxicas, como a deposição de β-amilóide, os níveis microgliais deste receptor aumentam consideravelmente (Van Sickle *et al.*, 2005; Gong *et al.*, 2006). De fato, o [^{11}C]A-836339 é um ligante que atualmente já foi investigado em um modelo animal de β-amilóide e é considerado promissor para o uso clínico no contexto da DA (Horti *et al.*, 2010). Além da ativação microglial, existem outros dois alvos moleculares de bastante interesse para avaliação via PET de neuroinflamação na DA: a reatividade astrocitária e a atividade cerebral da enzima fosfolipase A2 (PLA_2) (Lehtonen *et al.*, 1996; Verkhratsky *et al.*, 2010). A reatividade astrocitária pode ser medida pela expressão da enzima monoamino oxidase B (MAO-B) que é expressa predominantemente na membrana mitocondrial dos astrócitos. Neste sentido, o 11C-deuterium-L-deprenyl ([^{11}C]-DED) tem alta afinidade e especificidade pela MAO-B, e estudos já mostraram retenção aumentada de [^{11}C]-DED em pacientes MCI e DA (Carter *et al.*, 2012). A atividade da PLA_2 pode ser medida utilizando ácido araquidônico (AA) marcado com cabono-11 (1-[11]-AA), pois o metabolismo de AA parece estar aumentado na DA (Esposito *et al.*, 2008).

Cabe salientar que estudos epidemiológicos demonstraram uma menor incidência de DA em pacientes que utilizam NSAIDs (Mcgeer *et al.*, 1996; In T' Veld *et al.*, 2001). Apesar disso, um estudo clínico de grande escala denominado *Alzheimer's Disease Anti-inflammatory Prevention Trial* (ADAPT) não demonstrou eficácia no tratamento da DA, porém sugeriu que os NSAIDs podem ser eficazes se administrados nas fases inicias da DA (Breitner *et al.*, 2011; Group, 2015). Baseado no acima exposto, parece intuitivo que todos estes radiofármacos de PET para medir neuroinflamação devem ser incorporados em estudos clínicos de caráter longitudinal, e podem ser utilizados como indicadores da progressão da doença e eficácia de drogas anti-inflamatórias. Além disso, existe uma necessidade da inclusão destes processos inflamatórias nos modelos hipotéticos da DA, pois a neuroinflamação parece ser um processo chave no desencadeamento e exacerbação de eventos neurodegenerativos na DA (Zimmer *et al.*, 2014b).

Na pesquisa básica, estudos utilizando microPET em roedores têm sido utilizados majoritariamente para o desenvolvimento de novos radiofármacos, ou seja, para avaliar características farmacocinéticas e assim avançar no uso destes ligantes em pesquisas clínicas. Em dois estudos desta tese (parte II, capítulo X, *"MicroPET imaging and transgenic models: a blueprint for Alzheimer's disease clinical research"*, e capítulo XI, *"In vivo tracking of tau pathology using positron emission tomography (PET) molecular imaging in small animals"*) sugerimos o uso do microPET de maneira refinada com a finalidade de avançar em termos de fisiopatologia da DA e de outras taupatias. É importante ressaltar que os mesmos princípios metodológicos utilizados no PET em humanos são utilizados no microPET, o que confere um alto grau translacional aos estudos experimentais com microPET. Ainda, diversos modelos de roedores transgênicos

carregando mutações humanas replicam a deposição de placas (mutações humanas no APP e nas presenilinas) e a propagação dos agregados de tau (mutações humanas patológicas na tau) (Gotz e Ittner, 2008).

De fato, diversos estudos experimentais de microPET foram conduzidos com estes modelos animais para análise de placas de β-amilóide, neurodegeneração e neuroinflamação, e de maneira geral, estes estudos demonstram que estes animais conseguem replicar o fenótipo de imagem de PET esperado em pacientes portadores da DA e de outras taupatias (Zimmer *et al.*, 2014d). Neste sentido, estudos longitudinais oferecem uma grande oportunidade para avaliar os efeitos da deposição das placas de β-amilóide e de NFTs em função da progressão dos processos neurodegenerativos e declínio da função cognitiva. O primeiro estudo longitudinal de longa duração foi recentemente publicado em uma parceria entre os laboratórios dos Profs. Mathias Jucker e Bernd Pichler ambos da Universidade de Tubingen na Alemanha (Maier *et al.*, 2014). Neste estudo, camundongos APP23 (modelo carregando APP humana) foram escaneados com [^{11}C]PIB em 6 tempos: 2, 8, 18, 21, 27 e 30 meses, e a progressão do acúmulo de β-amilóide foi mensurada. Cabe salientar que a maioria dos estudos de microPET foram desenvolvidos em modelos transgênicos usando linhagens de camundongos. Recentemente, os primeiros modelos transgênicos utilizando engenharia genética em ratos foram desenvolvidos (Leon *et al.*, 2010; Cohen *et al.*, 2013), e oferecem uma oportunidade muito superior para estudos de microPET, simplesmente devido ao maior tamanho do cérebro e volume sanguíneo corporal. Devido a resolução atual dos microPETs (Goertzen *et al.*, 2012), o uso de ratos fornece resultados com maior precisão e facilita na identificação de regiões cerebrais. De fato, o que se faz altamente necessário

são estudos implantando plataformas multimodais nestes animais, ou seja, estudos que incorporem diversos radiofármacos de PET, outras modalidades de imagem como as imagens por MRI, análises bioquímicas de sangue ou LCR, e comportamentais de maneira longitudinal. Além disso, a maioria dos estudos com o PET [^{18}F]FDG ainda seguem utilizando o consumo cerebral de glicose como uma medida estática. Entretanto, baseados no conceito de acoplamento entre a atividade cerebral e o metabolismo de glicose (Choi *et al.*, 2014), o [^{18}F]FDG pode ser utilizado para estudo de redes metabólicas e consequente identificação de mecanismos de propagação do processo neurodegenerativo. De fato, um estudo recente aplicou análise de rede com [^{18}F]FDG em pacientes com MCI, e revelou que a deposição de placas de β-amilóide está associada a uma organização aberrante da rede metabólica cerebral (Carbonell *et al.*, 2014).

Além da proposta de se utilizar microPET de maneira longitudinal para seguir a progressão das alterações da DA, a pesquisa experimental oferece maior flexibilidade para se avaliar mecanismos fisiopatológicos e avançar na interpretação das imagens provenientes da ligação de radiofármacos. Nos próximos parágrafos discutiremos dois estudos onde utilizamos intervenções farmacológicas associadas a imagens por microPET com a finalidade de avançar no entendimento das propriedades do [^{11}C]ABP688 e do [^{18}F]FDG.

Estudos com PET para avaliar o sistema glutamatérgico oferecem oportunidades interessantes para se entender processos excitotóxicos na DA e em outras demências. Neste sentido, o [^{11}C]ABP688 é um radiofármaco que se liga no sítio alostérico do mGluR5 e possui características peculiares (Ametamey *et al.*, 2006). Apesar de ter sido desenvolvido para se estimar a concentração destes receptores, o [^{11}C]ABP688 parece ser

sensível a variações no sistema de neurotransmissão glutamatérgica (Delorenzo *et al.*, 2011). Mais especificamente, estudos demonstraram que a infusão intravenosa (IV) de N-acetilcisteína (NAC), uma droga que aumenta os níveis extracelulares de glutamato, antes do exame de imagem com PET em macacos diminui a retenção cerebral de [^{11}C]ABP688 (Miyake *et al.*, 2011; Sandiego *et al.*, 2013). Outro estudo, mostra que a quetamina, um antagonista do receptor NMDA que em doses sub-anestésicas aumenta a liberação de glutamato, também diminui o sinal das imagens com PET [^{11}C]ABP688 (Delorenzo *et al.*, 2015). Baseado nestes estudos, utilizamos a ceftriaxona, um antibiótico β-lactâmico que aumenta a captação de glutamato via ativação de GLT-1 astrocitário, e consequentemente diminui os níveis extracelulares de glutamato (Thone-Reineke *et al.*, 2008; Rasmussen *et al.*, 2011), antes do exame de imagem com microPET [^{11}C]ABP688 em ratos (ver parte II, capítulo XII, *"Imaging in vivo glutamate fluctuations with [^{11}C]ABP688: a GLT-1 challenge with ceftriaxone"*).

A ativação de GLT-1, via administração IV de ceftriaxona, aumentou a retenção de [^{11}C]ABP688 nos dois hemisférios cerebrais em uma região específica, o núcleo ventral anterior do tálamo (VA). Um estudo subsequente de microdiálise demonstrou que os níveis de glutamato estavam realmente reduzidos no VA. Os nossos dados contribuem para a conjectura de que o [^{11}C]ABP688 é sensível a flutuações na concentração de glutamato (Zimmer *et al.*, 2015b). Como o [^{11}C]ABP688 não compete pelo sítio de ligação do glutamato (ortostérico), acredita-se que a ligação do [^{11}C]ABP688 no cérebro dependa da conformação do mGlur5. O mGlur5 pode assumir diversas conformações entre elas dímeros, heterodímeros e ainda, por estar acoplado a proteínas G, pode estar em baixo ou alto estado de afinidade, o que provavelmente influencie na disponibilidade

do seu sítio alostérico, e contribua para esta dinâmica de ligação do [^{11}C]ABP688 (Romano *et al.*, 1996; Cabello *et al.*, 2009; Canela *et al.*, 2009). Esta propriedade interessante do [^{11}C]ABP688 tem potencial aplicação para o monitoramento do papel do sistema glutamatérgico na DA, em outras doenças neurodegenerativas e neuropsiquiátricas. De fato, em um estudo seguinte demonstramos um desacoplamento entre atrofia cerebral, captação de [^{18}F]FDG e retenção de [^{11}C]ABP688 em pacientes diagnosticados com a FTD variante comportamental (bvFTD, do inglês *behavioral variant frontotemporal dementia*). Mais especificamente, encontramos regiões cerebrais com retenção reduzida de [^{11}C]ABP688, porém, com metabolismo normal ([^{18}F]FDG) e sem sinais de atrofia (Leuzy *et al.*, 2015). Cabe salientar que utilizamos uma estratégia baseada na interação entre neurônios e astrócitos para investigar as propriedades do [^{11}C]ABP688, ou seja, ativamos o transportador astrocitária GLT-1 e conseguimos alterar a ligação do [^{11}C]ABP688 no sítio alostérico do mGluR5, que é predominantemente neuronal.

Esta interação neurônio-astrócito tem sido alvo de diversos debates principalmente em termos de metabolismo energético. Atualmente, acredita-se que o consumo de PET [^{18}F]FDG reflita atividade neuronal, ou seja, o consumo de glicose em neurônios (Mosconi *et al.*, 2010). De fato, o hipometabolismo cerebral característico da DA e de outras demências parece estar intimamente ligado a disfunção sináptica de natureza neuronal. Entretanto diversos estudos liderados pelos Drs. Pierre Magistretti e Luc Pellerin da Universidade de Lausanne na Suíça indicam um cenário um pouco distinto em termos de consumo cerebral de glicose (Pellerin e Magistretti, 2012). Eles postularam um mecanismo denominado a “lançadeira de lactato astrócito-neurônio”

(ANLS, do inglês *astrocyte-neuron lactate shuttle*). Baseado na ANLS, a captação de glicose é feita pelos astrócitos, que produzem lactato via glicólise anaeróbica, e enviam este lactato para suprir demandas energéticas neuronais. Ainda, cabe salientar que a ANLS propõe que o gatilho para a captação astrocitária de glicose seria a captação de glutamato via GLT-1 e GLAST (Pellerin e Magistretti, 1994; Voutsinos-Porche *et al.*, 2003). Porém este mecanismo nunca foi testado *in vivo* e não se sabe se a ativação do GLT-1 astrocitário seria capaz de alterar o sinal proveniente do PET [^{18}F]FDG.

Utilizando a mesma abordagem farmacológica do estudo anterior, administramos uma dose única de ceftriaxona IV antes do escaneamento de microPET com [^{18}F]FDG, e analisamos o impacto da ativação de GLT-1 no sinal de [^{18}F]FDG. A ativação de GLT-1 causou um aumento global no consumo de [^{18}F]FDG (parte II, capítulo XIII, *"[^{18}F]FDG PET signal is driven by astroglial glutamate transport"*). Uma análise um pouco mais refinada demonstrou que regiões com maior expressão de GLT-1, como o córtex pré-frontal e o hipocampo, foram as regiões onde a ativação do GLT-1 causou um aumento mais marcante no consumo de [^{18}F]FDG. Baseado no acoplamento entre fluxo sanguíneo cerebral e atividade neuronal (Lauritzen, 2001), analisamos o fluxo sanguíneo cerebral via *laser doppler* após a ativação de GLT-1. De fato, a administração de ceftriaxona não alterou o fluxo sanguíneo cerebral em estado de repouso, ou durante estimulação das vibrissas (do inglês *whiskers stimulation*). Além disso, a ativação de GLT-1 *per se* foi capaz de reorganizar a arquitetura metabólica e dessincronizar a captação de glicose entre diversas regiões cerebrais.

Nossos resultados são a primeira evidência *in vivo* via PET [^{18}F]FDG de que a captação de glutamato astrocitária via GLT-1 aumenta a captação de glicose. Nossos

dados associados a estudos anteriores (para revisão ver (Pellerin e Magistretti, 2012)) indicam que muito do sinal proveniente do PET [^{18}F]FDG tem natureza astrocitária. Estes resultados têm implicação direta na clínica, pois o [^{18}F]FDG PET tem sido utilizado como um índice metabólico de atividade neuronal. Mais especificamente, estes achados têm consequências diretas na interpretação de imagens com PET [^{18}F]FDG em doenças cerebrais. Por exemplo, regiões hipometabólicas captadas por PET [^{18}F]FDG são características presentes em diversas doenças neurodegenerativas, como a DA e as FTDs, e doenças neuropsiquiátricas, como depressão e transtorno obsessivo-compulsivo (para revisão ver (Magistretti e Pellerin, 1996)). Desta maneira, estas assinaturas metabólicas podem estar indicando disfunção astrocitária e não necessariamente disfunção neuronal, o que potencialmente desafia o conceito atual da interpretação das imagens com PET [^{18}F]FDG.

Conclusão

Na presente tese, avançamos no entendimento de vias de sinalização associadas com a hipersforforilação da proteína tau envolvendo a disfunção da PP2A e a excitotoxicidade glutamatérgica. Além disso, avaliamos o uso dos radiofármacos de PET para visualização *in vivo* e não invasiva da fisiopatologia da DA. Finalmente, sugerimos o PET [^{11}C]ABP688, para avaliar flutuações no sistema glutamatérgico *in vivo*, e propomos uma reconceptualização na interpretação do PET [^{18}F]FDG, o radiofármaco mais utilizado na clínica atualmente para visualização do metabolismo de glicose. Além de avançar em termos de fisiopatologia, os resultados dos nossos estudos com microPET têm alto potencial translacional e impacto direto na clínica. O PET [^{11}C]ABP688 pode ser

diretamente incluído em estudos clínicos e a nova intepretação do PET [^{18}F]FDG pode alterar a maneira atual como vemos o metabolismo de glicose na DA e em outras doenças neurodegenerativas.

Referências

AKIYAMA, H. et al. Inflammation and Alzheimer's disease. **Neurobiol Aging,** v. 21, n. 3, p. 383-421, May-Jun 2000.

ALZHEIMER'S, A. 2015 Alzheimer's disease facts and figures. **Alzheimers Dement,** v. 11, n. 3, p. 332-84, Mar 2015.

AMETAMEY, S. M. et al. Radiosynthesis and preclinical evaluation of 11C-ABP688 as a probe for imaging the metabotropic glutamate receptor subtype 5. **J Nucl Med,** v. 47, n. 4, p. 698-705, Apr 2006.

ARIF, M. et al. Tau pathology involves protein phosphatase 2A in parkinsonism-dementia of Guam. **Proc Natl Acad Sci U S A,** v. 111, n. 3, p. 1144-9, Jan 21 2014.

ARRIAGADA, P. V. et al. Neurofibrillary tangles but not senile plaques parallel duration and severity of Alzheimer's disease. **Neurology,** v. 42, n. 3 Pt 1, p. 631-9, Mar 1992.

AUGUSTINACK, J. C. et al. Specific tau phosphorylation sites correlate with severity of neuronal cytopathology in Alzheimer's disease. **Acta Neuropathol,** v. 103, n. 1, p. 26-35, Jan 2002.

AYTON, S. et al. Ferritin levels in the cerebrospinal fluid predict Alzheimer's disease outcomes and are regulated by APOE. **Nat Commun,** v. 6, p. 6760, 2015.

BALLATORE, C.; LEE, V. M.; TROJANOWSKI, J. Q. Tau-mediated neurodegeneration in Alzheimer's disease and related disorders. **Nat Rev Neurosci,** v. 8, n. 9, p. 663-72, Sep 2007.

BENILOVA, I.; DE STROOPER, B. An overlooked neurotoxic species in Alzheimer's disease. **Nat Neurosci,** v. 14, n. 8, p. 949-50, Aug 2011.

BIOMARKERS DEFINITIONS WORKING, G. Biomarkers and surrogate endpoints: preferred definitions and conceptual framework. **Clin Pharmacol Ther,** v. 69, n. 3, p. 89-95, Mar 2001.

BLENNOW, K. Cerebrospinal fluid protein biomarkers for Alzheimer's disease. **NeuroRx,** v. 1, n. 2, p. 213-25, Apr 2004.

BLENNOW, K. et al. Amyloid biomarkers in Alzheimer's disease. **Trends Pharmacol Sci,** v. 36, n. 5, p. 297-309, May 2015.

BLENNOW, K.; VANMECHELEN, E. CSF markers for pathogenic processes in Alzheimer's disease: diagnostic implications and use in clinical neurochemistry. **Brain Res Bull,** v. 61, n. 3, p. 235-42, Aug 15 2003.

BLENNOW, K.; ZETTERBERG, H.; FAGAN, A. M. Fluid biomarkers in Alzheimer disease. **Cold Spring Harb Perspect Med,** v. 2, n. 9, p. a006221, Sep 2012.

BRAAK, H.; BRAAK, E. Neuropathological stageing of Alzheimer-related changes. **Acta Neuropathol,** v. 82, n. 4, p. 239-59, 1991.

BREITNER, J. C. et al. Extended results of the Alzheimer's disease anti-inflammatory prevention trial. **Alzheimers Dement,** v. 7, n. 4, p. 402-11, Jul 2011.

BRUNDEN, K. R.; TROJANOWSKI, J. Q.; LEE, V. M. Advances in tau-focused drug discovery for Alzheimer's disease and related tauopathies. **Nat Rev Drug Discov,** v. 8, n. 10, p. 783-93, Oct 2009.

BUEE, L. et al. Tau protein isoforms, phosphorylation and role in neurodegenerative disorders. **Brain Res Brain Res Rev,** v. 33, n. 1, p. 95-130, Aug 2000.

BUERGER, K. et al. CSF tau protein phosphorylated at threonine 231 correlates with cognitive decline in MCI subjects. **Neurology,** v. 59, n. 4, p. 627-9, Aug 27 2002.

CABELLO, N. et al. Metabotropic glutamate type 5, dopamine D2 and adenosine A2a receptors form higher-order oligomers in living cells. **J Neurochem,** v. 109, n. 5, p. 1497-507, Jun 2009.

CANELA, L. et al. The association of metabotropic glutamate receptor type 5 with the neuronal Ca2+-binding protein 2 modulates receptor function. **J Neurochem,** v. 111, n. 2, p. 555-67, Oct 2009.

CARBONELL, F. et al. beta-Amyloid is associated with aberrant metabolic connectivity in subjects with mild cognitive impairment. **J Cereb Blood Flow Metab,** v. 34, n. 7, p. 1169-79, Jul 2014.

CARTER, S. F. et al. Evidence for astrocytosis in prodromal Alzheimer disease provided by 11C-deuterium-L-deprenyl: a multitracer PET paradigm combining 11C-Pittsburgh compound B and 18F-FDG. **J Nucl Med,** v. 53, n. 1, p. 37-46, Jan 2012.

CHOI, H. et al. Abnormal metabolic connectivity in the pilocarpine-induced epilepsy rat model: a multiscale network analysis based on persistent homology. **Neuroimage,** v. 99, p. 226-36, Oct 1 2014.

COHEN, P.; KLUMPP, S.; SCHELLING, D. L. An improved procedure for identifying and quantitating protein phosphatases in mammalian tissues. **FEBS Lett,** v. 250, n. 2, p. 596-600, Jul 3 1989.

COHEN, R. M. et al. A transgenic Alzheimer rat with plaques, tau pathology, behavioral impairment, oligomeric abeta, and frank neuronal loss. **J Neurosci,** v. 33, n. 15, p. 6245-56, Apr 10 2013.

Consensus report of the Working Group on: "Molecular and Biochemical Markers of Alzheimer's Disease". The Ronald and Nancy Reagan Research Institute of the Alzheimer's Association and the National Institute on Aging Working Group. **Neurobiol Aging,** v. 19, n. 2, p. 109-16, Mar-Apr 1998.

CULL-CANDY, S.; BRICKLEY, S.; FARRANT, M. NMDA receptor subunits: diversity, development and disease. **Curr Opin Neurobiol,** v. 11, n. 3, p. 327-35, Jun 2001.

DANBOLT, N. C. Glutamate uptake. **Prog Neurobiol,** v. 65, n. 1, p. 1-105, Sep 2001.

DANYSZ, W.; PARSONS, C. G. Alzheimer's disease, beta-amyloid, glutamate, NMDA receptors and memantine--searching for the connections. **Br J Pharmacol,** v. 167, n. 2, p. 324-52, Sep 2012.

DE LEON, M. J. et al. Prediction of cognitive decline in normal elderly subjects with 2-[(18)F]fluoro-2-deoxy-D-glucose/poitron-emission tomography (FDG/PET). **Proc Natl Acad Sci U S A,** v. 98, n. 19, p. 10966-71, Sep 11 2001.

DELORENZO, C. et al. In vivo ketamine-induced changes in [(1)(1)C]ABP688 binding to metabotropic glutamate receptor subtype 5. **Biol Psychiatry,** v. 77, n. 3, p. 266-75, Feb 1 2015.

DELORENZO, C. et al. In vivo variation in metabotropic glutamate receptor subtype 5 binding using positron emission tomography and [11C]ABP688. **J Cereb Blood Flow Metab,** v. 31, n. 11, p. 2169-80, Nov 2011.

DUBOIS, B. et al. Revising the definition of Alzheimer's disease: a new lexicon. **Lancet Neurol,** v. 9, n. 11, p. 1118-27, Nov 2010.

DUBOIS, B. et al. Research criteria for the diagnosis of Alzheimer's disease: revising the NINCDS-ADRDA criteria. **Lancet Neurol,** v. 6, n. 8, p. 734-46, Aug 2007.

EDISON, P. et al. Microglia, amyloid, and cognition in Alzheimer's disease: An [11C](R)PK11195-PET and [11C]PIB-PET study. **Neurobiol Dis,** v. 32, n. 3, p. 412-9, Dec 2008.

EIKELENBOOM, P. et al. Complement activation in amyloid plaques in Alzheimer's dementia. **Virchows Arch B Cell Pathol Incl Mol Pathol,** v. 56, n. 4, p. 259-62, 1989.

EIKELENBOOM, P.; STAM, F. C. Immunoglobulins and complement factors in senile plaques. An immunoperoxidase study. **Acta Neuropathol,** v. 57, n. 2-3, p. 239-42, 1982.

EIKELENBOOM, P.; VAN GOOL, W. A. Neuroinflammatory perspectives on the two faces of Alzheimer's disease. **J Neural Transm,** v. 111, n. 3, p. 281-94, Mar 2004.

ESPOSITO, G. et al. Imaging neuroinflammation in Alzheimer's disease with radiolabeled arachidonic acid and PET. **J Nucl Med,** v. 49, n. 9, p. 1414-21, Sep 2008.

FERREIRA, S. T. et al. Inflammation, defective insulin signaling, and neuronal dysfunction in Alzheimer's disease. **Alzheimers Dement,** v. 10, n. 1 Suppl, p. S76-83, Feb 2014.

FODERO-TAVOLETTI, M. T. et al. 18F-THK523: a novel in vivo tau imaging ligand for Alzheimer's disease. **Brain,** v. 134, n. Pt 4, p. 1089-100, Apr 2011.

FRISONI, G. B. et al. The clinical use of structural MRI in Alzheimer disease. **Nat Rev Neurol,** v. 6, n. 2, p. 67-77, Feb 2010.

FULLER, S.; STEELE, M.; MUNCH, G. Activated astroglia during chronic inflammation in Alzheimer's disease--do they neglect their neurosupportive roles? **Mutat Res,** v. 690, n. 1-2, p. 40-9, Aug 7 2010.

GAUGLER, J. E. et al. Characteristics of patients misdiagnosed with Alzheimer's disease and their medication use: an analysis of the NACC-UDS database. **BMC Geriatr,** v. 13, p. 137, 2013.

GENDREAU, K. L.; HALL, G. F. Tangles, Toxicity, and Tau Secretion in AD - New Approaches to a Vexing Problem. **Front Neurol,** v. 4, p. 160, 2013.

GOEDERT, M.; SPILLANTINI, M. G. A century of Alzheimer's disease. **Science,** v. 314, n. 5800, p. 777-81, Nov 3 2006.

GOERTZEN, A. L. et al. NEMA NU 4-2008 comparison of preclinical PET imaging systems. **J Nucl Med,** v. 53, n. 8, p. 1300-9, Aug 2012.

GONG, C. X.; IQBAL, K. Hyperphosphorylation of microtubule-associated protein tau: a promising therapeutic target for Alzheimer disease. **Curr Med Chem,** v. 15, n. 23, p. 2321-8, 2008.

GONG, C. X. et al. Phosphorylation of microtubule-associated protein tau is regulated by protein phosphatase 2A in mammalian brain. Implications for neurofibrillary degeneration in Alzheimer's disease. **J Biol Chem,** v. 275, n. 8, p. 5535-44, Feb 25 2000.

GONG, C. X. et al. Phosphatase activity toward abnormally phosphorylated tau: decrease in Alzheimer disease brain. **J Neurochem,** v. 65, n. 2, p. 732-8, Aug 1995.

GONG, C. X. et al. Phosphoprotein phosphatase activities in Alzheimer disease brain. **J Neurochem,** v. 61, n. 3, p. 921-7, Sep 1993.

GONG, J. P. et al. Cannabinoid CB2 receptors: immunohistochemical localization in rat brain. **Brain Res,** v. 1071, n. 1, p. 10-23, Feb 3 2006.

GOTZ, J. et al. A decade of tau transgenic animal models and beyond. **Brain Pathol,** v. 17, n. 1, p. 91-103, Jan 2007.

GOTZ, J.; ITTNER, L. M. Animal models of Alzheimer's disease and frontotemporal dementia. **Nat Rev Neurosci,** v. 9, n. 7, p. 532-44, Jul 2008.

GRIFFIN, W. S. et al. Brain interleukin 1 and S-100 immunoreactivity are elevated in Down syndrome and Alzheimer disease. **Proc Natl Acad Sci U S A,** v. 86, n. 19, p. 7611-5, Oct 1989.

GROUP, A.-F. R. Follow-up evaluation of cognitive function in the randomized Alzheimer's Disease Anti-inflammatory Prevention Trial and its Follow-up Study. **Alzheimers Dement,** v. 11, n. 2, p. 216-25 e1, Feb 2015.

GUILLOZET, A. L. et al. Neurofibrillary tangles, amyloid, and memory in aging and mild cognitive impairment. **Arch Neurol,** v. 60, n. 5, p. 729-36, May 2003.

HAASS, C.; SELKOE, D. J. Soluble protein oligomers in neurodegeneration: lessons from the Alzheimer's amyloid beta-peptide. **Nat Rev Mol Cell Biol,** v. 8, n. 2, p. 101-12, Feb 2007.

HAMPEL, H. Amyloid-beta and cognition in aging and Alzheimer's disease: molecular and neurophysiological mechanisms. **J Alzheimers Dis,** v. 33 Suppl 1, p. S79-86, 2013.

HAMPEL, H. et al. Correlation of cerebrospinal fluid levels of tau protein phosphorylated at threonine 231 with rates of hippocampal atrophy in Alzheimer disease. **Arch Neurol,** v. 62, n. 5, p. 770-3, May 2005.

HANSSON, O. et al. Prediction of Alzheimer's disease using the CSF Abeta42/Abeta40 ratio in patients with mild cognitive impairment. **Dement Geriatr Cogn Disord,** v. 23, n. 5, p. 316-20, 2007.

HARDY, J.; SELKOE, D. J. The amyloid hypothesis of Alzheimer's disease: progress and problems on the road to therapeutics. **Science,** v. 297, n. 5580, p. 353-6, Jul 19 2002.

HARDY, J. A.; HIGGINS, G. A. Alzheimer's disease: the amyloid cascade hypothesis. **Science,** v. 256, n. 5054, p. 184-5, Apr 10 1992.

HARRIS, K. A. et al. Okadaic acid induces hyperphosphorylated forms of tau protein in human brain slices. **Ann Neurol,** v. 33, n. 1, p. 77-87, Jan 1993.

HEEMELS, M. T. Ageing. **Nature,** v. 464, n. 7288, p. 503, Mar 25 2010.

HOLLMANN, M.; HEINEMANN, S. Cloned glutamate receptors. **Annu Rev Neurosci,** v. 17, p. 31-108, 1994.

HOOZEMANS, J. J. et al. Soothing the inflamed brain: effect of non-steroidal anti-inflammatory drugs on Alzheimer's disease pathology. **CNS Neurol Disord Drug Targets,** v. 10, n. 1, p. 57-67, Feb 2011.

HORN, R. et al. Atrophy of hippocampus in patients with Alzheimer's disease and other diseases with memory impairment. **Dementia,** v. 7, n. 4, p. 182-6, Jul-Aug 1996.

HORTI, A. G. et al. Synthesis and biodistribution of [11C]A-836339, a new potential radioligand for PET imaging of cannabinoid type 2 receptors (CB2). **Bioorg Med Chem,** v. 18, n. 14, p. 5202-7, Jul 15 2010.

IN T' VELD, B. A. et al. Nonsteroidal antiinflammatory drugs and the risk of Alzheimer's disease. **N Engl J Med,** v. 345, n. 21, p. 1515-21, Nov 22 2001.

INESTROSA, N. C.; ARENAS, E. Emerging roles of Wnts in the adult nervous system. **Nat Rev Neurosci,** v. 11, n. 2, p. 77-86, Feb 2010.

JACK, C. R., JR.; BARRIO, J. R.; KEPE, V. Cerebral amyloid PET imaging in Alzheimer's disease. **Acta Neuropathol,** v. 126, n. 5, p. 643-57, Nov 2013a.

JACK, C. R., JR. et al. Tracking pathophysiological processes in Alzheimer's disease: an updated hypothetical model of dynamic biomarkers. **Lancet Neurol,** v. 12, n. 2, p. 207-16, Feb 2013b.

JACK, C. R., JR. et al. Hypothetical model of dynamic biomarkers of the Alzheimer's pathological cascade. **Lancet Neurol,** v. 9, n. 1, p. 119-28, Jan 2010.

JAMES, M. L. et al. PET imaging of translocator protein (18 kDa) in a mouse model of Alzheimer's disease using N-(2,5-dimethoxybenzyl)-2-18F-fluoro-N-(2-phenoxyphenyl)acetamide. **J Nucl Med,** v. 56, n. 2, p. 311-6, Feb 2015.

JANSEN, W. J. et al. Prevalence of cerebral amyloid pathology in persons without dementia: a meta-analysis. **JAMA,** v. 313, n. 19, p. 1924-38, May 19 2015.

JOHN, C. S. et al. Blockade of the GLT-1 Transporter in the Central Nucleus of the Amygdala Induces both Anxiety and Depressive-Like Symptoms. **Neuropsychopharmacology,** v. 40, n. 7, p. 1700-8, Jun 2015.

JOHNSON, G. V.; STOOTHOFF, W. H. Tau phosphorylation in neuronal cell function and dysfunction. **J Cell Sci,** v. 117, n. Pt 24, p. 5721-9, Nov 15 2004.

JOHNSON, J. W.; KOTERMANSKI, S. E. Mechanism of action of memantine. **Curr Opin Pharmacol,** v. 6, n. 1, p. 61-7, Feb 2006.

JOHNSON, K. A. et al. Appropriate use criteria for amyloid PET: a report of the Amyloid Imaging Task Force, the Society of Nuclear Medicine and Molecular Imaging, and the Alzheimer's Association. **Alzheimers Dement,** v. 9, n. 1, p. e-1-16, Jan 2013a.

JOHNSON, K. A. et al. Update on appropriate use criteria for amyloid PET imaging: dementia experts, mild cognitive impairment, and education. **J Nucl Med,** v. 54, n. 7, p. 1011-3, Jul 2013b.

JUCKER, M. et al. **Alzheimer: 100 Years and Beyond**. Research and Perspectives in Alzheimer&#x2019 s Disease. Berlin, Heidelberg: Springer-Verlag Berlin Heidelberg, 2006.

KAMAT, P. K. et al. Mechanism of synapse redox stress in Okadaic acid (ICV) induced memory impairment: Role of NMDA receptor. **Neurochem Int,** v. 76, p. 32-41, Oct 2014.

KAMAT, P. K. et al. Mitochondrial dysfunction: a crucial event in okadaic acid (ICV) induced memory impairment and apoptotic cell death in rat brain. **Pharmacol Biochem Behav,** v. 100, n. 2, p. 311-9, Dec 2011.

KARUS, C. et al. Astrocytes restrict discharge duration and neuronal sodium loads during recurrent network activity. **Glia,** v. 63, n. 6, p. 936-57, Jun 2015.

KLUNK, W. E. et al. Imaging brain amyloid in Alzheimer's disease with Pittsburgh Compound-B. **Ann Neurol,** v. 55, n. 3, p. 306-19, Mar 2004.

LAURITZEN, M. Relationship of spikes, synaptic activity, and local changes of cerebral blood flow. **J Cereb Blood Flow Metab,** v. 21, n. 12, p. 1367-83, Dec 2001.

LEHTONEN, J. Y.; HOLOPAINEN, J. M.; KINNUNEN, P. K. Activation of phospholipase A2 by amyloid beta-peptides in vitro. **Biochemistry,** v. 35, n. 29, p. 9407-14, Jul 23 1996.

LEON, W. C. et al. A novel transgenic rat model with a full Alzheimer's-like amyloid pathology displays pre-plaque intracellular amyloid-beta-associated cognitive impairment. **J Alzheimers Dis,** v. 20, n. 1, p. 113-26, 2010.

LEUZY, A. et al. Amyloid imaging in Alzheimer’s disease: a potential new era of personalized medicine? **Translational Neuroscience,** v. 5, n. 1, p. 51-56, 2014/03/01 2014a.

LEUZY, A. et al. Imaging biomarkers for amyloid: a new generation of probes and what lies ahead. **Int Psychogeriatr,** v. 26, n. 5, p. 703-7, May 2014b.

LEUZY, A. et al. In vivo characterization of metabotropic glutamate receptor type 5 abnormalities in behavioral variant FTD. **Brain Struct Funct**, Jan 18 2015.

LEUZY, A. et al. Use of amyloid PET across the spectrum of Alzheimer's disease: clinical utility and associated ethical issues. **Amyloid,** v. 21, n. 3, p. 143-8, Sep 2014c.

LEWCZUK, P. et al. Amyloid-beta 42/40 cerebrospinal fluid concentration ratio in the diagnostics of Alzheimer's disease: validation of two novel assays. **J Alzheimers Dis,** v. 43, n. 1, p. 183-91, 2015.

LIPTON, S. A. Pathologically activated therapeutics for neuroprotection. **Nat Rev Neurosci,** v. 8, n. 10, p. 803-8, Oct 2007.

LIPTON, S. A.; CHEN, H. S. Paradigm shift in neuroprotective drug development: clinically tolerated NMDA receptor inhibition by memantine. **Cell Death Differ,** v. 11, n. 1, p. 18-20, Jan 2004.

LU, C. W.; LIN, T. Y.; WANG, S. J. Memantine depresses glutamate release through inhibition of voltage-dependent Ca2+ entry and protein kinase C in rat cerebral cortex nerve terminals: an NMDA receptor-independent mechanism. **Neurochem Int,** v. 57, n. 2, p. 168-76, Sep 2010.

MADEIRA, C. et al. d-serine levels in Alzheimer's disease: implications for novel biomarker development. **Transl Psychiatry,** v. 5, p. e561, 2015.

MAGISTRETTI, P. J.; PELLERIN, L. The contribution of astrocytes to the 18F-2-deoxyglucose signal in PET activation studies. **Mol Psychiatry,** v. 1, n. 6, p. 445-52, Dec 1996.

MAIER, F. C. et al. Longitudinal PET-MRI reveals beta-amyloid deposition and rCBF dynamics and connects vascular amyloidosis to quantitative loss of perfusion. **Nat Med,** v. 20, n. 12, p. 1485-92, Dec 2014.

MARK, L. P. et al. Pictorial review of glutamate excitotoxicity: fundamental concepts for neuroimaging. **AJNR Am J Neuroradiol,** v. 22, n. 10, p. 1813-24, Nov-Dec 2001.

MARUYAMA, M. et al. Imaging of tau pathology in a tauopathy mouse model and in Alzheimer patients compared to normal controls. **Neuron,** v. 79, n. 6, p. 1094-108, Sep 18 2013.

MAZZILOTTA, J. C. et al. Tomographic mapping of human cerebral metabolism: normal unstimulated state. **Neurology,** v. 31, n. 5, p. 503-16, May 1981.

MCDONALD, C. R. et al. Regional rates of neocortical atrophy from normal aging to early Alzheimer disease. **Neurology,** v. 73, n. 6, p. 457-65, Aug 11 2009.

MCGEER, P. L.; MCGEER, E. G. The amyloid cascade-inflammatory hypothesis of Alzheimer disease: implications for therapy. **Acta Neuropathol,** v. 126, n. 4, p. 479-97, Oct 2013.

MCGEER, P. L.; SCHULZER, M.; MCGEER, E. G. Arthritis and anti-inflammatory agents as possible protective factors for Alzheimer's disease: a review of 17 epidemiologic studies. **Neurology,** v. 47, n. 2, p. 425-32, Aug 1996.

MCKHANN, G. et al. Clinical diagnosis of Alzheimer's disease: report of the NINCDS-ADRDA Work Group under the auspices of Department of Health and Human Services Task Force on Alzheimer's Disease. **Neurology,** v. 34, n. 7, p. 939-44, Jul 1984.

MEHTA, A. et al. Excitotoxicity: bridge to various triggers in neurodegenerative disorders. **Eur J Pharmacol,** v. 698, n. 1-3, p. 6-18, Jan 5 2013.

MENENDEZ-GONZALEZ, M.; CALATAYUD, M. T.; BLAZQUEZ-MENES, B. Exacerbation of Lewy bodies dementia due to memantine. **J Alzheimers Dis,** v. 8, n. 3, p. 289-91, Dec 2005.

MIYAKE, N. et al. Imaging changes in glutamate transmission in vivo with the metabotropic glutamate receptor 5 tracer [11C] ABP688 and N-acetylcysteine challenge. **Biol Psychiatry,** v. 69, n. 9, p. 822-4, May 1 2011.

MOSCONI, L. Brain glucose metabolism in the early and specific diagnosis of Alzheimer's disease. FDG-PET studies in MCI and AD. **Eur J Nucl Med Mol Imaging,** v. 32, n. 4, p. 486-510, Apr 2005.

MOSCONI, L. et al. Pre-clinical detection of Alzheimer's disease using FDG-PET, with or without amyloid imaging. **J Alzheimers Dis,** v. 20, n. 3, p. 843-54, 2010.

MOSCONI, L. et al. Hippocampal hypometabolism predicts cognitive decline from normal aging. **Neurobiol Aging,** v. 29, n. 5, p. 676-92, May 2008.

MRAK, R. E.; GRIFFIN, W. S. Glia and their cytokines in progression of neurodegeneration. **Neurobiol Aging,** v. 26, n. 3, p. 349-54, Mar 2005.

MUKAETOVA-LADINSKA, E. B. et al. Biochemical and anatomical redistribution of tau protein in Alzheimer's disease. **Am J Pathol,** v. 143, n. 2, p. 565-78, Aug 1993.

NELISSEN, N. et al. Phase 1 study of the Pittsburgh compound B derivative 18F-flutemetamol in healthy volunteers and patients with probable Alzheimer disease. **J Nucl Med,** v. 50, n. 8, p. 1251-9, Aug 2009.

NISBET, R. M. et al. Tau aggregation and its interplay with amyloid-beta. **Acta Neuropathol,** v. 129, n. 2, p. 207-20, Feb 2015.

NUNAN, J.; SMALL, D. H. Regulation of APP cleavage by alpha-, beta- and gamma-secretases. **FEBS Lett,** v. 483, n. 1, p. 6-10, Oct 13 2000.

OKELLO, A. et al. Microglial activation and amyloid deposition in mild cognitive impairment: a PET study. **Neurology,** v. 72, n. 1, p. 56-62, Jan 6 2009.

OSSENKOPPELE, R. et al. Prevalence of amyloid PET positivity in dementia syndromes: a meta-analysis. **JAMA,** v. 313, n. 19, p. 1939-49, May 19 2015.

PAULA-LIMA, A. C.; BRITO-MOREIRA, J.; FERREIRA, S. T. Deregulation of excitatory neurotransmission underlying synapse failure in Alzheimer's disease. **J Neurochem,** v. 126, n. 2, p. 191-202, Jul 2013.

PELLERIN, L.; MAGISTRETTI, P. J. Glutamate uptake into astrocytes stimulates aerobic glycolysis: a mechanism coupling neuronal activity to glucose utilization. **Proc Natl Acad Sci U S A,** v. 91, n. 22, p. 10625-9, Oct 25 1994.

_____. Sweet sixteen for ANLS. **J Cereb Blood Flow Metab,** v. 32, n. 7, p. 1152-66, Jul 2012.

PESKIND, E. R. et al. Memantine treatment in mild to moderate Alzheimer disease: a 24-week randomized, controlled trial. **Am J Geriatr Psychiatry,** v. 14, n. 8, p. 704-15, Aug 2006.

PRATICO, D. et al. Increase of brain oxidative stress in mild cognitive impairment: a possible predictor of Alzheimer disease. **Arch Neurol,** v. 59, n. 6, p. 972-6, Jun 2002.

PRICE, J. C. et al. Kinetic modeling of amyloid binding in humans using PET imaging and Pittsburgh Compound-B. **J Cereb Blood Flow Metab,** v. 25, n. 11, p. 1528-47, Nov 2005.

RABINOVICI, G. D. et al. 11C-PIB PET imaging in Alzheimer disease and frontotemporal lobar degeneration. **Neurology,** v. 68, n. 15, p. 1205-12, Apr 10 2007.

RASMUSSEN, B. A. et al. beta-Lactam antibiotic produces a sustained reduction in extracellular glutamate in the nucleus accumbens of rats. **Amino Acids,** v. 40, n. 2, p. 761-4, Feb 2011.

REIMAN, E. M. et al. Brain imaging and fluid biomarker analysis in young adults at genetic risk for autosomal dominant Alzheimer's disease in the presenilin 1 E280A kindred: a case-control study. **Lancet Neurol,** v. 11, n. 12, p. 1048-56, Dec 2012.

REISBERG, B. et al. Memantine in moderate-to-severe Alzheimer's disease. **N Engl J Med,** v. 348, n. 14, p. 1333-41, Apr 3 2003.

REVETT, T. J. et al. Glutamate system, amyloid ss peptides and tau protein: functional interrelationships and relevance to Alzheimer disease pathology. **J Psychiatry Neurosci,** v. 38, n. 1, p. 6-23, Jan 2013.

ROCHER, A. B. et al. Resting-state brain glucose utilization as measured by PET is directly related to regional synaptophysin levels: a study in baboons. **Neuroimage,** v. 20, n. 3, p. 1894-8, Nov 2003.

ROMANO, C.; YANG, W. L.; O'MALLEY, K. L. Metabotropic glutamate receptor 5 is a disulfide-linked dimer. **J Biol Chem,** v. 271, n. 45, p. 28612-6, Nov 8 1996.

ROWE, C. C. et al. Imaging of amyloid beta in Alzheimer's disease with 18F-BAY94-9172, a novel PET tracer: proof of mechanism. **Lancet Neurol,** v. 7, n. 2, p. 129-35, Feb 2008.

ROWE, C. C. et al. Head-to-head comparison of 11C-PiB and 18F-AZD4694 (NAV4694) for beta-amyloid imaging in aging and dementia. **J Nucl Med,** v. 54, n. 6, p. 880-6, Jun 2013.

ROWE, C. C.; VILLEMAGNE, V. L. Brain amyloid imaging. **J Nucl Med Technol,** v. 41, n. 1, p. 11-8, Mar 2013.

SAFER, U.; DORUK, H.; TASCI, I. Memantine overdose in a non-demented older adult. **Geriatr Gerontol Int,** v. 15, n. 3, p. 383, Mar 2015.

SAMGARD, K. et al. Cerebrospinal fluid total tau as a marker of Alzheimer's disease intensity. **Int J Geriatr Psychiatry,** v. 25, n. 4, p. 403-10, Apr 2010.

SANDIEGO, C. M. et al. Studies of the metabotropic glutamate receptor 5 radioligand [(1)(1)C]ABP688 with N-acetylcysteine challenge in rhesus monkeys. **Synapse,** v. 67, n. 8, p. 489-501, Aug 2013.

SCAHILL, R. I. et al. Mapping the evolution of regional atrophy in Alzheimer's disease: unbiased analysis of fluid-registered serial MRI. **Proc Natl Acad Sci U S A,** v. 99, n. 7, p. 4703-7, Apr 2 2002.

SCHAEFFER, E.; DUPLANTIER, A. Glutamate and Neurodegenerative Disease. In: DOMINGUEZ, C. (Ed.). **Neurodegenerative Diseases**: Springer Berlin Heidelberg, v.6, 2010. cap. 11, p.91-147. (Topics in Medicinal Chemistry). ISBN 978-3-642-16757-7.

SCHAEFFER, E. L.; GATTAZ, W. F. Cholinergic and glutamatergic alterations beginning at the early stages of Alzheimer disease: participation of the phospholipase A2 enzyme. **Psychopharmacology (Berl),** v. 198, n. 1, p. 1-27, May 2008.

SCHILLING, L. P. et al. Nonamyloid PET biomarkers and Alzheimer's disease: current and future perspectives. **Future Neurology,** v. 9, n. 6, p. 597-613, 2014/11/01 2014.

SCHOEPFER, R. et al. Molecular biology of glutamate receptors. **Prog Neurobiol,** v. 42, n. 2, p. 353-7, Feb 1994.

SCHRAG, M. et al. Oxidative stress in blood in Alzheimer's disease and mild cognitive impairment: a meta-analysis. **Neurobiol Dis,** v. 59, p. 100-10, Nov 2013.

SCHUFF, N. et al. MRI of hippocampal volume loss in early Alzheimer's disease in relation to ApoE genotype and biomarkers. **Brain,** v. 132, n. Pt 4, p. 1067-77, Apr 2009.

SERRANO-POZO, A. et al. Reactive glia not only associates with plaques but also parallels tangles in Alzheimer's disease. **Am J Pathol,** v. 179, n. 3, p. 1373-84, Sep 2011.

SERRANO-POZO, A. et al. Differential relationships of reactive astrocytes and microglia to fibrillar amyloid deposits in Alzheimer disease. **J Neuropathol Exp Neurol,** v. 72, n. 6, p. 462-71, Jun 2013.

SHMAKOV, D. N.; ABROSIMOVA, G. V. [The process of heart ventricle depolarization and the formation of an electrocardiographic QRS complex in the frog]. **Fiziol Zh SSSR Im I M Sechenova,** v. 75, n. 8, p. 1116-20, Aug 1989.

SHULMAN, M. B. et al. Using AD biomarker research results for clinical care: a survey of ADNI investigators. **Neurology,** v. 81, n. 13, p. 1114-21, Sep 24 2013.

SILVERMAN, D. H. Brain 18F-FDG PET in the diagnosis of neurodegenerative dementias: comparison with perfusion SPECT and with clinical evaluations lacking nuclear imaging. **J Nucl Med,** v. 45, n. 4, p. 594-607, Apr 2004.

SPERLING, R. A. et al. Toward defining the preclinical stages of Alzheimer's disease: recommendations from the National Institute on Aging-Alzheimer's Association workgroups on diagnostic guidelines for Alzheimer's disease. **Alzheimers Dement,** v. 7, n. 3, p. 280-92, May 2011.

SPIRES-JONES, T. L. et al. Tau pathophysiology in neurodegeneration: a tangled issue. **Trends Neurosci,** v. 32, n. 3, p. 150-9, Mar 2009.

SUH, Y. H.; CHECLER, F. Amyloid precursor protein, presenilins, and alpha-synuclein: molecular pathogenesis and pharmacological applications in Alzheimer's disease. **Pharmacol Rev,** v. 54, n. 3, p. 469-525, Sep 2002.

TARIOT, P. N. et al. Memantine treatment in patients with moderate to severe Alzheimer disease already receiving donepezil: a randomized controlled trial. **JAMA,** v. 291, n. 3, p. 317-24, Jan 21 2004.

THAL, D. R. et al. Neuropathology and biochemistry of Abeta and its aggregates in Alzheimer's disease. **Acta Neuropathol,** v. 129, n. 2, p. 167-82, Feb 2015.

THOMPSON, P. M. et al. Dynamics of gray matter loss in Alzheimer's disease. **J Neurosci,** v. 23, n. 3, p. 994-1005, Feb 1 2003.

THONE-REINEKE, C. et al. The beta-lactam antibiotic, ceftriaxone, dramatically improves survival, increases glutamate uptake and induces neurotrophins in stroke. **J Hypertens,** v. 26, n. 12, p. 2426-35, Dec 2008.

TIAN, Q. et al. Injection of okadaic acid into the meynert nucleus basalis of rat brain induces decreased acetylcholine level and spatial memory deficit. **Neuroscience,** v. 126, n. 2, p. 277-84, 2004.

TOMASI, G. et al. Novel reference region model reveals increased microglial and reduced vascular binding of 11C-(R)-PK11195 in patients with Alzheimer's disease. **J Nucl Med,** v. 49, n. 8, p. 1249-56, Aug 2008.

TOYAMA, H. et al. Absolute quantification of regional cerebral glucose utilization in mice by 18F-FDG small animal PET scanning and 2-14C-DG autoradiography. **J Nucl Med,** v. 45, n. 8, p. 1398-405, Aug 2004.

TU, S. et al. Oligomeric Abeta-induced synaptic dysfunction in Alzheimer's disease. **Mol Neurodegener,** v. 9, p. 48, 2014.

VAN MARUM, R. J. Update on the use of memantine in Alzheimer's disease. **Neuropsychiatr Dis Treat,** v. 5, p. 237-47, 2009.

VAN SICKLE, M. D. et al. Identification and functional characterization of brainstem cannabinoid CB2 receptors. **Science,** v. 310, n. 5746, p. 329-32, Oct 14 2005.

VAUPEL, J. W. Biodemography of human ageing. **Nature,** v. 464, n. 7288, p. 536-42, Mar 25 2010.

VENNETI, S. et al. PK11195 labels activated microglia in Alzheimer's disease and in vivo in a mouse model using PET. **Neurobiol Aging,** v. 30, n. 8, p. 1217-26, Aug 2009.

VENNETI, S.; LOPRESTI, B. J.; WILEY, C. A. The peripheral benzodiazepine receptor (Translocator protein 18kDa) in microglia: from pathology to imaging. **Prog Neurobiol,** v. 80, n. 6, p. 308-22, Dec 2006.

VERKHRATSKY, A. et al. Astrocytes in Alzheimer's disease. **Neurotherapeutics,** v. 7, n. 4, p. 399-412, Oct 2010.

VILLEMAGNE, V. L. et al. In vivo evaluation of a novel tau imaging tracer for Alzheimer's disease. **Eur J Nucl Med Mol Imaging,** v. 41, n. 5, p. 816-26, May 2014.

VOUTSINOS-PORCHE, B. et al. Glial glutamate transporters mediate a functional metabolic crosstalk between neurons and astrocytes in the mouse developing cortex. **Neuron,** v. 37, n. 2, p. 275-86, Jan 23 2003.

WADE, J. et al. Biophysically based computational models of astrocyte ~ neuron coupling and their functional significance. **Front Comput Neurosci,** v. 7, p. 44, 2013.

WILLIAMS, D. R. Tauopathies: classification and clinical update on neurodegenerative diseases associated with microtubule-associated protein tau. **Intern Med J,** v. 36, n. 10, p. 652-60, Oct 2006.

WINBLAD, B.; PORITIS, N. Memantine in severe dementia: results of the 9M-Best Study (Benefit and efficacy in severely demented patients during treatment with memantine). **Int J Geriatr Psychiatry,** v. 14, n. 2, p. 135-46, Feb 1999.

WONG, D. F. et al. In vivo imaging of amyloid deposition in Alzheimer disease using the radioligand 18F-AV-45 (florbetapir [corrected] F 18). **J Nucl Med,** v. 51, n. 6, p. 913-20, Jun 2010.

WU, L. et al. Early-onset familial Alzheimer's disease (EOFAD). **Can J Neurol Sci,** v. 39, n. 4, p. 436-45, Jul 2012.

WYSS-CORAY, T.; MUCKE, L. Inflammation in neurodegenerative disease--a double-edged sword. **Neuron,** v. 35, n. 3, p. 419-32, Aug 1 2002.

XIA, C. F. et al. [(18)F]T807, a novel tau positron emission tomography imaging agent for Alzheimer's disease. **Alzheimers Dement,** v. 9, n. 6, p. 666-76, Nov 2013.

YASUNO, F. et al. Increased binding of peripheral benzodiazepine receptor in mild cognitive impairment-dementia converters measured by positron emission tomography with [(1)(1)C]DAA1106. **Psychiatry Res,** v. 203, n. 1, p. 67-74, Jul 30 2012.

ZHANG, Z.; SIMPKINS, J. W. An okadaic acid-induced model of tauopathy and cognitive deficiency. **Brain Res,** v. 1359, p. 233-46, Nov 4 2010.

ZIMMER, E. et al. [18F]NAV4694 shows higher binding and wider dynamic range compared with [11C]PiB in Alzheimer's disease postmortem tissue. **Alzheimer's & Dementia: The Journal of the Alzheimer's Association,** v. 9, n. 4, p. P22-P23, 2013.

ZIMMER, E. R. et al. Pretreatment with memantine prevents Alzheimer-like alterations induced by intrahippocampal okadaic acid administration in rats. **Curr Alzheimer Res,** v. 9, n. 10, p. 1182-90, Dec 2012.

ZIMMER, E. R. et al. IN VITRO PROPERTIES OF [18F]NAV4694: DYNAMIC RANGE, DISPLACEMENT, AND WHITE-MATTER BINDING. **Alzheimer's & Dementia: The Journal of the Alzheimer's Association,** v. 10, n. 4, p. P23-P24, 2014a.

ZIMMER, E. R. et al. Tracking neuroinflammation in Alzheimer's disease: the role of positron emission tomography imaging. **J Neuroinflammation,** v. 11, p. 120, 2014b.

ZIMMER, E. R. et al. Developments in Tau PET Imaging. **Can J Neurol Sci,** v. 41, n. 5, p. 547-53, Sep 2014c.

ZIMMER, E. R. et al. Inhibition of Protein Phosphatase 2A: Focus on the Glutamatergic System. **Mol Neurobiol**, Jul 4 2015a.

ZIMMER, E. R. et al. MicroPET imaging and transgenic models: a blueprint for Alzheimer's disease clinical research. **Trends Neurosci,** v. 37, n. 11, p. 629-41, Nov 2014d.

ZIMMER, E. R. et al. Imaging in vivo glutamate fluctuations with [(11)C]ABP688: a GLT-1 challenge with ceftriaxone. **J Cereb Blood Flow Metab,** v. 35, n. 7, p. 1169-74, Jul 2015b.

ZIMMER, E. R. et al. Long-term NMDAR antagonism correlates reduced astrocytic glutamate uptake with anxiety-like phenotype. **Front Cell Neurosci,** v. 9, p. 219, 2015c.

Anexos

ANEXO I: Artigos publicados durante o período de doutoramento cujos temas se relacionam a esta tese, mas não foram incluídos no corpo principal da tese.

ANEXO I-A. *Physical exercise exacerbates memory deficits induced by intracerebroventricular STZ but improves insulin regulation of H_2O_2 production in mice synaptosomes.*

No **ANEXO I-A** apresentamos o artigo publicado no periódico *Journal of Alzheimer's disease.*

Journal of Alzheimer's Disease 30 (2012) 889–898
DOI 10.3233/JAD-2012-112066
IOS Press

Physical Exercise Exacerbates Memory Deficits Induced by Intracerebroventricular STZ but Improves Insulin Regulation of H_2O_2 Production in Mice Synaptosomes

Alexandre P. Muller[a,1,*], Eduardo Rigon Zimmer[a,1], Eduardo Kalinine[a], Clarissa B. Haas[a], Jean Pierre Oses[a,b], Adriano Martimbianco de Assis[a], Antonio Galina[c], Diogo O. Souza[a] and Luis Valmor Portela[a]

[a]*Departamento de Bioquímica, ICBS, UFRGS, Programa de Pós Graduação em Ciências Biológicas-Bioquímica, Rua Ramiro Barcelos, Porto Alegre, RS, Brazil*
[b]*Programa de Pós-Graduação em Saúde & Comportamento Centro de Ciências da Vida e da Saúde Universidade Católica de Pelotas, Rua Almirante Barroso, Pelotas, Rio Grande do Sul, Brazil*
[c]*Instituto de Bioquímica Médica, Programa de Biofísica e Bioquímica Celular e Programa de Biologia Molecular e Biotecnologia, Universidade Federal do Rio de Janeiro, Laboratório de Bioenergética e Fisiologia Mitocondrial, Cidade Universitária, Rio de Janeiro, Brazil*

Accepted 11 March 2012

Abstract. Insulin brain resistant state is associated with cognitive deficits and Alzheimer's disease by mechanisms that may involve mitochondrial damage and oxidative stress. Conversely, physical exercise improves cognitive function and brain insulin signaling. The intracerebroventricular (i.c.v.) administration of streptozotocin (STZ) in rodents is an established model of insulin-resistant brain state. This study evaluates the effects of physical exercise on memory performance of i.c.v., STZ-treated mice (1 and 3 mg/kg) and whether insulin (50 and 100 ng/ml) modulates mitochondrial H_2O_2 generation in synaptosomes. S100B levels and SOD and CAT activities were assessed as markers of brain damage caused by STZ. Sedentary and exercise vehicle-treated mice demonstrated similar performance in object recognition memory task. In the water maze test, exercise vehicle-treated mice showed improvement performance in the acquisition and retrieval phases. The administration of STZ (1 mg/kg) before thirty days of voluntary physical exercise protocol impaired recognition and spatial memory only in exercised mice, whereas STZ (3 mg/kg) impaired the performance of sedentary and exercise groups. Moreover, STZ (3 mg/kg) increased hippocampal S100B levels in both groups and SOD/CAT ratio in the sedentary animals. Insulin decreased synaptosomal H_2O_2 production in exercised compared to sedentary mice; however, both STZ doses abolished this effect. Normal brain insulin signaling is mechanistically involved in the improvement of cognitive function induced by exercise through the regulation of mitochondrial H_2O_2 production. However, a prior blockade of brain insulin signaling with STZ abolished the benefits of exercise on memory performance and mitochondrial H_2O_2 regulation.

Keywords: Alzheimer's disease, cognitive performance, insulin, insulin-resistant brain state, mitochondria, physical exercise

INTRODUCTION

There has been growing interest in determining the importance of insulin signaling for normal brain function and whether a state of central insulin resistance is involved in the pathogenesis of neurodegenerative

[1]Both authors contributed equally to this work.

*Correspondence to: Alexandre Pastoris Muller, PhD, Departamento de Bioquímica, ICBS, UFRGS, Rua Ramiro Barcelos, 2600 Anexo, CEP 90035-003, Porto Alegre, RS, Brazil. Tel.: +55 51 33085557; Fax: +55 51 33085544; E-mail: alexandrep.muller@gmail.com.

ISSN 1387-2877/12/$27.50 © 2012 – IOS Press and the authors. All rights reserved

diseases and cognitive deficits [1–4]. According to these conjectures, several studies have demonstrated that impaired brain insulin/IGF1 pathways may cause mitochondrial dysfunction and increase oxidative stress damage to neural cells. The insulin-resistant brain state is thought to play a pivotal role in the pathogenesis of neurodegenerative disorders including Alzheimer's disease (AD) [5–7].

Alterations in many aspects of mitochondrial physiology has been linked with neurodegenerative disorders [8]. For instance, functional changes in the respiratory chain complexes affect brain energy supply, leading neural cells to degenerate [9]. Mitochondria have been previously shown to be a site of damage in neurodegenerative diseases [10]. Interestingly, amyloid-β can interact with various mitochondrial proteins causing reduction in respiratory chain complex activities and increase in generation of reactive oxygen species (ROS) [11]. Hydrogen peroxide (H_2O_2) is a ROS that can induce oxidative damage and regulates redox-sensitive signaling [12]. Under normal conditions, the majority of cellular H_2O_2 is produced by mitochondria and is promptly metabolized by antioxidant enzymes. However, in a scenario of decreased mitochondrial antioxidant capacity, an increase in H_2O_2 causes oxidative damage, impairs metabolism, and promotes neurodegeneration [10, 13]. Thus, mitochondrial dysfunction and ROS generation emerge as important factors associated with AD pathogenesis. Conversely, it has been shown that regular physical exercise positively modulates brain insulin signaling [14], protects against neurodegenerative disorders [15], and increases antioxidant defenses [16]. Moreover, physical exercise increases the number and activity of neuronal mitochondria, providing enough energy for exercise-induced neuroplasticity [16].

Streptozotocin (STZ) is commonly administered at high doses (>65 mg/kg, i.p.) peripherally to induce experimental diabetes mellitus in rats [17]. However, intracerebroventricular (i.c.v.) administration of STZ at very low doses (1–3 mg/kg) in rodents does not alter peripheral glucose levels and is considered as a reliable experimental model for late-onset sporadic Alzheimer's disease [18–21]. The proposed mechanisms for STZ-induced AD are multifactorial and include: i) impaired glucose metabolism, particularly in brain structures with high glucose demands and high insulin sensitivity [22]; ii) decreased intracellular insulin/IGF1 signaling [23, 24]; and iii) increased oxidative stress [20]. These alterations have been associated with the impaired learning and memory performance that have been reported in this AD model [25, 26].

The aim of this work was to evaluate the effects of physical exercise on memory performance of i.c.v., STZ-treated mice and to determine whether insulin modulates mitochondrial H_2O_2 generation. To test these hypotheses, we used spatial and recognition memory tasks and biochemical analyzes in brain tissue preparations. Our results indicate that i.c.v., administration of STZ causes cognitive impairment, which is exacerbated by physical exercise.

MATERIAL AND METHODS

Animals, surgical procedures, and exercise protocol

Two-months-old CF1 male mice were housed in standard cages (48 × 26 cm) with four animals per cage. To avoid social isolation, the animals were not confined to individual housing [27]. The animals were kept in a controlled room temperature (22°C), under a 12 h light/12 h dark cycle and had free access to food and water. Prior the voluntary exercise, the animals were anesthetized by intraperitoneal (i.p.) injection of ketamine (100 mg/kg body weight) and xylazine (10 mg/kg body weight) and underwent i.c.v., surgery procedures as previously described [14]. The STZ (1 mg/kg or 3 mg/kg) or saline was i.c.v., injected (2 μl/hemisphere) bilaterally into the lateral ventricle ($n = 20$ animals per group). Three days after surgery mice were divided into either the sedentary or exercise groups. In the exercise group, the animals had free access to a running wheel during 4 weeks. After 4 weeks, each mouse ran an average of approximately 3500 m. The animals still had free access to the running wheel during the behavioral experiments. All of the experiments were performed in accordance with the guidelines of the Committee on Care and Use of Experimental Animal Resources, UFRGS, Brazil.

Locomotor, recognition, and spatial memory tasks

The open field test is commonly used to evaluate spontaneous locomotor activity. The experiments were conducted in a sound-attenuated room under low-intensity light. The mice ($n = 10$ per group) were randomly placed into individual square wooden boxes (50 × 50 × 50 cm) that were positioned on the floor of a soundproof and diffusely illuminated room for

10 min. The locomotor activity, exploratory activity and anxiety-like behavior were recorded with a video camera for 10 min. The analysis of behavioral protocols was performed using a computer-operated tracking system (Any-maze, Stoelting, Woods Dale, IL).

The recognition memory was analyzed as previously described [28]. On the first day (day 1), the mice ($n = 10$–12 per group) were randomly placed into individual square wooden boxes ($50 \times 50 \times 50$ cm) that were positioned on the floor of a soundproof and diffusely illuminated room for 10 min. On day 2, the mice were familiarized with two identical plastic objects that were placed 8.5 cm from the walls of the cage. Each testing session lasted 3 min. Following the novel-place test trial, the mice were returned to their home cages for 24 h and were then placed in the arena for the novel object recognition test. In this test, one of the objects was replaced with a novel object that differed in shape, color, and texture. All of the objects and the arena were thoroughly cleaned with 10% ethanol between trials to remove any residual odors. The number of times that the animal explored each object during the familiarization training and the testing trials was recorded. Each exploration was defined as an act in which the mouse would approach the object with the nose (within 1 cm), sniff, and touch the object with the tip of its nose and/or with its paws. It was not considered to be explorative activity when the mouse either stood next to the object or on top of it.

To analyze the spatial memory, we performed the water maze task. We used an apparatus that was a black, circular pool (110 cm in diameter) with a water temperature of $21 \pm 1^{\circ}$C. The mice ($n = 12$–16 per group) were trained daily in a 4-trial water maze task for 4 consecutive days, with each trial lasting up to 60 s, followed by 20 s of rest on a hidden black platform. During the training, the mice learned to escape from the water by finding a hidden, rigid, black platform, which was submerged approximately 1 cm below the water surface in a fixed location. If the animal failed to find the platform within 60 s, it was manually placed on top of the platform and allowed to rest for 20 s. Each trial was separated by at least 12 min to avoid hypothermia (the variations of rectal temperature were equal in all of the groups) and facilitate memory acquisition. The maze was located in a well-lit white room with several visual stimuli hanging on the walls to provide spatial cues. The latency to find the platform during each trial was measured as an indicator of learning. A probe test without the platform was performed on the fourth day and the time spent in the target quadrant was measured as an indicator of memory retention.

Preparation of synaptosomes

The mice ($n = 5$–8 animals per group) were sacrificed by decapitation and the synaptosomes were isolated [29]. Briefly, the brains were rapidly removed and placed into ice-cold "isolation buffer" containing 0.32 M sucrose, 1 mM EDTA, and 10 mM Tris-HC1 (pH 7.4). The cerebellum and underlying structures were removed and the remaining tissue was used for the forebrain sample. The forebrain was also homogenized in isolation buffer.

The homogenate was centrifuged at 4,000 rpm (1,330 *g*) for 3 min. The supernatant was carefully decanted and the pellet was resuspended in isolation buffer. This homogenate was then re-centrifuged as described above, the supernatant retained, and the pellet discarded. Next, the pooled supernatant was centrifuged at 16,000 rpm (21,200 *g*) for 10 min. The decanted supernatant was discarded and the pellet was resuspended in 3 ml of 15% Percoll and a discontinuous density gradient was prepared (3.5 ml of 23% Percoll above 3.5 ml of 40% Percoll). The tubes were centrifuged for 5 min at 19,000 rpm (30,700 *g*). Fraction 2 was enriched in synaptosomes and fraction 3 was enriched in mitochondria. This protocol was described in more detail previously [29, 30].

Mitochondrial H_2O_2 production

Mitochondrial H_2O_2 production was assessed by the Amplex Red oxidation method. Synaptosomes (0.1 mg protein/mL) were incubated in the standard respiration buffer supplemented with 10 mM Amplex Red and 2 units/mL horseradish peroxidase. Succinate (10 mM) and ADP (2 mM) was used to analyze the mitochondrial response in our preparation. Vehicle or insulin (50 and 100 ng/ml) was incubated in each well. The doses of insulin and time of incubation to achieve a decrease in synaptosomes H_2O_2 production were previously standardized by our group (Muller et al. unpublished data). Similar doses of insulin were used by Chenal et al. in cell culture to improve the neuroenergetic status and to activate downstream intracellular signaling pathways involved in neuroprotective effects [31]. The fluorescence was monitored at the excitation and emission wavelengths of 563 nm (slit 5 nm) and 587 nm (slit5 nm), respectively, with the Spectra Max M5 multi-mode microplate reader (Molecular Devices). Each experiment was repeated at least five

times with different synaptosomal preparation. The maximal rate (100%) of mitochondrial H_2O_2 formation was assumed to be the difference between the rate of H_2O_2 formation in the absence of the oxidative substrate and that rate measured after the addition of succinate for up to 30 min.

S100B ELISA assay

After decapitation ($n = 8$ animals per group), the hippocampus was dissected and homogenized in PIK buffer (1% NP-40, 150 mM NaCl, 20 mM Tris, pH 7.4, 10% glycerol, 1 mM $CaCl_2$, 1 mM $MgCl_2$, 400 μM sodium vanadate, 0.2 mM PMSF, 1 μg/ml leupeptin, 1 μg/ml aprotinin, and 0.1% phosphatase inhibitor cocktails I and II. Sigma-Aldrich, USA). The homogenate was centrifuged and the supernatant was collected. The total protein content was measured using a method previously described by Peterson [32]. The homogenates were stored at −70°C until further analysis. S100B protocol was conducted according the instructions of the manufacturer (Diasorin, Italy).

Antioxidant enzyme activity

The antioxidant enzymes were evaluated in forebrain homogenates. The catalase (CAT) activity was measured as previously described [33]. The rate of

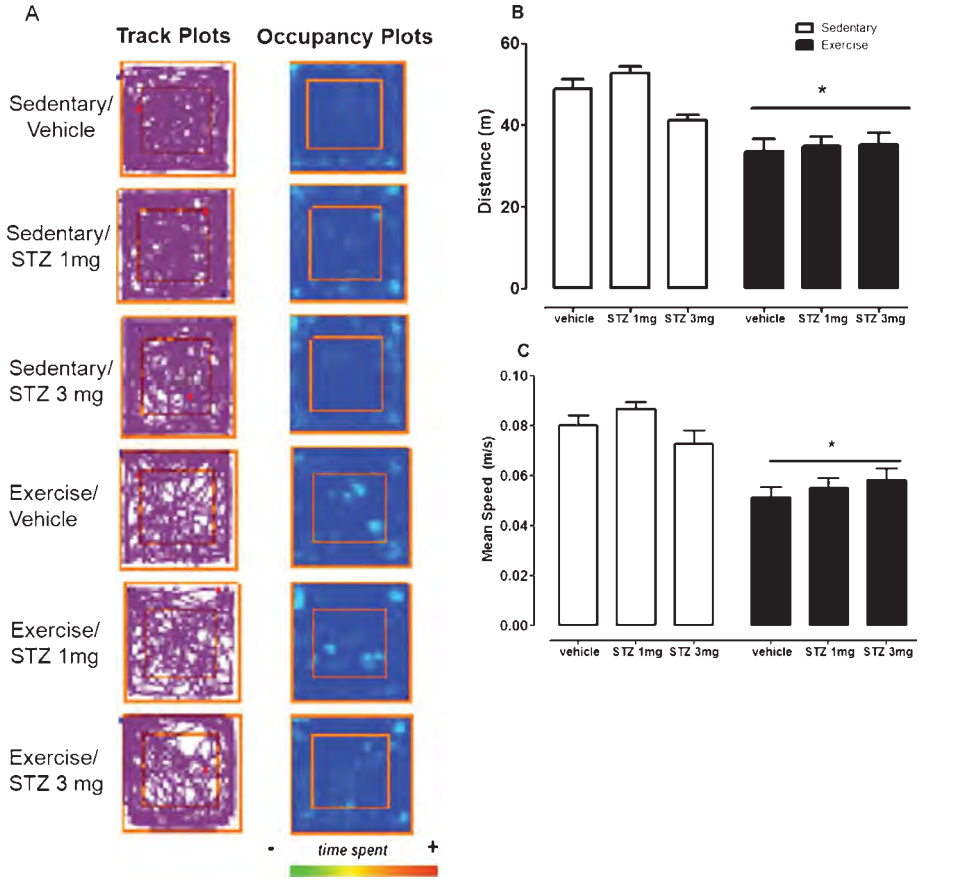

Fig. 1. Locomotor activity was evaluated in an open field task ($n = 10$ animals per group). A) Representative track and occupancy plots of the experimental groups obtained by video-tracking software (ANY-maze®, Stoelting CO, USA), displaying the specific patterns of their exploratory behavior during 10 min. B, C) Exercise decreased the distance and speed in all groups when compared with sedentary groups (*exercise < sedentary; $p < 0.05$). The administration of i.c.v., STZ had no effect on the locomotor activity.

the decrease in absorbance at 240 nm was measured as a function of the H_2O_2 degradation produced by the catalase. The superoxide dismutase (SOD) activity was assessed by quantifying the inhibition of the superoxide-dependent adrenaline auto-oxidation by recording the absorbance of the samples at 480 nm [34] ($n = 4$–6 animals per group for CAT and SOD).

Statistical analyses

The data were expressed as the means ± S.E.M., except for the object recognition task, which was expressed as the median ± interquartile ranges. The data from the water maze task was analyzed using a repeated-measures analysis of variance (ANOVA) followed by Tukey's *post-hoc* test. The Kruskal-Wallis One Way Analysis of Variance was used for object recognition, once the distribution was asymmetrical according to the Shapiro-Wilk analysis. To analyze the differences between the groups, we used a one-way ANOVA followed by Tukey's *post-hoc* test. The differences between the groups were analyzed by *t*-Test. The differences were considered statistically significant at a *p*-value <0.05.

RESULTS

Locomotor activity

Exercise animals of all groups demonstrated decreased locomotor activity and had lower mean speed than sedentary animals. Those parameters were not affected by STZ i.c.v., treatment in all groups (Fig. 1, exercise groups < sedentary groups; $p < 0.05$).

Recognition memory

There was no significant difference between the sedentary vehicle and exercise vehicle groups in the object recognition task. However, STZ 1 mg/kg before the physical exercise caused impairment in recognition memory when compared to exercise vehicle animals. Also, STZ 3 mg/kg administration impaired the recognition memory in both groups, exercise and sedentary (Fig. 2; $p < 0.05$).

Spatial memory performance

In the water maze task, the exercise vehicle animals showed improvement of memory performance in both the acquisition and retrieval phases, as revealed by the decrease latency to found the hidden platform and

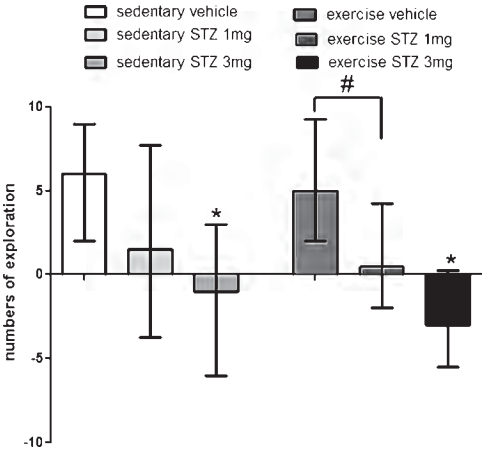

Fig. 2. The i.c.v., STZ administration and recognition memory deficits ($n = 10$–12 animals per group; median with interquartile ranges). Exercise and sedentary vehicle animals showed similar performance in the object recognition task. However, 1 mg/kg of STZ impaired recognition performance only in the exercise mice ($^{\#}$exercise vehicle > exercise STZ 1 mg/kg; $p < 0.05$). At a dose of STZ 3 mg/kg, both groups showed impairment in recognition memory (*sedentary vehicle and exercise vehicle > sedentary STZ 3 mg/kg and exercise STZ 3 mg/kg; $p < 0.05$).

increase in time spent in the target quadrant. Administration of STZ (1 mg/kg) before four weeks of exercise impaired spatial memory performance. However the sedentary animals were not affected. The administration of STZ 3 mg/kg impaired the recognition memory in both groups, exercise and sedentary (Fig. 3A, B; $p < 0.05$). The mean swim speed was not significantly different among the groups (Fig. 3C).

Mitochondrial H_2O_2 production

The forebrain synaptosomal fractions were tested to evaluate the mitochondrial production of H_2O_2 as proposed by Sims [35]. The addition of succinate builds up the proton gradient and increases mitochondrial H_2O_2 production in synaptosomes. ADP was used as substrate to generate ATP in the complex F_oF_1ATP synthase thus consuming the proton gradient and decreasing H_2O_2 production (Fig. 4A). These parameters allow us to predict that the synaptosomal preparation was responsive to manipulation and can be used to test insulin and exercise effects on H_2O_2 production. Insulin receptor signaling was reported to modulate many aspects of the mitochondrial physiology including biogenesis, metabolism and ROS generation [36]. Here we incubated

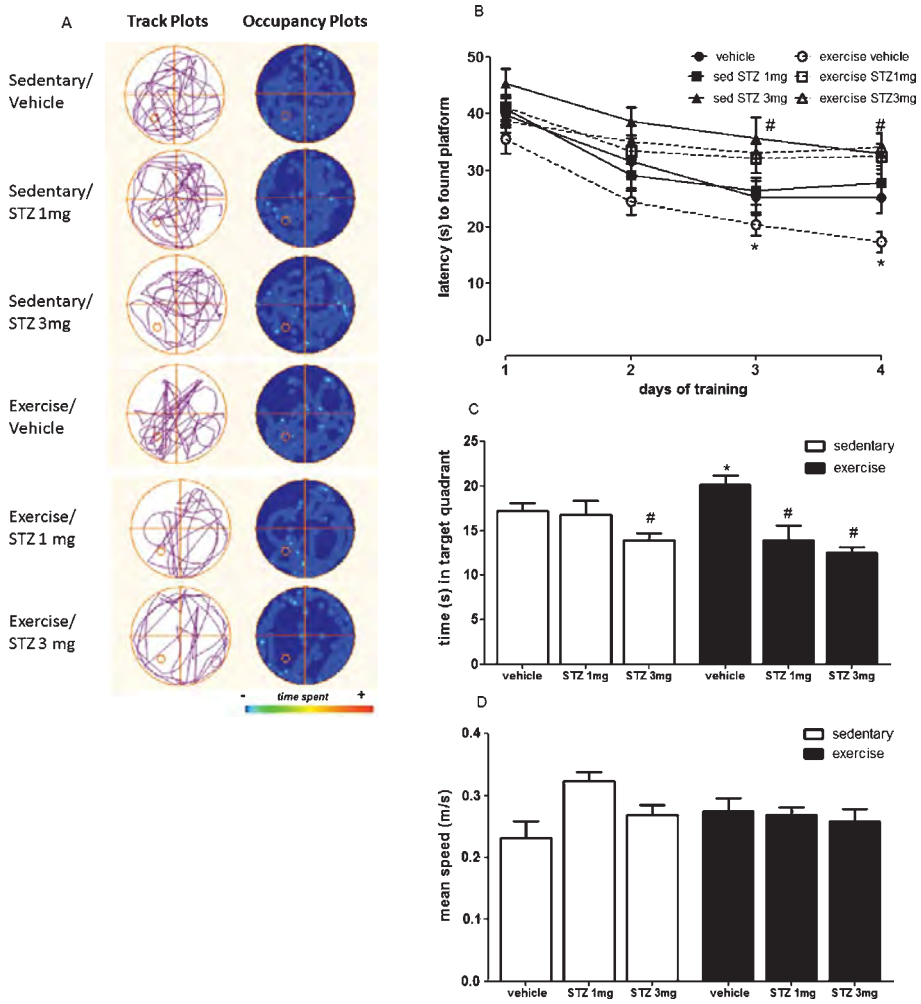

Fig. 3. The i.c.v., STZ administration and spatial memory deficits on Morris water maze task. A) Representative track and occupancy plots obtained by video-tracking software (ANY-mazeH, Stoelting CO, USA), displaying the retention phase during 60 seconds. B) The exercise mice showed improvement in spatial memory performance during the acquisition phase of the water maze task (*latency to the hidden platform exercise vehicle < other groups; $p < 0.05$). The administration of STZ (1 mg/kg) impaired the exercise effects on memory (a; latency to found the hidden platform = exercise 1 mg/kg > exercise vehicle; $p < 0.05$). The administration of STZ (3 mg/kg) impaired the performance in both groups when compared with their respective vehicles (b, c; latency to found the hidden platform = sedentary vehicle and exercise vehicle < sedentary STZ 3 mg/kg and exercise STZ 3 mg/kg; $p < 0.05$). C) In the retrieval phase, exercise improved spatial memory (*exercise vehicle > other groups; $p < 0.05$). The i.c.v., administration of STZ at 1 mg/kg decreased the time spent in the target quadrant in the exercise group when compared with the exercise vehicle ($^{\#}$exercise vehicle > exercise STZ 1 mg/kg and; $p < 0.05$). Administration of 3 mg/kg STZ decreased the time spent in the target quadrant in both of the groups ($^{\#}$sedentary STZ 3 mg/kg and exercise STZ 3 mg/kg < other groups). D) STZ-treatment did not affect the mean speed ($n = 12$–16 animals per group).

synaptosomal preparations with insulin at doses of 50 and 100 ng/ml that has been shown to induce neuroprotective responses in neural cell cultures [31]. Insulin decreased the H_2O_2 production induced by succinate in sedentary and exercise vehicle groups (Fig. 4B, C). Exercise increased the H_2O_2 production induced by succinate in the synaptosomes (Fig. 4C, **exercise vehicle > sedentary vehicle (dotted line); $p < 0.05$). The

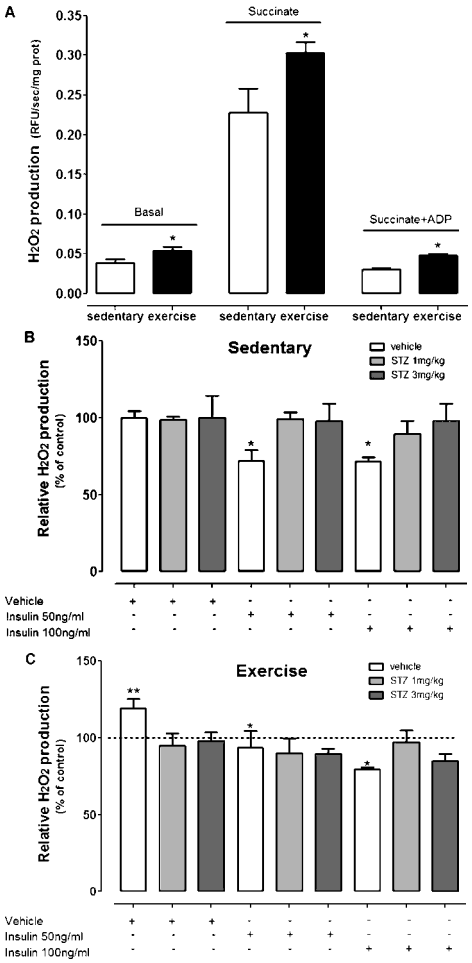

Fig. 4. Exercise increased the H_2O_2 production and insulin decreased the H_2O_2 production in synaptosome preparations. A) Synaptosomes were responsive to succinate and ADP treatment. Exercise increased the H_2O_2 production when compared with sedentary animals (*exercise vehicle > sedentary vehicle; $p < 0.05$. B) Insulin 50 and 100 ng/ml decreased the H_2O_2 production in synaptosme of the sedentary animals (*sedentary vehicle > sedentary insulin 50 and 100 ng/ml, $p < 0.05$). The STZ i.c.v. administration abolished the effect of insulin. C) Exercise animals showed increased H_2O_2 production induced by succinate in synaptosomes when compared with sedentary mice (**exercise > sedentary (dotted line), $p < 0.05$). Insulin at a doses of 50 and 100 ng/ml decreased H_2O_2 production induced by succinate in synaptosomes of exercise mice (*exercise vehicle > exercise 50 ng/ml > exercise 100 ng/ml; $p < 0.05$). The STZ i.c.v. administration prior to four weeks of physical activity abolished the increase of mitochondrial H_2O_2 production induced by exercise and the decreased H_2O_2 production induced by insulin (*exercise vehicle > exercise STZ 1 and 3 mg/kg, $p < 0.05$) ($n = 5$–8 animals per group).

ability of insulin to decrease H_2O_2 production was enhanced in the exercise group compared with the sedentary animals (38% versus 26%) (Fig. 4B, C). The STZ i.c.v., treatment at doses of 1 and 3 mg/kg abolished the effect of insulin on H_2O_2 production (Fig. 4B, C). Moreover, the STZ i.c.v., (1 and 3 mg/kg) administration before the physical activity abolished the effect of exercise in H_2O_2 production (Fig. 4C; *exercise vehicle > exercise 1 and 3 mg/kg; $p < 0.05$).

Glial reactivity and oxidative stress

We analyzed the content of hippocampal S100B as an indicator of glial response to the damage caused by STZ i.c.v., as previously demonstrated [37]. Exercise did not increase hippocampal S100B when compared with the sedentary group. However after thirty days of 3 mg/kg STZ i.c.v., there was an increase S100B content in the sedentary and exercise groups compared to their respective controls and 1 mg/kg group (Fig. 5A; $p < 0.05$). Furthermore, the evaluation of antioxidant enzymes showed that sedentary 3 mg/kg STZ mice exhibited a decrease hippocampal CAT (Fig. 5B; $p < 0.05$) and SOD (Fig. 5C; $p < 0.05$) activities; and an increase SOD/CAT ratio (Fig. 5D; $p < 0.05$) when compared with sedentary vehicle mice.

DISCUSSION

In this study, we demonstrated that voluntary physical exercise increased the sensitivity of the insulin-resistant brain state induced by one previous STZ i.c.v., administration. Accordingly, the administration of 3 mg/kg STZ caused impairment in the recognition and spatial memory of both sedentary and exercise animals, while the administration of 1 mg/kg STZ prior the physical activity caused memory deficits only in the exercise animals. Conversely, the ability of insulin to decrease mitochondrial H_2O_2 production induced by succinate in synaptosomal preparations was more prominent in the exercised animals. Furthermore, both STZ doses abolished the ability of insulin to decrease mitochondrial H_2O_2 production in sedentary and exercise mice, suggesting that this regulatory effect require normal brain insulin receptor signaling.

Brain insulin receptors are mainly localized in regions associated with learning and memory processes such as the cortex and hippocampus. Deficits in brain insulin signaling have been consistently linked with cognitive deficits in experimental animal disease models and in AD patients [38]. The data of memory deficits reported here corroborate this finding. On the

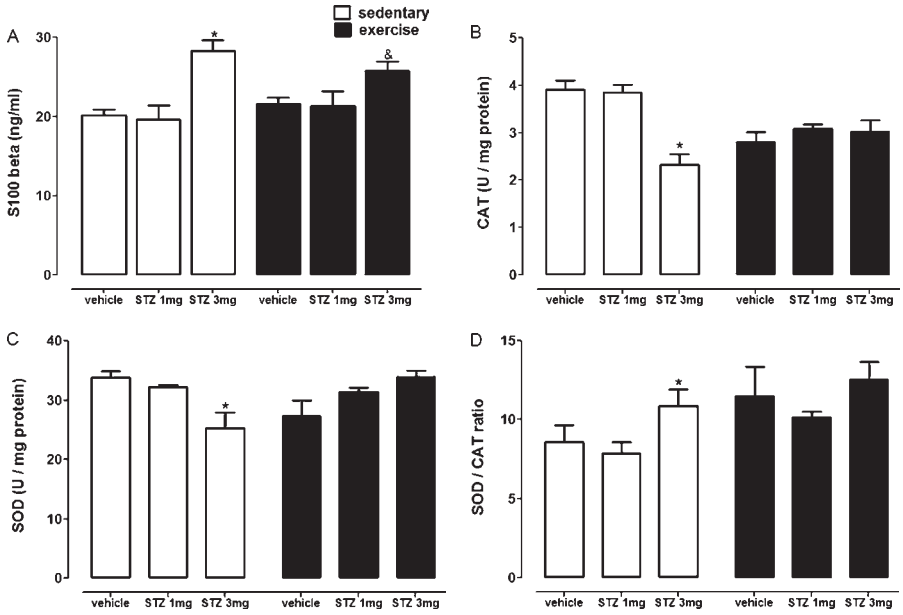

Fig. 5. A) Glial reactivity (S100B expression), and antioxidant enzymes, catalase (CAT) and superoxide dismutase (SOD), activities. The i.c.v., administration of STZ (3 mg/kg) increased the hippocampal S100B levels in both sedentary and exercise mice (*sedentary 3 mg/kg and &exercise 3 mg/kg > other groups, $p < 0.05$) ($n = 8$ animals per group). B) The i.c.v., administration of STZ (3 mg/kg) decreased CAT activity in sedentary animals (*sedentary 3 mg/kg < sedentary vehicle, $p < 0.05$). C) The i.c.v., administration of STZ (3 mg/kg) decreased the SOD activity in sedentary animals (*sedentary 3 mg/kg < sedentary vehicle, $p < 0.05$). D) The i.c.v., administration of STZ (3 mg/kg) increased the SOD/CAT ratio in sedentary animals (*sedentary 3 mg/kg < sedentary vehicle, $p < 0.05$) ($n = 4$–6 animals per group).

other hand, insulin administration at optimal doses has been shown to improve cognitive performance in both rodents and humans [39]. It is well established that voluntary exercise improves the hippocampal plasticity and spatial memory performance of rodents [14]. We previously showed that voluntary exercise increases insulin signaling in the hippocampus, a region known to be closely associated with spatial memory [14]. The i.c.v., administration of STZ causes a broad range of neural changes including impaired metabolism, decreases in insulin signaling, and increases in oxidative stress damage [25], which are associated with the undesired consequences for learning and memory processes [20, 25]. Interestingly, the cognitive deficits are long-term and progressive and can be observed as early as 2 weeks after i.c.v.,-STZ administration. Moreover, these changes are maintained for up to 12 weeks post treatment [3, 18, 40]. As expected, after four weeks of STZ i.c.v., administration, the animals still exhibited memory deficits, which were not reduced by an exercise intervention. Surprisingly, we showed that even low doses of the i.c.v., STZ (1 mg/kg) injected before the physical activity affected the memory performance of exercise animals in both tasks (recognition and spatial). The difference between our results and those obtained by others with regard the neuroprotective effects of exercise [41, 42] could be explained by the influence of different exercise regimens (voluntary or forced) on brain responses [43]. Further, it is attempt to propose that damaged caused by STZ i.c.v., abolished the effect of physical exercise on cognition which is associate with increased in insulin sensitivity in brain [14]. Although this postulation is merely speculative, our results support the idea that an intact hippocampal insulin signaling is important to attain the benefits of exercise on recognition and spatial memory processes [14].

To investigate potential mechanisms involved in cognitive impairment associated with STZ administration, we evaluated mitochondrial H_2O_2 generation. H_2O_2 is a major ROS produced by mitochondria that is important for oxidative damage [44] implicated in the aging processes [45] and AD pathogenesis [10]. Here we showed that exercise increases mitochondrial

H_2O_2 production induced by succinate in synaptosomes. This may represent one aspect of mitochondrial activation induced by exercise [46]. We also found that insulin did not reduce H_2O_2 production in synaptosomes of i.c.v., STZ mice but did in i.c.v., vehicle mice. The results presented reinforce the belief that physiological insulin signaling may have neuroprotective relevance for the modulation of brain mitochondrial H_2O_2 production. Indeed, perturbing insulin signaling by the administration of 3 mg/kg i.c.v., STZ, increased expression of S100B protein in the hippocampus of all groups, which may reflect the glial activation responses to the neurotoxic effects of STZ [37]. Furthermore, the decreased SOD and CAT activity [25, 41], associated with increased SOD/CAT ratio suggests a cellular environment favorable to oxidative stress damage. Interestingly, Chen et al. [47] previously demonstrated that transgenic mice overexpressing mitochondrial peroxiredoxin 3 (peroxidase activity) exhibited a decreased brain mitochondrial H_2O_2 generation as well as significant decrease in cognitive deficits induced by the paraquat [48]. Altogether, the results emphasize the significant role of mitochondrial H_2O_2 generation and metabolism in the impaired cognitive function and the important role of insulin and exercise on the modulation of mitochondrial function.

In summary, normal brain insulin signaling is mechanistically involved in the improvement of cognitive function induced by exercise. This may be associated with the regulation of mitochondrial H_2O_2 production. However, blockade of brain insulin signaling by STZ before the initial of physical activity abolished the benefits of exercise on memory performance and mitochondrial H_2O_2 regulation.

ACKNOWLEDGMENTS

This work was supported by the following Brazilian agencies and grants: CNPq, CAPES, FAPERGS-PPSUS, Brazilian Grants IBNet-FINEP, INCT-Excitotoxicity and neuroprotection.

Authors' disclosures available online (http://www.j-alz.com/disclosures/view.php?id=1220).

REFERENCES

[1] Hoyer S (2004) Causes and consequences of disturbances of cerebral glucose metabolism in sporadic Alzheimer disease: Therapeutic implications. *Adv Exp Med Biol* **541**, 135-152.

[2] de la Monte SM, Wands JR (2005) Review of insulin and insulin-like growth factor expression, signaling, and malfunction in the central nervous system: Relevance to Alzheimer's disease. *J Alzheimers Dis* **7**, 45-61.

[3] Salkovic-Petrisic M, Hoyer S (2007) Central insulin resistance as a trigger for sporadic Alzheimer-like pathology: An experimental approach. *J Neural Transm Suppl* 217-233.

[4] Fulop T, Larbi A, Douziech N (2003) Insulin receptor and ageing. *Pathol Biol (Paris)* **51**, 574-580.

[5] Muller AP, Cammarota M, Dietrich MO, Rotta LN, Portela LV, Souza DO, Izquierdo I, Bevilaqua LR, Perry ML (2008) Different effect of high fat diet and physical exercise in the hippocampal signaling. *Neurochem Res* **33**, 880-885.

[6] Dietrich MO, Muller A, Bolos M, Carro E, Perry ML, Portela LV, Souza DO, Torres-Aleman I (2007) Western style diet impairs entrance of blood-borne insulin-like growth factor-1 into the brain. *Neuromolecular Med* **9**, 324-330.

[7] Lin MT, Beal MF (2006) Alzheimer's APP mangles mitochondria. *Nat Med* **12**, 1241-1243.

[8] Davey GP, Peuchen S, Clark JB (1998) Energy thresholds in brain mitochondria. Potential involvement in neurodegeneration. *J Biol Chem* **273**, 12753-12757.

[9] Bowling AC, Mutisya EM, Walker LC, Price DL, Cork LC, Beal MF (1993) Age-dependent impairment of mitochondrial function in primate brain. *J Neurochem* **60**, 1964-1967.

[10] Manczak M, Anekonda TS, Henson E, Park BS, Quinn J, Reddy PH (2006) Mitochondria are a direct site of A beta accumulation in Alzheimer's disease neurons: Implications for free radical generation and oxidative damage in disease progression. *Hum Mol Genet* **15**, 1437-1449.

[11] Readnower RD, Sauerbeck AD, Sullivan PG (2011) Mitochondria, Amyloid beta, and Alzheimer's disease. *Int J Alzheimers Dis* **2011**, 104545.

[12] Murphy MP, Holmgren A, Larsson NG, Halliwell B, Chang CJ, Kalyanaraman B, Rhee SG, Thornalley PJ, Partridge L, Gems D, Nystrom T, Belousov V, Schumacker PT, Winterbourn CC (2011) Unraveling the biological roles of reactive oxygen species. *Cell Metab* **13**, 361-366.

[13] Du Y, Wooten MC, Wooten MW (2009) Oxidative damage to the promoter region of SQSTM1/p62 is common to neurodegenerative disease. *Neurobiol Dis* **35**, 302-310.

[14] Muller AP, Gnoatto J, Moreira JD, Zimmer ER, Haas CB, Lulhier F, Perry ML, Souza DO, Torres-Aleman I, Portela LV (2011) Exercise increases insulin signaling in the hippocampus: Physiological effects and pharmacological impact of intracerebroventricular insulin administration in mice. *Hippocampus* **21**, 1082-1092.

[15] Cotman CW, Berchtold NC (2002) Exercise: A behavioral intervention to enhance brain health and plasticity. *Trends Neurosci* **25**, 295-301.

[16] Radak Z, Chung HY, Goto S (2008) Systemic adaptation to oxidative challenge induced by regular exercise. *Free Radic Biol Med* **44**, 153-159.

[17] Szkudelski T (2001) The mechanism of alloxan and streptozotocin action in B cells of the rat pancreas. *Physiol Res* **50**, 537-546.

[18] Lannert H, Hoyer S (1998) Intracerebroventricular administration of streptozotocin causes long-term diminutions in learning and memory abilities and in cerebral energy metabolism in adult rats. *Behav Neurosci* **112**, 1199-1208.

[19] Prickaerts J, Fahrig T, Blokland A (1999) Cognitive performance and biochemical markers in septum, hippocampus and striatum of rats after an i.c.v., injection of streptozotocin: A correlation analysis. *Behav Brain Res* **102**, 73-88.

[20] Sharma M, Gupta YK (2001) Intracerebroventricular injection of streptozotocin in rats produces both oxidative stress in the brain and cognitive impairment. *Life Sci* **68**, 1021-1029.

[21] Plaschke K, Hoyer S (1993) Action of the diabetogenic drug streptozotocin on glycolytic and glycogenolytic metabolism in adult rat brain cortex and hippocampus. *Int J Dev Neurosci* **11**, 477-483.

[22] Henneberg N, Hoyer S (1995) Desensitization of the neuronal insulin receptor: A new approach in the etiopathogenesis of late-onset sporadic dementia of the Alzheimer type (SDAT)? *Arch Gerontol Geriatr* **21**, 63-74.

[23] Mayer G, Nitsch R, Hoyer S (1990) Effects of changes in peripheral and cerebral glucose metabolism on locomotor activity, learning and memory in adult male rats. *Brain Res* **532**, 95-100.

[24] Blokland A, Jolles J (1993) Spatial learning deficit and reduced hippocampal ChAT activity in rats after an ICV injection of streptozotocin. *Pharmacol Biochem Behav* **44**, 491-494.

[25] Agrawal R, Tyagi E, Shukla R, Nath C (2009) A study of brain insulin receptors, AChE activity and oxidative stress in rat model of ICV STZ induced dementia. *Neuropharmacology* **56**, 779-787.

[26] Agrawal R, Tyagi E, Shukla R, Nath C (2011) Insulin receptor signaling in rat hippocampus: A study in STZ (ICV) induced memory deficit model. *Eur Neuropsychopharmacol* **21**, 261-273.

[27] Leasure JL, Decker L (2009) Social isolation prevents exercise-induced proliferation of hippocampal progenitor cells in female rats. *Hippocampus* **19**, 907-912.

[28] Muller AP, Fernandez AM, Haas C, Zimmer E, Portela LV, Torres-Aleman I (2012) Reduced brain insulin-like growth factor I function during aging. *Mol Cell Neurosci* **49**, 9-12.

[29] Sims NR (1990) Rapid isolation of metabolically active mitochondria from rat brain and subregions using Percoll density gradient centrifugation. *J Neurochem* **55**, 698-707.

[30] Sims NR, Anderson MF (2008) Isolation of mitochondria from rat brain using Percoll density gradient centrifugation. *Nat Protoc* **3**, 1228-1239.

[31] Chenal J, Pierre K, Pellerin L (2008) Insulin and IGF-1 enhance the expression of the neuronal monocarboxylate transporter MCT2 by translational activation via stimulation of the phosphoinositide 3-kinase-Akt-mammalian target of rapamycin pathway. *Eur J Neurosci* **27**, 53-65.

[32] Peterson GL (1977) A simplification of the protein assay method of Lowry et al. Which is more generally applicable. *Anal Biochem* **83**, 346-356.

[33] Aebi H (1984) Catalase *in vitro*. *Methods Enzymol* **105**, 121-126.

[34] Misra HP, Fridovich I (1972) The role of superoxide anion in the autoxidation of epinephrine and a simple assay for superoxide dismutase. *J Biol Chem* **247**, 3170-3175.

[35] Sims NR, Blass JP (1986) Expression of classical mitochondrial respiratory responses in homogenates of rat forebrain. *J Neurochem* **47**, 496-505.

[36] Cheng Z, Tseng Y, White MF (2010) Insulin signaling meets mitochondria in metabolism. *Trends Endocrinol Metab* **21**, 589-598.

[37] Rodrigues L, Biasibetti R, Swarowsky A, Leite MC, Quincozes-Santos A, Quilfeldt JA, Achaval M, Goncalves CA (2009) Hippocampal alterations in rats submitted to streptozotocin-induced dementia model are prevented by aminoguanidine. *J Alzheimers Dis* **17**, 193-202.

[38] Craft S (2006) Insulin resistance syndrome and Alzheimer disease: Pathophysiologic mechanisms and therapeutic implications. *Alzheimer Dis Assoc Disord* **20**, 298-301.

[39] Park CR (2001) Cognitive effects of insulin in the central nervous system. *Neurosci Biobehav Rev* **25**, 311-323.

[40] Grunblatt E, Salkovic-Petrisic M, Osmanovic J, Riederer P, Hoyer S (2007) Brain insulin system dysfunction in streptozotocin intracerebroventricularly treated rats generates hyperphosphorylated tau protein. *J Neurochem* **101**, 757-770.

[41] Rodrigues L, Dutra MF, Ilha J, Biasibetti R, Quincozes-Santos A, Leite MC, Marcuzzo S, Achaval M, Goncalves CA (2010) Treadmill training restores spatial cognitive deficits and neurochemical alterations in the hippocampus of rats submitted to an intracerebroventricular administration of streptozotocin. *J Neural Transm* **117**, 1295-1305.

[42] Jee YS, Ko IG, Sung YH, Lee JW, Kim YS, Kim SE, Kim BK, Seo JH, Shin MS, Lee HH, Cho HJ, Kim CJ (2008) Effects of treadmill exercise on memory and c-Fos expression in the hippocampus of the rats with intracerebroventricular injection of streptozotocin. *Neurosci Lett* **443**, 188-192.

[43] Leasure JL, Jones M (2008) Forced and voluntary exercise differentially affect brain and behavior. *Neuroscience* **156**, 456-465.

[44] Stone JR, Yang S (2006) Hydrogen peroxide: A signaling messenger. *Antioxid Redox Signal* **8**, 243-270.

[45] Schriner SE, Linford NJ, Martin GM, Treuting P, Ogburn CE, Emond M, Coskun PE, Ladiges W, Wolf N, Van Remmen H, Wallace DC, Rabinovitch PS (2005) Extension of murine life span by overexpression of catalase targeted to mitochondria. *Science* **308**, 1909-1911.

[46] Dietrich MO, Andrews ZB, Horvath TL (2008) Exercise-induced synaptogenesis in the hippocampus is dependent on UCP2-regulated mitochondrial adaptation. *J Neurosci* **28**, 10766-10771.

[47] Chen L, Yoo SE, Na R, Liu Y, Ran Q (2012) Cognitive impairment and increased Abeta levels induced by paraquat exposure are attenuated by enhanced removal of mitochondrial H_2O_2. *Neurobiol Aging* **33**, 432.e15-26.

[48] Chen L, Na R, Gu M, Salmon AB, Liu Y, Liang H, Qi W, Van Remmen H, Richardson A, Ran Q (2008) Reduction of mitochondrial H_2O_2 by overexpressing peroxiredoxin 3 improves glucose tolerance in mice. *Aging Cell* **7**, 866-878.

ANEXO I-B. *In vivo characterization of metabotropic glutamate receptor type 5 abnormalities in behavioral variant FTD.*

No **ANEXO I-B** apresentamos o artigo publicado no periódico *Brain Structure and Function.*

Brain Struct Funct
DOI 10.1007/s00429-014-0978-3

ORIGINAL ARTICLE

In vivo characterization of metabotropic glutamate receptor type 5 abnormalities in behavioral variant FTD

Antoine Leuzy · Eduardo Rigon Zimmer · Jonathan Dubois · Jens Pruessner · Cory Cooperman · Jean-Paul Soucy · Alexey Kostikov · Esther Schirmaccher · René Désautels · Serge Gauthier · Pedro Rosa-Neto

Received: 14 August 2014 / Accepted: 22 December 2014
© Springer-Verlag Berlin Heidelberg 2015

Abstract Although the pathogenesis underlying behavioral variant frontotemporal dementia (bvFTD) has yet to be fully understood, glutamatergic abnormalities have been hypothesized to play an important role. The aim of the present study was to determine the availability of the metabotropic glutamate receptor type 5 (mGluR5) using a novel positron emission tomography (PET) radiopharmaceutical with high selectivity for mGluR5 ([^{11}C]ABP688) in a sample of bvFTD patients. In addition, we sought to determine the overlap between availability of mGluR5 and neurodegeneration, as measured using [^{18}F]FDG-PET and voxel-based morphometry (VBM). Availability of mGluR5 and glucose metabolism ([^{18}F]FDG) were measured in bvFTD ($n = 5$) and cognitively normal (CN) subjects ($n = 10$). [^{11}C]ABP688 binding potential maps (BP_{ND}) were calculated using the cerebellum as a reference region, with [^{18}F]FDG standardized uptake ratio maps (SUV_R) normalized to the pons. Grey matter (GM) concentrations were determined using VBM. Voxel-based group differences were obtained using RMINC. BvFTD patients showed widespread decrements in [^{11}C]ABP688 BP_{ND} throughout frontal, temporal and subcortical areas. These areas were likewise characterized by significant hypometabolism and GM loss, with overlap between reduced [^{11}C]ABP688 BP_{ND} and hypometabolism superior to that for GM atrophy. Several regions were characterized only by decreased binding of [^{11}C]ABP688. The present findings represent the first in vivo report of decreased availability of mGluR5 in bvFTD. This study suggests that glutamate excitotoxicity may play a role in the pathogenesis of bvFTD and that [^{11}C]ABP688 may prove a suitable marker of glutamatergic neurotransmission in vivo.

A. Leuzy · E. R. Zimmer · P. Rosa-Neto (✉)
Translational Neuroimaging Laboratory, McGill Centre for Studies in Aging, McGill University, 6825 LaSalle Blvd, Montreal, QC H4H 1R3, Canada
e-mail: pedro.rosa@mcgill.ca

A. Leuzy · E. R. Zimmer · S. Gauthier · P. Rosa-Neto
Alzheimer's Disease Research Unit, McGill Centre for Studies in Aging, McGill University, Montreal, Canada

E. R. Zimmer
Department of Biochemistry, Federal University of Rio Grande do Sul, Porto Alegre, Brazil

J. Dubois
Department of Neurology and Neurosurgery, Montreal Neurological Institute, McGill University, Montreal, Canada

J. Pruessner
McGill Centre for Studies in Aging, McGill University, Montreal, Canada

J. Pruessner · C. Cooperman
Department of Psychiatry, Douglas Mental Health University Institute, McGill University, Montreal, Canada

C. Cooperman
Department of Psychology, McGill University, Montreal, Canada

J.-P. Soucy · A. Kostikov · E. Schirmaccher
McConnell Brain Imaging Centre, Montreal Neurological Institute, McGill University, Montreal, Canada

R. Désautels
Division of Geriatric Psychiatry, Douglas Mental Health University Institute, Montreal, Canada

Published online: 18 January 2015

Keywords Behavioral variant frontotemporal dementia · Frontotemporal lobar degeneration · Positron emission tomography · ^{11}C-ABP688 · Metabotropic glutamate receptor type 5 · Excitotoxicity

Introduction

Behavioral variant frontotemporal dementia (bvFTD) is a progressive neurodegenerative syndrome characterized by change in personality, impaired social cognition, and executive dysfunction (Mendez et al. 2008; Swartz et al. 1997). Approaching Alzheimer's disease (AD) as the leading cause of early-onset (before 65 years of age) dementia (Ratnavalli et al. 2002; Rosso et al. 2003), bvFTD arises from a heterogeneous range of pathologies—referred to collectively as frontotemporal lobar degeneration (FTLD)—resulting in degenerative changes within frontal paralimbic, temporal and subcortical brain regions. In most cases, patients show either deposition of the microtubule associated protein tau (tau) or the TAR DNA-binding protein of 43 kDa (TDP) (Mackenzie et al. 2010). A minority, however, show a defect in metabolism of the tumor-associated protein fused in sarcoma (FUS). The majority of FTLDs can therefore be classified into FTLD-tau, FTLD-TDP, or FTLD-FUS, with further subclassification based predominantly on inclusion morphology and lesion distribution (Mackenzie et al. 2010).

Although the pathogenic mechanisms underlying bvFTD have yet to be fully elucidated, aberrant glutamatergic neurotransmission has been hypothesized to play a role. The primary excitatory neurotransmitter in the mammalian brain, glutamate acts via ionotropic and metabotropic receptors (Schaeffer and Duplantier 2010). Whereas ionotropic receptors mediate fast excitatory neurotransmission, metabotropic glutamate receptors (mGluRs) play an important role in synaptic modulation via regulation of neuronal excitability, transmitter release, synaptic plasticity and glial function. In the case of bvFTD, FTLD has been found to accumulate preferentially within paralimbic and homotypical heteromodal brain regions, areas rich in excitatory glutamatergic pyramidal cells. Indeed, several autoradiographic and immunohistochemical studies in post-mortem bvFTD tissue have provided evidence supporting this hypothesis (Dalfo et al. 2005; Ferrer 1999; Procter et al. 1999), highlighting reduced expression of the *N*-methyl-D-aspartate (NMDA) ionotropic glutamate receptor. Importantly, activation of mGluR5 was shown to regulate glutamatergic neurotransmission via modulation of NMDA receptor functionality (Llansola and Felipo 2010; Niswender and Conn 2010; Perroy et al. 2008). Moreover, mGluR5 signaling has been shown to be critically involved in the normal cognitive functioning of various neuronal populations (Schaeffer and Duplantier 2010), including those within FTLD predilection sites (Ferraguti and Shigemoto 2006).

Despite a strong in vitro evidence base, glutamatergic abnormalities in bvFTD have yet to be systematically characterized in vivo owing to the lack of suitable molecular probes. Using [^{11}C]ABP688—a novel positron emission tomography (PET) radiopharmaceutical with high selectivity for mGluR5 (Ametamey et al. 2006, 2007)—we sought to measure mGluR5 availability and to determine the topographic overlap with neurodegeneration within frontotemporal and subcortical brain regions, as indexed using [^{18}F]fluorodeoxyglucose ([^{18}F]FDG)-PET and voxel-based morphometry (VBM).

Methods

Subjects

Five patients meeting research criteria for probable bvFTD (Rascovsky et al. 2011) were recruited from the McGill Centre for Studies in Aging (MCSA) Alzheimer's Disease Research Unit. Exclusion criteria were (1) past or present use of memantine; (2) presence of other neurological diseases; (3) premorbid psychiatric disease or intellectual disability; (4) history of head injuries and loss of consciousness following head trauma; (5) current (within 1 month) use of psychoactive substances; (6) parkinsonism—as identified using the United Parkinson's Disease Rating Scale (Goetz et al. 2007)—and (7) the presence of any major structural anomaly or signs of major vascular pathology on magnetic resonance imaging (MRI) evaluation (Roman et al. 1993). All patients underwent neuropsychological assessment and behavioral testing. Global cognition was assessed using the Mini-Mental State Examination (MMSE) (Folstein et al. 1975), with language and visuospatial function measured using the Wechsler Abbreviated Scale of Intelligence, second edition (McCrimmon and Smith 2013). The Cogstate Research test battery was used to assess executive function, episodic memory, and social cognition (http://cogstate.com/tag/cogstate-brief-battery/). The choice of measures included in the overall assessment battery took into consideration test availability in both English and French. Behavioral measures included the Neuropsychiatric Inventory (NPI) (Cummings et al. 1994), and the Frontal Behavioral Inventory (FBI) (Kertesz et al. 1997). In addition, given that bvFTD and the frontal variant of AD are often difficult to differentiate on clinical grounds alone (Alladi et al. 2007), all patients underwent carbon-11 Pittsburgh Compound B ([^{11}C]PiB) PET to rule out the presence of

amyloid pathology. The diagnosis of bvFTD was determined during a multidisciplinary conference taking into consideration available medical, clinical, imaging, neuropsychological, and complementary laboratory information.

The bvFTD patients were matched by age and gender to a group of 10 cognitively normal (CN) controls, recruited via advertisements in a local newspaper. CN subjects were identified as individuals who (1) were independently functioning community dwellers; (2) did not have a personal or first degree relative history of psychiatric disorders; (3) had no cognitive complaints; (4) had a normal neurological and psychometric examination; (5) were not taking any psychoactive medications; (6) had no history of head trauma; (7) showed no signs of vascular pathology on MRI evaluation (Roman et al. 1993) and (8) had an MMSE score $\geq$29, an NPI score of 0, and an FBI score of 0.

Demographic and clinical data for all subjects are shown in Table 1, with ratings of lobar atrophy (Kipps et al. 2007) and hypometabolism (Poljansky et al. 2011) for bvFTD patients shown in Table 2. All subjects and their caregivers provided written informed consent. The study protocol, approved by the Research Ethics Board of the Montreal Neurological Institute as well as by the Faculty of Medicine Research Ethics Office, McGill University, was carried out in accordance with the Declaration of Helsinki.

Table 1 Demographic and clinical data for all subjects

	BvFTD ($n = 5$)	CN ($n = 10$)	p[a] value
Age at scan, Med (IQR), years	65 (7)	63 (2.75)	0.65
Education, Med (IQR), years	10 (5)	16 (4)	0.06
Sex, M/F	3/2	7/3	1.00
Handedness, R/L	5/0	9/1	0.52
MMSE, Med (IQR), max = 30	26 (1)	30 (1)	0.03
FBI, Med (IQR), max = 72	20 (0)	0 (0)	0.001
NPI Total, Med (IQR), max = 144	32 (8)	0 (0)	0.001

Due to the small group sizes, data are represented as Med (IQR) = median (interquartile range)

M/F male/female, *R/L* right/left, *MMSE* Mini-Mental State Examination, *FBI* Frontal Behavioral Inventory, *NPI* Neuropsychiatric Inventory

[a] The *t* test for continuous variables, Fischer's exact test for categorical variables

PET acquisition

3-(6-Methyl-pyridin-2-ylethynyl)-cyclohex-2-enone-*O*-^{11}C-methyl-oxime ([^{11}C]ABP688) was synthesized as described previously (Elmenhorst et al. 2010), with a radiochemical purity >99 %. The study was performed using a high-resolution research tomograph (HRRT) PET scanner (CTI/Siemens, Knoxville, Tennessee), a brain-dedicated tomograph combining high spatial image resolution with high sensitivity. Prior to radiopharmaceutical administration, a 6-min transmission scan was acquired for scatter and attenuation correction using a [^{137}Cs] rotating point source. A 60-min dynamic list-mode emission scan was started concomitantly with the venous injection of 370 MBq (mean specific activity >500 Ci/μmol) of [^{11}C]ABP688, with emission data acquired in list-mode format, and binned into 26 time frames. For each and every time frame, sets of fully 3D sinograms were generated from the list-mode data (2,209 sinograms, span 9, with 256 radial bins and 288 azimuthal angle samples). A time-series of 26 3D images (frame duration: 6 × 30 s, 4 × 60 s, 8 × 120 s, 3 × 240 s, 5 × 300 s) were then reconstructed from these sinograms, each 3D image being composed of 256 × 256 × 207 cubic voxels (voxel side-length of 1.21875 mm), using an expectation maximization image reconstruction algorithm with an ordinary Poisson model of the acquired PET data. The reconstruction included full accounting for the normalization, attenuation, and time-dependent scatter of random events. To reduce the partial volume effect, resolution modeling with point-spread function was implemented in the reconstruction (Comtat et al. 2008). Subject head-motion correction was

Table 2 Ratings of hypometabolism and lobar atrophy in patients with bvFTD

[^{18}F]FDG-PET								MRI	
Subject	Frontal lobe	Temporal lobe	Parietal lobe	Occipital lobe	Cerebellum	Basal ganglia	Thalamus	Frontal lobe	Anterior temporal lobe
1	2	2	1	0	0	0	1	3	2
2	2	2	1	0	0	0	0	1	1
3	2	2	1	0	0	0	0	3	3
4	2	2	1	0	0	0	0	1	2
5	2	2	1	0	0	0	1	1	2

Ratings for [^{18}F]FDG-PET: *0* absent, *1* mild, *2* moderate, *3* strong

Ratings for MRI: *1* very mild, *2* mild, *3* moderate

implemented using a data-driven motion estimation and correction method (Costes et al. 2009).

All patients underwent an [^{18}F]FDG-PET scan using a Siemens ECAT EXACT HR+ PET device (CTI/Siemens, Knoxville, TN, USA) as part of their clinical evaluation. In keeping with the ALARA radiation safety principle (Natarajan et al. 2013), data were not recollected on the HRRT. After fasting overnight, patients received a venous bolus injection of 185 MBq of ^{18}F-fluorodeoxyglucose ([^{18}F]FDG) in a quiet environment. A dynamic scan was performed in 3-dimensional mode for 10 min under standard resting-state conditions with eyes open, recording 63 transaxial slices simultaneously with an axial resolution of 5 mm full width at half maximum (FWHM) and an in-plane resolution of 4.6 mm. Each collected slice had a thickness of 2.45 mm and a matrix size of 128 × 128 voxels. After correction for attenuation, scatter, decay and scanner-specific dead time, the PET data were reconstructed by filtered back-projection using a Hann filter (4.9 mm FWHM).

CN subjects had their acquisition conducted on the HRRT, with acquisition parameters identical to those for [^{11}C]ABP688, as described above. Images were reconstructed taking into consideration data acquired between 45 and 60 min only, with reconstruction matching that used for the HR+ data. In order to compare data from the HRRT and HR+ PET scanners, the resolution of the HRRT was matched to the partial volume effect of the HR+. To do so, an anisotropic Gaussian kernel of 5.7 × 5.7 × 6.7 mm FWHM was used, which was found to be the best match of scanner resolutions through an internal phantom study (unpublished data). In the case of [^{18}F]FDG, two CN subjects were excluded owing to movement with one patient unable to return for the scan, reducing the sample size for [^{18}F]FDG to 4 bvFTD and 8 CN.

Magnetic resonance imaging

For anatomical co-registration and identification of the volumes of interest (VOI), all subjects underwent a high-resolution T-1 weighted MRI using a Siemens TRIO 3T scanner (Siemens Medical Solutions, Erlangen, Germany). Images were acquired in 3-D (voxel size = 1 mm^3; FOV = 256 × 256 mm; TR = 22 ms; TE = 9.2 ms; flip angle = 30°), with the scan performed on either on the same day or less than 2 weeks apart from the PET acquisitions, depending on the availability of the research slots.

Imaging analysis

[^{11}C]ABP688 binding potential, non-displaceable (BP_{ND}) values were obtained using the simplified reference tissue method (SRTM) (Gunn et al. 1997), using the cerebellum as a reference region (Elmenhorst et al. 2009; Minuzzi et al. 2009). [^{18}F]FDG-PET frames were summed and standardized uptake value ratio (SUV_R) maps calculated by normalizing the summed image to mean pontine activity for each subject. In order to correct for partial volume error (PVE), a modified version (Greve et al. 2014; Rousset et al. 2007) of the Muller-Gartner method (Muller-Gartner et al. 1992; Rousset et al. 1998) was implemented using the PVElab software package (https://nru.dk/downloads/software/pveout/pveout.html) (Quarantelli et al. 2004).

Following correction for field inhomogeneities (Sled and Evans 1998), native MRI volumes were nonlinearly resampled into standardized stereotaxic space, using the high-resolution ICBM template as reference (Fonov et al. 2009). Subsequently, normalized images were classified into grey matter (GM), white matter (WM) and cerebrospinal fluid (CSF) using an automatic algorithm (INSECT) (Zijdenbos and Evans 1998). Voxel-based morphometry (VBM) (Ashburner and Friston 2000) was carried out on the structural segmented GM images nonlinearly resampled to the standard stereotaxic space after blurring with an isotropic Gaussian kernel of 10 mm FWHM. Finally, classified images were resampled to an anatomical template and automatically labeled using a probabilistic atlas-based approach (ANIMAL) (Collins et al. 1999; Collins and Evans 1997). VOIs yielded by this procedure were subsequently applied to PET BP_{ND} (cerebellum) and SUV_R maps (pons).

Voxel-wise analysis maps of [^{11}C]ABP688 BP_{ND}, [^{18}F]FDG SUV_R, and VBM values were estimated using a basis functions approach (Gunn et al. 1997), with PET images convolved using an isotropic Gaussian kernel of 6 mm FWHM. Parametric maps created in native space were then normalized into MNI space in order to allow for group comparisons. The resulting t-maps, calculated using RMINC (Lerch 2006), show the areas with a significant difference in BP_{ND}, SUV_R, and relative concentration of GM between groups. Those areas were subsequently adjusted for a statistical cluster-wise threshold of $p < 0.05$, and corrected for multiple comparisons using random field theory (Worsley et al. 1998). [^{11}C]ABP688 BP_{ND} local maxima coordinates were used to extract [^{18}F]FDG SUV_R, and VBM values, in order to compare the magnitude of decline.

Brain regions where all patients differed significantly from controls on the basis of Z scores ≥ 2—calculated using the formula [(individual patient value) − (control mean)/(control standard deviation)]—were calculated for [^{11}C]ABP688 BP_{ND}, [^{18}F]FDG SUV_R, and VBM t-maps. These areas were then used to extract raw [^{11}C]ABP688 BP_{ND}, [^{18}F]FDG SUV_R, and VBM values, which, after reconversion to Z scores, were plotted using GraphPad Prism 5 software. Overlap maps—[^{11}C]ABP688 BP_{ND} and

[^{18}F]FDG SUV_R, [^{11}C]ABP688 BP_{ND} and VBM, [^{18}F]FDG SUV_R and VBM—as well as areas showing only reduced [^{11}C]ABP688 BP_{ND}, [^{18}F]FDG SUVR, and VBM—were created using MINC tools (http://www.bic.mni.mcgill.ca/ServicesSoftware/MINC). For overlap maps, binary masks were generated by applying the cluster-corrected t-map thresholds to each individual t-map—[^{11}C]ABP688 BP_{ND}, [^{18}F]FDG SUV_R, and VBM—setting voxels less than the given threshold to 0 and voxels greater than the threshold to 1. Binary masks were then summed, with voxels having a value of 2 indicating overlap. In order to show areas exhibiting only reductions (e.g., in availability of mGluR5) binary masks were subtracted (e.g., [^{11}C]ABP688 BP_{ND} − [^{18}F]FDG SUV_R − VBM), with the range of values in the resulting volume restricted to lie between 0 and 1, removing negative values generated as a result of the subtraction. Finally, volumes were visualized and color-coded using the software DISPLAY (http://www.bic.mni.mcgill.ca/software/Display/Display.html).

Results

Groups differed significantly in terms of MMSE, FBI and NPI (see Table 1). No differences were observed for age at scan, education, sex, or handedness. Since only two patients were capable of completing the entire neuropsychological assessment battery, quantitative assessment proved uninformative. Qualitative assessment based on the expert judgement of neuropsychologists (JP and CC) indicated clear deficits in executive and social cognitive measures in all bvFTD patients. Two patients displayed abnormal performance on measures of abstract and concrete language, with three showing deficits in visuospatial processing. While all patients showed moderate hypometabolism within frontotemporal regions, atrophy ranged from very mild to moderate (see Table 2).

Z score maps for regions with significantly reduced [^{11}C]ABP688 BP_{ND}, hypometabolism and atrophy common to all patients—along with plots showing *Z* scores relative to controls are shown in Fig. 1. Location and coordinates of local maxima for the contrast [^{11}C]ABP688 BP_{ND} CN > bvFTD] are reported in Table 3, along with values for [^{18}F]FDG SUV_R and VBM using these local maxima. Despite neurodegeneration being more widespread than declines in mGluR5 availability, reductions in metabolism and GM were found to be inferior to those for [^{11}C]ABP688 BP_{ND} across a wide range of FTLD predilection sites (see Table 3). Relative to controls, bvFTD patients showed reductions of 65, 30, and 15 %—for [^{11}C]ABP688 BP_{ND}, [^{18}F]FDG SUV_R, and VBM, respectively—on the basis of values extracted from common *Z* score maps.

Voxel-wise analysis of group differences in [^{11}C]ABP688 BP_{ND} revealed declines in mGluR5 availability (85,152 mm^3) in orbital, ventromedial, and

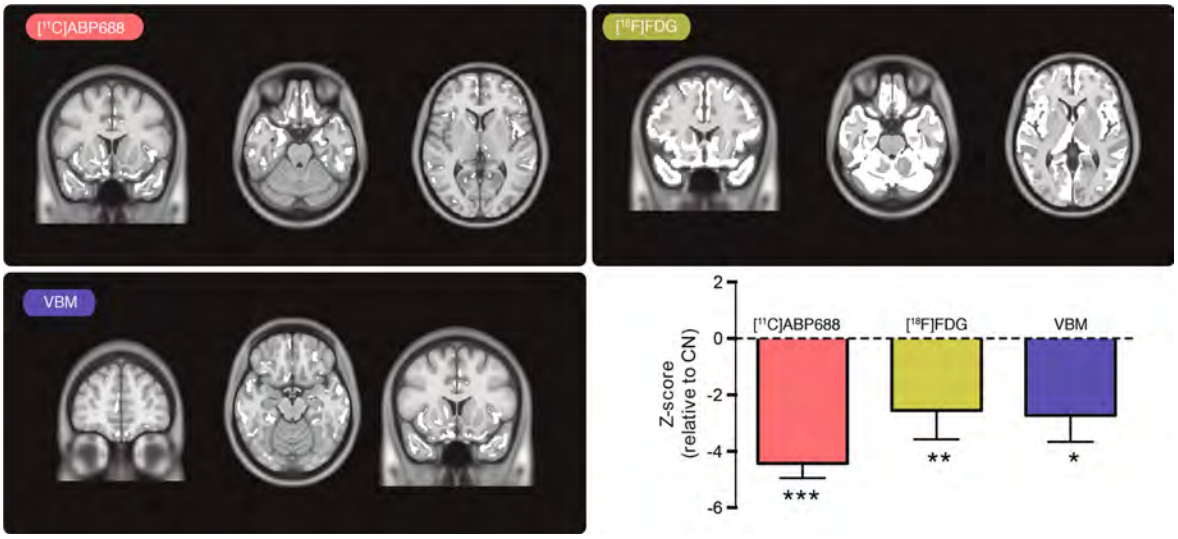

Fig. 1 *Z* score maps for all bvFTD patients were created for [^{11}C]ABP688 BP_{ND}, [^{18}F]FDG SUV_R, and VBM. These maps were then combined to show areas with significantly reduced [^{11}C]ABP688 BP_{ND}, [^{18}F]FDG SUV_R, and GM common to all bvFTD patients (*top left*, *top right*, *bottom left*, respectively). These common *Z* maps were then used to extract raw [^{11}C]ABP688 BP_{ND}, [^{18}F]FDG SUV_R, and VBM values. After conversion to *Z* scores, values were plotted, relative to CN subjects (*bottom right*). ***$p < 0.001$, **$p < 0.01$, *$p < 0.05$

Table 3 Location and Talairach coordinates of local maxima for areas of reduced [^{11}C]ABP688 BP_{ND} in patients with bvFTD, along with *t* values for [^{18}F]FDG SUV_R and VBM findings, using [^{11}C]ABP688 BP_{ND} maxima coordinates

Brain region	*x*	*y*	*z*	$t_{[11C]ABP688}$	*p*	$t_{[18F]FDG}$	*p*	t_{VBM}	*p*
Gyrus rectus L	−9.0	28.2	−24.7	−7.12	>0.0001	−4.19	>0.0001	−2.28	0.0401
Gyrus rectus R	13.8	26.2	−24.7	−6.52	>0.0001	−3.22	0.0092	−2.38	0.0333
Medial orbitofrontal cortex L	−16.0	23.1	−15.2	−8.49	>0.0001	−2.40	0.0373	−0.527	0.6071
Medial orbitofrontal cortex R	15.0	−15.2	−9.66	−9.73	>0.0001	−1.98	0.0076	−0.002	0.9998
Lateral orbitofrontal cortex L	−32.1	36.0	−15.2	−4.63	0.0005	−4.14	0.0020	−4.03	0.0014
Lateral orbitofrontal cortex R	28.1	47.2	−15.2	−5.21	0.0002	2.59	0.0269	−4.45	0.0007
Ventromedial prefrontal cortex L	−2.9	51.3	4.0	−7.42	>0.0001	−5.55	0.0002	−5.6t9	>0.0001
Ventromedial prefrontal cortex R	13.3	53.2	2.5	−4.42	0.0007	−2.01	0.0722	−3.32	0.0055
Dorsomedial prefrontal cortex L	−3.6	56.9	28.0	−6.14	>0.0001	−4.56	0.0010	−1.43	0.1763
Dorsomedial prefrontal cortex R	3.3	42.0	34.2	−4.11	0.0012	−4.88	0.0006	−4.29	0.0009
Anterior cingulate L	−2.4	37.0	14.7	−4.93	0.0003	−4.03	0.0024	−5.00	0.0002
Anterior cingulate R	5.0	40.2	14.7	−4.40	0.0007	−3.97	0.0026	−5.66	>0.0001
Frontal pole L	−10.1	71.1	3.0	−4.85	0.0003	−2.79	0.0191	−1.53	0.1500
Frontal pole R	14.2	72.0	3.0	−4.81	0.0003	−2.59	0.0269	−1.42	0.1791
Dorsolateral prefrontal cortex L	–	–	–	–	–	–	–	–	–
Dorsolateral prefrontal cortex R	52.1	25.1	21.8	−8.3	>0.0001	−5.01	0.0005	−1.51	0.1550
Ventrolateral prefrontal cortex L	–	–	–	–	–	–	–	–	–
Ventrolateral prefrontal cortex R	52.1	38.9	−4.9	−5.87	>0.0001	−5.28	0.0004	−0.96	0.3546
Paracentral lobule L	−4.6	−26.9	64.5	−5.09	0.0002	−1.98	0.0759	−2.34	0.0359
Paracentral lobule R	7.0	−35.9	−55.1	−4.11	0.0002	−1.98	0.0759	−1.52	0.0152
Thalamus L	−17.8	−31.3	1.8	−6.50	>0.0001	−3.11	0.0111	−8.74	>0.0001
Thalamus R	9.0	−15.9	1.8	−4.74	0.0004	−1.93	0.0824	−9.66	>0.0001
Hypothalamus L	−5.1	−5.9	−11.1	−4.18	0.0011	−2.32	0.0428	−8.49	>0.0001
Hypothalamus R	4.1	−5.9	−11.2	−4.26	0.0009	−2.67	0.0235	−8.34	>0.0001
Caudate L	−11.2	14.1	1.8	−5.43	0.0001	−4.65	0.0009	−5.89	>0.0001
Caudate R	9.0	9.1	7.3	−3.96	0.0016	−4.16	0.0019	−1.05	0.3128
Putamen L	−26.2	17.1	1.8	−4.74	0.0004	−3.64	0.0445	−3.81	0.0022
Putamen R	–	–	–	–	–	–	–	–	–
Insula L	−41.1	13.0	−9.8	−4.55	0.0005	−3.59	0.0049	−4.11	0.0012
Insula R	41.7	14.1	−2.0	−5.76	>0.0001	−4.32	0.0015	−5.78	>0.0001
Temporal pole L	−38.1	22.2	−35.9	−5.59	>0.0001	−4.13	0.0020	−2.02	0.0645
Temporal pole R	31.1	22.2	−39.0	−6.79	>0.0001	−2.75	0.0205	−1.56	0.1428
Superior temporal gyrus L	−58.2	−10.9	2.0	−3.96	0.0016	−4.07	0.0023	−1.74	0.1055
Superior temporal gyrus R	49.4	−2.4	−4.0	−6.61	>0.0001	−3.21	0.0093	−4.78	0.0004
Middle temporal gyrus L	−58.2	−16.0	−11.0	−4.60	0.0005	−4.00	0.0024	−1.29	0.2195
Middle temporal gyrus R	52.7	−12.1	−24.0	−6.99	>0.0001	−4.53	0.0011	−1.53	0.1500
Inferior temporal gyrus L	−58.2	−24.5	−25.4	−7.19	>0.0001	−3.95	0.0027	−0.16	0.8753
Inferior temporal gyrus R	52.7	−45.1	−22.9	−5.16	0.0002	−3.65	0.0045	−0.09	0.9297
Hippocampal formation L	−35.1	−11.8	−19.2	−4.94	0.0003	−1.00	0.3409	−1.62	0.1292
Hippocampal formation R	34.5	−14.6	−18.5	−1.99	0.0680	−2.77	0.0198	−3.26	0.0062
Cuneus L	−11.2	−92.9	15.9	−5.22	0.0002	−3.35	0.0074	−4.81	0.0003
Cuneus R	13.8	−90.8	15.9	−5.27	0.0002	−2.05	0.0611	−4.69	0.0004
Lingual gyrus L	−12.7	−73.7	−1.7	−6.87	>0.0001	−1.27	0.2328	−5.52	>0.0001
Lingual gyrus R	22.8	−79.1	−3.9	−7.17	>0.0001	−0.41	0.6905	−0.26	0.7983

standardized uptake ratio (SUV_R); voxel-based morphometry (VBM); non-displaceable binding potentials (BP_{ND}). Talairach coordinates (*x*, *y*, *z*) of [^{11}C]ABP688 BP_{ND} local maxima (*t* values, corrected for multiple comparisons, $p < 0.05$) were applied to [^{18}F]FDG SUV_R and VBM t-maps in order to extra *t* values. p values were determined using *t* values and degrees of freedom ([^{11}C]ABP688 $BP_{ND} = 14$, [^{18}F]FDG $SUV_R = 11$, VBM = 14). *R* right hemisphere, *L* Left hemisphere, – indicates no findings in that region

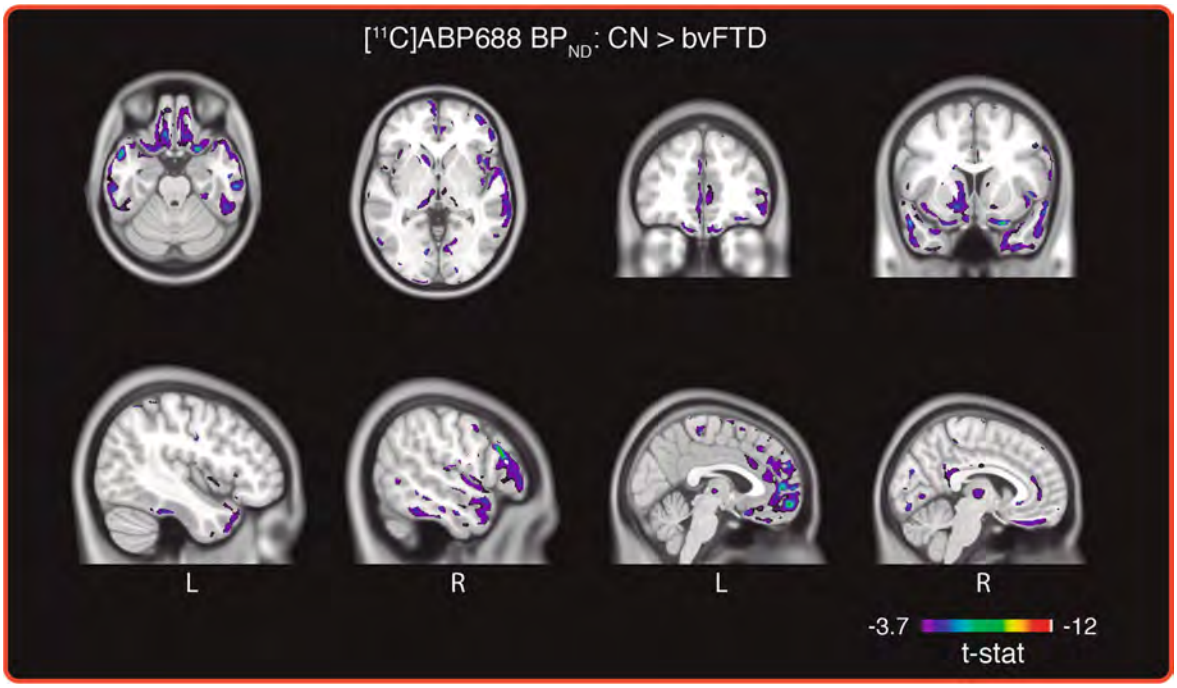

Fig. 2 Voxel-wise t-maps showing areas of decreased [^{11}C]ABP688 BP_{ND} in patients with bvFTD compared with CN subjects (85,152 mm^3; corrected for multiple comparisons, $p < 0.05$). Leftward asymmetry was noted in the anterior cingulate, superior frontal gyrus, paracentral lobule, caudate, putamen, and thalamus. Rightward asymmetry was found in the posterior cingulate, lingual gyrus, cuneus, dorsolateral/ventrolateral prefrontal cortex, superior/middle temporal gyri and the temporal poles. No significant increases in [^{11}C]ABP688 binding were observed in bvFTD patients

dorsomedial prefrontal areas (corrected for multiple comparisons, $p < 0.05$; see Fig. 2). Declines were likewise noted in the gyrus rectus, anterior cingulate (L > R), right posterior cingulate, superior frontal gyrus (L > R), paracentral lobule (L > R), caudate (L > R), left putamen, insula (R > L), thalamus (L > R), right lingual gyrus, and right cuneus. Additional declines were found in the right dorsolateral, right ventrolateral, and anterior prefrontal cortex, the right superior and middle temporal gyri, as well as in the temporal poles. No significant increases in [^{11}C]ABP688 binding were observed in bvFTD patients.

Significant hypometabolism was noted among bvFTD patients (116,742 mm^3) in extensive prefrontal areas, including the orbitofrontal (R > L), ventromedial and dorsomedial prefrontal (L > R), as well as the cingulate gyrus (L > R) (corrected for multiple comparisons, $p < 0.05$) (see Fig. 3). Metabolism was significantly reduced in the superior, middle, and inferior frontal gyri as well as in the precuneus and paracentral lobule (L > R). Hypometabolism was also found in the bilateral insula (R > L), uncus/amygdala, and parahippocampus (L > R), as well as in subcortical structures, including the head of the caudatum and the left thalamus. There was also hypometabolism in the superior, middle, and inferior temporal gyri, temporal poles, and cerebellar tonsils.

Among bvFTD patients, grey matter loss (88,845 mm^3) was predominantly focused in the striatum—including the putamen (L > R) and head of the caudate nucleus bilaterally (corrected for multiple comparisons, $p < 0.05$; see Fig. 4). There was significant involvement of the thalamus and insula bilaterally, as well as the amygdala, and parahippocampus. Atrophy was also observed in the anterior cingulate (L > R), precuneus (R > L) gyrus rectus, orbitofrontal gyrus, as well as the right superior/middle temporal gyri, though to a lesser degree (see Table 3).

Overlap between [^{11}C]ABP688 BP_{ND} and [^{18}F]FDG SUV_R t-maps was observed in the gyrus rectus (L > R), anterior cingulate/ventromedial prefrontal cortex (L > R), dorsomedial prefrontal cortex (L > R), thalamus (L > R) insula (R > L) and temporal poles (22 379 mm^3; see Fig. 5). [^{11}C]ABP688 BP_{ND} and VBM findings overlapped in the anterior cingulate/ventromedial prefrontal cortex (L > R), orbitofrontal cortex (R > L), thalamus (L > R), head of the caudate nucleus (L > R) and the insula (R > L) (13 463 mm^3; see Fig. 6). Overlap between hypometabolic regions and atrophy was noted in medial and lateral

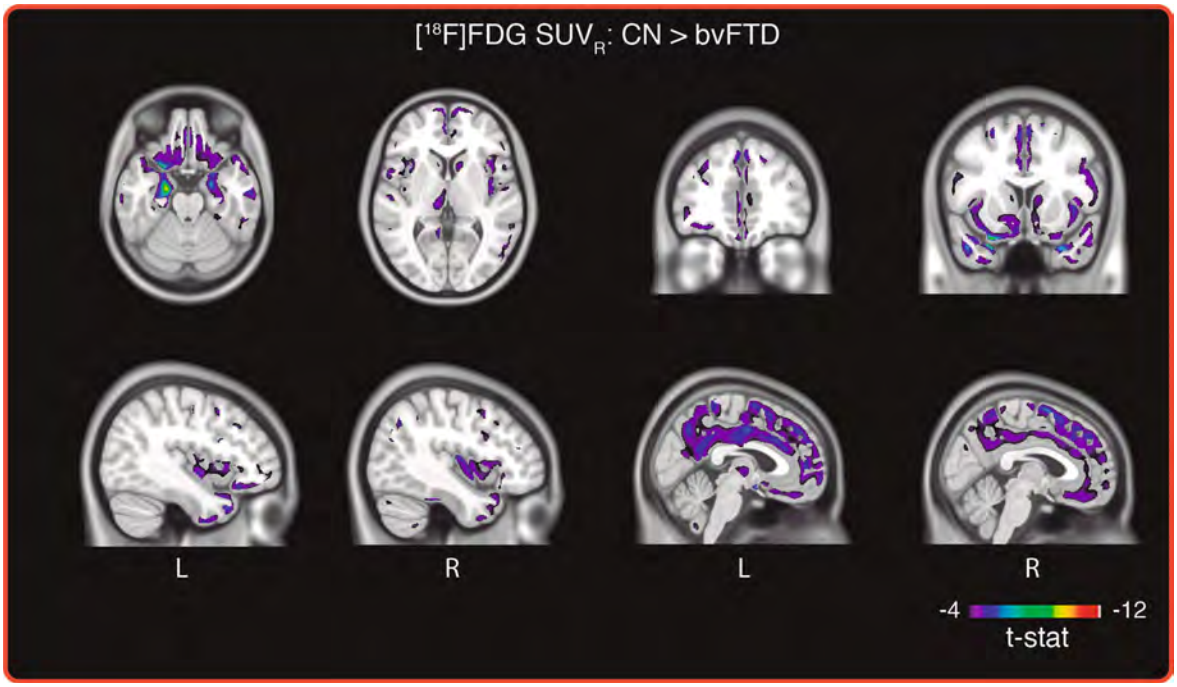

Fig. 3 Voxel-wise t-maps showing areas of decreased [^{18}F]FDG SUV_R in patients with bvFTD compared with CN subjects (116,742 mm^3; corrected for multiple comparisons, $p < 0.05$). The dorso/ventromedial prefrontal cortex, cingulate gyrus, frontal gyri, paracentral lobule, precuneus, parahippocampus, thalamus, caudate and temporal lobes were characterized by leftward asymmetry. Hypometabolism was also noted with rightward asymmetry in the insula and orbitofrontal gyrus and in the cerebellar tonsils bilaterally

orbitofrontal areas, anterior cingulate/ventromedial prefrontal cortex (L > R), dorsomedial prefrontal cortex (R > L), insula (R > L), thalamus (L > R), left amygdala, right hippocampal formation, and the head of the caudate nucleus (R > L) (14 179 mm^3; see Fig. 7). Though hypometabolism and atrophy were found in frontal, temporal, and subcortical brain regions, these declines were found to be inferior relative to those for [^{11}C]ABP688 BP_{ND} in a wide range of areas, including the gyrus rectus, medial and lateral orbitofrontal cortex, ventromedial prefrontal cortex, left dorsomedial prefrontal cortex, paracentral lobule, frontal pole, left putamen, left insula, lingual gyrus, cuneus, temporal poles, right superior temporal gyrus, inferior and middle temporal gyri, and the right dorso- and ventrolateral prefrontal cortex.

Subtraction of binarized t-maps ([^{11}C]ABP688 BP_{ND} − [^{18}F]FDG SUV_R − VBM) showed that decreased binding of [^{11}C]ABP688 was unique to the gyrus rectus (R > L), orbitofrontal cortex (R > L), lateral portion of the right head of the caudate nucleus, left putamen, left superior temporal lobe, inferior temporal lobes, temporal poles (R > L), right posterior cingulate, right ventral/dorsolateral prefrontal cortex, left paracentral lobule, right occipital cortex, and right lingual gyrus (55 742 mm^3; see Fig. 8). A similar subtraction yielded a volume of 86 616 mm^3 for regions displaying only hypometabolism ([^{18}F]FDG SUV_R − [^{11}C]ABP688 BP_{ND} − VBM)—including the uncus/amygdalae (L > R), the parahippocampus (L > R), bilateral cuneus, posterior cingulate/precuneus (L > R), bilateral insula, medial prefrontal cortex, left posterior paracentral lobule, left frontal operculum, anterior temporal poles, orbitofrontal gyrus/gyrus rectus (R > L), and bilateral cerebellar cortex (see Fig. 9). In addition, the orbitofrontal gyrus, the right middle temporal gyrus, right temporal operculum, left anterior insula, posterior insula bilaterally (R > L), ventral amygdala (L > R), left posterior inferior temporal gyrus, anterior cingulate gyrus (L > R), the putamen (L > R) and head of the caudate nucleus bilaterally, the thalamus as well as the posterior portion of the hippocampal formation, bilaterally, were found to be characterized only by GM reductions (VBM − [^{18}F]FDG SUV_R − [^{11}C]ABP688 BP_{ND}; 67 635 mm^3; see Fig. 10). Though changes in [^{11}C]ABP688 BP_{ND}, [^{18}F]FDG SUVR, and VBM were found to co-exist within the orbitofrontal cortex and temporal lobe, relative to [^{18}F]FDG and VBM, findings for [^{11}C]ABP688 were more ventral and lateral, respectively.

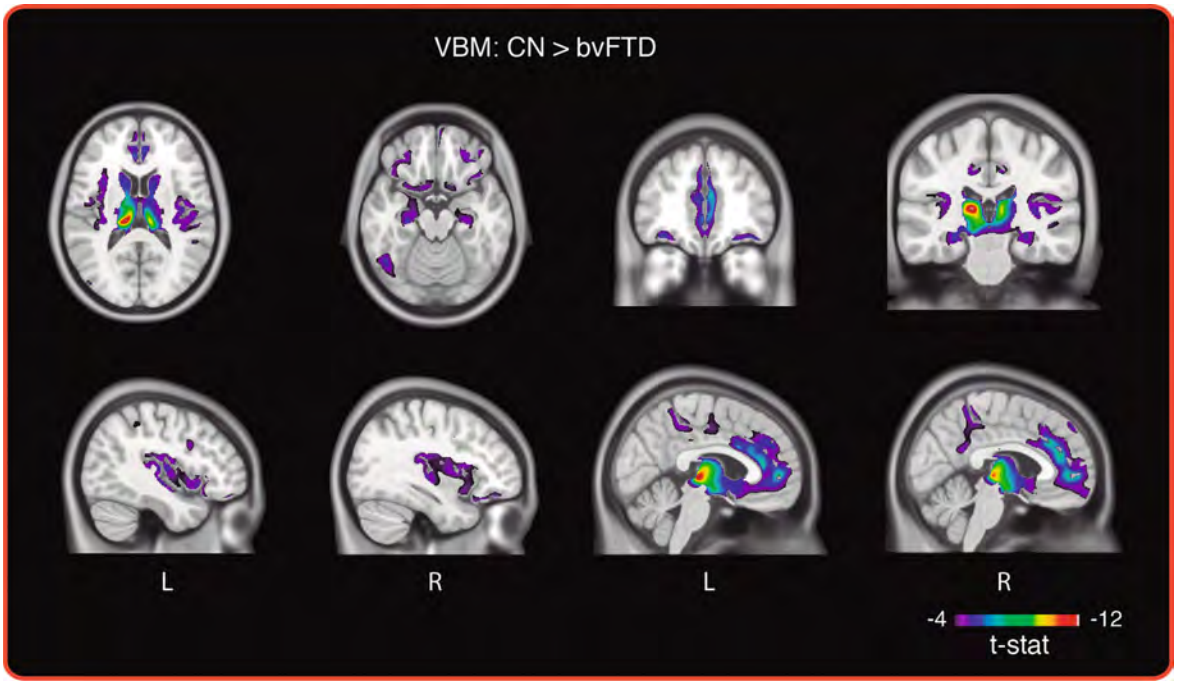

Fig. 4 Voxel-wise t-maps showing areas of reduced VBM derived GM concentration in patients with bvFTD compared with CN subjects (88,845 mm^3; corrected for multiple comparisons, $p < 0.05$). Atrophy was predominant in the thalami (L > R), head of caudate, insula, uncus/amygdala, and parahippocampus. GM loss was likewise noted in the putamen (L > R), precuneus (R > L), anterior cingulate (L > R), gyrus rectus, orbitofrontal gyrus and right superior/middle temporal gyri

Discussion

The present findings represent the first in vivo report of decreased availability of mGluR5 in bvFTD. In line with recent studies showing reduced binding of [^{11}C]ABP688 in disorders characterized by glutamate excitotoxicity—such as major depressive disorder and temporal lobe epilepsy (Choi et al. 2014; Deschwanden et al. 2011)—our findings may indicate altered glutamatergic neurotransmission in bvFTD, or conformational changes specific to the mGluR5 allosteric site. Further, we reproduced previous [^{18}F]FDG and VBM findings in terms of both the topography of neurodegeneration and its partially asymmetric distribution (Diehl-Schmid et al. 2007; Hornberger et al. 2012; Jeong et al. 2005; Pan et al. 2012). In addition, we showed that the volume of decreased mGluR5 availability was inferior to that for hypometabolism and GM atrophy, and that the overlap between reduced [^{11}C]ABP688 BP_{ND} and hypometabolism was superior to that for GM atrophy. Moreover, we showed that declines in mGluR5 availability were unique to several isocortical, limbic, and paralimbic areas, possibly representing an early sign of pyramidal cell dysfunction. In this respect, the focality of [^{11}C]ABP688 BP_{ND} reductions in the present study is striking given the widespread distribution of mGluR5. In addition, several frontotemporal areas showed hypometabolism and/or GM loss in the absence of reduced [^{11}C]ABP688 binding. Taken together, these findings suggest a differential neuronal vulnerability to FTLD pathology in bvFTD—similar to that seen in other neurodegenerative diseases (Double et al. 2010)—with reduced availability of mGluR5 possibly preceding neurodegeneration within select frontotemporal brain regions.

While at physiological concentrations glutamate is known to play a pivotal role in synaptic plasticity (Balschun et al. 2006; Huber et al. 2001)—with any given function of a given cortical region likely to depend on glutamatergic neurotransmission at some level (Francis 2009)—at high concentrations it has been shown to act as a neurotoxin, promoting neuronal injury and death in animal models (Rao et al. 2001; Rothstein 1996) and in neurodegenerative diseases, including AD (Francis 2003). In the case of AD, accumulation of β-amyloid is thought to inhibit astroglial glutamate uptake, resulting in increased extracellular levels of glutamate, which, under chronic conditions, lead to cell death via sustained elevations in intracellular calcium (Harkany et al. 2000). This excitotoxic scenario may explain decreased binding of

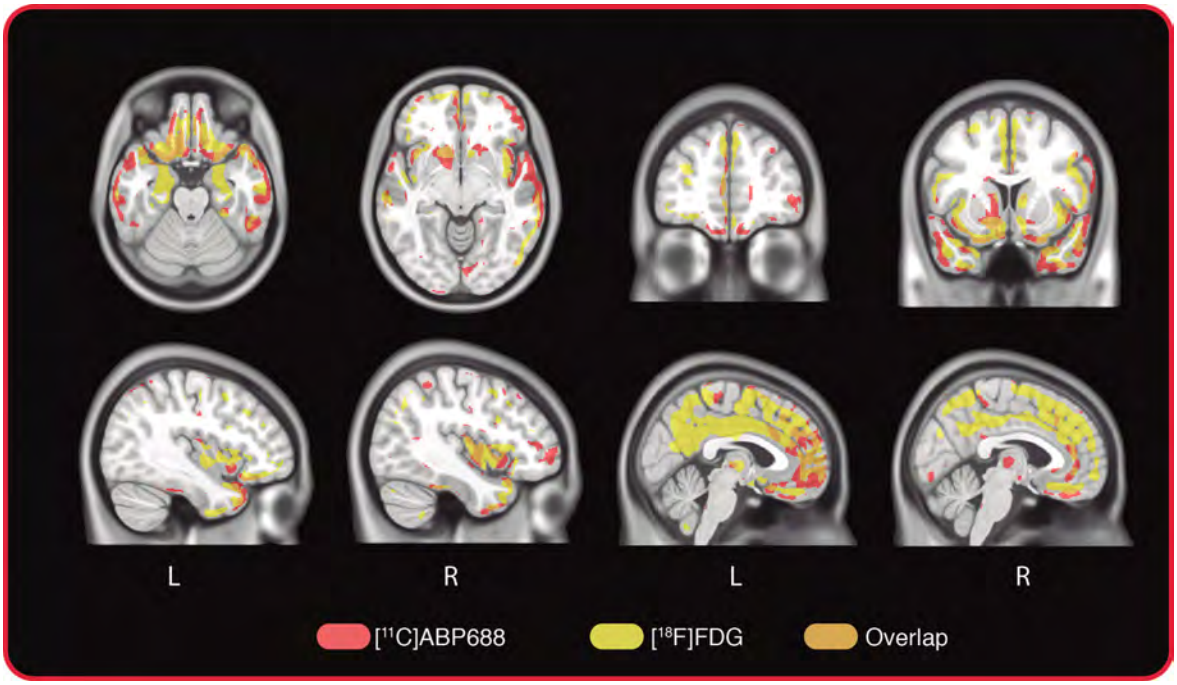

Fig. 5 Overlap (*orange*; 22,379 mm^3) between binarized [^{11}C]ABP688 BP_{ND} (*red*) and [^{18}F]FDG SUV_R (*yellow*) t-maps was found with leftward predominance in the gyrus rectus, anterior cingulate dorso/ventromedial prefrontal cortex, and thalamus. Overlap was also noted with rightward asymmetry in the insula and in the temporal poles bilaterally

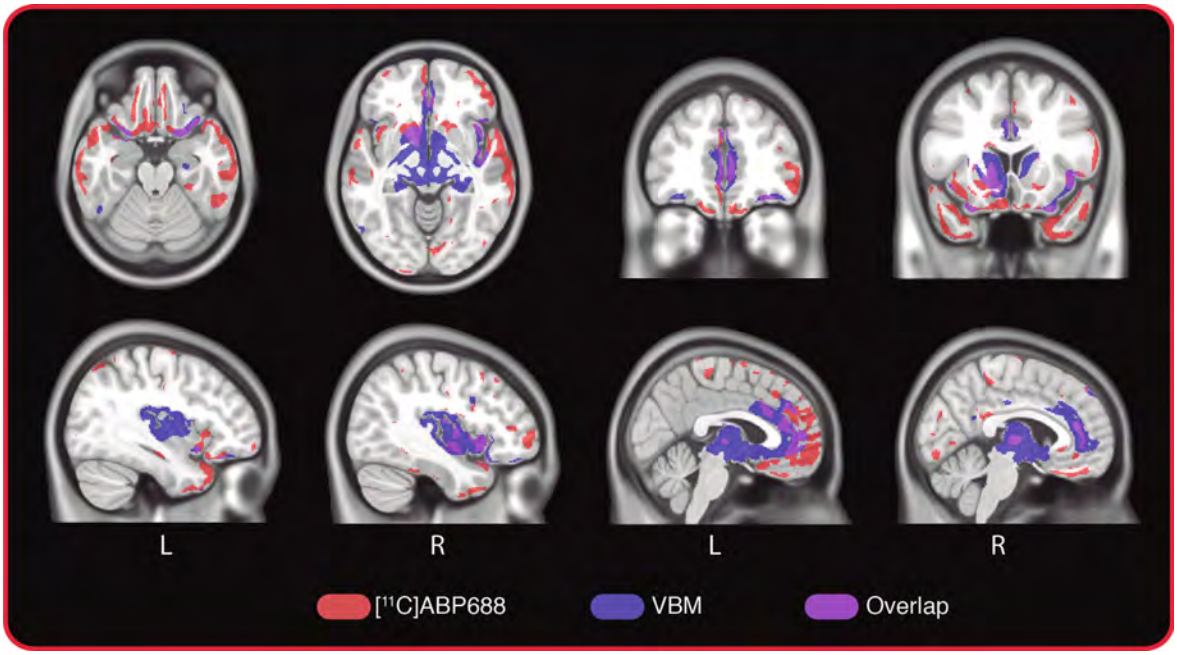

Fig. 6 Overlap (*purple*; 13,463 mm^3) between binarized [^{11}C]ABP688 BP_{ND} (*red*) and VBM (*blue*) t-maps was found with leftward asymmetry in the anterior cingulate, ventromedial prefrontal cortex, thalamus, and head of the caudate nucleus. Rightward asymmetry was noted in the insula and orbitofrontal cortex

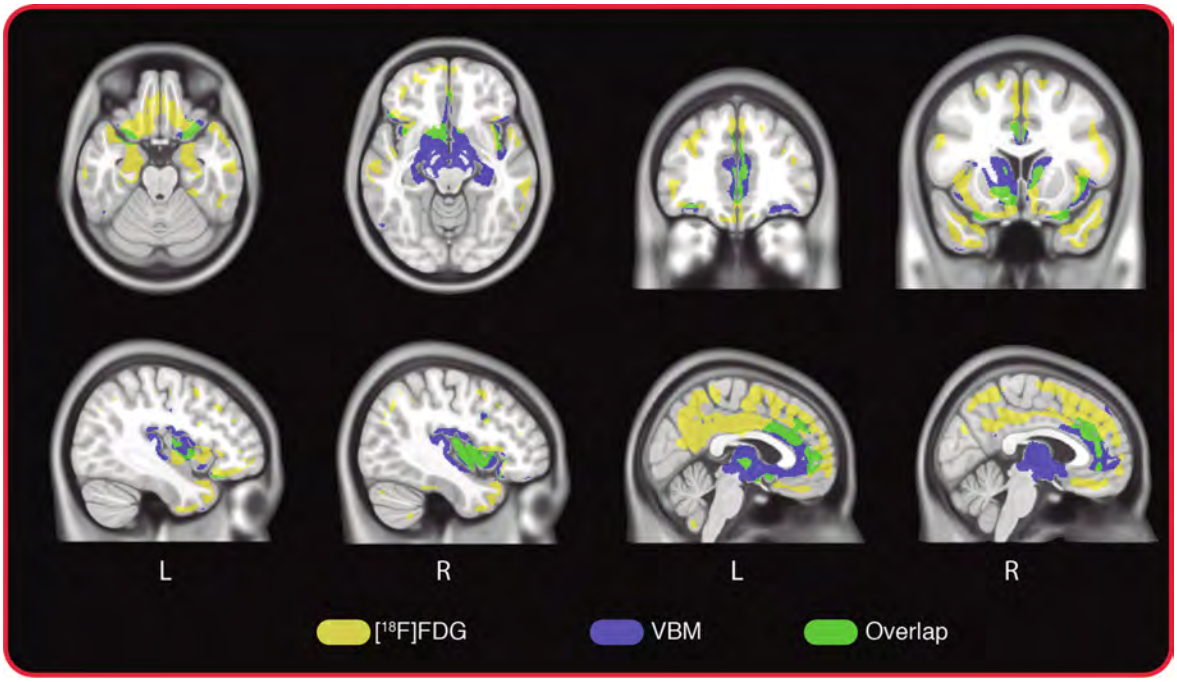

Fig. 7 Overlap (*green*; 14,179 mm^3) between binarized [^{18}F]FDG SUV_R (*red*) and VBM (*blue*) t-maps was observed with leftward asymmetry in the orbitofrontal cortex, anterior cingulate/ventromedial prefrontal cortex, thalamus and amygdala. Rightward asymmetry was found in the dorsomedial prefrontal cortex, insula, hippocampal formation, and head of the caudate

[^{11}C]ABP688 in that continued high levels of glutamate may alter the availability of its transmembrane allosteric binding site (Ametamey et al. 2007) by altering mGluR5 conformational states (Cabello et al. 2009; Canela et al. 2009; Changeux and Edelstein 2005; Romano et al. 1996). Indeed, affinity shifts in receptor–radioligand interactions have previously been described in the context of dopaminergic neurotransmission, where the affinity of a D2 PET radiopharmaceutical was altered following an amphetamine challenge (Narendran et al. 2004; Seneca et al. 2006; Wilson et al. 2005).

Recently, an expanded hexanucleotide repeat in the chromosome 9 open reading frame 72 (C9ORF72) was identified as the most common cause of familial FTD and amyotrophic lateral sclerosis (ALS), with mutations associated with deposition of TDP-43 pathology (DeJesus-Hernandez et al. 2011; Renton et al. 2011). While the pathogenic mechanism(s) by which this repeat expansion could cause disease remain unknown, induced pluripotent stem cell differentiated neurons from C9ORF72 ALS patients were shown to be highly susceptible to glutamate excitotoxicity (Donnelly et al. 2013). Related work on primary cells from TDP-43 transgenic mice showed an increased vulnerability to the toxic effects of excess glutamate (Swarup et al. 2011). Moreover, a recent study involving transgenic mice expressing the FTDP-17 mutation P301L in the human tau gene—resulting in the accumulation of hyperphosphorylated tau—showed a tau-dependent impairment of glutamate metabolism (Nilsen et al. 2013). These studies suggest that the pathogenicity of hyperphosphorylated tau and TDP-43—the molecular pathologies accounting for most cases of bvFTD (Mackenzie et al. 2011)—may involve glutamatergic excitotoxicity.

Certain methodological aspects, however, limit interpretation of the present findings. In addition to this study's cross-sectional design and small sample size, the absence of histopathological data precludes conclusions about the homogeneity of the sample from the perspective of underlying molecular pathology. As such we were not able to address the possible interplay between different FTLD subtypes and possibly differing effects on mGluR5 availability. Moreover, potential limitations may accompany the use of VBM when applied to atrophic brains (Good et al. 2002).

Despite these caveats, our findings shed light on the possible role of glutamate excitotoxicity in the pathogenesis of bvFTD and suggest that [^{11}C]ABP688 may prove a suitable non-invasive marker of glutamatergic neurotransmission in vivo. Larger prospective studies are required to

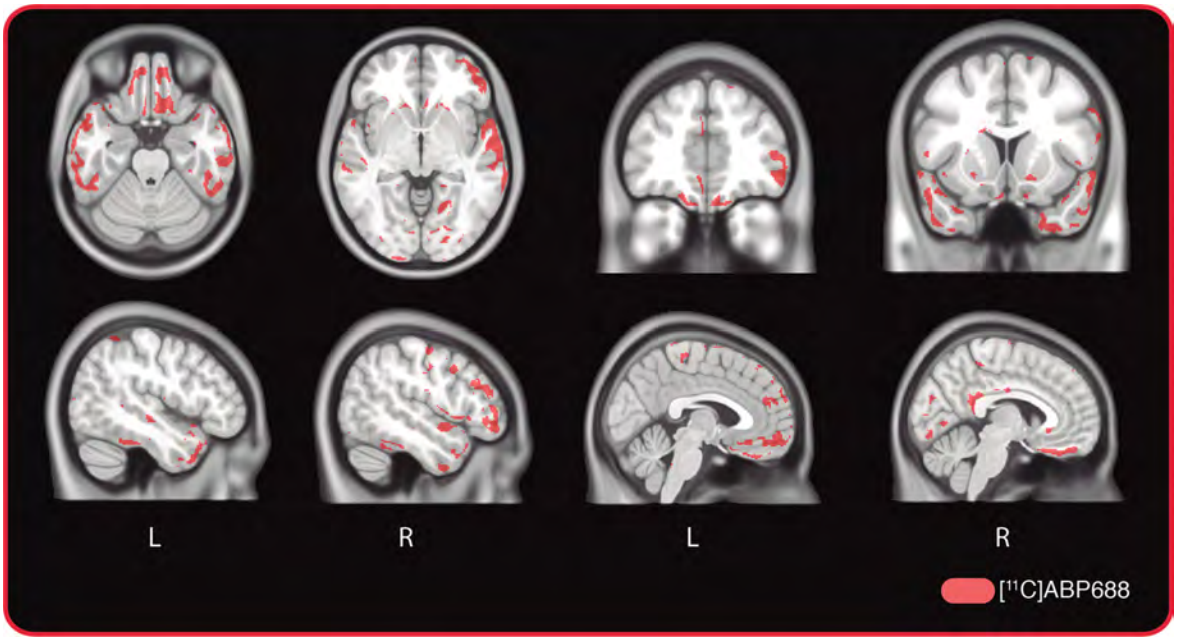

Fig. 8 Subtraction of binarized t-maps ([^{11}C]ABP688 BP_{ND} − [^{18}F]FDG SUV_R − VBM) showed areas characterized only by declines in [^{11}C]ABP688 BP_{ND} (55,742 mm^3). Areas characterized by rightward asymmetry included the inferior temporal lobes, temporal poles gyrus rectus, orbitofrontal cortex, head of the caudate nucleus, posterior cingulate, ventral/dorsolateral prefrontal cortex, lingual gyrus, and occipital cortex. Areas characterized by leftward asymmetry included the putamen, superior temporal lobe, and paracentral lobule

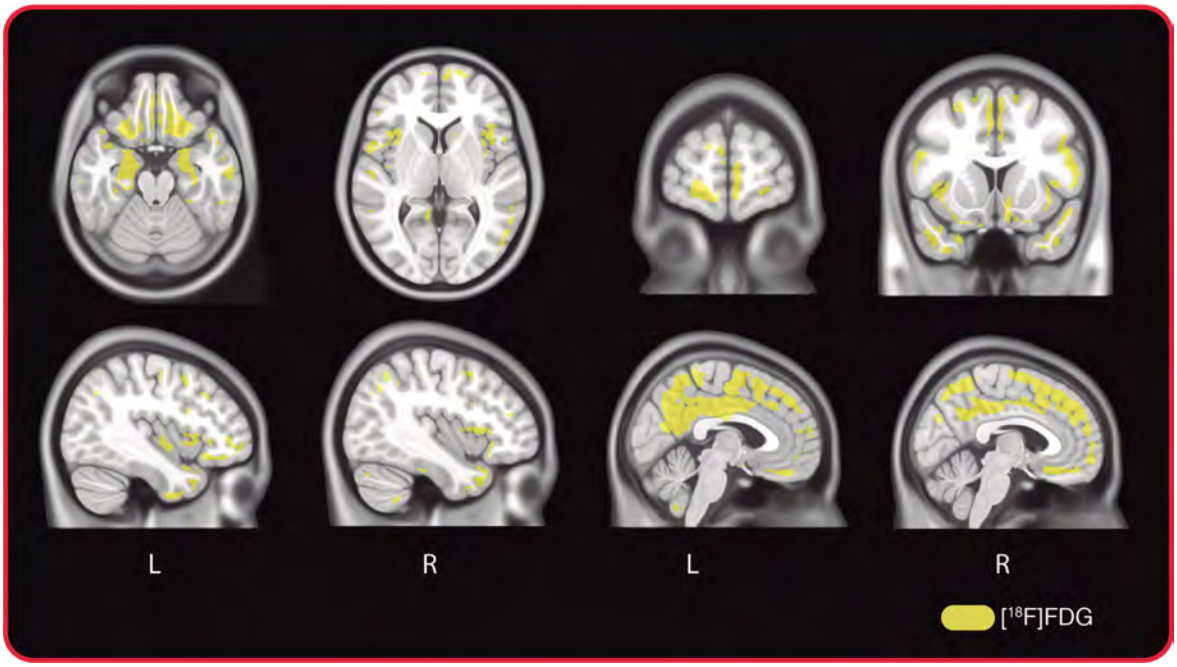

Fig. 9 Subtraction of binarized t-maps ([^{18}F]FDG SUV_R − [^{11}C]ABP688 BP_{ND} − VBM) showed areas characterized only by hypometabolism (86,616 mm^3), including the bilateral insula, medial prefrontal cortex, left posterior paracentral lobule, left frontal operculum, anterior temporal poles, and bilateral cerebellar cortex. Leftward asymmetry was noted for the uncus/amygdalae, parahippocampus, and posterior cingulate/precuneus. Rightward asymmetry was noted for the orbitofrontal gyrus/gyrus rectus

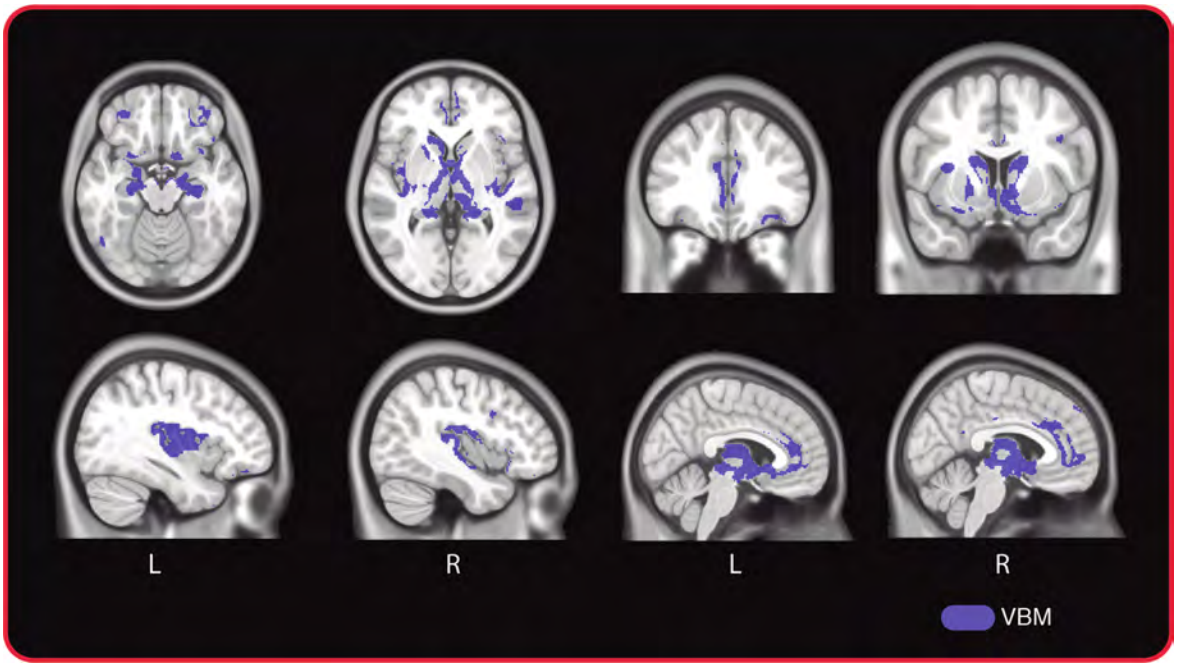

Fig. 10 Subtraction of binarized t-maps (VBM − [^{18}F]FDG SUV_R − [^{11}C]ABP688 BP_{ND}) showed areas characterized only by reductions in GM (67,635 mm^3), including the orbitofrontal gyrus, the right middle temporal gyrus, right temporal operculum, left anterior insula, head of the caudate nucleus bilaterally, left posterior inferior temporal gyrus, the thalamus as well as the posterior portion of the hippocampal formation, bilaterally. Leftward asymmetry was noted for the ventral amygdala, anterior cingulate gyrus, and putamina. Rightward asymmetry was noted for the posterior insula

validate these findings, to establish the trajectory of reduced mGluR5 availability relative to other biomarkers of neurodegeneration, and to address the potential link between the dysregulation of glutamatergic neurotransmission and bvFTD symptomatology.

Acknowledgments The authors wish to thank the patients and their families for participating in this study. This work was supported by the Canadian Institutes of Health Research (CIHR) [MOP-11-51-31], the Alan Tiffin Foundation, the Alzheimer's Association [NIRG-08-92090], and the Fonds de la recherche en santé du Québec (Chercheur boursier). The authors wish to acknowledge the help of the imaging staff at the Montreal Neurological Institute McConnell Brain Imaging Centre, including Reda Bouhachi, Simion Matei, Rick Fukasawa (PET Technologists), Ron Lopez, David Costa, Louise Marcotte (MRI Technologists), and André Cormier (Chief MRI Technologist).

Conflict of interest The authors declare no conflict of interest.

References

Alladi S, Xuereb J, Bak T, Nestor P, Knibb J, Patterson K, Hodges JR (2007) Focal cortical presentations of Alzheimer's disease. Brain J Neurol 130:2636–2645. doi:10.1093/brain/awm213

Ametamey SM, Kessler LJ, Honer M, Wyss MT, Buck A, Hintermann S, Auberson YP, Gasparini F, Schubiger PA (2006) Radiosynthesis and preclinical evaluation of 11C-ABP688 as a probe for imaging the metabotropic glutamate receptor subtype 5. J Nucl Med 47:698–705

Ametamey SM, Treyer V, Streffer J, Wyss MT, Schmidt M, Blagoev M, Hintermann S, Auberson Y, Gasparini F, Fischer UC, Buck A (2007) Human PET studies of metabotropic glutamate receptor subtype 5 with 11C-ABP688. J Nucl Med 48:247–252

Ashburner J, Friston KJ (2000) Voxel-based morphometry—the methods. NeuroImage 11:805–821. doi:10.1006/nimg.2000.0582

Balschun D, Zuschratter W, Wetzel W (2006) Allosteric enhancement of metabotropic glutamate receptor 5 function promotes spatial memory. Neuroscience 142:691–702. doi:10.1016/j.neuroscience.2006.06.043

Cabello N, Gandía J, Bertarelli DC, Watanabe M, Lluís C, Franco R, Ferré S, Luján R, Ciruela F (2009) Metabotropic glutamate type 5, dopamine D2 and adenosine A2a receptors form higher-order oligomers in living cells. J Neurochem 109:1497–1507. doi:10.1111/j.1471-4159.2009.06078.x

Canela L, Fernández-Dueñas V, Albergaria C, Watanabe M, Lluís C, Mallol J, Canela EI, Franco R, Luján R, Ciruela F (2009) The association of metabotropic glutamate receptor type 5 with the neuronal Ca^{2+}-binding protein 2 modulates receptor function. J Neurochem 111:555–567. doi:10.1111/j.1471-4159.2009.06348.x

Changeux J-P, Edelstein SJ (2005) Allosteric mechanisms of signal transduction. Science 308:1424–1428. doi:10.1126/science.1108595

Choi H, Kim YK, Oh SW, Im HJ, Hwang do W, Kang H, Lee B, Lee YS, Jeong JM, Kim EE, Chung JK, Lee DS (2014) In vivo imaging of mGluR5 changes during epileptogenesis using [11C]ABP688 PET in pilocarpine-induced epilepsy rat model. PLoS One 9:e92765. doi:10.1371/journal.pone.0092765

Collins DL, Evans AC (1997) Animal: validation and applications of non-linear registration-based segmentation. Int J Pattern Recogn Art Intell 11:1271–1294

Collins DL, Zijendos AP, Barré WFC, Evans AC (1999) ANIMAL + INSECT: inproved cortical structure segmentation. In: Kuba A, Samal M, Todd-Pokropek A (eds) Lecture Notes in Computer Science. Springer-Verlag, Berlin, Heidelberg, pp 210–223

Comtat C, Sureau FC, Sibomana M, Hong IK, Sjoholm N, Trebossen R (2008) Image based resolution modeling for the HRRT OSEM reconstructions software. In: IEEE Nuclear Science Symposium Conference Record, pp 4120–4123

Costes N, Dagher A, Larcher K, Evans AC, Collins DL, Reilhac A (2009) Motion correction of multi-frame PET data in neuroreceptor mapping: simulation based validation. Neuroimage 47:1496–1505. doi:10.1016/j.neuroimage.2009.05.052

Cummings JL, Mega M, Gray K, Rosenberg-Thompson S, Carusi DA, Gornbein J (1994) The Neuropsychiatric Inventory: comprehensive assessment of psychopathology in dementia. Neurology 44:2308–2314

Dalfo E, Albasanz JL, Rodriguez A, Martin M, Ferrer I (2005) Abnormal group I metabotropic glutamate receptor expression and signaling in the frontal cortex in Pick disease. J Neuropathol Exp Neurol 64:638–647

DeJesus-Hernandez M, Mackenzie IR, Boeve BF, Boxer AL, Baker M, Rutherford NJ, Nicholson AM, Finch NA, Flynn H, Adamson J, Kouri N, Wojtas A, Sengdy P, Hsiung GY, Karydas A, Seeley WW, Josephs KA, Coppola G, Geschwind DH, Wszolek ZK, Feldman H, Knopman DS, Petersen RC, Miller BL, Dickson DW, Boylan KB, Graff-Radford NR, Rademakers R (2011) Expanded GGGGCC hexanucleotide repeat in noncoding region of C9ORF72 causes chromosome 9p-linked FTD and ALS. Neuron 72:245–256. doi:10.1016/j.neuron.2011.09.011

Deschwanden A, Karolewicz B, Feyissa AM, Treyer V, Ametamey SM, Johayem A, Burger C, Auberson YP, Sovago J, Stockmeier CA, Buck A, Hasler G (2011) Reduced metabotropic glutamate receptor 5 density in major depression determined by [(11)C]ABP688 PET and postmortem study. Am J Psychiatry 168:727–734. doi:10.1176/appi.ajp.2011.09111607

Diehl-Schmid J, Grimmer T, Drzezga A, Bornschein S, Riemenschneider M, Förstl H, Schwaiger M, Kurz A (2007) Decline of cerebral glucose metabolism in frontotemporal dementia: a longitudinal 18F-FDG-PET-study. Neurobiol Aging 28:42–50. doi:10.1016/j.neurobiolaging.2005.11.002

Donnelly CJ, Zhang PW, Pham JT, Haeusler AR, Mistry NA, Vidensky S, Daley EL, Poth EM, Hoover B, Fines DM, Maragakis N, Tienari PJ, Petrucelli L, Traynor BJ, Wang J, Rigo F, Bennett CF, Blackshaw S, Sattler R, Rothstein JD (2013) RNA toxicity from the ALS/FTD C9ORF72 expansion is mitigated by antisense intervention. Neuron 80:415–428. doi:10.1016/j.neuron.2013.10.015

Double KL, Reyes S, Werry EL, Halliday GM (2010) Selective cell death in neurodegeneration: why are some neurons spared in vulnerable regions? Prog Neurobiol 92:316–329. doi:10.1016/j.pneurobio.2010.06.001

Elmenhorst D, Biagini M, Minuzzi L, Aliaga A, Massarweh G, Diksic M, Avoli M, Bauer A, Rosa-Neto P (2009) Evaluation of reference models for [11C]ABP688 targeting the metabotropic glutamate receptor 5 in rats-application to an epilepsy model. J Cerebr Blood Flow Metab 29:S71–S72

Elmenhorst D, Minuzzi L, Aliaga A, Rowley J, Massarweh G, Diksic M, Bauer A, Rosa-Neto P (2010) In vivo and in vitro validation of reference tissue models for the mGluR(5) ligand [(11)C]ABP688. J Cereb Blood Flow Metab 30:1538–1549. doi:10.1038/jcbfm.2010.65

Ferraguti F, Shigemoto R (2006) Metabotropic glutamate receptors. Cell Tissue Res 326:483–504. doi:10.1007/s00441-006-0266-5

Ferrer I (1999) Neurons and their dendrites in frontotemporal dementia. Dement Geriatr Cogn Disord 10(Suppl 1):55–60. doi:10.1159/000051214

Folstein MF, Folstein SE, McHugh PR (1975) "Mini-mental state". A practical method for grading the cognitive state of patients for the clinician. J Psychiatr Res 12:189–198

Fonov VS, Evans AC, McKinstry RC, Almli CR, Collins DL (2009) Unbiased nonlinear average age-appropriate brain templates from birth to adulthood. NeuroImage 47:S102. doi:10.1016/S1053-8119(09)70884-5

Francis PT (2003) Glutamatergic systems in Alzheimer's disease. Int J Geriatr Psychiatry 18:S15–S21. doi:10.1002/gps.934

Francis PT (2009) Altered glutamate neurotransmission and behaviour in dementia: evidence from studies of memantine. Curr Mol Pharmacol 2:77–82

Goetz CG, Fahn S, Martinez-Martin P, Poewe W, Sampaio C, Stebbins GT, Stern MB, Tilley BC, Dodel R, Dubois B, Holloway R, Jankovic J, Kulisevsky J, Lang AE, Lees A, Leurgans S, LeWitt PA, Nyenhuis D, Olanow CW, Rascol O, Schrag A, Teresi JA, Van Hilten JJ, LaPelle N (2007) Movement Disorder Society-sponsored revision of the Unified Parkinson's Disease Rating Scale (MDS-UPDRS): process, format, and clinimetric testing plan. Mov Disord 22:41–47. doi:10.1002/mds.21198

Good CD, Scahill RI, Fox NC, Ashburner J, Friston KJ, Chan D, Crum WR, Rossor MN, Frackowiak RS (2002) Automatic differentiation of anatomical patterns in the human brain: validation with studies of degenerative dementias. Neuroimage 17:29–46

Greve DN, Svarer C, Fisher PM, Feng L, Hansen AE, Baare W, Rosen B, Fischl B, Knudsen GM (2014) Cortical surface-based analysis reduces bias and variance in kinetic modeling of brain PET data. Neuroimage 92:225–236. doi:10.1016/j.neuroimage.2013.12.021

Gunn RN, Lammertsma AA, Hume SP, Cunningham VJ (1997) Parametric imaging of ligand-receptor binding in PET using a simplified reference region model. Neuroimage 6:279–287. doi:10.1006/nimg.1997.0303

Harkany T, Abrahám I, Timmerman W, Laskay G, Tóth B, Sasvári M, Kónya C, Sebens JB, Korf J, Nyakas C, Zarándi M, Soós K, Penke B, Luiten PG (2000) beta-amyloid neurotoxicity is mediated by a glutamate-triggered excitotoxic cascade in rat nucleus basalis. Eur J Neurosci 12:2735–2745

Hornberger M, Wong S, Tan R, Irish M, Piguet O, Kril J, Hodges JR, Halliday G (2012) In vivo and post-mortem memory circuit integrity in frontotemporal dementia and Alzheimer's disease. Brain 135:3015–3025. doi:10.1093/brain/aws239

Huber KM, Roder JC, Bear MF (2001) Chemical induction of mGluR5- and protein synthesis–dependent long-term depression in hippocampal area CA1. J Neurophysiol 86:321–325

Jeong Y, Cho SS, Park JM, Kang SJ, Lee JS, Kang E, Na DL, Kim SE (2005) 18F-FDG PET findings in frontotemporal dementia: an SPM analysis of 29 patients. J Nucl Med 46:233–239

Kertesz A, Davidson W, Fox H (1997) Frontal behavioral inventory: diagnostic criteria for frontal lobe dementia. Can J Neurol Sci 24:29–36

Kipps CM, Davies RR, Mitchell J, Kril JJ, Halliday GM, Hodges JR (2007) Clinical significance of lobar atrophy in frontotemporal dementia: application of an MRI visual rating scale. Dement Geriatr Cogn Disord 23:334–342. doi:10.1159/000100973

Lerch J (2006) Voxel-wise morphometry using RMINC. http://www.bic.mni.mcgill.ca/~samir/Brain_imaging/RMINC.pdf. Accessed 15 July 2014

Llansola M, Felipo V (2010) Metabotropic glutamate receptor 5, but not 1, modulates NMDA receptor-mediated activation of neuronal nitric oxide synthase. Neurochem Int 56:535–545. doi:10.1016/j.neuint.2009.12.016

Mackenzie IR, Neumann M, Bigio EH, Cairns NJ, Alafuzoff I, Kril J, Kovacs GG, Ghetti B, Halliday G, Holm IE, Ince PG, Kamphorst W, Revesz T, Rozemuller AJ, Kumar-Singh S, Akiyama H, Baborie A, Spina S, Dickson DW, Trojanowski JQ, Mann DM (2010) Nomenclature and nosology for neuropathologic subtypes of frontotemporal lobar degeneration: an update. Acta Neuropathol 119:1–4. doi:10.1007/s00401-009-0612-2

Mackenzie IR, Munoz DG, Kusaka H, Yokota O, Ishihara K, Roeber S, Kretzschmar HA, Cairns NJ, Neumann M (2011) Distinct pathological subtypes of FTLD-FUS. Acta Neuropathol 121:207–218. doi:10.1007/s00401-010-0764-0

McCrimmon AW, Smith AD (2013) Test Review: review of the Wechsler Abbreviated Scale of Intelligence, Second Edition (WASI-II). J Psychoeduc Assess 31:337–341. doi:10.1177/0734282912467756

Mendez MF, Lauterbach EC, Sampson SM, ANPA Committee on Research (2008) An evidence-based review of the psychopathology of frontotemporal dementia: a report of the ANPA Committee on Research. J Neuropsychiatry Clin Neurosci 20:130–149. doi:10.1176/appi.neuropsych.20.2.130

Minuzzi L, Diksic M, Gauthier S, Quirion R, Rosa-Neto P (2009) In vitro quantification of mGluR5 in pons and cerebellum of human brain using [H-3]ABP688. J Cerebr Blood F Met 29:S368–S369

Muller-Gartner HW, Links JM, Prince JL, Bryan RN, McVeigh E, Leal JP, Davatzikos C, Frost JJ (1992) Measurement of radiotracer concentration in brain gray matter using positron emission tomography: MRI-based correction for partial volume effects. J Cereb Blood Flow Metab 12:571–583. doi:10.1038/jcbfm.1992.81

Narendran R, Hwang DR, Slifstein M, Talbot PS, Erritzoe D, Huang Y (2004) In vivo vulnerability to competition by dopamine: comparison of the D2 receptor agonist radiotracer (−)-*N*-[11C]propyl-norapomorphine ([11C]NPA) with the D2 receptor antagonist radiotracer [11C]-raclopride. Synapse 52:188–208. doi:10.1002/syn.20013

Natarajan MK, Paul N, Mercuri M, Waller EJ, Leipsic J, Traboulsi M, Banijamali HS, Benson L, Sheth TN, Secondary Panel: Simpson CS, Brydie A, Love MP, Gallo R, Canadian Cardiovascular Society (2013) Canadian Cardiovascular Society position statement on radiation exposure from cardiac imaging and interventional procedures. Can J Cardiol 29:1361–1368. doi:10.1016/j.cjca.2013.06.002

Nilsen LH, Rae C, Ittner LM, Gotz J, Sonnewald U (2013) Glutamate metabolism is impaired in transgenic mice with tau hyperphosphorylation. J Cereb Blood Flow Metab 33:684–691. doi:10.1038/jcbfm.2012.212

Niswender CM, Conn PJ (2010) Metabotropic glutamate receptors: physiology, pharmacology, and disease. Annu Rev Pharmacol Toxicol 50:295–322. doi:10.1146/annurev.pharmtox.011008.145533

Pan PL, Song W, Yang J, Huang R, Chen K, Gong QY, Zhong JG, Shi HC, Shang HF (2012) Gray matter atrophy in behavioral variant frontotemporal dementia: a meta-analysis of voxel-based morphometry studies. Dement Geriatr Cogn Disord 33:141–148. doi:10.1159/000338176

Perroy J, Raynaud F, Homburger V, Rousset MC, Telley L, Bockaert J, Fagni L (2008) Direct interaction enables cross-talk between ionotropic and group I metabotropic glutamate receptors. J Biol Chem 283:6799–6805. doi:10.1074/jbc.M705661200

Poljansky S, Ibach B, Hirschberger B, Manner P, Klunemann H, Hajak G, Marienhagen J (2011) A visual [18F]FDG-PET rating scale for the differential diagnosis of frontotemporal lobar degeneration. Eur Arch Psychiatry Clin Neurosci 261:433–446. doi:10.1007/s00406-010-0184-0

Procter AW, Qurne M, Francis PT (1999) Neurochemical features of frontotemporal dementia. Dement Geriatr Cogn Disord 10(Suppl 1):80–84. doi:10.1159/000051219

Quarantelli M, Berkouk K, Prinster A, Landeau B, Svarer C, Balkay L, Alfano B, Brunetti A, Baron JC, Salvatore M (2004) Integrated software for the analysis of brain PET/SPECT studies with partial-volume-effect correction. J Nucl Med 45:192–201

Rao VL, Bowen KK, Dempsey RJ (2001) Transient focal cerebral ischemia down-regulates glutamate transporters GLT-1 and EAAC1 expression in rat brain. Neurochem Res 26:497–502

Rascovsky K, Hodges JR, Knopman D, Mendez MF, Kramer JH, Neuhaus J, van Swieten JC, Seelaar H, Dopper EG, Onyike CU, Hillis AE, Josephs KA, Boeve BF, Kertesz A, Seeley WW, Rankin KP, Johnson JK, Gorno-Tempini ML, Rosen H, Prioleau-Latham CE, Lee A, Kipps CM, Lillo P, Piguet O, Rohrer JD, Rossor MN, Warren JD, Fox NC, Galasko D, Salmon DP, Black SE, Mesulam M, Weintraub S, Dickerson BC, Diehl-Schmid J, Pasquier F, Deramecourt V, Lebert F, Pijnenburg Y, Chow TW, Manes F, Grafman J, Cappa SF, Freedman M, Grossman M, Miller BL (2011) Sensitivity of revised diagnostic criteria for the behavioural variant of frontotemporal dementia. Brain 134:2456–2477. doi:10.1093/brain/awr179

Ratnavalli E, Brayne C, Dawson K, Hodges JR (2002) The prevalence of frontotemporal dementia. Neurology 58:1615–1621

Renton AE, Majounie E, Waite A, Simón-Sánchez J, Rollinson S, Gibbs JR, Schymick JC, Laaksovirta H, van Swieten JC, Myllykangas L, Kalimo H, Paetau A, Abramzon Y, Remes AM, Kaganovich A, Scholz SW, Duckworth J, Ding J, Harmer DW, Hernandez DG, Johnson JO, Mok K, Ryten M, Trabzuni D, Guerreiro RJ, Orrell RW, Neal J, Murray A, Pearson J, Jansen IE, Sondervan D, Seelaar H, Blake D, Young K, Halliwell N, Callister JB, Toulson G, Richardson A, Gerhard A, Snowden J, Mann D, Neary D, Nalls MA, Peuralinna T, Jansson L, Isoviita VM, Kaivorinne AL, Hölttä-Vuori M, Ikonen E, Sulkava R, Benatar M, Wuu J, Chiò A, Restagno G, Borghero G, Sabatelli M, ITALSGEN Consortium, Heckerman D, Rogaeva E, Zinman L, Rothstein JD, Sendtner M, Drepper C, Eichler EE, Alkan C, Abdullaev Z, Pack SD, Dutra A, Pak E, Hardy J, Singleton A, Williams NM, Heutink P, Pickering-Brown S, Morris HR, Tienari PJ, Traynor BJ (2011) A hexanucleotide repeat expansion in C9ORF72 is the cause of chromosome 9p21-linked ALS-FTD. Neuron 72:257–268. doi:10.1016/j.neuron.2011.09.010

Roman GC, Tatemichi TK, Erkinjuntti T, Cummings JL, Masdeu JC, Garcia JH, Amaducci L, Orgogozo JM, Brun A, Hofman A, Moody DM, O'Brien MD, Yamaguchi T, Grafman J, Drayer BP, Bennett DA, Fisher M, Ogata J, Kokmen E, Bermejo F, Wolf PA, Gorelick PB, Bick KL, Pajeau AK, Bell MA, DeCarli C, Culebras A, Korczyn AD, Bogousslavsky J, Hartmann A, Scheinberg P (1993) Vascular dementia: diagnostic criteria for research studies. Report of the NINDS-AIREN International Workshop. Neurology 43:250–260

Romano C, Yang WL, O'Malley KL (1996) Metabotropic glutamate receptor 5 is a disulfide-linked dimer. J Biol Chem 271:28612–28616

Rothstein JD (1996) Excitotoxicity hypothesis. Neurology 47:S19–S26

Rousset OG, Ma Y, Evans AC (1998) Correction for partial volume effects in PET: principle and validation. J Nucl Med 39:904–911

Rousset O, Rahmim A, Alavi A, Zaidi H (2007) Partial volume correction strategies in PET. PET Clin 2:235–249

Rosso SM, Donker Kaat L, Baks T, Joosse M, de Koning I, Pijnenburg Y, de Jong D, Dooijes D, Kamphorst W, Ravid R, Niermeijer MF, Verheij F, Kremer HP, Scheltens P, van Duijn

CM, Heutink P, van Swieten JC (2003) Frontotemporal dementia in The Netherlands: patient characteristics and prevalence estimates from a population-based study. Brain 126:2016–2022. doi:10.1093/brain/awg204

Schaeffer E, Duplantier A (2010) Glutamate and Neurodegenerative Disease. In: Dominguez C (ed) Neurodegenerative Diseases. Springer-Verlag, Berlin, Heidelberg, pp 91–147

Seneca N, Finnema SJ, Farde L, Gulyas B, Wikstrom HV, Halldin C, Innis RB (2006) Effect of amphetamine on dopamine D2 receptor binding in nonhuman primate brain: a comparison of the agonist radioligand [11C]MNPA and antagonist [11C]raclopride. Synapse 59:260–269. doi:10.1002/syn.20238

Sled JGZA, Evans AC (1998) A nonparametric method for automatic correction of intensity nonuniformity in MRI data. IEEE Trans Med Imaging 17:87–97

Swartz JR, Miller BL, Lesser IM, Booth R, Darby A, Wohl M, Benson DF (1997) Behavioral phenomenology in Alzheimer's disease, frontotemporal dementia, and late-life depression: a retrospective analysis. J Geriatr Psychiatry Neurol 10:67–74

Swarup V, Phaneuf D, Dupre N, Petri S, Strong M, Kriz J, Julien JP (2011) Deregulation of TDP-43 in amyotrophic lateral sclerosis triggers nuclear factor kappaB-mediated pathogenic pathways. J Exp Med 208:2429–2447. doi:10.1084/jem.20111313

Wilson AA, McCormick P, Kapur S, Willeit M, Garcia A, Hussey D, Houle S, Seeman P, Ginovart N (2005) Radiosynthesis and evaluation of [11C]-(+)-4-propyl-3,4,4a,5,6,10b-hexahydro-2H-naphtho[1,2-b][1,4]oxazin-9-ol as a potential radiotracer for in vivo imaging of the dopamine D2 high-affinity state with positron emission tomography. J Med Chem 48:4153–4160. doi:10.1021/jm050155n

Worsley KJ, Cao J, Paus T, Petrides M, Evans AC (1998) Applications of random field theory to functional connectivity. Hum Brain Mapp 6:364–367

Zijdenbos AFR, Evans AC (1998) Automatic quantification of MS lesions in 3D MRI brain data sets: validation of INSECT. In: Wells M, Colchester A, Delp S (eds) Lecture Notes in Computer Science. Springer, Berlin, Heidelberg, New York, pp 438–448

ANEXO II: Artigos publicados durante o período de doutoramento cujos temas não se relacionam diretamente a esta tese.

ANEXO II-A. *Long-Term Oral Administration of Capsicum baccatum Extracts Does Not Alter Behavioral, Hematological, and Metabolic Parameters in CF1 Mice.*

No **ANEXO II-A** apresentamos o artigo publicado no periódico *Evidence-Based Complementary and Alternative Medicine.*

Hindawi Publishing Corporation
Evidence-Based Complementary and Alternative Medicine
Volume 2012, Article ID 196358, 9 pages
doi:10.1155/2012/196358

Research Article

Long-Term Oral Administration of *Capsicum baccatum* Extracts Does Not Alter Behavioral, Hematological, and Metabolic Parameters in CF1 Mice

Aline Rigon Zimmer,[1] Bianca Leonardi,[1] Eduardo Rigon Zimmer,[2] Eduardo Kalinine,[2] Diogo Onofre de Souza,[2] Luis Valmor Portela,[2] and Grace Gosmann[1]

[1] *Pharmaceutical Sciences Graduate Program, Faculty of Pharmacy, Federal University of Rio Grande do Sul (UFRGS), Ipiranga Avendia 2752, 90610-000 Porto Alegre, RS, Brazil*
[2] *Post-Graduate Program in Biological Science, Department of Biochemistry, ICBS, Federal University of Rio Grande do Sul (UFRGS), Ramiro Barcelos Street 2600, 90035-003 Porto Alegre, RS, Brazil*

Correspondence should be addressed to Luis Valmor Portela, roskaportela@gmail.com and Grace Gosmann, grace.gosmann@ufrgs.br

Received 13 August 2012; Revised 20 November 2012; Accepted 21 November 2012

Academic Editor: Jenny M. Wilkinson

Copyright © 2012 Aline Rigon Zimmer et al. This is an open access article distributed under the Creative Commons Attribution License, which permits unrestricted use, distribution, and reproduction in any medium, provided the original work is properly cited.

Our group showed that crude ethanol (CE) and butanol (BUT) extracts of *Capsicum baccatum* presented anti-inflammatory and antioxidant properties. Furthermore, the flavonoid and total phenolic contents were positively correlated with both of these properties observed for *C. baccatum* extracts. The present study demonstrated that 60 days of oral administration of CE and BUT (200 mg/kg) in mice did not cause significant differences in the following parameters evaluated: hematological profile, body weight and relative weight of visceral organs, systemic lipid profile, glucose homeostasis (GTT), kidney and hepatic biochemical markers, and spontaneous locomotion and anxiety-like behavior. Altogether, these results indicate for the first time that the long-term oral administration of *C. baccatum* extracts does not affect specific aspects of CF1 mice physiology, suggesting their safety, building up the venue to test their efficacy in animal models underlying persistent activation of oxidative and inflammatory pathways.

1. Introduction

Capsicum species, from Solanaceae family, are native to the tropical and humid zones of central and south America and include peppers of significant economic value and potential pharmacological application. The fruits vary widely in size, shape, flavor, and sensory heat. The five main species in the genus are *C. annuum*, *C. baccatum, C. chinense*, *C. frutescens,* and *C. pubescens*. These peppers are widely used as spices in the food industry and in a broad variety of medicinal applications worldwide [1, 2].

Capsicum annuum, *C. chinense,* and *C. frutescens* are remarkable sources of antioxidant compounds, including capsaicinoids [3, 4] and phenolic compounds, particularly flavonoids [5]. The consumption of these components has potential health benefits due to their activity as free-radical scavengers, which may help prevent inflammatory diseases and pathologies associated with oxidative damage, such as atherosclerosis and Alzheimer's disease [6–8]. These *Capsicum* species exert anti-inflammatory, antioxidant, antiplatelet, antihypertensive, hypoglycemic, and hypocholesterolemic properties *in vitro* and *in vivo* models [8–13]. The main pungent component, capsaicin, has been used clinically for its analgesic and anti-inflammatory properties [14, 15].

The red pepper *C. baccatum* var. *pendulum* is widely consumed in food preparations. Reports about the chemical composition of this species are very scarce, especially for this variety. Although the potential pharmacological properties of *C. baccatum* have been also less explored, there are some studies that suggest antioxidant and anti-inflammatory activities of the crude juice [16–18]. A crude juice of

C. baccatum fruit presented anti-inflammatory effects in a pleurisy model when 2 and 20 g/kg were administered via i.p. and s.c. to rats [19]. In a recent study, we prepared a crude ethanol extract (CE) of *C. baccatum* fruit and, after fractionation, a butanol extract (BUT) enriched in bioactive substances was obtained [20]. We showed that the oral acute administration of 200 mg/kg of BUT extract exhibited the highest antioxidant and anti-inflammatory activities in mice and this extract did not contain capsaicin by HPLC analysis. Furthermore, the flavonoid and total phenolic contents were positively correlated with the antioxidant and anti-inflammatory properties observed for CE and BUT [20]. Although the use of plant extracts as an alternative to conventional medications is widespread, the safety of the extracts needs to be determined before human use [21]. As in this case the constituent concentration intake of these enriched extracts is significantly higher than in the fruit, and considering their potential pharmacological properties previously described, it is relevant to evaluate their long-term oral administration adverse effects. Accordingly, in this study we evaluated the effects of *Capsicum baccatum* extracts on behavioral, hematological, and metabolic parameters of mice.

2. Materials and Methods

2.1. Plant Material and Extraction. *Capsicum baccatum* var. *pendulum* (Willd.) Eshbaugh (Solanaceae) fruit was obtained from a cultivated area in the city of Turuçu, Rio Grande do Sul, Brazil. This plant was certified by the Germoplasm Bank of the Brazilian Government Research Institute EMBRAPA (Empresa Brasileira de Pesquisa Agropecuária, Pelotas, RS, Brazil) which maintains botanical and chemical uniformity. A voucher specimen (number P278) was identified and deposited at the Herbarium of the Brazilian Government Research Institute EMBRAPA. The fruit of red pepper was dried in a circulating air stove (40°C) and triturated to powder. The fruit was extracted with 70% ethanol (plant : solvent, 1 : 10, w/v) under reflux for 4 hours to obtain the crude ethanol extract (CE). Then the fruit was also submitted to successive extractions in a soxhlet apparatus in order to obtain the dichloromethane, butanol (BUT), and aqueous dried extracts as described previously [20].

2.2. Phytochemical Study. The ethanol and butanol extracts were characterized according to the previous studies [20] as follows: the characterization of the phenolic compounds (quercetin and rutin) and capsaicin in *C. baccatum* was performed by HPLC on Agilent instrument (serie 1200) equipped with photodiode array detector (G1322A), autosampler (G1329A), and Agilent ChemStation software. An Ace RP-18 column (250 mm × 4.0 mm i.d., particle size 5 μm) and a linear gradient starting from methanol : acetonitrile : water (15 : 15 : 70) then changed to methanol : acetonitrile : water (30 : 30 : 40) over 25 min, were used. Capsaicin was determined at 280 nm and rutin and quercetin at 254 nm. The total phenolic content was estimated using the Folin-Ciocalteu method customized for 96-well microplates. Gallic acid was used to obtain the calibration curve, and the results were expressed as milligrams of gallic acid equivalents per gram of dried extract (GAE/g). The total content of flavonoids was determined by the $AlCl_3$ colorimetric method, using quercetin as standard. Results were expressed as milligrams of quercetin equivalents per gram of dried extract (QE/g).

2.3. Animals. Adult 2-month-old CF1 male mice weighing 25–35 g were used. The animals were maintained under controlled temperature (22 ± 2°C) and humidity (55% ± 10%) conditions on a 12 h light-dark cycle (7 : 00 AM and 7 : 00 PM) with free access to standard commercial diet and distilled water. To avoid social isolation two animals were maintained per cage [22]. All experiments complied with the international standards for animal protection and those of the Brazilian College of Animal Experimentation. The Ethical Committee on animal use of the Universidade Federal do Rio Grande do Sul, Brazil, approved all experiments (number 19446).

2.4. Experimental Design. The animals were randomized into three groups of 10 animals: distilled water (control group), ethanol extract (CE), and butanol extract (BUT). *C. baccatum* extracts (200 mg/kg body weight) were administered daily by gavage for 60 days. The extracts and dose of 200 mg/kg were selected considering that they presented the higher antioxidant and anti-inflammatory activities in our previous study [20]. Clinical signs of toxicity, general appearance, and mortality were monitored daily during the experimental period. Mean body weight gain and food intake were calculated and compared among groups. Body weights were recorded weekly throughout the study period. Mean daily food consumption was calculated twice per week by subtracting the weight of the remaining food from the weight of the supplied food. All behavioral tasks were performed between 1 : 00 PM and 5 : 00 PM Twenty-four hours after the behavioral tasks, the animals were anesthetized (ketamine:xylazine, 100 : 10 mg/kg, i.p.) to blood sampling for hematological and biochemical analysis. After that, animals were quickly sacrificed, dissected, and subjected to necropsy examination.

2.5. Open Field Task. The open field task is a widely used model for the evaluation of spontaneous locomotion and exploratory activities, as well as indicator of anxiety-like behavior [23]. The apparatus was a black-painted box (50 × 50 cm) surrounded by 50 cm high walls. The experiments were conducted in a quiet room under low-intensity light (12 lx). On the 59th day of administration, each mouse was placed in the center of the arena, and the distance travelled (total and central zone), time spent in the central zone, and mean speed were measured for 10 min. To analyze anxiety-like behavior, we created a virtual central zone (30 × 30 cm) using the analysis software and the time in the central zone was used as an indicator of anxiety-like behavior [24]. A video camera positioned above the arena was used to record all experimental sessions. The analysis was performed using

a computer-operated tracking system (ANY-maze, Stoelting, Woods Dale, IL).

2.6. Elevated Plus-Maze Task. The elevated plus-maze task measures anxiety-like behavior in rodents and was performed as previously described [25]. The apparatus was made of wood and consisted of four elevated arms (70 cm from the floor × 30 cm long × 5 cm wide) arranged in cross-like disposition and separated by a central zone (5 cm long × 5 cm wide). Two opposite arms were enclosed by 10 cm high walls, with an open roof, and the other two were open (no walls). The experiments were conducted in a sound-attenuated and temperature-controlled room under dim red light illumination. On the 60th day of administration, each mouse was placed individually on the central zone of the plus-maze facing one of the open arms (no walls) and recorded with a video camera for 5 min. The time spent in the open and closed arms, the number of entries into the arms, the total distance travelled, and the mean speed were analyzed. The time spent in open arms was considered a measurement of anxiety-like behavior. The analysis was performed using a computer-operated tracking system (ANY-maze, Stoelting, Woods Dale, IL).

2.7. Pathological Examination. All animals were firstly subjected to necropsy by examination of macroscopic external aspect of organs. Then mice were quickly dissected, and the stomach, liver, brain, heart, lung, and kidneys were excised and weighted individually. Fat tissues from the retroperitoneal and epididymal regions were dissected and weighed as previously described [26]. Organ/tissue absolute weight was compared with the final body weight of each mouse on the day of sacrifice to determine the relative organ/tissue weight (absolute organ/tissue weight (g) × 100/animal body weight (g)).

2.8. Hematological and Biochemical Analysis. The following hematological parameters were determined by using a semiautomatic blood analyzer (MS4, USA): hemoglobin (Hb), red blood cell (RBC) count, hematocrit (HCT), white blood cell (WBC) count, mean corpuscular volume (MCV), mean corpuscular hemoglobin (MCH), and mean corpuscular hemoglobin concentration (MCHC). For biochemical determinations, these were evaluated: total cholesterol, HDL-cholesterol, LDL-cholesterol, triglycerides, total protein, albumin, alanine aminotransferase (ALT), alkaline phosphatase (ALP), lactate dehydrogenase (LDH), creatinine, and urea. Glucose homeostasis was determined using the glucose tolerance test (GGT), which was performed five days prior to animal sacrifice to avoid metabolic and behavioral alterations. A glucose solution (2 mg/g i.p.) was injected into mice fasted for 12 h, and blood was collected from a small puncture on the tail at 0, 30, 60, and 120 min after injection. Blood glucose level was measured with glucometer (AccuChek Active, Roche Diagnostics, USA), and the area under the curve was used to compare the glucose tolerance among groups [7]. All biochemical determinations were performed using commercial kits (Labtest, MG, Brazil) in a Spectramax M5 (Molecular Devices, USA).

2.9. Statistical Analysis. Statistical analysis was performed using a one-way analysis of variance (ANOVA) followed by a Bonferroni test for multiple comparisons. We used the Software GraphPad Prism 5.0 for this analysis. The results are expressed as the mean ± standard error of mean (SEM). Differences were considered significant at $P < 0.05$.

3. Results

3.1. Phytochemical Study. The total phenolic content of *C. baccatum* was the same in CE and in BUT extracts, 180.08 ± 3.76 mg and 187.51 ± 2.34 mg GAE/g, respectively ($P > 0.05$). In contrast, the flavonoid contents present in BUT extract (54.68 ± 2.92 mg of QE/g) were significantly higher compared to CE extract (34.36 ± 4.04 mg QE/g) ($P < 0.05$). HPLC analysis did not identify the presence of flavonoids quercetin and rutin in any samples obtained from *C. baccatum* (Figure 1(b)). Furthermore, capsaicin was not detected in BUT extract (Figure 1(a)) [20].

3.2. Open Field Task. After the long-term administration of 200 mg/kg of CE and BUT there were no statistical differences among the groups in distance traveled (Figure 2(a)), mean speed (Figure 2(b)), time spent in the central zone (Figure 2(c)), and total distance travelled in central zone (Figure 2(d)). The representative occupancy plots (Figure 2(e)) illustrated a similar exploratory behavior profile among groups during 10 min recording.

3.3. Elevated Plus-Maze Task. There were no differences among groups in mean speed (Figure 3(a)), total distance travelled (Figure 3(b)), time spent in open arms (Figure 3(c)), closed arms (Figure 3(d)), and entries in open arms (Figure 3(e)) and in closed arms (Figure 3(f)). The representative occupancy plots (Figure 3(g)) illustrated a similar occupancy profile of the central zone and open and closed arms of the plus-maze apparatus among groups. These results reinforced the data obtained in the open field task (Figure 2) in which CE and BUT did not cause anxiety-like behavior.

3.4. Oral Toxicity Study. After 60 days of treatment, no clinical signs of toxicity, including hair loss, piloerection, changes in skin, eyes, or oral mucosa, or death, were observed in both treated groups. All animals appeared healthy at the end of the experiment. Visceral examinations of the control and treated mice revealed no visible lesions. There was no accumulation of the extracts, signs of hyperemia, or ulcerations in the gastric mucosa. The body weight increase throughout the administration period was similar in all groups (Figure 4). In addition, there was no statistical difference among groups in final mean body weight and food intake during the administration period. Furthermore, no significant alterations in the relative weights of the kidney, heart, brain, lung, stomach, or epididymal and

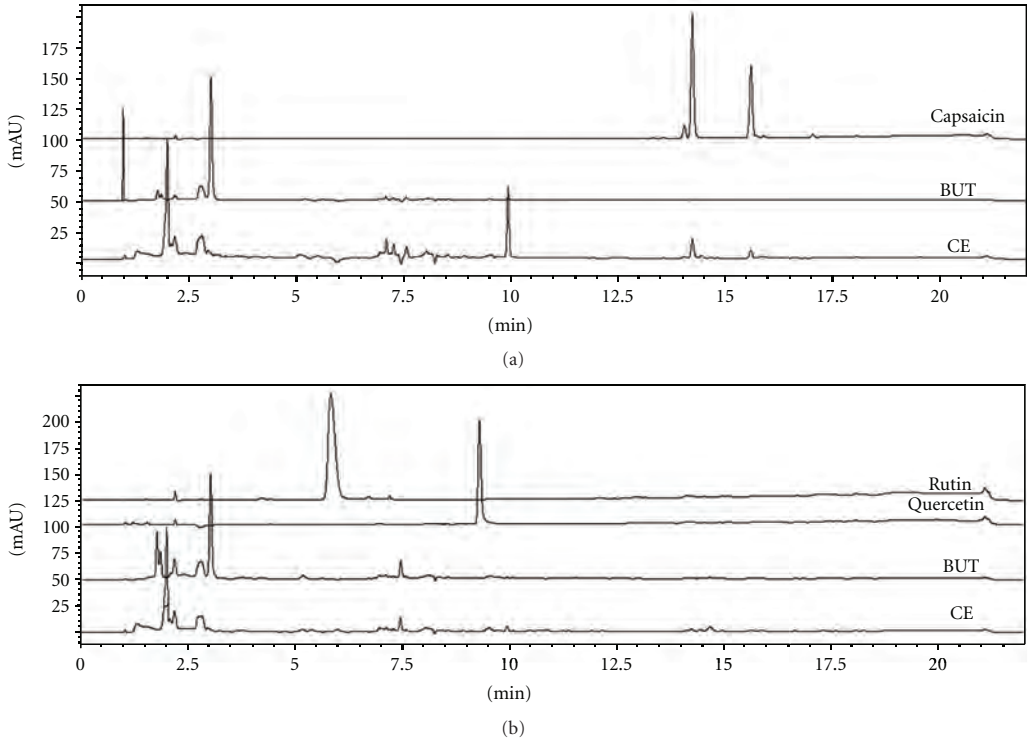

Figure 1: HPLC chromatograms of CE and BUT extracts of *C. baccatum*: (a) detection at 280 nm to capsaicin (Rt = 14.20 min); (b) detection at 254 nm to rutin and quercetin (Rt: 5.80 and 9.26 min, resp.). CE: crude ethanol extract; BUT: butanol extract.

retroperitoneal fat pads were observed among treated and control groups (Table 1). There was a reduction in the relative liver weight in animals that received CE extract; however at macroscopic examination we did not visualize signs of lesion.

3.5. Hematological and Biochemical Parameters. There were no significant differences among groups in hematological parameters analyzed: hemoglobin, red blood cells count, hematocrit, MCV, MCH, MCHC, WBC count, lymphocyte, and neutrophils content (Table 2). Furthermore, there was no significant difference among groups in biochemical parameters analyzed: ALT, ALP, total proteins and albumin, LDH, triglycerides, cholesterol, HDL and LDL, urea, and creatinine (Table 3) at the end of the experiment. Moreover, extracts administration did not cause alterations in glucose tolerance test (Figure 5, $P > 0.05$).

4. Discussion

The red pepper *C. baccatum* is widely used as spice and the few studies on its pharmacological activities were performed using crude extract or juice [16–19]. Previously our group demonstrated that CE and the enriched BUT extract showed the high antioxidant and anti-inflammatory activities. These latter extracts presented higher total phenolic and flavonoid contents than other *Capsicum* species, whose compounds were considered the main responsible for the antioxidant and anti-inflammatory properties imparted to *C. baccatum*. Another relevant issue raised by the former work revealed that BUT extract does not contain capsaicin, one component of other *Capsicum* species associated to anti-inflammatory activity. However, even without detectable presence of capsaicin in BUT, it still maintains significant anti-inflammatory effect. This latter extract represents a new potential therapeutic opportunity to identify novel, more effective, and safety components. Herein, CE and BUT at the daily dose of 200 mg/kg were chosen for investigating their effects on baseline aspects of mice physiology, considering their pharmacological activities described previously [20].

The present study demonstrated that long-term oral administration of CE and BUT had no negative effects on hematologic, metabolic, and behavioral outcomes in normal male CF1 mice. Some features in the normal physiology of rodents resemble to humans and can be used to understand the response to toxic/therapeutic agents, diseases, and pharmacological strategies. Usually mice show a high degree of exploratory behavior necessary to search for food and territory dominance and establish social interactions [27]. In the open field task, CE and BUT administration did not affect total distance traveled, mean speed, time, and distance travelled in the center zone. Similarly, in the elevated plus-maze task, no differences were observed among

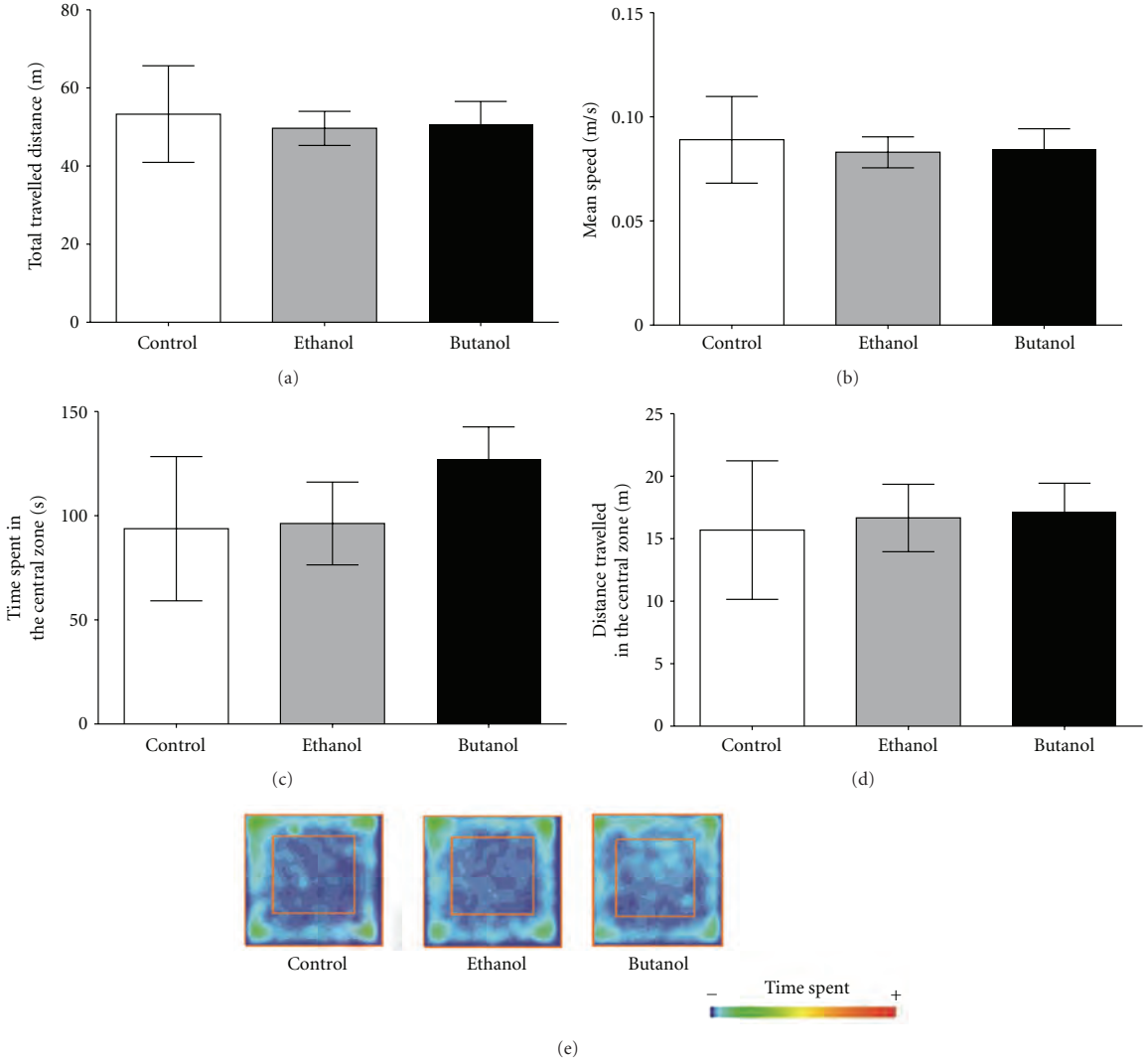

Figure 2: Open field task performed after sixty days of oral administration of *C. baccatum* extracts (200 mg/kg). Total distance travelled (a), mean speed (b), time spent in the central zone (c), and the distance travelled in the central zone of the apparatus (d). Representative occupancy plots obtained by video-tracking software (ANY-mazeH, Stoelting, CO, USA) (e). The results are presented as the mean ± SEM ($n = 10$) using one-way ANOVA. No significant differences were observed among groups.

the groups; they presented similar mean speed, total distance travelled, time spent, and number of entries in open and closed arms. Although in the plus-maze task CE group seems to spend more time in the open arms compared to other groups, the difference did not reach statistical significance. These results indicate that CE and BUT did not cause alterations in spontaneous locomotion and anxiety-like behavior, making it possible for mice to maintain social interactions and reach water and food. In accordance with this, no significant changes in food consumption, body weight gain/final weight, and mortality ratio were observed among groups. Further, during the course of administration, we did not observe mouth lesions or ulcerations caused by gavage procedures or reaction to extracts. Overall, these parameters were considered a preliminary indication that mice had normal absorption of nutrients, hormonal signaling, metabolic and organ-specific functions, which resulted in similar growth and development. In addition, a normal macroscopic appearance was noted in all organs, and there was no difference in organ/body weight among groups.

In this context, we conducted a more precise hematological, metabolic, and tissue assessments, searching for signs of undesirable effects induced by long-term administration of CE and BUT. We confirmed that biochemical profile related to lipid metabolism (serum triglycerides, total cholesterol,

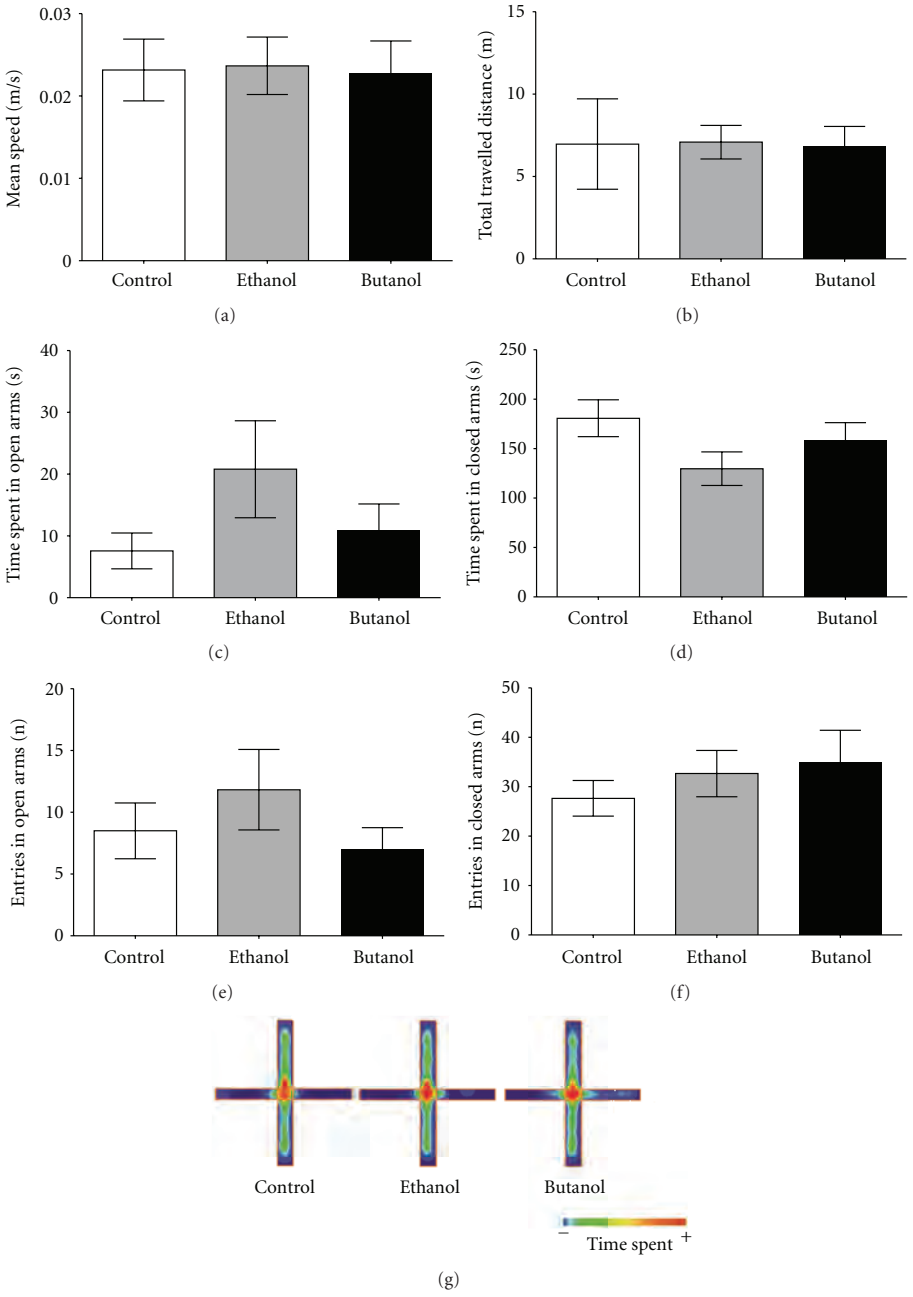

Figure 3: Elevated plus-maze task performed after the administration of *C. baccatum* extracts (200 mg/kg). Mean speed (a), total travelled distance (b), time spent in the open arms (c), time spent in the closed arms (d), number of entries into the closed arms (e), and the number of entries into the open arms (f). Representative occupancy plots obtained by video-tracking software (ANY-mazeH, Stoelting, CO, USA) (g). The results are presented as mean ± SEM ($n = 10$) after analysis by one-way ANOVA. No significant differences were observed among the groups.

Table 1: Effects of *C. baccatum* extracts on body weight (g), the relative weight of visceral organs and tissues (g/100 g b.w.), and food consumption (g/day) after a 60-day study in mice (200 mg/kg, *per os*).

Parameters	Control	Ethanol	Butanol
Initial weight (g)	33.7 ± 5.72	33.3 ± 4.03	30.7 ± 3.72
Final weight (g)	44.2 ± 4.68	43.1 ± 2.68	43.4 ± 6.63
Weight gained (g)	10.5 ± 3.63	9.8 ± 2.52	12.7 ± 3.33
Weight gained (%)	31.2	29.4	41.4
Food intake (g)/day	9.5 ± 1.9	9.0 ± 1.7	11.0 ± 2.2
Relative epididymal fat pad weight (%)	1.50 ± 0.48	1.02 ± 0.31	1.18 ± 0.34
Relative retroperitoneal fat pad weight (%)	0.50 ± 0.29	0.26 ± 0.13	0.38 ± 0.20
Relative liver weight (%)	5.52 ± 0.29	4.86 ± 0.17*	5.94 ± 0.44
Relative kidney weight (%)	1.82 ± 0.18	1.79 ± 0.15	1.78 ± 0.15
Relative heart weight (%)	0.47 ± 0.02	0.46 ± 0.05	0.45 ± 0.04
Relative brain weight (%)	1.07 ± 0.08	1.13 ± 0.04	1.08 ± 0.10
Relative lung weight (%)	0.52 ± 0.07	0.56 ± 0.04	0.63 ± 0.11
Relative stomach weight (%)	0.73 ± 0.07	0.69 ± 0.26	0.84 ± 0.15

* Significant difference compared with the control ($P < 0.05$). Values are mean ± SEM of 10 animals.

Table 2: Hematological profiles of mice following gavage administration of *C. baccatum* extracts for 60 days (200 mg/kg).

Parameters	Control	Ethanol	Butanol
Hb (g/dL)	13.1 ± 0.56	13.1 ± 0.95	13.1 ± 0.81
RBC count ($10^6/\mu$L)	8.5 ± 0.33	8.5 ± 0.43	8.3 ± 0.65
HCT (%)	40.1 ± 2.29	39.7 ± 3.53	39.1 ± 2.47
MCV (fl)	47.3 ± 1.57	46.6 ± 1.93	47.2 ± 1.82
MCH (pg)	15.5 ± 0.51	15.5 ± 0.44	15.8 ± 0.46
MCHC (g/dL)	32.9 ± 1.32	33.2 ± 0.72	33.5 ± 0.60
WBC count ($10^3/\mu$L)	6910 ± 2222.2	7818 ± 1639.2	8158 ± 2090.7
Lymphocyte (%)	74.5 ± 5.11	79.9 ± 7.06	70.3 ± 9.88
Neutrophils (%)	19.7 ± 7.0	12.2 ± 6.90	22.0 ± 7.97

Hb: hemoglobin; RBC: red blood cells; HCT: hematocrit; MCV: mean corpuscular volume; MCH: mean corpuscular hemoglobin; MCHC: Mean corpuscular hemoglobin concentration; WBC: white blood cells. No significant difference was observed among groups ($P > 0.05$). Values are mean ± SEM of 10 animals.

Table 3: Serum biochemical evaluations of mice following gavage administration of *C. baccatum* extracts for 60 days (200 mg/kg).

Parameters	Control	Ethanol	Butanol
ALT (IU/L)	29.0 ± 10.94	45.8 ± 40.52	42.2 ± 18.79
ALP (IU/L)	45.7 ± 21.74	28.5 ± 15.93	41.3 ± 14.68
Proteins (mg/dL)	4.9 ± 0.58	4.9 ± 0.42	4.8 ± 0.38
Albumin (mg/dL)	2.0 ± 0.45	2.0 ± 0.21	1.6 ± 0.38
LDH (IU/L)	150.2 ± 37.2	202.2 ± 83.93	148.0 ± 22.43
Triglycerides (mg/dL)	91.0 ± 25.63	76.4 ± 21.97	102.2 ± 31.42
Cholesterol (mg/dL)	129.5 ± 9.93	101.0 ± 13.58	119.4 ± 26.81
HDL-cholesterol (mg/dL)	63.5 ± 8.68	53.3 ± 7.69	56.7 ± 10.08
LDL-cholesterol (mg/dL)	47.8 ± 11.28	32.4 ± 11.08	42.3 ± 24.55
Glucose (mg/dL)	96.2 ± 44.45	133.5 ± 47.53	108.6 ± 34.70
Urea (mg/dL)	42.5 ± 3.15	45.6 ± 1.52	45.3 ± 12.53
Creatinine (mg/dL)	<0.20	0.20 ± 0.04	<0.20

ALT: alanine aminotransferase; ALP: alkaline phosphatase; LDH: lactate dehydrogenase. Neither of the treated groups was significantly different from the control group. Values are means ± SEM of 10 animals. No significant difference was observed among groups ($P > 0.05$).

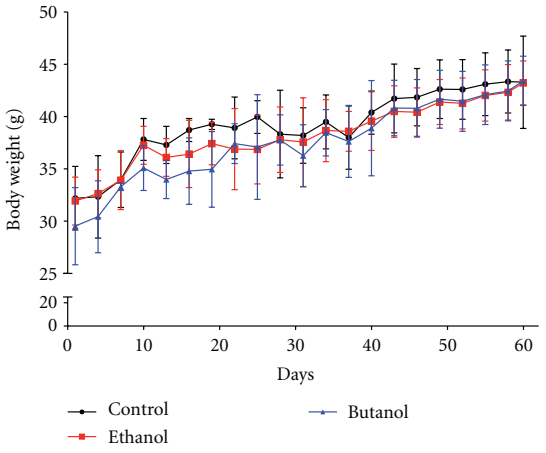

Figure 4: Growth curves of CF1 mice orally treated with *C. baccatum* extracts (200 mg/kg) during sixty days. No significant differences were observed among the groups.

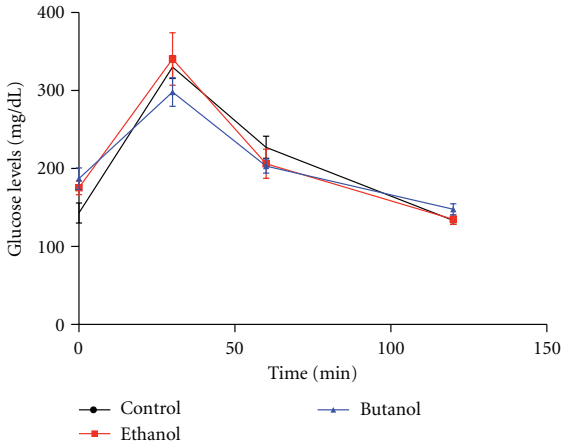

Figure 5: Glucose tolerance test: mice fasted for 8 h received glucose (2 mg/g of body weight, i.p.). Blood samples from the tail vein were taken at 0, 30, 60, and 120 min. Repeated measures of analysis of variance (ANOVA) were used to evaluate the statistical significance. The results are expressed as mean ± SEM No significant difference was observed among groups ($P > 0.05$).

HDL, and LDL-cholesterol) and glucose homeostasis (GTT) was similar among groups. There was no indication of cytotoxicity induced by the extracts on hematopoietic red and leucocytes cells. Further, under macroscopic evaluation, there was no sign of alterations in kidney and liver by CE and BUT extracts, which was confirmed by the levels of serum biochemical markers of function/damage of these organs. CE showed decreased liver weight with no significant changes in serum markers of liver damage (ALT, ALP) and functionality (total proteins, albumin, and urea) compared to other groups, which reinforces the lack of structural or functional abnormalities. However, this issue requires caution and additional examinations on liver through histochemical and immunohistochemical investigations.

This study provides evidence that sixty-days administration of *C. baccatum* extracts (CE and BUT) has a pharmacological level of safety. From these data, it is possible to envisage studies to understand its mechanism of action and obtain more data on the reproductive toxicity, genotoxicity, and carcinogenicity in order to proceed to clinical evaluation.

5. Conclusion

This work demonstrated for the first time that 60 days of oral administration of crude ethanol and butanol extracts of *C. baccatum* did not affect specific aspects of CF1 mice physiology. In fact, animals showed normal locomotor ability, blood cells counts, lipid and glucose homeostasis, as well as tissue-specific markers of functionality/damage suggesting a level of pharmacological safety. These normal outcomes build up the venue to test the effective dose of these extracts in animal models underlying persistent activation of oxidative and inflammatory pathways for a long-term period.

Conflict of Interests

The authors would like to declare that there is no conflict of interests.

Acknowledgments

The authors would like to thank Dr. Rosa LíaBarbieri, a biologist at the Brazilian Government Research Institute EMBRAPA (Empresa Brasileira de Pesquisa Agropecuária, Pelotas, RS, Brazil), for identifying the plants, and the Brazilian Government Agency CNPq (Conselho Nacional de Desenvolvimento Científico e Tecnológico, Brazil), INCT-Excitotoxicity, and Neuroprotection and IBN.Net (Brazil) for their financial support.

References

[1] V. S. Govindarajan, "*Capsicum* production, technology, chemistry, and quality. Part 1: History, botany, cultivation, and primary processing," *Critical Reviews in Food Science and Nutrition*, vol. 22, no. 2, pp. 109–176, 1985.

[2] J. Pino, M. González, L. Ceballos et al., "Characterization of total capsaicinoids, colour and volatile compounds of Habanero chilli pepper (*Capsicum chinense* Jack.) cultivars grown in Yucatan," *Food Chemistry*, vol. 104, no. 4, pp. 1682–1686, 2007.

[3] T. Ochi, Y. Takaishi, K. Kogure, and I. Yamauti, "Antioxidant activity of a new capsaicin derivative from *Capsicum annuum*," *Journal of Natural Products*, vol. 66, no. 8, pp. 1094–1096, 2003.

[4] A. Topuz and F. Ozdemir, "Assessment of carotenoids, capsaicinoids and ascorbic acid composition of some selected pepper cultivars (*Capsicum annuum* L.) grown in Turkey," *Journal of Food Composition and Analysis*, vol. 20, no. 7, pp. 596–602, 2007.

[5] M. Materska and I. Perucka, "Antioxidant activity of the main phenolic compounds isolated from hot pepper fruit (*Capsicum annuum* L.)," *Journal of Agricultural and Food Chemistry*, vol. 53, no. 5, pp. 1750–1756, 2005.

[6] F. Menichini, R. Tundis, M. Bonesi et al., "The influence of fruit ripening on the phytochemical content and biological activity of *Capsicum chinense* Jacq. cv Habanero," *Food Chemistry*, vol. 114, no. 2, pp. 553–560, 2009.

[7] A. P. Muller, J. Gnoatto, J. D. Moreira et al., "Exercise increases insulin signaling in the hippocampus: physiological effects and pharmacological impact of intracerebroventricular insulin administration in mice," *Hippocampus*, vol. 21, pp. 1082–1092, 2011.

[8] J. Barnes J, L. A. Anderson, and J. D. Phillipson, *Herbal Medicines*, Pharmaceutical Press, London, UK, 3rd edition, 2007.

[9] K. D. K. Ahuja, I. K. Robertson, D. P. Geraghty, and M. J. Ball, "The effect of 4-week chilli supplementation on metabolic and arterial function in humans," *European Journal of Clinical Nutrition*, vol. 61, no. 3, pp. 326–333, 2007.

[10] K. Aizawa and T. Inakuma, "Dietary capsanthin, the main carotenoid in paprika (*Capsicum annuum*), alters plasma high-density lipoprotein-cholesterol levels and hepatic gene expression in rats," *British Journal of Nutrition*, vol. 102, no. 12, pp. 1760–1766, 2009.

[11] Y. Liu and M. G. Nair, "Capsaicinoids in the hottest pepper Bhut Jolokia and its antioxidant and antiinflammatory activities," *Natural Product Communications*, vol. 5, no. 1, pp. 91–94, 2010.

[12] L. G. Ranilla, Y. I. Kwon, E. Apostolidis, and K. Shetty, "Phenolic compounds, antioxidant activity and in vitro inhibitory potential against key enzymes relevant for hyperglycemia and hypertension of commonly used medicinal plants, herbs and spices in Latin America," *Bioresource Technology*, vol. 101, no. 12, pp. 4676–4689, 2010.

[13] K. Srinivasan, "Spices as influencers of body metabolism: an overview of three decades of research," *Food Research International*, vol. 38, no. 1, pp. 77–86, 2005.

[14] R. D. Altman and H. R. Barthel, "Topical therapies for osteoarthritis," *Drugs*, vol. 71, no. 10, pp. 1259–1279, 2011.

[15] P. Donofrio, F. Walker, V. Hunt et al., "Treatment of painful diabetic neuropathy with topical capsaicin: a multicenter, double-blind, vehicle-controlled study," *Archives of Internal Medicine*, vol. 151, no. 11, pp. 2225–2229, 1991.

[16] V. D. Kappel, G. M. Costa, G. Scola et al., "Phenolic content and antioxidant and antimicrobial properties of fruits of *Capsicum baccatum* L. var. pendulum at different maturity stages," *Journal of Medicinal Food*, vol. 11, no. 2, pp. 267–274, 2008.

[17] H. Kollmannsberger, A. Rodríguez-Burruezo, S. Nitz, and F. Nuez, "Volatile and capsaicinoid composition of ají (*Capsicum baccatum*) and rocoto (*Capsicum pubescens*), two Andean species of chile peppers," *Journal of the Science of Food and Agriculture*, vol. 91, no. 9, pp. 1598–1611, 2011.

[18] A. Rodríguez-Burruezo, M. C. González-Mas, and F. Nuez, "Carotenoid composition and vitamin A value in ají(*Capsicum baccatum* L.) and rocoto (*C. pubescens* R. & P.), 2 pepper species from the andean region," *Journal of Food Science*, vol. 75, no. 8, pp. S446–S453, 2010.

[19] F. Spiller, M. K. Alves, S. M. Vieira et al., "Anti-inflammatory effects of red pepper (*Capsicum baccatum*) on carrageenan- and antigen-induced inflammation," *Journal of Pharmacy and Pharmacology*, vol. 60, no. 4, pp. 473–478, 2008.

[20] A. R. Zimmer, B. Leonardi, D. Miron, E. Schapoval, J. R. de Oliveira, and G. Gosmann, "Antioxidant and anti-inflammatory properties of *Capsicum baccatum*: from traditional use to scientific approach," *Journal of Ethnopharmacology*, vol. 139, pp. 228–233, 2012.

[21] L. O. Chuah, S. K. Yeap, W. Y. Ho, B. K. Beh, and N. B. Alitheen, "In vitro and in vivo toxicity of garcinia or hydroxycitric acid: a review," *Evidence-Based Complementary and Alternative Medicine*, vol. 2012, Article ID 197920, 12 pages, 2012.

[22] J. L. Leasure and L. Decker, "Social isolation prevents exercise-induced proliferation of hippocampal progenitor cells in female rats," *Hippocampus*, vol. 19, no. 10, pp. 907–912, 2009.

[23] A. E. Whimbey and V. H. Denenberg, "Two independent behavioral dimensions in open-field performance," *Journal of Comparative and Physiological Psychology*, vol. 63, no. 3, pp. 500–504, 1967.

[24] L. Prut and C. Belzung, "The open field as a paradigm to measure the effects of drugs on anxiety-like behaviors: a review," *European Journal of Pharmacology*, vol. 463, no. 1–3, pp. 3–33, 2003.

[25] S. Pellow, P. Chopin, S. E. File, and M. Briley, "Validation of open:closed arm entries in an elevated plus-maze as a measure of anxiety in the rat," *Journal of Neuroscience Methods*, vol. 14, no. 3, pp. 149–167, 1985.

[26] P. I. Parekh, A. E. Petro, J. M. Tiller, M. N. Feinglos, and R. S. Surwit, "Reversal of diet-induced obesity and diabetes in C57BL/6J mice," *Metabolism*, vol. 47, no. 9, pp. 1089–1096, 1998.

[27] V. Kazlauckas, N. Pagnussat, S. Mioranzza et al., "Enriched environment effects on behavior, memory and BDNF in low and high exploratory mice," *Physiology and Behavior*, vol. 102, no. 5, pp. 475–480, 2011.

ANEXO II-B. *Insulin prevents mitochondrial generation of H_2O_2 in rat brain.*

No **ANEXO II-B** apresentamos o artigo publicado no periódico *Experimental Neurology*.

Experimental Neurology 247 (2013) 66–72

Contents lists available at SciVerse ScienceDirect

Experimental Neurology

journal homepage: www.elsevier.com/locate/yexnr

Insulin prevents mitochondrial generation of H_2O_2 in rat brain

Alexandre Pastoris Muller [a,*,1], Clarissa Branco Haas [a,1], Juliana Camacho-Pereira [b], Andressa Wigner Brochier [a], Jussânia Gnoatto [a], Eduardo Rigon Zimmer [a], Diogo Onofre de Souza [a], Antonio Galina [b], Luis Valmor Portela [a]

[a] Departamento de Bioquímica, ICBS, UFRG, Programa de Pós Graduação em Ciências Biológicas-Bioquímica, Rua Ramiro Barcelos, 2600 anexo, CEP 90035-003, Porto Alegre, RS, Brazil
[b] Instituto de Bioquímica Médica, Programa de Biofísica e Bioquímica Celular e Programa de Biologia Molecular e Biotecnologia, Universidade Federal do Rio de Janeiro, Laboratório de Bioenergética e Fisiologia Mitocondrial, Cidade Universitária, Rio de Janeiro 21941-590, Brazil

ARTICLE INFO

Article history:
Received 16 January 2013
Revised 1 March 2013
Accepted 4 March 2013
Available online 13 March 2013

Keywords:
Brain metabolism
Mitochondria
H_2O_2 production
Insulin signaling

ABSTRACT

The mitochondrial electron transport system (ETS) is a main source of cellular ROS, including hydrogen peroxide (H_2O_2). The production of H_2O_2 also involves the mitochondrial membrane potential ($\Delta\Psi_m$) and oxygen consumption. Impaired insulin signaling causes oxidative neuronal damage and places the brain at risk of neurodegeneration. We evaluated whether insulin signaling cross-talks with ETS components (complexes I and F_oF_1ATP synthase) and $\Delta\Psi_m$ to regulate mitochondrial H_2O_2 production, in tissue preparations from rat brain. Insulin (50 to 100 ng/mL) decreased H_2O_2 production in synaptosomal preparations in high Na^+ buffer (polarized state), stimulated by glucose and pyruvate, without affecting the oxygen consumption. In addition, insulin (10 to 100 ng/mL) decreased H_2O_2 production induced by succinate in synaptosomes in high K^+ (depolarized state), whereas wortmannin and LY290042, inhibitors of the PI3K pathway, reversed this effect; heated insulin had no effect. Insulin decreased H_2O_2 production when complexes I and F_oF_1ATP synthase were inhibited by rotenone and oligomycin respectively suggesting a target effect on complex III. Also, insulin prevented the generation of maximum level of $\Delta\Psi_m$ induced by succinate. The PI3K inhibitors and heated insulin maintained the maximum level of $\Delta\Psi_m$ induced by succinate in synaptosomes in a depolarized state. Similarly, insulin decreased ROS production in neuronal cultures. In mitochondrial preparations, insulin neither modulated H_2O_2 production or oxygen consumption. In conclusion, the normal downstream insulin receptor signaling is necessary to regulate complex III of ETS avoiding the generation of maximal $\Delta\Psi_m$ and increased mitochondrial H_2O_2 production.

© 2013 Elsevier Inc. Open access under the Elsevier OA license.

Introduction

The brain consumes large amounts of oxygen to generate the ATP and phosphocreatine required for the maintenance of cellular functional homeostasis (Halliwell, 2006). However, part of the oxygen is physiologically diverted to the generation of reactive oxygen species (ROS) (Floyd and Hensley, 2002). Given their potentially harmful effects, the balance between ROS production and antioxidant defenses determines the degree of oxidative stress on cellular membranes, proteins and DNA; therefore a tight regulation is required to maintain a normal cell functioning (Nicholls and Budd, 2000).

Evidence indicates the complexes I and III, and F_oF_1ATP synthase of the mitochondrial electron transport system (ETS) as main sources of cellular ROS production, such as superoxide ($O_2^{\cdot-}$) and hydrogen peroxide (H_2O_2) (Meyer et al., 2006). Although all organs can potentially be modified by oxidative stress damage, brain comprises one especially sensitive tissue as consequence of its reduced antioxidant defenses and high metabolic rate. This is particularly relevant during brain aging, metabolic disorders and in the pathogenesis of neurodegenerative diseases including Alzheimer's disease (Reger et al., 2006). In this scenario, the mitochondrial membrane potential ($\Delta\Psi_m$) is at the center of the cell's interactions, controlling ATP synthesis, mitochondrial Ca^{2++} accumulation, superoxide generation and redox activity (Aldinucci et al., 2007). Thus, the mechanisms involved in the regulation of mitochondrial function could link ROS production and neurodegenerative process (Dumont and Beal, 2011).

Insulin was recognized as a neurotrophic factor that acts on insulin receptors (IRs) distributed in neurons from different brain regions (Zhao and Alkon, 2001). Activation of insulin receptor downstream signaling proteins (PI3K and AKT) modulates neuronal survival (Valenciano et al., 2006), synaptic plasticity, and inhibitory/excitatory neurotransmission (Dou et al., 2005; Lee et al., 2005; Stranahan et al., 2008; Zhao et al., 1999). Moreover, insulin signaling modulates the activity of AKT, GSK3, and cytochrome c proteins localized in mitochondrial compartment (Cheng et al., 2010; Mookherjee et al., 2007; Petit-Paitel et al., 2009). Consistent data of the literature have supported the concept that impaired peripheral and central IR

* Corresponding author at: Departamento de Bioquímica, ICBS, UFRGS, Rua Ramiro Barcelos, 2600 anexo, CEP 90035-003, Porto Alegre, RS, Brazil. Fax: +55 51 33085544.
E-mail address: alexandrep.muller@gmail.com (A.P. Muller).
[1] Both authors contributed equally to this work.

0014-4886 © 2013 Elsevier Inc. Open access under the Elsevier OA license.
http://dx.doi.org/10.1016/j.expneurol.2013.03.007

signaling is a risk factor for neurodegenerative diseases (Neumann et al., 2008; Ott et al., 1999). Indeed, it was recently proposed that impaired central insulin signaling is an early feature in AD, promoting cognitive decline independent of classic neuropathological alterations (Talbot et al., 2012). This places the downstream insulin signaling targets at the center of interest for preventive and therapeutic interventions.

Given the importance of mitochondria in different aspects of normal cell physiology several studies have tried to identify whether extracellular signals influence mitochondria function. Thus, the main objective of this work was to evaluate whether insulin signaling could modulate mitochondrial H_2O_2 production through the regulation of ETS components (complexes I, III and FoF1ATP synthase) and $\Delta\Psi_m$ in rat brain.

Materials and methods

Reagents

Insulin–Humulin was purchased from Lilly and bovine serum albumin, succinate, oligomycin, safranin-O, FCCP (carbonylcyanide-p-trifluoromethoxyphenylhydrazone), horseradish peroxidase, rotenone, oligomycin and wortmannin were purchased from Sigma. LY290042 was purchased from Cell Signaling. Amplex Red, Neurobasal, RPMI 1640 and B27 supplement medium were purchased from Invitrogen. Percoll was purchased from Amersham Biosciences and, hydrogen peroxide was purchased from Merck. CM-H2DCFDA was purchased from Molecular Probes.

Isolation of synaptosomes and mitochondria

The forebrain from male Wistar rats (3–4 months old) was rapidly removed and homogenized in isolation buffer containing 0.32 M sucrose, 1 mM EDTA (K^+ salt), and 10 mM Tris–HC1 (pH 7.4). The homogenate was centrifuged at 1330 ×*g* for 3 min. The supernatant was carefully retained and then centrifuged at 16,000 rpm (21,200 ×*g*) for 10 min. The pellet was resuspended and carefully layered on top of a discontinuous Percoll gradient and centrifuged for 5 min at 30,700 ×*g* (Sims, 1990; Sims and Anderson, 2008). The synaptosomal and mitochondrial fractions were incubated in depolarized buffer (high K^+) (100 mM KCI, 75 mM mannitol, 25 mM sucrose, 5 mM phosphate, 0.05 mM EDTA, and 10 mM Tris–HC1, pH 7.4) and synaptosomal was also incubated in polarized buffer (high Na^+) (20 mM HEPES, 10 mM D-glucose, 1.2 mM Na_2HPO_4, 1 mM $MgCl_2$, 5 mM $NaHCO_3$, 5 mM KCl, 140 mM NaCl, pH 7.4). Animal care followed the official governmental guidelines in compliance with the Federation of Brazilian Societies for Experimental Biology and was approved by the Ethics Committee of the Federal University of Rio Grande do Sul, Brazil at number 22436.

Glutamate uptake in synaptosomes

We evaluated glutamate uptake capacity to analyze the viability of synaptosomal preparations (Bole et al., 2002). Briefly, preparations were incubated in polarized (high Na^+) or depolarized (high K^+) buffer in the presence of 100 nM L-[^{3}H]glutamate, for 1 and 5 min at 37 °C. The filters were washed three times with 3 mL ice-cold 15 mM sucrose medium buffer (pH 7.4). The radioactivity retained by the filters was measured in a Wallac model 1409 liquid scintillation counter.

Oxygen (O_2) measurement

The O_2 consumption rates were measured polarographically using high-resolution respirometry (Oroboros Oxygraph-O2K). Synaptosomal fractions (0.1 mg/mL) were incubated with polarized buffer. The synaptosomes were incubated for 30 min at 37 °C with 50 or 100 ng/mL of insulin before the measurement of oxygen consumption. The oxygen consumption flow was monitored for 10 min with the ionic medium with 15 mM glucose or with 50 mM glucose plus 20 mM pyruvate; after that it was added to synaptosomes 0.5 μM of the proton ionophore FCCP to estimate the maximal ETS capacity.

ROS production and mitochondrial membrane potential ($\Delta\Psi_m$)

The mitochondrial release of H_2O_2 was assessed by the Amplex Red oxidation method. The synaptosomal or mitochondrial fractions (0.1 mg protein/mL) were incubated in the polarized or depolarized buffer supplemented with 10 μM Amplex Red and 2 units/mL horseradish peroxidase. The fluorescence was monitored at excitation (563 nm) and emission wavelengths (587 nm) in Spectra Max M5 microplate reader (Molecular Devices, USA). Each experiment was repeated five times with different synaptosomal and or mitochondrial preparations. The maximal rate (100%) of mitochondrial H_2O_2 formation in polarized state was assumed to be the difference between the rate of H_2O_2 formation in the polarized buffer and in polarized buffer plus substrates (50 mM glucose + 20 mM pyruvate) up to 30 min. The maximal rate (100%) of mitochondrial H_2O_2 formation in depolarized state was assumed to be the difference between the rate of H_2O_2 formation in the absence and in the presence of succinate up to 30 min.

The $\Delta\Psi_m$ was measured by using the fluorescence signal of the cationic dye, safranin-O. The synaptosomal and mitochondrial fractions (0.1 mg protein/mL) were incubated on respiration buffer in high K^+ supplemented with 10 μM safranin O. Fluorescence was detected with an excitation wavelength of 495 nm and an emission wavelength of 586 nm (Spectra Max M5, Molecular Devices). Data are reported as percentage of maximal polarization induced by succinate. Each experiment was repeated at least three times with different mitochondrial preparations.

In the experiments with 15 and 30 min with pre-incubation (insulin and PI3K inhibitors) there was no addition of mitochondrial substrates.

Western blotting

For Western blot analysis, 30 μg of protein (Peterson, 1977) from synaptosomal and mitochondrial fractions was separated by electrophoresis on a 10% polyacrylamide gel and electrotransferred to PVDF membranes. Polyclonal antibodies pAktser-473 (Cell Signaling Technology, 1:1000) and Akt (Cell Signaling Technology, 1:3000) were used to analyze downstream intracellular insulin signaling.

Neuronal cultures

Cortices from 16-day-old Wistar rat embryos were dissected and 150.000 cells/well was plated in 24 well/1 cm^2 (TPP, Switzerland) in neurobasal medium plus B27 supplement. After 7 days of culture, the neurobasal medium was replaced by RPMI 1640 medium, which contained 10 mM glucose without B27. To investigate the effects of glucose and insulin in ROS production, neurons were supplemented with different solutions to achieve the following final concentrations: 50 mM glucose; 50 mM glucose + insulin 10 ng/mL; 50 mM glucose + insulin 50 ng/mL; 50 mM glucose + insulin 100 ng/mL and 50 mM glucose + FCCP for 30 min. Afterwards, cells were incubated with 1 μM CM-H2DCFDA for 40 min at 35 °C and examined under a Nikon Eclipse TE300 epifluorescence microscope at a fixed exposure time. We performed three independent cortical neuron cultures and use triplicates for each treatment (see above).

Statistical analysis

To analyze the data distribution we used Shapiro–Wilk test. Data were analyzed by one-way analysis of variance (ANOVA) followed

by a post-hoc Tukey. Data showed in Fig. 3 were analyzed by repeated measures one-way ANOVA followed by a post-hoc Tukey test and are presented as mean ± S.E.M. P values < 0.05 were considered statistically different.

Results

Functional properties of synaptosomes

Synaptosomes incubated in the polarized state (high Na^+) showed Na^+-dependent L-[^{3}H]glutamate uptake (Fig. 1A). As expected, the glutamate uptake was impaired in depolarized state (high K^+) (Fig. 1A). The routine and uncoupled respiration (0.4 μM FCCP) was not different when 50 mM glucose was the only substrate in the polarized state, a condition that favors ROS formation by mitochondria in neurons (da-Silva et al., 2004) (Fig. 1B, glucose). However, the oxygen consumption increased by FCCP when 50 mM glucose + 20 mM pyruvate were included as substrate in the medium (Fig. 1B, glucose + pyruvate; *uncoupled > routine). Insulin had no effects on oxygen consumption routine and uncoupled respiration in synaptosomes (Fig. 1B). Glucose plus pyruvate increased H_2O_2 production in synaptosomes incubated in a polarized state. Also, the uncoupling agent FCCP decreased H_2O_2 production (Fig. 1C compared to 15 mM glucose, dotted line). Insulin at 50 and 100 ng/mL decreased H_2O_2 production in 50 mM glucose and/or 20 mM pyruvate compared to 15 mM glucose (basal level, dotted line) (Fig. 1C).

Insulin decreased H_2O_2 production and $\Delta\Psi_m$ levels in synaptosomes

To improve the capacity in generating H_2O_2 we used a buffer with high K^+ to depolarize the synaptosomes (Sims and Blass, 1986) and increase the H_2O_2 production compared to polarize buffer (data not shown). This experimental strategy changes the membrane permeability during the incubation time and permits the detection of classical mitochondrial responses (ROS production and $\Delta\Psi_m$) stimulated by anionic substrates, nucleotides (ADP and ATP) and succinate (Sims and Blass, 1986). Synaptosomes and mitochondria were responsive to succinate, succinate + ADP and oligomycin (inhibitor F_oF_1ATP synthase) (Figs. 2A and B). The fractions containing isolated mitochondria showed similar responses to substrates and oligomycin as observed in synaptosomal preparations, but showing a two-fold higher rate of H_2O_2 production as compared to synaptosomal preparation (Figs. 2A and B). Moreover, as shown in Fig. 2C, the downstream signaling proteins pAKT ser473 was activated in a dose-dependent manner by insulin in synaptosomes incubated during 15 min. Insulin did not affect the expression of AKT and pAKTser473 in mitochondrial enriched preparations (Fig. 2C).

Insulin decreased the synaptosomal H_2O_2 production induced by succinate (Fig. 3A, open square; dose effect: $F_{(3,75)} = 11.112$, $p = 0.0001$). Taking into consideration that some evidences pointed that insulin signaling remains increasing over time (Christie et al., 1999; Grillo et al., 2009) we tried to optimize its effects in synaptosomes using a pre-incubation strategy. A pre-incubation up to 30 min with

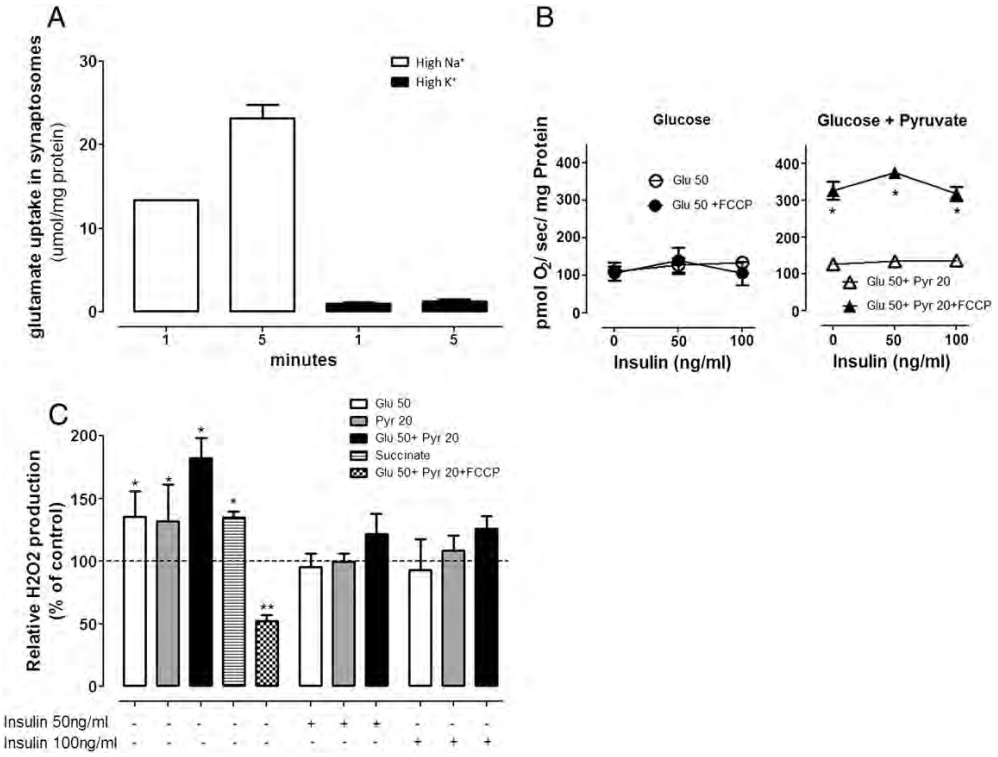

Fig. 1. Functional properties of synaptosomes. A) Sodium dependent L-[^{3}H] glutamate uptake capacity was evaluated during 1 and 5 min. The L-[^{3}H]glutamate uptake was negligible in the presence of high K^+. B) Oxygen consumption flow rate was determined after pre-incubation (30 min) with or without insulin (50–100 ng/mL). The routine respiration (open symbols) or oxidative phosphorylation uncoupled respiration (maximal ETS capacity) by addition of 0.4 μM of the proton ionophore FCCP (closed symbols) was determined polarographically. The oxygen consumption was increased only in a buffer containing 50 mM glucose + 20 mM pyruvate (closed triangles, right graph) in uncoupled respiration. Insulin had no effect in oxygen consumption in neither routine nor uncoupled respiration. C) H_2O_2 production increased in synaptosomes in high Na^+ buffer plus 50 mM glucose (Glu), 20 mM pyruvate and with bigger effect with Glu 50 + pyruvate 20 mM compared to 15 mM Glu (dotted line), such as 10 mM succinate (* < 0.05). Uncoupled agent FCCP decreased H_2O_2 production in synaptosomes compared to 15 mM Glu (** < 0.05). Insulin at 50 and 100 ng/mL decreased the H_2O_2 production induced by glucose and pyruvate ($p < 0.05$) ($n = 5$).

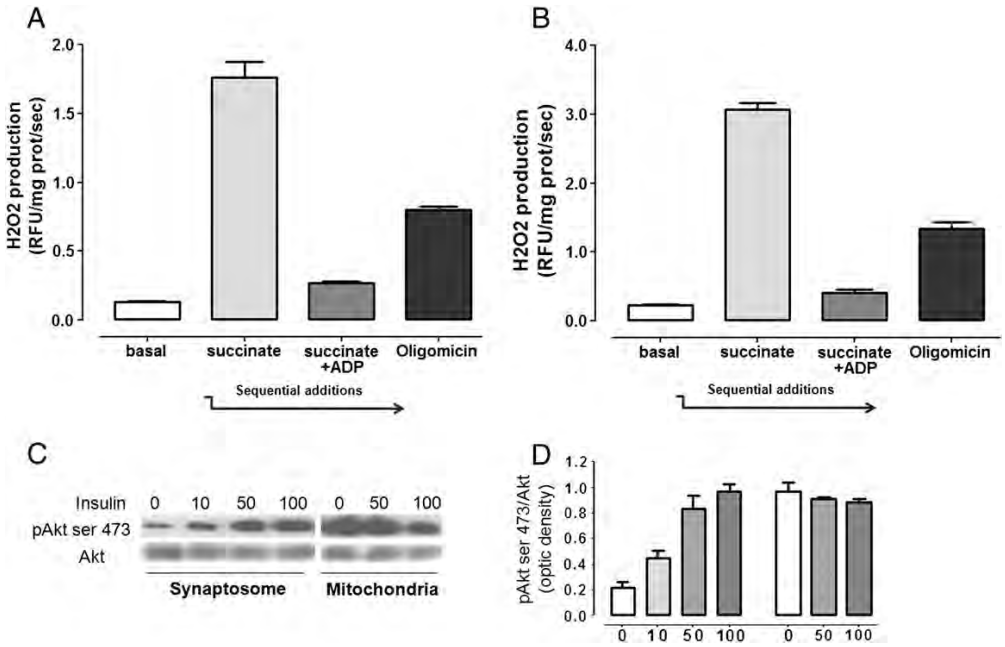

Fig. 2. H_2O_2 production by synaptosomes and mitochondria. A and B) Synaptosomes and mitochondria incubated with succinate increased H_2O_2 production when compared to the basal levels (* succinate > basal; $p < 0.05$). The addition of ADP decreased H_2O_2 production when compared to succinate (# succinate + ADP < succinate; $p < 0.05$). The addition of oligomycin decreased H_2O_2 production when compared to succinate (oligomycin < succinate; $p < 0.05$). C and D) Insulin at a dose of 10–100 ng/mL increased the phosphorylation state of Akt^{Ser473} in synaptosomes but not in mitochondria ($n = 5$) (Western blot bands and columns).

increasing doses of insulin caused a progressive inhibition in more than 60% of mitochondrial H_2O_2 generation in synaptosomes (Fig. 3A, open triangles and circles; incubation time effect: $F_{(2,75)} = 7.096$, $p = 0.002$). Interestingly, 30 min of pre-incubation with different doses of insulin did not cause any detectable decrease in H_2O_2 generation by mitochondrial preparations (Fig. 3A, closed circles, dose effect: $F_{(3,36)} = 0.056$, $p = 0.982$). The PI3K inhibitors, wortmannin (200 nM), LY290042 (10 μM) and heated insulin (90 °C for 15 min) (Marks et al., 2009), completely reversed the protective effect of insulin (from 10 to 100 ng/mL) at 15 min (Fig. 3B, open triangles, dose effect: $F_{(3,37)} = 1.887$, $p = 0.149$) and at 30 min (Fig. 3C, open circles, dose effect: $F_{(3,66)} = 1.927$, $p = 0.127$). PI3K inhibitors had no effect on isolated mitochondria (Fig. 3B, closed circles, dose effect: $F_{(3,16)} = 0.168$, $p = 0.916$; and Fig. 3C, closed circles, dose effect: $F_{(3,16)} = 0.130$, $p = 0.941$). In addition, heated insulin had no effect in H_2O_2 production induced by succinate in the synaptosomes (Fig. 3D, insulin dose: $F_{(3,36)} = 2.103$, $p = 0.110$).

We further tested if insulin-mediated H_2O_2 production is due to regulation on electron transfer system (ETS). Thus, we incubated synaptosomes in the presence of oligomycin (inhibitor F_oF_1ATP synthase). Additionally we used rotenone (inhibitor complex I) to measure reverse (complex III → complex I) electron transfer-mediated ROS production in the depolarized synaptosomes. As expected oligomycin increased the H_2O_2 production (Fig. 3E, open circles, $p < 0.05$), and insulin at 100 ng/mL significantly decreased the oligomycin-induced H_2O_2 production (Fig. 3E; oligomycin > oligomycin + 100 ng/mL, $p < 0.05$). Moreover, rotenone decreased the H_2O_2 production (Fig. 3E closed triangles, $p < 0.05$) and insulin at 10–100 ng/mL significantly improved the effect of rotenone (Fig. 3E; * rotenone > succinate + rotenone + 10–100 ng/mL, dose effect: $F_{(3,48)} = 5.084$, $^*p = 0.004$).

Subsequently, we induced $\Delta\Psi_m$ formation by succinate on both synaptosomes and mitochondrial preparations (Figs. 3F and G respectively) using high K^+ in the incubation medium. Insulin efficiently prevented the reaching of maximum level of $\Delta\Psi_m$ induced by succinate in synaptosomes (Fig. 3F open circles, insulin dose: $F_{(3,48)} = 8.821$, $p = 0.0001$). PI3K inhibitors, wortmannin and LY290042, and heated insulin maintain the maximum level of $\Delta\Psi_m$ induced by succinate in synaptosomes with or without 30 min pre-incubation with insulin (Fig. 3F). In the isolated mitochondrial fraction, insulin doses, wortmannin and LY290042 had no significant effect on $\Delta\Psi_m$, (Fig. 3G, insulin dose: $F_{(3,36)} = 0.219$, $p = 0.883$).

Furthermore, we analyzed whether ROS production in neurons is responsive to insulin regulation in neuronal cell cultures (Figs. 3H–O). Incubation with 50 mM glucose increased ROS production by neurons (Fig. 3I) when compared to 10 mM glucose (Fig. 3H). Insulin at 10, 50 and 100 ng/mL (Figs. 3J, K, and L respectively) decreased neuronal ROS production induced by glucose. The PI3K inhibitors reduced the effect of insulin (Figs. 3M and N), as well as FCCP reduced mitochondrial ROS production (Fig. 3O).

Discussion

Our results show that insulin signaling regulates the complex III of ETS and stability of $\Delta\Psi_m$ and thus decreasing the mitochondrial ROS production in synaptosomes without affecting oxygen consumption. However, when downstream insulin signaling is disrupting by PI3K inhibitors these regulatory effects on synaptosomes and neurons are missing. These findings support the previous belief that brain insulin signaling (Cole and Frautschy, 2007), has antioxidant functional roles (Duarte et al., 2004) and exerts regulatory actions on $\Delta\Psi_m$ (Huang et al., 2005). Conversely, insulin neither affected AKT phosphorylation nor H_2O_2 production in isolated mitochondrial preparations. This lack of insulin effects on mitochondria preparations might be caused by the breakdown of the molecular machinery during isolation procedure or reflect the absence of complete components of insulin signaling cascade in mitochondria. This later possibility deserves investigation.

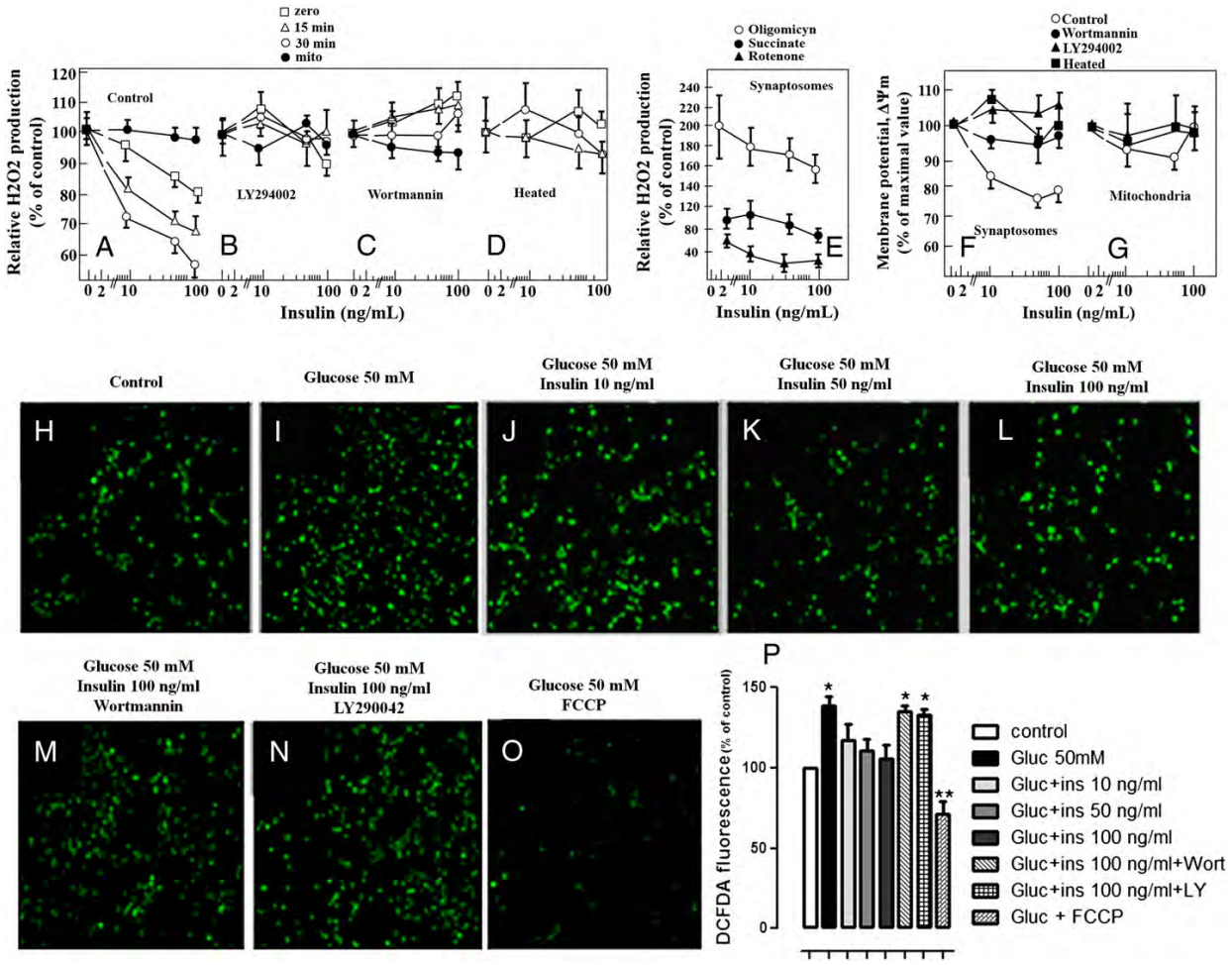

Fig. 3. Insulin decreases H_2O_2 production and efficiently prevents the formation of the maximal $\Delta\Psi_m$ induced by succinate in synaptosomes. A) Insulin decreased H_2O_2 production without pre-incubation (vehicle > insulin 100 ng/mL; $p < 0.05$; open squares, insulin dose: $F_{(3,75)} = 11.112$, $^*p = 0.0001$). Pre-incubation with insulin up to 30 min improved the insulin antioxidant effect (open triangle and open circle, incubation time: $F_{(2,75)} = 7.096$, $^*p = 0.002$). Insulin had no effect on mitochondrial-enriched fraction (Fig. 3A, closed circles, dose effect: $F_{(3,36)} = 0.056$, $p = 0.982$). B, C and D) The incubation or pre-incubation with the PI3K inhibitors wortmannin and LY294002, and heated insulin abolished the effect of insulin in regulated H_2O_2 production induced by succinate in synaptosomes. The PI3K inhibitors had no effect on mitochondrial-enriched fractions ($n = 5$). E) Oligomycin increased the H_2O_2 production in synaptosomes (* succinate + oligomycin > succinate; $p < 0.05$). Insulin at 100 ng/mL decreased H_2O_2 production induced by oligomycin (& succinate + oligomycin > succinate + oligomycin + insulin 100 ng/mL; $p < 0.05$). Rotenone alone decreased the H_2O_2 production in synaptosomes (* succinate + rotenone < succinate; $p < 0.05$). Insulin at 10–100 ng/mL further decreased the H_2O_2 production when incubated with rotenone (succinate + rotenone + insulin 10–100 ng/mL succinate + rotenone; insulin dose: $F_{(3,48)} = 5.084$, $^*p = 0.004$). (F) Pre-incubation with insulin for 30 min inhibited the maximal $\Delta\Psi_m$ (basal > insulin 10–100 ng/mL; open circles, insulin dose: $F_{(3,48)} = 8.821$, $p = 0.0001$). Incubation with PI3K inhibitors wortmannin, LY294002, and heated insulin abolished this effect. G) Neither insulin nor PI3K inhibitors affected the maximal $\Delta\Psi_m$ in mitochondrial-enriched fraction ($n = 5$). H–P) Neuronal cultures: insulin (10–100 ng/mL) decreased the ROS production induced by 50 mM Glu (H–L). PI3K inhibitors abolished the effect of insulin (M–N); and FCCP reduced the mitochondrial ROS production (O). P) The figure shows the CM-H2DCFDA immunofluorescence quantification of the images H–O.

Normal intracellular insulin signaling is putatively involved in several aspects of brain physiology (Plum et al., 2005) and alterations in this pathway have been consistently implicated in the etiology of neurodegenerative diseases (Hoyer and Lannert, 2007). We used drugs to disrupt downstream signaling trying to mimic a brain insulin resistance state. The results with or without PI3K inhibitors showed that an uninterrupted intracellular insulin signaling is necessary to achieve the effect of insulin in decreasing H_2O_2 production in synaptosomes. Moreover, synaptosomes pre-incubated with insulin (15 and 30 min) were more responsive to insulin-regulation of H_2O_2 production compared with no pre-incubation protocol. Based on this pre-incubation approach we suggest that similarly as observed for other insulin target proteins in cerebral tissue (Christie et al., 1999; Grillo et al., 2009), the time of exposition to insulin is important to achieve a maximal effect in the regulation of mitochondrial H_2O_2 production in synaptosomes.

In addition insulin was able to modulate the effects of oligomycin and rotenone on H_2O_2 production. When succinate is used as a substrate for mitochondrial respiration the majority of H_2O_2 production is generated by reverse-electron flow in complex I and complex III (Votyakova and Reynolds, 2001). Thus, the inhibition of complex I with rotenone in the presence of succinate causes increased proton leaks and ROS production by the complex III. Here we showed that this inhibitory experimental condition insulin (10–100 ng/mL) was efficient in decreasing the H_2O_2 production through the modulation of the complex III (Petit-Paitel et al., 2009) or cytochrome c release (Sanderson et al., 2008). Similarly, insulin also decreased H_2O_2 production induced by oligomycin reinforcing the regulatory role in the

reverse electron flow of ETS. Furthermore, insulin protects neurons against ROS production induced by high glucose levels (Russell et al., 2002). The cross-talk between insulin signaling and mitochondria is not completely understood; however some reports have shown possible connections involving the activation of AKT affecting some aspects of the mitochondrial physiology including closure of a permeability transition pore component, the voltage-dependent anion channel, and the decline in oxidative phosphorylation that precedes cytochrome c release (Gottlob et al., 2001; Sanderson et al., 2008).

The H_2O_2 production can also be influenced by changes in the $\Delta\Psi_m$. It is known that even a slight decrease in $\Delta\Psi_m$ avoids the semi-ubiquinone radical formation leading to a drastic impairment in the electron leaks from ETS to form superoxide anion, a substrate for H_2O_2 production (Korshunov et al., 1997). Here, we showed that insulin decreases the maximum $\Delta\Psi_m$ induced by succinate in synaptosomes; however, there were no differences with or without pre-incubation, pointing that insulin modulates the H_2O_2 production in different pathways. Moreover kinases (Meyer et al., 2006) and scavenger enzyme activities (Santiago et al., 2008) can regulate the homeostasis of H_2O_2 levels in brain. Thus, it seems that insulin can potentially act in different targets of mitochondrial compartment resulting in decrease H_2O_2 production and/or increase metabolism. One potential limitation of this work is related to the use of brain preparations from normal rat in which the disruption of insulin signaling was induced through pharmacological inhibitors. Thus additional studies are necessary to establish the functional relevance of these finding in animal models of impaired brain insulin signaling.

Considering the main findings of this study, we confirm that insulin may exert antioxidant properties in the brain. However, when brain insulin/IGF-I signaling is deficient, including aging (Muller et al., 2012), Alzheimer's disease and diabetes mellitus there is an increased H_2O_2 production which has been reported to contribute to cause neurological deficits (Kilbride et al., 2008) or beyond, to be an early main event in neurodegenerative processes (Talbot et al., 2012). In contrast, strategies designed to improve brain insulin signaling (Muller et al., 2011) and mitochondrial function (Dietrich et al., 2008) could be helpful to maintain the normal balance of the redox state in the brain and to avoid the development of neurodegenerative diseases. Our findings strongly suggest that normal insulin signaling is required for a normal mitochondrial function and metabolism (Cheng et al., 2009).

Conclusion

In conclusion, the normal downstream insulin receptor signaling is necessary to regulate complex III of ETS avoiding the generation of maximal $\Delta\Psi_m$ and increasing mitochondrial H_2O_2 production.

Acknowledgments

We would like to thank Danielle Abdala and Clara Rodrigues-Ferreira for their assistance with the oxygen consumption experiments. This work was supported by Brazilian agencies and grants: CNPq, CAPES, FAPERGS-PPSUS 10/1026.7, Brazil-Swiss 590011/2010-3, Brazilian Institute of Neuroscience — IBN Net FINEP, INCT — Excitotoxicity and Neuroprotection 573577/2008-5.

References

Aldinucci, C., Carretta, A., Ciccoli, L., Leoncini, S., Signorini, C., Buonocore, G., Pessina, G.P., 2007. Hypoxia affects the physiological behavior of rat cortical synaptosomes. Free Radic. Biol. Med. 42, 1749–1756.

Bole, D.G., Hirata, K., Ueda, T., 2002. Prolonged depolarization of rat cerebral synaptosomes leads to an increase in vesicular glutamate content. Neurosci. Lett. 322, 17–20.

Cheng, Z., Guo, S., Copps, K., Dong, X., Kollipara, R., Rodgers, J.T., Depinho, R.A., Puigserver, P., White, M.F., 2009. Foxo1 integrates insulin signaling with mitochondrial function in the liver. Nat. Med. 15, 1307–1311.

Cheng, Z., Tseng, Y., White, M.F., 2010. Insulin signaling meets mitochondria in metabolism. Trends Endocrinol. Metab. 21, 589–598.

Christie, J.M., Wenthold, R.J., Monaghan, D.T., 1999. Insulin causes a transient tyrosine phosphorylation of NR2A and NR2B NMDA receptor subunits in rat hippocampus. J. Neurochem. 72, 1523–1528.

Cole, G.M., Frautschy, S.A., 2007. The role of insulin and neurotrophic factor signaling in brain aging and Alzheimer's disease. Exp. Gerontol. 42, 10–21.

da-Silva, W.S., Gomez-Puyou, A., de Gomez-Puyou, M.T., Moreno-Sanchez, R., De Felice, F.G., de Meis, L., Oliveira, M.F., Galina, A., 2004. Mitochondrial bound hexokinase activity as a preventive antioxidant defense: steady-state ADP formation as a regulatory mechanism of membrane potential and reactive oxygen species generation in mitochondria. J. Biol. Chem. 279, 39846–39855.

Dietrich, M.O., Andrews, Z.B., Horvath, T.L., 2008. Exercise-induced synaptogenesis in the hippocampus is dependent on UCP2-regulated mitochondrial adaptation. J. Neurosci. 28, 10766–10771.

Dou, J.T., Chen, M., Dufour, F., Alkon, D.L., Zhao, W.Q., 2005. Insulin receptor signaling in long-term memory consolidation following spatial learning. Learn. Mem. 12, 646–655.

Duarte, A.I., Santos, M.S., Seica, R., Oliveira, C.R., 2004. Oxidative stress affects synaptosomal gamma-aminobutyric acid and glutamate transport in diabetic rats: the role of insulin. Diabetes 53, 2110–2116.

Dumont, M., Beal, M.F., 2011. Neuroprotective strategies involving ROS in Alzheimer disease. Free Radic. Biol. Med. 51, 1014–1026.

Floyd, R.A., Hensley, K., 2002. Oxidative stress in brain aging. Implications for therapeutics of neurodegenerative diseases. Neurobiol. Aging 23, 795–807.

Gottlob, K., Majewski, N., Kennedy, S., Kandel, E., Robey, R.B., Hay, N., 2001. Inhibition of early apoptotic events by Akt/PKB is dependent on the first committed step of glycolysis and mitochondrial hexokinase. Genes Dev. 15, 1406–1418.

Grillo, C.A., Piroli, G.G., Hendry, R.M., Reagan, L.P., 2009. Insulin-stimulated translocation of GLUT4 to the plasma membrane in rat hippocampus is PI3-kinase dependent. Brain Res. 1296, 35–45.

Halliwell, B., 2006. Oxidative stress and neurodegeneration: where are we now? J. Neurochem. 97, 1634–1658.

Hoyer, S., Lannert, H., 2007. Long-term abnormalities in brain glucose/energy metabolism after inhibition of the neuronal insulin receptor: implication of tau-protein. J. Neural Transm. Suppl. 195–202.

Huang, T.J., Verkhratsky, A., Fernyhough, P., 2005. Insulin enhances mitochondrial inner membrane potential and increases ATP levels through phosphoinositide 3-kinase in adult sensory neurons. Mol. Cell. Neurosci. 28, 42–54.

Kilbride, S.M., Telford, J.E., Davey, G.P., 2008. Age-related changes in H2O2 production and bioenergetics in rat brain synaptosomes. Biochim. Biophys. Acta 1777, 783–788.

Korshunov, S.S., Skulachev, V.P., Starkov, A.A., 1997. High protonic potential actuates a mechanism of production of reactive oxygen species in mitochondria. FEBS Lett. 416, 15–18.

Lee, C.C., Huang, C.C., Wu, M.Y., Hsu, K.S., 2005. Insulin stimulates postsynaptic density-95 protein translation via the phosphoinositide 3-kinase-Akt-mammalian target of rapamycin signaling pathway. J. Biol. Chem. 280, 18543–18550.

Marks, D.R., Tucker, K., Cavallin, M.A., Mast, T.G., Fadool, D.A., 2009. Awake intranasal insulin delivery modifies protein complexes and alters memory, anxiety, and olfactory behaviors. J. Neurosci. 29, 6734–6751.

Meyer, L.E., Machado, L.B., Santiago, A.P., da-Silva, W.S., De Felice, F.G., Holub, O., Oliveira, M.F., Galina, A., 2006. Mitochondrial creatine kinase activity prevents reactive oxygen species generation: antioxidant role of mitochondrial kinase-dependent ADP re-cycling activity. J. Biol. Chem. 281, 37361–37371.

Mookherjee, P., Quintanilla, R., Roh, M.S., Zmijewska, A.A., Jope, R.S., Johnson, G.V., 2007. Mitochondrial-targeted active Akt protects SH-SY5Y neuroblastoma cells from staurosporine-induced apoptotic cell death. J. Cell. Biochem. 102, 196–210.

Muller, A.P., Gnoatto, J., Moreira, J.D., Zimmer, E.R., Haas, C.B., Lulhier, F., Perry, M.L., Souza, D.O., Torres-Aleman, I., Portela, L.V., 2011. Exercise increases insulin signaling in the hippocampus: physiological effects and pharmacological impact of intracerebroventricular insulin administration in mice. Hippocampus 21, 1082–1092.

Muller, A.P., Fernandez, A.M., Haas, C., Zimmer, E., Portela, L.V., Torres-Aleman, I., 2012. Reduced brain insulin-like growth factor I function during aging. Mol. Cell. Neurosci. 49, 9–12.

Neumann, K.F., Rojo, L., Navarrete, L.P., Farias, G., Reyes, P., Maccioni, R.B., 2008. Insulin resistance and Alzheimer's disease: molecular links & clinical implications. Curr. Alzheimer Res. 5, 438–447.

Nicholls, D.G., Budd, S.L., 2000. Mitochondria and neuronal survival. Physiol. Rev. 80, 315–360.

Ott, A., Stolk, R.P., van Harskamp, F., Pols, H.A., Hofman, A., Breteler, M.M., 1999. Diabetes mellitus and the risk of dementia: the Rotterdam Study. Neurology 53, 1937–1942.

Peterson, G.L., 1977. A simplification of the protein assay method of Lowry et al. which is more generally applicable. Anal. Biochem. 83, 346–356.

Petit-Paitel, A., Brau, F., Cazareth, J., Chabry, J., 2009. Involvement of cytosolic and mitochondrial GSK-3beta in mitochondrial dysfunction and neuronal cell death of MPTP/MPP-treated neurons. PLoS One 4, e5491.

Plum, L., Schubert, M., Bruning, J.C., 2005. The role of insulin receptor signaling in the brain. Trends Endocrinol. Metab. 16, 59–65.

Reger, M.A., Watson, G.S., Frey II, W.H., Baker, L.D., Cholerton, B., Keeling, M.L., Belongia, D.A., Fishel, M.A., Plymate, S.R., Schellenberg, G.D., Cherrier, M.M., Craft, S., 2006. Effects of intranasal insulin on cognition in memory-impaired older adults: modulation by APOE genotype. Neurobiol. Aging 27, 451–458.

Russell, J.W., Golovoy, D., Vincent, A.M., Mahendru, P., Olzmann, J.A., Mentzer, A., Feldman, E.L., 2002. High glucose-induced oxidative stress and mitochondrial dysfunction in neurons. FASEB J. 16, 1738–1748.

Sanderson, T.H., Kumar, R., Sullivan, J.M., Krause, G.S., 2008. Insulin blocks cytochrome c release in the reperfused brain through PI3-K signaling and by promoting Bax/Bcl-XL binding. J. Neurochem. 106, 1248–1258.
Santiago, A.P., Chaves, E.A., Oliveira, M.F., Galina, A., 2008. Reactive oxygen species generation is modulated by mitochondrial kinases: correlation with mitochondrial antioxidant peroxidases in rat tissues. Biochimie 90, 1566–1577.
Sims, N.R., 1990. Rapid isolation of metabolically active mitochondria from rat brain and subregions using Percoll density gradient centrifugation. J. Neurochem. 55, 698–707.
Sims, N.R., Anderson, M.F., 2008. Isolation of mitochondria from rat brain using Percoll density gradient centrifugation. Nat. Protoc. 3, 1228–1239.
Sims, N.R., Blass, J.P., 1986. Expression of classical mitochondrial respiratory responses in homogenates of rat forebrain. J. Neurochem. 47, 496–505.
Stranahan, A.M., Norman, E.D., Lee, K., Cutler, R.G., Telljohann, R.S., Egan, J.M., Mattson, M.P., 2008. Diet-induced insulin resistance impairs hippocampal synaptic plasticity and cognition in middle-aged rats. Hippocampus 18, 1085–1088.
Talbot, K., Wang, H.Y., Kazi, H., Han, L.Y., Bakshi, K.P., Stucky, A., Fuino, R.L., Kawaguchi, K.R., Samoyedny, A.J., Wilson, R.S., Arvanitakis, Z., Schneider, J.A., Wolf, B.A., Bennett, D.A., Trojanowski, J.Q., Arnold, S.E., 2012. Demonstrated brain insulin resistance in Alzheimer's disease patients is associated with IGF-1 resistance, IRS-1 dysregulation, and cognitive decline. J. Clin. Invest. 122, 1316–1338.
Valenciano, A.I., Corrochano, S., de Pablo, F., de la Villa, P., de la Rosa, E.J., 2006. Proinsulin/insulin is synthesized locally and prevents caspase- and cathepsin-mediated cell death in the embryonic mouse retina. J. Neurochem. 99, 524–536.
Votyakova, T.V., Reynolds, I.J., 2001. DeltaPsi(m)-dependent and -independent production of reactive oxygen species by rat brain mitochondria. J. Neurochem. 79, 266–277.
Zhao, W.Q., Alkon, D.L., 2001. Role of insulin and insulin receptor in learning and memory. Mol. Cell. Endocrinol. 177, 125–134.
Zhao, W., Chen, H., Xu, H., Moore, E., Meiri, N., Quon, M.J., Alkon, D.L., 1999. Brain insulin receptors and spatial memory. Correlated changes in gene expression, tyrosine phosphorylation, and signaling molecules in the hippocampus of water maze trained rats. J. Biol. Chem. 274, 34893–34902.

ANEXO II-C. *Nandrolone-induced aggressive behavior is associated with alterations in extracellular glutamate homeostasis in mice.*

No **ANEXO II-C** apresentamos o artigo publicado no periódico *Hormones and Behavior.*

Hormones and Behavior 66 (2014) 383–392

Contents lists available at ScienceDirect

Hormones and Behavior

journal homepage: www.elsevier.com/locate/yhbeh

Regular article

Nandrolone-induced aggressive behavior is associated with alterations in extracellular glutamate homeostasis in mice

Eduardo Kalinine [a], Eduardo Rigon Zimmer [a], Kamila Cagliari Zenki [a], Iouri Kalinine [b], Vanessa Kazlauckas [a], Clarissa Branco Haas [a], Gisele Hansel [a], Aline Rigon Zimmer [c], Diogo Onofre Souza [a], Alexandre Pastoris Müller [d], Luis Valmor Portela [a,*]

[a] Department of Biochemistry, Post-Graduation Program in Biochemistry, ICBS, Federal University of Rio Grande do Sul (UFRGS), Rio Grande do Sul, Porto Alegre, Brazil
[b] Laboratory of Exercise Physiology and Human Performance, Federal University of Santa Maria (UFSM), Rio Grande do Sul, Santa Maria, Brazil
[c] Pharmaceutical Sciences Program, Faculty of Pharmacy, Federal University of Rio Grande do Sul (UFRGS), Porto Alegre, Brazil
[d] Laboratory of Exercise Biochemistry and Physiology, Health Sciences Unit, University of Extremo Sul Catarinense (UNESC), Criciúma, Santa Catarina, Brazil

ARTICLE INFO

Article history:
Received 30 November 2013
Revised 3 June 2014
Accepted 6 June 2014
Available online 14 June 2014

Keywords:
Aggressive behavior
Nandrolone decanoate
Glutamate transporter 1 (GLT-1)
N-methyl-D-aspartate receptor (NMDAr)
Memantine
MK-801

ABSTRACT

Nandrolone decanoate (ND), an anabolic androgenic steroid (AAS), induces an aggressive phenotype by mechanisms involving glutamate-induced N-methyl-D-aspartate receptor (NMDAr) hyperexcitability. The astrocytic glutamate transporters remove excessive glutamate surrounding the synapse. However, the impact of supraphysiological doses of ND on glutamate transporters activity remains elusive. We investigated whether ND-induced aggressive behavior is interconnected with GLT-1 activity, glutamate levels and abnormal NMDAr responses. Two-month-old untreated male mice (CF1, n = 20) were tested for baseline aggressive behavior in the resident–intruder test. Another group of mice (n = 188) was injected with ND (15 mg/kg) or vehicle for 4, 11 and 19 days (short-, mid- and long-term endpoints, respectively) and was evaluated in the resident–intruder test. Each endpoint was assessed for GLT-1 expression and glutamate uptake activity in the frontoparietal cortex and hippocampal tissues. Only the long-term ND endpoint significantly decreased the latency to first attack and increased the number of attacks, which was associated with decreased GLT-1 expression and glutamate uptake activity in both brain areas. These alterations may affect extracellular glutamate levels and receptor excitability. Resident males were assessed for hippocampal glutamate levels via microdialysis both prior to, and following, the introduction of intruders. Long-term ND mice displayed significant increases in the microdialysate glutamate levels only after exposure to intruders. A single intraperitoneal dose of the NMDAr antagonists, memantine or MK-801, shortly before the intruder test decreased aggressive behavior. In summary, long-term ND-induced aggressive behavior is associated with decreased extracellular glutamate clearance and NMDAr hyperexcitability, emphasizing the role of this receptor in mediating aggression mechanisms.

© 2014 Elsevier Inc. All rights reserved.

Introduction

Anabolic androgenic steroids (AAS), such as nandrolone decanoate (ND), are synthetic derivatives of testosterone that were developed to improve anabolic functions with fewer androgenic effects (Jones and Lopez, 2006; Shahidi, 2001). However, humans and rodents submitted to high AAS dose regimens may display exaggerated emotional reactivity and aggressive behavior, which ultimately is associated with glutamatergic hyperexcitability in brain areas such as the hypothalamus, cortex, and hippocampus (Breuer et al., 2001; Carrillo et al., 2009, 2011a; Diano et al., 1997; Kanayama et al., 2010; Le Greves et al., 1997; McGinnis, 2004; Ricci et al., 2007; Robinson et al., 2012; Talih et al., 2007).

The mechanism underlying the AAS-induced aggressive phenotype is dynamic and not restricted to proteins of the synaptic milieu. For instance, select hypothalamic neurons express dramatic increases in phosphate-activated glutaminase, the rate-limiting enzyme in the synthesis of glutamate, in aggressive, adolescent, AAS-treated, male Syrian hamsters (Fischer et al., 2007). Steroids also increase the rate of glutamate and aspartate release, thus increasing the binding probability of glutamate to NMDA or AMPA receptors (Brann and Mahesh, 1995; Ventriglia and Di Maio, 2013). Actually, AAS-induced aggression is mechanistically associated with glutamatergic hyperexcitability. This concept has been supported by studies on genetically modified animals and pharmacological studies addressing glutamate fast-acting ionotropic receptors, i.e. kainate (KAr), α-amino-3-hydroxy-5-methyl-4-isoxazolepropionic acid (AMPAr), and N-methyl-D-aspartate (NMDAr) (Fischer et al., 2007). To date, studies on knockout mice lacking the AMPAr 1 subunit (GluR1) show reduced aggressive behavior (Vekovischeva et al., 2004), whereas AAS-treated aggressive hamsters

* Corresponding author at: Department of Biochemistry, ICBS, UFRGS, 2600 Ramiro Barcelos, 90035-003 Porto Alegre, RS, Brazil. Fax: 55 51 33085544.
E-mail address: roskaportela@gmail.com (L.V. Portela).

http://dx.doi.org/10.1016/j.yhbeh.2014.06.005
0018-506X/© 2014 Elsevier Inc. All rights reserved.

display a significant increase in the number and density of GluR1-expressing hypothalamic neurons compared to non-aggressive, vehicle-treated controls (Fischer et al., 2007). Moreover, hypothalamic administration of a KAr agonist or L-glutamate stimulates aggressive attacks in rats and cats respectively (Brody et al., 1969; Haller et al., 1998). Although pharmacological antagonism of NMDAr may cause non-specific behavioral effects due to sedation, this receptor has multiple regulatory binding sites that may serve as anti-aggressive targets (Bortolato et al., 2012; Umukoro et al., 2013). Accordingly, the administration of memantine (MEM), a low-affinity uncompetitive NMDAr antagonist, decreases aggression induced by social isolation or morphine withdrawal in rodents (Belozertseva et al., 1999; Sukhotina and Bespalov, 2000). Moreover, knockout mice for monoamino oxidase 'A' exhibited pathological aggressive behavior mediated by the higher expression of NR2A and NR2B subunits of NMDAr in the prefrontal cortex (Bortolato et al., 2012). Remarkably, systemic administration of selective NR2A and NR2B antagonists as well as dizocilpine (MK-801) an uncompetitive high-affinity NMDAr antagonist, countered the enhanced aggression (Bortolato et al., 2012). Collectively, these studies highlight a positive correlation between heightened aggression and increased glutamatergic tonus in a range of animal models.

Because there are no extracellular enzymes that can degrade glutamate, the maintenance of physiological concentrations requires glutamate transporters activity present in both astrocytes and neurons. The high-affinity glutamate transporter 1 (GLT-1) is predominantly expressed in astrocytes and is responsible for more than 90% of glutamate clearance from the synaptic cleft (Lehre and Danbolt, 1998). Further, GLT-1 is highest expressed in the hippocampus and neocortical areas (Ullensvang et al., 1997). In contrast, glutamate transporter 3 (EAAC1) is widely distributed in neurons and even GLT-1 can be found at lower levels in neurons, particularly in axon terminals. Despite neuronal EAAC1 being quantitatively lower when compared to astrocytes, its functional role cannot be neglected. Notably, it can be assumed that astrocytes (via GLT-1) are the main regulators of extracellular glutamate levels (Danbolt, 2001). Although astrocytic glutamate uptake is recognized as an important mechanism to avoid excessive glutamate levels associated with prolonged receptor activation, the impact of supraphysiological doses of ND on glutamate transporters activity remains elusive.

Here, we investigate whether ND-induced aggression is mechanistically interconnected with GLT-1 activity, glutamate levels, and NMDAr response in the brains of male, gonad-intact CF1 mice.

Material and methods

Animals

Two-month old CF1 male mice (total n = 208) weighting 32–38 g were housed in standard polycarbonate cages (cm: 28 × 17.8 × 12.7), and kept in a temperature-controlled room (22 ± 1 °C) with a 12 h light/12 h dark cycle (light on at 7 a.m.). The animals were permitted free access to food and water. To avoid social isolation, both resident and intruder mice were housed at four per cage (Leasure and Decker, 2009). All experimental procedures were performed according to the *NIH Guide for Care and Use of Laboratory Animals* and the *Brazilian Society for Neuroscience and Behavior* (SBNeC). Recommendations for animal

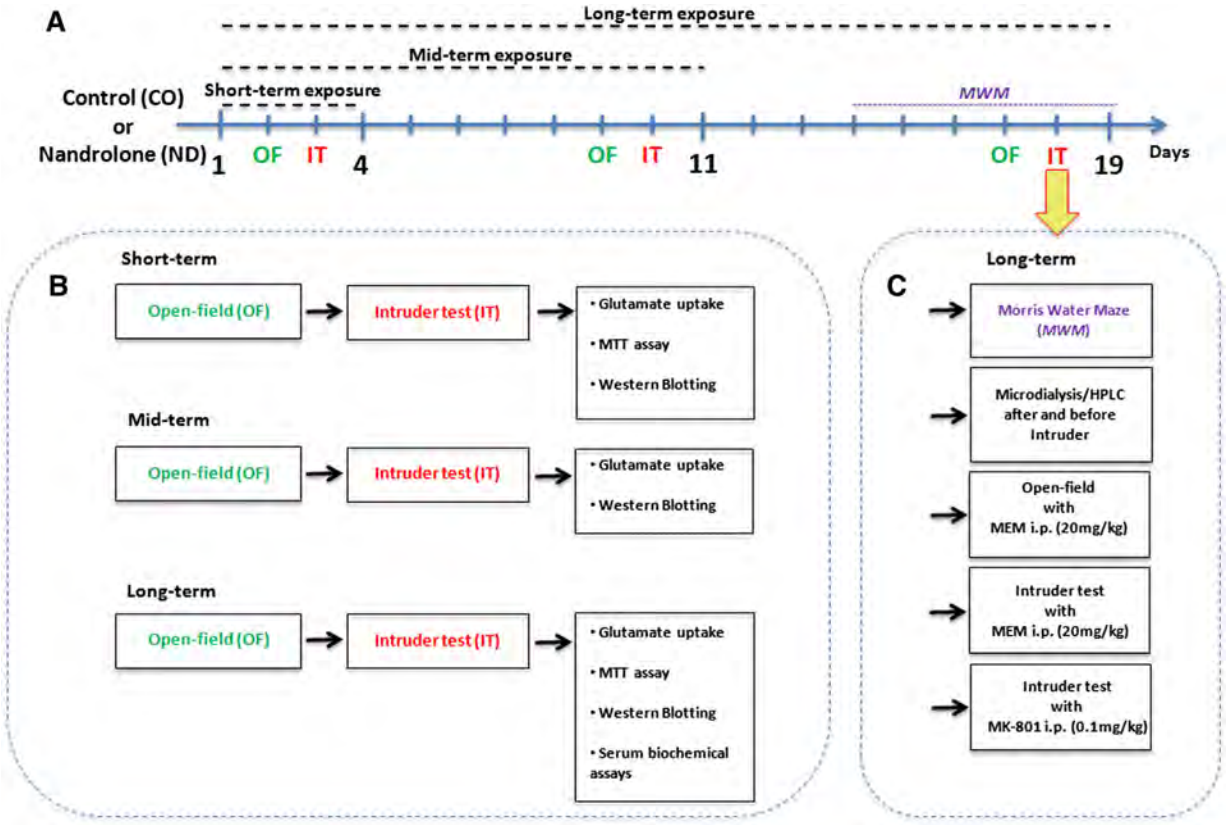

Fig. 1. Schematic experimental design. Behavioral and neurochemical endpoints in control (CO) and nandrolone (ND) groups: (A) The timeline showing each endpoint (short-, mid- and long-term exposure); (B) Flowchart representing behavioral and biochemical outcomes for each endpoint; (C) Boxes with arrows representing five independent experiments conducted after long-term exposure. Abbreviations: high-performance liquid chromatography (HPLC), memantine (MEM), dizocilpine (MK-801), intraperitoneal (i.p.).

care were followed throughout all the experiments in accordance with project approved by the ethical committee from the Federal University of Rio Grande do Sul-UFRGS #26739.

Experimental design and drug administration

All experimental procedures are shown in Fig. 1: (A) The timeline showing each endpoint (short-, mid- and long-term exposure); (B) Flowchart representing behavioral and biochemical outcomes for each endpoint; and (C) Boxes with arrows representing five independent experiments conducted after long-term exposure.

The mice home cages were allocated in one of the following groups; resident or intruder. Resident mice home cages were assigned to treatment groups. Animals received single daily subcutaneous injections of oil-vehicle (CO) or nandrolone decanoate 50 mg (ND; Deca-Durabolin®, Organon; 15 mg/kg/day in a volume of 1 ml/kg, dissolved in corn oil) for 4 days (short-term exposure), 11 days (mid-term exposure) and 19 days (long-term exposure). The ND and CO-treated animals were not housed in the same cage. This strategy avoids ND mice establishing social dominance over CO animals before the intruder test. The dose and treatment regimen were based on previous published works (Le Greves et al., 1997; Rossbach et al., 2007). All the behavioral experiments were conducted during light phase, from 9 a.m. to 3 p.m. (de Almeida et al., 2010) whereas the vehicle and ND were administered from 3 p.m. to 4 p.m. Thus, the last injection was performed on the day prior to the behavioral and neurochemical experiments.

The NMDAr antagonist memantine (MEM; Sigma-Aldrich, M183), and dizocilpine (MK-801; Sigma-Aldrich, M107) were dissolved in saline 0.9%, and were administered intraperitoneally (i.p.) using a single injection volume of 10 ml/kg. The time of peak concentration (60 min) in the rat brain after MEM administration was chosen based on the work of Kotermanski et al. (2013). The dose of MEM (20 mg/kg) was based on the neuroprotective effects achieved in a rat model of glutamatergic hyperexcitability (Zimmer et al., 2012b). The time and dose regimen of MK-801 (0.1 mg/kg) were based on previous published work (Bortolato et al., 2012).

Open-field test

Animals (n = 10 per group/n = 20 per endpoint) were tested for spontaneous and locomotor activity after short, mid and long-term CO or ND administration using a black box apparatus 50 cm × 50 cm × 50 cm. The experiments were conducted in a sound-attenuated room under low-intensity light (12 lx). Animals were placed in the right corner of the arena and locomotor activity was recorded with a video camera for 10 min (Prut and Belzung, 2003). All analyses were performed using a computer-operated tracking system (Any-maze, Stoelting, Woods Dale, IL) (see Supplementary material for detailed description).

Additionally, an independent group of mice were long-term treated with ND or vehicle (CO) and received an i.p. injection of MEM (20 mg/kg) or saline, 60 min before the open-field test (Kotermanski et al., 2013). Animals were assigned to one of the following groups: control + saline (CO + SAL), control + memantine (CO + MEM), ND + saline (ND + SAL) and ND + memantine (ND + MEM); n = 9 per group.

Morris water maze task

We performed the Morris water maze task (MWM) to evaluate spatial memory performance in one independent group of long-term treated animals. The apparatus was a black, circular pool (110 cm diameter) with a water temperature of 21 ± 1 °C. The long-term CO (n = 10) and ND mice (n = 10) were trained daily in a four-trial MWM for five consecutive days; each trial lasted up to 60 s and was followed by 20 s of rest on a hidden black platform. During training, mice learned to escape from the water by finding a hidden, rigid, black platform submerged about 1 cm below the water surface in a fixed location. If the animal failed to find the platform in 60 s, it was manually placed on the platform and allowed to rest for 20 s. Each trial was separated by at least 12 min to avoid hypothermia and facilitate memory acquisition (Muller et al., 2011), see Supplementary Fig. 2.

Resident–intruder test

In this test, aggressive behavior is tested by introducing an intruder into a resident's home cage. As expected, residents are typically more aggressive because they are familiar with the environment and are defending their home territory (Nelson and Trainor, 2007). The protocol of the intruder test used in this study was adapted from a previous work of our group (Kazlauckas et al., 2005). To date, dominant or subordinate animals were not distinguished before the test. If the intruder animal attacks the resident first (~10% of intruders) or showed an exacerbated offensive profile, both animals were excluded from the analysis and were not retested. Thus, all residents attacking the intruder were considered dominant. The test was performed during the light phase based on previous work of Bortolato et al. (2012) and in the proposed concept that light or dark phases produce reliable results in social behavior testing (Yang et al., 2008). As cited above the mice home cages were assigned as resident (ND or vehicle) or intruder.

Two days prior to the intruder test, the home cage sawdust of ND and CO groups was not changed in order for the animals to establish and maintain territoriality within their home cage. Before the test, three resident CF1 mice were removed to an identical and clean cage. One resident mouse remained alone for 2 min habituation prior to introducing the intruder mouse. After testing, the animal number one was moved to the clean cage. For each ND one CO mouse was assessed in the intruder test. The ND and CO animals were tested in their own home cages. The time-delay between each animal test was 15 min, including the first 2 min habituation. Observations of dominant and subordinate status, latency to the first aggressive attack, and the number of attacks of the resident toward the intruder were recorded during a period of 10 min maximum. In this work, an attack was defined as a bout of activity (fight) lasting up to several seconds during which the resident mouse bites the intruder at least once. The behaviors that can be displayed by mice consist of a stationary one-sided attack, frontal attack, chase, wrestle, lunge or boxing inflicted by the resident against the intruder. These components were then recorded as the number of aggressive acts (adapted from Thurmond, 1975).

The intruders did not receive any treatment and were housed in different home cages than were the residents (ND or CO). Residents and intruders were submitted to the resident–intruder test only once. For ethical reasons, if the aggressive behavior put the animals at risk of injuries like blooding or suffering the test was stopped earlier than the maximum test duration of 10 min and both resident and intruder animals were excluded from the analysis (Defensor et al., 2012; Kazlauckas et al., 2005; Simon and Whalen, 1986; Thurmond, 1975).

To characterize the baseline aggressive behavior, three groups of untreated two-month old male mice were subjected to the resident–intruder test for 10 min, with intervals of 48 h (day 1; n = 6, day 2; n = 7 and day 3; n = 7). The aggressive scores of each group did not vary significantly across three independent experiments. The mean latency to first attack was 471.5 ± 42.7 s (S.E.M.), and the mean number of attacks was 2.10 ± 0.65 (S.E.M.).

After that, another group of mice was injected with vehicle (CO) or ND and tested for aggressive behavior at short-, mid- and long-term exposures (n = 10 per group/per endpoint). In addition, another group of long-term ND and CO mice received a single i.p. injection of MEM (20 mg/kg) or saline 60 min before the resident–intruder test (Kotermanski et al., 2013). For this approach, animals were assigned to the following groups: CO + SAL, CO + MEM, ND + SAL and ND + MEM (n = 6 per group, total n = 24).

A separate group of long-term ND and CO mice were i.p. injected with MK-801 (0.1 mg/kg) or saline 30 min before the resident–intruder test (Bortolato et al., 2012). Animals were then assigned to the following groups: CO + SAL, CO + MK-801, ND + SAL and ND + MK-801 (n = 10 per group, total n = 40).

Sodium-dependent glutamate uptake activity

After short-, mid- and long-term vehicle (CO) or ND exposure (n = 6 per group) animals were decapitated and the right hippocampus and frontoparietal cortex were immediately dissected on ice (4 °C). Slices from the hippocampus and frontoparietal cortex (0.4 mm thick) were rapidly prepared using a McIlwain Tissue Chopper, separated in HBSS (in mM: 137 NaCl, 0.63 Na_2HPO_4, 4.17 $NaHCO_3$, 5.36 KCl, 0.44 KH_2PO_4, 1.26 $CaCl_2$, 0.41 $MgSO_4$, 0.49 $MgCl_2$ and 1.11 glucose, pH 7.2) at 4 °C. Hippocampal and frontoparietal cortical slices were pre-incubated with HBSS at 37 °C for 15 min, followed by the addition of 0.33 μCi ml^{-1} L-[^{3}H] glutamate (PerkinElmer®). Incubation was stopped after 5 min for hippocampus and 7 min for frontoparietal cortex with 2 ice-cold washes of 1 ml HBSS. After washing, 0.5 N NaOH was immediately added to the slices and they were stored overnight. Na^+-independent uptake was measured using the above-described protocol with alterations in the temperature (4 °C) and the composition of the medium (N-methyl-D-glucamine instead of NaCl). Results (Na^+-dependent uptake) were measured as the difference between the total uptake and the Na^+-independent uptake. Each incubation was performed in quadruplicate (Thomazi et al., 2004). Incorporated radioactivity was measured using a liquid scintillation counter (Hidex 300 SL).

Cell viability

Mice (n = 5 per group) were decapitated after long-term exposure and the right hippocampus and frontoparietal cortex were immediately dissected on ice (4 °C). Cellular viability was measured in brain slices (0.4 mm thick) by MTT (3-(4,5-dimethylthiazol-2-yl)-2,5-diphenyltetrazolium bromide) assay (Oliveira et al., 2002) (for detailed description of MTT assay, see Supplementary material). Active mitochondrial dehydrogenases from living cells are able to reduce MTT to form a purple formazan product. This is feasible method for measuring cell proliferation and neural cytotoxicity in response to drugs.

Western blotting

Mice (n = 6–8 per group) exposed to short-, mid- and long-term ND were decapitated and the left hippocampus and frontoparietal cortex were immediately dissected on ice (4 °C) and stored at −80 °C for homogenate preparations. Hippocampal and frontoparietal cortical homogenates were prepared in PIK buffer (1% NP-40, 150 mM NaCl, 20 mM Tris pH 7.4, 10% glycerol, 1 mM $CaCl_2$, 1 mM $MgCl_2$ and 0.1% phosphatase inhibitor cocktails I and II; Sigma-Aldrich, USA) at 4 °C, and centrifuged. Supernatants were collected and the total protein was measured using the method described by Peterson (1977). For Western blot analysis, 20 μg of protein from hippocampus and frontoparietal cortex homogenate preparations was loaded into each well, separated by electrophoresis on 8% polyacrylamide gel and electrotransferred to PVDF (polyvinyl difluoride, Thermo Scientific Pearce) membranes. Protein bands within each sample lane were compared to standard molecular weight markers (Precision Plus Protein™ Dual Color Standards, Bio-rad), which were used to identify the molecular weight of proteins of interest. Nonspecific binding sites were blocked with Tween-Tris buffered saline (TTBS, 100 mM Tris–HCl, pH 7.5) containing 5% bovine albumin serum (Sigma-Aldrich, USA) for 2 h and then incubated overnight at 4 °C with polyclonal antibody against GLT-1 dissolved in TTBS (1:1000, Alpha Diagnostic International) and monoclonal antibody anti-β-actin (1:3000, Sigma-Aldrich, USA). Membranes were then rinsed 3× for 10 min with TTBS and incubated with secondary antibodies horseradish peroxidase-conjugated secondary antibody (1:3000 dilution, anti-rabbit and 1:3000 dilution anti-mouse, GE Healthcare Life Sciences) for 2 h at room temperature, membranes were then rinsed 4× for 10 min with TTBS and incubated with enhanced chemiluminescent substrate (PerkinElmer®) for 1 min or 2 min at room temperature. The resulting reaction was displayed on autoradiographic film by chemiluminescence (Moreira et al., 2011; Muller et al., 2011). The X-ray films (Kodak X-Omat, Rochester, NY, USA) were scanned and band intensity was analyzed using Image J software (developed at the US National Institutes of Health and available on the Internet at http://rsb.info.nih.gov/nih-image).

Microdialysis

Long-term ND and CO mice (n = 4 per group) were implanted with a guide cannula under anesthesia with ketamine (100 mg/kg) and xylazine (10 mg/kg) using the following coordinates: anterior = 1.8 mm and lateral = 1.5 mm (both from the bregma), and ventral = 1.5 mm (from the skull) (Paxinos and Franklin, 2001). Animals assigned in each experimental group were randomly chosen from two different cages, and were not distinguished as being dominant or submissive. The mice were allowed to recover for 48 h after implantation of the guide cannula. The location of the dialysis probe was confirmed at the end of the experiment using a vibratome (Leica, Germany) and magnifying lens.

Animals used for microdialysis were allowed to move freely in their cages. A microdialysis probe was slowly inserted into the hippocampus (dentate gyrus-CA3 area) through the guide cannula. The animals were habituated to microdialysis for 1 h (1 μl/min with artificial extracellular fluid aECF; 124 mM NaCl, 3 mM KCl_2, 1 mM $MgSO_4$ $7H_2O$, $NaHCO_3$, 2 mM $CaCl_2$ H_2O, 1 mM glucose, buffered at pH 7.4) using BASi brain microdialysis probes (MD-2200-BR2, USA) (Garrido et al., 2012). To analyze baseline levels of extracellular glutamate, we collected 3 samples at 10 minute increments. Subsequently, individual animals were exposed to an intruder (as previously described) without aECF perfusion, and soon afterward four samples in fractions of 10 min were collected during 40 min to analyze post-test glutamate levels. These animals were used only for microdialysate sampling. Glutamate concentration was analyzed through high-performance liquid chromatography (HPLC).

HPLC procedure

HPLC was performed with cell-free supernatant aliquots to quantify glutamate levels (Schmidt et al., 2009). Briefly, samples were derivatized with *o*-phthalaldehyde and separation was carried out with a reverse phase column (Supelcosil LC-18, 250 mm × 4.6 mm, Supelco) in a Shimadzu Instruments liquid chromatograph (200 μl loop valve injection). The mobile phase flowed at a rate of 1.4 ml/min and column temperature was 24 °C. Buffer composition is A: 0.04 mol/l sodium dihydrogen phosphate monohydrate buffer, pH 5.5, containing 20% of methanol; and B: 0.01 mol/l sodium dihydrogen phosphate monohydrate buffer, pH 5.5, containing 80% of methanol. The gradient profile was modified according to the content of buffer B in the mobile phase: 0% at 0.00 min, 25% at 13.75 min, 100% at 15.00–20.00 min, and 0% at 20.01–25.00 min. Absorbance was read at 360 nm and 455 nm, excitation and emission respectively, in a Shimadzu fluorescence detector. Samples of 8 μl were used and concentration was expressed in μM.

Biochemical evaluations

After long-term exposure to ND or the vehicle (CO), the animals (n = 10 per group) were sacrificed by decapitation, and then blood was collected and centrifuged (10,000 × g, 10 min) to obtain serum samples. We evaluated serum biochemical parameters linked with metabolic profile (glucose tolerance test and lipids) and tissue-specific toxicity: kidney (urea, creatinine) and liver (albumin, AST; alanine

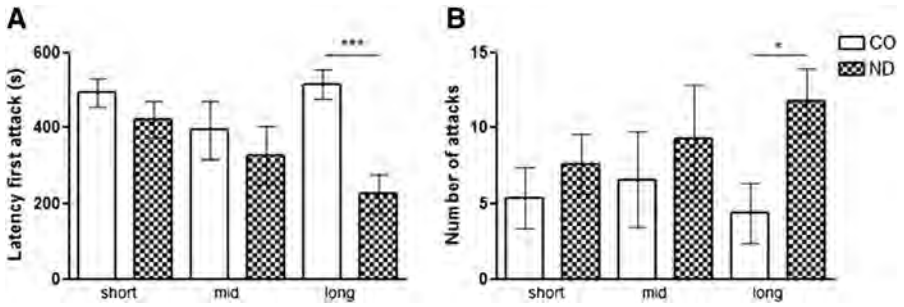

Fig. 2. Resident–intruder test. Long-term ND exposure (15 mg/kg) induced an exacerbated aggressive behavior in CF1 male mice. (A) Latency to first attack ($p < 0.0001$); (B) Number of attacks; ($p = 0.0168$). Data represented mean ± S.E.M. ($n = 10$ per group). *$p = 0.0168$ and ***$p < 0.0001$ indicate significant statistical difference between groups.

aminotransferase and ALT; aspartate aminotransferase) (Muller et al., 2011; Zimmer et al., 2012a) (for detailed description see Supplementary material).

Statistical analysis

Data distribution was analyzed using the Kolmogorov–Smirnov test. The Mann–Whitney *U*-test was used to analyze differences between each ND endpoint (short-, mid-, long-term) and its respective CO group in the resident–intruder test. Differences between groups in neurochemical and biochemical parameters were analyzed using Student's *t* test. Nonparametric comparisons were performed by the Kruskal–Wallis test, with Dunn's post-hoc test comparisons to analyze differences in the resident–intruder test with MEM and MK-801 administration. The differences between groups were considered statistically significant if $p < 0.05$. Results were presented as mean ± standard error of mean (S.E.M.).

The Cohen's *d* was used to estimate the effect size, which is the difference between means divided by standard deviation (S.D.). According to Cohen's *d*, effect size was classified as small ($d = 0.2$), medium ($d = 0.5$) and large ($d \geq 0.8$) (Sullivan and Feinn, 2012).

Results

Nandrolone-induced aggressive behavior

ND exposure did not cause significant decrease in the latency to first attack in short- ($p = 0.199$; Cohen's $d = 0.36$), and mid-term exposures ($p = 0.662$; Cohen's $d = 0.28$) compared to their respective CO groups (Fig. 2A). Also, there was no significant difference in the number of attacks in short- ($p = 0.372$; Cohen's $d = -0.25$), and mid-term exposures ($p = 0.525$; Cohen's $d = -0.26$) compared to their respective CO groups (Fig. 2B). In contrast, long-term administration of ND significantly decreased the latency to first attack (Fig. 2A, $p < 0.0001$; Cohen's $d = 1.41$), and increased the total number of attacks against an intruder compared to the CO group (Fig. 2B, $p = 0.0168$; Cohen's $d = -0.77$). For more detailed pairwise comparisons see Table 1.

Nandrolone decreased glutamate uptake and immunocontent of GLT-1

Long-term ND exposure significantly decreased glutamate uptake in slices of hippocampus (Fig. 3A, $p = 0.03$; Cohen's $d = 1.83$) and frontoparietal cortex (Fig. 3B, $p = 0.004$; Cohen's $d = 1.20$) when compared to the CO group. Moreover, the immunoquantification of the glutamate transporter 1 (GLT-1) by Western blotting revealed a significant decrease in hippocampus (Fig. 3C, $p = 0.03$; Cohen's $d = 1.26$) and frontoparietal cortex (Fig. 3D, $p = 0.0003$; Cohen's $d = 2.02$). For more detailed pairwise comparisons see Tables 2 and 3. The decreased glutamate uptake activity and GLT-1 expression may cause increases in the glutamate levels associated with hyperstimulation of glutamate receptors and cell damage and/or dysfunction. Thus, we performed analyses of cell viability through MTT assay in slices of frontoparietal cortex and hippocampus after short- and long-term ND exposures ($n = 5$ per group). There was no significant difference observed between the ND and CO groups, suggesting no overt signs of decreased neural cells' viability/damage in frontoparietal cortex (short-, $p = 0.577$; Cohen's $d = 0.39$ and long-term, $p = 0.682$; Cohen's $d = 0.61$) and hippocampus (short-, $p = 0.629$; Cohen's $d = -0.29$ and long-term, $p = 0.579$; Cohen's $d = 0.42$) (see Supplementary Table 2).

Short- and mid-term exposures to ND or vehicle (CO) ($n = 6$–8) did not cause significant changes, either in the immunocontent of GLT-1 in hippocampus (short-, $p = 0.785$; Cohen's $d = 0.10$ and mid-, $p = 0.086$; Cohen's $d = 0.81$) and frontoparietal cortex (short-, $p = 0.694$; Cohen's $d = 0.25$ and mid-term, $p = 0.069$; Cohen's $d = 0.88$), or in glutamate-uptake capacity in same brain areas (data not shown).

Long-term ND exposure increased hippocampal extracellular glutamate levels

The glutamate levels in the long-term (ND) group not exposed to intruder (baseline) did not show statistical significant difference compared to the control (CO) group (Fig. 4, $p = 0.06$; Cohen's $d = -1.70$). After exposure to the intruder test, the glutamate levels in the ND group significantly increase compared to CO animals (Fig. 4, $p =$

Table 1
Resident–intruder test after vehicle (CO) or nandrolone (ND) administration (short-, mid-, and long-term endpoints, $n = 10$ per group/per endpoint).

Behavior test	Time regimen	Parameters	Control (CO)	Nandrolone (ND)	Cohen's *d*	Statistical difference	n per group/per endpoint
Intruder test	Short-term exposure	Latency to first attack (s)	493.6 ± 172.0	422.7 ± 221.8	0.36	n.s.	10
	Mid-term exposure		393.7 ± 240.6	327.0 ± 240.8	0.28	n.s.	
	Long-term exposure		515.9 ± 176.9	227.2 ± 233.4	1.41	$p < 0.0001$	
	Short-term exposure	Number of attacks	5.4 ± 9.2	7.6 ± 9.1	−0.25	n.s.	
	Mid-term exposure		6.6 ± 10.0	9.3 ± 11.0	−0.26	n.s.	
	Long-term exposure		4.4 ± 9.2	11.8 ± 10.0	−0.77	$p = 0.0168$	
						n Total	*60*

Values are expressed as mean ± S.D.

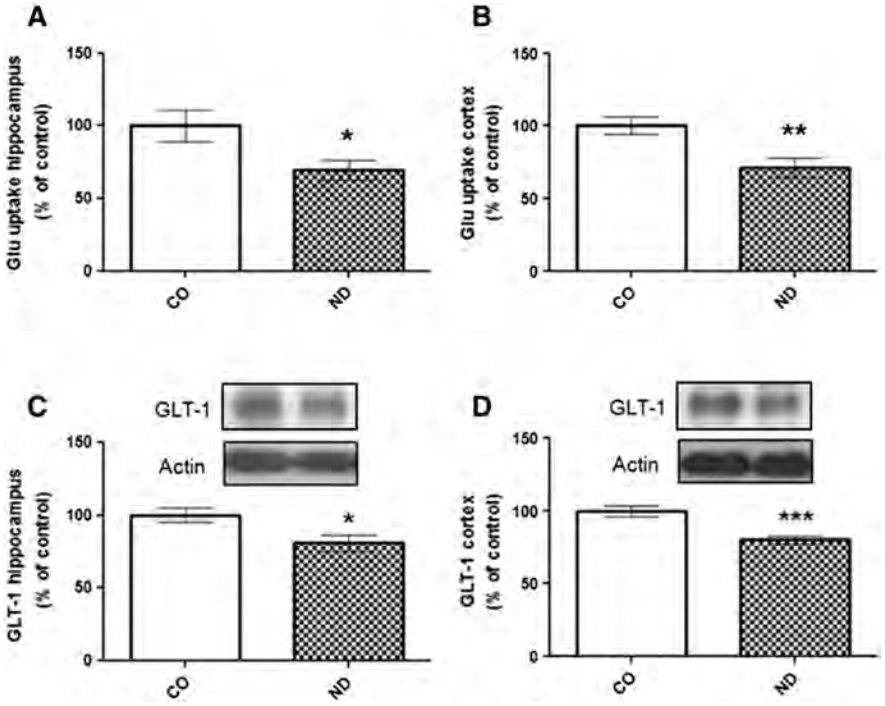

Fig. 3. Glutamate uptake and Western blotting. Nandrolone (ND) decreases glutamate uptake and immunocontent of GLT-1 in hippocampus and frontoparietal cortex. (A) Glutamate uptake in slices of hippocampus, and (B) frontoparietal cortex (n = 6). (C) Immunocontent of GLT-1 in hippocampus and, (D) frontoparietal cortex (n = 6–8). Data represented mean ± S.E.M. *p = 0.03, **p = 0.004 and ***p = 0.0003 indicate significant difference between groups. Short- and mid-term ND exposures were not significantly different from their respective control groups.

Table 2
Glutamate uptake in slices of hippocampus and cortex in long-term groups (CO and ND, n = 6 per group).

Neurochemical assay	Brain structure	Time regimen	Control (CO)	Nandrolone (ND)	Cohen's *d*	Statistical difference	n per group/per endpoint
Glutamate uptake	Hippocampus	Long-term exposure	100.0 ± 11.1	69.56 ± 22.2	1.83	p = 0.03	6
	Cortex	Long-term exposure	100.0 ± 22.7	70.93 ± 25.7	1.20	p = 0.004	
						n Total (hippocampus)	*12*
						n Total (cortex)	*12*

Values are expressed as mean ± S.D.

0.04; Cohen's $d = -3.00$). Extracellular microdialysate fluid was collected and glutamate was measured with HPLC. Data represent mean ± S.E.M. (n = 4 per group). For more detailed comparisons see Table 4.

Memantine and MK-801 decreases aggressive behavior induced by nandrolone

A single MEM administration after long-term ND exposure did not cause significant changes in the locomotor activity on open-field test (see results in the Supplementary Table 3). This indicates an absence of sedative effects, which could be a confounding factor in the resident–intruder.

We additionally investigated the possible connection between increased extracellular glutamate levels and NMDAr hyperexcitability mediating aggressive behavior. Thus, long-term ND + SAL group significantly decreased the latency to first attack and increased the number of attacks compared to CO + SAL group (Fig. 5A, p = 0.022; Cohen's $d = 2.97$ and Fig. 5B, p = 0.0457; Cohen's $d = -2.73$ respectively). The

Table 3
Immunocontent of GLT-1 in homogenates of hippocampus and frontoparietal cortex after vehicle (CO) or nandrolone (ND) administration (Short-, mid- and long-term endpoints).

Neurochemical assay	Brain structure	Time regimen	Control (CO)	Nandrolone (ND)	Cohen's *d*	Statistical difference	n per group
Western blotting	Hippocampus	Short-term exposure	100.0 ± 14.0	98.0 ± 24.4	0.10	n.s.	6
		Mid-term exposure	100.0 ± 18.9	84.1 ± 20.2	0.81	n.s.	
		Long-term exposure	100.0 ± 13.9	80.9 ± 16.5	1.26	0.03	
	Cortex	Short-term exposure	100.0 ± 15.4	96.01 ± 16.3	0.25	n.s.	8
		Mid-term exposure	100.0 ± 15.9	84.98 ± 18.3	0.88	n.s.	
		Long-term exposure	100.0 ± 11.3	80.25 ± 8.3	2.02	p = 0.0003	
						n Total (hippocampus)	*36*
						n Total (cortex)	*48*

Values are expressed as mean ± S.D., n = 6 for hippocampus and n = 8 for cortex per group/per endpoint (short-, mid- and long-term exposures).

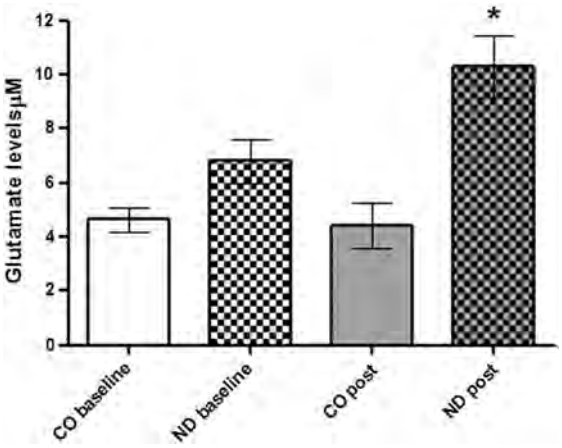

Fig. 4. Glutamate levels in extracellular fluid of hippocampus. The glutamate levels in long-term nandrolone (ND) and vehicle (CO) animals not exposed to intruder (baseline). After exposure to intruder test (post-test), the animals significantly increase the glutamate levels when compared to CO animals ($p = 0.04$). Extracellular microdialysate fluid was collected and glutamate was measured with HPLC. Data represent mean ± S.E.M. ($n = 4$ per group).

administration of MEM significantly increased the latency to first attack and decreased the number of attacks (Fig. 5A, $p = 0.017$; Cohen's $d = -2.99$ and Fig. 5B, $p = 0.003$; Cohen's $d = 3.50$) in ND + MEM compared to the ND + SAL group, respectively. The MEM per se did not significantly affect the latency to first attack or number of attacks in CO + SAL compared to CO + MEM (Figs. 5A and B, $p = 0.999$; Cohen's $d = 0.08$ and $d = -0.04$ respectively).

Additionally, long-term ND + SAL group significantly decreased the latency to first attack and increased the number of attacks compared to CO + SAL group (Fig. 5C, $p = 0.004$; Cohen's $d = 1.57$ and Fig. 5D, $p = 0.024$; Cohen's $d = -1.05$ respectively). The administration of MK-801 significantly increased the latency to first attack and decreased the number of attacks (Fig. 5C, $p = 0.004$; Cohen's $d = -1.32$ and Fig. 5D, $p = 0.002$; Cohen's $d = 1.38$) in ND + MK-801 compared to ND + SAL group, respectively. As expected, the MK-801 per se did not significantly affect the latency to first attack or number of attacks in CO + SAL compared to CO + MK-801 (Figs. 5C and D, $p = 0.999$; Cohen's $d = -0.10$ and $d = 0.22$ respectively). These pharmacological approaches with MEM or MK-801 reinforce the implication of NMDAr hyperexcitability in the mechanism of aggression For more detailed pairwise comparisons see Tables 5 and 6.

Biochemical evaluation

Serum biochemical results are presented in Supplementary Table 1. After long-term exposure, ND significantly increased serum levels of triglycerides ($p = 0.0468$; Cohen's $d = -1.32$) and decreased HDL-cholesterol serum levels ($p = 0.0017$; Cohen's $d = 1.46$) compared to the CO. The capacity of mice in regulating glucose homeostasis (GTT) was not affected by treatments (data not shown). Similarly, there were no significant alterations in serum biochemical markers of liver and kidney damage. The food consumption and body weight gain during short-term to long-term exposure were similar between groups. As expected, testicular weight (in grams) was significantly decreased in ND relative to CO (0.291 g ± 0.04 versus 0.251 g ± 0.04, $p = 0.007$; Cohen's $d = 1.00$).

Discussion

Our results demonstrate that long-term ND-induced aggressive behavior is associated with glutamatergic abnormalities like down-regulation of astrocytic glutamate uptake and increases in the glutamate levels mediating NMDAr hyperexcitability. In accordance to this, the administration of NMDAr antagonists MEM (uncompetitive low-affinity NMDAr antagonist) and MK-801 (uncompetitive high-affinity NMDAr antagonist), shortly before the intruder test reduce the aggressive behavior in long-term ND group.

Short-, mid- and long-term ND exposures did not affect locomotor and exploratory activity on open-field test (see Supplementary Fig. 1) indicating that there was no alteration in the motor components of aggressive responding. In fact, studies evaluating putative effects of AAS on spontaneous locomotion and exploratory profile in rodents have shown no significant changes (see review of Clark and Henderson, 2003). Similarly, the spatial memory performance on MWM in both acquisition and retention phases showed no significant differences between ND and CO groups suggesting normal spatial information processing (see Supplementary Fig. 2). As the hippocampus participates in both memory and aggressive behavior and is very sensitive to repetitive stress, this evaluation allows ruling out the overlap of hippocampal responses associated with long-term ND administration. In contrast to our findings, long-term administration of ND (15 mg/kg) impairs MWM performance in both acquisition and retention phases in rats (Magnusson et al., 2009; Tanehkar et al., 2013). Overall, these behavioral outcomes, associated with the lack of differences on kidney and liver serum biochemical markers (see Supplementary Table 1), strengthen the view that our long-term ND treatment regimen impacts central mechanisms associated with aggression without apparent toxic effects on these organs.

Also, the temporal aggressive profile reported here corroborates published data by Carrillo et al. (2011a), in which an AAS cocktail induced progressive alterations in the glutamatergic parameters associated with increased aggressive scores. Glutamatergic neurotransmission in the hypothalamus is an output aggressive system modulated by gonadal hormones and AAS (Brann and Mahesh, 1995; Brody et al., 1969; Diano et al., 1997; Fischer et al., 2007; Haller, 2013), which also receives many inputs from different brain areas and neurotransmitter systems. This implies that the neurobiology of aggressive behavior involves a complex and intricate collaborative network (Carrillo et al., 2011b; Ferris et al., 2008; Nelson and Trainor, 2007). Accordingly, a neural circuit composed of several regions including the prefrontal cortex, amygdala, hippocampus, hypothalamus, anterior cingulated cortex, and other interconnected structures has been implicated in emotion regulation. Consequently, functional or structural abnormalities in one or more of these regions or in the interconnections among them can increase the susceptibility for impulsive aggression and violence (Nelson and Chiavegatto, 2001). Considering these functional interconnections,

Table 4
Microdialysis/HPLC in long-term groups (CO and ND) at baseline and after exposed an intruder ($n = 4$ per group).

Behavior test	Time regimen	Parameters	Time period	CO	ND	Cohen's *d*	Statistical difference	n per group
Microdialysis/HPLC after and before intruder	Long-term exposure	Glutamate levels (µM)	Baseline	4.63 ± 0.92	6.80 ± 1.64	−1.70	$p = 0.06$	4
			Post-test	4.43 ± 1.65	10.30 ± 2.26	−3.00	$p = 0.04$	
							n Total	*8*

Values are expressed as mean ± S.D.

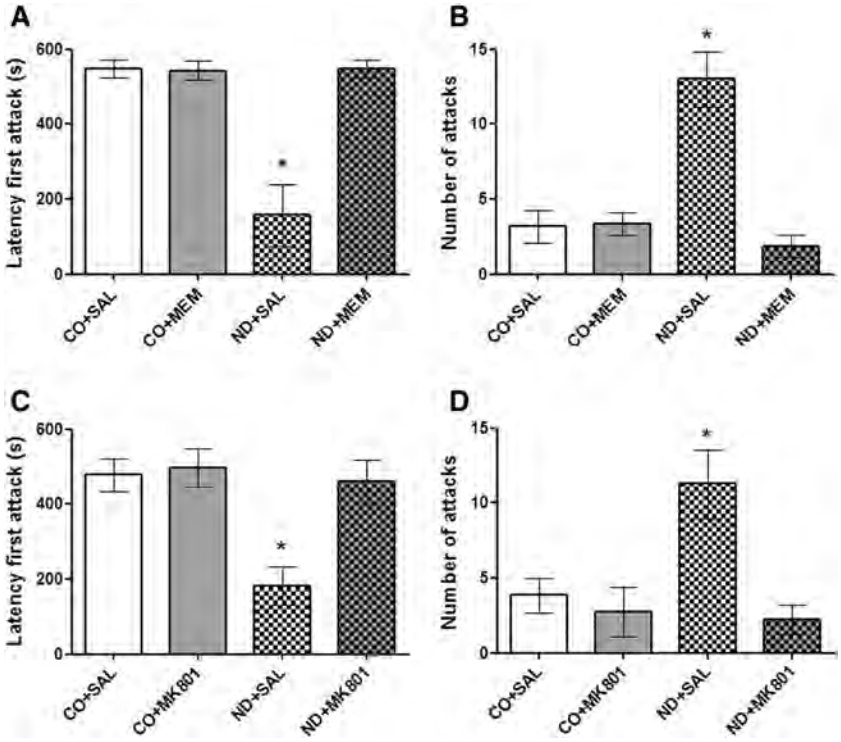

Fig. 5. N-methyl-D-aspartate receptor (NMDAr) antagonists and resident-intruder test. Memantine (20 mg/kg i.p.) or MK-801 (0.1 mg/kg i.p.) administration in long-term ND mice, 60 min and 30 min respectively prior to intruder test, restores the aggressive scores to levels of the CO group: (A) Latency to first attack (CO + SAL versus ND + SAL; $p = 0.0219$ and ND + SAL versus ND + MEM; $p = 0.0168$) and (B) Number of attacks (CO + SAL versus ND + SAL; $p = 0.0457$ and ND + SAL versus ND + MEM; $p = 0.0029$, $n = 6$ per group) after memantine administration; (C) Latency to first attack (CO + SAL versus ND + SAL; $p = 0.0041$ and ND + SAL versus ND + MK-801; $p = 0.0041$); and (D) Number of attacks (CO + SAL versus ND + SAL; $p = 0.0239$, and ND + SAL versus ND + MK-801; $p = 0.0015$, $n = 10$ per group) after MK-801 administration. Data represent mean ± S.E.M. $^*p < 0.05$ indicates significant statistical difference between groups.

Table 5
Resident–intruder test in long-term groups (CO and ND) after a single memantine (MEM) administration ($n = 6$ per group).

Behavior test	Time regimen	Parameters	CO/SAL	CO/MEM	ND/SAL	ND/MEM	Cohen's *d*	Statistical difference	n per group
Intruder test with MEM	Long-term exposure	Latency to first attack (s)	548.3 ± 59.6	543.3 ± 60.6			0.08	n.s.	6
					156.7 ± 203.8	547.7 ± 57.4	−2.99	$p = 0.017$	
			548.3 ± 59.6		156.7 ± 203.8		2.97	$p = 0.022$	
				543.3 ± 60.6		547.7 ± 57.4	−0.04	n.s.	
		Number of attacks	3.2 ± 2.6	3.3 ± 1.9			−0.07	n.s.	
					13.0 ± 4.6	1.8 ± 1.8	3.50	$p = 0.003$	
			3.2 ± 2.6		13.0 ± 4.6		−2.73	$p = 0.046$	
				3.3 ± 1.9		1.8 ± 1.8	0.81	n.s.	
								n Total	*24*

Values are expressed as mean ± S.D. Oil vehicle (CO), nandrolone (ND), saline (SAL) and memantine (MEM, 20 mg/kg). The MEM was administered (i.p.), 60 min before the test.

Table 6
Resident–intruder test in long-term groups (CO and ND) after a single MK-801 administration ($n = 10$ per group).

Behavior test	Time regimen	Parameters	CO/SAL	CO/MK-801	ND/SAL	ND/MK-801	Cohen's *d*	Statistical difference	n per group
Intruder test with MK-801	Long-term exposure	Latency to first attack (s)	478.4 ± 164.74	496.3 ± 194.64			−0.10	n.s.	10
					180.8 ± 215.39	460.6 ± 207.53	−1.32	$p = 0.004$	
			478.4 ± 164.74		180.8 ± 215.39		1.57	$p = 0.004$	
				496.3 ± 194.64		460.6 ± 207.53	0.18	n.s.	
		Number of attacks							
			3.86 ± 4.40	2.73 ± 6.39			0.22	n.s.	
					11.28 ± 9.66	2.23 ± 3.54	1.38	$p = 0.002$	
			3.86 ± 4.40		11.28 ± 9.66		−1.05	$p = 0.024$	
				2.73 ± 6.39		2.23 ± 3.54	0.10	n.s.	
								n Total	*40*

Values are expressed as mean ± S.D. Oil vehicle (CO), nandrolone (ND), saline (SAL); dizolcipine (MK-801). The MK-801 (0.1 mg/kg) was administered (i.p.), 30 min before the test.

it seems that the facilitating role attributed to glutamatergic system on aggressive responding is widespread in the brain (Ricci et al., 2007).

Furthermore, long-term ND exposure decreased the immunocontent of GLT-1 and Na^+-dependent glutamate uptake activity in the hippocampus and frontoparietal cortex, acting as contributory factors to the observed increase in hippocampal glutamate levels when animals were exposed to an intruder. These findings support the concept that the peak concentration and rate of clearance of glutamate from the synaptic cleft are important determinants of synaptic function (Clements et al., 1992), and also shed lights for the putative impact of glutamate transporters dysfunction in the mechanisms of aggression. Considering that high glutamate levels are implicated in the genesis of aggression and violent behavior (Munozblanco and Castillo, 1987), and that NMDAr is a candidate modulator of several behavioral phenotypes, we conjectured that ND mediates the aggressive responding through NMDAr.

Therefore, we administrated MEM and MK-801 antagonists to modulate NMDAr activity and aggression in long-term ND exposed mice. Although, the NMDAr antagonists may exhibit a sedative effect (Umukoro et al., 2013), long-term ND mice injected with MEM (20 mg/kg, 60 min before the test) did not show a significantly reduced locomotor profile in the open-field test, implying that MEM might modulate specific mechanisms of aggression without sedative effects. Indeed, the same dose and time regimen of MEM used in the open-field decreased the aggressive outcomes in the long-term ND mice. It seems clear that NMDAr antagonism is the primary mechanism of action of therapeutic relevance for MEM although additional effects at 5-HT3, α-7 nicotinic acetylcholine and dopamine D2 receptors may be supportive for therapeutic effects (Rammes et al., 2008). Thus, the significantly reduced aggressive behavior attained with MEM may also include the participation of these neurotransmitter systems. However, this issue was not addressed by this study. Similarly to MEM, acute injection of MK-801 mitigates the aggressive outcomes in long-term ND exposed mice. It is recognized that MK-801 increases spontaneous locomotion (Bortolato et al., 2012; Tort et al., 2004), albeit doses up to 0.15 mg/kg barely increase locomotor activity in mice (Su et al., 2007) and rats (Ouagazzal et al., 1993). Bortolato et al. (2012) showed that wild-type mice injected with MK-801 (0.1 mg/kg) caused hyperlocomotion and none antiaggressive effects; but despite this the same dose in our work decreased the aggressive outcomes in long-term ND mice. In contrast to our hypothesis, there are studies showing that NMDAr antagonism with phencyclidine or memantine increases rather than decrease aggressive behavior (Audet et al., 2009; Newman et al., 2012). Taken together, these results corroborate the functional relevance of increased brain glutamate levels and the NMDAr binding sites in the neurobiology of aggression.

Conclusion

In summary, long-term ND-induced aggressive behavior is associated with decreased extracellular glutamate clearance and NMDAr hyperexcitability emphasizing the role of this receptor in mediating mechanisms of aggression.

Supplementary data to this article can be found online at http://dx.doi.org/10.1016/j.yhbeh.2014.06.005.

Financial disclosures

The authors have no biomedical financial interests to disclose.

Conflict of interest

There are no conflicts of interest with other people or organizations.

Acknowledgments

This work was supported by the following Brazilian agencies: CNPq, CAPES, FAPERGS and by Grants of the Brazilian Institute of Neuroscience — IBNnet FINEP (550006/2011-7), INCT — Excitotoxicity and Neuroprotection (573677/2208-5).

References

Audet, M.C., Goulet, S., Dore, F.Y., 2009. Impaired social motivation and increased aggression in rats subchronically exposed to phencyclidine. Physiol. Behav. 96, 394–398.
Belozertseva, I., Bespalov, A., Gmiro, E., Danysz, W., Zvartau, E., 1999. Effects of NMDA receptor channel blockade on aggression in isolated male mice. Aggress. Behav. 25, 48–49.
Bortolato, M., Godar, S.C., Melis, M., Soggiu, A., Roncada, P., Casu, A., Flore, G., Chen, K., Frau, R., Urbani, A., Castelli, M.P., Devoto, P., Shih, J.C., 2012. NMDARs mediate the role of monoamine oxidase A in pathological aggression. J. Neurosci. 32, 8574–8582.
Brann, D.W., Mahesh, V.B., 1995. Glutamate: a major neuroendocrine excitatory signal mediating steroid effects on gonadotropin secretion. J. Steroid Biochem. Mol. Biol. 53, 325–329.
Breuer, M.E., McGinnis, M.Y., Lumia, A.R., Possidente, B.P., 2001. Aggression in male rats receiving anabolic androgenic steroids: effects of social and environmental provocation. Horm. Behav. 40, 409–418.
Brody, J.F., DeFeudis, P.A., DeFeudis, F.V., 1969. Effects of micro-injections of L-glutamate into the hypothalamus on attack and flight behaviour in cats. Nature 224, 1330.
Carrillo, M., Ricci, L.A., Melloni Jr., R.H., 2009. Adolescent anabolic androgenic steroids reorganize the glutamatergic neural circuitry in the hypothalamus. Brain Res. 1249, 118–127.
Carrillo, M., Ricci, L.A., Melloni, R.H., 2011a. Developmental and withdrawal effects of adolescent AAS exposure on the glutamatergic system in hamsters. Behav. Neurosci. 125, 452–464.
Carrillo, M., Ricci, L.A., Melloni, R.H., 2011b. Glutamate and the aggression neural circuit in adolescent anabolic steroid-treated Syrian hamsters (*Mesocricetus auratus*). Behav. Neurosci. 125, 753–763.
Clark, A.S., Henderson, L.P., 2003. Behavioral and physiological responses to anabolic–androgenic steroids. Neurosci. Biobehav. Rev. 27, 413–436.
Clements, J.D., Lester, R.A., Tong, G., Jahr, C.E., Westbrook, G.L., 1992. The time course of glutamate in the synaptic cleft. Science 258, 1498–1501.
Danbolt, N.C., 2001. Glutamate uptake. Prog. Neurobiol. 65, 1–105.
de Almeida, R.M., Saft, D.M., Rosa, M.M., Miczek, K.A., 2010. Flunitrazepam in combination with alcohol engenders high levels of aggression in mice and rats. Pharmacol. Biochem. Behav. 95, 292–297.
Defensor, E.B., Corley, M.J., Blanchard, R.J., Blanchard, D.C., 2012. Facial expressions of mice in aggressive and fearful contexts. Physiol. Behav. 107, 680–685.
Diano, S., Naftolin, F., Horvath, T.L., 1997. Gonadal steroids target AMPA glutamate receptor-containing neurons in the rat hypothalamus, septum and amygdala: a morphological and biochemical study. Endocrinology 138, 778–789.
Ferris, C.F., Stolberg, T., Kulkarni, P., Murugavel, M., Blanchard, R., Blanchard, D.C., Febo, M., Brevard, M., Simon, N.G., 2008. Imaging the neural circuitry and chemical control of aggressive motivation. BMC Neurosci. 9, 111.
Fischer, S.G., Ricci, L.A., Melloni Jr., R.H., 2007. Repeated anabolic/androgenic steroid exposure during adolescence alters phosphate-activated glutaminase and glutamate receptor 1 (GluR1) subunit immunoreactivity in hamster brain: correlation with offensive aggression. Behav. Brain Res. 180, 77–85.
Garrido, P., de Blas, M., Del Arco, A., Segovia, G., Mora, F., 2012. Aging increases basal but not stress-induced levels of corticosterone in the brain of the awake rat. Neurobiol. Aging 33, 375–382.
Haller, J., 2013. The neurobiology of abnormal manifestations of aggression — a review of hypothalamic mechanisms in cats, rodents, and humans. Brain Res. Bull. 93, 97–109.
Haller, J., Abraham, I., Zelena, D., Juhasz, G., Makara, G.B., Kruk, M.R., 1998. Aggressive experience affects the sensitivity of neurons towards pharmacological treatment in the hypothalamic attack area. Behav. Pharmacol. 9, 469–475.
Jones, R.E., Lopez, K.H., 2006. Human Reproductive Biology, 3rd ed. Elsevier Academic Press, Amsterdam Boston.
Kanayama, G., Hudson, J.I., Pope Jr., H.G., 2010. Illicit anabolic–androgenic steroid use. Horm. Behav. 58, 111–121.
Kazlauckas, V., Schuh, J., Dall'Igna, O.P., Pereira, G.S., Bonan, C.D., Lara, D.R., 2005. Behavioral and cognitive profile of mice with high and low exploratory phenotypes. Behav. Brain Res. 162, 272–278.
Kotermanski, S.E., Johnson, J.W., Thiels, E., 2013. Comparison of behavioral effects of the NMDA receptor channel blockers memantine and ketamine in rats. Pharmacol. Biochem. Behav. 109, 67–76.
Le Greves, P., Huang, W., Johansson, P., Thornwall, M., Zhou, Q., Nyberg, F., 1997. Effects of an anabolic–androgenic steroid on the regulation of the NMDA receptor NR1, NR2A and NR2B subunit mRNAs in brain regions of the male rat. Neurosci. Lett. 226, 61–64.
Leasure, J.L., Decker, L., 2009. Social isolation prevents exercise-induced proliferation of hippocampal progenitor cells in female rats. Hippocampus 19, 907–912.
Lehre, K.P., Danbolt, N.C., 1998. The number of glutamate transporter subtype molecules at glutamatergic synapses: chemical and stereological quantification in young adult rat brain. J. Neurosci. 18, 8751–8757.
Magnusson, K., Hanell, A., Bazov, I., Clausen, F., Zhou, Q., Nyberg, F., 2009. Nandrolone decanoate administration elevates hippocampal prodynorphin mRNA expression

and impairs Morris water maze performance in male rats. Neurosci. Lett. 467, 189–193.
McGinnis, M.Y., 2004. Anabolic androgenic steroids and aggression: studies using animal models. Ann. N. Y. Acad. Sci. 1036, 399–415.
Moreira, J.D., de Siqueira, L.V., Lague, V.M., Porciuncula, L.O., Vinade, L., Souza, D.O., 2011. Short-term alterations in hippocampal glutamate transport system caused by one-single neonatal seizure episode: implications on behavioral performance in adulthood. Neurochem. Int. 59, 217–223.
Muller, A.P., Gnoatto, J., Moreira, J.D., Zimmer, E.R., Haas, C.B., Lulhier, F., Perry, M.L., Souza, D.O., Torres-Aleman, I., Portela, L.V., 2011. Exercise increases insulin signaling in the hippocampus: physiological effects and pharmacological impact of intracerebroventricular insulin administration in mice. Hippocampus 21, 1082–1092.
Munozblanco, J., Castillo, A.P., 1987. Changes in neurotransmitter amino-acids content in several CNS areas from aggressive and nonaggressive bull strains. Physiol. Behav. 39, 453–457.
Nelson, R.J., Chiavegatto, S., 2001. Molecular basis of aggression. Trends Neurosci. 24, 713–719.
Nelson, R.J., Trainor, B.C., 2007. Neural mechanisms of aggression. Nat. Rev. Neurosci. 8, 536–546.
Newman, E.L., Chu, A., Bahamon, B., Takahashi, A., Debold, J.F., Miczek, K.A., 2012. NMDA receptor antagonism: escalation of aggressive behavior in alcohol-drinking mice. Psychopharmacology (Berlin) 224, 167–177.
Oliveira, I.J., Molz, S., Souza, D.O., Tasca, C.I., 2002. Neuroprotective effect of GMP in hippocampal slices submitted to an in vitro model of ischemia. Cell. Mol. Neurobiol. 22, 335–344.
Ouagazzal, A., Nieoullon, A., Amalric, M., 1993. Effects of dopamine D1 and D2 receptor blockade on MK-801-induced hyperlocomotion in rats. Psychopharmacology (Berlin) 111, 427–434.
Paxinos, G., Franklin, K.B.J., 2001. The Mouse Brain in Stereotaxic Coordinates, 2nd ed. Academic Press, San Diego.
Peterson, G.L., 1977. A simplification of the protein assay method of Lowry et al. which is more generally applicable. Anal. Biochem. 83, 346–356.
Prut, L., Belzung, C., 2003. The open field as a paradigm to measure the effects of drugs on anxiety-like behaviors: a review. Eur. J. Pharmacol. 463, 3–33.
Rammes, G., Danysz, W., Parsons, C.G., 2008. Pharmacodynamics of memantine: an update. Curr. Neuropharmacol. 6, 55–78.
Ricci, L.A., Grimes, J.M., Melloni Jr., R.H., 2007. Lasting changes in neuronal activation patterns in select forebrain regions of aggressive, adolescent anabolic/androgenic steroid-treated hamsters. Behav. Brain Res. 176, 344–352.
Robinson, S., Penatti, C.A., Clark, A.S., 2012. The role of the androgen receptor in anabolic androgenic steroid-induced aggressive behavior in C57BL/6J and TFM mice. Horm. Behav. 61, 67–75.
Rossbach, U.L., Steensland, P., Nyberg, F., Le Greves, P., 2007. Nandrolone-induced hippocampal phosphorylation of NMDA receptor subunits and ERKs. Biochem. Biophys. Res. Commun. 357, 1028–1033.
Schmidt, A.P., Tort, A.B., Silveira, P.P., Bohmer, A.E., Hansel, G., Knorr, L., Schallenberger, C., Dalmaz, C., Elisabetsky, E., Crestana, R.H., Lara, D.R., Souza, D.O., 2009. The NMDA antagonist MK-801 induces hyperalgesia and increases CSF excitatory amino acids in rats: reversal by guanosine. Pharmacol. Biochem. Behav. 91, 549–553.
Shahidi, N.T., 2001. A review of the chemistry, biological action, and clinical applications of anabolic–androgenic steroids. Clin. Ther. 23, 1355–1390.
Simon, N.G., Whalen, R.E., 1986. Hormonal-regulation of aggression — evidence for a relationship among genotype, receptor-binding, and behavioral sensitivity to androgen and estrogen. Aggress. Behav. 12, 255–266.
Su, Y.A., Si, T.M., Zhou, D.F., Guo, C.M., Wang, X.D., Yang, Y., Shu, L., Liang, J.H., 2007. Risperidone attenuates MK-801-induced hyperlocomotion in mice via the blockade of serotonin 5-HT 2A/2C receptors. Eur. J. Pharmacol. 564, 123–130.
Sukhotina, I.A., Bespalov, A.Y., 2000. Effects of the NMDA receptor channel blockers memantine and MRZ 2/579 on morphine withdrawal-facilitated aggression in mice. Psychopharmacology (Berlin) 149, 345–350.
Sullivan, G.M., Feinn, R., 2012. Using effect size-or why the p value is not enough. J. Grad. Med. Educ. 4, 279–282.
Talih, F., Fattal, O., Malone Jr., D., 2007. Anabolic steroid abuse: psychiatric and physical costs. Cleve. Clin. J. Med. 341–344 (346, 349–352).
Tanehkar, F., Rashidy-Pour, A., Vafaei, A.A., Sameni, H.R., Haghighi, S., Miladi-Gorji, H., Motamedi, F., Akhavan, M.M., Bavarsad, K., 2013. Voluntary exercise does not ameliorate spatial learning and memory deficits induced by chronic administration of nandrolone decanoate in rats. Horm. Behav. 63, 158–165.
Thomazi, A.P., Godinho, G.F., Rodrigues, J.M., Schwalm, F.D., Frizzo, M.E., Moriguchi, E., Souza, D.O., Wofchuk, S.T., 2004. Ontogenetic profile of glutamate uptake in brain structures slices from rats: sensitivity to guanosine. Mech. Ageing Dev. 125, 475–481.
Thurmond, J.B., 1975. Technique for producing and measuring territorial aggression using laboratory mice. Physiol. Behav. 14, 879–881.
Tort, A.B., Mantese, C.E., dos Anjos, G.M., Dietrich, M.O., Dall'Igna, O.P., Souza, D.O., Lara, D.R., 2004. Guanosine selectively inhibits locomotor stimulation induced by the NMDA antagonist dizocilpine. Behav. Brain Res. 154, 417–422.
Ullensvang, K., Lehre, K.P., Storm-Mathisen, J., Danbolt, N.C., 1997. Differential developmental expression of the two rat brain glutamate transporter proteins GLAST and GLT. Eur. J. Neurosci. 9, 1646–1655.
Umukoro, S., Aladeokin, A.C., Eduviere, A.T., 2013. Aggressive behavior: a comprehensive review of its neurochemical mechanisms and management. Aggress. Violent Behav. 18, 195–203.
Vekovischeva, O.Y., Aitta-Aho, T., Echenko, O., Kankaanpaa, A., Seppala, T., Honkanen, A., Sprengel, R., Korpi, E.R., 2004. Reduced aggression in AMPA-type glutamate receptor GluR-A subunit-deficient mice. Genes Brain Behav. 3, 253–265.
Ventriglia, F., Di Maio, V., 2013. Effects of AMPARs trafficking and glutamate-receptors binding probability on stochastic variability of EPSC. Biosystems 112, 298–304.
Yang, M., Weber, M.D., Crawley, J.N., 2008. Light phase testing of social behaviors: not a problem. Front. Neurosci. 2, 186–191.
Zimmer, A.R., Leonardi, B., Zimmer, E.R., Kalinine, E., de Souza, D.O., Portela, L.V., Gosmann, G., 2012a. Long-term oral administration of *Capsicum baccatum* extracts does not alter behavioral, hematological, and metabolic parameters in CF1 mice. Evid. Based Complement. Alternat. Med. 2012, 196358.
Zimmer, E.R., Kalinine, E., Haas, C.B., Torrez, V.R., Souza, D.O., Muller, A.P., Portela, L.V., 2012b. Pretreatment with memantine prevents Alzheimer-like alterations induced by intrahippocampal okadaic acid administration in rats. Curr. Alzheimer Res. 9, 1182–1190.

ANEXO II-D. *Changes in Brain 14-3-3 Proteins in Response to Insulin Resistance Induced by a High Palatable Diet.*

No **ANEXO II-D** apresentamos o artigo publicado no periódico *Molecular Neurobiology*.

Author's personal copy

Mol Neurobiol (2015) 52:710–718
DOI 10.1007/s12035-014-8905-4

Changes in Brain 14-3-3 Proteins in Response to Insulin Resistance Induced by a High Palatable Diet

Hugo Bock · Aline Rigon Zimmer · Eduardo Rigon Zimmer · Diogo Onofre Gomes de Souza · Luis Valmor Cruz Portela · Maria Luiza Saraiva-Pereira

Received: 23 March 2014 / Accepted: 24 September 2014 / Published online: 4 October 2014
© Springer Science+Business Media New York 2014

Abstract The 14-3-3 protein family takes part in a wide range of cellular processes and is expressed in all eukaryotic organisms. In mammals, seven isoforms (β, ε, η, γ, τ, ζ, and σ) have been identified. 14-3-3 proteins are suggested to modulate the insulin-signaling cascade in the brain. The aim of this study was to investigate whether insulin resistance state induced by high palatable diet modulates expression of the 14-3-3 proteins in brain. Wistar male rats ($n=8$) were divided into two experimental groups: insulin resistant (IR), induced by high palatable diet, and control (CO) group. Biochemical parameters (glucose tolerance test and plasma lipid profile) were evaluated after 130 days. Brain structures (cortex and hippocampus) were dissected for evaluation of messenger RNA (mRNA) and protein levels of different 14-3-3 proteins. Statistical analyses included Student t test and Pearson correlation. Significant decrease was observed in Ywhah and in Ywahq mRNA levels in the cortex of IR group, while no changes were observed in the hippocampus. Significant increase of θ isoform was observed in hippocampus IR group by immunodetection, while no differences were detected in the remaining isoforms. Inverse correlation was observed between blood glucose levels in cortex IR group and both Ywhah and Ywhaq mRNA levels. Protein levels of Creb and phosphatidylinositide 3-kinases (PI3K) showed to be increased in the hippocampus. These alterations may be due to a compensatory effect of impaired insulin signaling. We demonstrated differential expression of 14-3-3 isoforms throughout brain regions of rats with IR. As a whole, our results indicate that brain 14-3-3 levels are influenced by different diets.

Keywords 14-3-3 · Insulin resistance · Protein expression · mRNA levels · Rat brain

H. Bock · M. L. Saraiva-Pereira
Laboratório de Identificação Genética–Centro de Pesquisa Experimental e Serviço de Genética Médica–Hospital de Clínicas de Porto Alegre (HCPA), Porto Alegre, Brazil

H. Bock · E. R. Zimmer · D. O. G. de Souza · L. V. C. Portela · M. L. Saraiva-Pereira
Programa de Pós-Graduação em Ciências Biológicas: Bioquímica, Universidade Federal do Rio Grande do Sul—UFRGS, Porto Alegre, Brazil

A. R. Zimmer
Departamento de Produção de Matéria-Prima, Faculdade de Farmácia, Universidade Federal do Rio Grande do Sul—UFRGS, Porto Alegre, Brazil

D. O. G. de Souza · L. V. C. Portela · M. L. Saraiva-Pereira
Departamento de Bioquímica, Universidade Federal do Rio Grande do Sul—UFRGS, Porto Alegre, Brazil

M. L. Saraiva-Pereira (✉)
Serviço de Genética Médica, Hospital de Clínicas de Porto Alegre, Rua Ramiro Barcelos, 2350, Porto Alegre 90035-903, Brazil
e-mail: mlpereira@hcpa.ufrgs.br

Introduction

The 14-3-3 protein family consists of highly conserved regulatory molecules expressed in all eukaryotic cells [1, 2]. In mammals, seven isoforms (β, γ, ε, ζ, η, θ, and σ) have been identified to date, and they seem to be highly abundant in the mammalian nervous system [3]. 14-3-3 proteins participate in a wide range of cellular processes through binding interactions with hundreds of structurally and functionally diverse proteins [4]. These proteins are implicated in regulation and coordination of many cellular processes, including signaling pathways, transcriptional regulation of messenger RNA (mRNA) levels, apoptosis, and signaling cascades among others [5, 6].

In the brain, 14-3-3 proteins are suggested to modulate the insulin signaling cascade pathway through phosphorylation and interaction with key regulatory proteins such as insulin

Author's personal copy

receptor substrate-1 (IRS-1) and IRS-2, glycogen synthase kinase 3 (GSK3), and phosphatidylinositide 3-kinases (PI3K) [7–10].

Insulin is well known as the major and immediate regulator of blood glucose levels in peripheral tissues and has emerged as a major regulatory substance within the brain [11]. For instance, two major brain areas of behavior affected by insulin are those related to feeding and cognition [12]. Depressive-like behavior in rats can be explained by downregulation of hypothalamic insulin receptor signaling [13]. In addition, insulin receptor protein levels decrease with age, which suggests that insulin signaling and insulin receptor levels are involved in the aging process [14, 15]. Disease states such as dementia and Alzheimer are related to insulin resistance and to other aspects of metabolic syndrome [16]. High risk of dementia or significant cognitive decline has been associated to both insulin resistance alone and type 2 diabetes mellitus (T2DM) [17, 18]. Therefore, insulin resistance possibly enhances the synaptic loss and neurodegeneration associated with cognitive decline and dementia [19].

Many proteins that bind to 14-3-3 in response to insulin-activated signaling pathways have been identified [20]. Overall, a network of 14-3-3-phosphoprotein interactions has been shown to provide mechanistic insights into glucose uptake stimulated by insulin as well as other effects in intracellular events [21]. IRS proteins serve as intracellular docking and adapter molecules that integrate stimuli from different cellular pathways. IRS2 and 14-3-3 have been shown to interact on high cAMP levels, upon insulin and IGF-1 stimulation [8]. Recently, 14-3-3 mRNA and protein levels were shown to be affected in an isoform- and tissue-specific manner in a streptozotocin-induced diabetic animal model [22].

It is well recognized that insulin resistance and disrupted glucose metabolism occurs in peripheral tissues. However, recent publications support the view that insulin resistance is also present in the brain. This perspective coincides with the current concept that brain insulin receptors/signaling have physiological relevance for neuroplasticity and neuromodulation mechanisms [23–26]. We have previously demonstrated in an insulin resistance model that in addition to peripheral parameters, some neurological aspects are also modified. All of these observations point to the fact that brain insulin resistance is reasonably reliable [11, 27]. Thus, impaired signaling modifies the expression of a wide variety of other related proteins, including 14-3-3 proteins, taking into account that insulin is a pro-survival molecule. The extent of mRNA and protein reflects a dynamic balance among all cell processes, although the way this balance is achieved remains a challenge. Emerging evidence is changing the role for many regulatory mechanisms occurring after mRNA are manufactured. This has been examined to date in almost every organism; amount of transcript does not fully predict protein extent [28, 29].

Therefore, the purpose of the present study was to investigate whether insulin resistance state induced by high palatable diet modulates the expression of 14-3-3 isoforms in the brain of rats.

Experimental Procedures

Animals and Diet

Eight (n=8) adult male Wistar rats were housed under controlled temperature (22±2 °C) and humidity (55±10 %) conditions on a 12-h light-dark cycle (lights on at 7 a.m.), with food and water offered ad libitum. All experiments were performed in agreement with international standards and the Brazilian College of Animal Experimentation for animal protection. The project was approved by the Ethical Committee on animal use of the Universidade Federal do Rio Grande do Sul, Brazil (#19446). At 2 months old (ranging from 200 to 250 g of weight), animals were divided into two experimental groups (n=4): control (CO) and insulin resistant (IR). Administration of high palatable diet (also known as *cafeteria diet* or *Western-style diet*) during 130 days was used to induce insulin resistance in IR group [27, 28], while CO group was fed with standard laboratory diet.

Biochemical parameters were evaluated after 130 days. For glucose tolerance test, rats were deprived from food overnight (8 h) and blood samples were collected through a small puncture on the tail. Animals were anesthetized with ketamine/xylazine intraperitoneally (100/10 mg/kg), and blood was collected for plasma lipid profile. They were then decapitated, the cortex and hippocampus were rapidly dissected, and each structure was divided into two pieces. One was rapidly frozen and stored at −80 °C for proteome analysis; the other was submerged in RNAlater® (Ambion, USA) and stored at −20 °C for mRNA analysis.

Biochemical Profile

Glucose solution at 50 % (w/v) was administrated into rats (2 g/kg of body weight) for glucose tolerance test (GTT). Blood samples were collected at fasting and at 30, 60, and 120 min after glucose overload, and glycemia was measured with a commercial glucometer, Accu-Chek Active (Roche, USA).

Plasma lipid profile was performed by measuring levels of total content of triglycerides (TG), total cholesterol (TC), and fractions of high-density lipoprotein (HDL) and low-density lipoprotein (LDL). Analyses were performed using commercial kits (Katal®, MG, Brazil).

Author's personal copy

Evaluation of Protein Profile by Mass Spectrometry

Pieces of frozen tissue were homogenized in PBS using a homogenizer, and proteins were extracted with 10 % TCA in cold acetone. Protein extracts of all the groups (cortex IR, cortex CO, hippocampus IR, and hippocampus CO groups) were analyzed by mass spectrometry (MS) to identify differentially expressed proteins. A total of 100 μg of protein was digested with trypsin (Sigma-Aldrich, USA) at 1:50 (*w*/*w*) enzyme/protein ratio for 1 h at 37 °C. Reaction was then quenched, and tryptic digest was separated using a nanoLC Ultra-1D plus system (Eksigent, USA), followed by direct elution to a nanospray ion source connected to a hybrid mass spectrometer (LTQ-XL and LTQ Orbitrap Discovery, Thermo, USA). Flow rate was set at 300 nL/min using 2–98 % acetonitrile/0.1 % formic acid gradient during 5 h.

Tandem mass spectra were obtained by Proteome Discoverer 1.0 software (Thermo Fisher Scientific, USA), and all MS/MS samples were analyzed using SEQUEST software assuming the digestion by trypsin. Scaffold software v. 3.1.2 (Proteome Software Inc., USA) was used to validate MS/MS-based peptide and protein identifications. Proteomes were compared using DeconTools software v. 1 (Pacific Northwest National Laboratory, USA) and MultiAlign v. 5.0.3 (Pacific Northwest National Laboratory, USA). Protein quantitation was assessed by spectral counting, where the number of observed spectral counts for each protein is a frequency-based analysis approach that provides a rough measure of protein levels in complex protein mixtures, especially for more abundant proteins [30, 31].

Evaluation of mRNA Levels of 14-3-3 Isoforms

mRNA levels were measured by quantitative real-time PCR (qPCR) using gene-specific TaqMan® FAM/MGB inventoried or made to order assays (14-3-3 isoform β/α, gene Ywhab, assay Rn00695953_m1; ζ/δ, Ywhaz, Rn00755072_m1; η, Ywhah, Rn00755085_m1; θ, Ywhaq, Rn00820723_g1; Applied Biosystems, USA), using glyceraldehyde-3-phosphate dehydrogenase (GAPDH) as endogenous control (inventoried assay Rn99999916_s1, Applied Biosystems, USA). Total RNA was extracted using TRI Reagent® solution (Ambion, USA) according to manufacturer's protocol. RNA concentration was estimated using the fluorimetric method Quant-iT® RNA Assay (Invitrogen, USA) in the Qubit™ (Invitrogen, USA) equipment. Complementary DNA (cDNA) was synthesized by reverse transcription (RT) reaction using High-Capacity cDNA Reverse Transcription Kit (Applied Biosystems, USA). Two hundred nanograms of total RNA was placed in a total reaction volume of 20 μL containing 1× RT buffer, 4 mM of each dNTP, 1× RT Random Primers, and 0.05 units of MultiScribe™ Reverse Transcriptase. RT reaction was performed as follows: 10 min at 25 °C, 2 h at 37 °C, and 5 s at 85 °C. Subsequently, cDNA was kept at −20 °C until further use.

cDNA solution was diluted 1:5 in water, and reaction was carried out in a total volume of 12 μL containing 1 μL of diluted cDNA solution, 1× of gene-specific TaqMan® assay, 1× of endogenous control TaqMan® assay, and 1× PCR Master Mix (Applied Biosystems, USA). Cycling program was 2, 10 min at 95 °C, followed by 40 cycles of 15 s at 95 °C and 1 min at 60 °C. Reactions of each sample were performed in triplicate in an ABI Prism 7500 Fast Sequence Detector System (Applied Biosystems, USA).

Transcriptional profile of each 14-3-3 isoform was determined in both brain structures. The relative mRNA levels were calculated by the ΔΔCt method according to Livak and Schmittgen [32], using GAPDH as endogenous control and the control group of each structure as calibrator.

Evaluation of Protein Levels by Western Blot

Total protein extracts of each group were analyzed by Western blot (WB) for protein analysis. Twenty micrograms of protein were mixed with Bolt™ LDS Sample Buffer (4×) (Novex, USA) and Bolt™ Sample Reducing Agent (10×) (Novex, USA). Samples were then heated for 5 min at 95 °C and separated on a precasted Bolt™ Bis-Tris Plus Gel 4 to 12 % polyacrylamide gradient (Novex, USA) using Bolt™ MES SDS Running Buffer (Novex, USA) for 35 min. at 165 V. Following electrophoresis, protein content was transferred to a nitrocellulose membrane using iBlot® Transfer Stack (Novex, USA) in the iBlot® Gel Transfer Device (Invitrogen, USA) using the P3–7-min program.

Free sites were blocked with 5 % nonfat milk powder in tris-buffered saline containing 0.5 % Tween 20 (TBS-T) pH 7.3 to 7.5 for 1 h after blotting. Membranes were rinsed once for 10 min followed by three times for 5 min with TBS-T solution and then incubated for 1 h with 14-3-3 isoform primary antibodies (14-3-3 β/α, #9636, 1:2.000; 14-3-3 ζ/δ, #7413, 1:2.000; 14-3-3 θ, #9638, 1:1.1000; 14-3-3 η, #5521, 1:1.000; Cell Signaling Technology, USA) diluted in TBS-T with 1 % BSA solution. For Creb (#9104, Cell Signaling Technology) and PI3K p85 (#4257P, Cell Signaling Technology), the primary antibodies were diluted 1:1.000 and incubated overnight at 4 °C. Next to incubation with primary antibodies, membranes were rinsed again as previously described and incubated for 1 h with secondary antibody conjugated to horseradish peroxidase (anti-rabbit IgG HRP-linked, #7074, 1:4.000; Cell Signaling Technology, USA) diluted in TBS-T with 1 % BSA solution. All incubations and washes were performed at room temperature with gentle

Author's personal copy

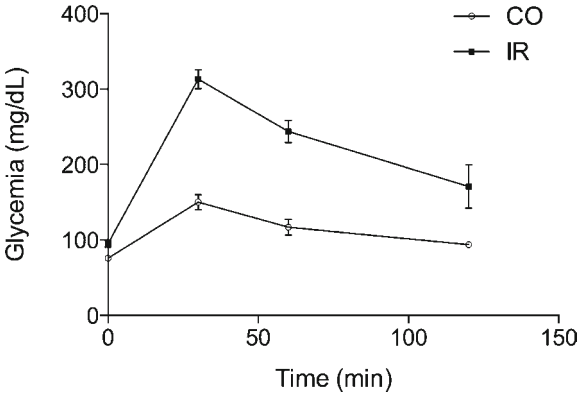

Fig. 1 Glucose tolerance test. High palatable diet during 130 days altered the glucose tolerance test (GTT). Measures were at fasting and at 30, 60, and 120 min after glucose overload. *CO* represents control group, and *IR* represents insulin-resistant group (n=4 per group)

agitation. Blots were developed using the Western Lightning ECL Pro (PerkinElmer, USA), and membranes were then imaged using the ImageQuant LAS 500 (General Electric Healthcare, USA). Same membranes were rinsed and blotted to housekeeping anti-β-actin HRP-linked antibody (#A3854, 1:30.000; Sigma-Aldrich, USA) and followed by the same treatment described above. Immunoreactive content was quantified using ImageJ software v. 1.47 (available from the National Institutes of Health, USA).

Statistical Analysis

Statistical analyses were performed using Student t test. Correlation between variables was calculated by Pearson correlation, and differences were considered statistically significant when $p<0.05$.

Results

Biochemical Profile Demonstrates Insulin Resistance in Animal Model

We demonstrated that the treatment with high palatable diet during 130 days altered results of the GTT. Blood glucose levels at 0, 30, 60, and 120 min after glucose overload were measured and are shown in Fig. 1. Area under the curve (AUC) showed a significant higher value in the IR group when compared to CO group ($p<0.0001$) (data not shown). We have also evaluated lipid parameters (TG, TC, HDL, and LDL), and TC as well as LDL was significantly increased in the IR group when compared to CO (Fig. 2).

Evaluation of mRNA Levels of 14-3-3 Isoforms and Correlation with Biochemical Parameters

Significant decrease of mRNA levels in cortex IR group was observed in Ywhah (14-3-3 η, $p=0.0118$) and Ywahq (14-3-3 θ, $p=0.0156$). Ywhab (14-3-3 β/α) and Ywhaz (14-3-3 ζ/δ) genes do not show significant differences in mRNA levels in cortex IR group, when compared to CO group. mRNA levels of all 14-3-3 isoforms analyzed do not show any significant difference in hippocampus (Fig. 3).

In the cortex, AUC of IR group in GTT has shown negative correlation to mRNA levels of Ywhah ($r=-0.7587$, $p=0.0291$) and Ywhaq ($r=-0.8063$, $p=0.0156$) when compared to the CO group. All remaining correlations with glucose levels were not statistically significant (Fig. 4).

No differences were found between each lipid parameters evaluated (TG, TC, HDL, and LDL) and mRNA levels of the four 14-3-3 isoforms in the cortex and hippocampus (Fig. 5).

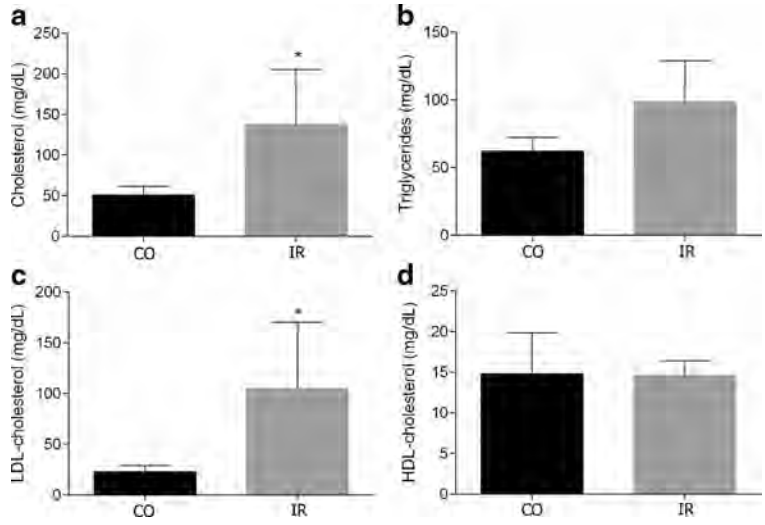

Fig. 2 Plasma lipid profile. Levels of total cholesterol (**a**), triglycerides (**b**), LDL-cholesterol (**c**), and HDL-cholesterol (**d**). *CO* represents control group (n=4), and *IR* represents insulin-resistant group (n=4). Means were compared by Student t test; *$p<0.05$

Author's personal copy

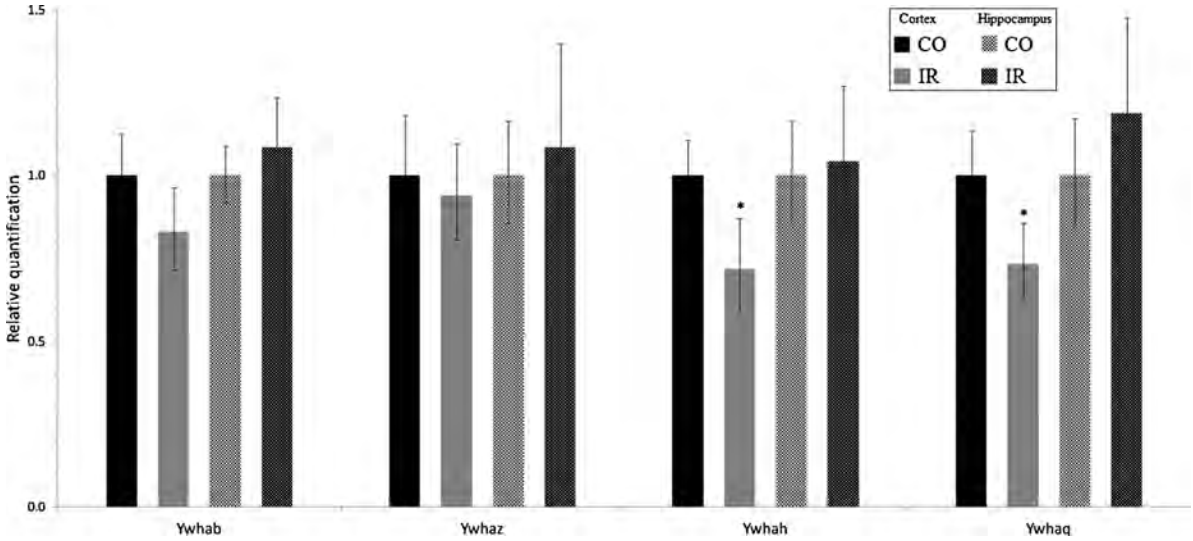

Fig. 3 Relative mRNA levels of 14-3-3 isoforms. Results are presented as mean±SD (n=4). Significant levels (*) were considered when $p<0.05$ Student t test. *CO* represents control group, and *IR* represents insulin resistant group

Evaluation of Protein Content of 14-3-3 Isoforms, Creb, and PI3K

Two (α/β and ζ/δ) of the four isoforms of 14-3-3 proteins analyzed showed alteration of expression pattern between test (IR) and control (CO) groups in MS experiment. Creb and PI3K were not detected, although total number of peptides found in MS was lower than expected for each group.

We observed significant increase of protein immunodetection in WB of the 14-3-3 θ isoform (p=0.0428) in hippocampus IR group, when compared to CO. No differences were found in the hippocampus for the other isoforms analyzed. In the cortex, all four isoforms analyzed do not show significant differences between the groups as well (Fig. 6). Creb and PI3K show a significant increase of protein immunodetection only in the hippocampus of IR group when compared to CO group (p=0.0090 and 0.0125, respectively). The cortex does not show significant changes (Fig. 7).

Discussion

In the present study, we have evaluated the effect of insulin resistance induced by high palatable diet on lipid and glucose parameters and on protein and mRNA levels of four 14-3-3 isoforms in adult male rats. Levels of TC and LDL and glucose intolerance showed to be significantly affected by diet, as expected.

mRNA levels and protein immunodetection of the four 14-3-3 isoforms (α/β, ζ/δ, η, and θ) were evaluated in the cortex and hippocampus of rats with induced insulin resistance and compared to rats fed with normal diet. We have then demonstrated that 14-3-3 isoforms

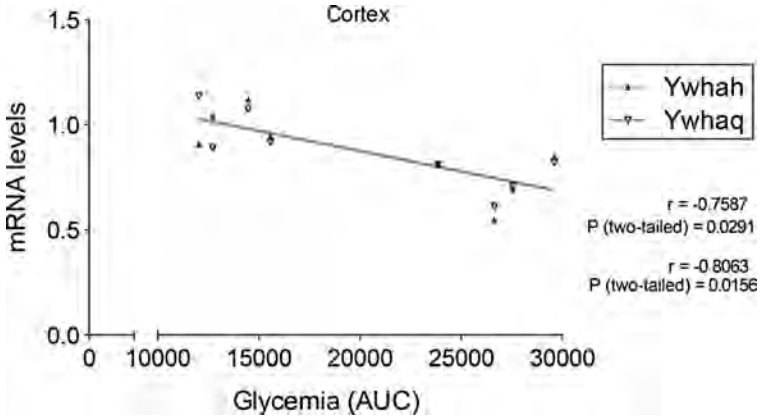

Fig. 4 Correlation of blood glucose versus mRNA levels. Correlation of glycemia (AUC) and mRNA levels of Ywhah and Ywhaq in cortex (Pearson correlation test)

Author's personal copy

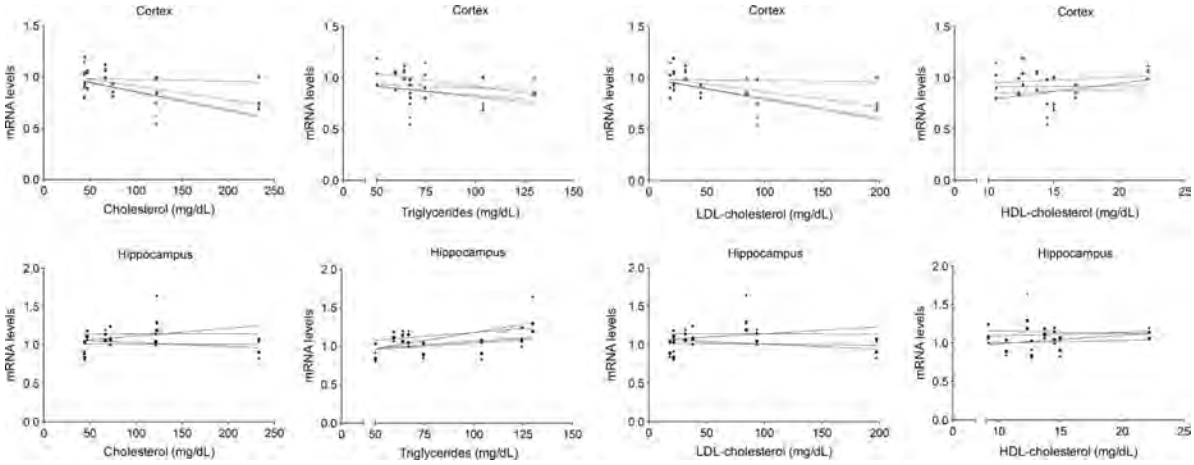

Fig. 5 Correlation of mRNA levels versus plasma lipid profile. mRNA levels of 14-3-3 isoforms (*black circle* Ywhab; *black square* Ywhaz; *black triangle* Ywhah; *black inverted triangle* Ywhaq) and total cholesterol, triglycerides, LDL cholesterol, and HDL cholesterol in the cortex (*upper set*) and in the hippocampus (*lower set*) per animal (n=4)

are differently expressed in the brain of rats with insulin resistance. As previously stated, 14-3-3 proteins are a family that can modulate interaction between proteins. Regulation of interaction usually involves phosphorylation of the interacting protein, and phosphorylation of 14-3-3 isoforms themselves may modulate interaction in some cases [2, 6, 33].

Proteome analysis revealed a decrease from 2 to 1 in peptide spectral count of 14-3-3 α/β in hippocampus IR group. These isoforms interact with the tuberous sclerosis 1/tuberous sclerosis 2 dimmer (TSC1/TSC2) and is involved in cell growth and morphology [34]. They form a protein complex that inhibits signal transduction to downstream effectors of the mammalian target of rapamycin (mTOR) [35]. The

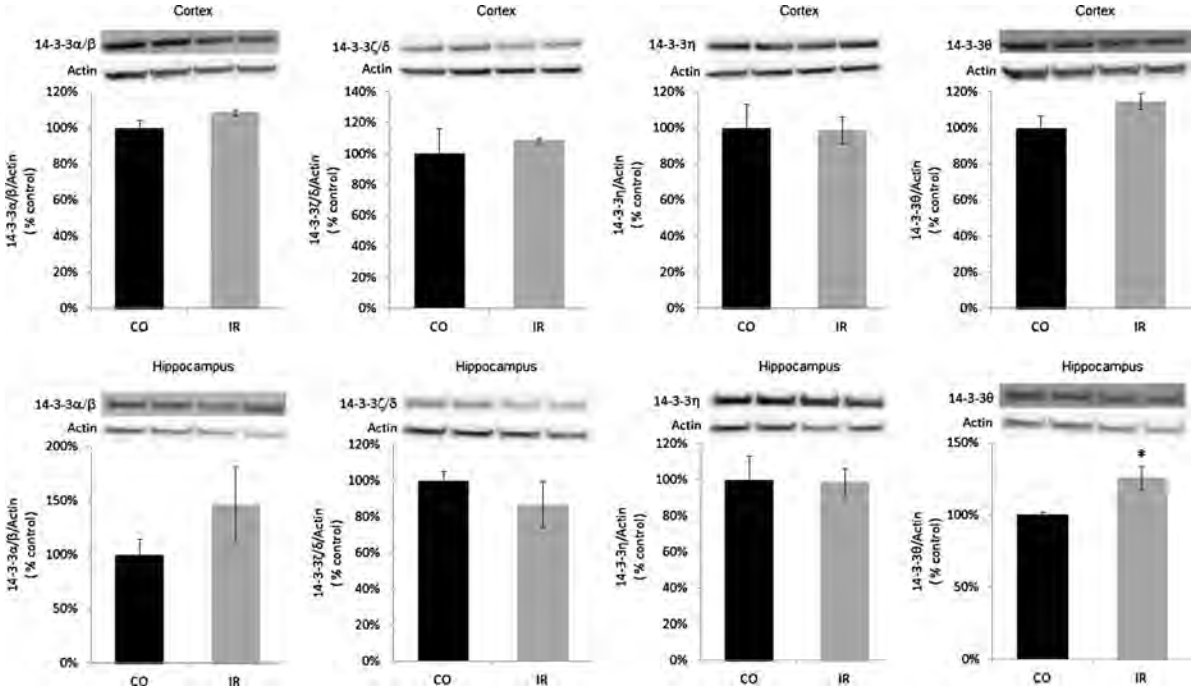

Fig. 6 Western blot analysis of 14-3-3 isoforms. Immunoreactive content was quantified by scanning densitometry, and density of each 14-3-3 antibody was normalized by actin content, in order to correct variations in protein loading. Upper panels represent results from the cortex, and lower panels represent results in the hippocampus. Results are presented as mean±SD (n=4). Means were compared using Student t test; *p<0.05

Author's personal copy

mTOR pathway is deregulated in diabetes, and a decrease of this isoform in insulin resistance state may be a consequence of the reduced signaling of insulin in the hippocampus that might be leading to a decreased inhibition of mTOR signaling [36].

We have also seen alterations in 14-3-3 ζ/δ isoforms in the proteome analysis. In cortex IR group, 3 counts in 14-3-3 ζ/δ isoforms were identified in peptide spectral while none were found in the CO. A small difference in peptide spectral count was also shown in the hippocampus, which increased from 4 to 5 counts when insulin resistance was induced. Interestingly, mRNA levels and immune content (WB) of this isoform remained unchanged. A recent study suggests that increasing 14-3-3 ζ/δ levels or activity could be a novel approach to the prevention of beta cell death that occurs in diabetes [37]. Other studies correlated 14-3-3 ζ/δ with IRS1 and IRS2 and with protein kinase B (Akt), but not in brain structures [7, 38]. IRS1, IRS2, and Akt are essential proteins in insulin pathway and may have a close interaction with 14-3-3 ζ/δ due to upregulation of this protein in insulin-resistant state.

mRNA levels of 14-3-3 η isoform were demonstrated to be significantly lower in cortex IR group. This isoform was previously shown to be important in long-term potentiation (LTP), more specifically as a downstream component of the pathway involved in presynaptic LTP [39]. Furthermore, 14-3-3 η has been associated with psychotic bipolar disorder [40]. In our study, despite no alterations in peptide and protein levels were present, we have demonstrated negative correlation of blood glucose levels and mRNA levels of this isoform. Therefore, we believe that this isoform can be involved in a fine tune regulation in the insulin pathway taking into account that variation was only found in mRNA levels in the cortex while no significant alteration was shown in the hippocampus.

mRNA levels of 14-3-3 θ isoform were shown to be downregulated in the present study. This isoform is involved in apoptosis and cell proliferation and promotes assembly and stability of microtubules. In addition, a protective effect in Parkinson disease has been demonstrated [41], and decrease observed here might be responsible for an increase in α-synuclein inclusion formation. It has been shown that overexpression of 14-3-3 θ protects against dopaminergic cell loss in a α-synuclein transgenic C. elegans model [42]. We demonstrate here a decrease in mRNA levels of Ywhaq only in the cortex, which is negatively correlated to AUC of blood

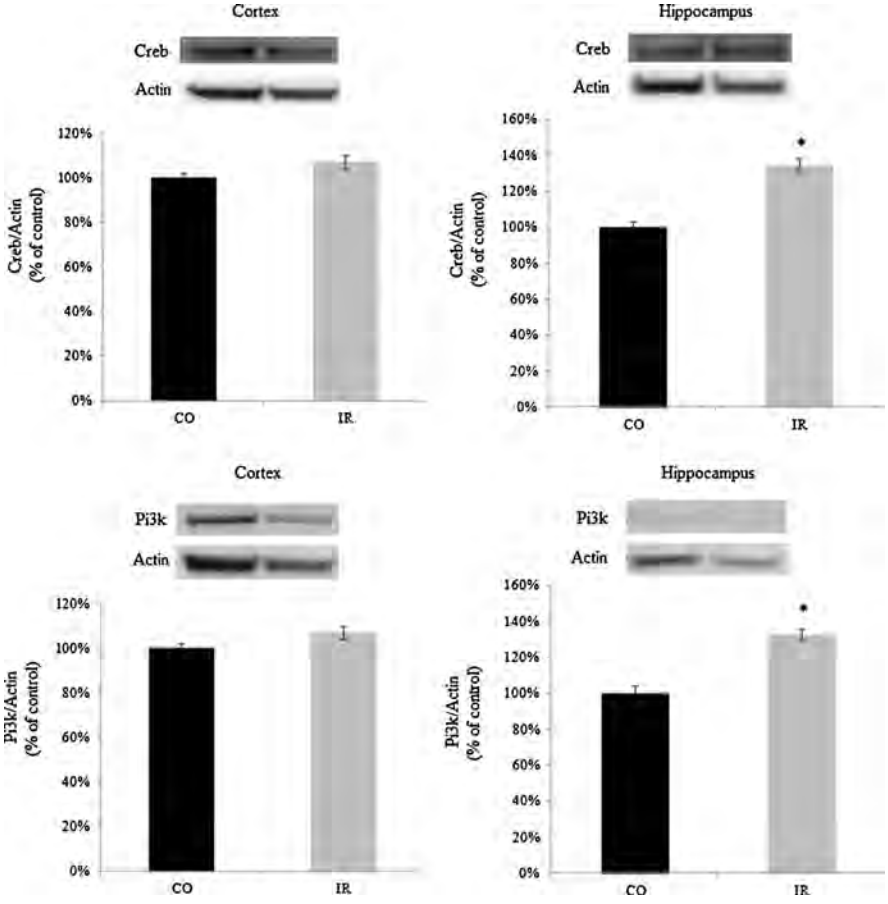

Fig. 7 Western blot analysis of Creb and PI3K in the cortex and hippocampus. Immunoreactive content was quantified by scanning densitometry, and density of each Creb (*upper set*) and PI3K (*lower set*) antibody was normalized by actin content, in order to correct variations in protein loading. Results are presented as mean±SD (n=4). Means were compared using Student t test; *p<0.05

Author's personal copy

glucose levels. Others studies have also shown downregulation in the cortex in association to bipolar disorder and schizophrenia [41]. Further, we have also seen an increase of almost 19 % in Ywhaq levels in the hippocampus, although no statistically significant difference was detected. Moreover, levels of 14-3-3 θ isoform detected by WB were significantly higher in hippocampus IR group. Involvement of 14-3-3 θ in the signaling pathway of growth factors, such as insulin, by stimulating the PI3K-Akt signal has been shown [43]. We then propose that insulin-resistant state may injure neurons, and these changes are an attempt to protect hippocampus by increasing 14-3-3 θ mRNA levels due to its protective effect. This data suggest that 14-3-3 θ isoform can play a key role in the insulin signaling pathway.

A recent work evaluated mRNA and protein levels of 14-3-3 proteins in a streptozotocin rat model of early DM1. Although they have assessed all forebrain and the model was of acute DM1, some results are in agreement with those presented in this work that show a decrease in mRNA levels of 14-3-3 3 η and θ and unchanged mRNA and protein levels of other isoforms. They demonstrated a decrease in protein levels of 14-3-3 θ in the brain cytosol while we observed an increase in protein levels of 14-3-3 θ in the hippocampus [22].

mRNA concentrations had represented concentrations and activities of the corresponding proteins, thereby assuming that transcript abundances are the main determinant of protein abundances. However, we observed a decrease in mRNA levels of 14-3-3 η and θ in the cortex and an increase in protein levels of 14-3-3 θ in the hippocampus. We also need to consider that when dealing with four isoforms and two distinct brain regions, it is plausible to expect differences in the molecular levels dependent on the isoform or the brain region. Insulin-resistant state can produce different responses in different structures, at different molecular levels, and in different molecules. There are many regulatory processes between transcription and translation, and protein stability is also an important issue. Data from transcription level can indicate whether the protein is present or not and, roughly, the levels of this protein. So, transcription data is useful for identifying potential candidates for follow-up at the protein level. However, changes in gene expression do not necessarily reflect alterations in protein level [44]. On the other hand, the discrepancies between mRNA and protein expression could be partially explained by differential tissue sensitivity pattern caused by insulin resistance.

We also evaluated the protein levels of Creb and PI3K by WB. Interestingly, the immunocontent of Creb and PI3K were increased in the hippocampus, but not in the cortex. This may be due to a compensatory effect of impaired insulin signaling in the structure. Creb is not only important in the direct transcriptional activation of gluconeogenic genes but also responsible for the progression of hepatic insulin resistance in the diet-induced or the genetic mouse models of obesity [45]. Despite the importance of Creb in diverse tissues, our study shows that Creb is also important in the CNS insulin-resistant state, mainly in the hippocampus. In turn, an increase of Creb levels seems to be essential to maintain CNS insulinergic pathway. Thus, further studies are necessary to delineate the diverse roles of Creb in the brain insulin resistance.

14-3-3 proteins have a number of binding partners involved in regulation of important basal functions in all cell types. The relevance of 14-3-3 proteins in the nervous tissue is based on the relevance of certain processes for proper neuronal development and function, such as synapse formation, and neuronal plasticity and development [46].

Improving brain insulin sensitivity might be a strategy for preventing or treating neurodegenerative disorders that correlate with brain insulin resistance [47]. Thus, drugs designed to increase the peripheral insulin sensitivity may potentially have similar effects in the brain; however, few studies have evaluated this hypothesis. In addition, 14-3-3 proteins are very important to many normal neurological functions as well as in neurological disorders. Connection between altered 14-3-3/ligand interaction and neural diseases suggests a pathological role for 14-3-3 proteins. It remains to be demonstrated alterations of specific isoforms in specific disease and/or injuries. However, results presented here provide further evidences to the involvement of 14-3-3 isoforms in the insulin signaling pathway.

Acknowledgments This study was partially supported by Conselho Nacional de Desenvolvimento Científico e Tecnológico (CNPq), Fundação de Amparo à Pesquisa do Estado do Rio Grande do Sul (FAPERGS), and Fundo de Incentivo a Pesquisa e Eventos do HCPA (FIPE-HCPA). HB was supported by Coordenação de Aperfeiçoamento de Pessoal de Nível Superior (CAPES). ERZ, DOGS, LVCP, and MLSP were supported by CNPq.

References

1. Wang W, Shakes DC (1996) Molecular evolution of the 14-3-3 protein family. J Mol Evol 43:384–398
2. Ferl RJ, Manak MS, Reyes MF (2002) The 14-3-3s. Genome Biol 3(7):3010.1–3010.7
3. Fu H, Subramanian RR, Masters SC (2000) 14-3-3 proteins: structure, function, and regulation. Annu Rev Pharmacol Toxicol 40:617–647
4. Obsil T, Obsilova V (2011) Structural basis of 14-3-3 protein functions. Semin Cell Dev Biol 22(7):663–672
5. Pozuelo Rubio M, Geraghty KM, Wong BH, Wood NT, Campbell DG, Morrice N, Mackintosh C (2004) 14-3-3-affinity purification of over 200 human phosphoproteins reveals new links to regulation of cellular metabolism, proliferation and trafficking. Biochem J 379: 395–408
6. Kleppe R, Martinez A, Døskeland SO, Haavik J (2011) The 14-3-3 proteins in regulation of cellular metabolism. Semin Cell Dev Biol 22:713–719
7. Ogihara T, Isobe T, Ichimura T, Taoka M, Funaki M, Sakoda H, Onishi Y, Inukai K, Anai M, Fukushima Y, Kikuchi M, Yazaki Y, Oka Y, Asano T (1997) 14-3-3 protein binds to insulin receptor substrate-1, one of the binding sites of which is in the phosphotyrosine binding domain. J Biol Chem 272:25267–25274

Author's personal copy

8. Neukamm SS, Ott J, Dammeier S, Lehmann R, Häring HU, Schleicher E, Weigert C (2013) Phosphorylation of serine 1137/1138 of mouse insulin receptor substrate (IRS) 2 regulates cAMP-dependent binding to 14-3-3 proteins and IRS2 protein degradation. J Biol Chem 288(23):16403–16415
9. Agarwal-Mawal A, Qureshi HY, Cafferty PW, Yuan Z, Han D, Lin R, Paudel HK (2003) 14-3-3 connects glycogen synthase kinase-3 beta to tau within a brain microtubule-associated tau phosphorylation complex. J Biol Chem 278(15):12722–12728
10. Dubois F, Vandermoere F, Gernez A, Murphy J, Toth R, Chen S, Geraghty KM, Morrice NA, MacKintosh C (2009) Differential 14-3-3 affinity capture reveals new downstream targets of phosphatidylinositol 3-kinase signaling. Mol Cell Proteomics 8(11):2487–2499
11. Muller AP, Gnoatto J, Moreira JD, Zimmer ER, Haas CB, Lulhier F, Perry ML, Souza DO, Torres-Aleman I, Portela LV (2011) Exercise increases insulin signaling in the hippocampus: physiological effects and pharmacological impact of intracerebroventricular insulin administration in mice. Hippocampus 21(10):1082–1092
12. Banks WA, Owen JB, Erickson MA (2012) Insulin in the brain: there and back again. Pharmacol Ther 136(1):82–93
13. Grillo CA, Piroli GG, Kaigler KF, Wilson SP, Wilson MA, Reagan LP (2011) Downregulation of hypothalamic insulin receptor expression elicits depressive-like behavior in rats. Behav Brain Res 222:230–235
14. Chung YH, Shin CM, Joo KM, Kim MJ, Cha CI (2002) Region-specific alterations in insulin-like growth factor receptor type I in the cerebral cortex and hippocampus of aged rats. Brain Res 946:307–313
15. Bosco D, Fava A, Plastino M, Montalcini T, Pujia A (2011) Possible implications of insulin resistance and glucose metabolism in Alzheimer's disease pathogenesis. J Cell Mol Med 15:1807–1821
16. Luschsinger JA, Tang MX, Shea S, Mayeux R (2004) Hyperinsulinemia and the risk of Alzheimer's disease. Neurology 63:1187–1192
17. Cole A, Astell A, Green C, Sutherland C (2007) Molecular connections between dementia and diabetes. Neurosci Biobehav Rev 31:1046–1063
18. Cukierman T, Gerstein HC, Williamson JD (2005) Cognitive decline and dementia in diabetes-systematic overview of prospective observational studies. Diabetologia 48:2460–2469
19. Williamson R, McNeilly A, Sutherland C (2012) Insulin resistance in the brain: an old-age or new-age problem? Biochem Pharmacol 84(6):737–745
20. Larance M, Rowland AF, Hoehn KL, Humphreys DT, Preiss T, Guilhaus M, James DE (2010) Global phosphoproteomics identifies a major role for AKT and 14-3-3 in regulating EDC3. Mol Cell Proteomics 9(4):682–694
21. Chen S, Synowsky S, Tinti M, MacKintosh C (2011) The capture of phosphoproteins by 14-3-3 proteins mediates actions of insulin. Trends Endocrinol Metab 22(11):429–436
22. Taurino F, Stanca E, Vonghia L, Siculella L, Sardanelli AM, Papa S, Zanotti F, Gnoni A (2014) Short-term type-1 diabetes differentially modulates 14-3-3 proteins in rat brain and liver. Eur J Clin Investig 44(4):350–358
23. Talbot K, Wang HY, Kazi H, Han LY, Bakshi KP, Stucky A, Fuino RL, Kawaguchi KR, Samoyedny AJ, Wilson RS, Arvanitakis Z, Schneider JA, Wolf BA, Bennett DA, Trojanowski JQ, Arnold SE (2012) Demonstrated brain insulin resistance in Alzheimer's disease patients is associated with IGF-1 resistance, IRS-1 dysregulation, and cognitive decline. J Clin Invest 122:1316–1338
24. Kern W, Peters A, Fruehwald-Schultes B, Deininger E, Born J, Fehm HL (2001) Improving influence of insulin on cognitive functions in humans. Neuroendocrinology 74:270–280
25. Bigornia SJ1, Farb MG, Mott MM, Hess DT, Carmine B, Fiscale A, Joseph L, Apovian CM, Gokce N (2012) Relation of depot-specific adipose inflammation to insulin resistance in human obesity. Nutr Diabetes 2((3):e30
26. Spielman LJ, Little JP, Klegeris A (2014) Inflammation and insulin/IGF-1 resistance as the possible link between obesity and neurodegeneration. J Neuroimmunol 273(1):8–21
27. Dietrich MO, Muller A, Bolos M, Carro E, Perry ML, Portela LV, Souza DO, Torres-Aleman I (2007) Western style diet impairs entrance of blood-borne insulin-like growth factor-1 into the brain. Neruomol Med 9(4):324–330
28. Schwartz MW, Porte D Jr (2005) Diabetes, obesity, and the brain. Science 307(5708):375–379
29. de Sousa AR, Penalva LO, Marcotte E, Vogel C (2009) Global signatures of protein and mRNA expression levels. Mol BioSyst 5:1512–1526
30. Liu H, Sadygov RG, Yates JR 3rd (2004) A model for random sampling and estimation of relative protein abundance in shotgun proteomics. Anal Chem 76(14):4193–4201
31. Fu X, Gharib SA, Green PS, Aitken ML, Frazer DA, Park DR, Vaisar T, Heinecke JW (2008) Spectral index for assessment of differential protein levels in shotgun proteomics. J Proteome Res 7(3):845–854
32. Livak KJ, Schmittgen TD (2001) Analysis of relative gene expression data using real-time quantitative PCR and the 2(−Delta Delta C(T)) method. Methods 25(4):402–408
33. Aitken A (2006) 14-3-3 proteins: a historic overview. Semin Cancer Biol 16:162–172
34. Shumway SD, Li Y, Xiong Y (2003) 14-3-3-beta binds to and negatively regulates the tuberous sclerosis complex 2 (TSC2) tumor suppressor gene product, tuberin. J Biol Chem 278:2089–2092
35. Inoki K, Li Y, Zhu T, Wu J, Guan K-L (2002) TSC2 is phosphorylated and inhibited by Akt and suppresses mTOR signalling. Nat Cell Biol 4:648–657
36. Zoncu R, Efeyan A, Sabatini DM (2011) mTOR: from growth signal integration to cancer, diabetes and ageing. Nat Rev Mol Cell Biol 12(1):21–35
37. Lim GE, Piske M, Johnson JD (2013) 14-3-3 proteins are essential signalling hubs for beta cell survival. Diabetologia 56(4):825–837
38. Powell DW, Rane MJ, Chen Q, Singh S, McLeish KR (2002) Identification of 14-3-3-zeta as a protein kinase B/Akt substrate. J Biol Chem 277:21639–21642
39. Simsek-Duran F, Linden DJ, Lonart G (2004) Adapter protein 14-3-3 is required for a pre-synaptic form of LTP in the cerebellum. Nat Neurosci 7:1296–1298
40. Grover D, Verma R, Goes FS, Mahon PL, Gershon ES, McMahon FJ (2009) Family based association of YWHAH in psychotic bipolar disorder. Am J Med Genet B Neuropsychiatr Genet 150B:977–983
41. Foote M, Zhou Y (2012) 14-3-3 proteins in neurological disorders. Int J Biochem Mol Biol 3(2):152–164
42. Yacoubian TA, Slone SR, Harrington AJ, Hamamichi S, Schieltz JM, Caldwell KA, Standaert DG (2010) Differential neuroprotective effects of 14-3-3 proteins in models of Parkinson's disease. Cell Death Differ 1(e2):1–13
43. Kakinuma N, Roy BC, Zhu Y, Wang Y, Kiyama R (2008) Kank regulates RhoA-dependent formation of actin stress fibers and cell migration via 14-3-3 in PI3K-Akt signaling. J Cell Biol 181(3):537–549
44. Vogel C, Marcotte EM (2012) Insights into the regulation of protein abundance from proteomic and transcriptomic analyses. Nat Rev Genet 13(4):227–232
45. Jitrapakdee S (2012) Transcription factors and coactivators controlling nutrient and hormonal regulation of hepatic gluconeogenesis. Int J Biochem Cell Biol 44(1):33–45
46. Steinacker P, Aitken A, Otto M (2011) 14-3-3 proteins in neurodegeneration. Semin Cell Dev Biol 22:696–704
47. Park CR (2001) Cognitive effects of insulin in the central nervous system. Neurosci Biobehav Rev 25:311–323

ANEXO II-E. *Intracerebroventricular metformin decreases body weight but has pro-oxidant effects and decreases survival.*

No **ANEXO II-E** apresentamos o artigo publicado no periódico *Neurochemical Research.*

Neurochem Res
DOI 10.1007/s11064-014-1496-7

ORIGINAL PAPER

Intracerebroventricular Metformin Decreases Body Weight But Has Pro-oxidant Effects and Decreases Survival

Luis Valmor Portela · Jussania Gnoatto · Andressa Wigner Brochier · Clarissa Branco Haas · Adriano Martimbianco de Assis · Afonso Kopczynski de Carvalho · Gisele Hansel · Eduardo Rigon Zimmer · Jean Pierre Oses · Alexandre Pastoris Muller

Received: 26 July 2014 / Revised: 24 November 2014 / Accepted: 2 December 2014
© Springer Science+Business Media New York 2014

Abstract Metformin (Met), which is an insulin-sensitizer, decreases insulin resistance and fasting insulin levels. The precise molecular target of Met is unknown; however, several reports have shown an inhibitory effect on mitochondrial complex I of the electron transport chain (ETC), which is a related site for reactive oxygen species production. In addition to peripheral effects, Met is capable of crossing the blood–brain barrier, thus regulating the central mechanism involved in appetite control. The present study explores the effects of intracerebroventricular (i.c.v.) infusion of Met on ROS production on brain, insulin sensitivity and metabolic and oxidative stress outcomes in CF1 mice. Metformin (Met 50 and 100 μg) was injected i.c.v. in mice daily for 7 days; the brain mitochondrial H_2O_2 production, food intake, body weight and fat pads were evaluated. The basal production of H_2O_2 of isolated mitochondria from the hippocampus and hypothalamus was significantly increased by Met (100 μg). There was increased peripheral sensitivity to insulin (Met 100 μg) and glucose tolerance tests (Met 50 and 100 μg). Moreover, Met decreased food intake, body weight, body temperature, fat pads and survival rates. Additionally, Met (1, 4 or 10 mM) decreased mitochondrial viability and increased the production of H_2O_2 in neuronal cell cultures. In summary, our data indicate that a high dose of Met injected directly into the brain has remarkable neurotoxic effects, as evidenced by hypothermia, hypoglycemia, disrupted mitochondrial ETC flux and decreased survival rate.

Keywords Brain metabolism · Food intake · Body weight · Body temperature · Insulin resistance · Fat pads · Mitochondrial function

L. V. Portela · J. Gnoatto · A. Wigner Brochier · C. B. Haas · A. M. de Assis · A. K. de Carvalho · G. Hansel · E. Rigon Zimmer
Departamento de Bioquímica, Programa de Pós Graduação em Ciências Biológicas-Bioquímica, ICBS, UFRGS, Rua: Ramiro Barcelos, 2600 anexo, Porto Alegre, Rio Grande do Sul CEP 90035-003, Brazil

J. P. Oses
Programa de Pós-Graduação em Saúde and Comportamento Centro de Ciências da Vida e da Saúde, Universidade Católica de Pelotas, Rua Almirante Barroso, 1202 sala G109, Pelotas, Rio Grande do Sul CEP 96010-280, Brazil

A. P. Muller (✉)
Unidade de Ciências da Saúde, Laboratório de Bioquímica e Fisiologia do Exercício-LAFIBE, Universidade do Extremo Sul Catarinense-UNESC, Av. Universitária, 1105-Bairro Universitário, Criciúma, Santa Catarina CEP 88806-000, Brazil
e-mail: alexandrep.muller@gmail.com

Introduction

Type 2 diabetes mellitus (T2D), which is a progressive and complex disorder, has a considerable impact on individuals and society. The majority of patients are unable to sustain normal glycemia without pharmacological interventions targeted at improving insulin receptor responsiveness [1]. Metformin (1,1-dimethylbiguanide) (Met), which is an oral insulin sensitizer, is widely prescribed for treating hyperglycemia in patients with T2D because it improves insulin sensitivity and peripheral glucose homeostasis [2, 3]. Although the precise molecular targets associated with these benefits have not been established, the increasing expression of insulin receptor and activity of tyrosine kinase present as likely candidates [4]. The inhibition of complex I of the mitochondrial electron transport chain

Published online: 10 December 2014

(ETC) [5], and prevention of erratic brain neovascularization induced by hyperglycemia [6] are also potential targets of the modulatory effect of Met. In contrast to these benefits, Met may affect the capacity of isolated mitochondria from liver in accumulate calcium by affecting the permeability transition pore opening thereby resulting in increased oxidation of thiol groups [7]. Therefore, Met may cause beneficial or harmful effects for mitochondrial physiology, which should be taken into consideration for pharmacological strategies aiming to improve brain insulin sensitivity.

Interestingly, patients with Alzheimer's disease (AD) share many age-related pathophysiological features of T2D, including insulin resistance and disrupted glucose metabolism in non-neural tissues, as well as peripheral oxidative and inflammatory stress associated with cognitive decline [8]. However, strong data from recent publications support the view that insulin resistance is not limited to peripheral tissues and that brain insulin receptors/signaling has physiological relevance for the mechanisms of neuroplasticity and memory [8]. Actually, It has been proposed that decreased brain insulin receptors responsiveness leads to cognitive deficits and neuropathological mechanisms like tau-hyperphosphorylation, oxidative stress, and apoptosis [9]. Also, brain insulin resistance was reported to be an early pathological event that precede cognitive decline [8]. Therefore, pharmacological strategies to improve brain insulin signaling might result in improvements of neuronal survival and cognitive function.

Although oral sensitizers, such as Met, can cross the blood–brain barrier [10] and has the potential for inducing similar therapeutic effects as insulin, its peripheral effects on glucose homeostasis limits such application in non-diabetic individuals [11]. In this context, few experimental studies have assessed the brain responses to Met, especially concerning delivery through intracerebral strategies. To date, intracerebroventricular (i.c.v.) infusion of Met attenuates salt-induced hypertension in hypertensive rats, thus connecting the central regulatory mechanism governed by insulin with the peripheral sympathetic nervous system [12]. Additionally, i.c.v. Met decreases food intake in a due to hypothalamic mechanisms [13, 14].

Another relevant issue is that both impaired brain insulin receptor response [15] and insulin receptor hyper activation may cause neurodegeneration and impaired cognitive function [16, 17]. Therefore, the neuromodulatory role exerted by insulin is under fine-tuning control and is not exclusively dependent on insulin levels but also on insulin receptor sensitivity. In the present study, we aimed to explore the effects of i.c.v. infusion of Met on reactive oxygen species (ROS) production on brain, insulin sensitivity and oxidative stress outcomes in CF1 wild type mice.

Materials and Methods

Animals

Male CF1 mice (weighing 40–50 g), aged 2 months old, were obtained from the Foundation for Health Science Research (FEPPS, Porto Alegre/RS, Brazil). The animals were placed in a temperature-controlled room (22 °C) under a 12-h light/12-h dark cycle (lights on at 7 am) and had free access to food and water. A total of 30 mice ($n = 30$) were randomly allocated to one of the following groups: control (vehicle, $n = 10$), Met 50 µg (Met 50, $n = 10$) and Met 100 µg (Met 100, $n = 10$). All of the experiments were conducted in agreement with the Committee on the Care and Use of Experimental Animal Resources, UFRGS, Brazil, project number 22436. Chloridrate of Met (EMS S/A) was dissolved in saline (NaCl, 0.9 %) at concentrations of 50 and 100 µg injected in 2 µL (1 µL/min).

Treatment and Surgical Procedure

The animals were anesthetized using an i.p. injection of ketamine (Cetamin, Schering-Plough Coopers, Brazil, 100 mg/kg body weight) and xylazine (Coopazine, Syntec, Brazil, 10 mg/kg body weight). A 27-gauge, 7-mm guide cannula was inserted 1 mm posterior to the bregma, 1 mm to the right from the midline and 1 mm above the lateral brain ventricle. Through a 2-mm hole made at the cranial bone, the cannula was implanted 1.5 mm ventral to the superior surface of the skull and fixed using jeweler's acrylic cement [16]. On day 3 post surgery, the mice exhibited normal food intake and water consumption as well as spontaneous locomotion; they were thus considered ready for in vivo experiments. The animals received a daily i.c.v. infusion of Met dissolve on saline (NaCl, 0.9 %) and filtered (Met 50 µg or Met 100 µg) or saline for seven consecutive days. The dose used was choose based on works that showed no damage caused by Met i.c.v. [14, 18].

Body Mass Parameters, Blood Sampling, Food Intake and Survival Rate

Body weight and food intake were measured daily for seven consecutive days. Each day, food was weighed and added to the cages. The ratio between these days was divided by the number of the animals per cage and was used to estimate food intake.

Body temperature was measured on the following days of administration: 1, 2, 4, 6 and 7. The animals were sacrificed by decapitation. Blood was collected and

centrifuged at 10,000*g* for 10 min to obtain serum samples. The serum samples were stored at −20 °C until analysis was performed. The hippocampus and hypothalamus were dissected to prepare homogenates. The fat tissues from the mesenteric and epididymal regions were dissected and weighed as previously described [19], briefly, between the lower part of the rib cage and mid-thigh was considered epididymal fat pad whereas all fat found along the mesentery starting at the lesser curvature of the stomach and ending at the sigmoid colon was considered mesenteric fat pad. The survival rate was evaluated during treatment.

Glucose Tolerance Test (GTT) and Insulin Sensitivity Test (IST)

One day after the Met/vehicle treatment one cohort of animal was used to GTT and other animals used to IST.

An intraperitoneal injection of glucose (2 mg/g body weight) was performed in 12-h fasted mice 24 h after the last i.c.v. Met injection. The blood samples were collected by a small puncture on the tail immediately before (0 min) and 30, 60, and 120 min after the injection [20]. At each time, glucose was measured using a glucosimeter (Accu-Chek Active, Roche Diagnostics®, USA).

An intraperitoneal injection of insulin (1 U/kg) was performed in 12-h fasted mice 24 h after the last i.c.v. Met injection. The blood samples were collected by a small puncture on the tail immediately before (0 min) and 30, 60, and 120 min after the injection [21]. At each time, glucose was measured using a glucosimeter (AccuChek Active, Roche Diagnostics®, USA).

ROS Production

The mitochondrial release of H_2O_2 was assessed using the Amplex Red oxidation method. The total homogenate from the hippocampus and hypothalamus (0.1 mg protein/mL) was incubated in standard respiration buffer supplemented with 10 µM Amplex Red and 2 U/mL horseradish peroxidase in polarized and depolarized buffers. Fluorescence was monitored at excitation (563 nm) and emission wavelengths (587 nm) using a Spectra Max M5 microplate reader (Molecular Devices) [22]. Each experiment was repeated at least three times with hippocampal and

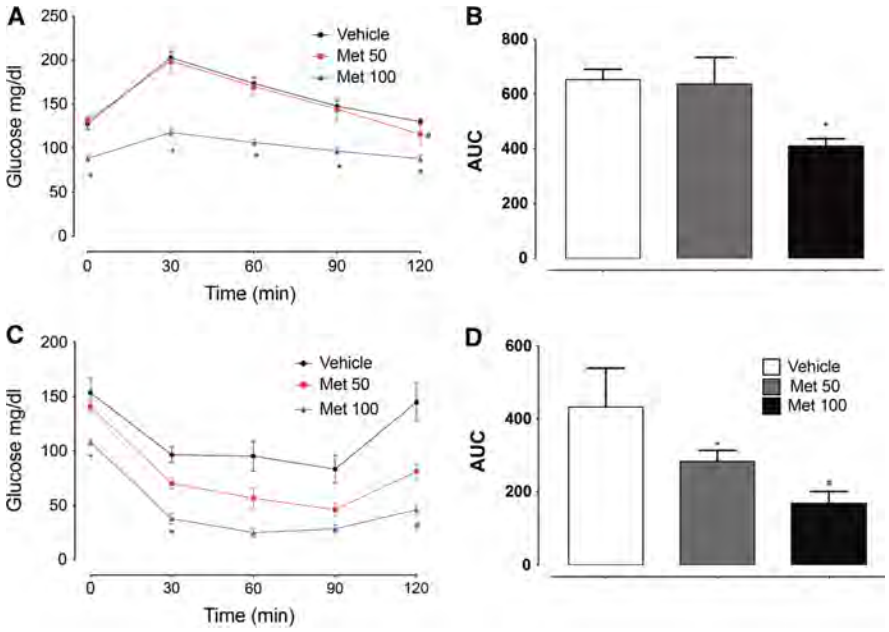

Fig. 1 Glucose tolerance test (GTT) and insulin sensitivity test (IST). **a** Met treatment altered the glucose tolerance test. At baseline (time 0) *Met 100 µg <Met 50 µg and vehicle. After glucose injection *Met 100 µg <Met 50 µg and vehicle until 120 min. #Met 50 µg <vehicle at time (120 min); one-way analysis of variance (ANOVA) with repeated measures followed by Bonferroni post hoc analysis; $p < 0.05$. **b** The treatment decreased the area under the curve (AUC) at Met 100 (*Met 100 µg <Met 50 µg and vehicle; one-way analysis of variance (ANOVA) with repeated measures followed by Bonferroni post hoc analysis; $p < 0.05$). **c** Met treatment altered the insulin sensitivity test. At baseline (time 0) and 30 min *Met 100 µg <vehicle, at 120 min. #Met 100 µg <Met 50 µg <vehicle; one-way analysis of variance (ANOVA) with repeated measures followed by Bonferroni post hoc analysis; $p < 0.05$. **d** The treatment decreased the area under the curve (AUC) (*Met 50 <vehicle and #Met 100 µg <Met 50 µg and vehicle; one-way analysis of variance (ANOVA) with repeated measures followed by Bonferroni post hoc analysis; $p < 0.05$)

hypothalamus preparations. The maximal rate (100 %) of mitochondrial H_2O_2 formation in a depolarized state was assumed to be the difference between the rate of H_2O_2 formation in the absence and in the presence of succinate up to 30 min. ADP was used for modulating the mitochondrial function by inhibiting ROS production.

Propidium Iodide (PI) and MTT Colorimetric Assay

Animals treated with saline or Met 50 and 100 ug after were killed by decapitation and after the hippocampal slices was cut in 300 µm using McIlwain tissue chopper.

On average, three slices from animal of the hippocampus were obtained and placed in a 96-well containing prewarmed HEPES-buffered saline (in mM: 120 NaCl, 5 KCl, 2 CaCl2, and 10 glucose; pH 7.4). The slices were incubated for 1 h before propidium iodide (PI) addition. Cell death was assessed by using uptake of the fluorescent exclusion dye PI, which is a polar compound that enters only into dead or dying cells with damaged membranes. Once inside the cells, PI binds to DNA, inducing intense red fluorescence (630 nm) when excited by green light (495 nm). The slices were incubated with 10 µg/mL PI for 1 h and then imaged on a standard inverted microscope by using a rhodamine filter set. The PI uptake was quantified by imageJ.

The assessment of slice viability was performed by the colorimetric [3(4,5-dimethylthiazol-2-yl)-2,5-diphenyl tetrazolium bromide]. Slices (400 µm) were pre-incubated for 1 h, then it was adding 0.5 mg/ml of MTT (PBS), followed by incubation at 37 °C during for 45 min. The formazan product generated during the incubation was solubilized in dimethyl sulfoxide and measured at 560 and 630 nm.

S100B ELISA Assay

The hippocampus was homogenate with PBS buffer (100 mM Tris/HCl, pH 7.4). The S100B level was assessed in hippocampus by a commercially available ELISA kits Millipore, USA (Cat #EZHS 100B-33K). All technical procedures were performed according to the manufacture.

Neuronal Cortex Cultures, Neuronal Viability and ROS Production

The cortices from 16-day-old Wistar rat embryos were dissected, and 150,000 cells/well were cultivated in neurobasal medium plus B27 supplement [23]. After 7 days of culture, the neurobasal medium was replaced by RPMI 1640

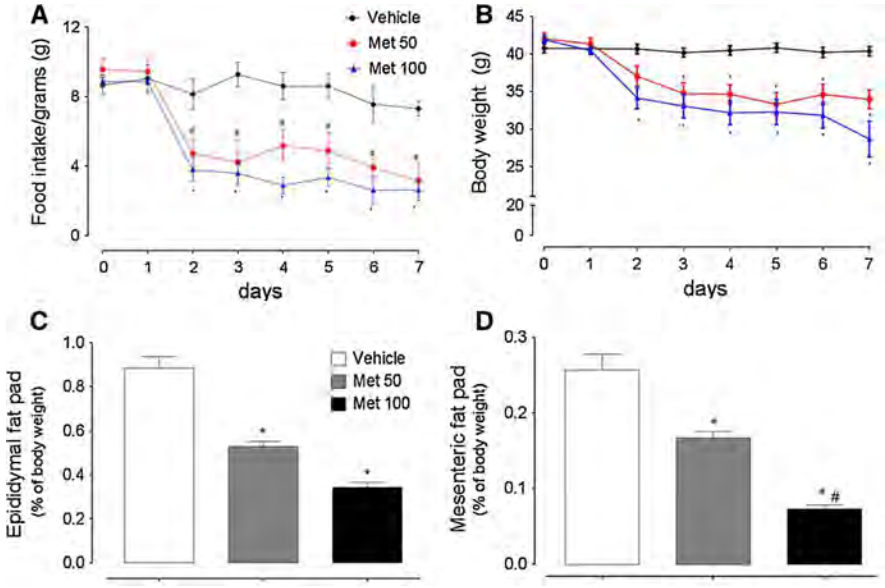

Fig. 2 Effects of i.c.v. metformin administration on food intake, body weight, epididymal and mesenteric fat pads. **a** Met treatment decreased food intake, #Met 50 µg <vehicle and *Met 100 µg <vehicle from days 2 to 7; **b** Met 50 µg decreased body weight: #Met 50 <vehicle from days 3 to 7. Met 100 µg decreased body weight: *Met 100 <vehicle from days 2 to 7. and Met 100 µg <Met 50 µg <vehicle on day 7. **c** Metformin treatment decreased the epididymal fat pad, *Met 100 µg and Met 50 µg <vehicle; one-way analysis of variance (ANOVA) followed by Bonferroni post hoc analysis; $p < 0.05$. **d** Metformin treatment decreased the mesenteric fat pad, *Met 100 µg and Met 50 µg <vehicle; #Met 100 µg <Met 50 µg; one-way analysis of variance (ANOVA) followed by Bonferroni post hoc analysis; $p < 0.05$

medium without B27, which contained glucose (10 mM). To investigate the effects of Met on neuronal mitochondrial viability, the neurons were supplemented with Met at doses of 1, 4 and 10 mM for 60 min [24]. The neuronal viability assay was performed using the colorimetric 3(4,5-dimethylthiazol-2-yl)-2-5-diphenyl tetrazolium bromide (MTT, Sigma) method. After treatment, the neurons were incubated with 0.5 mg/mL MTT at 37 °C for 45 min. The formazan product generated during the incubation was solubilized in dimethyl sulfoxide and measured at 560 and 630 nm. The results are expressed as a percentage of the control [25]. To investigate the effects of Met in ROS production, the neurons were supplemented with Met at doses of 1, 4 and 10 mM for 60 min. Subsequently, the cells were incubated with 2 μM CM-H2DCFDA for 40 min at 37 °C with 4 % CO_2. The cells were examined using a Nikon Eclipse TE300 epifluorescence microscope at a fixed exposure time [26].

Superoxide Dismutase Assay

Superoxide dismutase (SOD) activity was evaluated by quantifying the superoxide-dependent autoxidation inhibition of epinephrine, verifying the absorbance of the samples at 480 nm [27]. In a 96-well plate, we added tissue homogenates (30 μL), 150 μL of 50 mM glycine buffer pH 10.2, and 10 μL of 10 μM catalase. In the auto-oxidation wells, 180 μL of 50 mM glycine buffer, pH 10.2 and 10 μL of 10 μM catalase were added. The reaction was initiated by adding 10 μL of 60 mM epinephrine. The absorbance was obtained at 480 nm and recorded for 10 min at 32 °C. SOD activity was defined as the amount of enzyme required to decrease by 50 % the epinephrine oxidation using superoxide. The specific activity was expressed in units per mg of protein.

Glutathione Peroxidase (GPx) Activity

GPx activity was measured according to the technique described by Wendel [28] using tert-butyl-hydroperoxide as a substrate. Enzyme activity was determined by monitoring the NADPH disappearance at 340 nm in a medium containing 100 mM potassium phosphate buffer/1 mM ethylenediamine tetra acetic acid, pH 7.2, 2 mM GSH, 0.15 U/mL glutathione reductase, 0.4 mM Mazide, 0.5 mM tert-butyl-hydroperoxide, and 0.1 mM NADPH. One GPx unit (U) is defined as 1 μmol of NADPH consumed per minute. The specific activity was calculated as U/mg protein.

Statistical Analysis

The data are presented as the mean ± SEM values. The line graphs were analyzed using one-way analysis of variance (ANOVA) with repeated measures followed by Bonferroni post hoc analysis. The column bar graphs were analyzed using ANOVA followed by Bonferroni post hoc analysis. $p < 0.05$ was considered to be statistically significant. The cumulative survival probability was evaluated using a Kaplan–Meier plot.

Results

Insulin Sensitivity

Glucose Tolerance Test (GTT) and Insulin Sensitivity Test (IST)

Baseline (time 0) glucose levels of Met 100 μg group was decreased compared to the vehicle and Met 50 μg groups (Fig. 1a; *Met 100 μg <vehicle and Met 50 μg; $p < 0.05$). After glucose injection, the Met 100 μg group had lower glucose levels compared those of the other groups at 30, 60 and 120 min (Fig. 1a and b; *Met 100 μg <vehicle and Met 50 μg; $p < 0.05$). In the IST, the Met 100 μg group showed a lower glucose level compared to that of the vehicle and Met 50 μg groups. At 30, 60 and 120 min after insulin injection, the Met 50 μg and Met 100 μg groups showed lower glucose levels compared to that of the vehicle group. Moreover, the Met 100 μg group showed a lower glucose level compared to the Met 50 μg group (Fig. 1c and d; *Met 50 μg <vehicle; #Met 100 μg <Met 50 μg; $p < 0.05$).

Metabolic Parameters

Food Intake, Body Weight and Fat Pads

Food intake was decreased by Met 50 μg and Met 100 μg from days 2 to 7 of administration (Fig. 2a; *Met 100 <vehicle, #Met 50 <vehicle; $p < 0.05$). The vehicle group had normal food intake over 7 days (Fig. 2a). Met 50 μg decreased body weight from days 3 to 7 (Fig. 2b; Met 50 μg <vehicle; #$p < 0.05$). Met 100 μg decreased body weight from days 2 to 7 (Fig. 2b; Met 100 μg <vehicle; *$p < 0.05$). The body weight remained invariable in the vehicle group (Fig. 2b).

Met 50 μg and 100 μg decreased epididymal (Fig. 2c; Met 100 μg and 50 μg <vehicle; *$p < 0.05$) and mesenteric fat pads (Fig. 2d; Met 100 μg and 50 μg <vehicle; *$p < 0.05$) compared to those in the vehicle group. Moreover, the mesenteric fat pad in the Met 100 μg group was lower than that in the Met 50 μg group (Fig. 2d, Met 100 μg <Met 50 μg; #$p < 0.05$).

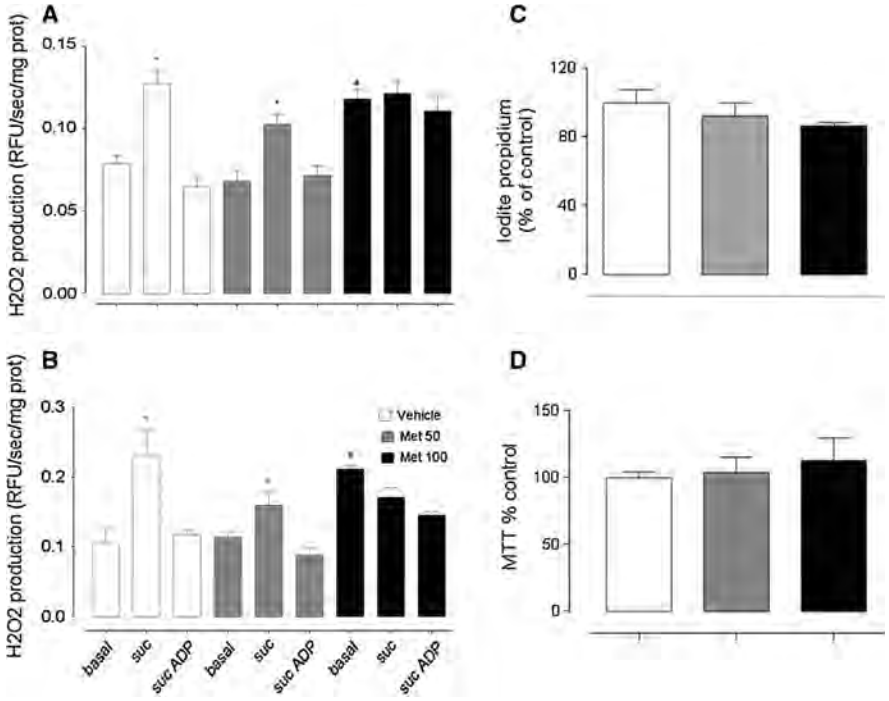

Fig. 3 Metformin treatment (100 µg) increased H_2O_2 production in the hippocampus and hypothalamus, however did not affect brain viability. **a** H_2O_2 production in hippocampus, *H_2O_2 production succinate >H_2O_2 production baseline in Met 50 µg and vehicle groups, #H_2O_2 production baseline in Met 100 µg >H_2O_2 production baseline in Met 50 µg and vehicle groups; one-way analysis of variance (ANOVA) followed by Bonferroni post hoc analysis; $p < 0.05$. **b** H_2O_2 production in hypothalamus, *H_2O_2 production succinate >H_2O_2 production baseline in Met 50 µg and vehicle groups, #H_2O_2 production baseline in Met 100 µg >H_2O_2 production baseline in Met 50 µg and vehicle groups; one-way analysis of variance (ANOVA) followed by Bonferroni post hoc analysis; $p < 0.05$. **c** Met i.c.v. had no effect on propidium iodide a marker of membrane damage. **d** Met i.c.v. had no effect on MTT assay a marker of mitochondrial viability

Oxidative Stress Parameters

Mitochondrial H_2O_2 Production in the Hippocampus and Hypothalamus

The hippocampus and hypothalamus homogenates were responsive to succinate, an activator of mitochondrial H_2O_2 production. ADP decreased H_2O_2 production in the vehicle and Met 50 µg groups (Fig. 3a and b; H_2O_2 production succinate >H_2O_2 production baseline; $*p < 0.05$). Met 100 µg induced increases in H_2O_2 production at basal levels (Fig. 3a and b; H_2O_2 production without substrate Met 100 µg >Met 50 µg and vehicle; $\#p < 0.05$). Succinate did not stimulate H_2O_2 production over basal levels (Fig. 3a and b) in the Met 100 µg group.

Neural Cell Damage and Mitochondrial Viability

Met i.c.v. at doses of 50 and 100 µg did not significantly affect neural cells integrity as showed by propidium iodite staining (Fig. 3c), and also did not affect brain mitochondrial viability as showed by MTT assay (Fig. 3d).

Protein Marker of Astrocyte Damage

Met i.c.v. in both doses (50 and 100 µg) did not significantly affect the hippocampal levels of S100B (Table 1).

Mitochondrial Viability and ROS Production in Neuronal Cell Cultures Exposed to Metformin

To analyze whether Met effects achieved in in vivo experiments affected isolated neurons, we evaluated mitochondrial viability and ROS production in neuronal cortical cultures. Met was added at doses of 1, 4 and 10 mM to each well for 60 min. The mitochondrial viability decreased in a dose-dependent manner [Fig. 4c vehicle >treated groups; $F(5, 18) = 168.135$ (dose–effect), $*p = 0.0001$; $R^2 = 0.973$ (linear regression)].

Total ROS production in neurons was measured using the fluorescent probe CM-H2DCFDA. Met was added to the neuron culture at doses of 1, 4 and 10 mM to each well for 60 min. ROS production increased in the Met groups in a dose-dependent manner [Fig. 3 D–H vehicle <Met 1, 4 and 10 mM; $F(3, 12) = 11.472$ (dose–effect); $^{*}p = 0.001$; $R^2 = 0.677$ (linear regression)].

Table 1 Antioxidant enzymes and S100B

	Vehicle	Met 50 μg	Met 100 μg
Glutathione peroxidase UGPx/mg protein			
Hippocampus	27 ± 1.5	35 ± 3.7	33 ± 3.9
Hypothalamus	48 ± 9.8	37 ± 7.9	44 ± 3.1
Serum	34 ± 7.1	25 ± 8.2	37 ± 8.3
Superoxide dismutase USOD/mg protein			
Hippocampus	11 ± 0.5	10 ± 0.2	11 ± 1.2
Hypothalamus	11 ± 0.2	10 ± 0.6	12 ± 1.5
Serum	5.0 ± 0.7	6.0 ± 0.5	6.0 ± 1.0
S100B (ng/mg protein)			
Hippocampus	1.8 ± 0.2	1.9 ± 0.1	1.6 ± 0.1

Oxidative Stress Damage and Antioxidant Enzymes

The antioxidant enzymes glutathione peroxidase and SOD were measured in the blood, hippocampus and hypothalamus. There were no significant differences between groups despite the pro-oxidant environment elicited by Met i.c.v. (Table 1).

Metformin Disturbs Body Temperature and Survival Rate

Met 50 μg decreased body temperature from treatment days 4 to 7 (Fig. 4a; #Met 50 μg <vehicle; $p < 0.05$), whereas Met 100 μg decreased body temperature from days 2 to 7 (Fig. 4a;*Met 100 μg <vehicle; and Met 100 μg <Met 50 μg <vehicle; $p < 0.05$). The vehicle group showed normal body temperature over 7 days (Fig. 5a). The survival rate curve showed that in the Met 50 μg group, the animals started to die on day 3 of administration; on day 7, only 60 % of the animals survived (Fig. 5b). Using Met 100 μg, the animals started to die on day 1 of administration; on the last day, only 40 % of the animals survived (Fig. 5b).

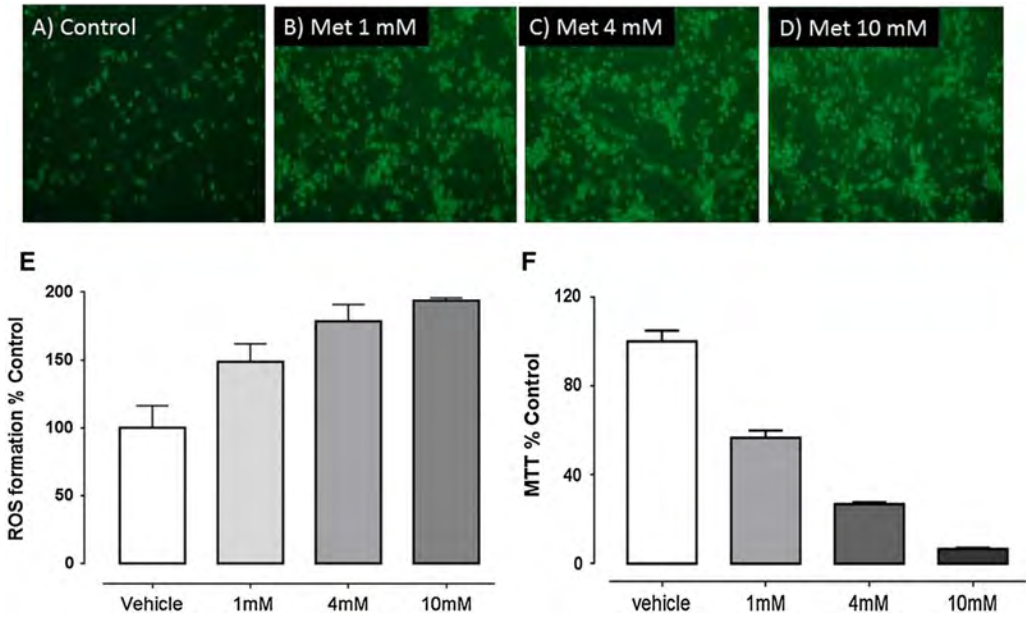

Fig. 4 Met affects the neuronal mitochondrial ROS production and the mitochondrial viability by the MTT assay in neurons. **a**–**d** Representative images of ROS production of neuronal cell culture at vehicle, Met 1 mM, Met 4 mM and Met 10 mM respectly. **e** Quantification of green fluorescence microscopy images (% of control). The ROS production in neurons was measured using fluorescent probe CM-H2DCFDA. Met increased ROS production in a dose-dependent manner, $F(3, 12) = 11.472$ (dose–effect), $p = 0.001$. $R^2 = 0.677$ (linear regression). **f** MTT, viability was altered by Met treatment in a dose-dependent manner, $F(5, 18) = 168.135$ (dose–effect), $p = 0.0001$. $R^2 = 0.973$ (linear regression). **d**–**f**

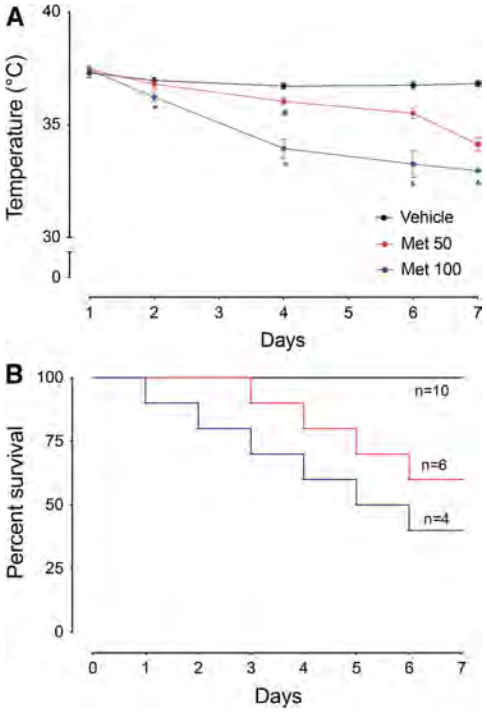

Fig. 5 Metformin treatment decreased temperature and survival rate. **a** Body temperature: The rectal body temperature was measured during Met i.c.v. administration. #Met 50 µg <vehicle on day 4, *Met 100 µg <vehicle on day 1 until 7 and & Met 100 µg <Met 50 µg <vehicle; one-way analysis of variance (ANOVA) with repeated measures followed by Bonferroni post hoc analysis; $p < 0.05$. **b** Survival: Metformin decreased survival; in Met 50 µg, 40 % of the mice died; in Met 100 µg, 60 % of the mice died. The cumulative survival probability was evaluated using a Kaplan–Meier plot; $p < 0.05$

Discussion

The present work showed that 7 days of Met (50–100 µg) i.c.v. administration down regulated body temperature, decreased food intake, body weight and survival rates. From the preclinical perspective, our results raised important concerns regarding undesirable effects of high doses of Met, mainly impaired brain mitochondrial ETC function associated to increased H_2O_2 production. Additionally, we should consider that Met consistently impaired glucose homeostasis, and decreased fat pads. Up to our knowledge, this is the first report using long-term i.c.v. treatment regimens, which intend to be more realistic strategy to test a candidate drug to be used chronically by patients.

Improving brain insulin sensitivity might be a feasible strategy for preventing or treating neurodegenerative disorders that correlate with brain insulin resistance [13]. Thus, medications designed to increase the peripheral insulin sensitivity may potentially exert similar effects on the brain; however, few studies have evaluated this hypothesis. Up to 24 h of Met treatment has been demonstrated to have dose-dependent anorexic effects, such as decreasing food intake and optimizing energy production by regulating hypothalamic circuits [29]. We showed for the first time that long-term i.c.v. treatment (7 days) decreased food intake, which paralleled decreased body weight and fats. This evidence may help reinforce the proposed role of Met in controlling food intake and energy expenditure by modulating agouti-related protein also called agouti-related peptide (AgRP) neurons [30]. Actually, Met i.c.v. increased the phosphorylation of signal transducer and activator of transcription 3 (STAT3), a hypothalamic protein involved in satiety response [11]; however, it did not affect the phosphatidylinositol-4,5-bisphosphate 3-kinase/5′ AMP-activated protein kinase (PI3K)/AMPK pathway. Although STAT3 is partially involved in Met-induced satiety control, the exact pathway has not been established. In another work Met i.c.v. decreased food intake by inhibition of phosphorylation of AMPK [14].

Met inhibits complex I, thus decreasing oxidative respiration [5] and increasing ROS production by the mitochondria. In the hippocampus and hypothalamus, i.c.v. Met (100 µg) disrupted the mitochondrial response to the substrate ADP. Under these circumstances, it seems that membrane lipids integrity and mitochondrial viability were not affected by treatment, probably implying that astrocytes are still able to provide neuroprotective mechanisms of defense to neurons. Similarly, we showed that the addition of Met to neuronal cultures increased ROS production and decreased mitochondrial viability. These results support the concept that mitochondrial hypofunction is the mechanistic basis behind disrupted energy homeostasis and neurotoxicity associated with high doses of Met.

The proposed effects of Met on adipose tissue are associated with the inhibition of lipogenesis and the stimulation of lipolysis [31]. We found decreased epididymal and mesenteric fat pads that appear to be caused by Met. However, these findings could be secondary to decreased food intake and impaired thermoregulation, which subsequently increased fat mobilization and oxidation. These results suggest that the administration of Met i.c.v. may be a promising strategy for experimental studies of obesity and diabetes [12]. The impact of Met on the hypothalamus, the primary brain regulatory center of feeding behavior and caloric expenditure, as well as on fat pads deserves additional exploration.

Met affects peripheral sympathetic nerve activity [32]. In the present study, we postulated that Met-induced hypothermia was attributed to impaired sympathetic nerve

activity, which can be considered the primary alteration associated with increased mortality rate. The integrity of the sympathetic nerve response is necessary for maintaining an adequate inflammatory response and thermoregulatory functions [33, 34]. Additionally, the doses used in this study demonstrated that Met affected the mechanisms involved in the regulation of glucose homeostasis, which resulted in hypoglycemia and impaired insulin sensitivity. However, one limitation of our work was the dose regimen. Thus, lower doses should be tested in preclinical studies to warrants better benefits with minimum side effects.

In conclusion, we demonstrated that the direct administration of Met on the brain up to seven days causes severe hypothermia and hypoglycemia and disturbs mitochondrial function/viability; these results parallel an increased mortality rate in mice.

Acknowledgments This work was supported by Brazilian agencies and grants: CNPq, CAPES 02/2102, FAPERGS0543/12-4-PPSUS, Brazil-Swiss 590011/2010-3, Brazilian Institute of Neuroscience-IBN Net FINEP, INCT-Excitotoxicity and Neuroprotection.

Conflict of interest The authors declare that they have no financial conflicts of interest.

References

1. Viollet B, Guigas B, Garcia NS, Leclerc J, Foretz M, Andreelli F (2012) Cellular and molecular mechanisms of metformin: an overview. Clin Sci (Lond) 122:253–270
2. Adler AI, Shaw EJ, Stokes T, Ruiz F (2009) New drugs for control of blood glucose in type 2 diabetes: summary of the NICE guidelines. Praxis (Bern 1994). 98:1161–1163
3. Nathan DM, Buse JB, Davidson MB, Ferrannini E, Holman RR, Sherwin R, Zinman B (2009) Medical management of hyperglycemia in type 2 diabetes: a consensus algorithm for the initiation and adjustment of therapy: a consensus statement of the American Diabetes Association and the European Association for the Study of Diabetes. Diabetes Care 32:193–203
4. Gunton JE, Delhanty PJ, Takahashi S, Baxter RC (2003) Metformin rapidly increases insulin receptor activation in human liver and signals preferentially through insulin-receptor substrate-2. J Clin Endocrinol Metab 88:1323–1332
5. El-Mir MY, Nogueira V, Fontaine E, Averet N, Rigoulet M, Leverve X (2000) Dimethylbiguanide inhibits cell respiration via an indirect effect targeted on the respiratory chain complex I. J Biol Chem 275:223–228
6. Prakash R1, Johnson M, Fagan SC, Ergul A. (2013) Cerebral neovascularization and remodeling patterns in two different models of type 2 diabetes. PLoS One 8(2):e56264
7. Carvalho C, Correia S, Santos MS, Seiça R, Oliveira CR, Moreira PI (2008) Metformin promotes isolated rat liver mitochondria impairment. Mol Cell Biochem 308:75–83
8. Talbot K, Wang HY, Kazi H, Han LY, Bakshi KP, Stucky A, Fuino RL, Kawaguchi KR, Samoyedny AJ, Wilson RS, Arvanitakis Z, Schneider JA, Wolf BA, Bennett DA, Trojanowski JQ, Arnold SE (2012) Demonstrated brain insulin resistance in Alzheimer's disease patients is associated with IGF-1 resistance, IRS-1 dysregulation, and cognitive decline. J Clin Invest 122:1316–1338
9. Reagan LP (2007) Insulin signaling effects on memory and mood. Curr Opin Pharmacol 7:633–637
10. Labuzek K, Suchy D, Gabryel B, Bielecka A, Liber S, Okopien B (2010) Quantification of metformin by the HPLC method in brain regions, cerebrospinal fluid and plasma of rats treated with lipopolysaccharide. Pharmacol Rep 62:956–965
11. Wilcock C, Wyre ND, Bailey CJ (1991) Subcellular distribution of metformin in rat liver. J Pharm Pharmacol 43:442–444
12. Petersen JS, Andersen D, Muntzel MS, Diemer NH, Holstein-Rathlou NH (2001) Intracerebroventricular metformin attenuates salt-induced hypertension in spontaneously hypertensive rats. Am J Hypertens 14:1116–1122
13. Lee CK, Choi YJ, Park SY, Kim JY, Won KC, Kim YW (2012) Intracerebroventricular injection of metformin induces anorexia in rats. Diabetes Metab J 36:293–299
14. Stevanovic D, Janjetovic K, Misirkic M, Vucicevic L, Sumarac-Dumanovic M, Micic D, Starcevic V, Trajkovic V (2012) Intracerebroventricular administration of metformin inhibits ghrelin-induced Hypothalamic AMP-kinase signalling and food intake. Neuroendocrinology 96:24–31
15. Park CR (2001) Cognitive effects of insulin in the central nervous system. Neurosci Biobehav Rev 25:311–323
16. Muller AP, Gnoatto J, Moreira JD, Zimmer ER, Haas CB, Lulhier F, Perry ML et al (2011) Exercise increases insulin signaling in the hippocampus: physiological effects and pharmacological impact of intracerebroventricular insulin administration in mice. Hippocampus 21:1082–1092
17. Grunblatt E, Salkovic-Petrisic M, Osmanovic J, Riederer P, Hoyer S (2007) Brain insulin system dysfunction in streptozotocin intracerebroventricularly treated rats generates hyperphosphorylated tau protein. J Neurochem 101:757–770
18. Menassol JB, Tautou C, Collet A, Chesneau D, Lomet D, Dupont J, Malpaux B, Scaramuzzi RJ (2011) The effect of an intracerebroventricular injection of metformin or AICAR on the plasma concentrations of melatonin in the ewe: potential involvement of AMPK? BMC Neurosci. 12:76. doi:10.1186/1471-2202-12-76
19. Parekh PI, Petro AE, Tiller JM, Feinglos MN, Surwit RS (1998) Reversal of diet-induced obesity and diabetes in C57BL/6J mice. Metabolism 47:1089–1096
20. Muller AP, Tort AH, Gnoatto J, Moreira JD, Vinade ER, Perry ML, Souza DO et al (2010) Metabolic and behavioral effects of chronic olanzapine treatment and cafeteria diet in rats. Behav Pharmacol 21:668–675
21. Berleze KJ, Muller AP, Schweigert ID, Longoni A, Sordi F, de Assis AM, Rotta LN et al (2009) Gestational and postnatal low protein diet alters insulin sensitivity in female rats. Exp Biol Med (Maywood) 234:1437–1444
22. Muller AP, Zimmer ER, Kalinine E, Haas CB, Oses JP, de Assis AM, Galina A et al (2012) Physical exercise exacerbates memory deficits induced by intracerebroventricular STZ but improves insulin regulation of H(2)O(2) production in mice synaptosomes. J Alzheimers Dis 30:889–898
23. Brewer GJ, Torricelli JR, Evege EK, Price PJ (1993) Optimized survival of hippocampal neurons in B27-supplemented Neurobasal, a new serum-free medium combination. J Neurosci Res 35:567–576
24. Williams T, Courchet J, Viollet B, Brenman JE, Polleux F (2011) AMP-activated protein kinase (AMPK) activity is not required for neuronal development but regulates axogenesis during metabolic stress. Proc Natl Acad Sci 108:5849–5854
25. Moreira JD, Knorr L, Thomazi AP, Simao F, Battu C, Oses JP, Gottfried C et al (2010) Dietary omega-3 fatty acids attenuate

cellular damage after a hippocampal ischemic insult in adult rats. J Nutr Biochem 21:351–356
26. da-Silva WS, Gomez-Puyou A, de Gomez-Puyou MT, Moreno-Sanchez R, De Felice FG, de Meis L, Oliveira MF et al (2004) Mitochondrial bound hexokinase activity as a preventive antioxidant defense: steady-state ADP formation as a regulatory mechanism of membrane potential and reactive oxygen species generation in mitochondria. J Biol Chem 279:39846–39855
27. Boveris A (1984) Determination of the production of superoxide radicals and hydrogen peroxide in mitochondria. Methods Enzymol 105:429–435
28. Wendel A (1981) Glutathione peroxidase. Methods Enzymol 77:325–333
29. Lv WS, Wen JP, Li L, Sun RX, Wang J, Xian YX, Cao CX et al (2012) The effect of metformin on food intake and its potential role in hypothalamic regulation in obese diabetic rats. Brain Res 1444:11–19
30. Gropp E, Shanabrough M, Borok E, Xu AW, Janoschek R, Buch T, Plum L et al (2005) Agouti-related peptide-expressing neurons are mandatory for feeding. Nat Neurosci 8:1289–1291
31. Luna B, Feinglos MN (2001) Oral agents in the management of type 2 diabetes mellitus. Am Fam Physician 63:1747–1756
32. Petersen JS, DiBona GF (1996) Acute sympathoinhibitory actions of metformin in spontaneously hypertensive rats. Hypertension 27:619–625
33. Trammell RA, Toth LA (2011) Markers for predicting death as an outcome for mice used in infectious disease research. Comp Med 61:492–498
34. Whitaker AM, Sulzer J, Walker E, Mathis K, Molina PE (2010) Sympathetic modulation of the host defense response to infectious challenge during recovery from hemorrhage. Neuroimmunomodulation 17:349–358

ANEXO II-F. *A new device for step-down inhibitory avoidance task--effects of low and high frequency in a novel device for passive inhibitory avoidance task that avoids bioimpedance variations.*

No **ANEXO II-F** apresentamos o artigo publicado no periódico *Plos One.*

PLOS | ONE

RESEARCH ARTICLE

A New Device for Step-Down Inhibitory Avoidance Task—Effects of Low and High Frequency in a Novel Device for Passive Inhibitory Avoidance Task That Avoids Bioimpedance Variations

Gilvan Luiz Borba Filho[1]*, Kamila Cagliari Zenki[2], Eduardo Kalinine[2,4], Suelen Baggio[2], Letícia Pettenuzzo[2], Eduardo Rigon Zimmer[2], Simone Nardin Weis[2], Maria Elisa Calcagnotto[2,3], Diogo Onofre de Souza[1,2,3]

1 Programa de Pós-Graduação em Educação em Ciências, ICBS—Universidade Federal do Rio Grande do Sul, Porto Alegre, Brasil, **2** Programa de Pós-Graduação em Ciências Biológicas-Bioquímica, ICBS—Universidade Federal do Rio Grande do Sul, Porto Alegre, Brasil, **3** Departamento de Bioquímica, ICBS—Universidade Federal do Rio Grande do Sul, Porto Alegre, Brasil, **4** Programa de Pós-Graduação em Ciências Fisiológicas—Universidade Federal de Sergipe, São Cristóvão, Sergipe, Brasil

* eng.gilvan@gmail.com

CrossMark
click for updates

OPEN ACCESS

Citation: Borba Filho GL, Zenki KC, Kalinine E, Baggio S, Pettenuzzo L, Zimmer ER, et al. (2015) A New Device for Step-Down Inhibitory Avoidance Task—Effects of Low and High Frequency in a Novel Device for Passive Inhibitory Avoidance Task That Avoids Bioimpedance Variations. PLoS ONE 10(2): e0116000. doi:10.1371/journal.pone.0116000

Academic Editor: Georges Chapouthier, Université Pierre et Marie Curie, FRANCE

Received: August 14, 2014

Accepted: December 3, 2014

Published: February 23, 2015

Copyright: © 2015 Borba Filho et al. This is an open access article distributed under the terms of the Creative Commons Attribution License, which permits unrestricted use, distribution, and reproduction in any medium, provided the original author and source are credited.

Data Availability Statement: All relevant data are within the paper.

Funding: This work was supported by Instituto Nacional de Ciência e Tecnologia (http://www.inct-inofar.ccs.ufrj.br/) (DOS); Fundação de Amparo à Pesquisa do Estado do Rio Grande do Sul (http://www.fapergs.rs.gov.br/) (DOS); Concelho Nacional de Desenvolvimento Científico e Tecnológico (http://www.cnpq.br/) (DOS); Coordenação de Aperfeiçoamento de Pessoal de Nível Superior (http://www.capes.gov.br/) (DOS); and Universidade

Abstract

Background

Step-down inhibitory avoidance task has been widely used to evaluate aversive memory, but crucial parameters inherent to traditional devices that may influence the behavior analysis (as stimulus frequency, animal's bioimpedance) are frequently neglected.

New Method

We developed a new device for step-down inhibitory avoidance task by modifying the shape and distribution of the stainless steel bars in the box floor where the stimuli are applied. The bars are 2mm wide, with rectangular shape, arranged in pairs at intervals of 1cm from the next pairs. Each pair makes an electrical dipole where the polarity inverts after each pulse. This device also presents a component that acquires and records the exact current received by the animal foot and precisely controls the frequency of stimulus applied during the entire experiment.

Result

Different from conventional devices, this new apparatus increases the contact surface with bars and animal´s paws, allowing the electric current pass through the animal´s paws only, drastically reducing the influence of animal's bioimpedance. The analysis of recorded data showed that the current received by the animal was practically the same as applied, independent of the animal´s body composition. Importantly, the aversive memory was observed at specific stimuli intensity and frequency (0.35 or 0.5 mA at 62 and 125Hz but not at

Federal do Rio Grande do Sul (http://www.ufrgs.br/ufrgs/inicial) (DOS).

Competing Interests: The authors have declared that no competing interests exist.

0.20 mA or 20 Hz). Moreover, with this device it was possible to observe the well-known step-down inhibitory avoidance task memory impairment induced by guanosine.

Conclusion

This new device offers a substantial improvement for behavioral analysis in step-down inhibitory avoidance task and allows us to precisely compare data from different animals with distinct body composition.

Introduction

In the last century many apparatus and protocols to study learning and memory have been created. One of these devices developed by Thorndike [1] consisted of small crates or 'problem boxes'. In the late 1930's, the task was performed with a box containing a lever and food supplier. In this device, the rat had to learn how to have access to the food by pressing the lever[2]. Later, Hudson and colleagues[3]presented a new one-trial protocol called Inhibitory Avoidance Task (IAT).In the 1960's, Jarvik and Kopp[4] modified the IAT by building a novel apparatus containing 2 compartments, a small lit chamber connected to a larger dark chamber, where the animal received a shock as it entered to the dark compartment. Thereafter, the protocol for IAT has been modified several times. These changes resulted in a well-established protocol of Step-down inhibitory (passive) avoidance task[5–16]

In step-down inhibitory avoidance task, one critical point was the application of various electric current intensities, ranging from 0.3mA to 3mA[17–20].The stimulus intensities reflect in the latency of step-down in the test trial (24 h after training). For male Wistar rats (age, 2–3 months, weight, 220–260 g), researchers showed the latency for step-down in the test of ±40–50 seconds with 2 seconds of stimulus in intensities of 0.3mA [7],0.4mA[15,21] and 0.5mA [22–26];step-down latencies of 180s in test applied 0.8mA (2s) in training[22,27] and 600 s for 1mA (2s)[28].

However, these apparatus did not consider the influence of animal's bioimpedance on the applied currents. Additionally, several other versions of protocol combine one or two-trials assessments during the task[21].Therefore, up to now there is no standardized protocol for IAT to properly evaluate aversive memory [29], principally for fresh researchers in the field.

Therefore our aim was to develop and standardize a new device for step-down inhibitory avoidance task, in which the applied electric current has the precise same intensity as the current passing through the animal paws, taking in consideration the animal bioimpedance; the stimulus frequency and intensity are controlled and recorded during the entire experiment. For further tasks, we challenged this new step-down inhibitory avoidance device using a known amnesic drug (guanosine,i.p.) [30,31].

Materials and Methods

Animals and experimental conditions

All experimental procedures were performed according to the Brazilian Law N° 11.794/2008. Recommendations for animal care were followed throughout all the experiments in accordance with project approved by the ethical committee from the Federal University of Rio Grande do Sul-UFRGS #5647. Adult Wistar female (3 months old, 280–300g, n = 20) and male (3–5 months old, 310–450g, n = 258) rats were used in the present study. Animals were allocated in

a controlled temperature (22°C ± 1°C) room under a 12h light/12h dark cycle. They were distributed, in groups of 5 in Plexiglas cages with free access to food and water. Previously to the experiment the animals were handled using gloves, for approximately 5 min, once a day for 7 consecutive days. This step is critical to habituate the animals to the experimenter and reduce the stress caused by manipulation. After the habituation period the animals were evaluated in the inhibitory avoidance apparatus between 3:00 to 5:00 PM. The animal behavioral performance was video recorded.

Two distinct protocol paradigms were used: in the first, the duration of the foot shocks was set in 3s[26,30,32] adapting the frequency and current applied; in the second, animals receive foot shock until they return to the platform[20]. The time parameters, including the step-down latency to the grid with the 4 paws during the training and the test sessions were accessed with a manual activated chronometer.

Inhibitory avoidance apparatus

The inhibitory avoidance apparatus consists of a 50 × 25 × 30 cm poly(methyl methacrylate) box. This box has a 48 × 30 cm transparent acrylic window, a 5 cm-high,12 cm-wide and 25 cm-long platform on the left facing a grid of a series of 20 pairs of stain steel bars (2mm diameter) spaced 2mm within bars and each pair spaced 1 cm apart (Fig. 1). Each pair of bars makes an electrical dipole where the polarity inverted after each pulse. All bars have insulating layer on the sides and bottom. This step-down inhibitory avoidance apparatus was built to avoid the variations of current intensity received by animals caused by the animal bioimpedance. With a new arrangement and bars design the electrical current pass through only the animals' paws that is in contact with each pair of bars. This allows us to control the current frequency and intensity and to record the current passing through the paw of the animal during the entire experiment.

Frequencies. Three different frequencies of current were applied, as shown in the Fig. 2: trains of pulses at 20Hz (10 pulses of 25ms every 500ms), 62Hz (10 pulses of 8ms every 167ms) and 125Hz (10 pulses of 4ms every 83ms). Thus, the period of shock applied in all selected frequency, in one second, was the same. Programing the current frequencies, we introduce one modulate frequency, which exposes the animal to pulse train followed by periods without

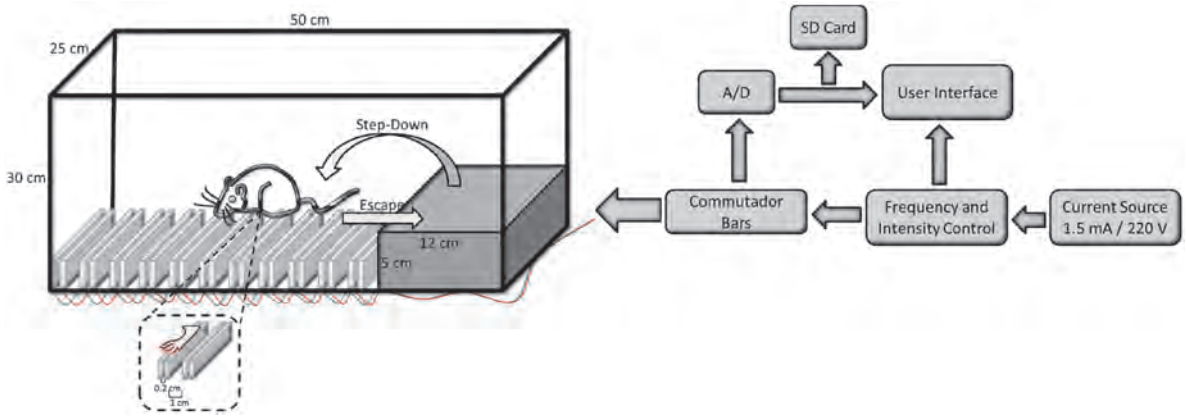

Fig 1. Schematic representation of the inhibitory avoidance apparatus. The inhibitory avoidance apparatus, including operating diagram with digital frequency control by microcontroller (PIC18F4520), an analog-digital (A/D) to measure and to control the intensity of stimulus and a data recorder on a SD card.

doi:10.1371/journal.pone.0116000.g001

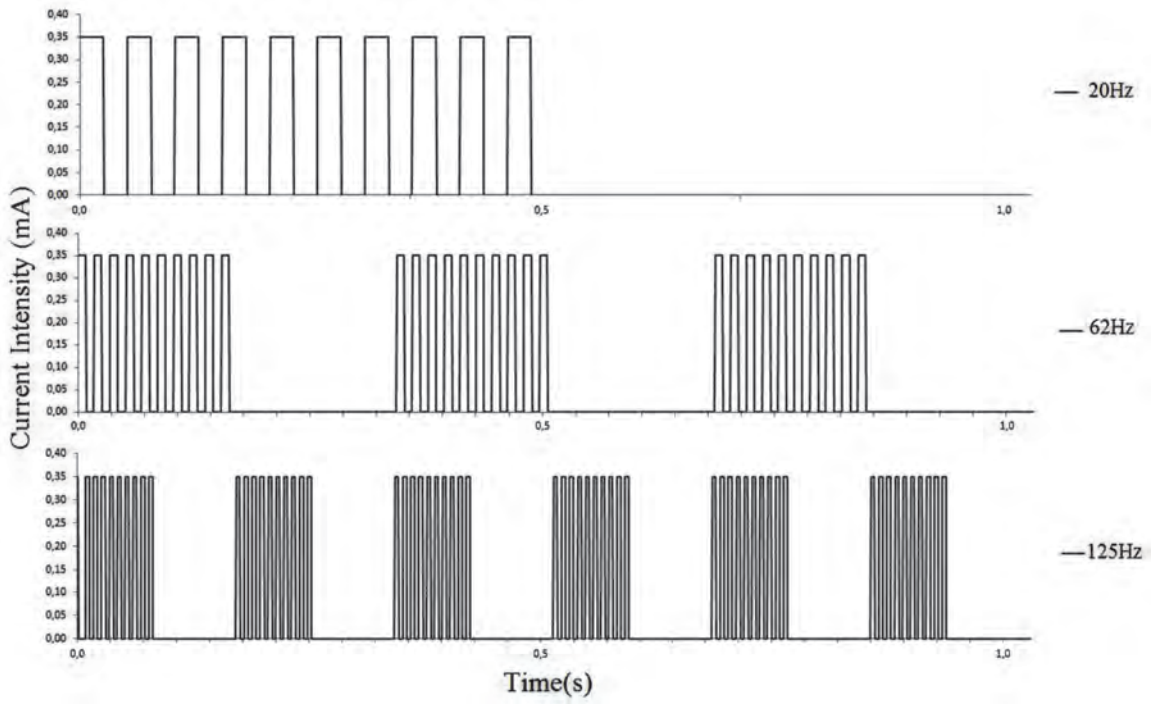

Fig 2. Positive phase of stimulus waveform for different frequencies (Hz) at 0.35mA current intensity.

doi:10.1371/journal.pone.0116000.g002

shock, it avoid the continuous animal muscle contraction provoked by passing of electric current and allows the animal to escape.

The choice of frequency was based in frequencies utilized in electric stimulation machines for physiotherapy proposes using 10–100Hz[33]. The frequency of 10Hz was used by Garin [20], and the value of frequency in major articles used the inhibitory avoidance apparatus wasn't specified.

These frequencies are controlled by a microcontroller PIC18F4520. The intensity of stimuli varied according to the protocol used and it is specified for voltage received by 100ohms resistor integrated in IAT circuit. This voltage was converted in a A/D port of microcontroller PIC18F4520 with 10bits resolution, in accordance with Nyquist-Shannon sampling theorem, converted in a ASCII number and recorded in a. txt file in a SD card (2Gb) using the fat16 library for C++.

Bioimpedance. Important aspects have to be considered when using the inhibitory avoidance apparatus. The voltage source is normally 110 or 220V and the resistance changes by a selector switch, the application of the direct current provided by batteries is used, however it result in an higher influence of bioimpedance of the animal [34]. According the Ohm's law, the bioimpedance decreases the effective current received by the animal when it steps on the grid [35]. There are three measures involved in bioimpedance value (using a frequency current below 1kHz): the conductivity value of animal's body (ρ), the contact area between animal's foot and iron bars (A) and the distance between bars (L). In frequencies below 1kHz the bioimpedance is equal as the body resistance $R = \rho.L/A$ [36]. We substantially increase the area (from 0.2cm² to 0.8cm²) modified the bars shape and decrease the distance (from ~15cm to 0,2cm) between ground and positive poles. As a result of our modifications we present a new

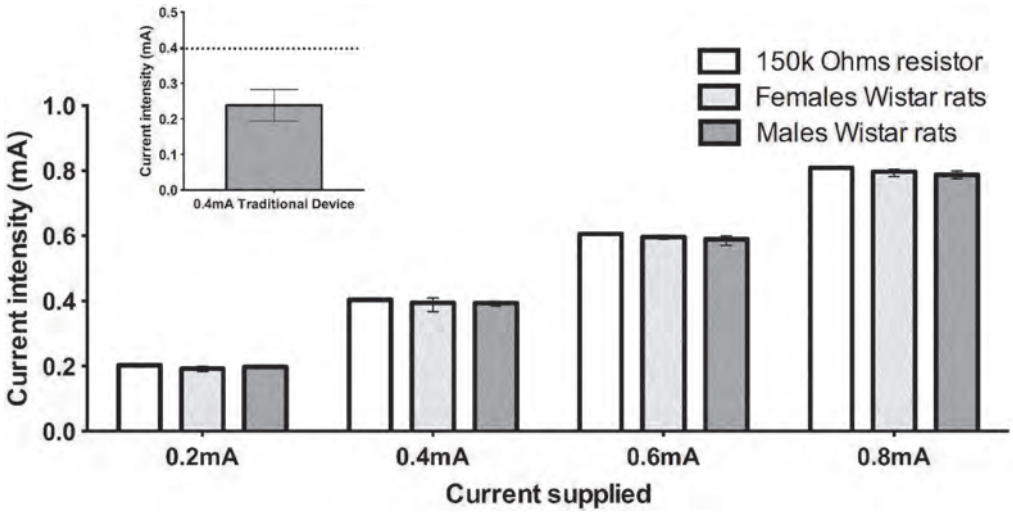

Fig 3. Plots of current intensity at 62Hz passing through the animal's paws or resistor. Different groups were represented by white, light gray or dark gray bars: 150Kohms resistor (no animal in the apparatus), female rats (3 months; 280–320g) or male rats (3 months; 310–360g), respectively. In insert graphic the effective current passing by animal body in traditional apparatus of inhibitory avoidance, nominal current 0.4mA. The standard data represents mean±S.D. Analyses by Mann-Whitney test; n = 5 animals/group/current supplied and 5 measurements for each animal. No significant difference was observed among the groups. Insert graphic, 8 animals, 3 measurements for each animal.

doi:10.1371/journal.pone.0116000.g003

device with a large (A) and small (L) resulting in a drastically decrease in the bioimpedance values of paw skin [37] from 1.7 Momhs to 32 Komhs.

In the traditional apparatus the skin bioimpedance of 1.7 Mohms/1mm^2 is very similar to the internal resistance of a current source of 1mA[37] and the bioimpedance of animal changes with body composition[38].This aspect has not been specified by many authors[3,20,30,39,40]. Indeed, we measured the value of current intensity in the traditional apparatus of Inhibitory Avoidance Task, with a floor containing parallel caliber stainless-steel bars (1mm diameter) spaced 1 cm apart [41,42]. So the effective current received by the animals´ paws in traditional apparatus usually is reduced by 21–58% of the selected value when the paws touch the bars (Fig. 3, insert).In simple words, a researcher selecting 0.5 mA in the traditional apparatus can be applying 0.25–0.4 mA, but not the choice intensity presenting a high variation in the final results.

In our Inhibitory Avoidance apparatus, we increased the contact area of the paws skin and the pair of bars by 0.8 cm^2 and we decrease the current route, consequently, we drastically decreased the impedance values of paw skin [37] from 1.7 Momhs to 32Komhs. By performing these changes we were able to reduce the decrement of effective current from 21–58% (traditional apparatus) to 0.1–3%.

To the electrical shock pass only in the paws and not through the body, in our apparatus, there are three position modes of bars: connected in phase, connected in ground, and off (no phase, no ground). We turn on the pars of bars, one by one, connected only one bar in phase and only one bar in ground each time, all others bars was off. The bars of pair were close enough for the animal touch, with one foot, the two bars at the same time (positive and ground bars), so the current pass from the positive bar to the ground bar by the pawn of the animal and not by the body as the traditional apparatus (Gauss Law).

Recording the current. It should be observed that, besides bioimpedance, electrical conduction also depends on "extra-corporeal factors" such as any dirt interposed between the paws

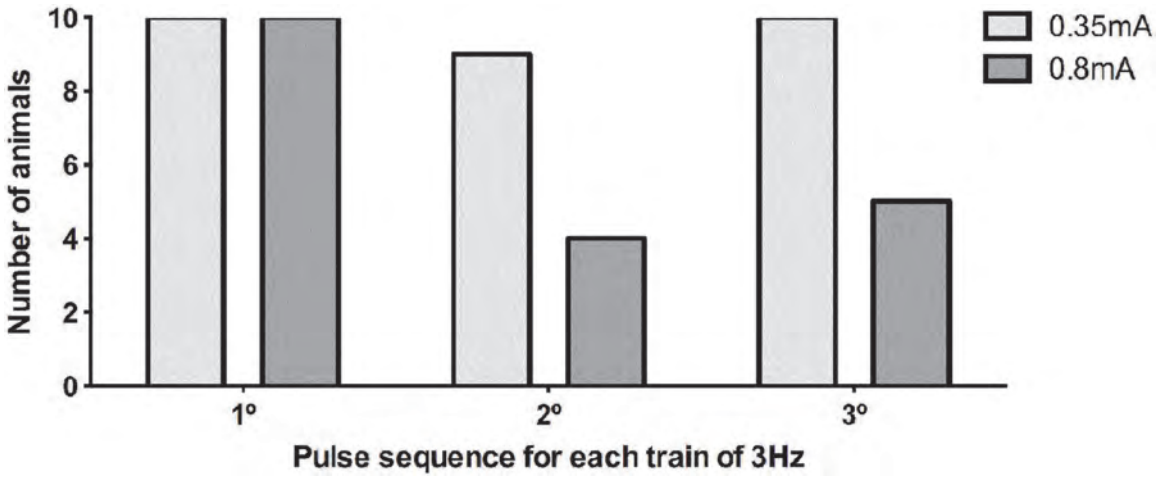

Fig 4. Number of animals (n = 10 per group) receiving 3 consecutive bursts of current (0.35 or 0.8mA, 62 Hz), measured for 1 s.

doi:10.1371/journal.pone.0116000.g004

and the bars during tests (faeces, etc.), another factor hard to quantify. This is the reason for measurement and record the current passing in the animal, if any extra-corporeal factors decrease the current intensity it will be visualized.

The current was recorded by an analog/digital converter (A/D) and the sampling rate followed the Nyquist-Shannon theorem. The sampling frequency of 400 Hz was used. We measured the current value by the voltage in a 100ohms resistor placed after the negative pole bar, so the current intensity value was registered only when the animal´s paw closed the circuit stepping on a pair of bars. The value measured (V_2) is the resultant of the voltage applied (V_1) divided by the summation of resistance in the switch (R_1), the bioimpedance of animal´s paws (R_2) and the 100ohms resistor (R_3), multiplied by 100ohms (see. 1).

$$V_2 = \frac{R_3 V_1}{(R_1 + R_2 + R_3)} \quad (1)$$

This value is then converted to ASCII character by the microcontroller and record on a SD Card.

Using this recording system, we were able to determine the number of stimuli received by each animal. The Fig. 4 shows the data of stimuli intensity of 0.35 and 0.8mA at trains of 62Hz. When the stimulus intensity were of 0.35 mA at trains of 62Hz or 125Hz, all animals received the exact given pulses, with no jumping. However, with stimulus intensity of 0.8mA, the number of jumps increased and consequently the exact given pulses received by the animals decreased, jeopardizing the experimental analysis. Therefore, to avoid the inconsistent amount of received stimuli due to the jumping, we decided to use the stimuli intensity of 0.2, 0.35 and 0.5 mA to evaluate the effect of different current frequencies on the performance of the animals (all data of the current intensity passing through the animal paws were recorded in a SD Card and analyzed offline).

Step-down Passive Inhibitory Avoidance Task

First protocol. For this protocol, we used the stimulus of 0.35mA at 62Hz. Each animal was gently placed on the platform facing the rear left corner of the inhibitory avoidance apparatus (training session).When the animal stepped-down on the grid with the 4 paws, it received the

footshock (stimulus) for 3 seconds. Afterwards, the animal was withdrawn from the apparatus. After 24h (test session), each animal was placed on the platform again. In this session no shock was applied when the animal stepped down on the grid. After stepping down, each animal was withdrawn from the apparatus and placed back to the home cage [43]. The time parameters were accessed during the training and the test sessions with a manual activated chronometer. The time to step down on the grid with the 4 paws was measured in both, training and test sessions. Step-down latencies were cut-off at 60s in the training session and at 180s in the test session.

Second protocol. During the training session, each animal was gently placed on the platform facing the rear left corner of the inhibitory avoidance apparatus. Immediately after stepping down with the 4paws on the grid the animal received continuous scrambled footshock (the current and frequency depended on the specific group) until it spontaneously step-up back to the platform (latency to escape). The animal was then withdrawn from the apparatus. The escape latencies were cut-off at 60s[20].After 24h (test session), the procedure was performed as described for the test session of first protocol. These time parameters were accessed during the training and the test sessions with a manual activated chronometer. Step-down latencies were cut-off at 60s in the training session and at 180s in the test session. The animals were divided at 11 groups according to the intensity and frequency stimuli applied (0.2mA; 20,62 and 125Hz), (0.35mA; 10,20,40,62 and 125Hz), and (0.5 mA; 20, 62 and 125 Hz).

Passive inhibitory avoidance performance (Score). To evaluate the performance in IAT, the latency to step-down in the training and test sessions are measured. According to previous studies, the memory was measured by the difference between the latency to step-down during the test session and the latency to step-down in the training session [30–32,43,44][22–26].In second protocol, the time to scape change for each animal, so we qualified the performance by the influence of the time to explore the platform (step-down latency in training session), the foot shock duration (latency to escape) and the latency for step-down in test (step-down latency in test)to evaluate the inhibitory avoidance performance(see 2).

$$f(t) = \frac{\log(k_1/SDT)}{(k_2.SU)}.SD24H \tag{2}$$

f(t): IAT function
SDT: step-down latency in training session
SD24:step-down latency in test
SU: latency to escape
k_1: 60s (maximum time in the platform during the training session)
k_2: 3s (minimum time in the platform during the training session)

The measure of "learning" was the same as all classic articles using the passive inhibitory avoidance task, so we measured the difference between step-down latency in train and the step-down latency in test after 24h.The value of latency to return to platform was used to qualify and compere animals with different time to return to platform in function of the leaning in task.

Using the equation *f(t)* we can compare the effect if a treatment that affects the latency to return to platform (ex: sensibility to the shock),do or do not affects learning. If the time to return to the platform is different among the animals, the equation balances this variable resulting in a value of performance.

Additionally any values of equation above 1 indicate the step-down latency in test (*SD24H*) is significant higher of step-down latency in training (*SDT*), independent of the escape latency.

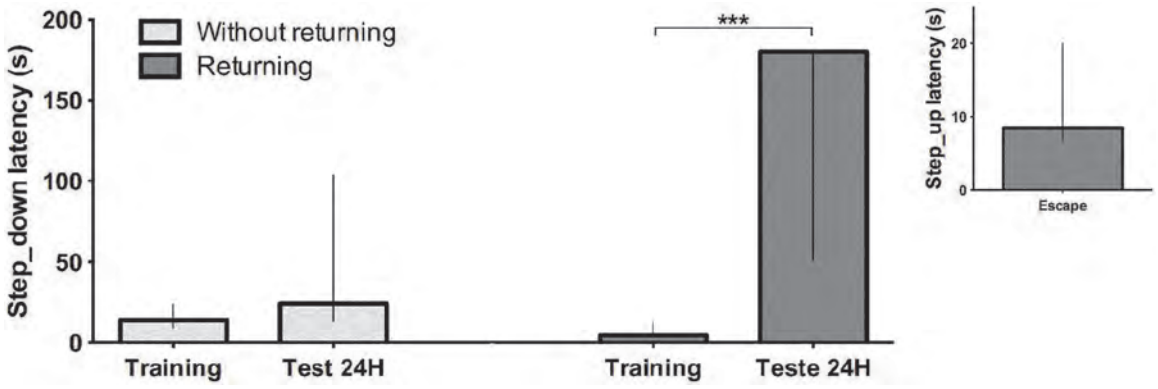

Fig 5. Step down latency (s) for training and test sessions. Light gray represents the group without returning (first protocol with 3s of stimulus), and dark gray represents the group returning (second protocol with escape latency) in the training session (0.35mA, 62Hz). The latency to escape in the second group is represented in the insert graphic. The data is expressed by median with interquartile range; analyses by Mann-Whitney test; (n = 10 per group) ***$p<0.001$ comparing to SDT.

doi:10.1371/journal.pone.0116000.g005

Drugs

Guanosine (GUO) from Sigma (St. Louis, MO, USA) was dissolved in NaCl 0.9%. The solutions were prepared immediately before use and were protected from the light[30,45].Thirty minutes before the training session the rats received a single intraperitoneal (i.p.) injection of 7.5mg/kg GUO (1ml/kg)or vehicle (NaCl—0.9%). The dose of GUO applied was based on previous studies from our group using *in vivo* protocols to investigate the anticonvulsant [46–49] and the amnesic effect on IAT [30].

Statistical analysis

The data are expressed as median and interquartile range, since the behavioral variables being analyzed (step- down and step up- latency) did not follow a normal distribution, using D'Agostino&Pearson omnibus test of normality. The observation was limited to 180 seconds. The data were analyzed using the Graphpad Prism 5 program. To compare the results we used One-Way ANOVA followed by Dunnett's, Mann-Whitney, or using Chi-square with significance level of $p< 0.05$.

Regarding total $n = 278$ we can divide in: current intensity measurement—48 animals (Fig. 3); measurement of consecutive bursts of current—20 animals (Fig. 4); protocol 1 and protocol 2 comparison–20 animals (Fig. 5); influence of current and intensity measurement—90 animals (Fig. 6); mapping of 0.35 mA effects—20 animals (Fig. 7); guanosine experiment—80 animals (Fig. 8).

Results

Using our new step-down inhibitory avoidance device, the current received by the animal through the paws was exactly the same current applied without any interference of the body bioimpedance for all stimuli intensities (0.2, 0.4, 0.6 or 0.8 mA) (Fig. 3). However, to obtain this result, it is necessary to turn on one pair of bars at a time. This is controlled by the microcontroller PIC18F4520that witches the pair of bars according the selected train of frequencies (20Hz, 62Hz or 125Hz) and the number of pair (20 pair in this apparatus).

In the second protocol (variable escape time), the median time that animals received shock was of 8.5s (interquartile range, 7.25–18.5 seconds) and the animals spent more time in the

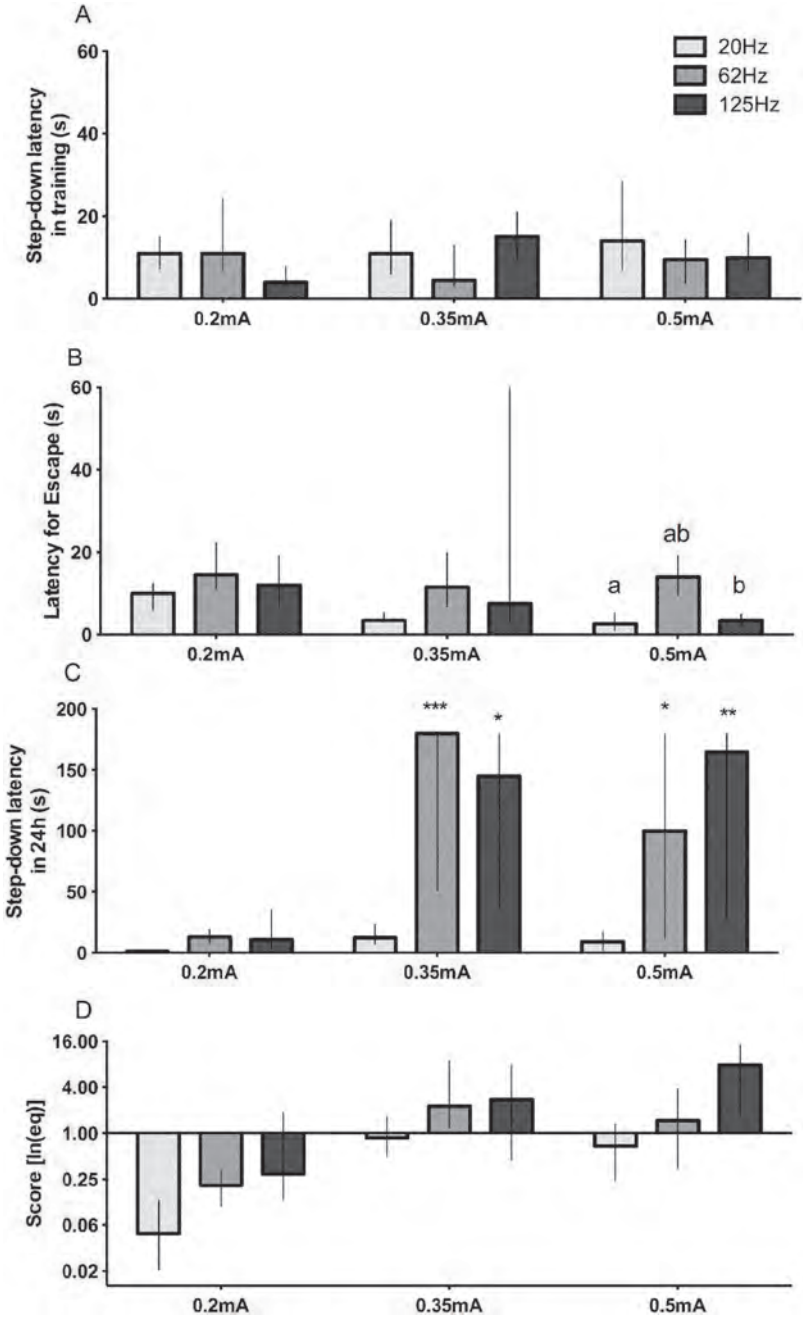

Fig 6. Effects of frequency (Hz) and current intensity (mA) in step-down inhibitory avoidance parameters. Effects of frequency (Hz) and current intensity (mA) on step down latency in training session—A, latency for escape—B, step down latency in test session—C, and score performance (D—the combination of the 3 graphs above by applying the Equation 2). In B, same letter represent statistical difference among groups; *$p<0.05$;**$P<0.01$;***$p<0.001$, by Mann-Whitney, comparing to the same group in A. Data represent median with interquartile range (n = 10/group).

doi:10.1371/journal.pone.0116000.g006

platform during the test session compared to the training session (Fig. 5). The learning was observed in the second protocol but not in the first protocol (applied the stimulus for 3s), using 0.35mA 62Hz.However, using current of 0.8mA 62Hz for 3s the animal behavior reflects the classic experiments (data not show). Therefore, we choose to use the second protocol for further experiments in this study.

There was no statistical difference among groups in the step-down period during the training session (Fig. 6A).There was statistical difference among groups 0.5mA 62Hz and 0.5mA 20–125Hz in the latency to escape from the grid (Fig. 6B). Moreover, for the stimuli intensity of 0.2mA at 20, 62 or 125Hz, and 0.35 or 0.5 mA at 20Hz there was no difference in step-down latency in test session when compared to the respective step-down latency in training (Fig. 6C). Animals receiving stimuli intensity of 0.35 and 0.5 mA at 62 and 125Hz had increased time spent in the platform in test session (Fig. 6C). Applying the Equation 2 we can observe the influence of all variables evaluated in this study that may contribute for the learning process. By these mathematical analyses all groups with a median above 1 are classified as presenting memory (Fig. 6D).

The Fig. 7 shows the effect of 0.35mA stimulus with different frequencies in step-down latency in test session. For 40Hz the step-down latency in test session is similar to observed when used 0.3–0.5mA in classic articles (median of 40–50 seconds), however, when we use 62Hz the step-down latency is comparable to 0.8mA (median of 180 seconds), and the behavioral response to the stimulus is more intense at higher frequencies (Table 1).

Using the second protocol we observed diminishing of memory in avoidance task by guanosine at i.p. 7.5mg/kg at 0.35mA, at 62Hzand 125 Hz stimulation (Fig. 8), even though the guanosine group presented different time to return to the platform among the animals of the group, there were still the amnesic effects of this compound. There was influence of latency to return to platform in test (escape latency) and the step-down latency in training on the performance score in both, saline (Fig. 9 A-C) and guanosine (Fig. 9 B-D) administration. We observed that 18% of animals treated with GUO and 17.5% of control group obtained a score ≥ 1 and < 2.99. However, the number of animals treated with GUO with score higher than 3 where significantly smaller than the control group (17%, 65%, respectively) ($p<0.0001$, Chi-square) (see Fig. 9).

Discussion

In our new apparatus, the electric stimulus does not depend of animal's bioimpedance (Fig. 3). It permits to evaluate the real effect of the stimulus among groups with different bioimpedance values, eliminate the influence of house conditions[50]the phenotype, genetic[34,35], treatments like exercise [51] and drugs[52], changing the bioimpedance value[53].

Further, our aim was to design an apparatus with stimulus frequency and intensity easily and clearly controlled and recorded during the entire experiment, as the studies using traditional apparatus designed to test step-down avoidance task do not evaluate the influence of animal's bioimpedance on the applied currents, nor frequency, neither the intensity of stimulus. These 3 points clearly alter the behavior of the animals, as confirmed by our results.

Among the advantages from these modifications we can sustain that the current applied during the task is the current arrived to the animals. In simple words, a researcher selecting 0.5 mA in the traditional apparatus can be applying 0.25–0.4 mA, which result in a high variation in the final performance of the animals. With this new apparatus, we were able to reduce the decrement of effective current from 21–58% (traditional apparatus) to 0.1–3% (Fig. 3). Using the traditional apparatus for step-down inhibitory avoidance task, each animal may receive different electric current intensity (due variations in body composition); so the

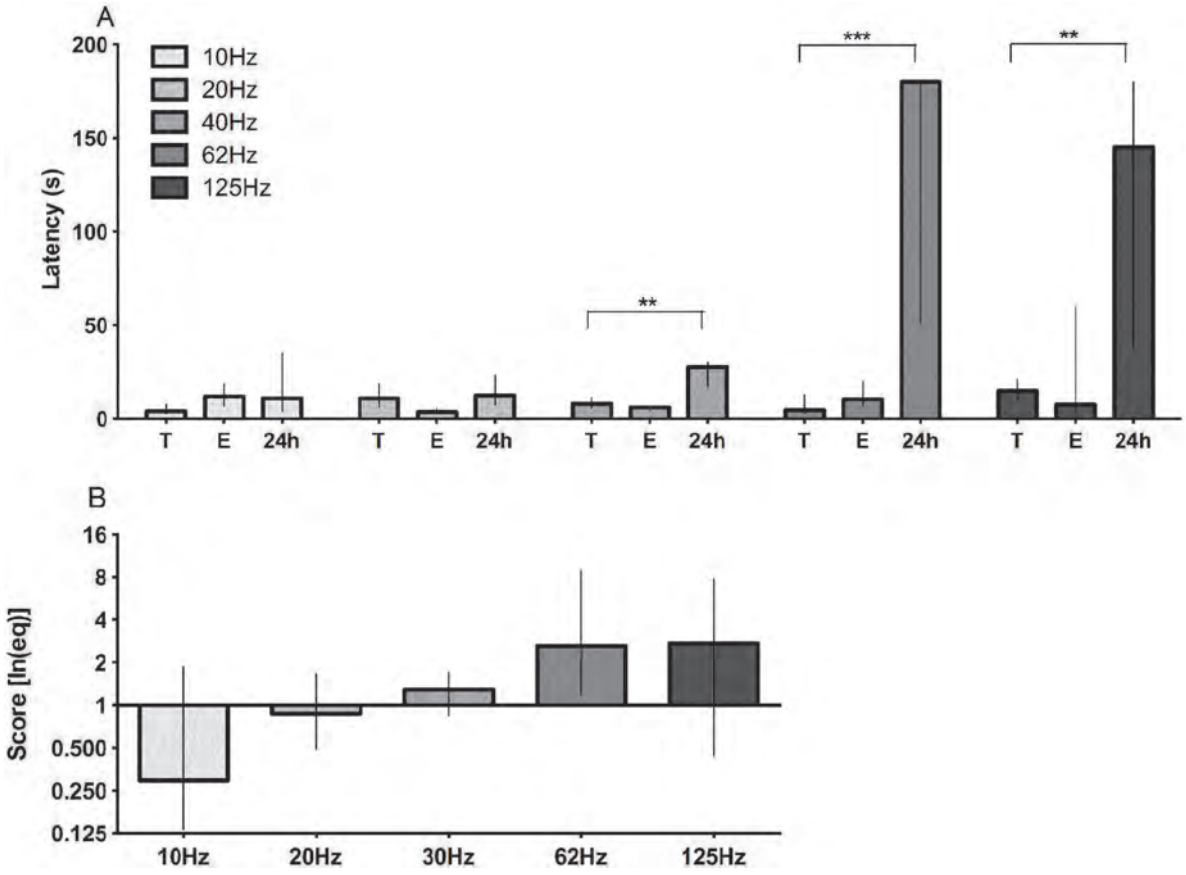

Fig 7. Effects of frequency (Hz) with 0.35mA current intensity in step-down inhibitory avoidance latencies. A- Effects of frequency (Hz) on step down latency in training session (T), latency for escape (E), step down latency in test session (24h), and score performance (B—the combination of the 3 parameters by applying the Equation 2).**P<0.01; ***p<0.001, by Mann-Whitney, comparing to the same group in A. Data represent median with interquartile range (n = 10/group).

doi:10.1371/journal.pone.0116000.g007

comparison among animals with different ages, sex or weight is jeopardized, due to the animals bioimpedance differences.

It should be observed that, besides bioimpedance, electrical conduction also depends on "extra-corporeal factors" such as any dirt interposed between the paws and the bars during tasks (faeces, etc.), another factor hard to quantify. This is an additional reason for measurement and recording of the current arriving to the animals, if any extra-corporeal factors decrease the current intensity it will be visualized.

The frequency modified the effect of current intensity on leaning in inhibitory avoidance task and the behavioral of the animal during the stimulus (Table 1). It's a nonstandard parameter and usually not cited in articles, but it is important as the current intensity confirmed by our data (Figs. 6 and 7).

The choice of frequency was based in frequencies utilized in electric stimulation machines for physiotherapy proposes using 10–100Hz[33]. The frequency of 10Hz was used by Garin [20], and the value of frequency in most articles used the inhibitory avoidance apparatus wasn't specified. Even using a battery as electric source, the stimulus should be given in form of

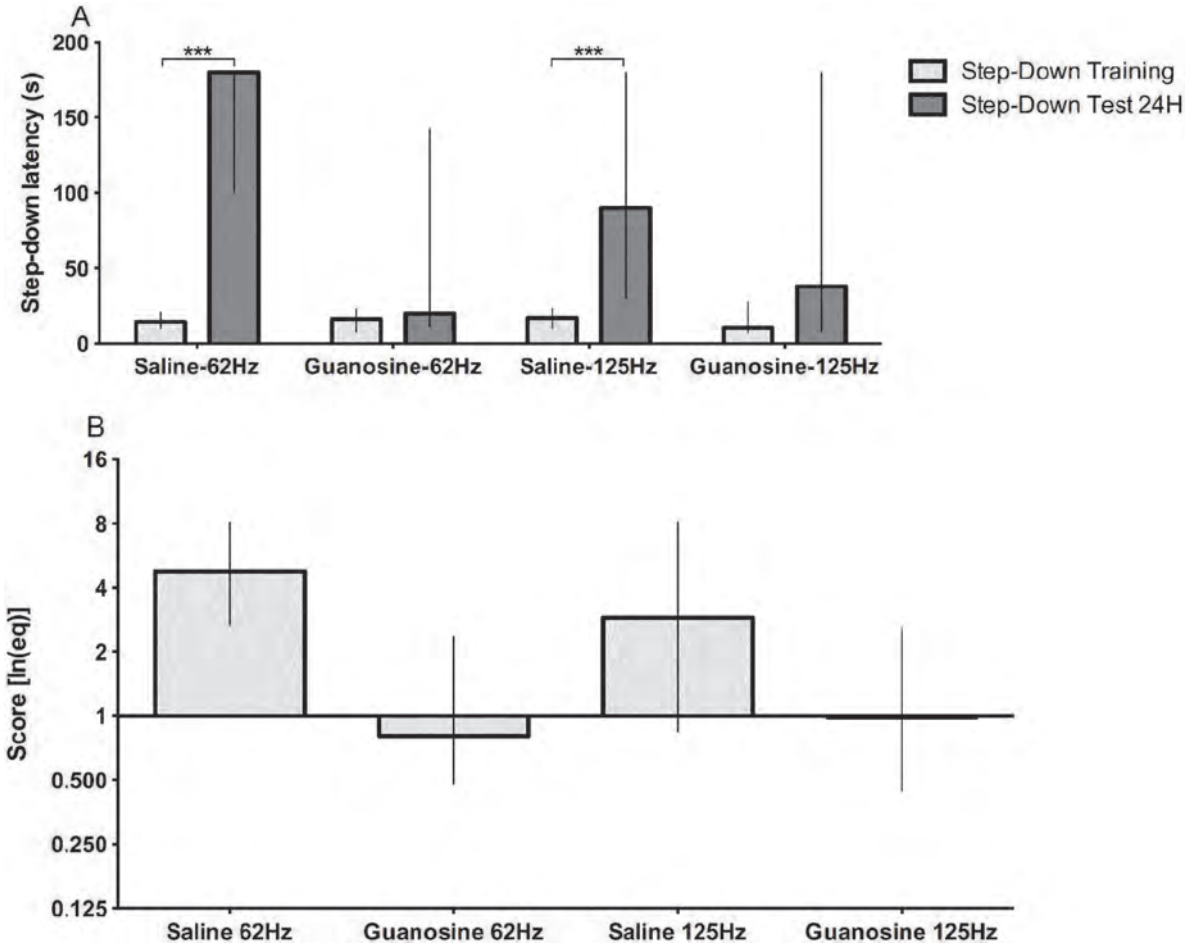

Fig 8. Effect of guanosine on the step-down inhibitory avoidance task. (A) Effect of guanosine (i.p.- 7.5mg/kg) on the step-down inhibitory avoidance task using 0.35 mA stimuli with different frequencies (62 Hz and 125 Hz). All groups displayed similar escape latency (data not shown). Bars express median (interquartile range). (B) Application of Equation 2 to the data of the graph A. The data were analyzed by Mann-Whitney test (n = 20 per group); ***$p<0.001$.

doi:10.1371/journal.pone.0116000.g008

pulses, the constant current (Gaussian current) promote fixed muscle contraction and can burn the skin (Joule effect). Moreover we need to have some kind of ideal frequency window to work. In this sense, we worked with a low frequency as 20 Hz to indirectly answer what could be the lesser frequency for the learning in this task.

Here, there was a relation between performance in step-down inhibitory avoidance task and the current frequency (Figs. 6 and 7). The behavioral escape, but not the performance in test session, was the same for 20 Hz and 125 Hz frequencies. This modified step-down inhibitory avoidance apparatus allowed us to control variables that have been not specified up to now [18,32,39,54]. Our data demonstrates that not only the intensity but also the frequency of the applied current plays a key role in the performance in a step-down inhibitory avoidance and learning. This data of frequency is one of missing information in other studies using IAT [19,41,55,56]. We observed learning with 0.35mA and 0.5mA at 62 and 125Hz but not at 20Hz (Fig. 6). The latency to step up back to the platform during the training session was

Table 1. Description of the observed behavioral responsesduring the test and training sessions.

0.35mA 20Hz								
	Training			Test				
ID	Vocalization	Flinch	Jump	Rearing	Turn Angle	Freez	Risk Acessment	Faeces
cx1 r1	-	+	-	2	0	0	0	0
cx1 r2	+	+	-	6	6	1	2	Ok
cx1 r3	-	+	-	3	2	0	2	Ok
cx2 r3	-	++	-	5	3	0	2	0
cx2 r4	+	+	-	2	1	0	1	Ok
cx3 r4	+	++	-	1	0	0	0	Ok
0.35mA 62Hz								
	Training			Test				
ID	Vocalization	Flinch	Jump	Rearing	Turn Angle	Freez	Risk Acessment	Faeces
cx1 r4	++	++	-	10	4	0	7	Ok
cx1 r5	+++	+++	+	5	5	0	5	Ok
cx2 r1	++	++	+	7	3	0	6	Ok
cx2 r2	++	++	+	3	2	0	5	0
cx3 r1	+++	+++	-	5	3	0	6	Ok
cx3 r2	+	+++	+	14	8	0	7	Ok
cx3 r3	+++	+++	+	2	1	0	3	Ok

+ one episode,

++ between two and four episodes,

+++ more than four episodes; in test the absolute number during the session.

doi:10.1371/journal.pone.0116000.t001

similar for all current intensities, even for the lowest applied current (0.2mA), regardless the frequency applied.

It is important to emphasize that the possibility to programing the current frequencies in our apparatus with one modulate frequency (Fig. 2) allows to avoid the continuous animal muscle contraction provoked by the passing of electricity by the animal body. Also, the shape of bar avoid that animal hold the bar during the stimulus (Fig. 1). In order to maintain this concept we needed to resolve the problem of bioimpedance influence in electric current. Thus, we changed the bars distribution, shape and turn on mode. In this way we cannot apply a scrambled footshock in this model, as the classical apparatus, because we need to turn off the bars. Furthermore, a comparison among traditional systems and the ours (with and without influence of bioimpedance, respectively), is difficult because we cannot control the frequency in traditional apparatus, nor to measure the real intensity through the animals

With the new apparatus presented here we were able:(1) to abolish the influence of bioimpedance in the intensity of the current received by the animal; (2) to precisely control the current received during the shocks delivery over the task; (3) to control and constantly record the intensity and frequency of the effective current applied, enabling a full record of the entire experiment. There was a clear reduction in the decrement of effective current to only 0.1–3%, indicating an insignificant interference of bioimpedance (Fig. 3).

The guanosine, a guanine-based purine, plays important roles in the Central Nervous System[49,57], and has a well establish amnesic effect *in vivo* in rodents[30,31,49]. Therefore we

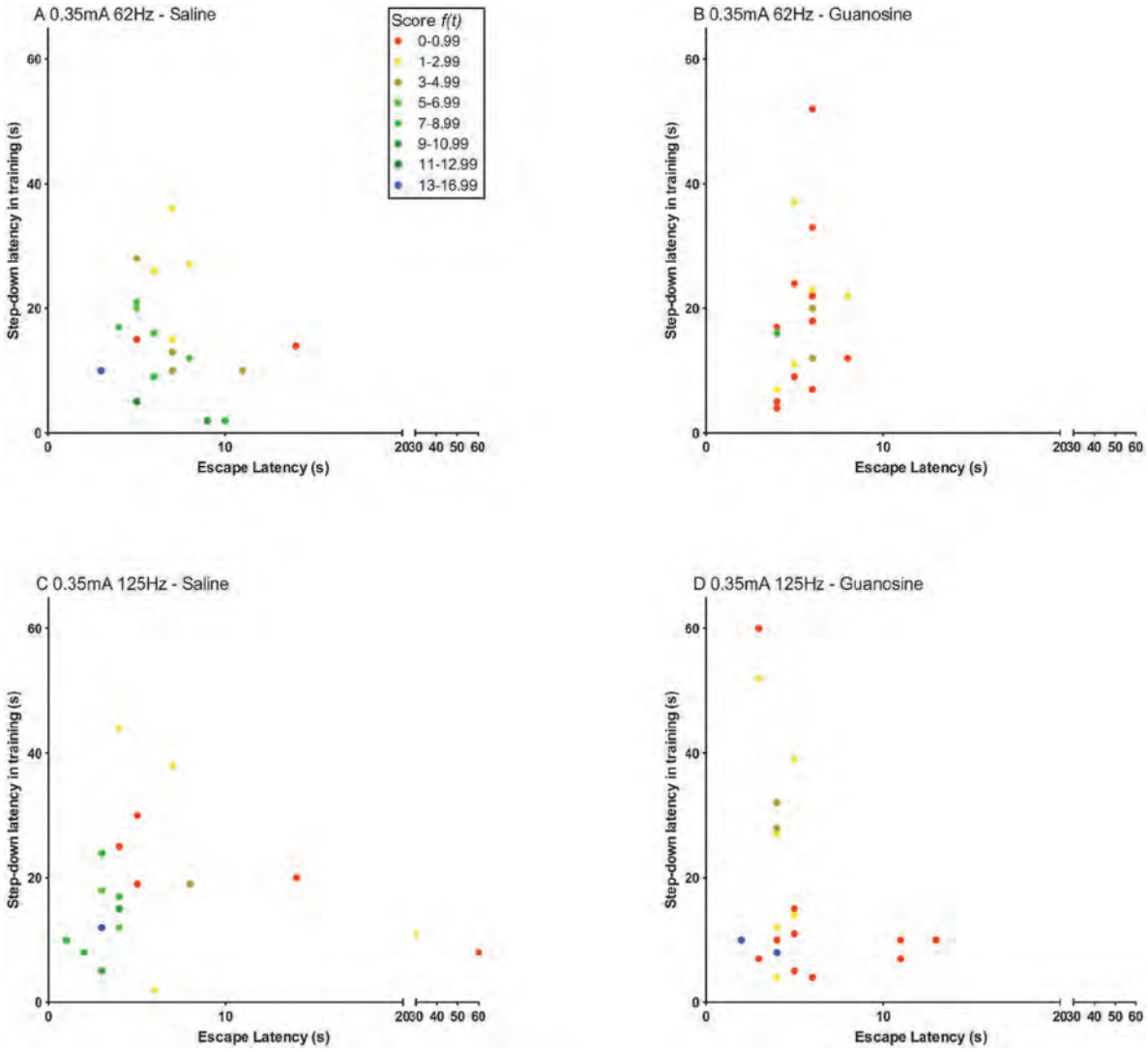

Fig 9. Platform exploration time in training (step-down latency in training) and time of stimulus (escape latency) influence on learning. The scale of colors indicates the animals score based in Equation 2. (A) Saline group exposed at 0.35mA, 62Hz. (B) Guanosine group exposed at 0.35mA, 62Hz. (C) Saline group exposed at 0.35mA, 125Hz. (D) Guanosine group exposed at 0.35mA, 125Hz. (n = 20/group).

doi:10.1371/journal.pone.0116000.g009

evaluated our new device using animals treated with i.p. injection of guanosine. We observed a significant diminishing effect of guanosine on step-down inhibitory avoidance memory even with a variable escape time.

Taken altogether, this new device offers a substantial improvement in behavioral analysis in the step-down inhibitory avoidance task, by considering crucial parameters that havebeen never stated before, such as frequency of stimulus application and principally the influence of the animal's bioimpedance. This influence was drastically reduced by the changes in the shape and distribution of the bars in the apparatus, which permitted to record the exact current passing precisely trough the paws of the animal during the task and to compare results among

animals with different body composition. Despite all these findings, only future studies with classical impaired memory diseases or potential memory modulators drugs could affirm the full potential of our new apparatus. Finally, we also propose a mathematical equation that could improve the analysis of animal performance in the inhibitory avoidance task.

Acknowledgments

The authors thank Ben Hur Marins Mussulini, MSc (UFRGS) for the scientific input and Gilvan Luiz Borba, PhD (UFRN) for helping with the mathematical modelling for the equation score.

Author Contributions

Conceived and designed the experiments: GLBF KCZ SNW MEC DOS. Performed the experiments: GLBF EK KCZ SB. Analyzed the data: GLBF EK KCZ LP MEC DOS. Contributed reagents/materials/analysis tools: GLBF. Wrote the paper: GLBF KCZ EK MEC ERZ DOS. Figure editing: ERZ. Contributed with reagents: ERZ. Statistics and animal manipulation: LP. Animal manipulation and habituation: SB.

References

1. Thorndike EL (1898) Animal intelligence: an experimental study of the associative processes in animals. New York; London: The Macmillan Company. 109 p. p.
2. Skinner BF (1938) The behavior of organisms. New York,: Appleton-Century-Crofts. xv, 457 p. p.
3. Hudson BB (1950) One-trial learning in the domestic rat. Genet Psychol Monogr 41: 99–145. PMID: 15411972
4. Jarvik ME, Kopp R (1967) An improved one-trial passive avoidance learning situation. Psychol Rep 21: 221–224. PMID: 6078370
5. Perry ML, Dias RD, Carrasco MA, Izquierdo I (1983) Step-down inhibitory avoidance training and beta-endorphin-like immunoreactivity of rat hypothalamus and plasma. Braz J Med Biol Res 16: 339–343. PMID: 6324942
6. Ardenghi P, Barros D, Izquierdo LA, Bevilaqua L, Schroder N, et al. (1997) Late and prolonged post-training memory modulation in entorhinal and parietal cortex by drugs acting on the cAMP/protein kinase A signalling pathway. Behav Pharmacol 8: 745–751. PMID: 9832961
7. Bernabeu R, Bevilaqua L, Ardenghi P, Bromberg E, Schmitz P, et al. (1997) Involvement of hippocampal cAMP/cAMP-dependent protein kinase signaling pathways in a late memory consolidation phase of aversively motivated learning in rats. Proc Natl Acad Sci U S A 94: 7041–7046. PMID: 9192688
8. Bianchin M, Walz R, Ruschel AC, Zanatta MS, Da Silva RC, et al. (1993) Memory expression is blocked by the infusion of CNQX into the hippocampus and/or the amygdala up to 20 days after training. Behav Neural Biol 59: 83–86. PMID: 8476386
9. Bliss TV, Collingridge GL (1993) A synaptic model of memory: long-term potentiation in the hippocampus. Nature 361: 31–39. PMID: 8421494
10. Izquierdo I, Barros DM, Mello e Souza T, de Souza MM, Izquierdo LA, et al. (1998) Mechanisms for memory types differ. Nature 393: 635–636. PMID: 9641675
11. Izquierdo I, Bianchin M, Silva MB, Zanatta MS, Walz R, et al. (1993) CNQX infused into rat hippocampus or amygdala disrupts the expression of memory of two different tasks. Behav Neural Biol 59: 1–4. PMID: 8095135
12. Izquierdo I, Medina JH, Vianna MR, Izquierdo LA, Barros DM (1999) Separate mechanisms for short- and long-term memory. Behav Brain Res 103: 1–11. PMID: 10475159
13. Izquierdo I, Quillfeldt JA, Zanatta MS, Quevedo J, Schaeffer E, et al. (1997) Sequential role of hippocampus and amygdala, entorhinal cortex and parietal cortex in formation and retrieval of memory for inhibitory avoidance in rats. Eur J Neurosci 9: 786–793. PMID: 9153585
14. Jerusalinsky D, Ferreira MB, Walz R, Da Silva RC, Bianchin M, et al. (1992) Amnesia by post-training infusion of glutamate receptor antagonists into the amygdala, hippocampus, and entorhinal cortex. Behav Neural Biol 58: 76–80. PMID: 1417675

15. Walz R, Roesler R, Quevedo J, Sant'Anna MK, Madruga M, et al. (2000) Time-dependent impairment of inhibitory avoidance retention in rats by posttraining infusion of a mitogen-activated protein kinase kinase inhibitor into cortical and limbic structures. Neurobiol Learn Mem 73: 11–20. PMID: 10686120

16. Cammarota M, Bernabeu R, Levi De Stein M, Izquierdo I, Medina JH (1998) Learning-specific, time-dependent increases in hippocampal Ca2+/calmodulin-dependent protein kinase II activity and AMPA GluR1 subunit immunoreactivity. Eur J Neurosci 10: 2669–2676. PMID: 9767396

17. Alonso M, Viola H, Izquierdo I, Medina JH (2002) Aversive experiences are associated with a rapid and transient activation of ERKs in the rat hippocampus. Neurobiol Learn Mem 77: 119–124. PMID: 11749089

18. Vinade ER, Izquierdo I, Lara DR, Schmidt AP, Souza DO (2004) Oral administration of guanosine impairs inhibitory avoidance performance in rats and mice. Neurobiol Learn Mem 81: 137–143. PMID: 14990233

19. Galindo LE, Garin-Aguilar ME, Medina AC, Serafin N, Quirarte GL, et al. (2008) Acquisition and retention of enhanced active avoidance are unaffected by interference with serotonergic activity. Behavioural Brain Research 195: 153–158. doi: 10.1016/j.bbr.2008.01.011 PMID: 18342379

20. Garin-Aguilar ME, Medina AC, Quirarte GL, McGaugh JL, Prado-Alcala RA (2014) Intense aversive training protects memory from the amnestic effects of hippocampal inactivation. Hippocampus 24: 102–112. doi: 10.1002/hipo.22210 PMID: 24123595

21. Quevedo J, Vianna MR, Roesler R, de-Paris F, Izquierdo I, et al. (1999) Two time windows of anisomycin-induced amnesia for inhibitory avoidance training in rats: protection from amnesia by pretraining but not pre-exposure to the task apparatus. Learn Mem 6: 600–607. PMID: 10641764

22. Cammarota M, Bevilaqua LR, Medina JH, Izquierdo I (2004) Retrieval does not induce reconsolidation of inhibitory avoidance memory. Learn Mem 11: 572–578. PMID: 15466311

23. Vianna MR, Szapiro G, McGaugh JL, Medina JH, Izquierdo I (2001) Retrieval of memory for fear-motivated training initiates extinction requiring protein synthesis in the rat hippocampus. Proc Natl Acad Sci U S A 98: 12251–12254. PMID: 11572949

24. Cammarota M, Bevilaqua LR, Kerr D, Medina JH, Izquierdo I (2003) Inhibition of mRNA and protein synthesis in the CA1 region of the dorsal hippocampus blocks reinstallment of an extinguished conditioned fear response. J Neurosci 23: 737–741. PMID: 12574401

25. Bevilaqua LR, da Silva WN, Medina JH, Izquierdo I, Cammarota M (2005) Extinction and reacquisition of a fear-motivated memory require activity of the Src family of tyrosine kinases in the CA1 region of the hippocampus. Pharmacol Biochem Behav 81: 139–145. PMID: 15894071

26. Vinade ER, Schmidt AP, Frizzo ME, Portela LV, Soares FA, et al. (2005) Effects of chronic administered guanosine on behavioral parameters and brain glutamate uptake in rats. J Neurosci Res 79: 248–253. PMID: 15558762

27. Bonini JS, Da Silva WC, Da Silveira CK, Kohler CA, Izquierdo I, et al. (2011) Histamine facilitates consolidation of fear extinction. Int J Neuropsychopharmacol 14: 1209–1217. doi: 10.1017/S1461145710001501 PMID: 21211106

28. Schmidt do Prado-Lima PA, Perrenoud MF, Kristensen CH, Cammarota M, Izquierdo I (2011) Topiramate diminishes fear memory consolidation and extinguishes conditioned fear in rats. J Psychiatry Neurosci 36: 250–255. doi: 10.1503/jpn.100115 PMID: 21392483

29. Brunner D, Nestler E, Leahy E (2002) In need of high-throughput behavioral systems. Drug Discov Today 7: S107–112. PMID: 12546875

30. Roesler R, Vianna MR, Lara DR, Izquierdo I, Schmidt AP, et al. (2000) Guanosine impairs inhibitory avoidance performance in rats. Neuroreport 11: 2537–2540. PMID: 10943718

31. Saute JA, da Silveira LE, Soares FA, Martini LH, Souza DO, et al. (2006) Amnesic effect of GMP depends on its conversion to guanosine. Neurobiol Learn Mem 85: 206–212. PMID: 16325434

32. Petronilho F, Perico SR, Vuolo F, Mina F, Constantino L, et al. (2012) Protective effects of guanosine against sepsis-induced damage in rat brain and cognitive impairment. Brain Behav Immun 26: 904–910. doi: 10.1016/j.bbi.2012.03.007 PMID: 22497789

33. Lloyd T, DED G, Strauss GR, Singer K (1986) A review of the use of electro-motor stimulation in human muscles. Aust J Physiother 32: 18–30. doi: 10.1016/S0004-9514(14)60640-1 PMID: 25026318

34. Wahlsten D (1972) Phenotypic and genetic relations between initial response to electric shock and rate of avoidance learning in mice. Behav Genet 2: 211–240. PMID: 4664210

35. Carran AB, Yeudall LT, Royce JR (1964) Voltage Level and Skin Resistance in Avoidance Conditioning of Inbred Strains of Mice. J Comp Physiol Psychol 58: 427–430. PMID: 14241059

36. Kyle UG, Bosaeus I, De Lorenzo AD, Deurenberg P, Elia M, et al. (2004) Bioelectrical impedance analysis—part I: review of principles and methods. Clin Nutr 23: 1226–1243. PMID: 15380917

37. Webster JG, Clark JW (2010) Medical instrumentation: application and design. Hoboken, NJ: John Wiley & Sons. xix, 713 p. p.

38. Smith D Jr, Johnson M, Nagy T (2009) Precision and accuracy of bioimpedance spectroscopy for determination of in vivo body composition in rats. Int J Body Compos Res 7: 21–26. PMID: 19668348

39. Farmer GE, Thompson LT (2012) Learning-dependent plasticity of hippocampal CA1 pyramidal neuron postburst afterhyperpolarizations and increased excitability after inhibitory avoidance learning depend upon basolateral amygdala inputs. Hippocampus 22: 1703–1719. doi: 10.1002/hipo.22005 PMID: 22367983

40. Nazari-Serenjeh F, Rezayof A (2013) Cooperative interaction between the basolateral amygdala and ventral tegmental area modulates the consolidation of inhibitory avoidance memory. Prog Neuropsychopharmacol Biol Psychiatry 40: 54–61. doi: 10.1016/j.pnpbp.2012.10.003 PMID: 23063440

41. Bach SA, de Siqueira LV, Muller AP, Oses JP, Quatrim A, et al. (2014) Dietary omega-3 deficiency reduces BDNF content and activation NMDA receptor and Fyn in dorsal hippocampus: Implications on persistence of long-term memory in rats. Nutr Neurosci 17: 186–192. doi: 10.1179/1476830513Y.0000000087 PMID: 24621058

42. Botton PH, Costa MS, Ardais AP, Mioranzza S, Souza DO, et al. (2010) Caffeine prevents disruption of memory consolidation in the inhibitory avoidance and novel object recognition tasks by scopolamine in adult mice. Behav Brain Res 214: 254–259. doi: 10.1016/j.bbr.2010.05.034 PMID: 20553765

43. Cline BH, Steinbusch HW, Malin D, Revishchin AV, Pavlova GV, et al. (2012) The neuronal insulin sensitizer dicholine succinate reduces stress-induced depressive traits and memory deficit: possible role of insulin-like growth factor 2. BMC Neurosci 13: 110. doi: 10.1186/1471-2202-13-110 PMID: 22989159

44. Detrait ER, Hanon E, Dardenne B, Lamberty Y (2009) The inhibitory avoidance test optimized for discovery of cognitive enhancers. Behav Res Methods 41: 805–811. doi: 10.3758/BRM.41.3.805 PMID: 19587195

45. Jiang S, Bendjelloul F, Ballerini P, D'Alimonte I, Nargi E, et al. (2007) Guanosine reduces apoptosis and inflammation associated with restoration of function in rats with acute spinal cord injury. Purinergic Signal 3: 411–421. doi: 10.1007/s11302-007-9079-6 PMID: 18404454

46. Lara DR, Schmidt AP, Frizzo ME, Burgos JS, Ramirez G, et al. (2001) Effect of orally administered guanosine on seizures and death induced by glutamatergic agents. Brain Res 912: 176–180. PMID: 11532434

47. Schmidt AP, Lara DR, de Faria Maraschin J, da Silveira Perla A, Onofre Souza D (2000) Guanosine and GMP prevent seizures induced by quinolinic acid in mice. Brain Res 864: 40–43. PMID: 10793184

48. Schmidt AP, Avila TT, Souza DO (2005) Intracerebroventricular guanine-based purines protect against seizures induced by quinolinic acid in mice. Neurochem Res 30: 69–73. PMID: 15756934

49. Schmidt AP, Lara DR, Souza DO (2007) Proposal of a guanine-based purinergic system in the mammalian central nervous system. Pharmacol Ther 116: 401–416. PMID: 17884172

50. Skalicky M, Narath E, Viidik A (2001) Housing conditions influence the survival and body composition of ageing rats. Exp Gerontol 36: 159–170. PMID: 11162919

51. Muller AP, Gnoatto J, Moreira JD, Zimmer ER, Haas CB, et al. (2011) Exercise increases insulin signaling in the hippocampus: physiological effects and pharmacological impact of intracerebroventricular insulin administration in mice. Hippocampus 21: 1082–1092. doi: 10.1002/hipo.20822 PMID: 20824731

52. Glick SD, Greenstein S, Goldfarb J (1973) Increased electrical impedance of mice following administration of scopolamine. Behav Biol 9: 771–775. PMID: 4764257

53. Hu L, Maslanik T, Zerebeckyj M, Plato CF (2012) Evaluation of bioimpedance spectroscopy for the measurement of body fluid compartment volumes in rats. J Pharmacol Toxicol Methods 65: 75–82. doi: 10.1016/j.vascn.2012.02.001 PMID: 22353670

54. Izquierdo LA, Barros DM, Ardenghi PG, Pereira P, Rodrigues C, et al. (2000) Different hippocampal molecular requirements for short- and long-term retrieval of one-trial avoidance learning. Behav Brain Res 111: 93–98. PMID: 10840135

55. Matte C, Pereira LO, Dos Santos TM, Mackedanz V, Cunha AA, et al. (2009) Acute homocysteine administration impairs memory consolidation on inhibitory avoidance task and decreases hippocampal brain-derived neurotrophic factor immunocontent: prevention by folic acid treatment. Neuroscience 163: 1039–1045. doi: 10.1016/j.neuroscience.2009.07.023 PMID: 19619620

56. Furini CR, Myskiw JC, Schmidt BE, Marcondes LA, Izquierdo I (2014) D1 and D5 dopamine receptors participate on the consolidation of two different memories. Behavioural Brain Research 271: 212–217. doi: 10.1016/j.bbr.2014.06.027 PMID: 24959860

57. Tarozzi A, Merlicco A, Morroni F, Bolondi C, Di Iorio P, et al. (2010) Guanosine protects human neuroblastoma cells from oxidative stress and toxicity induced by Amyloid-beta peptide oligomers. J Biol Regul Homeost Agents 24: 297–306. PMID: 20846477